

# Statistical Data Fusion for Hybrid Localization of Mobile Terminals

Dem Fachbereich 18  
Elektrotechnik und Informationstechnik  
der Technischen Universität Darmstadt  
zur Erlangung der Würde eines  
Doktor-Ingenieurs (Dr.-Ing.)  
vorgelegte Dissertation

von  
Dipl.-Ing. Carsten Fritsche  
geboren am 20.07.1978 in Groß-Gerau

Referent:	Prof. Dr.-Ing. Anja Klein
Korreferent:	Prof. Dr. Fredrik Gustafsson
Tag der Einreichung:	...
Tag der mündlichen Prüfung:	...



---

## Kurzfassung

In den letzten Jahren gibt es ein erhöhtes Interesse an drahtlosen Ortungssystemen, die zuverlässige Schätzungen des Ortes eines mobilen Endgerätes (ME) liefern. Dies liegt vor allem an den bereits vorhandenen sowie den kurz vor der Einführung stehenden ortsabhängigen Diensten, wie z.B. intelligente Transportsysteme, Gelbe Seiten, ortsabhängige Gebührenzahlungen und andere, viel versprechende Dienstleistungen, deren Anwendung eine genaue Schätzung des Ortes des ME erfordert. Bis heute sind eine Vielzahl an drahtlosen Ortungssystemen vorgeschlagen worden, die eine Ortsschätzungen des ME anbieten. Die viel versprechendsten Lösungen basieren auf dem globalen Navigations-Satellitensystem (GNSS) und dem zellularen Mobilfunknetz, da beide Systeme eine bereits existierende Infrastruktur ausnutzen. Üblicherweise stellen diese Systeme die Ortsschätzungen des ME unabhängig von einander zur Verfügung. Jedoch existieren Szenarien, in denen die Signale, die zwischen den Satelliten und des ME ausgetauscht werden, blockiert werden. Beispiele hierfür sind ein ME, das sich in innerstädtischen Umgebungen befindet, in denen hohe Gebäude die freie Sicht zu den Satelliten versperren oder ein ME, das sich innerhalb von Gebäuden befindet. In diesen Szenarien ist die Anzahl der zur Verfügung stehenden Messwerte meist nicht ausreichend, um mit Hilfe von GNSS den Ort des ME zu schätzen. Die Signale, die zwischen der Basisstation (BS) des zellularen Mobilfunknetzes und des ME ausgetauscht werden, stehen praktisch in jedem Szenario zur Verfügung, jedoch können diese Signale nicht die gleiche Lokalisierungs Genauigkeit liefern, wie die Signale des GNSS. In innerstädtischen Umgebungen und innerhalb von Gebäuden werden diese Signale häufig an den Hindernissen, wie z.B. Gebäuden oder Bäume reflektiert, so dass keine direkte Sichtverbindung (line-of-sight (LOS)) zwischen des ME und der BS existiert. In diesem Fall erreicht das Signal des ME die BS über einen indirekten Pfad, was in der Literatur als non-line-of-sight (NLOS) Ausbreitung bezeichnet wird. Die Fehler durch NLOS-Ausbreitung führen im Allgemeinen zu einer Verschlechterung der Lokalisierungs Genauigkeit, und sollten daher in den Lokalisierungs Algorithmen berücksichtigt werden.

Die vorliegende Arbeit behandelt das Problem der Bestimmung des Ortes des ME unter Verwendung von Pseudoentfernungs-Messwerte (PE), welche das Global Positioning System (GPS) zur Verfügung stellt, sowie Umlaufzeit-Messwerte (ULZ) und Empfangsfeldstärke-Messwerte (EFS), welche das Global System for Mobile communications (GSM) zur Verfügung stellt. Die zugrunde liegenden Messwerte werden heutzutage von jedem handelsüblichen Mobiltelefon sowie GPS-Empfänger zur Verfügung gestellt. Die verschiedenen Messwerte werden effektiv miteinander kombiniert unter der Verwendung von Verfahren der statistischen Datenfusion, was im

Folgenden als hybride Lokalisierung bezeichnet wird. Durch die Kombination von Messwerten ist es möglich, Ortsschätzungen des ME zu erhalten, auch wenn die Anzahl der von GPS zur Verfügung gestellten Messwerte nicht ausreicht. Die hybriden Lokisierungsalgorithmen sind so entworfen, dass eine gute Lokalisierungsgenauigkeit in Szenarien mit LOS Ausbreitungsbedingungen sowie in Szenarien in denen die Ausbreitungsbedingungen zwischen LOS und NLOS wechseln können, erreicht werden kann. Weiterhin wird untersucht, inwiefern Messwerte über die GNSS Referenzzeit (GRZ) den bestehenden Uhrenfehler zwischen den Uhren der Satelliten und des ME verringern und die Lokalisierungsgenauigkeit verbessern können. Um die hybriden Lokisierungsalgorithmen analysieren zu können, wird ein Modell eingeführt, das das hybride Lokalisierungsszenario mathematisch beschreibt. Statistische Modelle, die die Bewegung des ME sowie die Uhr des ME beschreiben, werden eingeführt. Die Messwerte werden ebenfalls statistisch beschrieben und enthalten Modelle die für LOS Ausbreitungsbedingungen gültig sind, sowie Modelle die zwischen LOS und NLOS Ausbreitungsbedingungen wechseln können. In dieser Arbeit werden die folgenden hybriden Lokisierungsalgorithmen vorgeschlagen:

- Nicht rekursive, hybride Lokisierungsalgorithmen, die Abhängigkeiten zwischen zeitlich aufeinanderfolgenden Orten des ME und zeitlich aufeinanderfolgenden Messwerten nicht berücksichtigen.
- Rekursive, hybride Lokisierungsalgorithmen, die Informationen über Schätzwerte des Ortes des ME aus zeitlich vorangegangenen Schätzungen sowie Messwerte von vorherigen Zeitschritten in die aktuellen Schätzung mit einfließen lassen.
- Rekursive, hybride Lokisierungsalgorithmen mit adaptiver LOS/NLOS Detektion, die Informationen über Schätzwerte des Ortes des ME aus zeitlich vorangegangenen Schätzungen sowie Messwerte von vorherigen Zeitschritten in die aktuellen Schätzung mit einfließen lassen, und darüber hinaus die aktuellen Ausbreitungsbedingungen schätzen.

Die nicht rekursiven hybriden Lokisierungsalgorithmen basieren auf dem Maximum Likelihood (ML) Prinzip. Für LOS Ausbreitungsbedingungen sowie für Ausbreitungsbedingungen, die zwischen LOS und NLOS wechseln können werden die ML Schätzer hergeleitet. Die ML Schätzwerte werden numerisch berechnet unter der Verwendung von suboptimalen Algorithmen. Um die theoretisch bestmögliche Performanz der nicht rekursiven Schätzer zu bestimmen, werden die Cramér-Rao Schranken (CRS) für die hybride Lokalisierung bestimmt. Die Ergebnisse mit simulierten Daten sowie Daten, die aus Feldversuchen stammen, haben gezeigt, dass durch die zusätzliche Berücksichtigung von PE Messwerte von GPS und GRT Messwerte von GSM die Lokalisierungsgenauigkeit erheblich verbessert werden kann, im Vergleich zu Algorithmen, die nur ULZ und EFS Messwerte von GSM auswerten.

Die rekursiven hybriden Lokalisierungsalgorithmen, die in dieser Arbeit entwickelt werden, beruhen auf Kalman Filter (KF)-basierte Schätzer und Partikelfilter (PF)-basierte Schätzer. Es werden verschiedene Schätzer für LOS Ausbreitungsbedingungen, sowie für Ausbreitungsbedingungen, die zwischen LOS und NLOS wechseln können, vorgeschlagen. Die PF-basierten Schätzer berücksichtigen zusätzlich Straßeninformationen, um die Lokalisierungsgenauigkeit weiter zu verbessern. Die a posteriori CRS (PCRS) für die hybride Lokalisierung wird hergeleitet, um die theoretisch bestmögliche Performanz der rekursiven Schätzer zu bestimmen. Es wird gezeigt, dass durch die Berücksichtigung von Straßeninformationen in den Schätzern die Lokalisierungsgenauigkeit erheblich verbessert werden kann. Des Weiteren wird gezeigt, dass die rekursiven hybriden Lokalisierungsalgorithmen eine höhere Lokalisierungsgenauigkeit liefern als die nicht rekursiven hybriden Lokalisierungsalgorithmen.

Die rekursiven hybriden Lokalisierungsalgorithmen mit adaptiver LOS/NLOS Detektion, die in dieser Arbeit vorgeschlagen werden, basieren auf einem interacing multiple model Algorithmus mit erweiterten KF Schätzern (IMM-EKF), sowie zwei multiple model PF-basierten Schätzer. Die multiple model PF-basierten Schätzer berücksichtigen zusätzlich Straßeninformationen, um die Lokalisierungsgenauigkeit weiter zu verbessern. Eine neue Methode wird vorgeschlagen, um die PCRS für rekursive Schätzer mit adaptiver LOS/NLOS Detektion zu bestimmen. Es wird gezeigt, dass multiple model PF-basierten Schätzer mit Straßeninformationen im Allgemeinen eine höhere Lokalisierungsgenauigkeit aufweisen als das IMM-EKF. Es wird weiterhin gezeigt, dass das IMM-EKF den besten Kompromiss zwischen Lokalisierungsgenauigkeit und Komplexität erzielt, solange keine Straßeninformation in den multiple model PF-basierten Schätzern berücksichtigt wird.



# Abstract

In recent years, there is an increased interest in wireless location systems offering reliable mobile terminal (MT) location estimates. This is mainly due to upcoming and already available Location Based Services, such as intelligent transport systems, yellow page services, location sensitive billing and other promising services that rely on accurate MT location estimates. So far, a multitude of wireless location systems have been proposed that offer MT location estimates. The most promising solutions are based on the Global Navigation Satellite System (GNSS) and the cellular radio network, since both systems utilize an already existing infrastructure. Conventionally, these systems provide MT location estimates independently from each other. However, there exist scenarios where the signals that are exchanged between the satellites and the MT are blocked, e.g., in urban environments where tall buildings surround the MT or in indoor environments. In these scenarios, the number of measurements available from GNSS is often insufficient to determine the MT location. The signals that are exchanged between the base stations (BSs) of the cellular radio network and the MT are available in these scenarios, but generally they cannot offer the same accuracy as the signals from GNSS. In urban and indoor scenarios, these signals are often reflected at obstacles such as buildings or trees, so that a direct, line-of-sight (LOS) path between MT and the BS does not exist. In this case, the signal of the MT arrive via an indirect path at the BS, which is known as non-line-of-sight (NLOS) propagation. The errors due to NLOS propagation generally result in a decreased localization performance, and should be therefore taken into account in the MT localization algorithms.

This thesis deals with the problem of estimating the MT location using pseudorange (PR) measurements from the Global Positioning System (GPS) and round trip time (RTT) and received signal strength (RSS) measurements from the Global System for Mobile communications (GSM), which is termed hybrid localization. The measurements, which are available from off-the-shelf mobile phones and conventional GPS receivers, are efficiently combined by using statistical data fusion, so that it is possible to obtain MT location estimates even if the number of measurements available from GPS is insufficient to determine the MT location. The corresponding hybrid localization algorithms are designed such that good performance can be achieved in situations when the measurements are affected by either LOS propagation conditions or propagation conditions that switch between LOS and NLOS. It is investigated how the existing offset between the satellite clocks and the MT clock can be mitigated and the localization accuracy can be improved by using GNSS reference time (GRT) measurements. In order to analyze the hybrid localization algorithms, a mathematical framework is introduced that describes the hybrid localization scenario. Statistical models for the

MT movement and MT clock, as well as models for the measurements assuming LOS and NLOS propagation conditions are introduced. In this work, the following three types of hybrid localization algorithms are introduced:

- Non-recursive hybrid localization algorithms, that do not take into account existing temporal dependencies between time consecutive MT locations and measurements.
- Recursive hybrid localization algorithms, that take into account the information of MT estimates and measurements from previous time steps.
- Recursive hybrid localization algorithms with adaptive LOS/NLOS detection, that take into account the information of MT estimates and measurements from previous time steps, and that estimate the current propagation conditions.

The non-recursive hybrid localization algorithms are based on the maximum likelihood (ML) principle. The ML estimators for LOS propagation conditions and for propagation conditions that switch between LOS and NLOS are newly derived, and ML estimates are numerically obtained using suboptimal algorithms. In order to assess the theoretical best achievable performance of non-recursive estimators, the Cramér-Rao lower bound (CRLB) for hybrid localization is evaluated. Simulation and field trial results have shown that additionally taking into account PR measurements from GPS and GRT from GSM in the algorithms can significantly improve the localization accuracy compared to algorithms that only take into account RTT and RSS measurements from GSM.

The recursive hybrid localization algorithms developed in this work are Kalman filter (KF)-based estimators and particle filter (PF)-based estimators. Different estimators for LOS propagation conditions and for propagation conditions that switch between LOS and NLOS are newly proposed. The PF-based estimators additionally take into account road information to further improve the localization accuracy. The theoretical best achievable performance of recursive estimators is found by evaluating the posterior CRLB (PCRLB). It is shown that additionally taking into account road information into the estimators can significantly improve the localization accuracy. It is further demonstrated that recursive hybrid localization algorithms outperform non-recursive hybrid localization algorithms.

The recursive hybrid localization algorithms with adaptive LOS/NLOS detection that are proposed in this work are based on the interacting multiple model (IMM) estimator that is combined with extended KFs (EKFs) and two multiple model PF-based estimators. The multiple model PF-based estimators additionally take into account road



information to further improve the localization accuracy. A novel method is presented to determine the PCRLB for recursive estimators with adaptive LOS/NLOS detection. It is shown that multiple model PF-based estimators with road constraints generally outperform the IMM-EKF. It is further demonstrated that the IMM-EKF achieves the best trade-off between performance and computational complexity, as long as road constraints are not considered in the multiple model PF-based estimators.



# Contents

<b>1</b>	<b>Introduction</b>	<b>1</b>
1.1	Localization of Mobile Terminals . . . . .	1
1.2	Hybrid Localization of Mobile Terminals . . . . .	4
1.3	State-of-the-art . . . . .	5
1.4	Open Issues . . . . .	10
1.5	Thesis Contributions and Overview . . . . .	11
<b>2</b>	<b>Hybrid Localization Scenario</b>	<b>15</b>
2.1	Introduction . . . . .	15
2.2	Scenario Assumptions . . . . .	15
2.3	Simulation Model . . . . .	16
2.3.1	Introduction . . . . .	16
2.3.2	State Model . . . . .	17
2.3.2.1	Introduction . . . . .	17
2.3.2.2	General State Model . . . . .	17
2.3.2.3	Mobile Terminal Kinematic State Model . . . . .	18
2.3.2.4	Mobile Terminal Clock State Model . . . . .	19
2.3.3	Measurement Model . . . . .	20
2.3.3.1	Introduction . . . . .	20
2.3.3.2	General Measurement Model . . . . .	20
2.3.3.3	General Measurement Model for Propagation Conditions that switch between LOS and NLOS . . . . .	21
2.3.3.4	Pseudorange . . . . .	24
2.3.3.5	Round Trip Time . . . . .	25
2.3.3.5.1	Introduction . . . . .	25
2.3.3.5.2	Model for Propagation Conditions that switch between LOS and NLOS . . . . .	25
2.3.3.5.3	Model for LOS Propagation Conditions . . . . .	27
2.3.3.6	Received Signal Strength . . . . .	28
2.3.3.6.1	Introduction . . . . .	28
2.3.3.6.2	Model for Propagation Conditions that switch between LOS and NLOS . . . . .	28
2.3.3.6.3	Model for LOS Propagation Conditions . . . . .	33
2.3.3.7	Global Navigation Satellite System Reference Time . . . . .	33
2.3.4	Simulation Scenario . . . . .	35
2.3.4.1	Introduction . . . . .	35
2.3.4.2	Scenario I . . . . .	35

2.3.4.3	Scenario II . . . . .	37
2.3.5	Monte Carlo Simulations . . . . .	39
2.4	Field Trial . . . . .	42
<b>3</b>	<b>Non-Recursive State Estimation for Hybrid Localization</b>	<b>45</b>
3.1	Introduction . . . . .	45
3.2	Concept of Non-Recursive State Estimation . . . . .	45
3.3	Cramér-Rao Lower Bound . . . . .	49
3.3.1	Introduction . . . . .	49
3.3.2	Cramér-Rao Lower Bound for LOS Propagation Conditions . . . . .	50
3.3.3	Cramér-Rao Lower Bound for Propagation Conditions that switch between LOS and NLOS . . . . .	60
3.4	Maximum Likelihood Estimator . . . . .	63
3.4.1	Introduction . . . . .	63
3.4.2	Maximum Likelihood Estimator for LOS Propagation Conditions	64
3.4.2.1	Introduction . . . . .	64
3.4.2.2	Gauss-Newton Algorithm . . . . .	65
3.4.2.3	Levenberg-Marquardt Algorithm . . . . .	67
3.4.3	Maximum Likelihood Estimator for Propagation Conditions that switch between LOS and NLOS . . . . .	69
3.5	Performance Evaluation . . . . .	74
3.5.1	Introduction . . . . .	74
3.5.2	Simulation Results for Scenario I . . . . .	75
3.5.2.1	Simulation Results for LOS Propagation Conditions . . . . .	75
3.5.2.2	Simulation Results for Propagation Conditions that switch between LOS and NLOS . . . . .	81
3.5.3	Field Trial Results . . . . .	83
3.5.4	Computational Complexity . . . . .	85
3.6	Conclusions . . . . .	88
<b>4</b>	<b>Recursive State Estimation for Hybrid Localization</b>	<b>91</b>
4.1	Introduction . . . . .	91
4.2	Concept of Recursive Bayesian Estimation . . . . .	91
4.3	Posterior Cramér-Rao Lower Bound . . . . .	93
4.3.1	Introduction . . . . .	93
4.3.2	Posterior Cramér-Rao Lower Bound for LOS propagation condi- tions . . . . .	95
4.3.3	Posterior Cramér-Rao Lower Bound for Propagation Conditions that switch between LOS and NLOS . . . . .	96
4.4	Kalman Filter-based Estimators . . . . .	98

---

4.4.1	Introduction . . . . .	98
4.4.2	Extended Kalman Filter . . . . .	99
4.4.3	Unscented Kalman Filter . . . . .	101
4.4.4	Cubature Kalman Filter . . . . .	105
4.5	Particle Filter-based Estimators . . . . .	107
4.5.1	Introduction . . . . .	107
4.5.2	Particle Filter . . . . .	109
4.5.2.1	Introduction . . . . .	109
4.5.2.2	Derivations . . . . .	109
4.5.2.3	Choice of Importance Density . . . . .	112
4.5.3	Rao-Blackwellized Particle Filter . . . . .	114
4.5.3.1	Introduction . . . . .	114
4.5.3.2	Derivations . . . . .	115
4.5.3.3	Choice of Importance Density . . . . .	121
4.5.3.4	Application to the Hybrid Localization Problem . . . . .	123
4.5.4	Auxiliary Particle Filter . . . . .	126
4.5.4.1	Introduction . . . . .	126
4.5.4.2	Derivations . . . . .	126
4.5.4.3	Choice of Importance Density . . . . .	128
4.5.5	Rao-Blackwellized Auxiliary Particle Filter . . . . .	129
4.5.5.1	Introduction . . . . .	129
4.5.5.2	Derivations . . . . .	129
4.5.5.3	Choice of Importance Density . . . . .	134
4.5.6	Particle Filter with Road Constraints . . . . .	137
4.5.6.1	Introduction . . . . .	137
4.5.6.2	Incorporation of Road Constraints . . . . .	137
4.5.7	Rao-Blackwellized Particle Filter with Road Constraints . . . . .	140
4.6	Performance Evaluation . . . . .	144
4.6.1	Introduction . . . . .	144
4.6.2	Simulation Results for Scenario I . . . . .	144
4.6.2.1	Simulation Results for LOS Propagation Conditions . . . . .	144
4.6.2.2	Simulation Results for Propagation Conditions that switch between LOS and NLOS . . . . .	155
4.6.3	Field Trial Results . . . . .	157
4.6.4	Computational Complexity . . . . .	163
4.7	Conclusions . . . . .	165
<b>5</b>	<b>Recursive State Estimation with Adaptive LOS/NLOS Detection</b>	<b>167</b>
5.1	Introduction . . . . .	167

5.2	Concept of Adaptive Recursive Bayesian Estimation . . . . .	168
5.2.1	Introduction . . . . .	168
5.2.2	Mode Sequence Conditioning . . . . .	168
5.2.3	State Vector Augmentation . . . . .	170
5.3	Posterior Cramér-Rao Lower Bound . . . . .	171
5.3.1	Introduction . . . . .	171
5.3.2	Enumeration Method . . . . .	172
5.3.3	Marginalization Method . . . . .	175
5.4	Interacting Multiple Model Algorithm-based Estimators . . . . .	179
5.4.1	Introduction . . . . .	179
5.4.2	Interacting Multiple Model Extended Kalman Filter . . . . .	179
5.5	Multiple Model Particle Filter-based Estimators . . . . .	183
5.5.1	Introduction . . . . .	183
5.5.2	Multiple Model Particle Filter . . . . .	184
5.5.2.1	Introduction . . . . .	184
5.5.2.2	Derivations . . . . .	185
5.5.2.3	Choice of Importance Density . . . . .	186
5.5.2.4	Incorporation of Road Constraints . . . . .	187
5.5.3	Multiple Model Rao-Blackwellized Particle Filter . . . . .	190
5.5.3.1	Introduction . . . . .	190
5.5.3.2	Derivations . . . . .	190
5.5.3.3	Choice of Importance Density . . . . .	196
5.5.3.4	Application to the Hybrid Localization Problem . . . . .	199
5.5.3.5	Incorporation of Road Constraints . . . . .	199
5.6	Performance Evaluation . . . . .	201
5.6.1	Introduction . . . . .	201
5.6.2	Simulation Results for Scenario II . . . . .	202
5.6.2.1	Simulation Results for LOS Propagation Conditions . . . . .	202
5.6.2.2	Simulation Results for Propagation conditions that switch between LOS and NLOS . . . . .	208
5.6.3	Comments on Computational Complexity . . . . .	212
5.7	Conclusions . . . . .	212
<b>6</b>	<b>Conclusions</b>	<b>215</b>
	<b>Appendix</b>	<b>217</b>
A.1	Coordinate Transformations for Hybrid Localization . . . . .	217
A.1.1	Introduction . . . . .	217
A.1.2	Transformation from Geodetic Coordinates to ECEF Coordinates	217
A.1.3	Transformation from ECEF Coordinates to ENU Coordinates . . . . .	218

---

A.2	Derivation of (3.19) describing the FIM for measurements corrupted by zero-mean Gaussian errors . . . . .	219
A.3	Derivation of (3.23) describing the FIM for PR measurements . . . . .	220
A.4	Derivation of (3.25) describing the FIM for RTT measurements . . . . .	222
A.5	Derivation of (3.28) describing the FIM for RSS measurements . . . . .	223
A.6	Derivation of (3.36) describing the MT location Fisher information submatrix for hybrid localization . . . . .	225
A.7	Derivation of (3.37) describing the numerator of the MT location CRLB	228
A.8	Derivation of (3.47) describing the denominator of the MT location CRLB	229
A.9	Proof showing that the MT location CRLBs of the Cellular and Hybrid 1 method are equal. . . . .	235
A.10	Monte Carlo Integration . . . . .	235
A.11	Proof of (5.28) showing that the Bayesian information submatrix can be calculated recursively. . . . .	236
<b>List of Acronyms</b>		<b>239</b>
<b>List of Symbols</b>		<b>243</b>
<b>Bibliography</b>		<b>257</b>
<b>Lebenslauf</b>		<b>271</b>





# Chapter 1

## Introduction

### 1.1 Localization of Mobile Terminals

In recent years, there has been an increased interest in wireless location systems offering reliable estimates of the geographical location of a user that is equipped with a Mobile Terminal (MT). On the one hand, this is due to upcoming and already available commercial services (also known as Location Based Services) such as social networking, intelligent transport systems, fraud detection, yellow page services, location sensitive billing and other promising services that rely on accurate MT location estimates [VWG<sup>+</sup>04, GG05, STK05, K up05, GP09]. On the other hand, the United States Federal Communications Commission issued an order, in which all wireless service providers are required to report the location of an enhanced 911 caller within a specified accuracy [Tri99]. In the European Union similar regulations are under way [KR99]. The emerging Location Based Services together with the regulations issued by the United States and the European Union have pushed further the research and standardization activities in the field of MT localization.

In the following, wireless location systems that are used in this context are categorized into the Global Navigation Satellite System (GNSS) and the cellular radio network. The GNSS consists of a number of satellites that circulate the Earth on predefined orbits. The satellites continuously broadcast radio signals containing information about their current location. The MT collects measurements by extracting important signal parameters from the received satellite signals that relate the MT location to the satellite location. The cellular radio network is composed of a number of Base Stations (BSs) which are installed at fixed points on Earth. The BSs generally transmit radio signals containing information about their current location to the MT and receive radio signals from the MT. From these signals, measurements are collected by either the MT or the BS by extracting important signal parameters that relate the MT location to the BS location. Depending on the investigated system, the location of the MT can be estimated by the MT itself (mobile-centric solution), or it can be estimated by a central entity in the cellular radio network that obtains the measurements via the BSs (network-centric solution) [GG05, STK05, SCGL05].

Important signal parameters that can be extracted from the received radio signal are, e.g., the Time of Arrival (ToA), Time Difference of Arrival (TDoA), Received Signal

Strength (RSS) or Angle of Arrival (AoA), which are called measurements in the following [Caf99, GG05, GP09]. These measurements have in common that they each do not provide unique information about the MT location. For example, the ToA measurement gives information about the time the radio signal requires to travel from the BS to the MT. By multiplying the ToA measurement with the speed of light, the measured distance to the MT can be obtained. Since a single measured distance to the MT gives an ambiguous solution for the MT location, several measurements from different satellites/BSs have to be collected, in order to obtain a unique solution for the MT location [Tor84, GG05]. The corresponding localization algorithms perform two tasks, that are conventionally processed using a two step approach [GP09]. In the first step, the localization algorithms estimate the signal parameters such as the ToA, TDoA, RSS or AoA from the received radio signal. These measurements are then used to estimate the MT location in a second step. In this work, only localization algorithms are developed for estimating the MT location. Algorithms for estimating the signal parameters are out of scope and are treated, for instance in [KV99, Caf99, Car05, GP09].

In Fig. 1.1 an example for the two-dimensional localization of an MT in a cellular network based on ToA measurements is given. It is assumed that the radio signals from different BSs arrive via the direct path at the MT, which is also known as Line-Of-Sight (LOS) propagation condition. The corresponding ToA measurements are assumed to be error-free and the BS locations are known. From Fig. 1.1 it can be seen that measuring the distance between the MT and a single BS limits the location of the MT to a circle drawn around the BS, with the measured distance being the

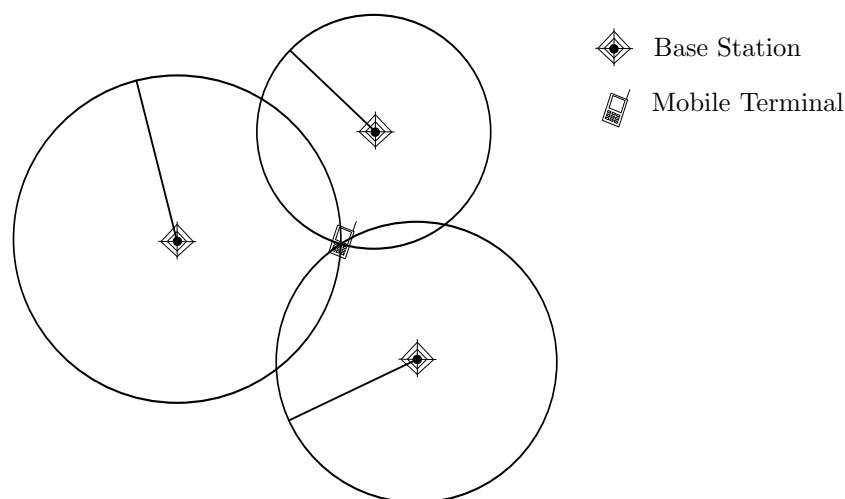


Figure 1.1. Principle of two dimensional MT localization using ToA measurements from the cellular radio network.

radius of the circle. If the measured distance to an additional BS is taken into account, then the MT location is restricted to the two points where both circles intersect. An unambiguous MT location can be finally found by taking into account the measured distance to a third BS.

In reality, however, the measured distances are affected by errors so that the circles in Fig. 1.1 will not intersect at a unique point. Further, obstacles such as hills, trees or buildings hinder the radio signals to arrive via the direct path at the MT, which is known as Non-Line-Of-Sight (NLOS) propagation. In this case, the radio signals are reflected, refracted, diffracted, absorbed or scattered at the obstacles resulting in estimated signal parameters that can completely differ from the ones that are expected under LOS propagation conditions. In Fig. 1.2, the LOS and NLOS propagation conditions are illustrated for a cellular radio network, where the radio signal of one BS arrives via the direct path at the MT and the radio signal of the other BS arrives via an indirect path at the MT. The deviations of the signal parameters in NLOS propagation conditions from the signal parameters in LOS propagation conditions can be very large and are generally different for each scenario [SM99, SPK01, FK09, YG09]. The NLOS problem has been identified as one of the most severe problems in wireless localization, and algorithms that do not take into account NLOS propagation will significantly degrade in localization accuracy when NLOS propagation occurs [WH96, Caf99, GG05].

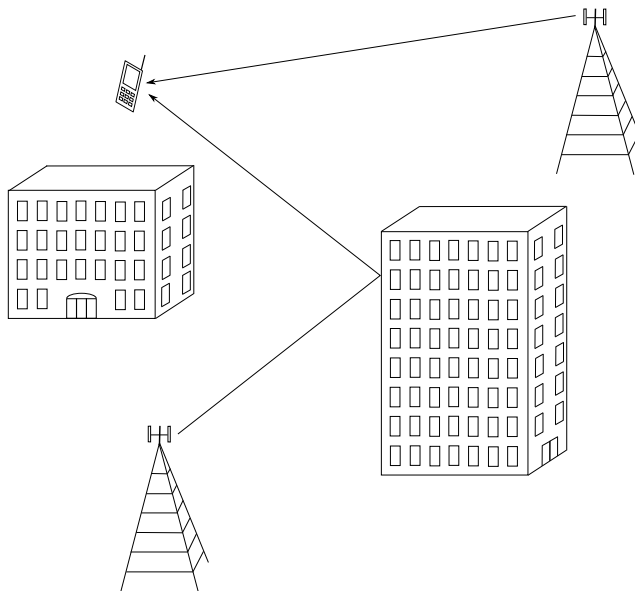


Figure 1.2. Scenario showing LOS and NLOS propagation conditions

## 1.2 Hybrid Localization of Mobile Terminals

Standard localization algorithms process only measurements of the same type, e.g., solely ToA measurements, in order to estimate the MT location. This strategy requires that a certain number of measurements of the same type are available at any time. In many situations, however, this is often not the case, so that localization algorithms are preferred that can efficiently combine different types of measurements. The combination of different types of measurements is also known as data fusion.

Nowadays, almost every MT is equipped with a GNSS receiver, that is used for navigation purposes. The GNSS, such as the Global Positioning System (GPS) and the prospective European counterpart Galileo, use ToA measurements to estimate the MT location. If the MT receives satellite signals from at least four different satellites, a three-dimensional MT location estimate can be found, where the fourth satellite signal is needed to resolve the unknown bias between the MT and the satellite clock [Kap96, ME06]. In a similar manner, one can obtain a two dimensional MT location estimate if the MT receives signals from at least three different satellites. However, there exist situations where the GNSS signals are blocked, e.g., when the MT is located indoors or in urban canyons. In these scenarios, the number of satellites in view is often not sufficient to obtain a three dimensional or even two dimensional MT location estimate.

An alternative to the GNSS is the exploitation of communication signals of the cellular radio network, in order to obtain MT location estimates. In the Global System for Mobile communications (GSM), for example, measurements such as the Timing Advance (TA), Enhanced Observed Time Difference (E-OTD), AoA or RSS exist that give information on the MT location [Küp05]. An appealing advantage of these measurements is that they are almost everywhere available. However, these measurement cannot offer the same accuracy as the GNSS-based measurements, and thus, the corresponding localization algorithms that are based on cellular radio network measurements cannot offer the same accuracy as their GNSS-based counterpart. The combination of measured values from the GNSS and the cellular radio network is, thus, a promising approach in order to obtain MT location estimates even if less than four or three satellites are in view [SAF<sup>+</sup>00, FKS06]. Instead of processing the measurements of each system independently, the measurements are processed jointly to estimate the MT location, which is termed hybrid localization in the following. The corresponding hybrid localization algorithms are expected to improve the accuracy and availability of MT location estimates, compared to the localization algorithms that either process the measurements from the cellular radio network or the GNSS.

In addition to that, there exist situations where additional information about the MT location is available. In automotive applications, for instance, this could be information about the infrastructure such as road maps, or information available from wheel speed sensors. Moreover, for a multitude of applications it is possible to approximate the MT movement with a statistical model, that takes into account that the MT can travel only a finite distance between two time consecutive time steps. These types of information with their different levels of accuracies should be additionally incorporated into the hybrid localization algorithms, in order to further improve the quality of the MT location estimates. The aim of this work is to develop hybrid localization algorithms that can efficiently combine RSS and TA measurements from GSM and Pseudorange (PR) measurements from GPS. These measurements can be easily obtained from off-the-shelf mobile phones and conventional GPS receivers, without the need to modify components of the satellite or cellular radio network. The performance of the hybrid localization algorithms should be further improved by taking into account models for the MT movement, models that take into account NLOS propagation conditions, and information available from a road map, in order to constrain the MT movement to roads in automotive applications.

### 1.3 State-of-the-art

This section presents a review of state-of-the-art in hybrid localization algorithms as well as localization algorithms that are robust against errors due to NLOS propagation conditions. In order to give a structured overview, the state-of-the-art in hybrid localization algorithms is presented first, which is followed by the survey of localization algorithms that are robust against errors due to NLOS propagation conditions.

In the following, the hybrid localization algorithms are further subdivided into two different categories. The first category contains hybrid localization algorithms that only use the information available from the measurements to estimate the MT location. These algorithms do not take into account information available from MT location estimates from previous time steps. In order to further improve the performance, the second category additionally takes into account information available from MT location estimates from previous time steps and a model for the MT movement. If the clocks of the satellites and the MT clock are assumed to be unsynchronized, which is usually the case, a model for the MT clock has to be additionally taken into account. The term hybrid is used in this section to describe the combination of different types of measurements as well as the combination of measurements from different systems.

Since it is not otherwise stated, all algorithms assume that the measurements are affected by LOS propagation conditions.

The state-of-the-art in hybrid localization algorithms belonging to the first category is presented next. In [HMD04], a hybrid localization algorithm based on the combination of PR measurements from GPS and TDoA measurements from the Universal Mobile Telecommunications System (UMTS) is presented, using a weighted least squares approach. In order to process the signals from GPS and UMTS simultaneously, a high-level joint receiver structure is proposed, but no performance results are presented. A similar approach is presented in [SLJ03], where PR measurements from GPS and TDoA measurements from a CDMA-2000 network are combined using a least squares approach. In contrast to [HMD04], the presented least squares algorithm is also tested on field trial data. In [SAF<sup>+</sup>00], a hybrid method is presented that is based on the fusion of PR measurements from GPS and Round Trip Time (RTT) measurements from a cellular radio network that is perfectly synchronized to GPS time. However, only a general description of the hybrid method is provided and no algorithms or theoretical performance bounds are given. Furthermore, the assumption that the radio network is perfectly synchronized to GPS is unrealistic, since the clocks installed in the satellite and radio network have a finite accuracy. A study on the influence of the timing accuracy on the performance of the hybrid localization algorithm is missing. A hybrid localization method combining PR measurements from GPS and E-OTD measurements from GSM is presented in [BGRS02]. Again, only general concepts concerning the radio network architecture are given and performance results are missing. The combination of MT location estimates from GPS and a wireless local area network is presented in [SGR04]. In [DKK00,KDTSP00], concepts for a hybrid localization system based on differential GPS and TDoA are presented and comments on the expected performance are given. A hybrid data fusion architecture that combines ToA, TDoA and AoA measurements in an optimal way is developed in [KOB01]. The combination of AoA and ToA measurements, where cross-correlation between the measurements is investigated, is presented in [PZV02]. The performance of hybrid systems combining TDoA and AoA measurements is addressed in [TCL01a,CZ02]. In [Spi01], ToA and TDoA measurements from a cellular radio network are combined and MT location estimates are obtained using a weighted least squares approach. The theoretical best achievable performance of this method is quantified by an accuracy measure, which turns out to be the Cramér-Rao Lower Bound (CRLB). Experimental results on combining TA and RSS measurements from a GSM network are presented in [SPK01]. Unfortunately, no localization algorithms are given. In [KGP05], a low cost positioning method for GSM networks is proposed. A cost function that combines TA and RSS measurements based on the Maximum Likelihood (ML) principle is proposed, which

is then solved using the Nelder-Mead simplex algorithm. A hybrid location estimation scheme for partially synchronized wireless sensor networks is presented in [SC04], where TDoA and RSS measurements are combined. The MT location estimates are obtained using the ML principle, but no formulas are provided. The estimation accuracy of the proposed scheme is further quantified by evaluating the corresponding CRLB. The results for the CRLB are extended to the case of combining ToA and RSS and are presented in [CS04]. In [MPV03,MPV05], a hybrid data fusion algorithm combining RSS and TDoA measurements from cellular radio networks is presented. The proposed algorithm uses nonparametric estimation methods, which are robust to variations of measurement noise due to NLOS propagation conditions and quantization. A hybrid system for accurate vehicular positioning combining signals from GSM and digital audio broadcast is presented in [RCC<sup>+</sup>00], and a hybrid positioning system that combines measurements from GPS and television is introduced in [Do08].

In the following a survey of state-of-the-art in hybrid localization algorithms belonging to the second category is given. In [MSD09], a hybrid data fusion approach is presented that combines PR measurements from the GNSS with TDoA measurements from future 3GPP-LTE communication systems using an Extended Kalman Filter (EKF). This work has been extended in [MSD10], where the hybrid data fusion problem is solved using a Particle Filter (PF). The application of so-called Gaussian mixture filters to hybrid localization is presented in [AL09], where PR measurements, PR rate measurements from GPS and range measurements from the cellular radio network are combined. In [PP07], the same combination of measurements as in [AL09] is used and a robust version of the EKF is proposed, in order to efficiently deal with measurement outliers due to NLOS propagation conditions. A modular software platform for testing hybrid position estimation algorithms has been presented in [RNALP08]. In [ZKUL06], a data fusion approach for improved positioning in GSM networks is presented. A method that combines TA and RSS measurements using an EKF is introduced, and the expected performance is evaluated in a simulation study. A Rao-Blackwellized variable rate particle filter for tracking the MT using PR measurements from GNSS, RSS measurements from a wireless sensor network and measurements from an inertial measurement unit is presented in [FPCFR07]. In this approach, the hybrid localization algorithm explicitly takes into account that measurements from different systems are available at different points in time. The expected performance of this approach is illustrated using computer simulations.

In the following, a review of state-of-the-art localization algorithms is given that are robust against errors due to NLOS propagation conditions. In order to give a structured overview, these algorithms are subdivided into two categories, namely algorithms for NLOS identification and algorithms for NLOS error mitigation.

The algorithms for NLOS identification detect and discard measurements that result from NLOS propagation conditions. The remaining measurements are then processed using localization algorithms that have been designed for LOS propagation conditions. Thus, these algorithms are especially useful for the case when a large number of measurements from different BS is available. In [BHM98], the NLOS identification problem for ToA measurements is formulated as a binary hypothesis test, where the errors due to NLOS are modeled statistically using different assumptions for the corresponding error probability density function (pdf). Depending on the assumption for the NLOS error pdf, various decision criteria are developed. In [GKP03], the pdf of the NLOS error is estimated from ToA measurements using non-parametric density estimation techniques. The estimated pdf is then compared to the known error pdf in LOS propagation conditions and an appropriate metric is introduced that decides whether the measurements result from LOS or NLOS propagation conditions. In [VC02], the error pdf of the ToA measurements remains unspecified and a composite hypothesis test is proposed to identify NLOS measurements. In [YG09], NLOS identification approaches based on the Neyman-Pearson theorem are proposed for AoA, ToA and RSS measurements. A simple NLOS identification approach for ultra-wideband localization systems is proposed in [SGKJ07].

In contrast to the algorithms for NLOS identification, the algorithms for NLOS error mitigation take into all available measurements to estimate the MT location. The algorithms for NLOS error mitigation can be subdivided into the following two categories. The first category contains algorithms for NLOS error mitigation that only use the information available from the measurements to estimate the MT location. These algorithms do not take into account information available from MT location estimates from previous time steps. The second category additionally take into account models for the MT movement and information available from MT location estimates from previous time steps to further improve the performance.

The state-of-the-art in algorithms for NLOS error mitigation belonging to the first category is presented next. In [RU04], an ML detection technique is applied to ToA measurements in order to mitigate NLOS errors. These approaches assume that the NLOS error pdf is a-priori known. In [CZ05], NLOS error mitigation algorithms for TDoA measurements and algorithms that combine TDoA and AoA measurements are developed. Depending on how much a-priori information about the NLOS error statistics is available, different algorithms are developed. In [QKS06], an analysis in terms of CRLBs is given for ToA, TDoA, AoA and RSS based localization methods assuming NLOS propagation conditions. Optimal estimators based on the ML and Maximum A Posteriori (MAP) principle are derived. A residual weighting algorithm to reduce



the NLOS error on MT location estimates is presented in [Che99]. In [MPV00], estimation techniques that are robust to some deviation from a presumed NLOS error pdf are applied to estimate the MT location from RSS measurements. In [SG04], a similar technique is applied to mitigate NLOS errors in ToA measurements. A NLOS error mitigation algorithm for ToA measurements which is based on a constrained linear least squares approach is proposed in [WWO03]. Estimation methods that approximate the pdf of ToA and TDoA measurements non-parametrically are proposed in [MPV03]. It is shown by means of simulations for a cellular radio network that the non-parametric estimators always outperform the parametric ML estimators. A similar technique is proposed in [HWZ08] to mitigate the NLOS errors in ToA measurements. The algorithms presented in [Che99, MPV00, MPV03, WWO03, SG04, HWZ08] all have in common, that there is no assumption on the NLOS error pdf. NLOS error mitigation algorithms that are based on multipath scattering models are presented in [TCL01b, AJC02, ZLB08]. A two stage approach for NLOS error mitigation for ToA/TDoA measurements is presented in [WH96, CZ01, GAM05]. In these algorithms, the first stage consists of identifying, which measurements are affected by errors due to NLOS propagation. In the second stage, these measurements are then corrected by the NLOS errors and the MT location is estimated.

In the following, a survey of state-of-the-art in algorithms for NLOS error mitigation belonging to the second category is given. In [NV03, NHVC04], an EKF based algorithm that mitigates NLOS errors in TDoA measurements and combined ToA and AoA measurements is proposed. In this algorithm, the NLOS errors are assumed to be Gaussian distributed with unknown mean value, which is additionally estimated by the EKF. Simulation and experimental results show, that the MT location can be efficiently estimated with this algorithm. An approach, where non-parametric density estimation methods are incorporated into the EKF framework to efficiently estimate the MT location with ToA measurements is proposed in [HWZ09]. An algorithm for mitigating the NLOS errors in ToA measurements which is based on probabilistic data association is presented in [HZ10]. In this algorithm, different subgroups of ToA measurements are constructed, which are fed into a least-squares estimator to determine the MT location. The MT location estimates together with the corresponding covariance matrices are then used in a hypothesis test for NLOS detection. The accepted MT location estimates are weighted with different probabilities in a Kalman filter (KF) based probabilistic data association framework to yield the final MT location estimate. A somewhat different approach is followed in [LC06, HGVT07, CYLL09], where LOS and NLOS propagation conditions are modeled as discrete events. A Markov chain is then used to describe the switching between LOS and NLOS propagation conditions probabilistically. Since it is generally unknown at which time instances the measure-

ments are affected by either LOS or NLOS propagation conditions, the current state of the Markov chain is estimated together with the MT location in the corresponding algorithms. In [HGVT07], the problem of jointly estimating the current state of the Markov chain and the MT location from ToA measurements is divided into two interdependent subproblems. It is proposed to solve the problem of estimating the current state of the Markov chain using a PF. The estimation result of the PF is then used in an Unscented Kalman Filter (UKF) to solve the problem of estimating the MT location. In [LC06], the problem of jointly estimating the current state of the Markov chain and the MT location from ToA measurements is solved using a decentralized approach. In the decentralized approach, an Interacting Multiple Model (IMM) algorithm is proposed at each BS that is capable to distinguish among a fixed number of discrete states. The IMM algorithm consists of two KFs, whose measurement noise statistics are matched to the different LOS and NLOS propagation conditions. The KF estimates are then combined, in order to determine the distance between the MT and the BS, but without taking into account the useful MT location information available from the other BSs. The final MT location estimate is obtained from the combination of the distance estimates from all BSs by using a geometric method. In [CYLL09], the decentralized approach is further extended and includes the combination of ToA and RSS measurements that are available from the BSs. In [LLP09], the Posterior Cramér-Rao Lower Bound (PCRLB) has been calculated for the joint estimation problem of the current state of the Markov chain and the MT location from ToA measurements. In this approach, the Markovian state sequence that models the switching between LOS and NLOS propagation conditions is assumed a-priori known. This assumption, however, will yield performance bounds that are overly optimistic, since in reality the state of the Markov chain is treated in the corresponding algorithms as unknown. The computation of the PCRLB, where the state sequence of the Markov chain is assumed unknown and exclusively related to the measurements is still an unsolved problem.

## 1.4 Open Issues

In the previous sections, it has been shown that hybrid localization is one of the most promising localization methods, when MT location estimates from GNSS are not available. However, it has been also shown that errors due to NLOS propagation conditions are one of the most severe problems in wireless localization. Thus, in the design of hybrid localization algorithms the aspect of NLOS propagation has to be taken into account. In this section, the open issues for hybrid localization using measurements from GPS and GSM arising from the review of the state-of-the-art in hybrid local-

ization algorithms and NLOS error mitigation algorithms presented in Section 1.3 are summarized:

1. How can hybrid localization algorithms be designed that efficiently combine different types of measurements with different accuracies from GPS and GSM, and which take into account that the measurements are affected by propagation conditions that generally switch between LOS and NLOS?
2. How can additional timing information about GPS reference time from the cellular radio network help to improve the performance of hybrid localization algorithms, and what accuracy is required for the timing information to yield performance improvements?
3. How can theoretical performance bounds be established for hybrid localization algorithms that take into account different types of measurements from GPS and GSM?
4. How can hybrid localization algorithms be designed that satisfy Question 1 and that additionally take into account information from road maps and models for the MT movement and the MT clock?
5. How can theoretical performance bounds be established for hybrid localization algorithms that take into account different types of measurements from GPS and GSM and models for the MT movement and clock?
6. How can hybrid localization algorithms be designed that satisfy Question 3 and that model the switching between LOS and NLOS propagation conditions with a Markov chain?
7. How can theoretical performance bounds be established for hybrid localization algorithms that take into account different types of measurements from GPS and GSM, a Markov chain model for the switching between LOS and NLOS propagation conditions and models for the MT movement and clock?

## 1.5 Thesis Contributions and Overview

In this section, an overview about the structure of the thesis is given and the main contributions which solve the open problems introduced in Section 1.4 are summarized. The contents of each chapter together with the main contributions are briefly described in the following.

In Chapter 2, the hybrid localization scenario is explained that is required to evaluate the corresponding hybrid localization algorithms. Statistical models for the MT movement, MT clock and statistical models for the measurements that take into account LOS propagation conditions as well as NLOS propagation conditions are presented. It is explained how measurements and MT trajectories can be generated from these models, so that the performance of the proposed hybrid localization algorithms can be evaluated via Monte Carlo simulations. For the simulations, it is assumed that the measurements are either affected by LOS propagation conditions or by propagation conditions that switch between LOS and NLOS. Since the proposed hybrid algorithms will be also tested on data that is available from a field trial, the corresponding field trial scenario is also explained.

In Chapter 3, new hybrid localization algorithms are introduced that efficiently combine different types of measurements from GPS and GSM. The combination of different types of measurements in this chapter and the following chapters is based on the combination of information that is available from statistical models for the measurements, which is also known as statistical data fusion [Gus10b]. In this chapter, answers to the Questions 1, 2 and 3 stated in Section 1.4 are given:

1. The ML estimator for hybrid localization is newly derived for the case that measurements are affected by LOS propagation conditions. For measurements, where the propagation conditions switch between LOS and NLOS, an approximate ML estimator is newly proposed. Since for both ML estimators, closed-form solutions are not available, three different suboptimal algorithms are proposed to solve the ML optimization problem.
2. The influence of the accuracy of GPS reference time information on the performance of the proposed hybrid localization algorithms is analyzed in terms of simulations.
3. The CRLB for hybrid localization is introduced. For measurements affected by LOS propagation conditions, an analytical expression for the bound of the MT location Mean Square Error (MSE) is newly derived and a new geometrical interpretation of the bound is presented. For measurements, where the propagation conditions switch between LOS and NLOS, the CRLB is evaluated numerically.

The performance of the newly introduced hybrid localization algorithms is evaluated by means of simulations and experimental data. For the simulations, the performance of the different algorithms is further compared to the corresponding CRLBs.

In Chapter 4, new hybrid localization algorithms are introduced that combine different types of measurements, information available from road maps and models for the MT movement and clock. This Chapter answers Questions 4 and 5 of the open issues:

4. KF-based estimators and PF-based estimators are proposed to solve the hybrid localization problem. For measurements affected by LOS propagation conditions as well as for propagation conditions that switch between LOS and NLOS, four different PF-based estimators are derived. Road map information is included into these estimators, to further improve the performance. For measurements affected by LOS propagation conditions, three different KF-based estimators are proposed that do not take into account road map information.
5. The PCRLB for hybrid localization is introduced. For LOS propagation conditions as well as for propagation conditions that switch between LOS and NLOS, the PCRLB is evaluated numerically.

The performance of the newly introduced hybrid localization algorithms is evaluated by means of simulations and experimental data. For the simulations, the performance of the different algorithms is compared to the PCRLBs. The simulations performed in this chapter give also an answer to Question 2 of the open issues.

Chapter 5 introduces new hybrid localization algorithms that model the switching between LOS and NLOS propagation conditions with a Markov chain. This chapter addresses the open Questions 6 and 7 by the following contributions:

6. An IMM-based estimator and two multiple model-based estimators are newly proposed to solve the hybrid localization problem using a centralized approach. In the centralized approach, all measurements are processed jointly in order to estimate the MT location. Road constraints are included into the multiple model-based estimators to further improve the performance.
7. The PCRLB for hybrid localization is introduced, where the switching between LOS and NLOS propagation conditions is modeled with a Markov chain. Two different approaches for approximately evaluating the PCRLB are proposed and compared to each other.

The performance of the newly introduced hybrid localization algorithms is evaluated by means of simulations and is further compared to the PCRLBs and the performance of the PF-based estimators introduced in Chapter 4.

Finally, a summary of the main conclusions of the thesis is given in Chapter 6.



---

## Chapter 2

# Hybrid Localization Scenario

### 2.1 Introduction

In this chapter, the hybrid localization scenario that is used for the derivation and evaluation of the different proposed hybrid localization algorithms is presented. The hybrid localization scenario is subdivided into the simulations and the field trial. In the simulations, models describing the MT movement and MT clock, as well as models for the measurements from the cellular radio and GNSS network are introduced, from which synthetic measurements are generated. In the field trial, the measurements from the cellular radio network and the corresponding MT locations are available from a field trial, while for the GNSS network, synthetic measurements are generated. For the simulations, single path propagation is assumed, i.e., the radio signals from the MT arrive at the BS either via the direct path (LOS propagation) or via an indirect path (NLOS propagation). Two different models for generating the measurements from the cellular radio network are considered. The first model assumes that the measurements are only affected by LOS propagation conditions. The second model assumes that the measurements are affected by either LOS or NLOS propagation conditions, and that the propagation conditions will switch in time between LOS and NLOS.

The chapter is organized as follows. In Section 2.2, the scenario assumptions for the simulations and the field trial are discussed. The simulation model together with the simulation scenario are introduced in Section 2.3, and the field trial together with the corresponding scenario is explained in Section 2.4.

### 2.2 Scenario Assumptions

The hybrid localization scenario is composed of the BSs of the cellular radio network, the Satellites (SATs) of the GNSS and the MT. The BS and satellite locations are assumed known and the MT location has to be estimated. The locations of the BSs, the satellites and the MT are defined in a three-dimensional (3-D) Cartesian space given by  $\mathbb{R}^3$ , where  $\mathbb{R}$  is the set of real numbers. A common assumption is to disregard the height information of the BSs and MT, so that in the following the BSs and MT can be assumed to be located in the  $xy$ -plane [PST97].

The cellular radio network is composed of  $N_{\text{BS}}$  BSs, which may be equipped with directional antennas. Each BS collects measurements by extracting important signal parameters from the received MT signal that relate the MT location to the BS location. The measurements are assumed to be available at discrete time steps  $k \cdot T_{\text{S}}$ , with  $k \in \mathbb{N}$ , where index  $k$  is assigned to a continuous-time instant  $t_k$ ,  $T_{\text{S}} \triangleq t_k - t_{k-1}$  denotes the sampling interval,  $\mathbb{N}$  is the set of natural numbers and " $\triangleq$ " denotes equal by definition. In the following, only RSS and RTT measurements will be considered, since both measurements are available from ordinary GSM mobile terminals [EVB01, K p05]. The BS locations are assumed to be fixed and are given by  $\mathbf{x}_{\text{BS}}^{(n)} = [x_{\text{BS}}^{(n)}, y_{\text{BS}}^{(n)}]^{\text{T}} \in \mathbb{R}^2$ ,  $n = 1, \dots, N_{\text{BS}}$ , where  $[\cdot]^{\text{T}}$  denotes the transpose of a vector or matrix. The MT generally moves in space, so that the MT location at time step  $k$  is given by  $\mathbf{x}_{\text{MT},k} = [x_{\text{MT},k}, y_{\text{MT},k}]^{\text{T}} \in \mathbb{R}^2$ .

The GNSS is composed of  $N_{\text{SAT}}$  satellites. The MT collects measurements by extracting important signal parameters from the received satellite signals that relate the MT location to the satellite locations. The measurements are available at discrete time steps  $k \cdot T'_{\text{S}}$ , where  $T'_{\text{S}}$  denotes the sampling time of the GNSS measurements. For simplicity, it is assumed that  $T'_{\text{S}} = T_{\text{S}}$ . In the following, only PR measurements will be considered, since these measurements are available from conventional GNSS receivers [Kap96, ME06]. Here, it is worth noting that the PR measurements are affected by a common MT clock bias from GNSS reference time, which has to be additionally estimated. The satellites generally move in space, so that the satellite locations at time step  $k$  are given by  $\mathbf{x}_{\text{SAT},k}^{(l)} = [x_{\text{SAT},k}^{(l)}, y_{\text{SAT},k}^{(l)}, z_{\text{SAT},k}^{(l)}]^{\text{T}} \in \mathbb{R}^3$ ,  $l = 1, \dots, N_{\text{SAT}}$ .

In addition to the RSS and RTT measurements, it is assumed that the cellular radio network provides GNSS Reference Time (GRT) measurements to the MT [3GP09]. The GRT measurements are used to estimate the unknown MT clock bias inherent in the PR measurements and are assumed to be available at discrete time steps  $k \cdot T_{\text{S}}$ .

## 2.3 Simulation Model

### 2.3.1 Introduction

In this section, the simulation model for the hybrid localization is presented. The simulation model is described in the following by a state model and a measurement model, which is also known as state-space approach [Jaz70, BSLK01, Sim06]. It is assumed that both models are formulated in discrete-time and are assumed to be



available in a probabilistic form. In the state-space approach, the MT is represented by a state vector that contains all relevant information to describe the MT in a hybrid localization scenario. The corresponding model describing the evolution in time of the MT state is given by the state model. The measurements that are available to the MT give information about the MT state. The corresponding model relating the measurements from the cellular radio and GNSS network to the MT state is given by the measurement model. The state model and the measurement model are both used to generate the simulation environment for the hybrid localization, in order to evaluate the performance of the hybrid localization algorithms that are developed in this thesis.

This section is organized as follows. In Section 2.3.2, the state model for the hybrid localization is presented. The models for the measurements from the cellular radio and GNSS network are introduced in Section 2.3.3. In Section 2.3.4, the simulation scenario for the hybrid localization is explained.

## 2.3.2 State Model

### 2.3.2.1 Introduction

The evolution in time of the MT state is described by a state model <sup>1</sup>. The MT state is in general a vector composed of state variables that provide a complete representation of the internal condition or status of the MT at a given time instant [Sim06]. A general state model describing the evolution in time of the MT state is introduced in section 2.3.2.2. For the hybrid localization scenario, the variables that entirely describe the MT state are assumed to be the two-dimensional MT position and velocity coordinates, as well as the MT clock bias and clock drift. The corresponding kinematic model, that is assumed to describe the MT movement is given in Section 2.3.2.3, and the model characterizing the MT clock is presented in Section 2.3.2.4.

### 2.3.2.2 General State Model

In this section, a general model is introduced that relates the MT state at time  $k$  to the MT state at time  $k - 1$ . It is assumed that the MT state is given by an  $n_x$ -dimensional vector  $\mathbf{x}_k = [x_k^{(1)}, \dots, x_k^{(n_x)}]^\top \in \mathbb{R}^{n_x}$ . The current state is generally affected

<sup>1</sup>In the literature, the state model is also known as dynamic model, plant model or process model [BSLK01].

by errors that take into account any mismodeling effects or unforeseen disturbances in the model for the MT state. These errors are commonly described statistically by an  $n_w$ -dimensional random variable  $\mathbf{w}_{k-1} = [w_{k-1}^{(1)}, \dots, w_{k-1}^{(n_w)}]^\top \in \mathbb{R}^{n_w}$  ( $n_w \leq n_x$ ) with probability density function  $p_{\mathbf{w}_{k-1}}(\mathbf{w}_{k-1})$ . The vector sequence  $\{\mathbf{w}_{k-1}, k = 1, 2, \dots\}$  is assumed to be white, i.e, the  $\mathbf{w}_{k-1}$ 's are mutually independent for all  $k \in \mathbb{N}$  [Jaz70]. The MT state  $\mathbf{x}_{k-1}$  and the errors  $\mathbf{w}_{k-1}$  at time  $k - 1$  are related to the state  $\mathbf{x}_k$  at time  $k$  through a vector of known, real-valued, in general nonlinear functions denoted by  $\mathbf{f}_{k-1}(\cdot)$ . The corresponding general model for the state is, thus, given by

$$\mathbf{x}_k = \mathbf{f}_{k-1}(\mathbf{x}_{k-1}, \mathbf{w}_{k-1}). \quad (2.1)$$

In the following, it is assumed that the errors  $\mathbf{w}_{k-1}$  affecting the current state are additive. Let  $\mathbf{\Gamma}_{k-1}$  denote the noise gain matrix of dimension  $n_x \times n_w$  that maps the  $n_w$ -dimensional noise vector  $\mathbf{w}_{k-1}$  to the  $n_x$ -dimensional state vector  $\mathbf{x}_k$ . Then, the state model simplifies to

$$\mathbf{x}_k = \mathbf{f}_{k-1}(\mathbf{x}_{k-1}) + \mathbf{\Gamma}_{k-1} \cdot \mathbf{w}_{k-1}. \quad (2.2)$$

### 2.3.2.3 Mobile Terminal Kinematic State Model

The movement of the MT can be generally described by a model, in order to predict the MT position at the next time step. Until now, various mathematical models have been developed to describe the movement of an MT. These models range from very simple ones assuming an nonmaneuvering MT movement to very complicated models that take into account possible MT maneuvers, cf. [LJ03] for a detailed survey of motion models.

In the following, the nearly Constant Velocity (CV) model is used to describe the MT kinematics [BSLK01, LJ03]. Other, more complicated motion models could have been used to model MT movement, but this is beyond the scope of this work. The nearly constant velocity model is one of the simplest motion models, where in addition to the MT position the MT velocity enters as another unknown into the state vector and slight changes due to accelerations are modeled with an additive noise term. Let  $\dot{\mathbf{x}}_{\text{MT},k} = [\dot{x}_{\text{MT},k}, \dot{y}_{\text{MT},k}]^\top$  denote the discrete-time 2-D MT velocity vector, which can be concatenated together with  $\mathbf{x}_{\text{MT},k}$  into a single state vector given by  $\mathbf{x}_{\text{CV},k} = [\mathbf{x}_{\text{MT},k}^\top, \dot{\mathbf{x}}_{\text{MT},k}^\top]^\top$  and let  $\mathbf{F}_{\text{CV}}$  denote the state transition matrix describing the movement of the MT between two consecutive time steps. Let further  $\mathbf{Q}_{\text{CV}}$  denote the covariance matrix of a vector-valued, zero-mean white Gaussian noise sequence

$\mathbf{w}_{\text{CV},k-1} = [w_{x,k-1}, w_{y,k-1}]^\top$  and let the matrix  $\mathbf{\Gamma}_{\text{CV}}$  describe the mapping of the random accelerations contained in  $\mathbf{w}_{\text{CV},k-1}$  to the MT position and velocity components. Then, the discrete-time MT kinematic state model can be written as

$$\mathbf{x}_{\text{CV},k} = \mathbf{F}_{\text{CV}} \cdot \mathbf{x}_{\text{CV},k-1} + \mathbf{\Gamma}_{\text{CV}} \cdot \mathbf{w}_{\text{CV},k-1}, \quad (2.3)$$

with

$$\mathbf{F}_{\text{CV}} = \begin{bmatrix} \mathbf{I}_2 & T_S \cdot \mathbf{I}_2 \\ 0 & \mathbf{I}_2 \end{bmatrix}, \mathbf{\Gamma}_{\text{CV}} = \begin{bmatrix} T_S^2/2 \cdot \mathbf{I}_2 \\ T_S \cdot \mathbf{I}_2 \end{bmatrix}, \quad (2.4)$$

where  $\mathbf{I}_n$  is the  $n \times n$  identity matrix [BSLK01, LJ03]. In the following, the covariance matrix  $\mathbf{Q}_{\text{CV}}$  is further specified, which describes the uncertainty on the motion model. It is assumed that the random variables  $w_{x,k-1}$  and  $w_{y,k-1}$  are statistically independent. Let  $\sigma_x^2$  and  $\sigma_y^2$  denote the noise variances in the  $x$ - and  $y$ - directions. Furthermore, let  $\text{diag}[a_1, a_2, \dots, a_K]$  denote a diagonal matrix whose  $\kappa_1$ -th entry on the main diagonal is given by  $a_{\kappa_1}$ ,  $\kappa_1 = 1, \dots, K$ . Then, the covariance matrix  $\mathbf{Q}_{\text{CV}}$  can be written as  $\mathbf{Q}_{\text{CV}} = \text{diag}[\sigma_x^2, \sigma_y^2]$ .

### 2.3.2.4 Mobile Terminal Clock State Model

While GNSS satellites use accurate atomic clocks, the MTs are generally equipped with inexpensive and inaccurate quartz clocks [ME06]. The main drawback of using quartz clocks is that the MT clock is not time-synchronized to the clocks of the GNSS satellites. The resulting unknown MT Clock Offset (CO) cannot be neglected and has to be additionally estimated (e.g. an MT clock offset of  $1 \mu\text{s}$  results in a range offset of 300 m). In the following, a model for the MT clock offset is introduced, in order to describe the behavior of the MT clock offset over time.

The MT clock offset is modeled using two state components: clock bias  $\delta t$  and clock drift  $\delta \dot{t}$ , which represent the phase and frequency errors in the MT clock. The relationship between the clock bias and clock drift is commonly modeled with a second-order Gauss-Markov process [BSLK01, vDBB84]. Let  $\mathbf{x}_{\text{CO},k} = [c_0 \cdot \delta t_k, c_0 \cdot \delta \dot{t}_k]^\top$  denote the vector of discrete-time MT clock states multiplied by the speed of light  $c_0 = 3 \cdot 10^8$  m/s and let  $\mathbf{F}_{\text{CO}}$  denote the state transition matrix describing the MT clock offset between two consecutive time steps. Let further  $\mathbf{Q}_{\text{CO}}$  denote the covariance matrix of a vector-valued zero-mean white Gaussian noise sequence  $\mathbf{w}_{\text{CO},k-1} = [w_{\delta t,k-1}, w_{\delta \dot{t},k-1}]^\top$  and let the matrix  $\mathbf{\Gamma}_{\text{CO}}$  describe the mapping of the noise vector  $\mathbf{w}_{\text{CO},k-1}$  to the MT clock states. Then, the discrete-time MT clock state model can be written as

$$\mathbf{x}_{\text{CO},k} = \mathbf{F}_{\text{CO}} \cdot \mathbf{x}_{\text{CO},k-1} + \mathbf{\Gamma}_{\text{CO}} \cdot \mathbf{w}_{\text{CO},k-1}, \quad (2.5)$$

with

$$\mathbf{F}_{\text{CO}} = \begin{bmatrix} 1 & T_S \\ 0 & 1 \end{bmatrix}, \mathbf{\Gamma}_{\text{CO}} = \begin{bmatrix} c_0 & 0 \\ 0 & c_0 \end{bmatrix}. \quad (2.6)$$

The covariance matrix  $\mathbf{Q}_{\text{CO}}$  models the MT clock uncertainty and depends on which clock type is used. The uncertainty of the different clock types is generally characterized by the Allan variance, which can be directly related to the covariance matrix  $\mathbf{Q}_{\text{CO}}$  [vDBB84]. Let  $h_0$ ,  $h_{-1}$  and  $h_{-2}$  denote the Allan variance parameters. Then, the elements of the covariance matrix  $\mathbf{Q}_{\text{CO}}$  are given by

$$Q_{11} = h_0 \frac{T_S}{2} + 2h_{-1}T_S^2 + \frac{2}{3}\pi^2 h_{-2}T_S^3, \quad (2.7a)$$

$$Q_{21} = Q_{12} = 2h_{-1}T_S + \pi^2 h_{-2}T_S^2, \quad (2.7b)$$

$$Q_{22} = \frac{h_0}{2T_S} + 2h_{-1} + \frac{8}{3}\pi^2 h_{-2}T_S. \quad (2.7c)$$

## 2.3.3 Measurement Model

### 2.3.3.1 Introduction

The relationship between the MT state and the measurements available from the GNSS and cellular radio network is described in the following by a measurement model. The measurements available from the GNSS are assumed to be the PRs and the measurements available from the cellular radio network are assumed to be the RTT, RSS and GRT. In general, the signals exchanged between the MT and the BSs are subject to propagation conditions that may switch in time between LOS and NLOS. Since the different propagation conditions may considerably affect the measurements, it is important to take the different propagation conditions into account in the measurement model.

In Section 2.3.3.2, a general measurement model is introduced that relates the actual measurements to the unknown MT state. A general measurement model that takes into account the switching between LOS and NLOS propagation conditions is presented in Section 2.3.3.3, where the switching is modeled with a Markov chain. In Sections 2.3.3.4 to 2.3.3.7, the measurement models for the PR, RTT, RSS and GRT measurements are presented.

### 2.3.3.2 General Measurement Model

In this section, a general model is introduced that relates the actual measurements to the unknown MT state. It is assumed that  $n_z$  measurements  $\mathbf{z}_k = [z_k^{(1)}, \dots, z_k^{(n_z)}]^\top \in$

$\mathbb{R}^{n_z}$  are available, each depending on the MT state  $\mathbf{x}_k$ . The measurements  $\mathbf{z}_k$  are generally affected by errors that are commonly described statistically by an  $n_v$ -dimensional random variable  $\mathbf{v}_k = [v_k^{(1)}, \dots, v_k^{(n_v)}]^\top \in \mathbb{R}^{n_v}$  ( $n_v \leq n_z$ ) with probability density function  $p_{\mathbf{v}_k}(\mathbf{v}_k)$ . The vector sequence  $\{\mathbf{v}_k, k = 1, 2, \dots\}$  is assumed to be white, i.e., the  $\mathbf{v}_k$ 's are mutually independent for all  $k \in \mathbb{N}$ . Furthermore, it is assumed that  $\mathbf{v}_k$  and  $\mathbf{w}_k$ , which is defined in (2.1), are mutually independent for all  $k \in \mathbb{N}$ . The MT state  $\mathbf{x}_k$  and the errors  $\mathbf{v}_k$  are related to the measurements  $\mathbf{z}_k$  through a vector of known, real-valued, in general nonlinear functions denoted by  $\mathbf{h}_k(\cdot)$ . The corresponding general model for the measurement is, thus, given by

$$\mathbf{z}_k = \mathbf{h}_k(\mathbf{x}_k, \mathbf{v}_k). \quad (2.8)$$

In the following, it is assumed that the errors  $\mathbf{v}_k$  affecting the measurements are additive and that the dimensions of the measurement and error vectors are equal, i.e.  $n_z = n_v$ . Let the vector of functions  $\mathbf{h}_k(\mathbf{x}_k)$  be given by  $\mathbf{h}_k(\mathbf{x}_k) = [h_k^{(1)}(\mathbf{x}_k), \dots, h_k^{(n_z)}(\mathbf{x}_k)]^\top$ . Then, the measurement model simplifies to

$$\mathbf{z}_k = \mathbf{h}_k(\mathbf{x}_k) + \mathbf{v}_k. \quad (2.9)$$

### 2.3.3.3 General Measurement Model for Propagation Conditions that switch between LOS and NLOS

In this section, a general measurement model is introduced that takes into account that measurements in LOS or NLOS propagation conditions can be described by different models, and that takes into account that between consecutive time steps the propagation conditions may switch between LOS and NLOS [DC99, Qi03, LC06]. The switching between LOS and NLOS is assumed to be time-dependent and is modeled for each measurement by a discrete-time 2-state stochastic process. The stochastic process is assumed to satisfy the Markov property [Pap84], i.e., the future states of the process depend only upon the present state and not on the past. The resulting discrete-time 2-state Markov process is termed Markov chain. The state of the Markov chain for the  $m$ -th measurement is described by a discrete-valued random variable  $r_k^{(m)}$ , called mode variable in the following, which is in effect during the sampling period  $(t_{k-1}, t_k]$ . The variable  $r_k^{(m)}$  is assumed to be among the  $s^{(m)} = 2$  possible modes  $r_k^{(m)} \in \{1, 2\}$ , where  $r_k^{(m)} = 1$  is assigned to the event "LOS" and  $r_k^{(m)} = 2$  is assigned to the event "NLOS". The Markov chain is characterized by the transition probabilities describing the conditional probability for switching to mode  $r_k^{(m)} = j$  at time  $k$  given that mode  $r_{k-1}^{(m)} = i$  is in effect at time  $k-1$ . In the following, it is assumed that the transition probabilities are independent of  $k$ , i.e., the Markov chain is time-homogeneous, and

are given by

$$\pi_{ij}^{(m)} = \Pr\{r_k^{(m)} = j | r_{k-1}^{(m)} = i\}, \quad \forall i, j = 1, 2, \quad \text{and} \quad m = 1, \dots, n_z. \quad (2.10)$$

The corresponding Transition Probability Matrix (TPM) is, thus, also independent of  $k$  and is given by

$$\mathbf{\Pi}_m = \begin{bmatrix} \pi_{11}^{(m)} & \pi_{12}^{(m)} \\ \pi_{21}^{(m)} & \pi_{22}^{(m)} \end{bmatrix}, \quad (2.11)$$

where the elements of the TPM are assumed to satisfy the following conditions for  $m = 1, \dots, n_z$ :

$$\pi_{ij}^{(m)} \geq 0 \quad \forall i, j = 1, 2, \quad \text{and} \quad \sum_{j=1}^2 \pi_{ij}^{(m)} = 1, \quad \text{for} \quad i = 1, 2. \quad (2.12)$$

The initial mode probabilities of the Markov chain, i.e., the probability of being in mode LOS or NLOS at time  $k = 1$ , are given by

$$\pi_i^{(m)} = \Pr\{r_1^{(m)} = i\}, \quad \text{for} \quad i = 1, 2, \quad \text{and} \quad m = 1, \dots, n_z, \quad (2.13)$$

where the following conditions for  $m = 1, \dots, n_z$ , hold:

$$\pi_i^{(m)} \geq 0 \quad \text{and} \quad \sum_{i=1}^2 \pi_i^{(m)} = 1, \quad \text{for} \quad i = 1, 2. \quad (2.14)$$

Furthermore, it is assumed that the Markov chain is regular, i.e., for every  $k$ , the  $k$ -th power of the TPM, given by the matrix  $\check{\mathbf{\Pi}} = (\mathbf{\Pi}_m)^k$ , contains only positive entries [Lip74]. From this it follows that as  $k \rightarrow \infty$  the Markov chain converges to a unique stationary distribution, regardless of which initial mode probabilities  $\pi_i^{(m)}$  are assumed. The stationary distribution is characterized by the probabilities of being in the mode LOS or NLOS as  $k \rightarrow \infty$  which are denoted by  $p_{\text{LOS}}^{(m)}$  and  $p_{\text{NLOS}}^{(m)}$ , where  $p_{\text{LOS}}^{(m)} \geq 0$ ,  $p_{\text{NLOS}}^{(m)} \geq 0$  and  $p_{\text{LOS}}^{(m)} + p_{\text{NLOS}}^{(m)} = 1$  for  $m = 1, \dots, n_z$ , hold. The probabilities of the stationary distribution can be related to the elements of the TPM and are given by

$$\lim_{k \rightarrow \infty} \Pr\{r_k^{(m)} = 1\} = \frac{\pi_{21}^{(m)}}{\pi_{12}^{(m)} + \pi_{21}^{(m)}} = p_{\text{LOS}}^{(m)}, \quad (2.15a)$$

$$\lim_{k \rightarrow \infty} \Pr\{r_k^{(m)} = 2\} = \frac{\pi_{12}^{(m)}}{\pi_{12}^{(m)} + \pi_{21}^{(m)}} = p_{\text{NLOS}}^{(m)}, \quad (2.15b)$$

[Lip74]. In Fig. 2.1, the mode transition diagram of the Markov chain modeling the switching between LOS and NLOS propagation conditions for the  $m$ -th measurement is shown. The circles in the diagram represent the modes of the process and the

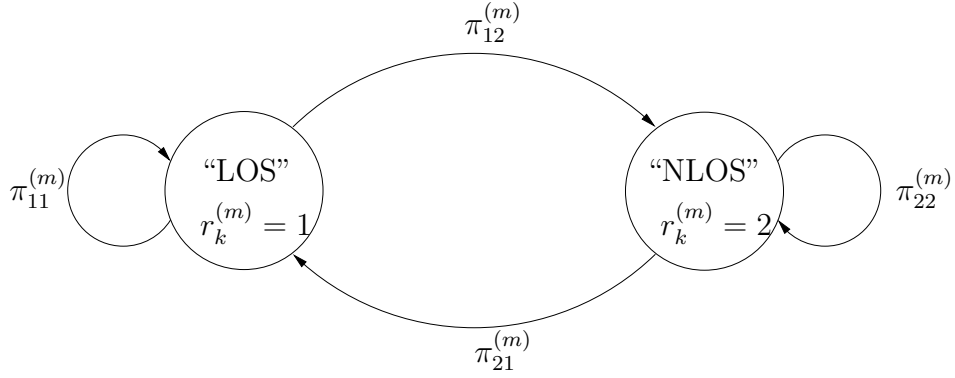


Figure 2.1. Mode transition model for Markov chain modeling the switching between LOS and NLOS propagation conditions for the  $m$ -th measurement.

arrows between circles represent the transition between modes and are labeled with the respective transition probabilities.

In the following, a general measurement model for a vector of  $n_z$  measurements is developed that takes into account that the switching between LOS and NLOS propagation conditions for each measurement can occur at different time steps. For  $n_z$  measurements, one has to consider  $n_z$  different 2-state Markov chains, which can be combined into a single, augmented Markov chain consisting of  $s = 2^{n_z}$  different states. In the following, it is assumed that the LOS/NLOS transitions among the different measurements are independent. Let  $\mathbf{\Pi}$  denote the TPM of the augmented Markov chain combining  $n_z$  different 2-state Markov chains and let the operator  $\otimes$  denote the Kronecker product. Then, the TPM  $\mathbf{\Pi}$  can be expressed in terms of the TPMs  $\mathbf{\Pi}_m$  of the different Markov chains with  $m = 1, \dots, n_z$ , according to:

$$\mathbf{\Pi} = \mathbf{\Pi}_1 \otimes \mathbf{\Pi}_2 \otimes \dots \otimes \mathbf{\Pi}_{n_z}. \quad (2.16)$$

The state of the augmented Markov chain is now described by the mode variable  $r_k$  that is assumed to be among the  $s = 2^{n_z}$  possible modes  $r_k \in \{1, \dots, 2^{n_z}\}$ . Thus, the general measurement model, that takes into account the switching between LOS and NLOS propagation conditions of  $n_z$  different measurements, can be determined by additionally considering the discrete mode variable  $r_k$  of the augmented Markov chain in the measurement equation  $\mathbf{h}_k(\cdot)$  according to

$$\mathbf{z}_k = \mathbf{h}_k(\mathbf{x}_k, r_k, \mathbf{v}_k). \quad (2.17)$$

In the following, it is assumed that the errors affecting the measurements are additive and that the dimensions of the measurement and error vectors are equal, i.e.  $n_z = n_v$ . Then, the measurement model simplifies to

$$\mathbf{z}_k = \mathbf{h}_k(\mathbf{x}_k, r_k) + \mathbf{v}_k(r_k), \quad (2.18)$$

where both the function  $\mathbf{h}_k(\cdot)$  and the error  $\mathbf{v}_k$  may depend on the mode variable  $r_k$ . In the same way, a mode variable can also be incorporated into the general state model, cf. Section 2.3.2.2, in order to model possible MT maneuvers but which is out of scope in this work [BSLK01].

### 2.3.3.4 Pseudorange

In GNSS, the MT measures the time the satellite signal requires to travel from the satellite to the MT [ME06]. The time measurements are generally affected by delays due to the propagation of the satellite signal through the ionosphere and the troposphere and due to errors such as receiver noise, relativity effects or multipath propagation [ME06]. In addition to that, the MT's clock is generally not time-synchronized to the clocks of the GNSS satellites, resulting in an unknown receiver clock bias that has to be taken into account in the measurement model. The biased time measurements are generally converted into biased range measurements, hereinafter referred to as PR measurements, that can be obtained from multiplying the time measurements by the speed of light  $c_0$ .

In the following, it is assumed that each measured PR is corrected for the known errors such as satellite clock offset, relativity effect and ionospheric delay using parameter values in the navigation message from the satellite [ME06]. Due to the fact that the clock offsets of the different GNSS satellites can be corrected, it can be assumed that these clocks are mutually synchronized, so that each PR measurement is affected by the same bias  $\delta t_k$ . It is further assumed that the signal strength of the satellite signal affected by NLOS propagation falls below the minimum detectable signal strength with which the GNSS receiver can acquire the satellite signal [ME06]. Thus, the MT can only receive signals from satellites in LOS, so that errors due to NLOS propagation are not considered in the PR measurement model.

Let  $\mathbf{z}_{\text{PR},k}$  denote the vector of  $M_{\text{PR}}$  PR measurements, where the  $m$ -th PR measurement is related to the satellite signal exchanged between the MT and the  $m$ -th satellite. Let  $d_{\text{SAT},k}^{(m)}(\mathbf{x}_{\text{MT},k})$  denote the Euclidean distance between the MT and the  $m$ -th satellite which is given by

$$d_{\text{SAT},k}^{(m)}(\mathbf{x}_{\text{MT},k}) = \sqrt{(x_{\text{MT},k} - x_{\text{SAT},k}^{(m)})^2 + (y_{\text{MT},k} - y_{\text{SAT},k}^{(m)})^2 + (z_{\text{SAT},k}^{(m)})^2}, \quad (2.19)$$

with  $m = 1, \dots, M_{\text{PR}}$ . Let further  $\mathbf{h}_{\text{PR}}(\mathbf{x}_{\text{MT},k}, \delta t_k)$  denote a vector of  $M_{\text{PR}}$  functions relating the MT state to the PR measurements, which is given by

$$\mathbf{h}_{\text{PR},k}(\mathbf{x}_{\text{MT},k}, c_0 \cdot \delta t_k) = \left[ d_{\text{SAT}}^{(1)}(\mathbf{x}_{\text{MT},k}), \dots, d_{\text{SAT}}^{(M_{\text{PR}})}(\mathbf{x}_{\text{MT},k}) \right]^T + c_0 \cdot \delta t_k, \quad (2.20)$$



and let the  $M_{\text{PR}}$ -dimensional random variable  $\mathbf{v}_{\text{PR},k} = [v_{\text{PR},k}^{(1)}, \dots, v_{\text{PR},k}^{(M_{\text{PR}})}]^\text{T}$  describe unmodeled effects, modeling errors and measurement errors affecting each PR measurement. Then, the PR measurement model can be written as

$$\mathbf{z}_{\text{PR},k} = \mathbf{h}_{\text{PR},k}(\mathbf{x}_{\text{MT},k}, c_0 \cdot \delta t_k) + \mathbf{v}_{\text{PR},k}. \quad (2.21)$$

In the following, it is assumed that  $\mathbf{v}_{\text{PR},k}$  is a white, zero-mean Gaussian distributed random sequence with covariance matrix  $\mathbf{R}_{\text{PR},k}$ . The errors affecting each PR measurement are generally assumed to be uncorrelated and the standard deviation  $\sigma_{\text{PR},k}^{(l)}$  from the PR measurement of the  $l$ -th satellite can be approximated by the user equivalent range error [Kap96, ME06]. Thus, the corresponding covariance matrix is given by  $\mathbf{R}_{\text{PR},k} = \text{diag}[\sigma_{\text{PR},k}^{(1),2}, \dots, \sigma_{\text{PR},k}^{(M_{\text{PR}}),2}]$ .

### 2.3.3.5 Round Trip Time

#### 2.3.3.5.1 Introduction

In cellular radio networks, there exist parameters such as the RTT, i.e., the time the radio signal requires to propagate from the BS to the MT and back, that give information about the MT location. Even though this parameter was not primarily designed for localization purposes, e.g., in GSM the RTT is used to synchronize the transmitted bursts of the MTs to the frame of the receiving BS, it provides an estimate of the distance between the BS and the MT [EVB01, K up05]. The accuracies of the distance estimates strongly depend on the current propagation conditions, i.e., whether the signals from the MT arrive via the direct (LOS) path or indirect (NLOS) path at the BS. Since the indirect path is longer than the direct path, the value of the RTT measurement will be significantly increased compared to the value of the RTT measurement under the LOS assumption. As the propagation conditions between consecutive time steps may switch between LOS and NLOS for each RTT measurement, and the errors due to NLOS propagation can lead to large errors in the RTT measurements, it is important that the RTT measurement model accounts for both LOS and NLOS propagation conditions.

#### 2.3.3.5.2 Model for Propagation Conditions that switch between LOS and NLOS

In the following, let  $\mathbf{z}_{\text{RTT},k}$  denote the vector of  $M_{\text{RTT}}$  RTT measurements multiplied by  $c_0/2$ , where the  $m$ -th RTT measurement is related to the radio signal exchanged

between the MT and the  $m$ -th BS. The switching between LOS and NLOS propagation conditions is modeled for each RTT measurement with a 2-state Markov chain which is represented by a discrete mode variable  $r_k^{(m)}$  with  $m = 1, \dots, M_{\text{RTT}}$ . The switching between LOS and NLOS for  $M_{\text{RTT}}$  RTT measurements is, thus, modeled with a  $2^{M_{\text{RTT}}}$ -state Monte Carlo, cf. section 2.3.3.3, where the discrete mode variable  $r_k$  is assumed to be among the  $2^{M_{\text{RTT}}}$  possible modes  $r_k \in \{1, \dots, 2^{M_{\text{RTT}}}\}$ . The Euclidean distance between the MT and the  $m$ -th BS is given by

$$d_{\text{BS},k}^{(m)}(\mathbf{x}_{\text{MT},k}) = \sqrt{(x_{\text{MT},k} - x_{\text{BS},k}^{(m)})^2 + (y_{\text{MT},k} - y_{\text{BS},k}^{(m)})^2}, \quad (2.22)$$

and the vector of  $M_{\text{RTT}}$  functions relating the MT state to the RTT measurements, which is assumed to be independent of  $r_k$ , is given by

$$\mathbf{h}_{\text{RTT},k}(\mathbf{x}_{\text{MT},k}) = \left[ d_{\text{BS}}^{(1)}(\mathbf{x}_{\text{MT},k}), \dots, d_{\text{BS}}^{(M_{\text{RTT}})}(\mathbf{x}_{\text{MT},k}) \right]^{\text{T}}. \quad (2.23)$$

The RTT measurements are generally affected by errors due to quantization, inaccuracies in the measurement equipment, changing propagation conditions - LOS and NLOS situations - and other measurement errors. These errors together with modeling errors are described by an  $M_{\text{RTT}}$ -dimensional, mode-dependent random variable  $\mathbf{v}_{\text{RTT},k}(r_k) = [v_{\text{RTT},k}(r_k^{(1)}), \dots, v_{\text{RTT},k}(r_k^{(M_{\text{RTT}})})]^{\text{T}}$ , where the discrete mode variable  $r_k$  takes into account that the propagation conditions between consecutive time steps may switch between LOS and NLOS. Thus, the corresponding model for the RTT measurements is given by

$$\mathbf{z}_{\text{RTT},k} = \mathbf{h}_{\text{RTT},k}(\mathbf{x}_{\text{MT},k}) + \mathbf{v}_{\text{RTT},k}(r_k). \quad (2.24)$$

In the following, it is assumed that  $\mathbf{v}_{\text{RTT},k}(r_k)$  is a white random sequence and that the errors affecting each of the  $M_{\text{RTT}}$  RTT measurements are mutually independent, so that for each RTT measurement the model for the mode-dependent random variable  $v_{\text{RTT},k}(r_k^{(m)})$  can be determined separately. It is assumed that the errors affecting each RTT measurement in LOS propagation conditions can be described by the random variable  $v_{\text{RTT,LOS},k}^{(m)}$ . In NLOS situations, the RTT measurements are additionally affected by errors due to NLOS propagation, that are modeled by the random variable  $v_{\text{RTT,NLOS},k}^{(m)}$ . Thus, the mode-dependent error model can be written as

$$v_{\text{RTT},k}(r_k^{(m)}) = \begin{cases} v_{\text{RTT,LOS},k}^{(m)} & \text{for } r_k^{(m)} = 1, \\ v_{\text{RTT,LOS},k}^{(m)} + v_{\text{RTT,NLOS},k}^{(m)} & \text{for } r_k^{(m)} = 2. \end{cases} \quad (2.25)$$

The random variable  $v_{\text{RTT,LOS},k}^{(m)}$  is generally described by a zero-mean Gaussian distribution with standard deviation  $\sigma_{\text{RTT,LOS},k}^{(m)}$  [SR96, WH96, FK09]. For the random variable  $v_{\text{RTT,NLOS},k}^{(m)}$  describing the NLOS error, several models have been proposed in the literature, such as random variables with exponential distributions or shifted Gaussian

distributions with positive mean value [SR96,CZ01,GG05]. Which error model best fits reality depends on different factors such as the investigated environment, e.g., indoor, urban or rural areas, and the cellular radio network, e.g., GSM or UMTS network. In the following, the NLOS error is described by a Gaussian random variable with positive mean value  $\mu_{\text{RTT,NLOS},k}^{(m)}$  and standard deviation  $\sigma_{\text{RTT,NLOS},k}^{(m)}$ , which is in accordance with the results that have been obtained from field-trial measurements in GSM networks [SR96,FK09]. Furthermore, the random variables  $v_{\text{RTT,LOS},k}^{(m)}$  and  $v_{\text{RTT,NLOS},k}^{(m)}$  are assumed to be independent. Then, the mode-dependent random variable  $v_{\text{RTT},k}(r_k^{(m)})$  for each RTT measurement is Gaussian distributed with mode-dependent mean value

$$\mu_{\text{RTT},k}(r_k^{(m)}) = \begin{cases} 0 & \text{for } r_k^{(m)} = 1, \\ \mu_{\text{RTT,NLOS},k}^{(m)} & \text{for } r_k^{(m)} = 2, \end{cases} \quad (2.26)$$

and mode-dependent variance

$$\sigma_{\text{RTT},k}^2(r_k^{(m)}) = \begin{cases} (\sigma_{\text{RTT,LOS},k}^{(m)})^2 & \text{for } r_k^{(m)} = 1, \\ (\sigma_{\text{RTT,LOS},k}^{(m)})^2 + (\sigma_{\text{RTT,NLOS},k}^{(m)})^2 & \text{for } r_k^{(m)} = 2. \end{cases} \quad (2.27)$$

Since the errors for the  $M_{\text{RTT}}$  RTT measurements are mutually independent and Gaussian distributed, the  $M_{\text{RTT}}$ -dimensional, mode-dependent random variable  $\mathbf{v}_{\text{RTT},k}(r_k)$  is also Gaussian distributed with mode-dependent mean vector  $\boldsymbol{\mu}_{\text{RTT},k}(r_k) = [\mu_{\text{RTT},k}(r_k^{(1)}), \dots, \mu_{\text{RTT},k}(r_k^{(M_{\text{RTT}})})]^\top$  and mode-dependent covariance matrix  $\mathbf{R}_{\text{RTT},k}(r_k) = \text{diag}[\sigma_{\text{RTT},k}^2(r_k^{(1)}), \dots, \sigma_{\text{RTT},k}^2(r_k^{(M_{\text{RTT}})})]$ .

### 2.3.3.5.3 Model for LOS Propagation Conditions

The model for the RTT measurement assuming LOS propagation conditions can be deduced from the model introduced in section 2.3.3.5.2. Let  $\mathbf{z}_{\text{RTT,LOS},k}$  denote the vector of  $M_{\text{RTT}}$  RTT measurements affected by LOS propagation conditions and let the  $M_{\text{RTT}}$ -dimensional, zero-mean Gaussian distributed random variable  $\mathbf{v}_{\text{RTT,LOS},k} = [v_{\text{RTT},k}(r_k^{(1)} = 1), \dots, v_{\text{RTT},k}(r_k^{(M_{\text{RTT}})} = 1)]^\top$  describe the corresponding errors with covariance matrix  $\mathbf{R}_{\text{RTT,LOS},k} = \text{diag}[\sigma_{\text{RTT},k}^2(r_k^{(1)} = 1), \dots, \sigma_{\text{RTT},k}^2(r_k^{(M_{\text{RTT}})} = 1)]$ . Then, the model for the RTT measurements assuming LOS propagation conditions is given by

$$\mathbf{z}_{\text{RTT,LOS},k} = \mathbf{h}_{\text{RTT},k}(\mathbf{x}_{\text{MT},k}) + \mathbf{v}_{\text{RTT,LOS},k}. \quad (2.28)$$

### 2.3.3.6 Received Signal Strength

#### 2.3.3.6.1 Introduction

In cellular radio networks, the MT measures the power of the received radio signal, which is known as RSS value. Although the RSS value was not primarily designed for localization purposes, e.g., in GSM the RSS values from multiple BS are used for the handover procedure, it provides information about the MT location [EVB01, K up05]. The RSS measurements are generally affected by the current propagation conditions, i.e., LOS or NLOS propagation, that have a direct influence on the achievable accuracy of the MT location estimates. Since in NLOS situations, the signal propagation is subject to reflection and diffraction from surrounding objects, such as buildings and trees, the value of the RSS measurement will be significantly decreased compared to the value of the RSS measurement under the LOS assumption. As the propagation conditions between consecutive time steps may switch between LOS and NLOS for each RSS measurement, and the errors due to NLOS propagation can lead to large errors in the RSS measurements, it is important that the RSS measurement model accounts for both LOS and NLOS propagation conditions.

#### 2.3.3.6.2 Model for Propagation Conditions that switch between LOS and NLOS

In the following, let  $\mathbf{z}_{\text{RSS},k}$  denote the vector of  $M_{\text{RSS}}$  RSS measurements, where the  $m$ -th RSS measurement is related to the radio signal exchanged between the MT and the  $m$ -th BS. The switching between LOS and NLOS propagation conditions is modeled for each RSS measurement with a 2-state Markov chain which is represented by a discrete mode variable  $r_k^{(m)}$  with  $m = 1, \dots, M_{\text{RSS}}$ . The switching between LOS and NLOS for  $M_{\text{BS}}$  RSS measurements is, thus, modeled with a  $2^{M_{\text{RSS}}}$ -state Markov chain, cf. section 2.3.3.3, where the discrete mode variable  $r_k$  is assumed to be among the  $2^{M_{\text{RSS}}}$  possible modes  $r_k \in \{1, \dots, 2^{M_{\text{RSS}}}\}$ .

The radio signal, that is exchanged between the  $m$ -th BS and the MT generally experiences attenuation. The attenuation of the signal strength through a mobile radio channel is mainly caused by three factors, namely multipath fading, shadowing and path loss [Qi03]. Multipath fading is caused by the reception of multiple copies of a transmitted signal through multipath propagation and results in a rapid fluctuation of the complex envelope of the received signal. However, the attenuation due to multipath fading is generally not considered in the RSS measurement model, since the

RSS value is obtained by averaging the received signal power over some time interval [Qi03]. Shadowing represents a slow variation in the received signal strength and is caused by events where the direct signal path between the MT and the BS is obscured, e.g., by large buildings. Experimental results have shown that shadowing can be described by a random variable with log-normal distribution [Rap02, Qi03]. The path loss describes the attenuation of the signal power as a function of the distance  $d_{\text{BS}}(\mathbf{x}_{\text{MT},k})$  between the MT and the BS. In the literature, various models for the path loss exist [Rap02, DC99, Hat80, OOKF68]. In the following, the log-distance path loss model is used, since it forms the basis of most of the models available in the literature [Rap02, DC99]. The log-distance path loss model assumes that the average received signal power decreases logarithmically with distance and is characterized by the path loss exponent and the reference path loss. The path loss exponent describes the rate at which the signal power decays with increasing MT to BS distance. The reference path loss is measured at a predetermined BS to MT reference distance (1 km in cellular radio networks) and depends on factors such as the specific propagation environment, BS antenna settings and the frequency band at which the cellular radio network is operating. Experimental and theoretical investigations have shown that the values for the reference path loss and the path loss exponent depend on the current propagation conditions [DC99]. In order to take into account the different propagation conditions in the path loss model, the reference path loss and the path loss exponent are assumed to be mode-dependent and are given by  $A(r_k^{(m)})$  and  $B(r_k^{(m)})$ . Let  $L^{(m)}(\mathbf{x}_{\text{MT},k}, r_k^{(m)})$  denote the path loss corresponding to the  $m$ -th RSS measurement. Then, the mode-dependent path loss model in dB scale is given by

$$L^{(m)}(\mathbf{x}_{\text{MT},k}, r_k^{(m)}) = A(r_k^{(m)}) + 10 \cdot B(r_k^{(m)}) \cdot \log_{10} \left( \frac{d_{\text{BS}}^{(m)}(\mathbf{x}_{\text{MT},k})}{1 \text{ km}} \right). \quad (2.29)$$

Let  $A_{\text{LOS}}^{(m)}$  and  $A_{\text{NLOS}}^{(m)}$  denote the reference path loss values for LOS and NLOS propagation conditions. Let further  $B_{\text{LOS}}^{(m)}$  and  $B_{\text{NLOS}}^{(m)}$  denote the path loss exponent for LOS and NLOS propagation conditions. Then, the mode-dependent reference path loss is given by

$$A(r_k^{(m)}) = \begin{cases} A_{\text{LOS}}^{(m)} & \text{for } r_k^{(m)} = 1, \\ A_{\text{NLOS}}^{(m)} & \text{for } r_k^{(m)} = 2, \end{cases} \quad (2.30)$$

and the mode-dependent path loss exponent is given by

$$B(r_k^{(m)}) = \begin{cases} B_{\text{LOS}}^{(m)} & \text{for } r_k^{(m)} = 1, \\ B_{\text{NLOS}}^{(m)} & \text{for } r_k^{(m)} = 2. \end{cases} \quad (2.31)$$

The specific values for the mode-dependent parameters  $A(r_k^{(m)})$  and  $B(r_k^{(m)})$  can be either determined from field trial measurements or from well known path loss models as, e.g., COST 231 Walfisch-Ikegami [DC99].

In real systems, the BSs may be equipped with several directional antennas (also known as sector antennas) in order to increase the cell's capacity. The employment of directional antennas at the BSs, however, will considerably affect the corresponding RSS measurements, since these antennas concentrate their signal power in one direction at the expense of other directions. Thus, it is important to incorporate the influence of directional antennas into the RSS measurement model. Directional antennas are commonly characterized by the antenna gain. In the following, it is assumed that 2-D models for the antenna gain are available. The antenna gain generally depends on the azimuth angle, which is given in the units of radians (rad) in the following. The azimuth angle  $\varphi_{\text{BS}}^{(m)}(\mathbf{x}_{\text{MT},k})$  denotes the angle between the vector pointing into the boresight direction of the  $m$ -th BS antenna and the vector that is directed towards the propagation path (LOS or NLOS) of the radio signal that is received by the MT. Since the indirect (NLOS) path is generally pointing into a different direction than the direct (LOS) path, the azimuth angle is assumed to be mode-dependent in the following. In LOS situations, the azimuth angle can be described deterministically. Let  $\varphi_0^{(m)}$  denote the azimuth angle between the positive  $x$ -axis of the Cartesian coordinate system with the  $m$ -th BS location as origin, and the vector pointing in the boresight direction of the  $m$ -th BS antenna. Then, the model for the azimuth angle in LOS situations is given by

$$\varphi_{\text{LOS}}^{(m)}(\mathbf{x}_{\text{MT},k}) = \arctan \left( \frac{y_{\text{BS}}^{(m)} - y_{\text{MT},k}}{x_{\text{BS}}^{(m)} - x_{\text{MT},k}} \right) - \varphi_0^{(m)}. \quad (2.32)$$

In NLOS situations, it is impractical to derive a deterministic model for the azimuth angle, as it would require additional information about the propagation environment such as the location and orientation of buildings. In these situations, it is much more convenient to model the azimuth angle statistically by a random variable [YG09, JCS98]. In the following, it is assumed that the azimuth angle in NLOS situations is uniformly distributed in the interval  $(-\pi - \varphi_0^{(m)}, \pi - \varphi_0^{(m)})$ , which corresponds to the assumption that can be often found in the literature [YG09, JCS98]. Thus, the mode-dependent azimuth angle can be written as

$$\varphi_{\text{BS}}^{(m)}(\mathbf{x}_{\text{MT},k}, r_k^{(m)}) = \begin{cases} \varphi_{\text{LOS}}^{(m)}(\mathbf{x}_{\text{MT},k}) & \text{for } r_k^{(m)} = 1, \\ \varphi_{\text{NLOS}}^{(m)} & \text{for } r_k^{(m)} = 2. \end{cases} \quad (2.33)$$

For the sake of clarity, the relationship between the different azimuth angles and the boresight direction of the BS antenna is depicted in Fig. 2.2. Note that the origin of the coordinate system is equal to the location of the  $m$ -th BS. In the following, the model for the antenna gain is further specified. Let the normalized antenna gain in dB scale be denoted as  $G_{\text{ANT}}^{(m)}(\varphi_{\text{BS}}^{(m)}(\mathbf{x}_{\text{MT},k}, r_k^{(m)}))$ . Let further  $G_{\text{min}}^{(m)}$  and  $\varphi_{3\text{dB}}^{(m)}$  denote the minimum gain and 3 dB beamwidth of the BS antenna and let  $\min\{a, b\}$  denote the smallest value in the set  $\{a, b\}$ . Then, a model for the normalized antenna gain is given

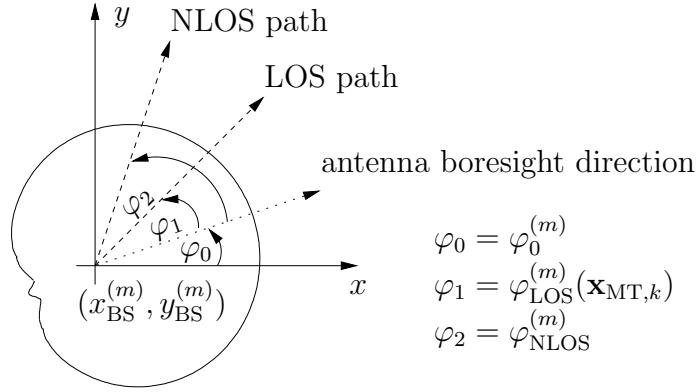


Figure 2.2. Relationship between the different azimuth angles and the antenna's boresight direction for the  $m$ -th BS antenna.

by

$$G_{\text{ANT}}^{(m)}(\varphi_{\text{BS}}^{(m)}(\mathbf{x}_{\text{MT},k}, r_k^{(m)})) = -\min \left\{ 12 \cdot \left( \frac{\varphi_{\text{BS}}^{(m)}(\mathbf{x}_{\text{MT},k}, r_k^{(m)})}{\varphi_{3\text{dB}}^{(m)}} \right)^2, G_{\text{min}}^{(m)} \right\}, \quad (2.34)$$

[3GP07]. Since the azimuth angle  $\varphi_{\text{NLOS}}^{(m)}$  in NLOS situations is modeled with a random variable, the corresponding antenna gain  $G_{\text{ANT}}^{(m)}(\varphi_{\text{BS}}^{(m)}(\mathbf{x}_{\text{MT},k}, r_k^{(m)} = 2))$  is also a random variable, whose pdf can be found from the transformation of random variables [Pap84]. For simplicity, the pdf of the antenna gain in NLOS situations is approximated in the following with a Gaussian pdf. Thus, the mean and variance of the Gaussian pdf are given by

$$\mu_{\text{ANT}}^{(m)} = -G_{\text{min}}^{(m)} \cdot \left( 1 - \frac{1}{3\pi\sqrt{3}} \sqrt{G_{\text{min}}^{(m)}} \cdot \varphi_{3\text{dB}}^{(m)} \right), \quad \text{and} \quad (2.35a)$$

$$\sigma_{\text{ANT}}^{(m),2} = G_{\text{min}}^{(m),2} \cdot \left( 1 - \frac{2}{5\pi\sqrt{3}} \sqrt{G_{\text{min}}^{(m)}} \cdot \varphi_{3\text{dB}}^{(m)} \right) - \mu_{\text{ANT},k}^{(m),2}, \quad (2.35b)$$

respectively. The corresponding mode-dependent antenna gain model can be rewritten as

$$G^{(m)}(\mathbf{x}_{\text{MT},k}, r_k^{(m)}) = \begin{cases} G_{\text{ANT}}^{(m)}(\varphi_{\text{BS}}^{(m)}(\mathbf{x}_{\text{MT},k}, r_k^{(m)})) & \text{for } r_k^{(m)} = 1, \\ \mu_{\text{ANT}}^{(m)} & \text{for } r_k^{(m)} = 2. \end{cases} \quad (2.36)$$

The models for the antenna gain and the path loss are used to determine the model relating the MT state to the  $m$ -th RSS measurement. Let  $P_{\text{T}}^{(m)}$  denote the equivalent isotropic radiated power of the  $m$ -th BS antenna in dB. Then, the mode-dependent model relating the MT state to the  $m$ -th RSS measurement is given by

$$h_{\text{RSS},k}^{(m)}(\mathbf{x}_{\text{MT},k}, r_k^{(m)}) = P_{\text{T}}^{(m)} - \left\{ L^{(m)}(\mathbf{x}_{\text{MT},k}, r_k^{(m)}) - G^{(m)}(\mathbf{x}_{\text{MT},k}, r_k^{(m)}) \right\}. \quad (2.37)$$

As a result, the vector of  $M_{\text{RSS}}$  mode-dependent functions relating the MT state to the  $M_{\text{RSS}}$  RSS measurements can be written as

$$\mathbf{h}_{\text{RSS},k}(\mathbf{x}_{\text{MT},k}, r_k) = \left[ h_{\text{RSS},k}^{(1)}(\mathbf{x}_{\text{MT},k}, r_k^{(1)}), \dots, h_{\text{RSS},k}^{(M_{\text{RSS}})}(\mathbf{x}_{\text{MT},k}, r_k^{(M_{\text{RSS}})}) \right]^{\text{T}}. \quad (2.38)$$

In general, the RSS measurements are affected by errors due to quantization, slow fading, changing propagation conditions - LOS and NLOS situations - and other measurement errors. These errors together with modeling errors are described by an  $M_{\text{RSS}}$ -dimensional, mode-dependent random variable  $\mathbf{v}_{\text{RSS},k}(r_k) = [v_{\text{RSS},k}(r_k^{(1)}), \dots, v_{\text{RSS},k}(r_k^{(M_{\text{RSS}})})]^{\text{T}}$ , where the discrete mode variable  $r_k$  takes into that between consecutive time steps the propagation conditions may switch between LOS and NLOS. Thus, the corresponding model for the RSS measurements in dB is given by

$$\mathbf{z}_{\text{RSS},k} = \mathbf{h}_{\text{RSS},k}(\mathbf{x}_{\text{MT},k}, r_k) + \mathbf{v}_{\text{RSS},k}(r_k). \quad (2.39)$$

In the following, it is assumed that  $\mathbf{v}_{\text{RSS},k}(r_k)$  is a white random sequence and that the errors affecting each of the  $M_{\text{RSS}}$  RSS measurements are mutually independent, so that for each RSS measurement the model for the mode-dependent random variable  $v_{\text{RSS},k}(r_k^{(m)})$  can be determined separately. The errors affecting each RSS measurement in LOS propagation conditions are described by the random variable  $v_{\text{RSS,LOS},k}^{(m)}$ . In NLOS situations, the RSS measurements are additionally affected by errors due to NLOS propagation, that are modeled by the random variable  $v_{\text{RSS,NLOS},k}^{(m)}$ . Thus, the mode-dependent error model can be written as

$$v_{\text{RSS},k}(r_k^{(m)}) = \begin{cases} v_{\text{RSS,LOS},k}^{(m)} & \text{for } r_k^{(m)} = 1, \\ v_{\text{RSS,LOS},k}^{(m)} + v_{\text{RSS,NLOS},k}^{(m)} & \text{for } r_k^{(m)} = 2. \end{cases} \quad (2.40)$$

The random variable  $v_{\text{RSS,LOS},k}^{(m)}$  is assumed to be zero-mean Gaussian distributed with standard deviation  $\sigma_{\text{RSS,LOS},k}^{(m)}$  [YG09]. In NLOS situations, shadowing as well as the randomly varying antenna gain predominate the errors. Shadowing is generally described by a random variable with log-normal distribution. Since the error model is in dB units, the random variable describing shadowing is zero-mean Gaussian distributed with standard deviation  $\sigma_{\text{SHA},k}^{(m)}$  [DC99, Rap02, YG09]. The random variable describing the antenna gain is Gaussian distributed with mean  $\mu_{\text{ANT}}^{(m)}$  and standard deviation  $\sigma_{\text{ANT}}^{(m)}$ . Since the mean  $\mu_{\text{ANT}}^{(m)}$  has been already considered in (2.36), the random variable describing the antenna gain is zero-mean Gaussian distributed. The random variables describing shadowing and the antenna gain are assumed to be independent, so that  $v_{\text{RSS,NLOS},k}^{(m)}$  is zero-mean Gaussian distributed with standard deviation  $\sigma_{\text{RSS,NLOS},k}^{(m)} = \sqrt{\sigma_{\text{SHA},k}^{(m),2} + \sigma_{\text{ANT}}^{(m),2}}$ . Assuming further that the random variables  $v_{\text{RSS,LOS},k}^{(m)}$  and  $v_{\text{RSS,NLOS},k}^{(m)}$  are independent, the mode-dependent random variable  $v_{\text{RSS},k}(r_k^{(m)})$  for



each RSS measurement is zero-mean Gaussian distributed with mode-dependent variance

$$\sigma_{\text{RSS},k}^2(r_k^{(m)}) = \begin{cases} \sigma_{\text{RSS,LOS},k}^{(m),2} & \text{for } r_k^{(m)} = 1, \\ \sigma_{\text{RSS,LOS},k}^{(m),2} + \sigma_{\text{RSS,NLOS},k}^{(m),2} & \text{for } r_k^{(m)} = 2. \end{cases} \quad (2.41)$$

Since the errors for the  $M_{\text{RSS}}$  RSS measurements are mutually independent and zero-mean Gaussian distributed, the  $M_{\text{RSS}}$ -dimensional, mode-dependent random variable  $\mathbf{v}_{\text{RSS},k}(r_k)$  is also zero-mean Gaussian distributed with mode-dependent covariance matrix  $\mathbf{R}_{\text{RSS},k}(r_k) = \text{diag}[\sigma_{\text{RSS},k}^2(r_k^{(1)}), \dots, \sigma_{\text{RSS},k}^2(r_k^{(M_{\text{RSS}})})]$ .

### 2.3.3.6.3 Model for LOS Propagation Conditions

The model for the RSS measurement assuming LOS propagation conditions can be deduced from the model introduced in section 2.3.3.6.2. Let  $\mathbf{z}_{\text{RSS,LOS},k}$  denote the vector of  $M_{\text{RSS}}$  RSS measurements affected by LOS propagation conditions and let the  $M_{\text{RSS}}$ -dimensional, zero-mean Gaussian distributed random variable  $\mathbf{v}_{\text{RSS,LOS},k} = [v_{\text{RSS},k}(r_k^{(1)} = 1), \dots, v_{\text{RSS},k}(r_k^{(M_{\text{RTT}})} = 1)]^T$  describe the corresponding errors with covariance matrix  $\mathbf{R}_{\text{RSS,LOS},k} = \text{diag}[\sigma_{\text{RSS},k}^2(r_k^{(1)} = 1), \dots, \sigma_{\text{RSS},k}^2(r_k^{(M_{\text{RSS}})} = 1)]$ . Furthermore, let  $\mathbf{h}_{\text{RSS,LOS},k}(\mathbf{x}_{\text{MT},k}) = [h_{\text{RSS},k}^{(1)}(\mathbf{x}_{\text{MT},k}, r_k^{(1)} = 1), \dots, h_{\text{RSS},k}^{(M_{\text{RSS}})}(\mathbf{x}_{\text{MT},k}, r_k^{(M_{\text{RSS}})} = 1)]^T$  denote the  $M_{\text{RSS}}$ -vector function relating the MT state to the  $M_{\text{RSS}}$  RSS measurements. Then, the model for the RSS measurements assuming LOS propagation conditions is given by

$$\mathbf{z}_{\text{RSS,LOS},k} = \mathbf{h}_{\text{RSS,LOS},k}(\mathbf{x}_{\text{MT},k}) + \mathbf{v}_{\text{RSS,LOS},k}. \quad (2.42)$$

### 2.3.3.7 Global Navigation Satellite System Reference Time

In GNSS, the satellite clocks are generally not time-synchronized to the clock of the MT. The resulting bias  $\delta t_k$  enters as an additional unknown into the pseudorange equations, cf. (2.21). In cellular radio networks, there exists the possibility to provide the MT with timing information that can be used to estimate the unknown clock bias  $\delta t_k$  in the pseudorange equations. In GSM, for example, the available Radio Resource Location Protocol (RRLP) provides timing information for GPS [3GP09]. In the following, a model is derived that relates the timing information available from the cellular radio network to the unknown clock bias  $\delta t_k$ .

In GNSS, there are basically three time scales to deal with. The two time scales corresponding to the times kept by the GNSS satellite and MT clocks, and a common time reference, denoted as GNSS reference time, which is a composite time scale derived

from the times kept by atomic clocks at the GNSS monitor stations and aboard the GNSS satellites [ME06]. The time scales of the GNSS satellite clocks are assumed to coincide with the GNSS reference time scale, since the GNSS satellite clocks are assumed to be mutually synchronized to GNSS reference time, cf. Section 2.3.3.4. Let  $t_{\text{GNSS},k}$  and  $t_{\text{MTC},k}$  denote the GNSS reference time scale and MT clock time scale at time step  $k$ , respectively. Then, the offset between these two time scales describes the clock bias  $\delta t_k$ , which is given by

$$\delta t_k = t_{\text{GNSS},k} - t_{\text{MTC},k}. \quad (2.43)$$

The timing information available from the cellular radio network is the GNSS reference time, which is marked on the radio signal that is transmitted to the MT. The GNSS reference time, however, can be provided to the MT only with a specified accuracy [3GP09]. On the one hand, this is due to errors affecting the GNSS reference time such as inaccurate clocks in the cellular radio network and other errors. On the other hand, the GNSS reference time information that is received by the MT is generally outdated by the amount of time the radio signal requires to propagate from the BS to the MT. The sum of these errors affecting the GNSS reference time is modeled in the following by a random variable  $v_{\text{GRT},k}$ . If the number of errors affecting the GNSS reference time is sufficiently large, the central limit theorem can be used and  $v_{\text{GRT},k}$  can be assumed to be Gaussian distributed with standard deviation  $\sigma_{\text{GRT},k}$  [Pap84]. In the following, it is assumed that  $v_{\text{GRT},k}$  is zero-mean and the corresponding sequence of random variables is white. Let  $z_{\text{GRT},k}$  denote the GRT measurement that is received by the MT. Then, the model for the GRT is given by

$$z_{\text{GRT},k} = t_{\text{GNSS},k} + v_{\text{GRT},k}. \quad (2.44)$$

The GRT measurement model can be directly converted into an MT clock bias model, since the MT time scale  $t_{\text{MTC},k}$  at time step  $k$  is known. Let  $z_{\text{BIAS},k}$  denote the MT clock bias measurement. Then, the model for the MT clock bias measurement is given by

$$z_{\text{BIAS},k} = c_0 \cdot (z_{\text{GRT},k} - t_{\text{MTC},k}) = c_0 \cdot \delta t_k + c_0 \cdot v_{\text{GRT},k} = h_{\text{BIAS},k}(c_0 \cdot \delta t_k) + v_{\text{BIAS},k}, \quad (2.45)$$

where the second equality follows from the insertion of (2.44) into (2.45) and taking into account (2.43). The error  $v_{\text{BIAS},k}$  is zero-mean Gaussian distributed with standard deviation  $\sigma_{\text{BIAS},k} = c_0 \cdot \sigma_{\text{GRT},k}$ . Instead of using the GRT measurement model, the MT clock bias measurement model is used in the following, since it gives a direct relationship to the MT clock bias  $\delta t_k$ , which is inherent in the PR measurement equations.

## 2.3.4 Simulation Scenario

### 2.3.4.1 Introduction

In this section, the simulation scenario for the hybrid localization is presented. In this work, two different simulation scenarios will be investigated. The first simulation scenario (Scenario I) is described in Section 2.3.4.2 and the second simulation scenario (Scenario II) is described in Section 2.3.4.3. For both simulation scenarios, it is assumed that the radio signals are either affected by LOS propagation conditions or propagation conditions that may switch between LOS or NLOS, whereas the satellite signals are assumed to be affected by LOS propagation conditions. The generation of the sequence of measurements and states together with the simulation parameters is presented in Section 2.3.5.

### 2.3.4.2 Scenario I

Scenario I that is investigated in this thesis has a size of  $3 \text{ km} \times 2 \text{ km}$  and is shown in Fig. 2.3. It is assumed that a car is equipped with an MT that is capable of providing PR measurements from GNSS and RSS, RTT and GRT measurements from the cellular radio network. In Fig. 2.3, the trajectory of the car together with the road network and the BS locations is shown. The car is assumed to move with a constant speed of 45 km/h on the trajectory. For simplicity, it is assumed that the car maintains its speed when it enters into a curve. The cellular radio network is composed of  $N_{\text{BS}} = 7$  BSs, where the serving BS is assumed to be the BS located at  $[-500 \text{ m}, 0 \text{ m}]^T$ . It is further assumed that the BSs are either equipped with omni-directional or sector antennas. The satellite locations are assumed to be fixed and are taken from a real GNSS satellite constellation. In order to investigate the effect of the relative satellite to MT geometry on the achievable accuracy of the MT location estimates, different satellite geometries are introduced. The influence of the geometry on the achievable accuracy is expressed by the 2-D Geometric Dilution of Precision (GDOP) value, which is further illustrated in Fig. 2.4 [Lev00]. When GNSS satellites are close together in the sky, the geometry is said to be weak and the GDOP value is high ( $\text{GDOP} > 5$ ). When GNSS satellites are far apart, the geometry is said to be strong and the GDOP value is low ( $\text{GDOP} \leq 5$ ). The satellite locations for different 2-D GDOP values are summarized in Table 2.1.

In order to evaluate the performance of the hybrid localization method, different combinations of measurements are proposed. In cellular radio networks, the RTT and RSS measurements are available only from a limited number of surrounding BSs. In GSM,

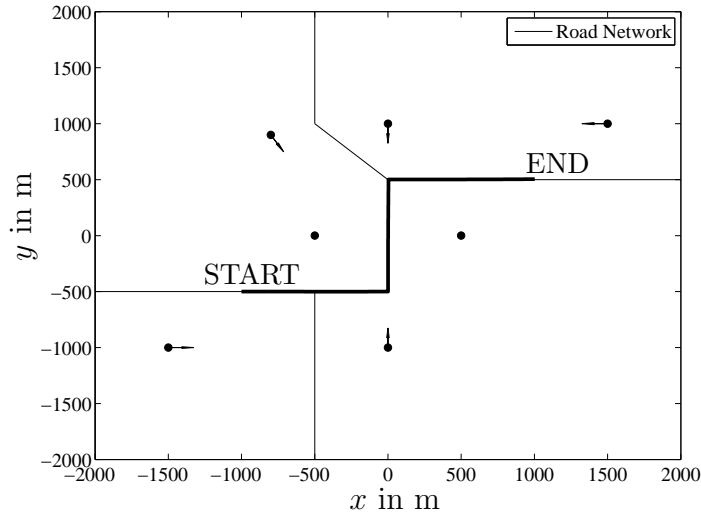


Figure 2.3. Scenario I with MT trajectory (bold line), road network and  $N_{\text{BS}} = 7$  BSs ( $\bullet$ ). The arrows ( $\rightarrow$ ) indicate BSs equipped with sector antennas, where only the sector antenna that is used in the simulations is shown.

for example, the RTT and RSS measurements from the serving BS and between one and six strongest RSS measurements from the neighboring BSs are available [EVB01]. In order to better reflect reality, these restrictions are taken into account in the combination of measurements. Beside the hybrid methods, the cellular method and the satellite method are introduced. The cellular method combines only measurements from the cellular radio network, while the satellite method combines only measurements from the GNSS network. It is assumed that in the satellite method, three PR measurements from three different GNSS satellites are combined, since this is the minimum number of PR measurements to obtain a 2-D MT location estimate. For the sake of clarity, the different considered methods are summarized as follows:

- Cellular method: One RTT measurement from the serving BS and a total of seven RSS measurements from serving and neighboring BS antennas,
- Hybrid 1 method: Measurements of cellular method and, in addition, one PR measurement from one GNSS satellite,
- Hybrid 1+ method: Measurements of Hybrid 1 method and, in addition, the GRT measurement from the cellular radio network,
- Hybrid 2 method: Measurements of cellular method and, in addition, two PR measurements from two different GNSS satellites,

- Hybrid 2+ method: Measurements of Hybrid 2 method and, in addition, the GRT measurement from the cellular radio network,
- Hybrid 3 method: Measurements of cellular method and, in addition, three PR measurements from three different GNSS satellites,
- Satellite method: Three PR measurements from three different GNSS satellites.

Scenario I is used to investigate the performance of the hybrid localization algorithms proposed in Chapter 3 and Chapter 4.

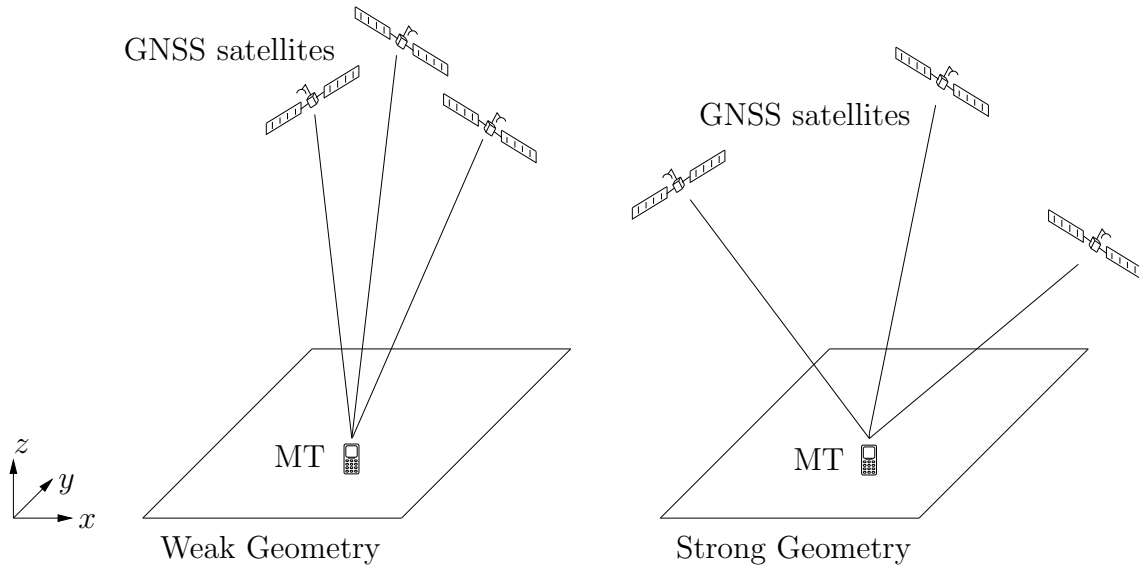


Figure 2.4. GNSS satellite to MT geometry for two different scenarios.

### 2.3.4.3 Scenario II

Scenario II that is investigated in this thesis has a size of  $3 \text{ km} \times 2 \text{ km}$  and is shown in Fig. 2.5. It is assumed that a car is equipped with an MT that is capable of providing PR measurements from GNSS and RSS and RTT measurements from the cellular radio network. In Fig. 2.5, the trajectory of the car together with the road network and the BS locations is shown. The car is assumed to move with a constant speed of  $45 \text{ km/h}$  on the trajectory as depicted in Fig. 2.5. For simplicity, it is assumed that the car maintains its speed when it enters into a curve. The cellular radio network is composed of  $N_{\text{BS}} = 3$  BSs and each BS is equipped with an omni-directional antenna. The satellite locations are assumed to be fixed and are taken from a real GNSS satellite constellation

Table 2.1. Satellite Locations for different 2-D GDOP values

Satellite Location	2-D GDOP			
	2	10	20	50
$x_{\text{SAT}}^{(1)}$ in m	14443484	17953574	18268005	18456147
$y_{\text{SAT}}^{(1)}$ in m	16934083	5296417.60	4395498.20	3856190.30
$z_{\text{SAT}}^{(1)}$ in m	8607443.69	12778466	12698276	12626966
$x_{\text{SAT}}^{(2)}$ in m	-13737497	13802799	-6961925.70	-7136389
$y_{\text{SAT}}^{(2)}$ in m	2341650.60	-771094.86	-12403207	-12874647
$z_{\text{SAT}}^{(2)}$ in m	16441855	16321784	16243256	15919980
$x_{\text{SAT}}^{(3)}$ in m	11017598	-6649567.10	13064925	12612713
$y_{\text{SAT}}^{(3)}$ in m	-4214169.60	-11609720	-388905.30	-176502.05
$z_{\text{SAT}}^{(3)}$ in m	17323090	16757534	16759635	17009222

according to Table 2.1. The performance of the hybrid localization method is evaluated based on different combinations of measurements. In contrast to Scenario I, it is now assumed that RTT measurements are available from all BSs. In GSM, for example, this can be accomplished by initiating forced handovers [SM99]. The different methods that are investigated are summarized as follows:

- Cellular method: Three RTT and RSS measurements from three different BS antennas,
- Hybrid 1 method: Measurements of cellular method and, in addition, one PR measurement from one GNSS satellite,
- Hybrid 2 method: Measurements of cellular method and, in addition, two PR measurements from two different GNSS satellites,
- Hybrid 3 method: Measurements of cellular method and, in addition, three PR measurements from three different GNSS satellites,
- Satellite method: Three PR measurements from three different GNSS satellites.

Scenario II is used to investigate the performance of the hybrid localization algorithms proposed in Chapter 4 and Chapter 5. The number of BS is decreased from  $N_{\text{BS}} = 7$  in Scenario I to  $N_{\text{BS}} = 3$ , since the computational complexity of the algorithms developed in Chapter 5 increases exponentially with  $N_{\text{BS}}$ . Since more measurements generally yield an improved localization performance, the number of RTT measurements is increased from  $M_{\text{RTT}} = 1$  in Scenario I to  $M_{\text{RTT}} = 3$ .

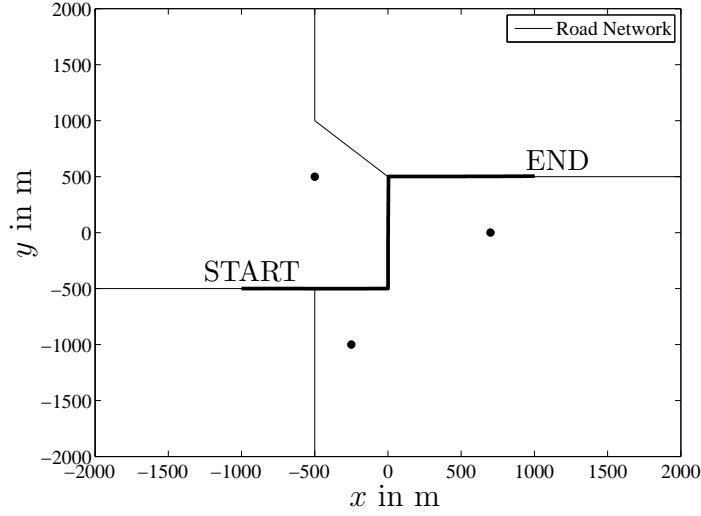


Figure 2.5. Scenario II with MT trajectory (bold line), road network and  $N_{\text{BS}} = 3$  BSs ( $\bullet$ ).

### 2.3.5 Monte Carlo Simulations

In this section, the need of performing Monte Carlo (MC) simulations (runs) is motivated. Models with which the MT state and the measurements can be generated for a single Monte Carlo run are presented, as well as the parameters that are used in the Monte Carlo simulations are given.

In order to compare different hybrid localization algorithms with each other, it is necessary to introduce a performance measure. In general, the performance of an algorithm is quantified by the expected value of a cost function  $C$  [BSLK01]. For localization algorithms, the most frequently chosen cost function is the squared error in the estimation of the MT location  $\mathbf{x}_{\text{MT},k}$ . Let  $\hat{\mathbf{x}}_{\text{MT},k}(\mathbf{z}_k)$  denote an estimate of the MT location based on the current measurements. Let further  $\mathbb{E}\{\cdot\}$  denote the expectation operator and let  $\|\mathbf{s}\|$  denote the 2-norm of the vector  $\mathbf{s}$ . Then, the MSE of the MT location is given by

$$\mathbb{E}\{C\} \triangleq \text{MSE} = \mathbb{E}\{\|\hat{\mathbf{x}}_{\text{MT},k}(\mathbf{z}_k) - \mathbf{x}_{\text{MT},k}\|^2\}. \quad (2.46)$$

For the hybrid localization algorithms investigated in this work, the performance cannot be evaluated analytically. In such a case, Monte Carlo simulations are performed to obtain an estimate of  $\mathbb{E}\{C\}$  from a sample average of  $N_{\text{MC}}$  independent realizations  $C_i$ ,  $i = 1, \dots, N_{\text{MC}}$ , of the cost  $C$ . The variability of the resulting estimate will become smaller for an increasing number of Monte Carlo simulations  $N_{\text{MC}}$ . Let  $\mathbf{x}_{\text{MT},k,i}$  and

$\hat{\mathbf{x}}_{\text{MT},k,i}(\mathbf{z}_{k,i})$  denote the true and estimated MT location at the  $i$ -th Monte Carlo run, respectively. Then, the estimate of the performance from  $N_{\text{MC}}$  independent runs is the sample mean of the  $N_{\text{MC}}$  realizations of the cost  $C$  or, equivalently,

$$\text{MSE} \approx \frac{1}{N_{\text{MC}}} \sum_{i=1}^{N_{\text{MC}}} \|\hat{\mathbf{x}}_{\text{MT},k,i}(\mathbf{z}_{k,i}) - \mathbf{x}_{\text{MT},k,i}\|^2. \quad (2.47)$$

In order to evaluate the average performance of the hybrid localization algorithms by means of simulations, it is, thus, necessary to generate for the MT trajectory depicted in Figs. 2.3 and 2.5  $N_{\text{MC}}$  independent realizations of the MT state and the measurements. The MT state vector for the hybrid localization is given by  $\mathbf{x}_k = [\mathbf{x}_{\text{CV},k}^{\text{T}}, \mathbf{x}_{\text{CO},k}^{\text{T}}]^{\text{T}}$ , and can be generated from the models introduced in Section 2.3.2. In the following, the model that is used to generate  $\mathbf{x}_k$  is written more compactly. Let  $\mathbf{w}_k = [\mathbf{w}_{\text{CV},k}^{\text{T}}, \mathbf{w}_{\text{CO},k}^{\text{T}}]^{\text{T}}$  denote a vector of random variables, where  $\mathbf{w}_{\text{CV},k}$  and  $\mathbf{w}_{\text{CO},k}$  are assumed to be statistically independent. Let  $\text{diag}_{\text{b}}[\mathbf{A}_1, \mathbf{A}_2, \dots, \mathbf{A}_K]$  denote a block diagonal matrix given by

$$\text{diag}_{\text{b}}[\mathbf{A}_1, \mathbf{A}_2, \dots, \mathbf{A}_K] = \begin{bmatrix} \mathbf{A}_1 & \mathbf{0} & \mathbf{0} & \cdots & \mathbf{0} \\ \mathbf{0} & \mathbf{A}_2 & \mathbf{0} & \cdots & \mathbf{0} \\ \mathbf{0} & \mathbf{0} & \ddots & \mathbf{0} & \vdots \\ \vdots & \vdots & \mathbf{0} & \mathbf{A}_{K-1} & \mathbf{0} \\ \mathbf{0} & \mathbf{0} & \cdots & \mathbf{0} & \mathbf{A}_K \end{bmatrix}, \quad (2.48)$$

where the all-zero matrices  $\mathbf{0}$  have to be adapted to the sizes of the arbitrarily sized real matrices  $\mathbf{A}_{\kappa_1}$ ,  $\kappa_1 = 1, \dots, K$ . Let further  $\mathbf{F} = \text{diag}_{\text{b}}[\mathbf{F}_{\text{CV}}, \mathbf{F}_{\text{CO}}]$  and  $\mathbf{\Gamma} = \text{diag}_{\text{b}}[\mathbf{\Gamma}_{\text{CV}}, \mathbf{\Gamma}_{\text{CO}}]$  denote the overall state transition and noise mapping matrices, respectively, and let  $\mathbf{Q} = \text{diag}_{\text{b}}[\mathbf{Q}_{\text{CV}}, \mathbf{Q}_{\text{CO}}]$  denote the covariance matrix of the noise vector  $\mathbf{w}_{k-1}$ . Then, the model for generating the MT state for the hybrid localization is given by

$$\mathbf{x}_k = \mathbf{F} \cdot \mathbf{x}_{k-1} + \mathbf{\Gamma} \cdot \mathbf{w}_{k-1}. \quad (2.49)$$

For the generation of the measurements, two different models are used:

- The first model assumes that both, the radio signals and satellite signals are affected by LOS propagation conditions. Let  $\mathbf{z}_{\text{LOS},k} = [\mathbf{z}_{\text{PR},k}^{\text{T}}, \mathbf{z}_{\text{RTT,LOS},k}^{\text{T}}, \mathbf{z}_{\text{RSS,LOS},k}^{\text{T}}, z_{\text{BIAS},k}]^{\text{T}}$  denote the vector of  $M$  measurements, and let  $\mathbf{h}_{\text{LOS},k}(\mathbf{x}_k) = [\mathbf{h}_{\text{PR},k}^{\text{T}}(\mathbf{x}_{\text{MT},k}, c_0 \cdot \delta t_k), \mathbf{h}_{\text{RTT},k}^{\text{T}}(\mathbf{x}_{\text{MT},k}), \mathbf{h}_{\text{RSS,LOS},k}^{\text{T}}(\mathbf{x}_{\text{MT},k}), h_{\text{BIAS},k}(c_0 \cdot \delta t_k)]^{\text{T}}$  denote the vector of  $M$  functions relating the MT state to the  $M$  measurements, where  $M = M_{\text{PR}} + M_{\text{RTT}} + M_{\text{RSS}} + 1$ . Furthermore, let  $\mathbf{v}_{\text{LOS},k} = [\mathbf{v}_{\text{PR},k}^{\text{T}}, \mathbf{v}_{\text{RTT,LOS},k}^{\text{T}}, \mathbf{v}_{\text{RSS,LOS},k}^{\text{T}}, v_{\text{BIAS},k}]^{\text{T}}$  denote the vector of  $M$  random variables. It is assumed that the random variables  $\mathbf{v}_{\text{PR},k}$ ,  $\mathbf{v}_{\text{RTT,LOS},k}$ ,  $\mathbf{v}_{\text{RSS,LOS},k}$  and  $v_{\text{BIAS},k}$  are statistically independent, so that the covariance matrix of  $\mathbf{v}_{\text{LOS},k}$  is given by  $\mathbf{R}_{\text{LOS},k} =$



$\text{diag}_{\text{b}}[\mathbf{R}_{\text{PR},k}, \mathbf{R}_{\text{RTT,LOS},k}, \mathbf{R}_{\text{RSS,LOS},k}, \sigma_{\text{BIAS},k}^2]$ . Then, the model for generating the measurements for the case of LOS propagation conditions can be written as

$$\mathbf{z}_{\text{LOS},k} = \mathbf{h}_{\text{LOS},k}(\mathbf{x}_k) + \mathbf{v}_{\text{LOS},k}. \quad (2.50)$$

- The second model assumes that the satellite signals are affected by LOS propagation conditions and that the radio signals are affected by propagation conditions that may switch between LOS and NLOS. The switching between LOS and NLOS propagation conditions is modeled for each radio signal that is exchanged between the  $m$ -th BS and the MT with a 2-state Markov chain  $r_k^{(m)}$ , with  $m = 1, \dots, N_{\text{BS}}$ . Here, it is worth noting that the RTT and RSS measurements that are related to the radio signal of the same BS are modeled with a single Markov chain, since both RTT and RSS parameters are extracted from the same radio signal. The TPM for each Markov chain is assumed to be given by

$$\mathbf{\Pi}_m = \begin{bmatrix} 0.95 & 0.05 \\ 0.05 & 0.95 \end{bmatrix}, \quad (2.51)$$

and the mode probabilities to initialize each Markov chain are chosen as  $\pi_1^{(m)} = 0.5$  and  $\pi_2^{(m)} = 0.5$ . In the following, the model for generating the measurements is written more compactly. The  $N_{\text{BS}}$  different 2-state Markov chains are combined into a single Markov chain consisting of  $2^{N_{\text{BS}}}$  different states. The state of the augmented Markov chain is now described by the mode variable  $r_k$  that is among the  $2^{N_{\text{BS}}}$  possible modes  $r_k \in \{1, \dots, 2^{N_{\text{BS}}}\}$ . The transition between LOS and NLOS propagation conditions is modeled for each radio signal independently, so that the TPM of the augmented Markov chain is given by

$$\mathbf{\Pi} = \mathbf{\Pi}_1 \otimes \mathbf{\Pi}_2 \otimes \dots \otimes \mathbf{\Pi}_{N_{\text{BS}}}. \quad (2.52)$$

Let  $\mathbf{z}_k = [\mathbf{z}_{\text{PR},k}^{\text{T}}, \mathbf{z}_{\text{RTT},k}^{\text{T}}, \mathbf{z}_{\text{RSS},k}^{\text{T}}, z_{\text{BIAS},k}]^{\text{T}}$  denote the vector of  $M$  measurements, and let  $\mathbf{h}_k(\mathbf{x}_k, r_k) = [\mathbf{h}_{\text{PR},k}^{\text{T}}(\mathbf{x}_{\text{MT},k}, \delta t_k), \mathbf{h}_{\text{RTT},k}^{\text{T}}(\mathbf{x}_{\text{MT},k}), \mathbf{h}_{\text{RSS},k}^{\text{T}}(\mathbf{x}_{\text{MT},k}, r_k), h_{\text{BIAS},k}(\delta t_k)]^{\text{T}}$  denote the mode-dependent vector of  $M$  functions relating the MT state to the  $M$  measurements. Furthermore, let  $\mathbf{v}_k(r_k) = [\mathbf{v}_{\text{PR},k}^{\text{T}}, \mathbf{v}_{\text{RTT},k}^{\text{T}}(r_k), \mathbf{v}_{\text{RSS},k}^{\text{T}}(r_k), v_{\text{BIAS},k}]^{\text{T}}$  denote the mode-dependent vector of random variables. It is assumed that the random variables  $\mathbf{v}_{\text{PR},k}$ ,  $\mathbf{v}_{\text{RTT},k}(r_k)$ ,  $\mathbf{v}_{\text{RSS},k}(r_k)$  and  $v_{\text{BIAS},k}$  are statistically independent. From this it follows that  $\mathbf{v}_k(r_k)$  is Gaussian distributed with mode-dependent mean vector  $\boldsymbol{\mu}_k(r_k) = [\mathbf{0}_{1 \times M_{\text{PR}}}, \boldsymbol{\mu}_{\text{RTT},k}^{\text{T}}(r_k), \mathbf{0}_{1 \times M_{\text{RSS}}}, 0]^{\text{T}}$  and mode-dependent covariance matrix  $\mathbf{R}_k(r_k) = \text{diag}_{\text{b}}[\mathbf{R}_{\text{PR},k}, \mathbf{R}_{\text{RTT},k}(r_k), \mathbf{R}_{\text{RSS},k}(r_k), \sigma_{\text{BIAS},k}^2]$ , where  $\mathbf{0}_{i \times j}$  denotes the all-zeros matrix with  $i$  rows and  $j$  columns. Thus, the model for generating the measurements that considers the switching between LOS and NLOS propagation conditions is given by

$$\mathbf{z}_k = \mathbf{h}_k(\mathbf{x}_k, r_k) + \mathbf{v}_k(r_k). \quad (2.53)$$

In order to generate the vectors  $\mathbf{x}_k$ ,  $\mathbf{z}_{\text{LOS},k}$  and  $\mathbf{z}_k$  for a single Monte Carlo run, the unknown parameters inherent in the corresponding models have to be further specified. For the sake of simplicity, it is assumed that these parameters are independent of  $k$  and equal for all BSs and satellites and are summarized in Table 2.2.

Table 2.2. Simulation parameters

Parameter	Equation	Value
$\sigma_x$ in $\text{m/s}^2$	(2.3)	$10^{-2}$
$\sigma_y$ in $\text{m/s}^2$	(2.3)	$10^{-2}$
$T_S$ in s	(2.4), (2.6), (2.7)	0.5
$h_0$ in s [vDBB84]	(2.7)	$9.4 \cdot 10^{-20}$
$h_{-1}$ [vDBB84]	(2.7)	$1.8 \cdot 10^{-19}$
$h_{-2}$ in $1/\text{s}$ [vDBB84]	(2.7)	$3.8 \cdot 10^{-21}$
$\sigma_{\text{PR}}$ in m [Kap96, ME06]	(2.21)	10
$\mu_{\text{RTT,NLOS}}$ in m [SR96, LC06]	(2.26)	513
$\sigma_{\text{RTT,LOS}}$ in m [SR96, LC06]	(2.27)	150
$\sigma_{\text{RTT,NLOS}}$ in m [SR96, LC06]	(2.27)	409
$A_{\text{LOS}}$ in dB [DC99]	(2.30)	101.7
$A_{\text{NLOS}}$ in dB [DC99]	(2.30)	132.8
$B_{\text{LOS}}$ in dB [DC99]	(2.31)	2.6
$B_{\text{NLOS}}$ in dB [DC99]	(2.31)	3.8
$\varphi_{3\text{dB}}$ in rad	(2.34)	$\pi/3$
$G_{\text{min}}$ in dB	(2.34)	17
$P_T$ in dBm	(2.37)	50
$\sigma_{\text{RSS,LOS}}$ in dB	(2.41)	2
$\sigma_{\text{RSS,NLOS}}$ in m	(2.41)	8

## 2.4 Field Trial

In this section, the field trial for the hybrid localization is explained. The field trial was conducted in an operating GSM network in the city center of a German city with a test area which has a size of approximately  $2 \text{ km} \times 2 \text{ km}$ . During the field trial, a car equipped with a standard cellular phone collected Received Signal Level (RXLEV) and TA measurements from GSM every  $T_S = 0.48 \text{ s}$ . Here, it is worth noting that RXLEV

measurements are quantized RSS measurements and TA measurements are quantized RTT measurements. In addition, it should be noted that the TA measurement is only available from the serving BS, while the RXLEV is available from the serving BS and between one and six strongest RXLEVs are available from the neighboring BSs [EVB01]. Since GRT measurements have not been collected during the field trial, this issue is not further elaborated. The GSM network is composed of  $N_{\text{BS}} = 13$  fixed BSs with known locations. The BSs are either equipped with directional antennas or a single omni-directional antenna, which may operate at different frequency bands (GSM 900 or GSM 1800). The antenna boresight directions, equivalent isotropic radiated powers and half-power beamwidths are a-priori known. The true MT location during the field trial was obtained from detailed maps and from GPS, where GPS was available.

For the GPS network, PR measurements collected from a field trial are not available, so that synthetic PR measurement data have been generated with the PR model presented in Section 2.3.3.4, the MT clock model described in Section 2.3.2.4 and the parameters given in Table 2.2. The constellation of the GPS satellites during the field trial is reconstructed by taking true satellite locations from the real satellite constellation. The satellite's visibility status cannot be reproduced subsequently, so that it is assumed that either  $N_{\text{SAT}} = 1$  or  $N_{\text{SAT}} = 2$  are visible to the MT. However, this assumption is only made in order to demonstrate the potential improvements that can be achieved by the hybrid localization. In reality, the number of visible satellites changes with time, so that there will be situations where  $N_{\text{SAT}} \geq 3$  and, thus, GPS is available. The satellite locations are chosen based on the expected visibility status during the field trial. As the MT antenna is located inside the car, the roof of the car prevents the MT to receive signals from satellites at high elevation angles. Here, the elevation angle refers to the angle that is measured in radians counterclockwise from the  $xy$ -plane (0 elevation) towards the  $z$ -axis ( $\pi/2$  elevation) of a Cartesian coordinate system, whose origin is defined to be the location of the MT. The resulting elevation angles, where the satellite signal is not blocked, is given by the so-called satellite elevation angle mask  $\theta_{\text{MASK}}$ . For the field trial, the satellite elevation angle mask in radians is chosen as  $\pi/9 \leq \theta_{\text{MASK}} \leq \pi/6$ . In general, the expected satellite visibility status also depends on the azimuth angle. However, for simplicity, the corresponding satellite azimuth elevation angle mask is not considered.

When it comes to the processing of real data from field trials, the locations of the MT, BSs and satellites are often expressed in different coordinate systems. The satellite locations, for example, are often expressed in Earth Centered Earth Fixed (ECEF) coordinates, while the true MT location as well as the BS locations are conventionally given in the geodetic coordinate system [RAG04, GWA07]. In order to apply the hybrid localization algorithms to the data from the field trial, it is, thus, necessary to define

a common Cartesian coordinate system. In the following, a fixed local East-North-Up (ENU) rectangular coordinate system with coordinates  $x_{\text{ENU}}$ ,  $y_{\text{ENU}}$  and  $z_{\text{ENU}}$  is used, which is determined by the fitting of a tangent plane to the Earth's surface at a fixed reference point [RAG04, GWA07]. The reference point is the origin of the local ENU coordinate system and is chosen to be in the vicinity of the field trial scenario where the data was collected. The  $x_{\text{ENU}}$ -axis points to true east, the  $y_{\text{ENU}}$ -axis points north and the  $z_{\text{ENU}}$ -axis points up, in order to complete the right-handed coordinate system. For completeness, the transformations between the different coordinate systems are summarized in Appendix A.1. The field trial scenario showing the BS locations, the road network, as well as the MT trajectory in the ENU coordinate system is presented in Fig. 2.6.

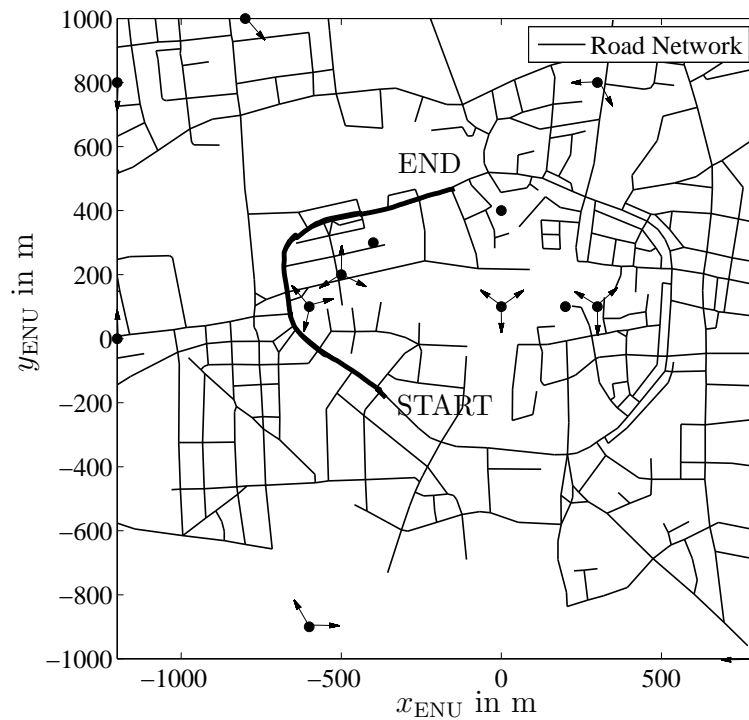


Figure 2.6. Field trial scenario with MT trajectory (bold line), road network and  $N_{\text{BS}} = 13$  BSs (●). Due to confidentiality reasons only approximate BS locations are shown. Arrows (→) indicate BSs equipped with sector antennas.

## Chapter 3

# Non-Recursive State Estimation for Hybrid Localization

### 3.1 Introduction

In this chapter, the hybrid localization problem is solved using non-recursive state estimation techniques<sup>1</sup>. In non-recursive state estimation, the MT state is estimated for each time step  $k$  independently, i.e., without taking into account information on measurements and MT state estimates from previous time steps. The estimation of the MT state is, thus, done in a snap-shot manner, based on the measurements available at a particular time step.

The concept of non-recursive state estimation is introduced in Section 3.2, where the ML estimator is chosen as a solution for the hybrid localization problem. In order to assess the theoretically best achievable performance of the estimator, the CRLB for hybrid localization is evaluated in Section 3.3. For measurements affected by LOS propagation conditions, a novel analytical expression for the CRLB is derived and a novel geometric interpretation of the bound is given. For measurements affected by propagation conditions that may switch between LOS and NLOS, a numerical solution for the CRLB is provided. The ML estimators for the hybrid localization problem assuming LOS propagation conditions and for propagation conditions that may switch between LOS and NLOS are newly proposed in Section 3.4. Since in both cases, analytical solutions to the ML estimators do not exist, suboptimal algorithms for approximately solving the ML estimation problem are proposed. The performance of the proposed hybrid localization algorithms is analyzed by means of simulations and experimental data in Section 3.5. Finally, the main conclusions of this chapter are drawn in Section 3.6. Several parts of this Chapter 3 have been originally published by the author in [FKS06, FKSP07, FK08].

### 3.2 Concept of Non-Recursive State Estimation

In this section, the concept of non-recursive state estimation for the hybrid localization is derived starting from the concept of static Bayesian estimation [vT68, Kay93,

<sup>1</sup>In the literature, non-recursive state estimation is also known as static estimation or parameter estimation [GG05, BSLK01].

BSLK01,GG05]. For static Bayesian estimation, temporal correlations between time consecutive MT states and measurements are not taken into account, so that the MT state and the measurements can be regarded as a sequence of uncorrelated parameters. In the following, the discrete mode variable  $r_k$  is not additionally estimated, so that the only unknown is the MT state  $\mathbf{x}_k$ , which is estimated for each time step  $k$  independently by using the information available from the current measurements  $\mathbf{z}_k$ .

In static Bayesian estimation, the problem of estimating the MT state from different measurements is equivalent to the construction of the posterior pdf of the MT state over an  $n_x$ -dimensional space given the measurements, from which the MT state can be then estimated [vT68,Kay93,BSLK01,GG05]. In the Bayesian approach, the MT state  $\mathbf{x}_k$  is assumed to be a random variable with prior pdf  $p(\mathbf{x}_k)$ . Let  $p(\mathbf{x}_k|\mathbf{z}_k)$  denote the posterior pdf of the MT state given the measurements. Let further  $p(\mathbf{z}_k|\mathbf{x}_k)$  denote the pdf of the measurements conditioned on the MT state, hereinafter called the likelihood function. Then, according to Bayes' theorem [Pap84], the posterior pdf can be found from the following relationship

$$p(\mathbf{x}_k|\mathbf{z}_k) = \frac{p(\mathbf{x}_k) \cdot p(\mathbf{z}_k|\mathbf{x}_k)}{\int_{\mathbb{R}^{n_x}} p(\mathbf{x}_k) \cdot p(\mathbf{z}_k|\mathbf{x}_k) d\mathbf{x}_k}, \quad (3.1)$$

where the denominator in (3.1) ensures that the posterior pdf  $p(\mathbf{x}_k|\mathbf{z}_k)$  integrates to unity [Kay93]. For the hybrid localization, the elements of the vector  $\mathbf{z}_k$  are assumed to be mutually independent. Let  $p_\nu(z_k^{(\nu)}|\mathbf{x}_k)$  denote the likelihood function of the  $\nu$ -th measurement. Then, the joint conditional pdf  $p(\mathbf{z}_k|\mathbf{x}_k)$  can be written as a product of the marginal pdfs  $p_\nu(z_k^{(\nu)}|\mathbf{x}_k)$  according to

$$p(\mathbf{z}_k|\mathbf{x}_k) = \prod_{\nu=1}^{n_z} p_\nu(z_k^{(\nu)}|\mathbf{x}_k), \quad (3.2)$$

[vT68]. For the measurement model given by (2.9) and under the additional assumption that the components of the vector of random variables  $\mathbf{v}_k$  are statistically independent, (3.2) holds and the marginal likelihood function  $p_\nu(z_k^{(\nu)}|\mathbf{x}_k)$  can be determined by

$$p_\nu(z_k^{(\nu)}|\mathbf{x}_k) = p_{v_k^{(\nu)}}(z_k^{(\nu)} - h_k^{(\nu)}(\mathbf{x}_k)), \quad \text{for } \nu = 1, \dots, n_z, \quad (3.3)$$

[Jaz70]. For the measurement model given by (2.18) and under the additional assumption that the components of the vector  $\mathbf{v}_k(r_k)$  of random variables are statistically independent, (3.2) holds and the marginal likelihood function  $p_\nu(z_k^{(\nu)}|\mathbf{x}_k)$  can be determined according to the following approach. For  $\nu = 1, \dots, n_z$ , the marginal likelihood function  $p_\nu(z_k^{(\nu)}|\mathbf{x}_k)$  can be found from the law of total probability [Pap84], yielding

$$p(z_k^{(\nu)}|\mathbf{x}_k) = \sum_{r_k^{(\nu)}=1}^2 p(z_k^{(\nu)}, r_k^{(\nu)}|\mathbf{x}_k) = \sum_{r_k^{(\nu)}=1}^2 \Pr\{r_k^{(\nu)}\} \cdot p(z_k^{(\nu)}|\mathbf{x}_k, r_k^{(\nu)}), \quad (3.4)$$

where the mode-dependent likelihood function is given by

$$p_\nu(z_k^{(\nu)}|\mathbf{x}_k, r_k^{(\nu)}) = p_{v_k^{(\nu)}(r_k^{(\nu)})}(z_k^{(\nu)} - h_k^{(\nu)}(\mathbf{x}_k, r_k^{(\nu)})), \quad \text{for } r_k^{(\nu)} = 1, 2. \quad (3.5)$$

It can be seen that the likelihood function  $p(z_k^{(\nu)}|\mathbf{x}_k)$  is given by a weighted sum of pdfs with mode dependent weights summing up to unity, which is also known as mixture pdf [BSLK01]. The mode probabilities  $\Pr\{r_k^{(\nu)}\}$  can be updated from the following recursive (temporal) relationship:

$$\Pr\{r_k^{(\nu)}\} = \sum_{r_{k-1}^{(\nu)}=1}^2 \Pr\{r_k^{(\nu)}|r_{k-1}^{(\nu)}\} \cdot \Pr\{r_{k-1}^{(\nu)}\}, \quad \text{for } \nu = 1, \dots, n_z. \quad (3.6)$$

Since in this chapter the mode variable  $r_k^{(\nu)}$  is not additionally estimated, suitable approximations to (3.6) have to be introduced. In the following, the unknown mode probabilities  $\Pr\{r_k^{(\nu)}\}$  are replaced with the stationary values  $p_{\text{LOS}}^{(\nu)}$  and  $p_{\text{NLOS}}^{(\nu)}$  of the Markov chain, cf. (2.15), which are assumed to be known a-priori. Thus, the marginal likelihood function can be approximated as

$$p(z_k^{(\nu)}|\mathbf{x}_k) \approx p_{\text{LOS}}^{(\nu)} \cdot p(z_k^{(\nu)}|\mathbf{x}_k, r_k^{(\nu)} = 1) + p_{\text{NLOS}}^{(\nu)} \cdot p(z_k^{(\nu)}|\mathbf{x}_k, r_k^{(\nu)} = 2), \quad (3.7)$$

for  $\nu = 1, \dots, n_z$ . Here, it is worth noting that the expression in (3.4) reduces to (3.7) for time-homogeneous Markov chains with symmetric TPMs which are initialized with their stationary values.

Having the prior pdf  $p(\mathbf{x}_k)$  and the likelihood functions  $p_\nu(z_k^{(\nu)}|\mathbf{x}_k)$  of the  $n_z$  measurements available, the posterior pdf can be determined. Knowledge of the posterior pdf  $p(\mathbf{x}_k|\mathbf{z}_k)$  allows to obtain MT state estimates with respect to any optimality criterion. A well known criterion is to minimize the mean square error for each component of the unknown MT state vector. Let  $g(x)$  denote an integrable function, where  $x$  is a real-valued random variable with pdf  $p(x)$ . Then, the expected value of  $g(x)$  is denoted as

$$\mathbb{E}_{p(x)}\{g(x)\} = \int_{\mathbb{R}} g(x) \cdot p(x) dx. \quad (3.8)$$

Whenever necessary, a subscript on  $\mathbb{E}$  is introduced, in order to clarify which pdf to use in the integral. Let  $\hat{\mathbf{x}}_{\text{MMSE},k}(\mathbf{z}_k)$  denote the Minimum Mean Square Error (MMSE) estimate. Then, the MMSE estimator is given by

$$\hat{\mathbf{x}}_{\text{MMSE},k}(\mathbf{z}_k) = \mathbb{E}_{p(\mathbf{x}_k|\mathbf{z}_k)}\{\mathbf{x}_k\} = \int_{\mathbb{R}^{n_x}} \mathbf{x}_k \cdot p(\mathbf{x}_k|\mathbf{z}_k) d\mathbf{x}_k, \quad (3.9)$$

[Kay93]. Note that  $\hat{\mathbf{x}}_{\text{MMSE},k}(\mathbf{z}_k)$  is a random variable since it depends on the random measurements  $\mathbf{z}_k$ . Finding the MMSE estimate  $\hat{\mathbf{x}}_{\text{MMSE},k}(\mathbf{z}_k)$  requires to evaluate the

multi-dimensional integrals in (3.1) and (3.9). For the hybrid localization, closed-form solutions for these integrals do not exist and the MMSE estimate  $\hat{\mathbf{x}}_{\text{MMSE},k}(\mathbf{z}_k)$  has to be calculated numerically by using Monte Carlo integration techniques [MU49,RC99]. The implementation of Monte Carlo integration techniques is computationally intensive, which often prevents the use of the MMSE estimator in practice. In the following, the MMSE estimator is not further treated in this chapter and the focus is put to estimators that are better suited for practical applications.

A criterion that does not require an evaluation of the multi-dimensional integral given in (3.1) is to determine the maximum of the posterior pdf. The corresponding estimator is called the MAP estimator [vT68,BSLK01]. Let  $\hat{\mathbf{x}}_{\text{MAP},k}(\mathbf{z}_k)$  denote the MAP estimate. Then, the MAP estimator is given by

$$\hat{\mathbf{x}}_{\text{MAP},k}(\mathbf{z}_k) = \arg \max_{\mathbf{x}_k} [p(\mathbf{x}_k) \cdot p(\mathbf{z}_k|\mathbf{x}_k)]. \quad (3.10)$$

The choice of the prior pdf  $p(\mathbf{x}_k)$  is critical in Bayesian estimation. If prior information about the unknown MT state is available, it should be incorporated into the estimator by an appropriate choice of  $p(\mathbf{x}_k)$ . However, in most situations prior information is not available or it is not clear how to model the prior information. In these cases, it is better to choose  $p(\mathbf{x}_k)$  as being uniformly distributed over an infinite interval, which is also known as noninformative prior pdf [BSLK01].

In the following, it is assumed that no prior information about the MT state is available, so that  $p(\mathbf{x}_k)$  is chosen to be uniformly distributed over  $\mathbb{R}^{n_x}$ . From this, the important property follows that the posterior pdf  $p(\mathbf{x}_k|\mathbf{z}_k)$  becomes proportional to its likelihood function. The corresponding estimator that determines the maximum of the likelihood function is known as the ML estimator [vT68,BSLK01]. Let  $\hat{\mathbf{x}}_{\text{ML},k}(\mathbf{z}_k)$  denote the ML estimate. Then, with  $p(\mathbf{x}_k)$  being noninformative, the MAP estimator reduces to the ML estimator, which is given by

$$\hat{\mathbf{x}}_{\text{ML},k}(\mathbf{z}_k) = \arg \max_{\mathbf{x}_k} p(\mathbf{z}_k|\mathbf{x}_k). \quad (3.11)$$

Since no prior information is incorporated into the ML estimator, the MT state can be regarded as an unknown (deterministic) constant. Instead of maximizing the likelihood function, one can equivalently minimize the negative log-likelihood function, since the logarithm is a monotonic transformation. This yields

$$\hat{\mathbf{x}}_{\text{ML},k}(\mathbf{z}_k) = \arg \min_{\mathbf{x}_k} [-\log_e (p(\mathbf{z}_k|\mathbf{x}_k))]. \quad (3.12)$$

Finding the ML estimate  $\hat{\mathbf{x}}_{\text{ML},k}(\mathbf{z}_k)$  requires the evaluation of (3.12). For the hybrid localization, a closed-form solution for the ML estimator does not exist and one has to resort to suboptimal, numerical optimization algorithms, in order to carry out the minimization of the log-likelihood function [BSLK01].



## 3.3 Cramér-Rao Lower Bound

### 3.3.1 Introduction

In this section, the CRLB for nonrandom parameters is introduced which is used to assess the theoretical performance bound for the non-recursive hybrid localization algorithms investigated in this work. Let  $\hat{\mathbf{x}}_k(\mathbf{z}_k)$  denote an unbiased estimate of the unknown deterministic MT state  $\mathbf{x}_k$  and let the estimation error be given by  $\hat{\mathbf{x}}_k(\mathbf{z}_k) - \mathbf{x}_k$ . The CRLB is defined to give a lower bound for the covariance matrix of the estimation error [Rao46, vT68, Kay93]. Let  $[\cdot]^{-1}$  denote the inverse of a matrix and let  $\mathcal{F}(\mathbf{x}_k)$  denote the Fisher Information Matrix (FIM) evaluated at the true value of the vector parameter  $\mathbf{x}_k$  [Fis22, Fis25]. Let further  $\mathcal{P}(\mathbf{x}_k)$  denote the CRLB matrix which is defined to be the inverse of the FIM. Then, the covariance matrix of the estimation error satisfies the following inequality:

$$\mathbb{E}_{p(\mathbf{z}_k|\mathbf{x}_k)}\{(\hat{\mathbf{x}}_k(\mathbf{z}_k) - \mathbf{x}_k)(\hat{\mathbf{x}}_k(\mathbf{z}_k) - \mathbf{x}_k)^\top\} \geq [\mathcal{F}(\mathbf{x}_k)]^{-1} \equiv \mathcal{P}(\mathbf{x}_k), \quad (3.13)$$

where the matrix inequality  $\mathbf{A} \geq \mathbf{B}$  should be interpreted as the matrix  $(\mathbf{A} - \mathbf{B})$  being positive semidefinite. Let us introduce the following operators:

$$\nabla_{\mathbf{a}} = \left[ \frac{\partial}{\partial a^{(1)}}, \frac{\partial}{\partial a^{(2)}}, \dots, \frac{\partial}{\partial a^{(n)}} \right]^\top, \quad (3.14)$$

$$\Delta_{\mathbf{a}}^{\mathbf{b}} = \nabla_{\mathbf{a}} \nabla_{\mathbf{b}}^\top, \quad (3.15)$$

for any vectors  $\mathbf{a}$  and  $\mathbf{b}$ . Using this notation, the FIM is defined as

$$\mathcal{F}(\mathbf{x}_k) = \mathbb{E}_{p(\mathbf{z}_k|\mathbf{x}_k)} \{ [\nabla_{\mathbf{x}_k} \log_e p(\mathbf{z}_k|\mathbf{x}_k)] [\nabla_{\mathbf{x}_k} \log_e p(\mathbf{z}_k|\mathbf{x}_k)]^\top \} \quad (3.16a)$$

$$= \mathbb{E}_{p(\mathbf{z}_k|\mathbf{x}_k)} \{ -\Delta_{\mathbf{x}_k}^{\mathbf{x}_k} \log_e p(\mathbf{z}_k|\mathbf{x}_k) \} \quad (3.16b)$$

$$= \mathbb{E}_{p(\mathbf{z}_k|\mathbf{x}_k)} \left\{ \frac{[\nabla_{\mathbf{x}_k} p(\mathbf{z}_k|\mathbf{x}_k)] [\nabla_{\mathbf{x}_k} p(\mathbf{z}_k|\mathbf{x}_k)]^\top}{[p(\mathbf{z}_k|\mathbf{x}_k)]^2} \right\}. \quad (3.16c)$$

The CRLB exists, if the pdf  $p(\mathbf{z}_k|\mathbf{x}_k)$  satisfies the regularity conditions [LC98]. Let  $[\mathbf{A}]_{i,j}$  denote the element at the  $i$ -th row and  $j$ -th column of the matrix  $\mathbf{A}$ . The elements on the main diagonal of the CRLB matrix given in (3.13) provide a lower bound on the MSEs of the individual components of  $\mathbf{x}_k$ , i.e.,

$$\mathbb{E}_{p(\mathbf{z}_k|\mathbf{x}_k)} \{ (\hat{x}_k^{(i)}(\mathbf{z}_k) - x_k^{(i)})^2 \} \geq [[\mathcal{F}(\mathbf{x}_k)]^{-1}]_{i,i}, \quad i = 1, \dots, n_x. \quad (3.17)$$

In the following, a lower bound on the MSE of the MT location is introduced, since it gives a bound on the best achievable localization accuracy. The MSE of the MT location satisfies the following inequality:

$$\mathbb{E}_{p(\mathbf{z}_k|\mathbf{x}_k)} \{ \|\hat{\mathbf{x}}_{\text{MT},k}(\mathbf{z}_k) - \mathbf{x}_{\text{MT},k}\|^2 \} \geq [[\mathcal{F}(\mathbf{x}_k)]^{-1}]_{1,1} + [[\mathcal{F}(\mathbf{x}_k)]^{-1}]_{2,2}. \quad (3.18)$$

The right-hand side of the inequality is termed hereinafter the MT location CRLB. In Section 3.3.2, an analytical expression for the MT location CRLB is derived assuming that the measurements are affected by LOS propagation conditions. For measurements affected by propagation conditions that may switch between LOS and NLOS, the MT location CRLB is evaluated numerically, which is presented in Section 3.3.3.

### 3.3.2 Cramér-Rao Lower Bound for LOS Propagation Conditions

In this section, a closed-form expression for the MT location CRLB is derived for measurements affected by LOS propagation conditions. For LOS propagation conditions, the  $n_z$  measurements are assumed to be mutually independent and corrupted by additive errors that are zero-mean Gaussian distributed with variance  $\sigma_{\text{LOS},k}^2$  for  $\nu = 1, \dots, n_z$ , cf. Section 2.3.5. In this case, the  $(i, j)$ -th element of  $\mathcal{F}(\mathbf{x}_k)$  is given by

$$[\mathcal{F}(\mathbf{x}_k)]_{i,j} = \sum_{\nu=1}^{n_z} \sigma_{\text{LOS},k}^{(\nu,-2)} \cdot \left[ \frac{\partial h_{\text{LOS},k}^{(\nu)}(\mathbf{x}_k)}{\partial x_k^{(i)}} \cdot \frac{\partial h_{\text{LOS},k}^{(\nu)}(\mathbf{x}_k)}{\partial x_k^{(j)}} \right], \quad i, j = 1, \dots, n_x. \quad (3.19)$$

A proof is given in Appendix A.2. Since the PR, RTT, RSS, and GRT measurements provide only information about the MT location and clock bias components, cf. (2.47), the FIM entries that are dependent on the MT velocity and MT clock drift are all zero. In this case, the FIM is not invertible, i.e., the FIM is singular, since several rows and columns of the FIM are zero. In the following, the FIM is evaluated for a reduced state vector  $\tilde{\mathbf{x}}_k = [\tilde{x}_k^{(1)}, \tilde{x}_k^{(2)}, \dots, \tilde{x}_k^{(n_{\tilde{x}})}]^\top$  with dimension  $n_{\tilde{x}}$ , that only consists of the elements that are contained in the corresponding measurements. Let  $\mathcal{F}_{\text{PR}}(\tilde{\mathbf{x}}_k)$ ,  $\mathcal{F}_{\text{RTT}}(\tilde{\mathbf{x}}_k)$ ,  $\mathcal{F}_{\text{RSS}}(\tilde{\mathbf{x}}_k)$  and  $\mathcal{F}_{\text{GRT}}(\tilde{\mathbf{x}}_k)$  denote the FIMs of the PR, RTT, RSS and GRT measurements for the reduced state vector  $\tilde{\mathbf{x}}_k = [\mathbf{x}_{\text{MT},k}^\top, c_0 \cdot \delta t_k]^\top$ . As long as the measurements are assumed to be mutually independent, the corresponding FIMs of the different measurements can be added up [Kay93]. Thus, the resulting FIM for the hybrid localization is given by

$$\mathcal{F}(\tilde{\mathbf{x}}_k) = \mathcal{F}_{\text{PR}}(\tilde{\mathbf{x}}_k) + \mathcal{F}_{\text{RTT}}(\tilde{\mathbf{x}}_k) + \mathcal{F}_{\text{RSS}}(\tilde{\mathbf{x}}_k) + \mathcal{F}_{\text{GRT}}(\tilde{\mathbf{x}}_k). \quad (3.20)$$

The FIM of the  $M_{\text{PR}}$  PR measurements can be determined from (2.21) and (3.19). The derivation of the FIM for the PR measurements can be found in Appendix A.3. Let  $\mathbf{u}_{\text{SAT},k}^{(m)}$  denote the unit vector originating at the true MT location and directed towards the  $m$ -th satellite, given by

$$\mathbf{u}_{\text{SAT},k}^{(m)} = u_{\text{SAT}_x,k}^{(m)} \cdot \mathbf{u}_x + u_{\text{SAT}_y,k}^{(m)} \cdot \mathbf{u}_y + u_{\text{SAT}_z,k}^{(m)} \cdot \mathbf{u}_z, \quad (3.21)$$

where  $\mathbf{u}_x$ ,  $\mathbf{u}_y$  and  $\mathbf{u}_z$  are the unit vectors in the  $x$ ,  $y$  and  $z$  directions. The vector  $\mathbf{p}_{\text{SAT},k}^{(m)}$  defines the projection of the unit vector  $\mathbf{u}_{\text{SAT},k}^{(m)}$  into the  $xy$ -plane and is given by

$$\mathbf{p}_{\text{SAT},k}^{(m)} = u_{\text{SAT},k}^{(m)} \cdot \mathbf{u}_x + u_{\text{SAT},k}^{(m)} \cdot \mathbf{u}_y. \quad (3.22)$$

Then, the elements of the FIM of PR measurements are given by

$$[\mathcal{F}_{\text{PR}}(\tilde{\mathbf{x}}_k)]_{1,1} = \sum_{m=1}^{M_{\text{PR}}} \sigma_{\text{PR},k}^{(m),-2} \cdot u_{\text{SAT},k}^{(m),2}, \quad (3.23a)$$

$$[\mathcal{F}_{\text{PR}}(\tilde{\mathbf{x}}_k)]_{1,2} = [\mathcal{F}_{\text{PR}}(\tilde{\mathbf{x}}_k)]_{2,1} = \sum_{m=1}^{M_{\text{PR}}} \sigma_{\text{PR},k}^{(m),-2} \cdot u_{\text{SAT},k}^{(m)} \cdot u_{\text{SAT},k}^{(m)}, \quad (3.23b)$$

$$[\mathcal{F}_{\text{PR}}(\tilde{\mathbf{x}}_k)]_{2,2} = \sum_{m=1}^{M_{\text{PR}}} \sigma_{\text{PR},k}^{(m),-2} \cdot u_{\text{SAT},k}^{(m),2}, \quad (3.23c)$$

$$[\mathcal{F}_{\text{PR}}(\tilde{\mathbf{x}}_k)]_{1,3} = [\mathcal{F}_{\text{PR}}(\tilde{\mathbf{x}}_k)]_{3,1} = \sum_{m=1}^{M_{\text{PR}}} \sigma_{\text{PR},k}^{(m),-2} \cdot u_{\text{SAT},k}^{(m)}, \quad (3.23d)$$

$$[\mathcal{F}_{\text{PR}}(\tilde{\mathbf{x}}_k)]_{2,3} = [\mathcal{F}_{\text{PR}}(\tilde{\mathbf{x}}_k)]_{3,2} = \sum_{m=1}^{M_{\text{PR}}} \sigma_{\text{PR},k}^{(m),-2} \cdot u_{\text{SAT},k}^{(m)}, \quad (3.23e)$$

$$[\mathcal{F}_{\text{PR}}(\tilde{\mathbf{x}}_k)]_{3,3} = \sum_{m=1}^{M_{\text{PR}}} \sigma_{\text{PR},k}^{(m),-2}. \quad (3.23f)$$

The FIM of the  $M_{\text{RTT}}$  RTT measurements can be determined from (2.28) and (3.19). The derivation of the FIM for the RTT measurements can be found in Appendix A.4. Let  $\mathbf{u}_{\text{BS},k}^{(m)}$  denote the unit vector originating at the true MT location and directed towards the  $m$ -th BS, given by

$$\mathbf{u}_{\text{BS},k}^{(m)} = u_{\text{BS},k}^{(m)} \cdot \mathbf{u}_x + u_{\text{BS},k}^{(m)} \cdot \mathbf{u}_y. \quad (3.24)$$

Then, the non-zero elements of the FIM of RTT measurements are given by

$$[\mathcal{F}_{\text{RTT}}(\tilde{\mathbf{x}}_k)]_{1,1} = \sum_{m=1}^{M_{\text{RTT}}} \sigma_{\text{RTT,LOS},k}^{(m),-2} \cdot u_{\text{BS},k}^{(m),2}, \quad (3.25a)$$

$$[\mathcal{F}_{\text{RTT}}(\tilde{\mathbf{x}}_k)]_{1,2} = [\mathcal{F}_{\text{RTT}}(\tilde{\mathbf{x}}_k)]_{2,1} = \sum_{m=1}^{M_{\text{RTT}}} \sigma_{\text{RTT,LOS},k}^{(m),-2} \cdot u_{\text{BS},k}^{(m)} \cdot u_{\text{BS},k}^{(m)}, \quad (3.25b)$$

$$[\mathcal{F}_{\text{RTT}}(\tilde{\mathbf{x}}_k)]_{2,2} = \sum_{m=1}^{M_{\text{RTT}}} \sigma_{\text{RTT,LOS},k}^{(m),-2} \cdot u_{\text{BS},k}^{(m),2}. \quad (3.25c)$$

Note, that all other elements of  $\mathcal{F}_{\text{RTT}}(\tilde{\mathbf{x}}_k)$  are zero, since  $\mathbf{h}_{\text{RTT},k}(\mathbf{x}_{\text{MT},k})$  only depends on the MT location. The FIM of the  $M_{\text{RSS}}$  RSS measurements can be determined from

(2.42) and (3.19). The derivation of the FIM for the RSS measurements can be found in Appendix A.5. Let  $b^{(m)}$  and  $g^{(m)}$  be defined as

$$b^{(m)} = \frac{10 \cdot B_{\text{LOS}}^{(m)}}{\log_e(10)} \quad (3.26)$$

and

$$g^{(m)} = \frac{\partial G_{\text{ANT}}^{(m)}(\varphi_{\text{LOS}}^{(m)}(\mathbf{x}_{\text{MT},k}))}{\partial \varphi_{\text{LOS}}^{(m)}(\mathbf{x}_{\text{MT},k})}. \quad (3.27)$$

Then, the non-zero elements of the FIM of RSS measurements are given by

$$[\mathcal{F}_{\text{RSS}}(\tilde{\mathbf{x}}_k)]_{1,1} = \sum_{m=1}^{M_{\text{RSS}}} \sigma_{\text{RSS,LOS},k}^{(m),-2} \cdot \left[ \frac{b^{(m)} \cdot u_{\text{BSx},k}^{(m)} + g^{(m)} \cdot u_{\text{BSy},k}^{(m)}}{d_{\text{BS},k}^{(m)}(\mathbf{x}_{\text{MT},k})} \right]^2, \quad (3.28a)$$

$$[\mathcal{F}_{\text{RSS}}(\tilde{\mathbf{x}}_k)]_{1,2} = [\mathcal{F}_{\text{RSS}}(\tilde{\mathbf{x}}_k)]_{2,1} = \sum_{m=1}^{M_{\text{RSS}}} \sigma_{\text{RSS,LOS},k}^{(m),-2} \cdot \left[ \left( \frac{b^{(m)} \cdot u_{\text{BSx},k}^{(m)} + g^{(m)} \cdot u_{\text{BSy},k}^{(m)}}{d_{\text{BS},k}^{(m)}(\mathbf{x}_{\text{MT},k})} \right) \cdot \left( \frac{b^{(m)} \cdot u_{\text{BSy},k}^{(m)} - g^{(m)} \cdot u_{\text{BSx},k}^{(m)}}{d_{\text{BS},k}^{(m)}(\mathbf{x}_{\text{MT},k})} \right) \right], \quad (3.28b)$$

$$[\mathcal{F}_{\text{RSS}}(\tilde{\mathbf{x}}_k)]_{2,2} = \sum_{m=1}^{M_{\text{RSS}}} \sigma_{\text{RSS,LOS},k}^{(m),-2} \cdot \left[ \frac{b^{(m)} \cdot u_{\text{BSy},k}^{(m)} - g^{(m)} \cdot u_{\text{BSx},k}^{(m)}}{d_{\text{BS},k}^{(m)}(\mathbf{x}_{\text{MT},k})} \right]^2. \quad (3.28c)$$

Note, that all other elements of  $\mathcal{F}_{\text{RSS}}(\tilde{\mathbf{x}}_k)$  are zero, since  $\mathbf{h}_{\text{RSS,LOS}}(\mathbf{x}_{\text{MT},k})$  only depends on the MT location. The FIM of the GRT measurement can be found from (2.45) and (3.19). The non-zero element of the FIM of the GRT measurement is given by

$$[\mathcal{F}_{\text{GRT}}(\tilde{\mathbf{x}}_k)]_{3,3} = \sigma_{\text{BIAS},k}^{-2}. \quad (3.29)$$

Note, that all other elements of  $\mathcal{F}_{\text{GRT}}(\tilde{\mathbf{x}}_k)$  are zero, since  $h_{\text{BIAS},k}(c_0 \cdot \delta t_k)$  only depends on the MT clock bias.

The FIM  $\mathcal{F}(\tilde{\mathbf{x}}_k)$  for hybrid localization can be found from adding up the FIMs of the PR, RTT, RSS and GRT measurements according to (3.20). For evaluating the MT location CRLB, the upper-left  $2 \times 2$  diagonal submatrix of  $[\mathcal{F}(\tilde{\mathbf{x}}_k)]^{-1}$  (or equivalently the upper-left  $2 \times 2$  diagonal submatrix of  $\mathcal{P}(\tilde{\mathbf{x}}_k)$ ) is of primary interest, cf. (3.18). Let the FIM be partitioned as follows

$$\mathcal{F}(\tilde{\mathbf{x}}_k) = \begin{bmatrix} [\mathcal{F}(\tilde{\mathbf{x}}_k)]_{1,1} & [\mathcal{F}(\tilde{\mathbf{x}}_k)]_{1,2} & [\mathcal{F}(\tilde{\mathbf{x}}_k)]_{1,3} \\ [\mathcal{F}(\tilde{\mathbf{x}}_k)]_{2,1} & [\mathcal{F}(\tilde{\mathbf{x}}_k)]_{2,2} & [\mathcal{F}(\tilde{\mathbf{x}}_k)]_{2,3} \\ [\mathcal{F}(\tilde{\mathbf{x}}_k)]_{3,1} & [\mathcal{F}(\tilde{\mathbf{x}}_k)]_{3,2} & [\mathcal{F}(\tilde{\mathbf{x}}_k)]_{3,3} \end{bmatrix} \equiv \begin{bmatrix} \mathcal{F}_1(\tilde{\mathbf{x}}_k) & \mathcal{F}_2(\tilde{\mathbf{x}}_k) \\ \mathcal{F}_3(\tilde{\mathbf{x}}_k) & \mathcal{F}_4(\tilde{\mathbf{x}}_k) \end{bmatrix}. \quad (3.30)$$

Then, the inverse of the matrix  $\mathcal{F}(\tilde{\mathbf{x}}_k)$  can be found from block matrix inversion [Ber09]

$$[\mathcal{F}(\tilde{\mathbf{x}}_k)]^{-1} = \left[ \left[ \begin{array}{c|c} \mathcal{F}_1(\tilde{\mathbf{x}}_k) & \mathcal{F}_2(\tilde{\mathbf{x}}_k) \\ \hline \mathcal{F}_3(\tilde{\mathbf{x}}_k) & \mathcal{F}_4(\tilde{\mathbf{x}}_k) \end{array} \right] \right]^{-1} \equiv \left[ \begin{array}{c|c} \mathcal{P}_1(\tilde{\mathbf{x}}_k) & \mathcal{P}_2(\tilde{\mathbf{x}}_k) \\ \hline \mathcal{P}_3(\tilde{\mathbf{x}}_k) & \mathcal{P}_4(\tilde{\mathbf{x}}_k) \end{array} \right], \quad (3.31)$$

where the upper-left  $2 \times 2$  submatrix of  $\mathcal{P}(\tilde{\mathbf{x}}_k)$  is given by

$$\mathcal{P}_1(\tilde{\mathbf{x}}_k) = [\mathcal{F}_1(\tilde{\mathbf{x}}_k) - \mathcal{F}_2(\tilde{\mathbf{x}}_k)\mathcal{F}_4^{-1}(\tilde{\mathbf{x}}_k)\mathcal{F}_3(\tilde{\mathbf{x}}_k)]^{-1} \triangleq [\mathcal{F}_L(\tilde{\mathbf{x}}_k)]^{-1}. \quad (3.32)$$

The MT location CRLB can be now expressed in terms of the equivalent FIM  $\mathcal{F}_L(\tilde{\mathbf{x}}_k)$  instead of  $\mathcal{F}(\tilde{\mathbf{x}}_k)$ , cf. (3.18). Let  $\text{tr}[\mathbf{A}]$  denote the trace and let  $\det[\mathbf{A}]$  denote the determinant of the matrix  $\mathbf{A}$ . Then, the MT location CRLB is given by

$$\mathcal{P}_{\text{CRLB},k} \triangleq \text{tr}[\mathcal{P}_1(\tilde{\mathbf{x}}_k)] = \frac{[\mathcal{F}_L(\tilde{\mathbf{x}}_k)]_{1,1} + [\mathcal{F}_L(\tilde{\mathbf{x}}_k)]_{2,2}}{\det[\mathcal{F}_L(\tilde{\mathbf{x}}_k)]}. \quad (3.33)$$

In order to derive a closed-form expression for  $\mathcal{P}_{\text{CRLB},k}$ , it is, thus, necessary to evaluate the expression in (3.33). Let two auxiliary variables be given by

$$c^{(\kappa_1, \kappa_2)} = \frac{\sigma_{\text{PR},k}^{(\kappa_1),-2} \cdot \sigma_{\text{PR},k}^{(\kappa_2),-2}}{\sigma_{\text{BIAS},k}^{-2} + \sum_{\kappa_3=1}^{M_{\text{PR}}} \sigma_{\text{PR},k}^{(\kappa_3),-2}}, \quad \kappa_1, \kappa_2 = 1, \dots, M_{\text{PR}}, \quad (3.34)$$

and

$$e^{(\kappa_1)} = \frac{\sigma_{\text{PR},k}^{(\kappa_1),-2} \cdot \sigma_{\text{BIAS},k}^{-2}}{\sigma_{\text{BIAS},k}^{-2} + \sum_{\kappa_3=1}^{M_{\text{PR}}} \sigma_{\text{PR},k}^{(\kappa_3),-2}}, \quad \kappa_1 = 1, \dots, M_{\text{PR}}, \quad (3.35)$$

respectively. Then, the elements of the matrix  $\mathcal{F}_L(\tilde{\mathbf{x}}_k)$  are given as follows

$$\begin{aligned} [\mathcal{F}_L(\tilde{\mathbf{x}}_k)]_{1,1} &= \sum_{\kappa_1=1}^{M_{\text{PR}}} e^{(\kappa_1)} \cdot u_{\text{SAT}_x,k}^{(\kappa_1),2} + \sum_{\kappa_1=1}^{M_{\text{RTT}}} \sigma_{\text{RTT,LOS},k}^{(\kappa_1),-2} \cdot u_{\text{BS}_x,k}^{(\kappa_1),2} \\ &\quad + \sum_{\kappa_1=1}^{M_{\text{PR}}} \sum_{\kappa_2=1}^{M_{\text{PR}}} c^{(\kappa_1, \kappa_2)} \cdot (u_{\text{SAT}_x,k}^{(\kappa_1),2} - u_{\text{SAT}_x,k}^{(\kappa_1)} \cdot u_{\text{SAT}_x,k}^{(\kappa_2)}) \\ &\quad + \sum_{\kappa_1=1}^{M_{\text{RSS}}} \sigma_{\text{RSS,LOS},k}^{(\kappa_1),-2} \cdot \left[ \frac{b^{(\kappa_1)} \cdot u_{\text{BS}_x,k}^{(\kappa_1)} + g^{(\kappa_1)} \cdot u_{\text{BS}_y,k}^{(\kappa_1)}}{d_{\text{BS},k}^{(\kappa_1)}(\mathbf{x}_{\text{MT},k})} \right]^2, \end{aligned} \quad (3.36a)$$

$$\begin{aligned}
[\mathcal{F}_L(\tilde{\mathbf{x}}_k)]_{1,2} &= \sum_{\kappa_1=1}^{M_{\text{PR}}} e^{(\kappa_1)} \cdot u_{\text{SAT}_x,k}^{(\kappa_1)} \cdot u_{\text{SAT}_y,k}^{(\kappa_1)} + \sum_{\kappa_1=1}^{M_{\text{RTT}}} \sigma_{\text{RTT,LOS},k}^{(\kappa_1),-2} \cdot u_{\text{BS}_x,k}^{(\kappa_1)} \cdot u_{\text{BS}_y,k}^{(\kappa_1)} \\
&+ \sum_{\kappa_1=1}^{M_{\text{PR}}} \sum_{\kappa_2=1}^{M_{\text{PR}}} c^{(\kappa_1,\kappa_2)} \cdot (u_{\text{SAT}_x,k}^{(\kappa_1)} \cdot u_{\text{SAT}_y,k}^{(\kappa_1)} - u_{\text{SAT}_y,k}^{(\kappa_1)} \cdot u_{\text{SAT}_x,k}^{(\kappa_2)}) \\
&+ \sum_{\kappa_1=1}^{M_{\text{RSS}}} \sigma_{\text{RSS,LOS},k}^{(\kappa_1),-2} \cdot \left[ \left( \frac{b^{(\kappa_1)} \cdot u_{\text{BS}_x,k}^{(\kappa_1)} + g^{(\kappa_1)} \cdot u_{\text{BS}_y,k}^{(\kappa_1)}}{d_{\text{BS},k}^{(\kappa_1)}(\mathbf{x}_{\text{MT},k})} \right) \right. \\
&\cdot \left. \left( \frac{b^{(\kappa_1)} \cdot u_{\text{BS}_y,k}^{(\kappa_1)} - g^{(\kappa_1)} \cdot u_{\text{BS}_x,k}^{(\kappa_1)}}{d_{\text{BS},k}^{(\kappa_1)}(\mathbf{x}_{\text{MT},k})} \right) \right] = [\mathcal{F}_L(\tilde{\mathbf{x}}_k)]_{2,1}, \quad (3.36b)
\end{aligned}$$

$$\begin{aligned}
[\mathcal{F}_L(\tilde{\mathbf{x}}_k)]_{2,2} &= \sum_{\kappa_1=1}^{M_{\text{PR}}} e^{(\kappa_1)} \cdot u_{\text{SAT}_y,k}^{(\kappa_1),2} + \sum_{\kappa_1=1}^{M_{\text{RTT}}} \sigma_{\text{RTT,LOS},k}^{(\kappa_1),-2} \cdot u_{\text{BS}_y,k}^{(\kappa_1),2} \\
&+ \sum_{\kappa_1=1}^{M_{\text{PR}}} \sum_{\kappa_2=1}^{M_{\text{PR}}} c^{(\kappa_1,\kappa_2)} \cdot (u_{\text{SAT}_y,k}^{(\kappa_1),2} - u_{\text{SAT}_y,k}^{(\kappa_1)} \cdot u_{\text{SAT}_y,k}^{(\kappa_2)}) \\
&+ \sum_{\kappa_1=1}^{M_{\text{RSS}}} \sigma_{\text{RSS,LOS},k}^{(\kappa_1),-2} \cdot \left[ \frac{b^{(\kappa_1)} \cdot u_{\text{BS}_y,k}^{(\kappa_1)} - g^{(\kappa_1)} \cdot u_{\text{BS}_x,k}^{(\kappa_1)}}{d_{\text{BS},k}^{(\kappa_1)}(\mathbf{x}_{\text{MT},k})} \right]^2. \quad (3.36c)
\end{aligned}$$

The derivation of (3.36) can be found in Appendix A.6. The numerator of (3.33) can be found from the addition of  $[\mathcal{F}_L(\tilde{\mathbf{x}}_k)]_{1,1}$  and  $[\mathcal{F}_L(\tilde{\mathbf{x}}_k)]_{2,2}$ , and is given by

$$\begin{aligned}
[\mathcal{F}_L(\tilde{\mathbf{x}}_k)]_{1,1} + [\mathcal{F}_L(\tilde{\mathbf{x}}_k)]_{2,2} &= \sum_{\kappa_1=1}^{M_{\text{PR}}} e^{(\kappa_1)} \cdot \|\mathbf{p}_{\text{SAT},k}^{(\kappa_1)}\|^2 + \sum_{\kappa_1=1}^{M_{\text{RTT}}} \sigma_{\text{RTT,LOS},k}^{(\kappa_1),-2} \\
&+ \sum_{\kappa_1=1}^{M_{\text{PR}}} \sum_{\substack{\kappa_2=1 \\ \kappa_2 > \kappa_1}}^{M_{\text{PR}}} c^{(\kappa_1,\kappa_2)} \cdot \|\mathbf{p}_{\text{SAT},k}^{(\kappa_1)} - \mathbf{p}_{\text{SAT},k}^{(\kappa_2)}\|^2 \\
&+ \sum_{\kappa_1=1}^{M_{\text{RSS}}} \sigma_{\text{RSS,LOS},k}^{(\kappa_1),-2} \cdot \left[ \frac{b^{(\kappa_1),2} + g^{(\kappa_1),2}}{d_{\text{BS},k}^{(\kappa_1),2}(\mathbf{x}_{\text{MT},k})} \right]. \quad (3.37)
\end{aligned}$$

The derivation of (3.37) can be found in Appendix A.7. The denominator of (3.33) can be found from evaluating the determinant

$$\det[\mathcal{F}_L(\tilde{\mathbf{x}}_k)] = [\mathcal{F}_L(\tilde{\mathbf{x}}_k)]_{1,1} \cdot [\mathcal{F}_L(\tilde{\mathbf{x}}_k)]_{2,2} - [\mathcal{F}_L(\tilde{\mathbf{x}}_k)]_{1,1} \cdot [\mathcal{F}_L(\tilde{\mathbf{x}}_k)]_{2,2}. \quad (3.38)$$

Let  $\mathbf{a} \times \mathbf{b}$  denote the cross product of the two vectors  $\mathbf{a}$  and  $\mathbf{b}$  and let  $\mathcal{A}^{(\kappa_1,\kappa_2)}$  be given by

$$\mathcal{A}^{(\kappa_1,\kappa_2)} = [\mathbf{p}_{\text{SAT},k}^{(\kappa_1)} \times \mathbf{p}_{\text{SAT},k}^{(\kappa_2)}]^\top \cdot \mathbf{u}_z, \quad \kappa_1 = \kappa_2 = 1, \dots, N_{\text{SAT}}. \quad (3.39)$$

The magnitude  $\|\mathcal{A}^{(\kappa_1,\kappa_2)}\|$  denotes the positive area of the parallelogram determined by the two vectors  $\mathbf{p}_{\text{SAT},k}^{(\kappa_1)}$  and  $\mathbf{p}_{\text{SAT},k}^{(\kappa_2)}$  and  $\mathcal{A}^{(\kappa_1,\kappa_2)}$  is commonly referred to as signed

area of the parallelogram (i.e. positive or negative area of parallelogram). The signed area of the parallelogram determined by  $\mathbf{u}_{\text{BS},k}^{(\kappa_1)}$  and  $\mathbf{p}_{\text{SAT},k}^{(\kappa_2)}$  is given by

$$\mathcal{B}^{(\kappa_1, \kappa_2)} = [\mathbf{u}_{\text{BS},k}^{(\kappa_1)} \times \mathbf{p}_{\text{SAT},k}^{(\kappa_2)}]^\top \cdot \mathbf{u}_z, \quad \kappa_1 = 1, \dots, N_{\text{BS}}, \quad \kappa_2 = 1, \dots, N_{\text{SAT}}, \quad (3.40)$$

and the signed area of the parallelogram determined by  $\mathbf{u}_{\text{BS},k}^{(\kappa_1)}$  and  $\mathbf{u}_{\text{BS},k}^{(\kappa_2)}$  is given by

$$\mathcal{C}^{(\kappa_1, \kappa_2)} = [\mathbf{u}_{\text{BS},k}^{(\kappa_1)} \times \mathbf{u}_{\text{BS},k}^{(\kappa_2)}]^\top \cdot \mathbf{u}_z, \quad \kappa_1 = \kappa_2 = 1, \dots, N_{\text{BS}}. \quad (3.41)$$

Let further  $\mathcal{D}^{(\kappa_1, \kappa_2)}$  denote the dot product of the two vectors  $\mathbf{u}_{\text{BS},k}^{(\kappa_1)}$  and  $\mathbf{p}_{\text{SAT},k}^{(\kappa_2)}$ , given by

$$\mathcal{D}^{(\kappa_1, \kappa_2)} = \mathbf{u}_{\text{BS},k}^{(\kappa_1)} \cdot \mathbf{p}_{\text{SAT},k}^{(\kappa_2)}, \quad \kappa_1 = 1, \dots, N_{\text{BS}}, \quad \kappa_2 = 1, \dots, N_{\text{SAT}}, \quad (3.42)$$

and let  $\mathcal{E}^{(\kappa_1, \kappa_2)}$  denote the dot product of the two vectors  $\mathbf{u}_{\text{BS},k}^{(\kappa_1)}$  and  $\mathbf{u}_{\text{BS},k}^{(\kappa_2)}$ , given by

$$\mathcal{E}^{(\kappa_1, \kappa_2)} = \mathbf{u}_{\text{BS},k}^{(\kappa_1)} \cdot \mathbf{u}_{\text{BS},k}^{(\kappa_2)}, \quad \kappa_1 = \kappa_2 = 1, \dots, N_{\text{BS}}. \quad (3.43)$$

The signed area of the rectangle determined by  $[\mathbf{p}_{\text{SAT},k}^{(\kappa_1)} - \mathbf{p}_{\text{SAT},k}^{(\kappa_2)}]^\top \cdot \mathbf{u}_x$  and  $[\mathbf{p}_{\text{SAT},k}^{(\kappa_3)} - \mathbf{p}_{\text{SAT},k}^{(\kappa_4)}]^\top \cdot \mathbf{u}_x$  is given by

$$\mathcal{G}_1^{(\kappa_1, \kappa_2, \kappa_3, \kappa_4)} = [\mathbf{p}_{\text{SAT},k}^{(\kappa_1)} - \mathbf{p}_{\text{SAT},k}^{(\kappa_2)}]^\top \cdot \mathbf{u}_x \cdot [\mathbf{p}_{\text{SAT},k}^{(\kappa_3)} - \mathbf{p}_{\text{SAT},k}^{(\kappa_4)}]^\top \cdot \mathbf{u}_y, \quad (3.44)$$

with  $\kappa_1 = \dots = \kappa_4 = 1, \dots, N_{\text{SAT}}$ . The signed area of the parallelogram determined by  $(\mathbf{p}_{\text{SAT},k}^{(\kappa_1)} - \mathbf{p}_{\text{SAT},k}^{(\kappa_2)})$  and  $(\mathbf{p}_{\text{SAT},k}^{(\kappa_3)} - \mathbf{p}_{\text{SAT},k}^{(\kappa_4)})$  is given by

$$\mathcal{G}_2^{(\kappa_1, \kappa_2, \kappa_3, \kappa_4)} = [(\mathbf{p}_{\text{SAT},k}^{(\kappa_1)} - \mathbf{p}_{\text{SAT},k}^{(\kappa_2)}) \times (\mathbf{p}_{\text{SAT},k}^{(\kappa_3)} - \mathbf{p}_{\text{SAT},k}^{(\kappa_4)})]^\top \cdot \mathbf{u}_z, \quad (3.45)$$

with  $\kappa_1 = \dots = \kappa_4 = 1, \dots, N_{\text{SAT}}$ . Furthermore, let  $\mathcal{G}^{(\kappa_1, \kappa_2, \kappa_3, \kappa_4)}$  be given by

$$\mathcal{G}^{(\kappa_1, \kappa_2, \kappa_3, \kappa_4)} = \mathcal{G}_1^{(\kappa_1, \kappa_2, \kappa_3, \kappa_4)} \cdot \mathcal{G}_2^{(\kappa_1, \kappa_2, \kappa_3, \kappa_4)}, \quad \kappa_1 = \dots = \kappa_4 = 1, \dots, N_{\text{SAT}}. \quad (3.46)$$

Then, the denominator of (3.33) can be written as

$$\begin{aligned}
\det[\mathcal{F}_L(\tilde{\mathbf{x}}_k)] &= \sum_{\kappa_1=1}^{M_{\text{PR}}} \sum_{\substack{\kappa_2=1 \\ \kappa_2 > \kappa_1}}^{M_{\text{PR}}} e^{(\kappa_1)} \cdot e^{(\kappa_2)} \cdot \mathcal{A}^{(\kappa_1, \kappa_2), 2} \\
&+ \sum_{\kappa_1=1}^{M_{\text{RTT}}} \sum_{\kappa_2=1}^{M_{\text{PR}}} \sigma_{\text{RTT,LOS},k}^{(\kappa_1), -2} \cdot e^{(\kappa_2)} \cdot \mathcal{B}^{(\kappa_1, \kappa_2), 2} \\
&+ \sum_{\kappa_1=1}^{M_{\text{PR}}} \sum_{\kappa_2=1}^{M_{\text{PR}}} \sum_{\substack{\kappa_3=1 \\ \kappa_3 > \kappa_2}}^{M_{\text{PR}}} e^{(\kappa_1)} \cdot c^{(\kappa_2, \kappa_3)} \cdot [\mathcal{A}^{(\kappa_1, \kappa_2)} - \mathcal{A}^{(\kappa_1, \kappa_3)}]^2 \\
&+ \sum_{\kappa_1=1}^{M_{\text{RSS}}} \sum_{\kappa_2=1}^{M_{\text{PR}}} \sigma_{\text{RSS,LOS},k}^{(\kappa_1), -2} \cdot e^{(\kappa_2)} \cdot \left[ \frac{b^{(\kappa_1)} \cdot \mathcal{B}^{(\kappa_1, \kappa_2)} + g^{(\kappa_1)} \cdot \mathcal{D}^{(\kappa_1, \kappa_2)}}{d_{\text{BS},k}^{(\kappa_1)}(\mathbf{x}_{\text{MT},k})} \right]^2 \\
&+ \sum_{\kappa_1=1}^{M_{\text{RTT}}} \sum_{\substack{\kappa_2=1 \\ \kappa_2 > \kappa_1}}^{M_{\text{RTT}}} \sigma_{\text{RTT,LOS},k}^{(\kappa_1), -2} \cdot \sigma_{\text{RTT,LOS},k}^{(\kappa_2), -2} \cdot \mathcal{C}^{(\kappa_1, \kappa_2), 2} \\
&+ \sum_{\kappa_1=1}^{M_{\text{RTT}}} \sum_{\kappa_2=1}^{M_{\text{PR}}} \sum_{\substack{\kappa_3=1 \\ \kappa_3 > \kappa_2}}^{M_{\text{PR}}} \sigma_{\text{RTT,LOS},k}^{(\kappa_1), -2} \cdot c^{(\kappa_2, \kappa_3)} \cdot [\mathcal{B}^{(\kappa_1, \kappa_2)} - \mathcal{B}^{(\kappa_1, \kappa_3)}]^2 \\
&+ \sum_{\kappa_1=1}^{M_{\text{RTT}}} \sum_{\kappa_2=1}^{M_{\text{RSS}}} \sigma_{\text{RTT,LOS},k}^{(\kappa_1), -2} \cdot \sigma_{\text{RSS,LOS},k}^{(\kappa_2), -2} \cdot \left[ \frac{b^{(\kappa_2)} \cdot \mathcal{C}^{(\kappa_1, \kappa_2)} - g^{(\kappa_2)} \cdot \mathcal{E}^{(\kappa_1, \kappa_2)}}{d_{\text{BS},k}^{(\kappa_2)}(\mathbf{x}_{\text{MT},k})} \right]^2 \\
&+ \sum_{\kappa_1=1}^{M_{\text{PR}}} \sum_{\substack{\kappa_2=1 \\ \kappa_2 > \kappa_1}}^{M_{\text{PR}}} \sum_{\kappa_3=1}^{M_{\text{PR}}} \sum_{\substack{\kappa_4=1 \\ \kappa_4 > \kappa_3}}^{M_{\text{PR}}} c^{(\kappa_1, \kappa_2)} \cdot c^{(\kappa_3, \kappa_4)} \cdot \mathcal{G}^{(\kappa_1, \kappa_2, \kappa_3, \kappa_4)} \\
&+ \sum_{\kappa_1=1}^{M_{\text{RSS}}} \sum_{\kappa_2=1}^{M_{\text{PR}}} \sum_{\substack{\kappa_3=1 \\ \kappa_3 > \kappa_2}}^{M_{\text{PR}}} \sigma_{\text{RSS,LOS},k}^{(\kappa_1), -2} \cdot c^{(\kappa_2, \kappa_3)} \cdot \left[ \frac{b^{(\kappa_1)} \cdot \mathcal{B}^{(\kappa_1, \kappa_2)} + g^{(\kappa_1)} \cdot \mathcal{D}^{(\kappa_1, \kappa_2)}}{d_{\text{BS},k}^{(\kappa_1)}(\mathbf{x}_{\text{MT},k})} \right. \\
&\quad \left. + \frac{b^{(\kappa_1)} \cdot \mathcal{B}^{(\kappa_1, \kappa_3)} + g^{(\kappa_1)} \cdot \mathcal{D}^{(\kappa_1, \kappa_3)}}{d_{\text{BS},k}^{(\kappa_1)}(\mathbf{x}_{\text{MT},k})} \right]^2 \\
&+ \sum_{\kappa_1=1}^{M_{\text{RSS}}} \sum_{\substack{\kappa_2=1 \\ \kappa_2 > \kappa_1}}^{M_{\text{RSS}}} \sigma_{\text{RSS,LOS},k}^{(\kappa_1), -2} \cdot \sigma_{\text{RSS,LOS},k}^{(\kappa_2), -2} \cdot \left[ \frac{(b^{(\kappa_1)} \cdot b^{(\kappa_2)} + g^{(\kappa_1)} \cdot g^{(\kappa_2)}) \cdot \mathcal{C}^{(\kappa_1, \kappa_2)}}{d_{\text{BS},k}^{(\kappa_1)}(\mathbf{x}_{\text{MT},k}) \cdot d_{\text{BS},k}^{(\kappa_2)}(\mathbf{x}_{\text{MT},k})} \right. \\
&\quad \left. + \frac{(b^{(\kappa_2)} \cdot g^{(\kappa_1)} - b^{(\kappa_1)} \cdot g^{(\kappa_2)}) \cdot \mathcal{E}^{(\kappa_1, \kappa_2)}}{d_{\text{BS},k}^{(\kappa_1)}(\mathbf{x}_{\text{MT},k}) \cdot d_{\text{BS},k}^{(\kappa_2)}(\mathbf{x}_{\text{MT},k})} \right]^2. \tag{3.47}
\end{aligned}$$

The derivation of (3.47) can be found in Appendix A.8.



The MT location CRLB in dependence of the PR, RTT, RSS and GRT measurements is, thus, given by

$$\mathcal{P}_{\text{CRLB},k} = \frac{\sum_{\kappa_1=1}^{M_{\text{RTT}}} \sigma_{\text{RTT,LOS},k}^{(\kappa_1),-2} + \sum_{\kappa_1=1}^{M_{\text{RSS}}} \sigma_{\text{RSS,LOS},k}^{(\kappa_1),-2} \cdot \left[ \frac{b^{(\kappa_1),2} + g^{(\kappa_1),2}}{d_{\text{BS},k}^{(\kappa_1),2}(\mathbf{x}_{\text{MT},k})} \right]}{\det[\mathcal{F}_{\text{L}}(\tilde{\mathbf{x}}_k)]} + \frac{\sum_{\kappa_1=1}^{M_{\text{PR}}} e^{(\kappa_1)} \cdot \|\mathbf{p}_{\text{SAT},k}^{(\kappa_1)}\|^2 + \sum_{\kappa_1=1}^{M_{\text{PR}}} \sum_{\substack{\kappa_2=1 \\ \kappa_2 > \kappa_1}}^{M_{\text{PR}}} c^{(\kappa_1,\kappa_2)} \cdot \|\mathbf{p}_{\text{SAT},k}^{(\kappa_1)} - \mathbf{p}_{\text{SAT},k}^{(\kappa_2)}\|^2}{\det[\mathcal{F}_{\text{L}}(\tilde{\mathbf{x}}_k)]}. \quad (3.48)$$

Depending on the number of available measurements, several special cases can be deduced from the above expression that correspond to the methods investigated in this thesis, cf. Section 2.3.4. In the following, the expression in (3.48) is explained in more detail and a geometric interpretation of the CRLB is given:

- The CRLB depends on the accuracy of the PR, RTT, RSS and GRT measurements, which is represented by the noise variances  $\sigma_{\text{RTT,LOS},k}^2$  and  $\sigma_{\text{RSS,LOS},k}^2$  and the noise variances  $\sigma_{\text{PR},k}^2$  and  $\sigma_{\text{BIAS},k}^2$  inherent in  $e^{(\kappa_1)}$  and  $c^{(\kappa_1,\kappa_2)}$ , cf. (3.34) and (3.35). For small variances and, thus, accurate measurements, the CRLB will be lower than for inaccurate measurements with large variances.
- The CRLB depends on the path loss exponent inherent in the constant  $b^{(\kappa_1)}$ , the derivative of the normalized antenna gain given by  $g^{(\kappa_1)}$  and the distance between the MT and the BSs. Note that if omni-directional antennas are employed at the BSs, then  $g^{(\kappa_1)} = 0$  holds. The distance dependency exclusively results from the RSS measurements. For small distances, the bound will be generally lower than for large distances. This in turn means that the contribution of the RSS measurements to the CRLB is large when the BSs are located close to each other.
- The CRLB depends on the relative geometry between the MT and the BS given by  $\mathcal{C}^{(\kappa_1,\kappa_2)}$  and  $\mathcal{E}^{(\kappa_1,\kappa_2)}$ , whose relationship is further illustrated in Fig. 3.1. From Fig. 3.1, it can be seen that the values of  $\mathcal{C}^{(\kappa_1,\kappa_2)}$  and  $\mathcal{E}^{(\kappa_1,\kappa_2)}$  strongly depend on the relative orientation of the unit vectors  $\mathbf{u}_{\text{BS},k}^{(\kappa_1)}$  and  $\mathbf{u}_{\text{BS},k}^{(\kappa_2)}$ . For instance, if the two vectors are parallel,  $\mathcal{C}^{(\kappa_1,\kappa_2)} = 0$  holds, and if the two vectors are orthogonal,  $\mathcal{E}^{(\kappa_1,\kappa_2)} = 0$  holds. Thus,  $\mathcal{C}^{(\kappa_1,\kappa_2)}$  and  $\mathcal{E}^{(\kappa_1,\kappa_2)}$  can be interpreted as a measure for the geometric contribution to the MT location accuracy [Spi01].

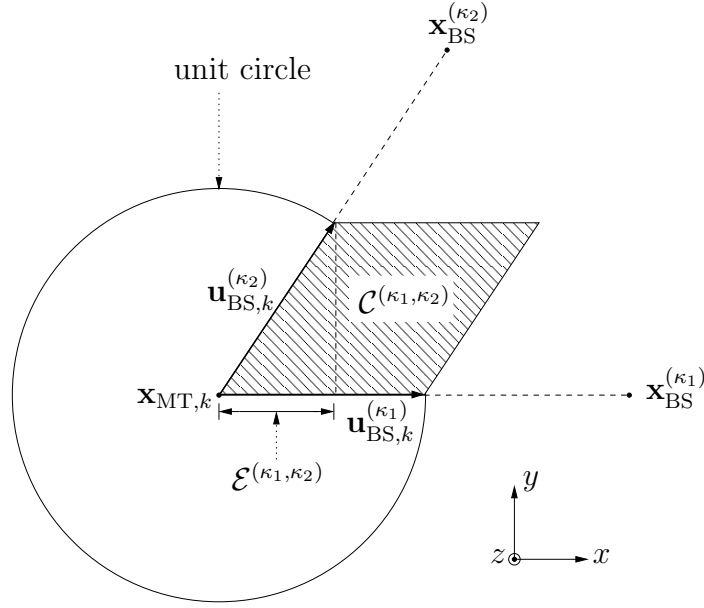


Figure 3.1. Relationship between  $\mathcal{C}^{(\kappa_1, \kappa_2)}$ ,  $\mathcal{E}^{(\kappa_1, \kappa_2)}$  and the unit vectors  $\mathbf{u}_{\text{BS},k}^{(\kappa_1)}$  and  $\mathbf{u}_{\text{BS},k}^{(\kappa_2)}$  [Spi01].

- The CRLB depends on the magnitude of the projection vector  $\mathbf{p}_{\text{SAT},k}^{(\kappa_1)}$  given by  $\|\mathbf{p}_{\text{SAT},k}^{(\kappa_1)}\|^2$ , which itself depends on the satellite elevation angle. For a satellite at a low elevation angle, the magnitude will be larger than for a satellite at a high elevation angle. For the special case that the satellite is located directly above the MT, the magnitude will be zero.
- The CRLB is influenced by the relative geometry between the MT, the BS and the satellite, given by  $\mathcal{B}^{(\kappa_1, \kappa_2)}$  and  $\mathcal{D}^{(\kappa_1, \kappa_2)}$ , whose relationship is illustrated in Fig. 3.2. From Fig. 3.2, it can be seen that the values of  $\mathcal{B}^{(\kappa_1, \kappa_2)}$  and  $\mathcal{D}^{(\kappa_1, \kappa_2)}$  strongly depend on the relative orientation of the unit vector  $\mathbf{u}_{\text{BS},k}^{(\kappa_1)}$  and the projection vector  $\mathbf{p}_{\text{SAT},k}^{(\kappa_2)}$ . For instance, if the two vectors are parallel,  $\mathcal{B}^{(\kappa_1, \kappa_2)} = 0$  holds, and if the two vectors are orthogonal  $\mathcal{D}^{(\kappa_1, \kappa_2)} = 0$  holds.
- The CRLB is influenced by the relative geometry between the MT and the satellites, given by  $\mathcal{A}^{(\kappa_1, \kappa_2)}$ ,  $\|\mathbf{p}_{\text{SAT},k}^{(\kappa_1)} - \mathbf{p}_{\text{SAT},k}^{(\kappa_2)}\|^2$  and  $\mathcal{G}^{(\kappa_1, \kappa_2, \kappa_3, \kappa_4)}$ . In Fig. 3.3, the geometrical relationship between the projection vectors  $\mathbf{p}_{\text{SAT},k}^{(\kappa_1)}$  and  $\mathbf{p}_{\text{SAT},k}^{(\kappa_2)}$  and the signed area of the parallelogram  $\mathcal{A}^{(\kappa_1, \kappa_2)}$  is shown. It can be seen that the values of  $\mathcal{A}^{(\kappa_1, \kappa_2)}$  strongly depend on the relative orientation of the projection vectors  $\mathbf{p}_{\text{SAT},k}^{(\kappa_1)}$  and  $\mathbf{p}_{\text{SAT},k}^{(\kappa_2)}$ . For example, if  $\mathbf{p}_{\text{SAT},k}^{(\kappa_1)}$  and  $\mathbf{p}_{\text{SAT},k}^{(\kappa_2)}$  are parallel,  $\mathcal{A}^{(\kappa_1, \kappa_2)} = 0$  holds. In Fig. 3.4, the relationship between the vectors  $(\mathbf{p}_{\text{SAT},k}^{(\kappa_1)} - \mathbf{p}_{\text{SAT},k}^{(\kappa_2)})$ ,  $(\mathbf{p}_{\text{SAT},k}^{(\kappa_3)} - \mathbf{p}_{\text{SAT},k}^{(\kappa_4)})$  and  $\mathcal{G}_1^{(\kappa_1, \kappa_2, \kappa_3, \kappa_4)}$ ,  $\mathcal{G}_2^{(\kappa_1, \kappa_2, \kappa_3, \kappa_4)}$  is shown, cf. (3.46). From Fig. 3.4, it can be seen that the sizes of the areas  $\mathcal{G}_1^{(\kappa_1, \kappa_2, \kappa_3, \kappa_4)}$  and  $\mathcal{G}_2^{(\kappa_1, \kappa_2, \kappa_3, \kappa_4)}$  strongly depend on the magnitude of the two vectors  $(\mathbf{p}_{\text{SAT},k}^{(\kappa_1)} - \mathbf{p}_{\text{SAT},k}^{(\kappa_2)})$  and  $(\mathbf{p}_{\text{SAT},k}^{(\kappa_3)} - \mathbf{p}_{\text{SAT},k}^{(\kappa_4)})$ .

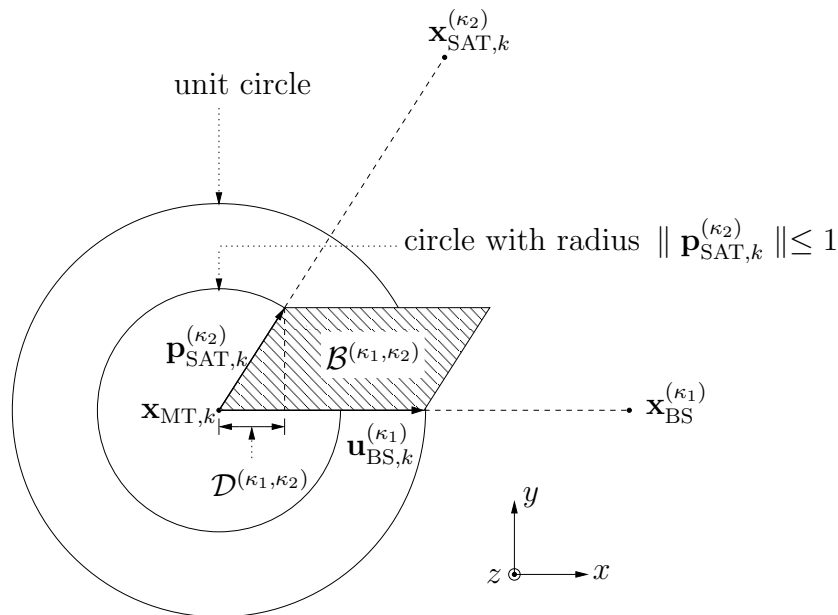


Figure 3.2. Relationship between  $\mathcal{B}^{(\kappa_1, \kappa_2)}$ ,  $\mathcal{D}^{(\kappa_1, \kappa_2)}$  and the vectors  $\mathbf{u}_{\text{BS},k}^{(\kappa_1)}$  and  $\mathbf{p}_{\text{SAT},k}^{(\kappa_2)}$ .

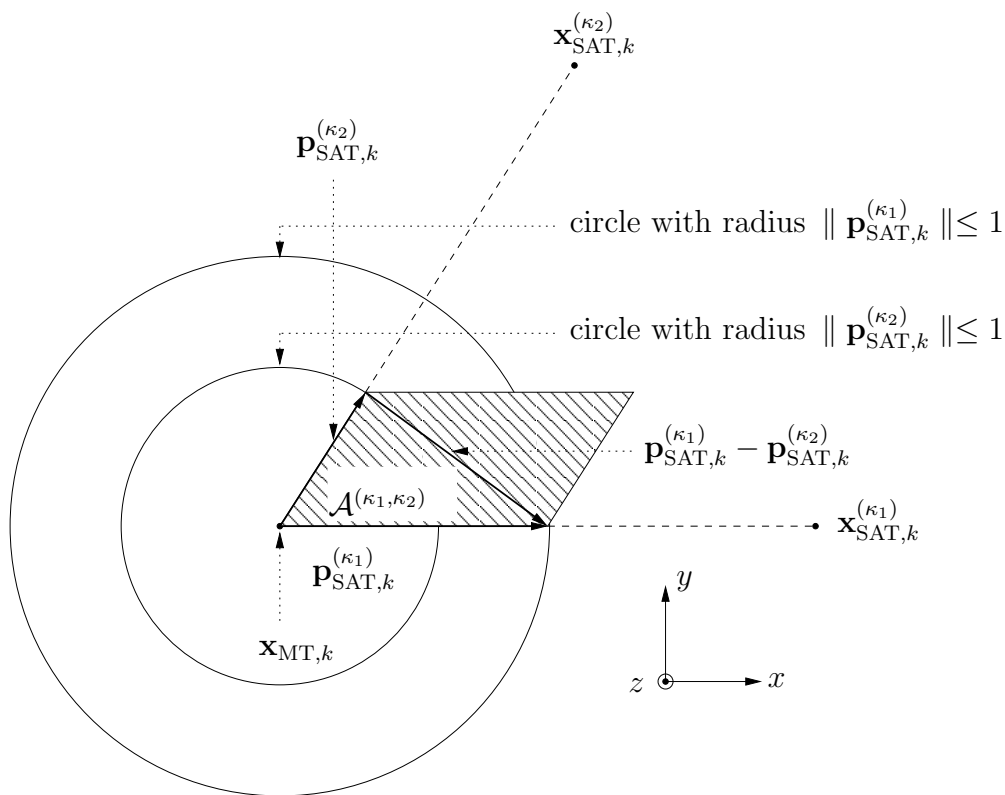


Figure 3.3. Relationship between  $\mathcal{A}^{(\kappa_1, \kappa_2)}$  and the vectors  $\mathbf{p}_{\text{SAT},k}^{(\kappa_1)}$  and  $\mathbf{p}_{\text{SAT},k}^{(\kappa_2)}$ .

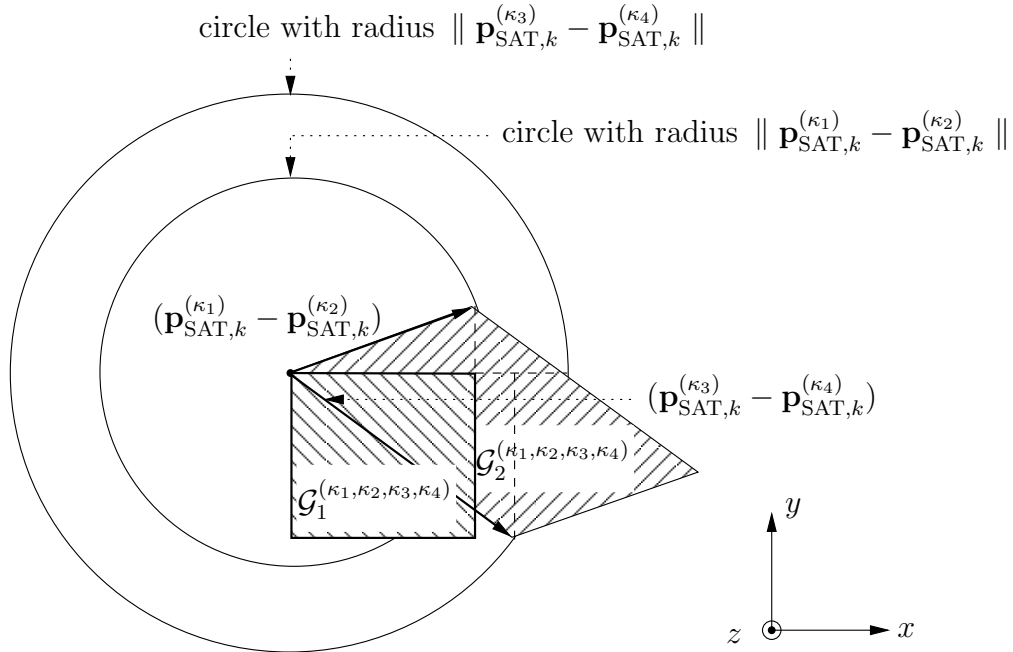


Figure 3.4. Relationship between the vectors  $(\mathbf{p}_{\text{SAT},k}^{(\kappa_1)} - \mathbf{p}_{\text{SAT},k}^{(\kappa_2)})$ ,  $(\mathbf{p}_{\text{SAT},k}^{(\kappa_3)} - \mathbf{p}_{\text{SAT},k}^{(\kappa_4)})$  and  $\mathcal{G}_1^{(\kappa_1, \kappa_2, \kappa_3, \kappa_4)}$ ,  $\mathcal{G}_2^{(\kappa_1, \kappa_2, \kappa_3, \kappa_4)}$ .

### 3.3.3 Cramér-Rao Lower Bound for Propagation Conditions that switch between LOS and NLOS

In this section, the MT location CRLB is determined for measurements affected by propagation conditions that may switch between LOS and NLOS. Let  $p(\mathbf{z}_{\text{PR},k}|\mathbf{x}_k)$  and  $p(z_{\text{BIAS},k}|\mathbf{x}_k)$  denote the likelihood function of the PR and GRT measurements. Let further  $p(z_{\text{RTT},k}^{(m)}|\mathbf{x}_k)$  and  $p(z_{\text{RSS},k}^{(m)}|\mathbf{x}_k)$  denote the likelihood function of the  $m$ -th RTT and RSS measurement. Since the measurements are assumed to be statistically independent, cf. (2.53), the joint likelihood function  $p(\mathbf{z}_k|\mathbf{x}_k)$  of the measurements can be factorized as follows

$$p(\mathbf{z}_k|\mathbf{x}_k) = p(\mathbf{z}_{\text{PR},k}|\mathbf{x}_k) \cdot p(z_{\text{BIAS},k}|\mathbf{x}_k) \cdot \prod_{\kappa_1=1}^{M_{\text{RTT}}} p(z_{\text{RTT},k}^{(\kappa_1)}|\mathbf{x}_k) \cdot \prod_{\kappa_2=1}^{M_{\text{RSS}}} p(z_{\text{RSS},k}^{(\kappa_2)}|\mathbf{x}_k). \quad (3.49)$$

The FIM for the hybrid localization method assuming measurements affected by propagation conditions that may switch between LOS and NLOS can be found from inserting (3.49) into (3.16). Since the measurements are assumed to be statistically independent,

the FIMs are additive. Let  $\mathcal{F}_{\text{RTT}}^{(m)}(\tilde{\mathbf{x}}_k)$  denote the FIM of the  $m$ -th RTT measurement given by

$$\mathcal{F}_{\text{RTT}}^{(m)}(\tilde{\mathbf{x}}_k) = \mathbb{E}_{p(z_{\text{RTT},k}^{(m)}|\mathbf{x}_k)} \left\{ \frac{\nabla_{\tilde{\mathbf{x}}_k} p(z_{\text{RTT},k}^{(m)}|\mathbf{x}_k) [\nabla_{\tilde{\mathbf{x}}_k} p(z_{\text{RTT},k}^{(m)}|\mathbf{x}_k)]^\top}{[p(z_{\text{RTT},k}^{(m)}|\mathbf{x}_k)]^2} \right\}, \quad (3.50)$$

and let  $\mathcal{F}_{\text{RSS}}^{(m)}(\tilde{\mathbf{x}}_k)$  denote the FIM of the  $m$ -th RSS measurement given by

$$\mathcal{F}_{\text{RSS}}^{(m)}(\tilde{\mathbf{x}}_k) = \sum_{m=1}^{M_{\text{RSS}}} \mathbb{E}_{p(z_{\text{RSS},k}^{(m)}|\mathbf{x}_k)} \left\{ \frac{\nabla_{\tilde{\mathbf{x}}_k} p(z_{\text{RSS},k}^{(m)}|\mathbf{x}_k) [\nabla_{\tilde{\mathbf{x}}_k} p(z_{\text{RSS},k}^{(m)}|\mathbf{x}_k)]^\top}{[p(z_{\text{RSS},k}^{(m)}|\mathbf{x}_k)]^2} \right\}, \quad (3.51)$$

Then, the corresponding FIM for the hybrid localization assuming propagation conditions that may switch between LOS and NLOS can be written as

$$\mathcal{F}(\tilde{\mathbf{x}}_k) = \mathcal{F}_{\text{PR}}(\tilde{\mathbf{x}}_k) + \mathcal{F}_{\text{GRT}}(\tilde{\mathbf{x}}_k) + \sum_{\kappa_1=1}^{M_{\text{RTT}}} \mathcal{F}_{\text{RTT}}^{(\kappa_1)}(\tilde{\mathbf{x}}_k) + \sum_{\kappa_2=1}^{M_{\text{RSS}}} \mathcal{F}_{\text{RSS}}^{(\kappa_2)}(\tilde{\mathbf{x}}_k). \quad (3.52)$$

Since the PR and GRT measurements are independent of  $r_k$ , the corresponding FIMs are given by (3.23) and (3.29). The likelihood functions  $p(z_{\text{RTT},k}^{(m)}|\mathbf{x}_k)$  and  $p(z_{\text{RSS},k}^{(m)}|\mathbf{x}_k)$  implicitly depend on  $r_k$ , cf. (3.4). Since the purpose of this chapter is to develop estimators that do not additionally estimate  $r_k$ , it is convenient to approximate the corresponding likelihood functions with the pdf given in (3.7). Let  $\mathcal{N}(z; \mu_z, \sigma_z^2)$  denote a Gaussian density with argument  $z$ , mean  $\mu_z$  and variance  $\sigma_z^2$ , that is,

$$\mathcal{N}(z; \mu_z, \sigma_z^2) = \frac{1}{\sqrt{2\pi\sigma_z^2}} \cdot \exp \left\{ -\frac{1}{2\sigma_z^2} (z - \mu_z)^2 \right\}. \quad (3.53)$$

Then, the likelihood function of the  $m$ -th RTT measurement for  $m = 1, \dots, M_{\text{RTT}}$  is given by

$$\begin{aligned} p(z_{\text{RTT},k}^{(m)}|\mathbf{x}_k) &\approx p_{\text{LOS}}^{(m)} \cdot \mathcal{N}(z_{\text{RTT},k}^{(m)}; h_{\text{RTT},k}^{(m)}(\mathbf{x}_{\text{MT},k}) + \mu_{\text{RTT},k}(r_k^{(m)}=1), \sigma_{\text{RTT},k}^2(r_k^{(m)}=1)) \\ &\quad + p_{\text{NLOS}}^{(m)} \cdot \mathcal{N}(z_{\text{RTT},k}^{(m)}; h_{\text{RTT},k}^{(m)}(\mathbf{x}_{\text{MT},k}) + \mu_{\text{RTT},k}(r_k^{(m)}=2), \sigma_{\text{RTT},k}^2(r_k^{(m)}=2)). \end{aligned} \quad (3.54)$$

Similarly, the likelihood function of the  $m$ -th RSS measurement for  $m = 1, \dots, M_{\text{RSS}}$  is given by

$$\begin{aligned} p(z_{\text{RSS},k}^{(m)}|\mathbf{x}_k) &\approx p_{\text{LOS}}^{(m)} \cdot \mathcal{N}(z_{\text{RSS},k}^{(m)}; h_{\text{RSS},k}^{(m)}(\mathbf{x}_{\text{MT},k}, r_k^{(m)}=1), \sigma_{\text{RSS},k}^2(r_k^{(m)}=1)) \\ &\quad + p_{\text{NLOS}}^{(m)} \cdot \mathcal{N}(z_{\text{RSS},k}^{(m)}; h_{\text{RSS},k}^{(m)}(\mathbf{x}_{\text{MT},k}, r_k^{(m)}=2), \sigma_{\text{RSS},k}^2(r_k^{(m)}=2)). \end{aligned} \quad (3.55)$$

The FIMs of the RTT and RSS measurements can be found from inserting (3.54) and (3.55) into (3.50) and (3.51) and evaluating the expected value. Calculating the FIM for a Gaussian mixture pdf is difficult, and in general no analytic expression exists. In the following, a Monte Carlo integration approach is used to obtain numerical approximations for the FIMs of the RTT and RSS measurements [MU49, RC99]. Since Monte Carlo integration will be used several times in this work, the approach and its most important properties are reviewed in Appendix A.10.

The application of Monte Carlo integration techniques involves the generation of realizations of a random variable from a previously specified pdf, for which a compact notation is introduced in the sequel. Let  $\{z^{(n)}\}_{n=1}^N$ , denote a sample of  $N$  realizations of a random variable that is drawn from the pdf  $p(z)$ . Then, for each realization one can write more compactly  $z^{(n)} \sim p(z)$ . In this work, the generation of realizations of a random variable from a pdf is denoted as sampling and the realizations are called samples, or particles. Using Monte Carlo Integration, the expected value in (3.50) for  $m = 1, \dots, M_{\text{RTT}}$ , can be approximated as

$$\mathcal{F}_{\text{RTT}}^{(m)}(\tilde{\mathbf{x}}_k) \approx \frac{1}{N} \sum_{n=1}^N \frac{\nabla_{\tilde{\mathbf{x}}_k} p(z_{\text{RTT},k}^{(m,n)} | \mathbf{x}_k) [\nabla_{\tilde{\mathbf{x}}_k} p(z_{\text{RTT},k}^{(m,n)} | \mathbf{x}_k)]^\top}{\left[ p(z_{\text{RTT},k}^{(m,n)} | \mathbf{x}_k) \right]^2}, \quad (3.56)$$

where  $z_{\text{RTT},k}^{(m,n)}$ ,  $n = 1, \dots, N$  are independent and identically distributed (i.i.d.) samples, such that  $z_{\text{RTT},k}^{(m,n)} \sim p(z_{\text{RTT},k}^{(m)} | \mathbf{x}_k)$ . The gradient is given by

$$\nabla_{\tilde{\mathbf{x}}_k} p(z_{\text{RTT},k}^{(m,n)} | \mathbf{x}_k) = p_{\text{LOS}}^{(m)} \cdot [\nabla_{\tilde{\mathbf{x}}_k} p(z_{\text{RTT},k}^{(m)} | \mathbf{x}_k, r_k^{(m)} = 1)] + p_{\text{NLOS}}^{(m)} \cdot [\nabla_{\tilde{\mathbf{x}}_k} p(z_{\text{RTT},k}^{(m)} | \mathbf{x}_k, r_k^{(m)} = 2)], \quad (3.57)$$

where

$$\begin{aligned} \nabla_{\tilde{\mathbf{x}}_k} p(z_{\text{RTT},k}^{(m)} | \mathbf{x}_k, r_k^{(m)}) &= \sigma_{\text{RTT},k}^{-2}(r_k^{(m)}) \cdot (z_{\text{RTT},k}^{(m)} - h_{\text{RTT},k}^{(m)}(\mathbf{x}_{\text{MT},k}) - \mu_{\text{RTT},k}(r_k^{(m)})) \\ &\quad \cdot p(z_{\text{RTT},k}^{(m)} | \mathbf{x}_k, r_k^{(m)}) \cdot \left[ \nabla_{\tilde{\mathbf{x}}_k} h_{\text{RTT},k}^{(m)}(\mathbf{x}_{\text{MT},k}) \right]. \end{aligned} \quad (3.58)$$

Similarly, the expected value in (3.51) for  $m = 1, \dots, M_{\text{RSS}}$ , can be approximated as

$$\mathcal{F}_{\text{RSS}}^{(m)}(\tilde{\mathbf{x}}_k) \approx \frac{1}{N} \sum_{n=1}^N \frac{\nabla_{\tilde{\mathbf{x}}_k} p(z_{\text{RSS},k}^{(m,n)} | \mathbf{x}_k) [\nabla_{\tilde{\mathbf{x}}_k} p(z_{\text{RSS},k}^{(m,n)} | \mathbf{x}_k)]^\top}{\left[ p(z_{\text{RSS},k}^{(m,n)} | \mathbf{x}_k) \right]^2}, \quad (3.59)$$

where  $z_{\text{RSS},k}^{(m,n)}$ ,  $n = 1, \dots, N$  are i.i.d. samples, such that  $z_{\text{RSS},k}^{(m,n)} \sim p(z_{\text{RSS},k}^{(m)} | \mathbf{x}_k)$ . The gradient is given by

$$\nabla_{\tilde{\mathbf{x}}_k} p(z_{\text{RSS},k}^{(m,n)} | \mathbf{x}_k) = p_{\text{LOS}}^{(m)} \cdot [\nabla_{\tilde{\mathbf{x}}_k} p(z_{\text{RSS},k}^{(m)} | \mathbf{x}_k, r_k^{(m)} = 1)] + p_{\text{NLOS}}^{(m)} \cdot [\nabla_{\tilde{\mathbf{x}}_k} p(z_{\text{RSS},k}^{(m)} | \mathbf{x}_k, r_k^{(m)} = 2)], \quad (3.60)$$

where

$$\begin{aligned} \nabla_{\tilde{\mathbf{x}}_k} p(z_{\text{RSS},k}^{(m)} | \mathbf{x}_k, r_k^{(m)}) &= \sigma_{\text{RSS},k}^{-2}(r_k^{(m)}) \cdot (z_{\text{RSS},k}^{(m)} - h_{\text{RSS},k}^{(m)}(\mathbf{x}_{\text{MT},k}, r_k^{(m)})) \\ &\quad \cdot p(z_{\text{RSS},k}^{(m)} | \mathbf{x}_k, r_k^{(m)}) \cdot \left[ \nabla_{\tilde{\mathbf{x}}_k} h_{\text{RSS},k}^{(m)}(\mathbf{x}_{\text{MT},k}, r_k^{(m)}) \right]. \end{aligned} \quad (3.61)$$

In order to evaluate the numerical approximations of the expectation given in (3.56) and (3.59), it is necessary to draw i.i.d. samples from a Gaussian mixture pdf. Samples from a Gaussian mixture can be obtained by sampling the mode based on the previously specified mode probabilities and then drawing samples from the Gaussian distribution indicated by the mode. The MT location CRLB for propagation conditions that may switch between LOS and NLOS can be finally found from evaluating (3.52) and (3.18).

## 3.4 Maximum Likelihood Estimator

### 3.4.1 Introduction

In this section, the ML estimator for hybrid localization is determined. In order to find the ML estimate  $\hat{\mathbf{x}}_{\text{ML},k}$ , it is required to evaluate the expression in (3.12). For the hybrid localization, a closed-form solution for the ML estimator does not exist. In this case, one has to resort to numerical search algorithms, in order to carry out the minimization of the negative log-likelihood function [BSLK01]. Until now, a large number of numerical search algorithms have been developed, see [JEDS83, Kel99] for a survey. Which algorithm can be applied to the optimization problem given in (3.12) strongly depends on the structure of the log-likelihood function. Since the structure of the log-likelihood function for the case of LOS propagation conditions generally differs from the structure of the log-likelihood function for the case of propagation conditions that may switch between LOS and NLOS, different numerical search algorithms have to be applied to evaluate (3.12).

In Section 3.4.2, the log-likelihood function for LOS propagation conditions is evaluated and the Gauss-Newton and Levenberg-Marquardt algorithms [JEDS83, Lev44, Mar63] are proposed to approximately solve the optimization problem. In Section 3.4.3, the log-likelihood function for propagation conditions that may switch between LOS and NLOS is evaluated and the Nelder-Mead simplex algorithm [NM65, LRWW98] is proposed to approximately solve the optimization problem.

### 3.4.2 Maximum Likelihood Estimator for LOS Propagation Conditions

#### 3.4.2.1 Introduction

In this section, the ML estimator for LOS propagation conditions is determined. The ML estimator can be found from evaluating the likelihood function given in (3.12). For the hybrid localization assuming LOS propagation conditions, the random variables describing the errors of the measurements are assumed to be i.i.d., cf. (2.50). Since for a given  $\mathbf{x}_k$ ,  $\mathbf{z}_{\text{LOS},k}$  is a linear function of  $\mathbf{v}_{\text{LOS},k}^{(\nu)}$ , the likelihood function  $p(\mathbf{z}_{\text{LOS},k}|\mathbf{x}_k)$  can be found from the transformation of random variables [Jaz70] and is given by

$$p(\mathbf{z}_{\text{LOS},k}|\mathbf{x}_k) = p_{\mathbf{v}_{\text{LOS},k}}(\mathbf{z}_{\text{LOS},k} - \mathbf{h}_{\text{LOS},k}(\mathbf{x}_k)), \quad (3.62)$$

where  $p_{\mathbf{v}_{\text{LOS},k}}(\mathbf{v}_{\text{LOS},k})$  denotes the pdf of the vector of random variables  $\mathbf{v}_{\text{LOS},k}$ . Let  $\mathcal{N}(\mathbf{z}; \boldsymbol{\mu}_z, \mathbf{P}_z)$  denote a Gaussian density with argument  $\mathbf{z}$ , mean vector  $\boldsymbol{\mu}_z$  and covariance matrix  $\mathbf{P}_z$ , that is,

$$\mathcal{N}(\mathbf{z}; \boldsymbol{\mu}_z, \mathbf{P}_z) = \frac{1}{|2\pi\mathbf{P}_z|^{1/2}} \cdot \exp\left\{-\frac{1}{2}(\mathbf{z} - \boldsymbol{\mu}_z)^\top \mathbf{P}_z^{-1}(\mathbf{z} - \boldsymbol{\mu}_z)\right\}. \quad (3.63)$$

Then,  $p_{\mathbf{v}_{\text{LOS},k}}(\mathbf{v}_{\text{LOS},k}) = \mathcal{N}(\mathbf{v}_{\text{LOS},k}; \mathbf{0}_{1 \times M}, \mathbf{R}_{\text{LOS},k})$  holds, and the likelihood function can be rewritten as

$$p(\mathbf{z}_{\text{LOS},k}|\mathbf{x}_k) = \mathcal{N}(\mathbf{z}_{\text{LOS},k}; \mathbf{h}_{\text{LOS},k}(\mathbf{x}_k), \mathbf{R}_{\text{LOS},k}). \quad (3.64)$$

The ML estimator is found from inserting (3.64) into (3.12). By omitting the irrelevant additive constants, the ML estimator can be written as

$$\hat{\tilde{\mathbf{x}}}_{\text{ML},k} = \arg \min_{\tilde{\mathbf{x}}_k} V_1(\tilde{\mathbf{x}}_k), \quad (3.65)$$

or equivalently

$$\nabla_{\tilde{\mathbf{x}}_k} V_1(\tilde{\mathbf{x}}_k)|_{\tilde{\mathbf{x}}_k = \hat{\tilde{\mathbf{x}}}_{\text{ML},k}} = \mathbf{0}_{n_{\tilde{\mathbf{x}}} \times 1}, \quad (3.66)$$

where the cost function to be minimized is given by

$$V_1(\tilde{\mathbf{x}}_k) = (\mathbf{z}_{\text{LOS},k} - \mathbf{h}_{\text{LOS},k}(\tilde{\mathbf{x}}_k))^\top \mathbf{R}_{\text{LOS},k}^{-1} (\mathbf{z}_{\text{LOS},k} - \mathbf{h}_{\text{LOS},k}(\tilde{\mathbf{x}}_k)). \quad (3.67)$$

Note that the minimization of  $V_1(\tilde{\mathbf{x}}_k)$  is with respect to the reduced state vector  $\tilde{\mathbf{x}}_k$ , since no information about the MT velocity components and the MT clock drift is contained in the measurements. A closed-form solution for the ML estimator does not exist, since  $\mathbf{h}_{\text{LOS},k}(\tilde{\mathbf{x}}_k)$  is nonlinear. Thus, one has to find approximate solutions by using e.g. numerical optimization algorithms. In the following, two gradient-based search algorithms, namely the Gauss-Newton and the Levenberg-Marquardt algorithm, are used to solve the minimization problem. These methods have been chosen due to their fast convergence to a local solution and relatively low computational complexity. Other, more complex numerical search methods could have been used, but this is beyond the scope of this work.



### 3.4.2.2 Gauss-Newton Algorithm

The Gauss-Newton algorithm is an iterative method that is based on a first-order Taylor series approximation of  $\mathbf{h}_{\text{LOS},k}(\tilde{\mathbf{x}}_k)$  [JEDS83]. Let  $\hat{\mathbf{x}}_k^{(\eta)}$  denote the estimate of the reduced state vector obtained from the Gauss-Newton algorithm at the  $\eta$ -th iteration. Let further  $\mathbf{H}_{\text{LOS},k}(\tilde{\mathbf{x}}_k)$  denote the Jacobian matrix of  $\mathbf{h}_{\text{LOS},k}(\tilde{\mathbf{x}}_k)$  with respect to the reduced state vector, which is given by

$$\mathbf{H}_{\text{LOS},k}(\tilde{\mathbf{x}}_k) = \begin{bmatrix} \frac{\partial h_{\text{LOS},k}^{(1)}(\tilde{\mathbf{x}}_k)}{\partial \tilde{x}_k^{(1)}} & \frac{\partial h_{\text{LOS},k}^{(1)}(\tilde{\mathbf{x}}_k)}{\partial \tilde{x}_k^{(2)}} & \dots & \frac{\partial h_{\text{LOS},k}^{(1)}(\tilde{\mathbf{x}}_k)}{\partial \tilde{x}_k^{(n_{\tilde{x}})}} \\ \frac{\partial h_{\text{LOS},k}^{(2)}(\tilde{\mathbf{x}}_k)}{\partial \tilde{x}_k^{(1)}} & \frac{\partial h_{\text{LOS},k}^{(2)}(\tilde{\mathbf{x}}_k)}{\partial \tilde{x}_k^{(2)}} & \dots & \frac{\partial h_{\text{LOS},k}^{(2)}(\tilde{\mathbf{x}}_k)}{\partial \tilde{x}_k^{(n_{\tilde{x}})}} \\ \vdots & \vdots & & \vdots \\ \frac{\partial h_{\text{LOS},k}^{(M)}(\tilde{\mathbf{x}}_k)}{\partial \tilde{x}_k^{(1)}} & \frac{\partial h_{\text{LOS},k}^{(M)}(\tilde{\mathbf{x}}_k)}{\partial \tilde{x}_k^{(2)}} & \dots & \frac{\partial h_{\text{LOS},k}^{(M)}(\tilde{\mathbf{x}}_k)}{\partial \tilde{x}_k^{(n_{\tilde{x}})}} \end{bmatrix}. \quad (3.68)$$

Then, the first-order Taylor series approximation of  $\mathbf{h}_{\text{LOS},k}(\tilde{\mathbf{x}}_k)$  about  $\hat{\mathbf{x}}_k^{(\eta)}$  is given by

$$\mathbf{h}_{\text{LOS},k}(\tilde{\mathbf{x}}_k) = \mathbf{h}_{\text{LOS},k}(\hat{\mathbf{x}}_k^{(\eta)}) + \mathbf{H}_{\text{LOS},k}(\tilde{\mathbf{x}}_k)|_{\tilde{\mathbf{x}}_k=\hat{\mathbf{x}}_k^{(\eta)}} \cdot (\tilde{\mathbf{x}}_k - \hat{\mathbf{x}}_k^{(\eta)}), \quad (3.69)$$

which is a good approximation of  $\mathbf{h}_{\text{LOS},k}(\tilde{\mathbf{x}}_k)$ , when  $\|\tilde{\mathbf{x}}_k - \hat{\mathbf{x}}_k^{(\eta)}\|$  is small. In the Gauss-Newton algorithm, a local-linearized version of the cost function  $V_1(\tilde{\mathbf{x}}_k)$  is minimized which can be found from inserting (3.69) into (3.67), yielding

$$\begin{aligned} \tilde{V}_1(\tilde{\mathbf{x}}_k) &= \left( \mathbf{z}_{\text{LOS},k} - \mathbf{h}_{\text{LOS},k}(\hat{\mathbf{x}}_k^{(\eta)}) + \mathbf{H}_{\text{LOS},k}(\hat{\mathbf{x}}_k^{(\eta)}) \cdot (\tilde{\mathbf{x}}_k - \hat{\mathbf{x}}_k^{(\eta)}) \right)^\top \mathbf{R}_{\text{LOS},k}^{-1} \\ &\quad \cdot \left( \mathbf{z}_{\text{LOS},k} - \mathbf{h}_{\text{LOS},k}(\hat{\mathbf{x}}_k^{(\eta)}) + \mathbf{H}_{\text{LOS},k}(\hat{\mathbf{x}}_k^{(\eta)}) \cdot (\tilde{\mathbf{x}}_k - \hat{\mathbf{x}}_k^{(\eta)}) \right). \end{aligned} \quad (3.70)$$

Minimizing the local linearized cost function  $\tilde{V}_1(\tilde{\mathbf{x}}_k)$  according to (3.66) results in what is known as the Gauss-Newton algorithm which is given by

$$\hat{\mathbf{x}}_k^{(\eta+1)} = \hat{\mathbf{x}}_k^{(\eta)} + \left[ \mathbf{D}(\hat{\mathbf{x}}_k^{(\eta)}) \right]^{-1} \cdot \mathbf{g}(\hat{\mathbf{x}}_k^{(\eta)}) \quad (3.71)$$

where

$$\mathbf{D}(\hat{\mathbf{x}}_k^{(\eta)}) = \mathbf{H}_{\text{LOS},k}^\top(\hat{\mathbf{x}}_k^{(\eta)}) \mathbf{R}_{\text{LOS},k}^{-1} \mathbf{H}_{\text{LOS},k}(\hat{\mathbf{x}}_k^{(\eta)}) \quad (3.72)$$

and

$$\mathbf{g}(\hat{\mathbf{x}}_k^{(\eta)}) = \mathbf{H}_{\text{LOS},k}^\top(\hat{\mathbf{x}}_k^{(\eta)}) \mathbf{R}_{\text{LOS},k}^{-1} \cdot (\mathbf{z}_{\text{LOS},k} - \mathbf{h}_{\text{LOS},k}(\hat{\mathbf{x}}_k^{(\eta)})). \quad (3.73)$$

Since the Gauss-Newton algorithm is an iterative method, it is necessary to define certain stopping criteria to terminate the algorithm. In the following, three stopping criteria are introduced. Let

$$V_1'(\tilde{\mathbf{x}}_k) = \nabla_{\tilde{\mathbf{x}}_k} V_1(\tilde{\mathbf{x}}_k) = -2 \mathbf{H}_{\text{LOS},k}^\top(\tilde{\mathbf{x}}_k) \mathbf{R}_{\text{LOS},k}^{-1} (\mathbf{z}_{\text{LOS},k} - \mathbf{h}_{\text{LOS},k}(\tilde{\mathbf{x}}_k)) = -2 \cdot \mathbf{g}(\tilde{\mathbf{x}}_k), \quad (3.74)$$

denote the gradient of the cost function. It is well known that the ML estimate  $\hat{\mathbf{x}}_{\text{ML},k}$  is located at the global minimum of the cost function, so that a necessary condition for convergence is given by (3.66). Even though this criterion indicates the convergence of the method to the ML solution, it cannot be used in practice, since  $\hat{\mathbf{x}}_{\text{ML},k}$  is not known. Instead, one has to use an approximate condition to stop the algorithm which is given by

$$\|V_1'(\hat{\mathbf{x}}_k^{(\eta)})\|_\infty \leq \epsilon_1, \quad (3.75)$$

[MNT04], where  $\|\mathbf{a}\|_\infty$  denotes the infinite norm of vector  $\mathbf{a}$  and  $\epsilon_1$  is a small, positive number. Another useful criterion is to stop the algorithm if the difference between  $\hat{\mathbf{x}}_k^{(\eta+1)}$  and  $\hat{\mathbf{x}}_k^{(\eta)}$  is small, i.e.,

$$\|\hat{\mathbf{x}}_k^{(\eta+1)} - \hat{\mathbf{x}}_k^{(\eta)}\| \leq \epsilon_2(\|\hat{\mathbf{x}}_k^{(\eta)}\| + \epsilon_2), \quad (3.76)$$

where  $\epsilon_2$  is a small, positive number [MNT04]. The last stopping criterion defines the maximum number of iterations  $\eta_{\text{max}}$ , in order to avoid that (3.71) is evaluated infinitely often, i.e.,  $\eta \geq \eta_{\text{max}}$ . The Gauss-Newton algorithm applied to the hybrid localization in LOS propagation conditions is summarized in Algorithm 3.1. For certain geometric constellations of the MT, BSs and satellites, the matrix  $\mathbf{D}(\hat{\mathbf{x}}_k^{(\eta)})$  becomes rank-deficient, and thus, is not-invertible. In this case, the Gauss-Newton algorithm diverges. In order to avoid this drawback, the Levenberg-Marquardt algorithm is proposed for the hybrid localization method, which is introduced in the next section.

---

**Algorithm 3.1** Gauss-Newton
 

---

- 1:  $\eta := 0$
  - 2:  $\hat{\mathbf{x}}_k^{(0)} := \mathbb{E}\{\tilde{\mathbf{x}}_k\}$
  - 3:  $\mathbf{D}(\hat{\mathbf{x}}_k^{(0)}) := \mathbf{H}_{\text{LOS},k}^\top(\hat{\mathbf{x}}_k^{(0)}) \mathbf{R}_{\text{LOS},k}^{-1} \mathbf{H}_{\text{LOS},k}(\hat{\mathbf{x}}_k^{(0)})$
  - 4:  $\mathbf{g}(\hat{\mathbf{x}}_k^{(0)}) := \mathbf{H}_{\text{LOS},k}^\top(\hat{\mathbf{x}}_k^{(0)}) \mathbf{R}_{\text{LOS},k}^{-1} \cdot (\mathbf{z}_{\text{LOS},k} - \mathbf{h}_{\text{LOS},k}(\hat{\mathbf{x}}_k^{(0)}))$
  - 5:  $V_1'(\hat{\mathbf{x}}_k^{(0)}) := -2 \cdot \mathbf{g}(\hat{\mathbf{x}}_k^{(0)})$
  - 6:  $\hat{\mathbf{x}}_k^{(1)} := \hat{\mathbf{x}}_k^{(0)} + [\mathbf{D}(\hat{\mathbf{x}}_k^{(0)})]^{-1} \cdot \mathbf{g}(\hat{\mathbf{x}}_k^{(0)})$
  - 7: **while**  $\|V_1'(\hat{\mathbf{x}}_k^{(\eta)})\|_\infty > \epsilon_1$  **and**  $\|\hat{\mathbf{x}}_k^{(\eta+1)} - \hat{\mathbf{x}}_k^{(\eta)}\| > \epsilon_2(\|\hat{\mathbf{x}}_k^{(\eta)}\| + \epsilon_2)$  **and**  $\eta < \eta_{\text{max}}$  **do**
  - 8:    $\eta := \eta + 1$
  - 9:    $\mathbf{D}(\hat{\mathbf{x}}_k^{(\eta)}) := \mathbf{H}_{\text{LOS},k}^\top(\hat{\mathbf{x}}_k^{(\eta)}) \mathbf{R}_{\text{LOS},k}^{-1} \mathbf{H}_{\text{LOS},k}(\hat{\mathbf{x}}_k^{(\eta)})$
  - 10:    $\mathbf{g}(\hat{\mathbf{x}}_k^{(\eta)}) := \mathbf{H}_{\text{LOS},k}^\top(\hat{\mathbf{x}}_k^{(\eta)}) \mathbf{R}_{\text{LOS},k}^{-1} \cdot (\mathbf{z}_{\text{LOS},k} - \mathbf{h}_{\text{LOS},k}(\hat{\mathbf{x}}_k^{(\eta)}))$
  - 11:    $V_1'(\hat{\mathbf{x}}_k^{(\eta)}) := -2 \cdot \mathbf{g}(\hat{\mathbf{x}}_k^{(\eta)})$
  - 12:    $\hat{\mathbf{x}}_k^{(\eta+1)} := \hat{\mathbf{x}}_k^{(\eta)} + [\mathbf{D}(\hat{\mathbf{x}}_k^{(\eta)})]^{-1} \cdot \mathbf{g}(\hat{\mathbf{x}}_k^{(\eta)})$
  - 13: **end while**
-

### 3.4.2.3 Levenberg-Marquardt Algorithm

The Gauss-Newton algorithm provides good performance for the case that  $\|\tilde{\mathbf{x}}_k - \hat{\mathbf{x}}_k^{(\eta)}\|$  is small. However, when  $\|\tilde{\mathbf{x}}_k - \hat{\mathbf{x}}_k^{(\eta)}\|$  is large, then (3.69) is a poor approximation to  $\mathbf{h}_{\text{LOS},k}(\tilde{\mathbf{x}}_k)$  and the performance is worse. The Levenberg-Marquardt algorithm tries to solve this problem by introducing an additional damping term in the cost function, that should control the performance of the algorithm when  $\|\tilde{\mathbf{x}}_k - \hat{\mathbf{x}}_k^{(\eta)}\|$  is too large [Lev44, Mar63]. Let  $\zeta^{(\eta)} > 0$  denote the damping parameter at the  $\eta$ -th iteration. Then, the modified cost function is given by

$$\check{V}_1(\tilde{\mathbf{x}}_k) = \tilde{V}_1(\tilde{\mathbf{x}}_k) + \frac{1}{2} \cdot \zeta^{(\eta)} \cdot \|\tilde{\mathbf{x}}_k - \hat{\mathbf{x}}_k^{(\eta)}\|^2. \quad (3.77)$$

where  $\tilde{V}_1(\tilde{\mathbf{x}}_k)$  is given in (3.70) and the damping term  $\zeta^{(\eta)}/2 \cdot \|\tilde{\mathbf{x}}_k - \hat{\mathbf{x}}_k^{(\eta)}\|^2$  involves higher costs when  $\|\tilde{\mathbf{x}}_k - \hat{\mathbf{x}}_k^{(\eta)}\|^2$  is large. Minimizing the modified cost function according to (3.66) yields the Levenberg-Marquardt algorithm which is given by

$$\hat{\mathbf{x}}_k^{(\eta+1)} = \hat{\mathbf{x}}_k^{(\eta)} + \left[ \mathbf{D}(\hat{\mathbf{x}}_k^{(\eta)}) + \zeta^{(\eta)} \cdot \mathbf{I}_M \right]^{-1} \cdot \mathbf{g}(\hat{\mathbf{x}}_k^{(\eta)}) \quad (3.78)$$

where  $\mathbf{D}(\cdot)$  and  $\mathbf{g}(\cdot)$  are defined in (3.72) and (3.73). The additional damping parameter  $\zeta^{(\eta)}$  makes sure that the matrix inversion in (3.78) is always possible, yielding a much more robust implementation compared to the Gauss-Newton algorithm. The influence of the damping term on the cost function is further controlled by the damping parameter  $\zeta^{(\eta)}$  which is updated at each iteration step. The value of  $\zeta^{(\eta)}$  is chosen based on the so-called gain ratio  $\rho$  which is the ratio between the actual and predicted decrease in cost function value and is given by

$$\rho = \frac{V_1(\hat{\mathbf{x}}_k^{(\eta)}) - V_1(\hat{\mathbf{x}}_k^{(\eta+1)})}{\check{V}_1(\hat{\mathbf{x}}_k^{(\eta)}) - \check{V}_1(\hat{\mathbf{x}}_k^{(\eta+1)})} = \frac{V_1(\hat{\mathbf{x}}_k^{(\eta)}) - V_1(\hat{\mathbf{x}}_k^{(\eta+1)})}{(\hat{\mathbf{x}}_k^{(\eta+1)} - \hat{\mathbf{x}}_k^{(\eta)})^\top \cdot [\mathbf{g}(\hat{\mathbf{x}}_k^{(\eta)}) + \zeta^{(\eta)} \cdot (\hat{\mathbf{x}}_k^{(\eta+1)} - \hat{\mathbf{x}}_k^{(\eta)})]}. \quad (3.79)$$

A small value of  $\rho$  indicates that  $\check{V}_1(\hat{\mathbf{x}}_k^{(\eta+1)})$  is a poor approximation to  $V_1(\hat{\mathbf{x}}_k^{(\eta+1)})$  and the damping factor  $\zeta^{(\eta)}$  should be increased. A large value of  $\rho$  indicates that  $\check{V}_1(\hat{\mathbf{x}}_k^{(\eta+1)})$  is a good approximation to  $V_1(\hat{\mathbf{x}}_k^{(\eta+1)})$  and the damping factor  $\zeta^{(\eta)}$  may be decreased. For updating  $\zeta^{(\eta)}$ , the following strategy is widely used:

$$\zeta^{(\eta+1)} := \begin{cases} \zeta^{(\eta)} \cdot \max\{1/3, 1 - (2\rho - 1)^3\} & \text{for } \rho > 0 \\ \zeta^{(\eta)} \cdot \rho^{(\eta)} & \text{else,} \end{cases} \quad (3.80a)$$

where

$$\rho^{(\eta)} := \begin{cases} 2 & \text{for } \rho > 0 \\ 2 \cdot \rho^{(\eta-1)} & \text{else,} \end{cases} \quad (3.80b)$$

[Nie99]. Since the Levenberg-Marquardt algorithm is iterative, the values of  $\zeta^{(\eta)}$  and  $\rho^{(\eta)}$  have to be initialized. The initial  $\rho$ -value is given by  $\rho^{(0)} = 2$ . The choice of the

initial  $\zeta$ -value is related to the size of the elements of  $\mathbf{D}(\hat{\mathbf{x}}_k^{(0)})$  and is given by

$$\zeta^{(0)} = \tau \cdot \max_i \left\{ \left[ \mathbf{D}(\hat{\mathbf{x}}_k^{(0)}) \right]_{i,i} \right\}, \quad \text{for } i = 1, \dots, M, \quad (3.81)$$

where  $\tau$  is a small positive number [Nie99]. In order to terminate the Levenberg-Marquardt algorithm, the same stopping criteria are used as they were introduced for the Gauss-Newton algorithm. The Levenberg-Marquardt algorithm applied to the hybrid localization in LOS propagation conditions is summarized in Algorithm 3.2.

---

**Algorithm 3.2** Levenberg-Marquardt

---

- 1:  $\eta := 0$
  - 2:  $\rho^{(0)} := 2$
  - 3:  $\hat{\mathbf{x}}_k^{(0)} := \mathbb{E}\{\tilde{\mathbf{x}}_k\}$
  - 4:  $\mathbf{D}(\hat{\mathbf{x}}_k^{(0)}) := \mathbf{H}_{\text{LOS},k}^{\text{T}}(\hat{\mathbf{x}}_k^{(0)}) \mathbf{R}_{\text{LOS},k}^{-1} \mathbf{H}_{\text{LOS},k}(\hat{\mathbf{x}}_k^{(0)})$
  - 5:  $\mathbf{g}(\hat{\mathbf{x}}_k^{(0)}) := \mathbf{H}_{\text{LOS},k}^{\text{T}}(\hat{\mathbf{x}}_k^{(0)}) \mathbf{R}_{\text{LOS},k}^{-1} \cdot (\mathbf{z}_{\text{LOS},k} - \mathbf{h}_{\text{LOS},k}(\hat{\mathbf{x}}_k^{(0)}))$
  - 6:  $V_1'(\hat{\mathbf{x}}_k^{(0)}) := -2 \cdot \mathbf{g}(\hat{\mathbf{x}}_k^{(0)})$
  - 7:  $\zeta^{(0)} := \tau \cdot \max_i \{ [\mathbf{D}(\hat{\mathbf{x}}_k^{(0)})]_{i,i} \}$
  - 8:  $\hat{\mathbf{x}}_k^{(1)} := \hat{\mathbf{x}}_k^{(0)} + \left[ \mathbf{D}(\hat{\mathbf{x}}_k^{(0)}) + \zeta^{(0)} \cdot \mathbf{I}_M \right]^{-1} \cdot \mathbf{g}(\hat{\mathbf{x}}_k^{(0)})$
  - 9: **while**  $\| V_1'(\hat{\mathbf{x}}_k^{(\eta)}) \|_{\infty} > \epsilon_1$  **and**  $\| \hat{\mathbf{x}}_k^{(\eta+1)} - \hat{\mathbf{x}}_k^{(\eta)} \| > \epsilon_2 (\| \hat{\mathbf{x}}_k^{(\eta)} \| + \epsilon_2)$  **and**  $\eta < \eta_{\text{max}}$  **do**
  - 10:    $\mathbf{d} := \hat{\mathbf{x}}_k^{(\eta+1)} - \hat{\mathbf{x}}_k^{(\eta)}$
  - 11:   Evaluate  $V_1(\hat{\mathbf{x}}_k^{(\eta)})$  according to (3.67)
  - 12:   Evaluate  $V_1(\hat{\mathbf{x}}_k^{(\eta+1)})$  according to (3.67)
  - 13:    $\varrho := \frac{V_1(\hat{\mathbf{x}}_k^{(\eta)}) - V_1(\hat{\mathbf{x}}_k^{(\eta+1)})}{\mathbf{d}^{\text{T}} \cdot [\mathbf{g}(\hat{\mathbf{x}}_k^{(\eta)}) + \zeta^{(\eta)} \cdot \mathbf{d}]}$
  - 14:   **if**  $\varrho > 0$  **then**
  - 15:      $\zeta^{(\eta+1)} := \zeta^{(\eta)} \cdot \max\{1/3, 1 - (2\varrho - 1)^3\}$
  - 16:      $\rho^{(\eta+1)} := 2$
  - 17:   **else**
  - 18:      $\zeta^{(\eta+1)} := \zeta^{(\eta)} \cdot \rho^{(\eta)}$
  - 19:      $\rho^{(\eta+1)} := 2 \cdot \rho^{(\eta)}$
  - 20:   **end if**
  - 21:    $\eta := \eta + 1$
  - 22:    $\mathbf{D}(\hat{\mathbf{x}}_k^{(\eta)}) := \mathbf{H}_{\text{LOS},k}^{\text{T}}(\hat{\mathbf{x}}_k^{(\eta)}) \mathbf{R}_{\text{LOS},k}^{-1} \mathbf{H}_{\text{LOS},k}(\hat{\mathbf{x}}_k^{(\eta)})$
  - 23:    $\mathbf{g}(\hat{\mathbf{x}}_k^{(\eta)}) := \mathbf{H}_{\text{LOS},k}^{\text{T}}(\hat{\mathbf{x}}_k^{(\eta)}) \mathbf{R}_{\text{LOS},k}^{-1} \cdot (\mathbf{z}_{\text{LOS},k} - \mathbf{h}_{\text{LOS},k}(\hat{\mathbf{x}}_k^{(\eta)}))$
  - 24:    $V_1'(\hat{\mathbf{x}}_k^{(\eta)}) := -2 \cdot \mathbf{g}(\hat{\mathbf{x}}_k^{(\eta)})$
  - 25:    $\hat{\mathbf{x}}_k^{(\eta+1)} := \hat{\mathbf{x}}_k^{(\eta)} + \left[ \mathbf{D}(\hat{\mathbf{x}}_k^{(\eta)}) + \zeta^{(\eta)} \cdot \mathbf{I}_M \right]^{-1} \cdot \mathbf{g}(\hat{\mathbf{x}}_k^{(\eta)})$
  - 26: **end while**
-

### 3.4.3 Maximum Likelihood Estimator for Propagation Conditions that switch between LOS and NLOS

In this section, the ML estimator for propagation conditions that may switch between LOS and NLOS is determined. The ML estimator for the hybrid localization can be found from evaluating the likelihood function according to (3.12). The likelihood function  $p(\mathbf{z}_k|\mathbf{x}_k)$  is given in (3.49), which can be rewritten by concatenating the PR and GRT measurements into a single measurement vector. Define  $\mathbf{z}_{\text{SAT},k} = [\mathbf{z}_{\text{PR},k}^\top, z_{\text{BIAS},k}]^\top$ ,  $\mathbf{h}_{\text{SAT},k}(\mathbf{x}_k) = \mathbf{h}_{\text{SAT},k}(\tilde{\mathbf{x}}_k = [\mathbf{h}_{\text{PR},k}^\top(\tilde{x}_k), h_{\text{BIAS},k}(c_0 \cdot \delta t_k)]^\top)$  and  $\mathbf{R}_{\text{SAT},k} = \text{diag}_b[\mathbf{R}_{\text{PR},k}, \sigma_{\text{BIAS},k}^2]$ . Then, the likelihood function of  $\mathbf{z}_{\text{SAT},k}$  is given by

$$p(\mathbf{z}_{\text{SAT},k}|\mathbf{x}_k) = \mathcal{N}(\mathbf{z}_{\text{SAT},k}; \mathbf{h}_{\text{SAT},k}(\mathbf{x}_k), \mathbf{R}_{\text{SAT},k}), \quad (3.82)$$

and the joint likelihood function of the measurement vector  $\mathbf{z}_k$  can be written more compactly, yielding

$$p(\mathbf{z}_k|\mathbf{x}_k) = p(\mathbf{z}_{\text{SAT},k}|\mathbf{x}_k) \cdot \prod_{\kappa_1=1}^{M_{\text{RTT}}} p(z_{\text{RTT},k}^{(\kappa_1)}|\mathbf{x}_k) \cdot \prod_{\kappa_2=1}^{M_{\text{RSS}}} p(z_{\text{RSS},k}^{(\kappa_2)}|\mathbf{x}_k), \quad (3.83)$$

where  $p(z_{\text{RTT},k}^{(\kappa_1)}|\mathbf{x}_k)$  and  $p(z_{\text{RSS},k}^{(\kappa_2)}|\mathbf{x}_k)$  are given by (3.54) and (3.55). The ML estimator can be found from inserting (3.83) into (3.12). By omitting the irrelevant additive constants, the ML estimator can be written as

$$\hat{\tilde{\mathbf{x}}}_{\text{ML},k} = \arg \min_{\tilde{\mathbf{x}}_k} V_2(\tilde{\mathbf{x}}_k), \quad (3.84)$$

where the cost function to be minimized is given by

$$V_2(\tilde{\mathbf{x}}_k) = [\mathbf{z}_{\text{SAT},k} - \mathbf{h}_{\text{SAT},k}(\tilde{\mathbf{x}}_k)]^\top \mathbf{R}_{\text{SAT},k}^{-1} [\mathbf{z}_{\text{SAT},k} - \mathbf{h}_{\text{SAT},k}(\tilde{\mathbf{x}}_k)] - \left[ \sum_{\kappa_1=1}^{M_{\text{RTT}}} \log_e(p(z_{\text{RTT},k}^{(\kappa_1)}|\tilde{\mathbf{x}}_k)) + \sum_{\kappa_2=1}^{M_{\text{RSS}}} \log_e(p(z_{\text{RSS},k}^{(\kappa_2)}|\tilde{\mathbf{x}}_k)) \right]. \quad (3.85)$$

Note that the minimization of  $V_2(\tilde{\mathbf{x}}_k)$  is with respect to the reduced state vector  $\tilde{\mathbf{x}}_k$ , since no information about the MT velocity components and the MT clock drift is contained in the measurements. A closed-form solution for the ML estimator does not exist, since  $\mathbf{h}_{\text{PR},k}(\tilde{\mathbf{x}}_k)$ ,  $h_{\text{RTT},k}^{(m)}(\mathbf{x}_{\text{MT},k})$ ,  $h_{\text{RSS},k}^{(m)}(\mathbf{x}_{\text{MT},k}, r_k^{(m)})$  are nonlinear and the likelihood functions of the RTT and RSS measurements are Gaussian mixtures. Thus, one has to find approximate solutions by using, e.g., numerical optimization algorithms. Since the cost function  $V_2(\tilde{\mathbf{x}}_k)$  has a different structure than the cost function  $V_1(\tilde{\mathbf{x}}_k)$ , the algorithms proposed in Section 3.4.2 cannot be used to solve the minimization problem without introducing further simplifications.

In the following, the Nelder-Mead simplex algorithm [NM65,LRWW98] is used to solve the minimization problem, which can be directly applied to the cost function  $V_2(\tilde{\mathbf{x}}_k)$ . The Nelder-Mead simplex algorithm is a direct search method for multi-dimensional unconstrained minimization which has the appealing advantage over gradient-based search methods, that no derivatives (implicit or explicit) are required. In the Nelder-Mead simplex algorithm, an essential role is played by the simplex which is a geometric figure in  $n_{\tilde{x}}$  dimensions that is the convex hull of  $n_{\tilde{x}} + 1$  vertices. In the case  $n_{\tilde{x}} = 2$ , the figure is a triangle, while when  $n_{\tilde{x}} = 3$  it is a tetrahedron. The Nelder-Mead simplex algorithm attempts to iteratively minimize a scalar valued nonlinear cost function of  $n_{\tilde{x}}$  variables, by comparing function values at the  $n_{\tilde{x}} + 1$  vertices of the simplex. The vertex with the largest function value is then replaced by another point so that some form of descent condition is satisfied. The  $n_{\tilde{x}} + 1$  vertices of the simplex given by the vectors  $\tilde{\mathbf{x}}_{i,k}^{(\eta)}$  for  $i = 1, \dots, n_{\tilde{x}}$ , are collected in the set  $S_1^{(\eta)} = \{\tilde{\mathbf{x}}_{0,k}^{(\eta)}, \dots, \tilde{\mathbf{x}}_{n_{\tilde{x}},k}^{(\eta)}\}$  and the  $n_{\tilde{x}} + 1$  cost function values evaluated at the corresponding vertices are collected in the set  $S_2^{(\eta)} = \{V_2(\tilde{\mathbf{x}}_{0,k}^{(\eta)}), \dots, V_2(\tilde{\mathbf{x}}_{n_{\tilde{x}},k}^{(\eta)})\}$ . The Nelder-Mead simplex algorithm is given as follows:

1. For  $\eta = 0$ , an initial simplex is formed as follows. Given a vector  $\tilde{\mathbf{x}}_{0,k}^{(0)}$  and an edge length  $l_1$ , an initial regular simplex with edge length  $l_1$  can be constructed. Let  $\mathbf{i}_n$  denote the  $n$ -th column of the matrix  $\mathbf{I}_{n_{\tilde{x}}}$ . Then, the vectors defining the vertices of the initial regular simplex with edge length  $l_1$  are given as follows

$$\tilde{\mathbf{x}}_{n,k}^{(0)} = \tilde{\mathbf{x}}_{0,k}^{(0)} + \frac{l_1}{2} \cdot \frac{\sqrt{n_{\tilde{x}} + 1} - 1}{n_{\tilde{x}}} \cdot \mathbf{1}_{n_{\tilde{x}} \times 1} + \frac{l_1}{\sqrt{2}} \cdot \mathbf{i}_n, \quad \text{for } n = 1, \dots, n_{\tilde{x}}. \quad (3.86)$$

The  $n_{\tilde{x}} + 1$  vectors are collected in the set  $S_1^{(0)} = \{\tilde{\mathbf{x}}_{0,k}^{(0)}, \dots, \tilde{\mathbf{x}}_{n_{\tilde{x}},k}^{(0)}\}$  and the  $n_{\tilde{x}} + 1$  cost function values evaluated at the corresponding vertices are collected in the set  $S_2^{(0)} = \{V_2(\tilde{\mathbf{x}}_{0,k}^{(0)}), \dots, V_2(\tilde{\mathbf{x}}_{n_{\tilde{x}},k}^{(0)})\}$ .

2. Each iteration  $\eta$  starts with the definition of the vector  $\tilde{\mathbf{x}}_{H,k}^{(\eta)}$  providing the largest function value  $V_2(\tilde{\mathbf{x}}_{H,k}^{(\eta)})$ , the vector  $\tilde{\mathbf{x}}_{S,k}^{(\eta)}$  providing the second largest function value  $V_2(\tilde{\mathbf{x}}_{S,k}^{(\eta)})$ , and the vector  $\tilde{\mathbf{x}}_{L,k}^{(\eta)}$  providing the smallest function value  $V_2(\tilde{\mathbf{x}}_{L,k}^{(\eta)})$ . This can be equivalently written as

$$\tilde{\mathbf{x}}_{H,k}^{(\eta)} = \arg \max_{\tilde{\mathbf{x}}_k \in S_1^{(\eta)}} V_2(\tilde{\mathbf{x}}_k), \quad (3.87a)$$

$$\tilde{\mathbf{x}}_{S,k}^{(\eta)} = \arg \max_{\tilde{\mathbf{x}}_k \in \tilde{S}_1^{(\eta)}} V_2(\tilde{\mathbf{x}}_k), \quad (3.87b)$$

$$\tilde{\mathbf{x}}_{L,k}^{(\eta)} = \arg \min_{\tilde{\mathbf{x}}_k \in S_1^{(\eta)}} V_2(\tilde{\mathbf{x}}_k), \quad (3.87c)$$

where  $\tilde{S}_1^{(\eta)} = \{S_1^{(\eta)} \setminus \tilde{\mathbf{x}}_{H,k}^{(\eta)}\}$  denotes the set of vectors excluding  $\tilde{\mathbf{x}}_{H,k}^{(\eta)}$ . Similarly, define  $\tilde{S}_2^{(\eta)} = \{S_2^{(\eta)} \setminus V_2(\tilde{\mathbf{x}}_{H,k}^{(\eta)})\}$ . At each iteration  $\eta$ , the vector  $\tilde{\mathbf{x}}_{H,k}^{(\eta)}$  providing

the largest function value is replaced by a new vector with a (hopefully) smaller function value. The new vector is found by the application of at least one of three basic operations to  $\tilde{\mathbf{x}}_{H,k}^{(\eta)}$ . These operations are reflection, expansion and contraction, which are further explained in step 3, 4 and 5. In order to perform one of these operations, it is necessary to define  $\tilde{\mathbf{x}}_{M,k}^{(\eta)}$  which is the centroid of all  $\tilde{\mathbf{x}}_{i,k}^{(\eta)}$  except  $\tilde{\mathbf{x}}_{H,k}^{(\eta)}$ , and is given by

$$\tilde{\mathbf{x}}_{M,k}^{(\eta)} = \frac{1}{n_{\tilde{x}}} \cdot \sum_{i=0}^{n_{\tilde{x}}} \left[ \tilde{\mathbf{x}}_{i,k}^{(\eta)} - \tilde{\mathbf{x}}_{H,k}^{(\eta)} \right]. \quad (3.88)$$

If all these operations do not result in a smaller cost function value, the simplex is shrunk which is explained in step 6.

3. Reflection: Calculate the reflection vector  $\tilde{\mathbf{x}}_{R,k}^{(\eta)}$  and evaluate the corresponding cost function  $V_2(\tilde{\mathbf{x}}_{R,k}^{(\eta)})$ . Let  $\alpha_1$  denote the reflection coefficient, where  $\alpha_1 > 0$  holds. Then, the reflection vector  $\tilde{\mathbf{x}}_{R,k}^{(\eta)}$  can be determined from

$$\tilde{\mathbf{x}}_{R,k}^{(\eta)} = (1 + \alpha_1) \cdot \tilde{\mathbf{x}}_{M,k}^{(\eta)} - \alpha_1 \cdot \tilde{\mathbf{x}}_{H,k}^{(\eta)}. \quad (3.89)$$

If  $V_2(\tilde{\mathbf{x}}_{L,k}^{(\eta)}) \leq V_2(\tilde{\mathbf{x}}_{R,k}^{(\eta)}) < V_2(\tilde{\mathbf{x}}_{S,k}^{(\eta)})$ , then set  $\tilde{\mathbf{x}}_{H,k}^{(\eta)} := \tilde{\mathbf{x}}_{R,k}^{(\eta)}$  and terminate the iteration. Set  $S_1^{(\eta+1)} := \{\tilde{S}_1^{(\eta)}, \tilde{\mathbf{x}}_{H,k}^{(\eta)}\}$  and  $S_2^{(\eta+1)} := \{\tilde{S}_2^{(\eta)}, V_2(\tilde{\mathbf{x}}_{H,k}^{(\eta)})\}$  and go to step 2.

4. Expansion: If  $V_2(\tilde{\mathbf{x}}_{R,k}^{(\eta)}) < V_2(\tilde{\mathbf{x}}_{L,k}^{(\eta)})$ , then calculate the expansion vector  $\tilde{\mathbf{x}}_{E,k}^{(\eta)}$  and evaluate the corresponding cost function  $V(\tilde{\mathbf{x}}_{E,k}^{(\eta)})$ . Let  $\alpha_2$  denote the expansion coefficient, where  $\alpha_2 > 1$  and  $\alpha_2 > \alpha_1$  holds. Then, the expansion vector  $\tilde{\mathbf{x}}_{E,k}^{(\eta)}$  can be determined from

$$\tilde{\mathbf{x}}_{E,k}^{(\eta)} = \alpha_2 \cdot \tilde{\mathbf{x}}_{R,k}^{(\eta)} + (1 - \alpha_2) \cdot \tilde{\mathbf{x}}_{M,k}^{(\eta)}. \quad (3.90)$$

If  $V_2(\tilde{\mathbf{x}}_{E,k}^{(\eta)}) < V_2(\tilde{\mathbf{x}}_{R,k}^{(\eta)})$ , then set  $\tilde{\mathbf{x}}_{H,k}^{(\eta)} := \tilde{\mathbf{x}}_{E,k}^{(\eta)}$ . If  $V_2(\tilde{\mathbf{x}}_{E,k}^{(\eta)}) \geq V_2(\tilde{\mathbf{x}}_{R,k}^{(\eta)})$ , then set  $\tilde{\mathbf{x}}_{H,k}^{(\eta)} := \tilde{\mathbf{x}}_{R,k}^{(\eta)}$ . In both cases terminate the iteration, set  $S_1^{(\eta+1)} := \{\tilde{S}_1^{(\eta)}, \tilde{\mathbf{x}}_{H,k}^{(\eta)}\}$  and  $S_2^{(\eta+1)} := \{\tilde{S}_2^{(\eta)}, V_2(\tilde{\mathbf{x}}_{H,k}^{(\eta)})\}$  and go to step 2.

- 5.a Outside contraction: If  $V_2(\tilde{\mathbf{x}}_{S,k}^{(\eta)}) \leq V_2(\tilde{\mathbf{x}}_{R,k}^{(\eta)}) < V_2(\tilde{\mathbf{x}}_{H,k}^{(\eta)})$ , then calculate the outside contraction vector  $\tilde{\mathbf{x}}_{OC,k}^{(\eta)}$  and evaluate the corresponding cost function  $V(\tilde{\mathbf{x}}_{OC,k}^{(\eta)})$ . Let  $\alpha_3$  denote the contraction coefficient where  $0 < \alpha_3 < 1$  holds. Then, the outside contraction vector  $\tilde{\mathbf{x}}_{OC,k}^{(\eta)}$  can be determined from

$$\tilde{\mathbf{x}}_{OC,k}^{(\eta)} = \alpha_3 \cdot \tilde{\mathbf{x}}_{R,k}^{(\eta)} + (1 - \alpha_3) \cdot \tilde{\mathbf{x}}_{M,k}^{(\eta)}. \quad (3.91)$$

If  $V_2(\tilde{\mathbf{x}}_{OC,k}^{(\eta)}) \leq V_2(\tilde{\mathbf{x}}_{R,k}^{(\eta)})$ , then set  $\tilde{\mathbf{x}}_{H,k}^{(\eta)} := \tilde{\mathbf{x}}_{OC,k}^{(\eta)}$  and terminate the iteration. Set  $S_1^{(\eta+1)} := \{\tilde{S}_1^{(\eta)}, \tilde{\mathbf{x}}_{H,k}^{(\eta)}\}$  and  $S_2^{(\eta+1)} := \{\tilde{S}_2^{(\eta)}, V_2(\tilde{\mathbf{x}}_{H,k}^{(\eta)})\}$  and go to step 2. If  $V_2(\tilde{\mathbf{x}}_{OC,k}^{(\eta)}) > V_2(\tilde{\mathbf{x}}_{R,k}^{(\eta)})$ , then go to step 6.

5.b Inside contraction: If  $V_2(\tilde{\mathbf{x}}_{\mathbf{R},k}^{(\eta)}) \geq V_2(\tilde{\mathbf{x}}_{\mathbf{H},k}^{(\eta)})$ , then calculate the inside contraction vector  $\tilde{\mathbf{x}}_{\mathbf{IC},k}^{(\eta)}$  and evaluate the corresponding cost function  $V_2(\tilde{\mathbf{x}}_{\mathbf{IC},k}^{(\eta)})$ . The inside contraction vector  $\tilde{\mathbf{x}}_{\mathbf{IC},k}^{(\eta)}$  can be determined from

$$\tilde{\mathbf{x}}_{\mathbf{IC},k}^{(\eta)} = \alpha_3 \cdot \tilde{\mathbf{x}}_{\mathbf{H},k}^{(\eta)} + (1 - \alpha_3) \cdot \tilde{\mathbf{x}}_{\mathbf{M},k}^{(\eta)}. \quad (3.92)$$

If  $V_2(\tilde{\mathbf{x}}_{\mathbf{IC},k}^{(\eta)}) < V_2(\tilde{\mathbf{x}}_{\mathbf{R},k}^{(\eta)})$ , then set  $\tilde{\mathbf{x}}_{\mathbf{H},k}^{(\eta)} := \tilde{\mathbf{x}}_{\mathbf{IC},k}^{(\eta)}$  and terminate the iteration. Set  $S_1^{(\eta+1)} := \{\tilde{S}_1^{(\eta)}, \tilde{\mathbf{x}}_{\mathbf{H},k}^{(\eta)}\}$  and  $S_2^{(\eta+1)} := \{\tilde{S}_2^{(\eta)}, V_2(\tilde{\mathbf{x}}_{\mathbf{H},k}^{(\eta)})\}$  and go to step 2. If  $V_2(\tilde{\mathbf{x}}_{\mathbf{IC},k}^{(\eta)}) \geq V_2(\tilde{\mathbf{x}}_{\mathbf{H},k}^{(\eta)})$ , then go to step 6.

6. Shrinkage: If  $V_2(\tilde{\mathbf{x}}_{\mathbf{OC},k}^{(\eta)}) > V_2(\tilde{\mathbf{x}}_{\mathbf{R},k}^{(\eta)})$  or if  $V_2(\tilde{\mathbf{x}}_{\mathbf{IC},k}^{(\eta)}) \geq V_2(\tilde{\mathbf{x}}_{\mathbf{H},k}^{(\eta)})$ , then evaluate  $n_{\tilde{x}}$  new vectors  $\tilde{\mathbf{n}}_{i,k}^{(\eta)}$  for  $i = 0, \dots, n_{\tilde{x}}$ . Let  $\alpha_4$  denote the shrinkage coefficient, where  $0 < \alpha_4 < 1$  holds. Then, the new vectors can be determined from

$$\tilde{\mathbf{n}}_{i,k}^{(\eta)} = \tilde{\mathbf{x}}_{\mathbf{L},k}^{(\eta)} + \alpha_4 \cdot (\tilde{\mathbf{x}}_{i,k}^{(\eta)} - \tilde{\mathbf{x}}_{\mathbf{L},k}^{(\eta)}), \quad \text{for } i = 0, \dots, n_{\tilde{x}}. \quad (3.93)$$

Evaluate  $V_2(\cdot)$  at the  $n_{\tilde{x}}$  vectors  $\tilde{\mathbf{n}}_{i,k}^{(\eta)}$ , set  $S_1^{(\eta+1)} := \{\tilde{\mathbf{n}}_{0,k}^{(\eta)}, \dots, \tilde{\mathbf{n}}_{n_{\tilde{x}},k}^{(\eta)}\}$  and  $S_2^{(\eta+1)} := \{V_2(\tilde{\mathbf{n}}_{0,k}^{(\eta)}), \dots, V_2(\tilde{\mathbf{n}}_{n_{\tilde{x}},k}^{(\eta)})\}$  and go to step 2.

Since the Nelder-Mead simplex algorithm is an iterative method, it is necessary to define certain stopping criteria to terminate the algorithm. In the following, the stopping criterion proposed in [NM65] is used, which is given by

$$\left\{ \frac{1}{n_{\tilde{x}}} \cdot \sum_{i=0}^{n_{\tilde{x}}} \left( V_2(\tilde{\mathbf{x}}_{i,k}^{(\eta)}) - V_2(\tilde{\mathbf{x}}_{\mathbf{M},k}^{(\eta)}) \right)^2 \right\}^{1/2} < \epsilon_3, \quad (3.94)$$

where  $\epsilon_3$  is a preset small positive number. In order to avoid that the algorithm is evaluated infinitely often, a second stopping criterion is introduced that stops the algorithm if a maximum number of iterations  $\eta_{\max}$  is reached. The vector providing the smallest cost function value is finally denoted as the estimate of the Nelder-Mead simplex method, cf. (3.87c). A pseudocode description of the Nelder-Mead simplex algorithm is given in Algorithm 3.3.

---

**Algorithm 3.3** Nelder-Mead simplex

---

- 1:  $\eta := 0$
- 2:  $\tilde{\mathbf{x}}_{0,k}^{(0)} := \mathbb{E}\{\tilde{\mathbf{x}}_k\}$
- 3: Determine initial simplex according to (3.86)
- 4:  $S_1^{(0)} := \{\tilde{\mathbf{x}}_{0,k}^{(0)}, \dots, \tilde{\mathbf{x}}_{n_{\tilde{x}},k}^{(0)}\}$ ,  $S_2^{(0)} := \{V_2(\tilde{\mathbf{x}}_{0,k}^{(0)}), \dots, V_2(\tilde{\mathbf{x}}_{n_{\tilde{x}},k}^{(0)})\}$
- 5: Define  $\tilde{\mathbf{x}}_{\mathbf{H},k}^{(0)}$ ,  $\tilde{\mathbf{x}}_{\mathbf{S},k}^{(0)}$  and  $\tilde{\mathbf{x}}_{\mathbf{L},k}^{(0)}$  according to (3.87)
- 6:  $\tilde{S}_1^{(0)} := \{S_1^{(0)} \setminus \tilde{\mathbf{x}}_{\mathbf{H},k}^{(0)}\}$ ,  $\tilde{S}_2^{(0)} := \{S_2^{(0)} \setminus V_2(\tilde{\mathbf{x}}_{\mathbf{H},k}^{(0)})\}$



7:  $\tilde{\mathbf{x}}_{M,k}^{(0)} := \frac{1}{n_{\tilde{x}}} \cdot \sum_{i=0}^{n_{\tilde{x}}} [\tilde{\mathbf{x}}_{i,k}^{(0)} - \tilde{\mathbf{x}}_{H,k}^{(0)}]$ , Evaluate  $\mathbf{V}_2(\tilde{\mathbf{x}}_{M,k}^{(0)})$  according to (3.85)

8:  $\hat{\tilde{\mathbf{x}}}_k^{(0)} := \tilde{\mathbf{x}}_{0,k}^{(0)}$

9: **while**  $\left\{ \frac{1}{n_{\tilde{x}}} \cdot \sum_{i=0}^{n_{\tilde{x}}} \left( V_2(\tilde{\mathbf{x}}_{i,k}^{(\eta)}) - V_2(\tilde{\mathbf{x}}_{M,k}^{(\eta)}) \right)^2 \right\}^{1/2} \geq \epsilon_3$  **and**  $\eta < \eta_{\max}$  **do**

10:  $\tilde{\mathbf{x}}_{R,k}^{(\eta)} = (1 + \alpha_1) \cdot \tilde{\mathbf{x}}_{M,k}^{(\eta)} - \alpha_1 \cdot \tilde{\mathbf{x}}_{H,k}^{(\eta)}$ , Evaluate  $\mathbf{V}_2(\tilde{\mathbf{x}}_{R,k}^{(\eta)})$  according to (3.85)

11: **if**  $\mathbf{V}_2(\tilde{\mathbf{x}}_{L,k}^{(\eta)}) \leq \mathbf{V}_2(\tilde{\mathbf{x}}_{R,k}^{(\eta)}) < \mathbf{V}_2(\tilde{\mathbf{x}}_{S,k}^{(\eta)})$  **then**

12:  $\tilde{\mathbf{x}}_{H,k}^{(\eta)} := \tilde{\mathbf{x}}_{R,k}^{(\eta)}$

13:  $S_1^{(\eta+1)} := \{\tilde{S}_1^{(\eta)}, \tilde{\mathbf{x}}_{H,k}^{(\eta)}\}$ ,  $S_2^{(\eta+1)} := \{\tilde{S}_2^{(\eta)}, V_2(\tilde{\mathbf{x}}_{H,k}^{(\eta)})\}$

14: **else if**  $\mathbf{V}_2(\tilde{\mathbf{x}}_{R,k}^{(\eta)}) < \mathbf{V}_2(\tilde{\mathbf{x}}_{L,k}^{(\eta)})$  **then**

15:  $\tilde{\mathbf{x}}_{E,k}^{(\eta)} := \alpha_2 \cdot \tilde{\mathbf{x}}_{R,k}^{(\eta)} + (1 - \alpha_2) \cdot \tilde{\mathbf{x}}_{M,k}^{(\eta)}$ , Evaluate  $\mathbf{V}_2(\tilde{\mathbf{x}}_{E,k}^{(\eta)})$  according to (3.85)

16: **if**  $\mathbf{V}_2(\tilde{\mathbf{x}}_{E,k}^{(\eta)}) < \mathbf{V}_2(\tilde{\mathbf{x}}_{R,k}^{(\eta)})$  **then**

17:  $\tilde{\mathbf{x}}_{H,k}^{(\eta)} := \tilde{\mathbf{x}}_{E,k}^{(\eta)}$

18: **else**

19:  $\tilde{\mathbf{x}}_{H,k}^{(\eta)} := \tilde{\mathbf{x}}_{R,k}^{(\eta)}$

20: **end if**

21:  $S_1^{(\eta+1)} := \{\tilde{S}_1^{(\eta)}, \tilde{\mathbf{x}}_{H,k}^{(\eta)}\}$ ,  $S_2^{(\eta+1)} := \{\tilde{S}_2^{(\eta)}, V_2(\tilde{\mathbf{x}}_{H,k}^{(\eta)})\}$

22: **else if**  $\mathbf{V}_2(\tilde{\mathbf{x}}_{S,k}^{(\eta)}) \leq \mathbf{V}_2(\tilde{\mathbf{x}}_{R,k}^{(\eta)}) < \mathbf{V}_2(\tilde{\mathbf{x}}_{H,k}^{(\eta)})$  **then**

23:  $\tilde{\mathbf{x}}_{OC,k}^{(\eta)} := \alpha_3 \cdot \tilde{\mathbf{x}}_{R,k}^{(\eta)} + (1 - \alpha_3) \cdot \tilde{\mathbf{x}}_{M,k}^{(\eta)}$ , Evaluate  $\mathbf{V}_2(\tilde{\mathbf{x}}_{OC,k}^{(\eta)})$  according to (3.85)

24: **if**  $\mathbf{V}_2(\tilde{\mathbf{x}}_{OC,k}^{(\eta)}) \leq \mathbf{V}_2(\tilde{\mathbf{x}}_{R,k}^{(\eta)})$  **then**

25:  $\tilde{\mathbf{x}}_{H,k}^{(\eta)} := \tilde{\mathbf{x}}_{OC,k}^{(\eta)}$

26:  $S_1^{(\eta+1)} := \{\tilde{S}_1^{(\eta)}, \tilde{\mathbf{x}}_{H,k}^{(\eta)}\}$ ,  $S_2^{(\eta+1)} := \{\tilde{S}_2^{(\eta)}, V_2(\tilde{\mathbf{x}}_{H,k}^{(\eta)})\}$

27: **else**

28: **for**  $i = 0$  **to**  $n_{\tilde{x}}$  **do**

29:  $\tilde{\mathbf{n}}_{i,k}^{(\eta)} := \tilde{\mathbf{x}}_{L,k}^{(\eta)} + \alpha_4 \cdot (\tilde{\mathbf{x}}_{i,k}^{(\eta)} - \tilde{\mathbf{x}}_{L,k}^{(\eta)})$ , Evaluate  $\mathbf{V}_2(\tilde{\mathbf{n}}_{i,k}^{(\eta)})$  according to (3.85)

30: **end for**

31:  $S_1^{(\eta+1)} := \{\tilde{\mathbf{n}}_{0,k}^{(\eta)}, \dots, \tilde{\mathbf{n}}_{n_{\tilde{x},k}}^{(\eta)}\}$ ,  $S_2^{(\eta+1)} := \{V_2(\tilde{\mathbf{n}}_{0,k}^{(\eta)}), \dots, V_2(\tilde{\mathbf{n}}_{n_{\tilde{x},k}}^{(\eta)})\}$

32: **end if**

33: **else if**  $\mathbf{V}_2(\tilde{\mathbf{x}}_{R,k}^{(\eta)}) \geq \mathbf{V}_2(\tilde{\mathbf{x}}_{H,k}^{(\eta)})$  **then**

34:  $\tilde{\mathbf{x}}_{IC,k}^{(\eta)} := \alpha_3 \cdot \tilde{\mathbf{x}}_{H,k}^{(\eta)} + (1 - \alpha_3) \cdot \tilde{\mathbf{x}}_{M,k}^{(\eta)}$ , Evaluate  $\mathbf{V}_2(\tilde{\mathbf{x}}_{IC,k}^{(\eta)})$  according to (3.85)

35: **if**  $\mathbf{V}_2(\tilde{\mathbf{x}}_{IC,k}^{(\eta)}) \leq \mathbf{V}_2(\tilde{\mathbf{x}}_{R,k}^{(\eta)})$  **then**

36:  $\tilde{\mathbf{x}}_{H,k}^{(\eta)} := \tilde{\mathbf{x}}_{IC,k}^{(\eta)}$

37:  $S_1^{(\eta+1)} := \{\tilde{S}_1^{(\eta)}, \tilde{\mathbf{x}}_{H,k}^{(\eta)}\}$ ,  $S_2^{(\eta+1)} := \{\tilde{S}_2^{(\eta)}, V_2(\tilde{\mathbf{x}}_{H,k}^{(\eta)})\}$

38: **else**

39: **for**  $i = 0$  **to**  $n_{\tilde{x}}$  **do**

40:  $\tilde{\mathbf{n}}_{i,k}^{(\eta)} := \tilde{\mathbf{x}}_{L,k}^{(\eta)} + \alpha_4 \cdot (\tilde{\mathbf{x}}_{i,k}^{(\eta)} - \tilde{\mathbf{x}}_{L,k}^{(\eta)})$ , Evaluate  $\mathbf{V}_2(\tilde{\mathbf{n}}_{i,k}^{(\eta)})$  according to (3.85)

41: **end for**

42:  $S_1^{(\eta+1)} := \{\tilde{\mathbf{n}}_{0,k}^{(\eta)}, \dots, \tilde{\mathbf{n}}_{n_{\tilde{x},k}}^{(\eta)}\}$ ,  $S_2^{(\eta+1)} := \{V_2(\tilde{\mathbf{n}}_{0,k}^{(\eta)}), \dots, V_2(\tilde{\mathbf{x}}_{n_{\tilde{x},k}}^{(\eta)})\}$

---

```

43:   end if
44:   end if
45:    $\eta := \eta + 1$ 
46:   Define  $\tilde{\mathbf{x}}_{H,k}^{(\eta)}$ ,  $\tilde{\mathbf{x}}_{S,k}^{(\eta)}$  and  $\tilde{\mathbf{x}}_{L,k}^{(\eta)}$  according to (3.87)
47:    $\tilde{S}_1^{(\eta)} := \{S_1^{(\eta)} \setminus \tilde{\mathbf{x}}_{H,k}^{(\eta)}\}$ ,  $\tilde{S}_2^{(\eta)} := \{S_2^{(\eta)} \setminus V_2(\tilde{\mathbf{x}}_{H,k}^{(\eta)})\}$ 
48:    $\tilde{\mathbf{x}}_{M,k}^{(\eta)} := \frac{1}{n_{\tilde{x}}} \cdot \sum_{i=0}^{n_{\tilde{x}}} [\tilde{\mathbf{x}}_{i,k}^{(\eta)} - \tilde{\mathbf{x}}_{H,k}^{(\eta)}]$ , Evaluate  $\mathbf{V}_2(\tilde{\mathbf{x}}_{M,k}^{(\eta)})$  according to (3.85)
49:    $\hat{\tilde{\mathbf{x}}}_k^{(\eta)} := \tilde{\mathbf{x}}_{L,k}^{(\eta)}$ 
50: end while

```

---

## 3.5 Performance Evaluation

### 3.5.1 Introduction

In this Section 3.5, the hybrid localization algorithms of Sections 3.4.2 and 3.4.3 are evaluated by means of simulations and their average performance is compared to the CRLB. The comparison of algorithms is based on a set of  $N_{MC}$  Monte Carlo simulations, cf. Section 2.3.5. The performance metrics that will be used are the Root Mean Square Error (RMSE) of the MT location and time averaged RMSE of the MT location. Recall that  $\mathbf{x}_{MT,k,i}$  and  $\hat{\mathbf{x}}_{MT,k,i}$  denote the true and estimated MT location at time  $k$  at the  $i$ -th Monte Carlo run. Then, the RMSE of the MT location at time  $k$  can be computed as

$$\text{RMSE}_k = \sqrt{\frac{1}{N_{MC}} \sum_{i=1}^{N_{MC}} \|\hat{\mathbf{x}}_{MT,k,i} - \mathbf{x}_{MT,k,i}\|^2} \quad (3.95)$$

Let  $k_{\max}$  denote the total number of time steps. Then, the time averaged RMSE of the MT location is given by

$$\overline{\text{RMSE}} = \frac{1}{k_{\max}} \sum_{k=1}^{k_{\max}} \sqrt{\frac{1}{N_{MC}} \sum_{i=1}^{N_{MC}} \|\hat{\mathbf{x}}_{MT,k,i} - \mathbf{x}_{MT,k,i}\|^2} \quad (3.96)$$

The corresponding CRLBs for the metrics (3.95) and (3.96) can be written as

$$\text{CRLB}_k = \sqrt{[[\mathcal{F}(\mathbf{x}_k)]^{-1}]_{1,1} + [[\mathcal{F}(\mathbf{x}_k)]^{-1}]_{2,2}} \quad (3.97)$$

and

$$\overline{\text{CRLB}} = \frac{1}{k_{\max}} \sum_{k=1}^{k_{\max}} \sqrt{[[\mathcal{F}(\mathbf{x}_k)]^{-1}]_{1,1} + [[\mathcal{F}(\mathbf{x}_k)]^{-1}]_{2,2}} \quad (3.98)$$

where the FIM  $\mathcal{F}(\mathbf{x}_k)$  is defined in (3.16). The Monte Carlo simulations are performed for Scenario I, cf. Section 2.3.4.2, and the results are presented in Section 3.5.2. The algorithm of Section 3.4.3 is further evaluated for experimental data available from a field trial, which is presented in Section 3.5.3. Finally, the computational complexity of the different algorithms is investigated in Section 3.5.4.

## 3.5.2 Simulation Results for Scenario I

### 3.5.2.1 Simulation Results for LOS Propagation Conditions

In this section, the performance of the Gauss-Newton algorithm and Levenberg-Marquardt algorithm introduced in Sections 3.4.2.2 and 3.4.2.3 is evaluated for the different combinations of measurements of Scenario I as given in Section 2.3.4.2. The CRLBs for the different combinations of measurements are computed to indicate the best possible performance that one can expect for the given scenario and set of parameters.

In order to apply the algorithms to the hybrid localization problem, the parameters included in the measurement model  $\mathbf{h}_{\text{LOS},k}(\mathbf{x}_k)$  and the covariance matrix  $\mathbf{R}_{\text{LOS},k}$  have to be specified. It is assumed that these parameters are equal to the parameters, with which the measurements have been generated. In practice, however, these parameters are unknown and have to be estimated in advance from field trial data. The parameters of the stopping criteria necessary to terminate the Gauss-Newton and Levenberg-Marquardt algorithm are summarized in Table 3.1. The results for each investigated method are obtained from  $N_{\text{MC}} = 500$  Monte Carlo runs. Since both algorithms are iterative, an initial guess  $\hat{\mathbf{x}}_k^{(0)}$  is required to start the iterations. For nonlinear measurement models, the cost function  $V_1(\tilde{\mathbf{x}}_k)$  to be minimized might have, besides the global minimum, multiple local minima to which the algorithm might converge. Thus, to avoid convergence to a local minimum, the initial guess should be chosen close to the global minimum. Convergence to a local optimum due to a bad initial guess has been identified as one of the most severe problems that can affect the performance of

Table 3.1. Parameters of the Gauss-Newton and Levenberg-Marquardt Algorithms

Parameter	Value	Parameter	Value
$\epsilon_1$	$10^{-10}$	$\epsilon_2$	$10^{-10}$
$\tau$	$10^{-6}$	$\eta_{max}$	200

iterative algorithms. It has been found out that for hybrid localization, the choice of the initial value is critical for both proposed algorithms and generally will yield biased estimates for the MT location. In the following, however, this issue is not further elaborated, since we are interested in the performance of the algorithms under "optimal" conditions. In the simulations, the algorithms are therefore initialized with the true state vector, i.e.  $\hat{\mathbf{x}}_k^{(0)} = \tilde{\mathbf{x}}_k$ , which can be expected to be located close to the global optimum. In practice, however, the true state vector is not available and one has to develop other approaches that are based on, e.g., non-iterative solutions or geometric concepts [Ban85, CSMC06].

In Fig. 3.5, the MT location RMSE in m vs. the time index  $k$  for the Cellular, Hybrid 1 and Hybrid 2 methods are shown for the Gauss-Newton algorithm together with the corresponding CRLBs. For the Gauss-Newton algorithm, the Cellular method provides the worst performance in terms of RMSE together with the Hybrid 1 method. The RMSE cannot be further improved with the Hybrid 1 method due to the fact that one PR measurement is not enough to resolve the unknown clock bias inherent in the PR measurement equation. The same result can be deduced from the corresponding CRLBs that coincide with each other in this case. The fact that the CRLBs of the Cellular and Hybrid 1 method are equivalent can be also proven mathematically which is given in Appendix A.9. In contrast to the Hybrid 1 method, the Hybrid 2 method takes into account two PR measurements from two different satellites. Since in this method an additional PR measurement is available, it is possible to resolve the unknown clock bias which in turn results in an improved MT location RMSE. The performance of the Hybrid 2 method using the Gauss-Newton algorithm is very close to the best achievable performance indicated by the corresponding CRLB, while for the Cellular and Hybrid 1 method this is not the case. This means that the first-order Taylor series approximation of the nonlinear measurement equation, introduced in the Gauss-Newton algorithm, has a larger influence on the Cellular and Hybrid 1 method than on the Hybrid 2 method. The variations in the MT location RMSE for the three methods can be explained by the fact that the achievable RMSE strongly depends on the geometric constellation of the BSs and satellites relative to the MT location.

In Fig. 3.6, the MT location RMSE in m vs. the time index  $k$  for the Cellular, Hybrid 1 and Hybrid 2 methods are shown for the Levenberg-Marquardt algorithm together with the corresponding CRLBs. It can be seen that for the Hybrid 2 method the performance of the Levenberg-Marquardt and Gauss-Newton algorithm is similar. However, for the Cellular and Hybrid 1 method small improvements can be achieved by using the Levenberg-Marquardt algorithm.

In the following, it is investigated how additional GNSS reference time information

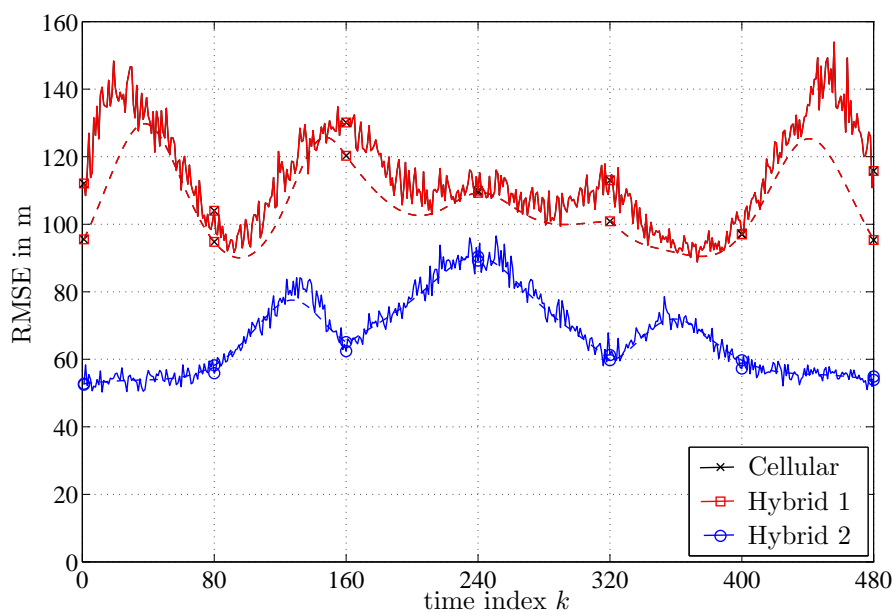


Figure 3.5. MT location RMSE vs. time index  $k$  for Cellular, Hybrid 1 and Hybrid 2 method, solid lines: Gauss-Newton algorithm, dashed lines: CRLB.

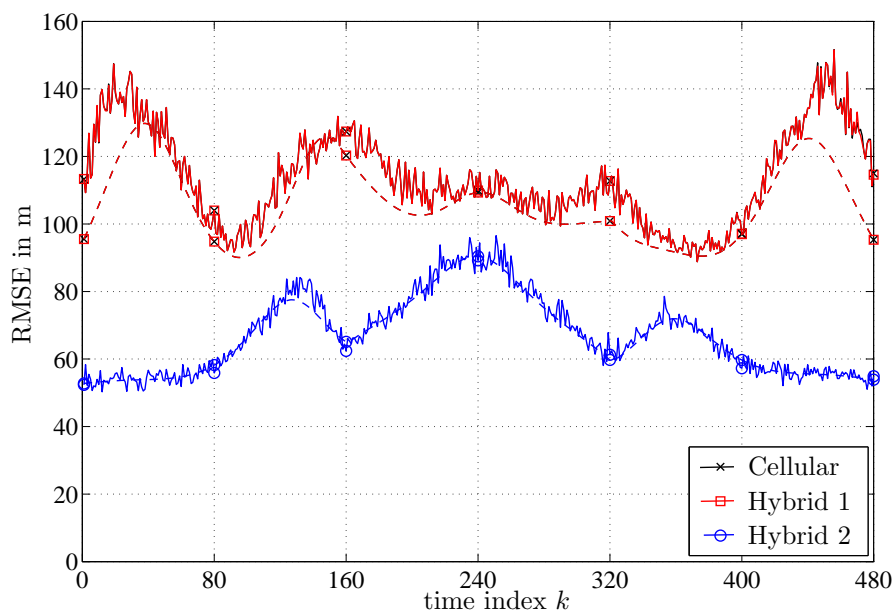


Figure 3.6. MT location RMSE vs. time index  $k$  for Cellular, Hybrid 1 and Hybrid 2 method, solid lines: Levenberg-Marquardt algorithm, dashed lines: CRLB.

available from the cellular radio network helps to improve the Hybrid 1 and Hybrid 2 methods. Here, the important question is investigated, what accuracy of the GNSS reference time measurements is needed in order to improve the MT location RMSE. In Fig. 3.7, the MT location  $\overline{\text{RMSE}}$  in m vs. the GRT error standard deviation  $\sigma_{\text{GRT}}$  in s for the Hybrid 1+ and Hybrid 2+ method are shown for the Gauss-Newton and Levenberg-Marquardt algorithm together with the corresponding  $\overline{\text{CRLBs}}$ . For  $\sigma_{\text{GRT}} \geq 5 \cdot 10^{-6}$ , the performance of the Hybrid 1+ method reaches an upper bound which is equivalent to the performance of the Hybrid 1 method as  $\sigma_{\text{GRT}} \rightarrow \infty$ . This fact can be proven mathematically by setting  $M_{\text{PR}} = 1$  and  $e^{(1)} = 0$ , cf. (3.35), in (3.48). Large performance improvements can be obtained for  $\sigma_{\text{GRT}} < 5 \cdot 10^{-6}$ . For  $\sigma_{\text{GRT}} < 10^{-8}$  the Hybrid 1+ method reaches a lower bound and no significant performance improvements are possible. The performance improvements of the Levenberg-Marquardt algorithm compared to the Gauss-Newton algorithm are very small. It can be further observed that both algorithms cannot achieve the CRLB. However, for decreasing values of  $\sigma_{\text{GRT}}$  the performance of the Hybrid 1+ method is very close to the CRLB. For  $\sigma_{\text{GRT}} \geq 5 \cdot 10^{-7}$ , the performance of the Hybrid 2+ method reaches an upper bound which is equivalent to the performance of the Hybrid 2 method as  $\sigma_{\text{GRT}} \rightarrow \infty$ . Large performance improvements are obtained for  $\sigma_{\text{GRT}} < 5 \cdot 10^{-7}$ . For  $\sigma_{\text{GRT}} < 10^{-9}$  the Hybrid 2+ method reaches a lower bound. The performance of the Gauss-Newton and

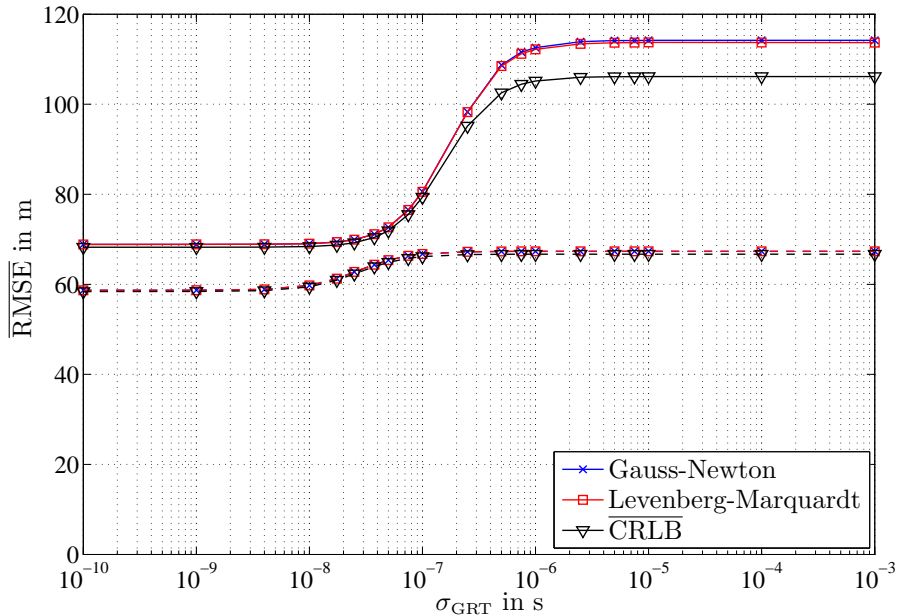


Figure 3.7. MT location  $\overline{\text{RMSE}}$  vs. GRT error standard deviation  $\sigma_{\text{GRT}}$  for Gauss-Newton algorithm, Levenberg-Marquardt algorithm and corresponding CRLB, solid lines: Hybrid 1+ method, dashed lines: Hybrid 2+ method.

Levenberg-Marquardt algorithm is practically equivalent and very close to the  $\overline{\text{CRLB}}$ . The performance improvements of the Hybrid 2+ method compared to the Hybrid 2 method are smaller than the relative performance improvements of the Hybrid 1+ method compared to the Hybrid 1 method.

The impact of the geometric constellation of the satellites relative to the MT location on the achievable MT location RMSE for the Satellite method and Hybrid 3 method is investigated next. Here, the important question is investigated, if it is necessary to take into account measurements from the cellular radio network when three PR measurements are available. In Fig. 3.8, the MT location RMSE in m vs. time index  $k$  for the Satellite and Hybrid 3 method and three different GDOP values, namely  $\text{GDOP} = 2$ ,  $\text{GDOP} = 5$  and  $\text{GDOP} = 10$ , are shown for the Gauss-Newton algorithm together with the corresponding CRLBs. Here, it is worth noting that the GDOP is defined and calculated only for the Satellite method and then the performance is compared to the Hybrid 3 method. The results for the Gauss-Newton algorithm show that for  $\text{GDOP} = 2$  the Satellite and Hybrid 3 method have a similar performance and only very small performance improvements can be achieved. This means, that the additional consideration of measurements from the cellular radio network does not help to improve the performance, if the geometric constellation between the satellites and the MT is good. However, for  $\text{GDOP} = 5$  and  $\text{GDOP} = 10$ , a significant difference in

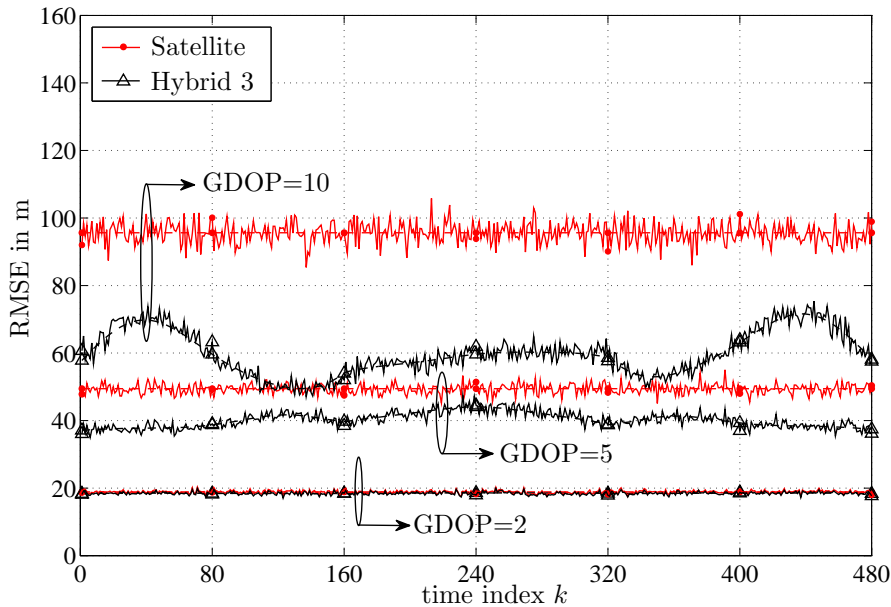


Figure 3.8. MT location RMSE vs. time index  $k$  for Satellite and Hybrid 3 method,  $\text{GDOP} = 2$ ,  $\text{GDOP} = 5$  and  $\text{GDOP} = 10$  values, solid lines: Gauss-Newton algorithm, dashed lines: CRLB.

performance can be observed. In this case, the Hybrid 3 method clearly outperforms the Satellite method. Furthermore, a comparison of the algorithms to the CRLBs show that a performance very close to these bounds can be achieved. In Fig. 3.9, the MT location  $\overline{\text{RMSE}}$  in m vs. GDOP for the Satellite and Hybrid 3 method are shown for the Gauss-Newton and Levenberg-Marquardt algorithms together with the corresponding  $\overline{\text{CRLB}}$ . The results show that there is practically no difference between the performance of the Gauss-Newton algorithm and the Levenberg-Marquardt algorithm. For the different GDOP values, it can be observed that the performance of these algorithms is very close to the CRLB. For small GDOP values, the performance improvements of the Hybrid 3 method compared to the Satellite method are small. However, for large GDOP values, the Hybrid 3 method significantly outperforms the Satellite method. From this it follows, that the additional consideration of measurements from the cellular radio network is expected to significantly improve the performance in scenarios where the value of GDOP is large.

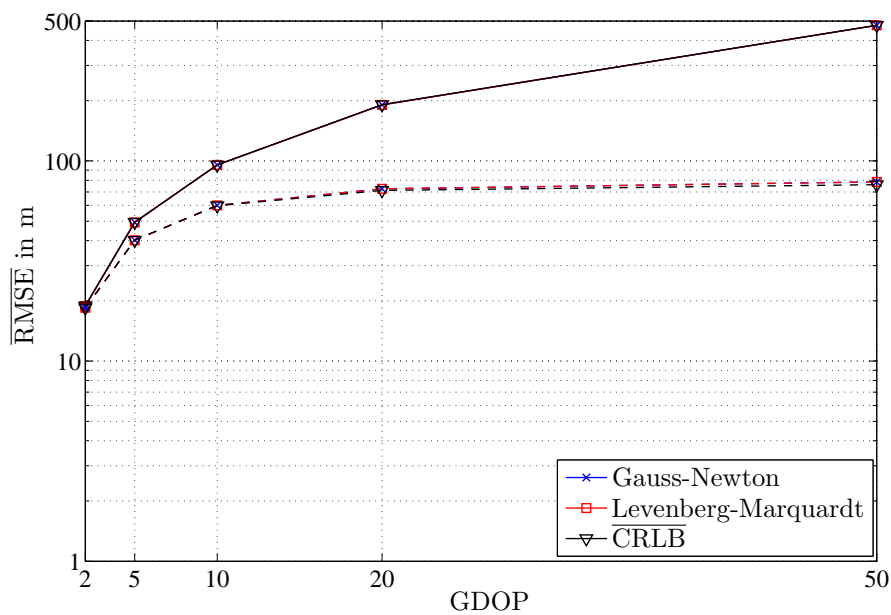


Figure 3.9. MT location  $\overline{\text{RMSE}}$  vs. GDOP for Gauss-Newton algorithm, Levenberg-Marquardt algorithm and  $\overline{\text{CRLB}}$ , solid lines: Satellite method, dashed lines: Hybrid 3 method.



### 3.5.2.2 Simulation Results for Propagation Conditions that switch between LOS and NLOS

In this section, the performance of the Nelder-Mead simplex algorithm introduced in Section 3.4.3 is evaluated for the different combinations of measurements of Scenario I as given in Section 2.3.4.2. In contrast to Section 3.5.2.1, it is now assumed that the RSS and RTT measurements are affected by propagation conditions that switch between LOS and NLOS. The CRLBs for the different combinations of measurements are computed according to Section 3.3.3 using  $N = 10000$  samples, in order to indicate the best possible performance that one can expect for the given scenario and set of parameters. In order to apply the algorithm to the hybrid localization problem, the parameters included in cost function  $V_2(\cdot)$ , cf. (3.85) have to be specified. For the simulations, it is assumed that these parameters are equal to the parameters, with which the measurements have been generated. In practice, however, these parameters are unknown and have to be estimated in advance from field trial data. The parameters of the stopping criteria, necessary to terminate the Nelder-Mead simplex algorithm are summarized in Table 3.2. Since the Nelder-Mead simplex algorithm requires a large number of iterations to converge to the minimum of the cost function, only  $N_{MC} = 100$  Monte Carlo runs are performed. The performance of the Nelder-Mead simplex algorithm may also suffer from a poor initial guess  $\hat{\mathbf{x}}_k^{(0)}$ . For the same reasons as those stated in Section 3.5.2.1, the algorithm is initialized with the true state vector, i.e.,  $\hat{\mathbf{x}}_k^{(0)} = \tilde{\mathbf{x}}_k$ .

In Fig. 3.10, the MT location RMSE in m vs. the time index  $k$  for the Cellular, Hybrid 1 and Hybrid 2 methods are shown for the Nelder-Mead simplex algorithm together with the corresponding CRLBs. For the results, the same conclusions as those for the Gauss-Newton algorithm, cf. Fig. 3.5, can be drawn. It can be noticed that the performance of the Cellular method is different to the Hybrid 1 method. These differences can be explained by the fact that the algorithm converges to different local solutions of the reduced state vector. The risk that the algorithm is ending up in a local minimum is higher for the Hybrid 1 method, since the algorithm has to additionally estimate the unknown MT clock bias. Comparing the results of the Nelder-Mead simplex method to the best achievable performance indicated by the corresponding CRLB, it can be

Table 3.2. Parameters of the Nelder-Mead Simplex Algorithm

Parameter	Value	Parameter	Value	Parameter	Value
$\alpha_1$	1	$\alpha_2$	2	$\alpha_3$	1/2
$\alpha_4$	1/2	$\epsilon_3$	$10^{-10}$	$\eta_{max}$	200

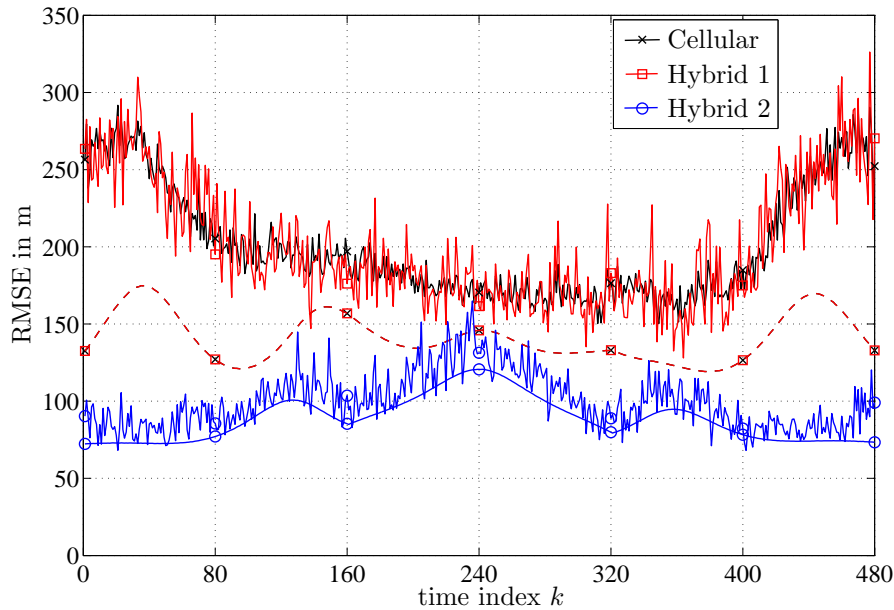


Figure 3.10. MT location RMSE vs. time index  $k$  for Cellular, Hybrid 1 and Hybrid 2 method, solid lines: Nelder-Mead simplex algorithm, dashed lines: CRLB.

observed that for the Hybrid 2 method the performance is close to the CRLB bound, while for the Cellular and Hybrid 1 method this is not the case.

In Fig. 3.11, the MT location  $\overline{\text{RMSE}}$  in m vs. the GRT error standard deviation  $\sigma_{\text{GRT}}$  in s for the Hybrid 1+ and Hybrid 2+ method are shown for the Nelder-Mead simplex algorithm together with the corresponding  $\overline{\text{CRLBs}}$ . The same conclusions as those for the Gauss-Newton algorithm, cf. Fig. 3.7, can be drawn from these results. It can be also noticed that the Nelder-Mead simplex algorithm cannot achieve the  $\overline{\text{CRLB}}$ . However, for decreasing values of  $\sigma_{\text{GRT}}$  the algorithm approaches the  $\overline{\text{CRLB}}$ .

In Fig. 3.12, the MT location  $\overline{\text{RMSE}}$  in m vs. GDOP for the Satellite and Hybrid 3 method are shown for the Nelder-Mead simplex algorithm together with the corresponding  $\overline{\text{CRLBs}}$ . For the results, the same conclusions as those for the Gauss-Newton algorithm, cf. Fig. 3.9, can be drawn. It can be noticed that for the Hybrid 3 method, the Nelder-Mead simplex algorithm cannot achieve the  $\overline{\text{CRLB}}$ . However, for decreasing values of GDOP the algorithm approaches the  $\overline{\text{CRLB}}$ .

The results for the Cellular and Hybrid methods in terms of the CRLBs, RMSEs and  $\overline{\text{RMSE}}$ s presented in this section are worse than the results obtained for the scenario with LOS propagation conditions. This can be explained by the fact that the RTT and RSS measurements affected by LOS propagation conditions are more accurate than the

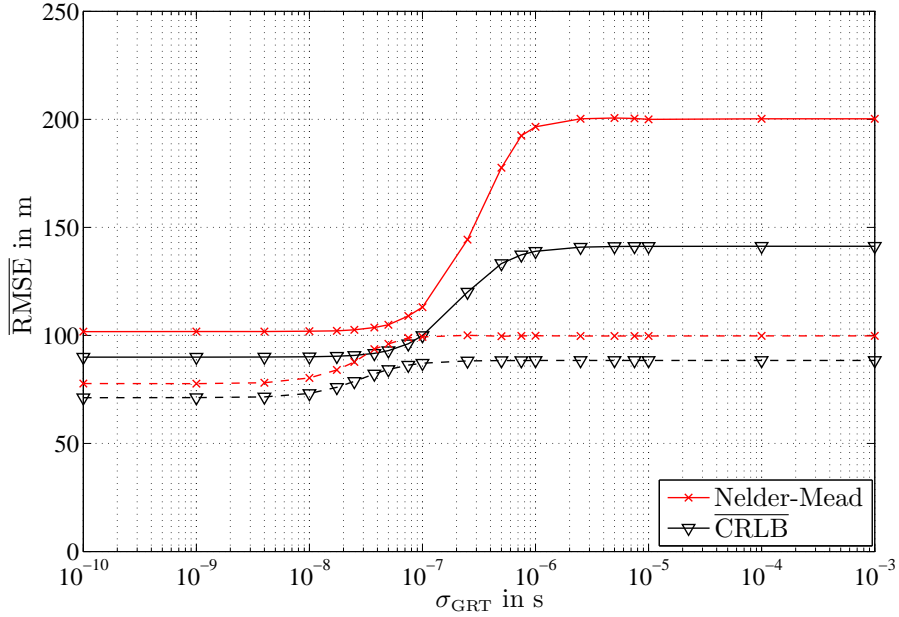


Figure 3.11. MT location  $\overline{\text{RMSE}}$  vs. GRT error standard deviation  $\sigma_{\text{GRT}}$  for Nelder-Mead simplex algorithm, solid lines: Hybrid 1+ method, dashed lines: Hybrid 2+ method.

same measurements affected by NLOS propagation conditions. Since both propagation conditions occur in the scenario that is investigated in this section, the results are on average worse than the results that can be obtained when using only measurements affected by LOS propagation conditions.

### 3.5.3 Field Trial Results

In this section, the expected performance of the hybrid localization method is tested on experimental data available from a field trial. Since the RTT and RSS measurements are highly affected by propagation conditions that switch between LOS and NLOS, the Nelder-Mead simplex algorithm has been used for the hybrid localization method. The unknown parameters of the RTT and RSS model, cf. (2.24) and (2.39), have been estimated from the available field trial data using the Expectation-Maximization algorithm [DLR77, MK97]. The parameters for the stopping criteria of the algorithm are chosen as in Table 3.2. The initial value is chosen as the mean value of the locations of all involved BSs, i.e.

$$\hat{\mathbf{x}}_{\text{MT},k}^{(0)} = \frac{1}{N_{\text{BS}}} \sum_{\nu=1}^{N_{\text{BS}}} \mathbf{x}_{\text{BS},k}^{(\nu)}. \quad (3.99)$$

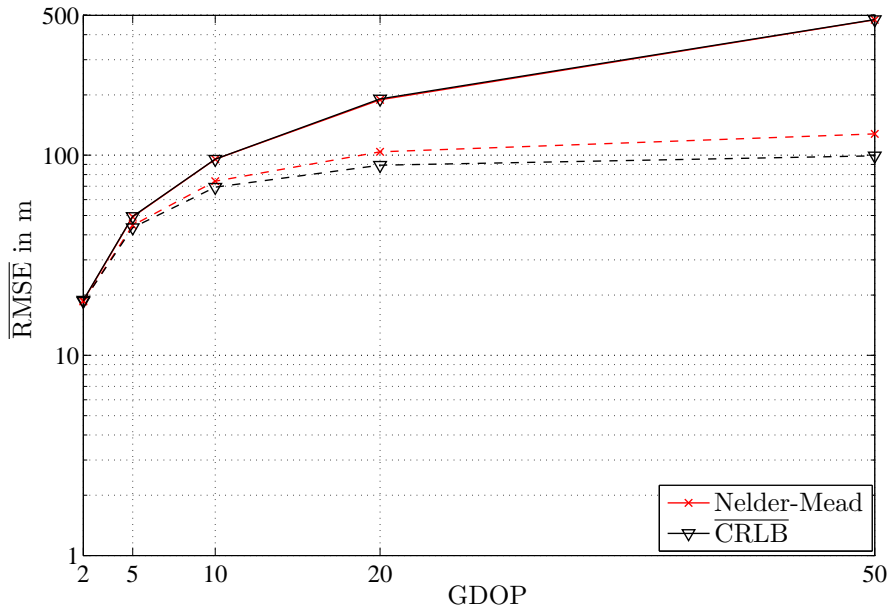


Figure 3.12. MT location  $\overline{\text{RMSE}}$  vs. GDOP for Nelder-Mead simplex algorithm and  $\overline{\text{CRLB}}$ , solid lines: Satellite method, dashed lines: Hybrid 3 method.

and the bias is initialized with  $c_o \cdot \hat{\delta} t_k^{(0)} = z_{\text{PR},k}^{(1)} - d_{\text{SAT},k}^{(1)}(\hat{\mathbf{x}}_{\text{MT},k}^{(0)})$ , which is denoted as suboptimal initial value. Since the performance of the Nelder-Mead simplex algorithm may suffer from a poor initial guess  $\hat{\mathbf{x}}_k^{(0)}$ , the performance has been additionally evaluated assuming  $\hat{\mathbf{x}}_k^{(0)} = \tilde{\mathbf{x}}_k$ , which is referred to as the optimal initial value in the following. In Fig. 3.13, the MT location error in m vs. time index  $k$  for the Cellular, Hybrid 1 and Hybrid 2 method are shown for the Nelder-Mead simplex algorithm using the optimal initial values. Note that the MT location error can be determined from (3.95) by setting  $N_{\text{MC}} = 1$ . The results show that the Cellular and Hybrid 1 method provide the worst performance. The performance can be significantly improved using the Hybrid 2 method. Even though from a theoretical point of view the performance of the Cellular and Hybrid 1 method should be equivalent, small performance differences can be observed. These differences can be explained by the fact that the Nelder-Mead simplex algorithm is converging to different minima of the respective cost functions. This is also the reason why the Cellular method sometimes outperforms the Hybrid 2 method. The results also show that distinct peaks occur in the MT location error for the different methods. These peaks result mainly from bad geometric conditions between the MT and the BSs. For example, it is possible that the MT receives measurements from only one BS, due to the fact that multiple antennas are deployed at the BSs. Another reason is that the algorithm does not converge to the global minimum due to a badly chosen initial value.

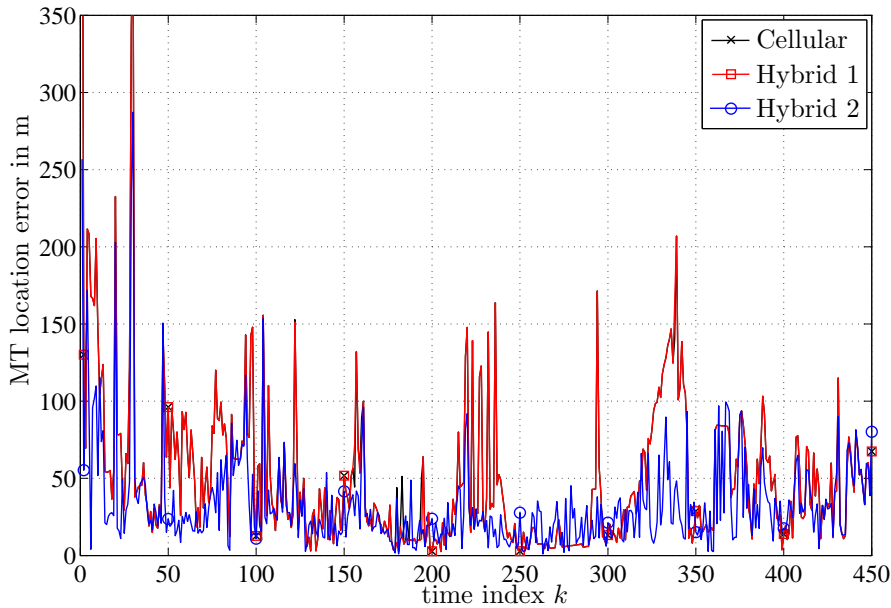


Figure 3.13. MT location error vs. time index  $k$  for Cellular, Hybrid 1 and Hybrid 2 method using the Nelder-Mead simplex algorithm and assuming optimal initial values.

The influence of the chosen initial value on the achievable performance is investigated next. In Fig. 3.14, the MT location error in m vs. time index  $k$  for the Cellular, Hybrid 1 and Hybrid 2 method are shown for the Nelder-Mead simplex algorithm using suboptimal initial values. The results show that the number of distinct peaks occurring in the MT location error for the different methods has increased. The algorithm is obviously converging to different local minima of the corresponding cost functions. Comparing the different localization methods with each other, the same conclusions can be drawn as for the case of initializing the algorithm with the optimal values. Table 3.3 summarizes the time averaged MT location error in m for the different localization methods and initialization strategies. Note that the time averaged MT location error can be determined from (3.96) assuming  $N_{MC} = 1$ . The results show that irrespective of the initialization strategy, the Hybrid 2 method significantly outperforms the Cellular and Hybrid 1 method. However, Table 3.3 also shows that the achievable performance strongly depends on the chosen initial values.

### 3.5.4 Computational Complexity

In order to complement the performance analysis, this section deals with the complexity of the different hybrid localization algorithms. With the obtained results, it

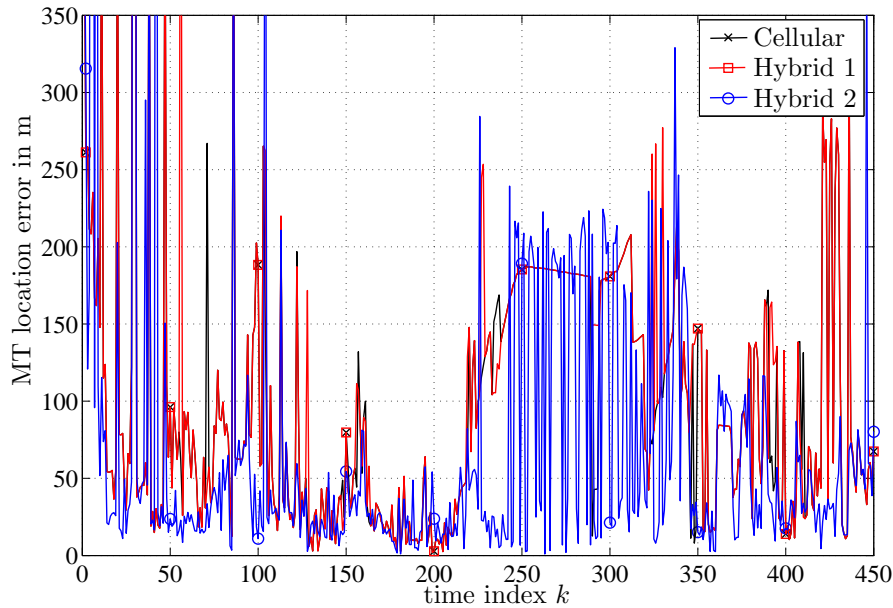


Figure 3.14. MT location error vs. time index  $k$  for Cellular, Hybrid 1 and Hybrid 2 method using the Nelder-Mead simplex algorithm and assuming suboptimal initial values.

is possible to identify which algorithm presents the best trade-off between complexity and performance.

In the following, the complexity of the Gauss-Newton algorithm and Levenberg-Marquardt algorithm, proposed for the solution of the hybrid localization problem in LOS propagation scenarios, is investigated. Even though the Nelder-Mead simplex algorithm could have been used to solve the optimization problem given in (3.66), it is generally orders of magnitude more complex due to its very slow convergence properties. The complexity analysis of the Nelder-Meads simplex algorithm can be found in [SS99] and is not further investigated in this section.

The Gauss-Newton algorithm and Levenberg-Marquardt algorithm are investigated in terms of Floating-Point Operations (FLOPs) per iteration, which is as one addition, subtraction, multiplication, or division of two floating-point numbers. Repeated operations do not increase the complexity, i.e., when the same computation is carried out at several points within the algorithm, its computational cost is computed only once, since its result can be stored in memory and reused when necessary. In the Gauss-Newton algorithm as well as in the Levenberg-Marquardt algorithm, there are certain steps that cannot be measured in FLOPs. In both algorithms, one has to evaluate the Jacobian matrix  $\mathbf{H}_{\text{LOS},k}(\cdot)$  and the nonlinear function  $\mathbf{h}_{\text{LOS},k}(\cdot)$  and in the Levenberg-Marquardt

Table 3.3. Time averaged MT location error for the Cellular, Hybrid 1 and Hybrid 2 method using the Nelder-Mead simplex algorithm and different initial values.

Method	Time Averaged MT Location Error in m	
	optimal initial values	suboptimal initial values
Cellular	50.73	101.02
Hybrid 1	50.53	103.16
Hybrid 2	32.93	74.28

method, it is further necessary to evaluate a conditional if-statement, cf. Algorithms 3.1 and 3.2. In the following, the cost of evaluating the nonlinear function and Jacobian matrix as well as the costs of evaluating conditional statements is neglected. Furthermore, the computational cost of the initialization for the two filters can be neglected, since this step is evaluated only once. Then, the computational complexity in FLOPs per iteration of the Gauss-Newton algorithm is given by

$$\mathcal{C}_{\text{GN}}(n_{\bar{x}}, n_z) = n_z^3 + n_{\bar{x}}^3 + 2n_z^2 n_{\bar{x}} + 2n_{\bar{x}}^2 n_z + n_{\bar{x}} n_z, + n_{\bar{x}}^2 + n_z - n_{\bar{x}} \quad (3.100)$$

and that of the Levenberg-Marquardt algorithm is given by

$$\mathcal{C}_{\text{LM}}(n_{\bar{x}}, n_z) = n_z^3 + n_{\bar{x}}^3 + 2n_z^2 n_{\bar{x}} + 2n_{\bar{x}}^2 n_z + n_{\bar{x}} n_z + 3n_{\bar{x}}^2 + 4n_{\bar{x}} + n_z + 9. \quad (3.101)$$

Here, it is worth noting that the FLOPs for the Levenberg-Marquardt are based on a worst case scenario with  $\rho > 0$  for all iteration steps, cf. Algorithm 3.2. Table 3.4 shows the complexity of the algorithms in terms of FLOPs per iteration for the different methods together with the average number of iterations, until the algorithms converge to a local solution. The results show that the Gauss-Newton algorithm has a lower complexity per iteration than the Levenberg-Marquardt algorithm for all investigated methods. When comparing the number of iterations the algorithms require to converge, it can be observed that these numbers are in the same order of magnitude. However, it can be also observed that for the different methods the numbers of iterations vary. In general, one cannot easily draw conclusions from the average number of iterations, since these values strongly depend on the investigated scenario, the initial guess  $\hat{\mathbf{x}}_k^{(0)}$  and the parameters of the stopping criteria, cf. Table 3.1.

Table 3.4. Computational complexity of the hybrid localization algorithms. Numbers in parentheses denote the average number of algorithm iterations until convergence.

Method	Complexity in FLOPs per Iteration	
	Gauss-Newton	Levenberg-Marquardt
Cellular	866 (19)	893 (21)
Hybrid 1	1446 (17)	1488 (14)
Hybrid 1+	1853 (13)	1895 (13)
Hybrid 2	1853 (10)	1895 (11)
Hybrid 2+	2332 (8)	2374 (10)
Hybrid 3	2332 (6)	2374 (5)
Satellite	180 (4)	222 (3)

### 3.6 Conclusions

In this chapter, the hybrid localization problem has been reformulated as an ML estimation problem, where temporal dependencies between MT states and between measurements are not taken into account explicitly. The ML estimators have been newly derived for measurements affected by LOS propagation conditions and measurements affected by propagation conditions that switch between LOS and NLOS. For both cases, the ML estimates are determined numerically using suboptimal algorithms. For the case of LOS propagation conditions, the Gauss-Newton and Levenberg-Marquardt algorithm have been proposed to solve the ML estimation problem. For the case of propagation conditions that switch between LOS and NLOS, the Nelder-Mead simplex algorithm has been proposed to solve the ML estimation problem. The performance of these algorithms have been compared to the theoretically best achievable performance, which is given by the CRLB. For the case of LOS propagation conditions, an analytical solution of the CRLB has been newly derived and a novel geometric interpretation of the bound is given. For the case of propagation conditions that may switch between LOS and NLOS, a numerical solution of the CRLB based on Monte Carlo integration has been newly proposed. Additionally, the Nelder-Mead simplex algorithm has been applied to experimental data available from a field trial. All presented algorithms have been extensively analyzed in terms of performance and complexity. If it is not otherwise stated, the following main conclusions hold for both cases assuming LOS propagation conditions and propagation conditions that switch between LOS and NLOS:

- The performance of the Cellular method and Hybrid 1 method are equivalent, and the Hybrid 2 method outperforms the Cellular and Hybrid 1 methods.



- 
- The performance improvements of the Hybrid 1+ and Hybrid 2+ strongly depend on the accuracy with which the GRT measurements can be provided.
  - The performance improvement of the Hybrid 3 method compared to the Satellite method strongly depends on the GDOP value. While for small GDOP values the performance improvements are small, significant performance improvements can be obtained for large GDOP values.
  - For the case of LOS propagation conditions, the Gauss-Newton algorithm presents the best trade-off between complexity and performance. However, for certain MT, BS and satellite geometries the Gauss-Newton algorithm diverges due to a rank-deficient matrix. In this case, the Levenberg-Marquardt algorithm converges to a solution, yielding a much more robust implementation.
  - The achievable performance of the different iterative algorithms strongly depends on the chosen initial values.
  - The CRLBs for LOS propagation conditions are always lower than the CRLBs for propagation conditions that switch between LOS and NLOS.
  - The performance of the Gauss-Newton and Levenberg-Marquardt algorithm for LOS propagation conditions are close to the CRLB. For propagation conditions that switch between LOS and NLOS, larger performance differences between the Nelder-Mead simplex algorithm and the CRLB can be observed.



---

## Chapter 4

# Recursive State Estimation for Hybrid Localization

### 4.1 Introduction

In this chapter, the hybrid localization problem is solved using recursive state estimation techniques <sup>1</sup>. In recursive state estimation, the MT state is estimated for each time step  $k$  recursively, by taking into account information about measurements and MT state estimates from previous time steps.

The concept of recursive Bayesian state estimation is introduced in Section 4.2 and the optimal recursive Bayesian solution is presented. In order to assess the theoretical best achievable performance of recursive estimators, the PCRLB is evaluated for the hybrid localization problem in Section 4.3. Since an analytical solution of the optimal recursive Bayesian solution for hybrid localization does not exist, suboptimal recursive estimators are proposed. In Section 4.4, KF-based estimators are introduced to solve the hybrid localization problem, and in Section 4.5, PF-based estimators are proposed. The performance of the different hybrid localization algorithms is analyzed by means of simulations and experimental data in Section 4.6. Finally, the main conclusions of this chapter are drawn in Section 4.7.

### 4.2 Concept of Recursive Bayesian Estimation

In this section, the concept of recursive Bayesian estimation is introduced. The idea of recursive estimation is to include information available from state estimates of previous time steps into the estimation process. In order to avoid that all previous state estimates have to be processed in the recursive estimator at each time step, it is common to assume that the MT state is a Markov process [Jaz70, RAG04]. With this strategy, only the information from the current measurement and the state estimate of the previous time step is processed in the recursive estimator.

---

<sup>1</sup>In the literature, recursive state estimation is also known as state estimation or filtering [GG05, BSLK01, RAG04].

The aim in recursive Bayesian estimation is to recursively compute estimates of the state  $\mathbf{x}_k$  using the sequence of all available measurements  $\mathbf{Z}_k = \{\mathbf{z}_1, \dots, \mathbf{z}_k\}$  up to and including time  $k$ . From a Bayesian point of view, the aim is to recursively compute the posterior pdf  $p(\mathbf{x}_k|\mathbf{Z}_k)$ , since it provides a complete statistical description of the state  $\mathbf{x}_k$  at that time. The optimal recursive Bayesian solution is divided into a time update step and measurement update step [Jaz70]. In the time update step, the prediction density  $p(\mathbf{x}_k|\mathbf{Z}_{k-1})$  is computed according to

$$p(\mathbf{x}_k|\mathbf{Z}_{k-1}) = \int_{\mathbb{R}^{n_x}} p(\mathbf{x}_k, \mathbf{x}_{k-1}|\mathbf{Z}_{k-1}) d\mathbf{x}_{k-1} \quad (4.1a)$$

$$= \int_{\mathbb{R}^{n_x}} p(\mathbf{x}_k|\mathbf{x}_{k-1}, \mathbf{Z}_{k-1}) \cdot p(\mathbf{x}_{k-1}|\mathbf{Z}_{k-1}) d\mathbf{x}_{k-1} \quad (4.1b)$$

$$= \int_{\mathbb{R}^{n_x}} p(\mathbf{x}_k|\mathbf{x}_{k-1}) \cdot p(\mathbf{x}_{k-1}|\mathbf{Z}_{k-1}) d\mathbf{x}_{k-1}, \quad (4.1c)$$

where (4.1b) follows from repeated application of Bayes' theorem, and (4.1c) follows from the fact that  $\mathbf{x}_k$  is Markov, i.e., the current state  $\mathbf{x}_k$  is conditionally independent of the previous measurements  $\mathbf{Z}_{k-1}$  given the previous state  $\mathbf{x}_k$ . Equation (4.1c) gives the time update equation, which is widely known as Chapman-Kolmogorov equation [Pap84]. For state-space models of the form (2.2), the transitional pdf  $p(\mathbf{x}_k|\mathbf{x}_{k-1})$  is given by

$$p(\mathbf{x}_k|\mathbf{x}_{k-1}) = p_{\mathbf{F}_{k-1} \cdot \mathbf{w}_{k-1}}(\mathbf{x}_k - \mathbf{f}_{k-1}(\mathbf{x}_{k-1})), \quad (4.2)$$

[Jaz70]. When a new measurement becomes available at time step  $k$ , the measurement update step is performed. Using Bayes' theorem, the posterior pdf  $p(\mathbf{x}_k|\mathbf{Z}_k)$  can be updated according to

$$p(\mathbf{x}_k|\mathbf{Z}_k) = p(\mathbf{x}_k|\mathbf{Z}_{k-1}, \mathbf{z}_k) = \frac{p(\mathbf{z}_k|\mathbf{x}_k, \mathbf{Z}_{k-1}) \cdot p(\mathbf{x}_k|\mathbf{Z}_{k-1})}{p(\mathbf{z}_k|\mathbf{Z}_{k-1})} \quad (4.3a)$$

$$= \frac{p(\mathbf{z}_k|\mathbf{x}_k) \cdot p(\mathbf{x}_k|\mathbf{Z}_{k-1})}{p(\mathbf{z}_k|\mathbf{Z}_{k-1})} \quad (4.3b)$$

$$= \frac{p(\mathbf{z}_k|\mathbf{x}_k) \cdot p(\mathbf{x}_k|\mathbf{Z}_{k-1})}{\int_{\mathbb{R}^{n_x}} p(\mathbf{z}_k|\mathbf{x}_k) \cdot p(\mathbf{x}_k|\mathbf{Z}_{k-1}) d\mathbf{x}_k}, \quad (4.3c)$$

where (4.3b) follows from the fact that  $\mathbf{x}_k$  is Markov, i.e., the current measurement  $\mathbf{z}_k$  is conditionally independent of the previous measurements  $\mathbf{Z}_{k-1}$ , given the current state  $\mathbf{x}_k$ . For measurement models of the form (2.9), the pdf  $p(\mathbf{z}_k|\mathbf{x}_k)$  (or likelihood function) is given by

$$p(\mathbf{z}_k|\mathbf{x}_k) = p_{\mathbf{v}_k}(\mathbf{x}_k - \mathbf{h}_k(\mathbf{x}_k)), \quad (4.4)$$

and the recursions are initiated with the pdf  $p(\mathbf{x}_0)$  [Jaz70]. Note if  $\mathbf{x}_k$  and  $\mathbf{x}_{k-1}$  are assumed to be statistically independent, i.e.,  $p(\mathbf{x}_k|\mathbf{x}_{k-1}) = p(\mathbf{x}_k)$  holds, then the recursive

Bayesian estimation solution given by (4.1c) and (4.3c) reduces to the non-recursive Bayesian estimation solution given by (3.1). Knowledge of the posterior pdf  $p(\mathbf{x}_k|\mathbf{Z}_k)$  enables one to obtain MT state estimates with respect to any criterion. In this work, only the MMSE criterion will be further elaborated, which has been introduced for non-recursive state estimation in Section 3.2. In order to better distinguish between non-recursive and recursive state estimation, the notation  $\hat{\mathbf{x}}_{k|k}$  is introduced in the following, which describes the estimate of the MT state  $\mathbf{x}_k$  at time  $k$ , given the measurements  $Z_k$  up to and including time  $k$ . The MMSE estimator for recursive estimation and the corresponding covariance is, thus, given by

$$\hat{\mathbf{x}}_{\text{MMSE},k|k} = \mathbb{E}_{p(\mathbf{x}_k|\mathbf{Z}_k)}\{\mathbf{x}_k\} = \int_{\mathbb{R}^{n_x}} \mathbf{x}_k \cdot p(\mathbf{x}_k|\mathbf{Z}_k) d\mathbf{x}_k, \quad (4.5a)$$

$$\begin{aligned} \mathbf{P}_{\text{MMSE},k|k} &= \mathbb{E}_{p(\mathbf{x}_k|\mathbf{Z}_k)}\{(\mathbf{x}_k - \hat{\mathbf{x}}_{\text{MMSE},k|k}) \cdot (\mathbf{x}_k - \hat{\mathbf{x}}_{\text{MMSE},k|k})^\top\} \\ &= \int_{\mathbb{R}^{n_x}} (\mathbf{x}_k - \hat{\mathbf{x}}_{\text{MMSE},k|k}) \cdot (\mathbf{x}_k - \hat{\mathbf{x}}_{\text{MMSE},k|k})^\top \cdot p(\mathbf{x}_k|\mathbf{Z}_k) d\mathbf{x}_k. \end{aligned} \quad (4.5b)$$

It is well known that the optimal solution in the MMSE sense of the recursive Bayesian estimation problem only allows analytical solutions in a few special cases. The most important special case is when the models  $\mathbf{f}_{k-1}(\cdot)$  and  $\mathbf{h}_k(\cdot)$ , cf. (2.1) and (2.8), are linear, and when the pdfs  $p(\mathbf{x}_0)$ ,  $p_{\mathbf{w}_{k-1}}(\mathbf{w}_{k-1})$ ,  $p_{\mathbf{v}_k}(\mathbf{v}_k)$  are Gaussian. In this case, a closed-form solution for the recursion equations (4.1) and (4.3) exist, which is known as the KF [Kal60, HL64, AM79, WB01].

However, if one of the functions  $\mathbf{f}_{k-1}(\cdot)$  or  $\mathbf{h}_k(\cdot)$  is nonlinear or one of the pdfs  $p(\mathbf{x}_0)$  or  $p(\mathbf{x}_k|\mathbf{x}_{k-1})$  or  $p(\mathbf{z}_k|\mathbf{x}_k)$  are non-Gaussian, the multidimensional integrals involved in the recursions often cannot be solved analytically and a closed-form solution for  $p(\mathbf{x}_k|\mathbf{Z}_k)$  becomes intractable. For the hybrid localization problem assuming LOS propagation conditions, this is the case, since the measurement models  $\mathbf{h}_{\text{LOS},k}(\cdot)$  are nonlinear. Furthermore, for the case of switching LOS/NLOS propagation conditions, the likelihood function  $p(\mathbf{z}_k|\mathbf{x}_k)$  is non-Gaussian, cf. (3.83). In both cases, an analytical solution for  $p(\mathbf{x}_k|\mathbf{Z}_k)$  is not available and one has to resort to suboptimal approaches.

## 4.3 Posterior Cramér-Rao Lower Bound

### 4.3.1 Introduction

In this section, the PCRLB for recursive Bayesian estimation is introduced, which is used to assess the theoretical performance bound for the recursive hybrid localization

algorithms investigated in this work <sup>2</sup>. Let the sequence of states be given by  $\mathbf{X}_k = \{\mathbf{x}_0, \mathbf{x}_1, \dots, \mathbf{x}_k\}$ . Let further  $\hat{\mathbf{X}}_{k|k}(\mathbf{Z}_k)$  denote an unbiased estimate of  $\mathbf{X}_k$  and let the estimation error be given by  $\hat{\mathbf{X}}_{k|k}(\mathbf{Z}_k) - \mathbf{X}_k$ . The PCRLB is defined to give a lower bound for the covariance matrix of the estimation error [vT68, TMN98]. Let  $\mathbf{I}_{B,k}$  denote the Bayesian Information Matrix (BIM) and its inverse is denoted as PCRLB matrix [vT68]. Then, the covariance matrix of the estimation error satisfies the following inequality

$$\mathbb{E}_{p(\mathbf{x}_k, \mathbf{z}_k)} \left\{ (\hat{\mathbf{X}}_{k|k}(\mathbf{Z}_k) - \mathbf{X}_k)(\hat{\mathbf{X}}_{k|k}(\mathbf{Z}_k) - \mathbf{X}_k)^\top \right\} \geq [\mathbf{I}_{B,k}]^{-1}. \quad (4.6)$$

The BIM for estimating the sequence of states  $\mathbf{X}_k$  is defined as

$$\mathbf{I}_{B,k} = \mathbb{E}_{p(\mathbf{x}_k, \mathbf{z}_k)} \left\{ \Delta_{\mathbf{x}_k}^{\mathbf{x}_k} \log_e(p(\mathbf{X}_k, \mathbf{Z}_k)) \right\}. \quad (4.7)$$

The PCRLB exists, if the derivatives and expectations in (4.6) and (4.7) exist. The proof is given in [vT68]. The BIM as well as the PCRLB matrix are  $(k+1)n_x \times (k+1)n_x$  matrices, whose dimension grows with time  $k$ . Since the computation of the PCRLB involves the inversion of the BIM, the computational complexity grows with time  $k$ . In general, however, one is interested in a recursive computation of the PCRLB, where the computational complexity is constant over time. In [TMN98], an elegant method is described, how the PCRLB can be computed recursively, while the computational complexity is kept constant over time. The idea of this approach is to evaluate the Bayesian information submatrix for estimating  $\mathbf{x}_k$ , which is denoted as  $\mathbf{J}_k$ , instead of the BIM for estimating  $\mathbf{X}_k$ . According to [TMN98],  $\mathbf{J}_k$  is given as the inverse of the  $n_x \times n_x$  right-lower block of  $[\mathbf{I}_{B,k}]^{-1}$ , whose dimension is independent of time  $k$ . The matrix  $[\mathbf{J}_k]^{-1}$ , then gives a lower bound on the mean square error of estimating  $\mathbf{x}_k$ . Let  $\hat{\mathbf{x}}_{k|k}(\mathbf{Z}_k)$  denote an unbiased estimate of  $\mathbf{x}_k$  and let the estimation error be given by  $\hat{\mathbf{x}}_{k|k}(\mathbf{Z}_k) - \mathbf{x}_k$ . Then, the covariance matrix of the estimation error satisfies the following inequality

$$\mathbb{E}_{p(\mathbf{x}_k, \mathbf{z}_k)} \left\{ (\hat{\mathbf{x}}_{k|k}(\mathbf{Z}_k) - \mathbf{x}_k)(\hat{\mathbf{x}}_{k|k}(\mathbf{Z}_k) - \mathbf{x}_k)^\top \right\} \geq [\mathbf{J}_k]^{-1}. \quad (4.8)$$

According to [TMN98], the Bayesian information submatrix  $\mathbf{J}_k$  for estimating the state vector  $\mathbf{x}_k$  can be calculated recursively using the following formula

$$\mathbf{J}_k = \mathbf{D}_{k-1}^{22} - \mathbf{D}_{k-1}^{21}[\mathbf{J}_{k-1} + \mathbf{D}_{k-1}^{11}]^{-1}\mathbf{D}_{k-1}^{12} + \mathbf{D}_{k-1}^{33}, \quad (k \geq 1) \quad (4.9)$$

where

$$\mathbf{D}_{k-1}^{11} = \mathbb{E}_{p(\mathbf{x}_k)} \left\{ -\Delta_{\mathbf{x}_{k-1}}^{\mathbf{x}_{k-1}} \log_e p(\mathbf{x}_k | \mathbf{x}_{k-1}) \right\}, \quad (4.10a)$$

$$\mathbf{D}_{k-1}^{12} = \mathbb{E}_{p(\mathbf{x}_k)} \left\{ -\Delta_{\mathbf{x}_{k-1}}^{\mathbf{x}_k} \log_e p(\mathbf{x}_k | \mathbf{x}_{k-1}) \right\} = [\mathbf{D}_{k-1}^{21}]^\top, \quad (4.10b)$$

$$\mathbf{D}_{k-1}^{22} = \mathbb{E}_{p(\mathbf{x}_k)} \left\{ -\Delta_{\mathbf{x}_k}^{\mathbf{x}_k} \log_e p(\mathbf{x}_k | \mathbf{x}_{k-1}) \right\}, \quad (4.10c)$$

$$\mathbf{D}_{k-1}^{33} = \mathbb{E}_{p(\mathbf{x}_k, \mathbf{z}_k)} \left\{ -\Delta_{\mathbf{x}_k}^{\mathbf{x}_k} \log_e p(\mathbf{z}_k | \mathbf{x}_k) \right\}. \quad (4.10d)$$

<sup>2</sup>Another name for the Posterior Cramér-Rao Lower Bound that can be often found in the literature is the Bayesian Cramér-Rao (Lower) Bound [vT68].

The expectation in (4.10d) can be rewritten by first taking the expectation with respect to the conditional pdf  $p(\mathbf{Z}_k|\mathbf{X}_k)$  and then with respect to the marginal pdf  $p(\mathbf{X}_k)$ . Then, it is possible to express  $\mathbf{D}_{k-1}^{33}$  in terms of the FIM  $\mathcal{F}(\mathbf{x}_k)$  introduced in Section 3.3.1, yielding

$$\begin{aligned}\mathbf{D}_{k-1}^{33} &= \mathbb{E}_{p(\mathbf{x}_k)} \left\{ \mathbb{E}_{p(\mathbf{z}_k|\mathbf{x}_k)} \left\{ -\Delta_{\mathbf{x}_k}^{\mathbf{x}_k} \log_e p(\mathbf{z}_k|\mathbf{x}_k) \right\} \right\} \\ &= \mathbb{E}_{p(\mathbf{x}_k)} \left\{ \mathbb{E}_{p(\mathbf{z}_k|\mathbf{x}_k)} \left\{ -\Delta_{\mathbf{x}_k}^{\mathbf{x}_k} \log_e p(\mathbf{z}_k|\mathbf{x}_k) \right\} \right\} = \mathbb{E}_{p(\mathbf{x}_k)} \left\{ \mathcal{F}(\mathbf{x}_k) \right\}.\end{aligned}\quad (4.11)$$

The initial Bayesian information submatrix  $\mathbf{J}_0$  can be calculated from the pdf  $p(\mathbf{x}_0)$  and is given by

$$\mathbf{J}_0 = \mathbb{E}_{p(\mathbf{x}_0)} \left\{ -\Delta_{\mathbf{x}_0}^{\mathbf{x}_0} \log_e(p(\mathbf{x}_0)) \right\}.\quad (4.12)$$

Note that for a Gaussian pdf  $p(\mathbf{x}_0)$  with mean  $\hat{\mathbf{x}}_{0|0}$  and covariance matrix  $\mathbf{P}_{0|0}$ ,  $\mathbf{J}_0 = [\mathbf{P}_{0|0}]^{-1}$  holds [RAG04]. Similar to (3.18), the MSE of the MT location satisfies the following inequality

$$\mathbb{E}_{p(\mathbf{x}_k, \mathbf{z}_k)} \left\{ \left\| \hat{\mathbf{x}}_{\text{MT},k|k}(\mathbf{Z}_k) - \mathbf{x}_{\text{MT},k} \right\|^2 \right\} \geq [[\mathbf{J}_k]^{-1}]_{1,1} + [[\mathbf{J}_k]^{-1}]_{2,2},\quad (4.13)$$

which is termed hereinafter the MT location PCRLB. In Section 4.3.2, the MT location PCRLB is determined for measurements affected by LOS propagation conditions. In Section 4.3.3, the MT location PCRLB is determined for measurements affected by switching LOS/NLOS propagation conditions. In both cases, the PCRLB is evaluated numerically using a Monte Carlo integration approach.

### 4.3.2 Posterior Cramér-Rao Lower Bound for LOS propagation conditions

In this section, the posterior Cramér-Rao lower bound for measurements affected by LOS propagation conditions is determined. In order to evaluate the PCRLB according to (4.13), it is necessary to determine the unknown matrices  $\mathbf{D}_{k-1}^{11}$ ,  $\mathbf{D}_{k-1}^{12}$ ,  $\mathbf{D}_{k-1}^{21}$ ,  $\mathbf{D}_{k-1}^{22}$  and  $\mathbf{D}_{k-1}^{33}$ , cf. (4.10). The hybrid localization method assuming LOS propagation conditions, is fully described by the models given in (2.49) and (2.50). The transitional pdf can be determined from inserting (2.49) into (3.2), yielding

$$p(\mathbf{x}_k|\mathbf{x}_{k-1}) = p_{\mathbf{\Gamma} \cdot \mathbf{w}_{k-1}}(\mathbf{x}_k - \mathbf{F} \cdot \mathbf{x}_{k-1}) = \mathcal{N}(\mathbf{x}_k; \mathbf{F} \cdot \mathbf{x}_{k-1}, \mathbf{\Gamma} \cdot \mathbf{Q} \cdot \mathbf{\Gamma}^\top).\quad (4.14)$$

Since the model in (2.49) is linear Gaussian, the matrices  $\mathbf{D}_{k-1}^{11}$ ,  $\mathbf{D}_{k-1}^{12}$ ,  $\mathbf{D}_{k-1}^{21}$  and  $\mathbf{D}_{k-1}^{22}$  greatly simplify to

$$\mathbf{D}_{k-1}^{11} = \mathbb{E}_{p(\mathbf{x}_k)} \left\{ -\Delta_{\mathbf{x}_{k-1}}^{\mathbf{x}_{k-1}} \log_e p(\mathbf{x}_k|\mathbf{x}_{k-1}) \right\} = \mathbf{F}^\top \cdot [\tilde{\mathbf{Q}}]^{-1} \cdot \mathbf{F},\quad (4.15a)$$

$$\mathbf{D}_{k-1}^{12} = \mathbb{E}_{p(\mathbf{x}_k)} \left\{ -\Delta_{\mathbf{x}_{k-1}}^{\mathbf{x}_k} \log_e p(\mathbf{x}_k|\mathbf{x}_{k-1}) \right\} = [\mathbf{D}_{k-1}^{21}]^\top = -\mathbf{F}^\top \cdot [\tilde{\mathbf{Q}}]^{-1},\quad (4.15b)$$

$$\mathbf{D}_{k-1}^{22} = \mathbb{E}_{p(\mathbf{x}_k)} \left\{ -\Delta_{\mathbf{x}_k}^{\mathbf{x}_k} \log_e p(\mathbf{x}_k|\mathbf{x}_{k-1}) \right\} = [\tilde{\mathbf{Q}}]^{-1},\quad (4.15c)$$

where  $\tilde{\mathbf{Q}} = \mathbf{\Gamma} \cdot \mathbf{Q} \cdot \mathbf{\Gamma}^\top$ . Recall that the joint likelihood function  $p(\mathbf{z}_{\text{LOS},k} | \mathbf{x}_k)$  is given by (3.64). Then, according to (A.9) the matrix  $\mathbf{D}_{k-1}^{33}$  can be written as

$$\mathbf{D}_{k-1}^{33} = \mathbb{E}_{p(\mathbf{x}_k)} \{ \mathcal{F}(\mathbf{x}_k) \} = \mathbb{E}_{p(\mathbf{x}_k)} \{ \mathbf{H}_{\text{LOS},k}^\top(\mathbf{x}_k) \cdot [\mathbf{R}_{\text{LOS},k}]^{-1} \cdot \mathbf{H}_{\text{LOS},k}(\mathbf{x}_k) \}, \quad (4.16)$$

where  $\mathbf{H}_{\text{LOS},k}(\mathbf{x}_k)$  denotes the Jacobian matrix of the measurements, cf. (3.68), but now evaluated for the complete MT state vector. Substitution of (4.15) and (4.16) into the recursion (4.9) yields

$$\begin{aligned} \mathbf{J}_k &= [\tilde{\mathbf{Q}}]^{-1} - [\tilde{\mathbf{Q}}]^{-1} \cdot \mathbf{F} \cdot \left[ \mathbf{J}_{k-1} + \mathbf{F}^\top \cdot [\tilde{\mathbf{Q}}]^{-1} \cdot \mathbf{F} \right]^{-1} \cdot \mathbf{F}^\top \cdot [\tilde{\mathbf{Q}}]^{-1} \\ &\quad + \mathbb{E}_{p(\mathbf{x}_k)} \{ \mathbf{H}_{\text{LOS},k}^\top(\mathbf{x}_k) \cdot [\mathbf{R}_{\text{LOS},k}]^{-1} \cdot \mathbf{H}_{\text{LOS},k}(\mathbf{x}_k) \}. \end{aligned} \quad (4.17)$$

Using the matrix inversion lemma

$$[\mathbf{A} + \mathbf{B}\mathbf{C}\mathbf{B}^\top]^{-1} = \mathbf{A}^{-1} - \mathbf{A}^{-1}\mathbf{B}[\mathbf{C}^{-1} + \mathbf{B}^\top\mathbf{A}^{-1}\mathbf{B}]^{-1}\mathbf{B}^\top\mathbf{A}^{-1} \quad (4.18)$$

[Ber09], the matrix  $\mathbf{J}_k$  can be rewritten as

$$\mathbf{J}_k = [\mathbf{\Gamma} \cdot \mathbf{Q} \cdot \mathbf{\Gamma}^\top + \mathbf{F} \cdot [\mathbf{J}_{k-1}]^{-1} \cdot \mathbf{F}^\top]^{-1} + \mathbb{E}_{p(\mathbf{x}_k)} \{ \mathbf{H}_{\text{LOS},k}^\top(\mathbf{x}_k) \cdot [\mathbf{R}_{\text{LOS},k}]^{-1} \cdot \mathbf{H}_{\text{LOS},k}(\mathbf{x}_k) \}. \quad (4.19)$$

Note that in the absence of a state model, i.e.  $\mathbf{F} = \mathbf{0}_{n_x \times n_x}$  and assuming zero process noise, i.e.  $\mathbf{Q} = \mathbf{0}_{n_w \times n_w}$ , the expectation in (4.19) can be dropped and the Bayesian information submatrix is equal to the FIM. In this case, the PCRLB reduces to the CRLB for nonrandom parameters, cf. (3.13). The most difficult problem in determining the PCRLB is the evaluation of the expectation in (4.19). In the following, a Monte Carlo integration approach, cf. Appendix A.10, is used to approximate the expected value of the FIM, yielding

$$\mathbb{E}_{p(\mathbf{x}_k)} \{ \mathcal{F}(\mathbf{x}_k) \} \approx \frac{1}{N_{\text{MC}}} \sum_{n=1}^{N_{\text{MC}}} \mathbf{H}_{\text{LOS},k}^\top(\mathbf{x}_k^{(n)}) \cdot [\mathbf{R}_{\text{LOS},k}]^{-1} \cdot \mathbf{H}_{\text{LOS},k}(\mathbf{x}_k^{(n)}), \quad (4.20)$$

where  $\mathbf{x}_k^{(n)}$ ,  $n = 1, \dots, N_{\text{MC}}$ , are i.i.d. state vector realizations, such that  $\mathbf{x}_k^{(n)} \sim p(\mathbf{x}_k)$ . Finally, by insertion of (4.19) into (4.13), the MT location PCRLB for measurements affected by LOS propagation conditions can be evaluated.

### 4.3.3 Posterior Cramér-Rao Lower Bound for Propagation Conditions that switch between LOS and NLOS

In this section, the posterior Cramér-Rao lower bound for measurements affected by switching LOS/NLOS propagation conditions is determined. The evaluation of the



PCRLB according to (4.13) requires the determination of the matrices  $\mathbf{D}_{k-1}^{11}$ ,  $\mathbf{D}_{k-1}^{12}$ ,  $\mathbf{D}_{k-1}^{21}$ ,  $\mathbf{D}_{k-1}^{22}$  and  $\mathbf{D}_{k-1}^{33}$ , cf. (4.10). The hybrid localization method assuming switching LOS/NLOS propagation conditions, is fully described by the models given in (2.49) and (2.51). Since the state model is equivalent to the LOS case, the matrices  $\mathbf{D}_{k-1}^{11}$ ,  $\mathbf{D}_{k-1}^{12}$ ,  $\mathbf{D}_{k-1}^{21}$ ,  $\mathbf{D}_{k-1}^{22}$  are given by (4.15). Thus, the only difference in determining the PCRLB is the computation of the matrix  $\mathbf{D}_{k-1}^{33}$ . Recall that the joint likelihood function  $p(\mathbf{z}_k|\mathbf{x}_k)$  in this case is given by (3.49). Then, the matrix  $\mathbf{D}_{k-1}^{33}$  can be written as

$$\begin{aligned} \mathbf{D}_{k-1}^{33} &= \mathbb{E}_{p(\mathbf{x}_k)}\{\mathcal{F}(\mathbf{x}_k)\} = \mathbb{E}_{p(\mathbf{x}_k)}\{\mathcal{F}_{\text{PR}}(\mathbf{x}_k)\} + \mathbb{E}_{p(\mathbf{x}_k)}\{\mathcal{F}_{\text{GRT}}(\mathbf{x}_k)\} \\ &\quad + \mathbb{E}_{p(\mathbf{x}_k)}\left\{\sum_{\kappa_1=1}^{M_{\text{RTT}}}\mathcal{F}_{\text{RTT}}^{(\kappa_1)}(\mathbf{x}_k)\right\} + \mathbb{E}_{p(\mathbf{x}_k)}\left\{\sum_{\kappa_2=1}^{M_{\text{RSS}}}\mathcal{F}_{\text{RSS}}^{(\kappa_2)}(\mathbf{x}_k)\right\}, \end{aligned} \quad (4.21)$$

where all involved FIMs are evaluated with respect to the complete state vector. Note, that the FIM  $\mathcal{F}(\mathbf{x}_k)$  for the complete state vector and the FIM for the reduced state vector  $\mathcal{F}(\tilde{\mathbf{x}}_k)$  are related to each other. For hybrid localization, the available measurements do not give information about the MT velocity states  $\dot{\mathbf{x}}_{\text{MT},k}$  and the MT clock drift state  $c_0 \cdot \delta \dot{t}_k$ . In this case, the following relationship holds:

$$\mathcal{F}(\mathbf{x}_k) = \begin{bmatrix} [\mathcal{F}(\tilde{\mathbf{x}}_k)]_{1,1} & [\mathcal{F}(\tilde{\mathbf{x}}_k)]_{1,2} & 0 & 0 & [\mathcal{F}(\tilde{\mathbf{x}}_k)]_{1,3} & 0 \\ [\mathcal{F}(\tilde{\mathbf{x}}_k)]_{2,1} & [\mathcal{F}(\tilde{\mathbf{x}}_k)]_{2,2} & 0 & 0 & [\mathcal{F}(\tilde{\mathbf{x}}_k)]_{2,3} & 0 \\ 0 & 0 & 0 & 0 & 0 & 0 \\ 0 & 0 & 0 & 0 & 0 & 0 \\ [\mathcal{F}(\tilde{\mathbf{x}}_k)]_{3,1} & [\mathcal{F}(\tilde{\mathbf{x}}_k)]_{3,2} & 0 & 0 & [\mathcal{F}(\tilde{\mathbf{x}}_k)]_{3,3} & 0 \\ 0 & 0 & 0 & 0 & 0 & 0 \end{bmatrix}. \quad (4.22)$$

Thus, determining the FIM of the complete state vector is nothing more than rearranging the elements of the FIM of the reduced state vector according to (4.22). Substitution of (4.15) into the recursion (4.9) and application of the matrix inversion lemma (4.18) yields,

$$\mathbf{J}_k = [\mathbf{\Gamma} \cdot \mathbf{Q} \cdot \mathbf{\Gamma}^T + \mathbf{F} \cdot [\mathbf{J}_{k-1}]^{-1} \cdot \mathbf{F}^T]^{-1} + \mathbf{D}_{k-1}^{33}. \quad (4.23)$$

The matrix  $\mathbf{D}_{k-1}^{33}$  is given by (4.21) and is evaluated approximately using a Monte Carlo integration approach, cf. Appendix A.10, yielding

$$\mathbf{D}_{k-1}^{33} \approx \frac{1}{N_{\text{MC}}} \sum_{n=1}^{N_{\text{MC}}} \left\{ \mathcal{F}_{\text{PR}}(\mathbf{x}_k^{(n)}) + \mathcal{F}_{\text{GRT}}(\mathbf{x}_k^{(n)}) + \sum_{\kappa_1=1}^{M_{\text{RTT}}}\mathcal{F}_{\text{RTT}}^{(\kappa_1)}(\mathbf{x}_k^{(n)}) + \sum_{\kappa_2=1}^{M_{\text{RSS}}}\mathcal{F}_{\text{RSS}}^{(\kappa_2)}(\mathbf{x}_k^{(n)}) \right\}, \quad (4.24)$$

where  $\mathbf{x}_k^{(n)}$ ,  $n = 1, \dots, N_{\text{MC}}$ , are i.i.d. state vector realizations, such that  $\mathbf{x}_k^{(n)} \sim p(\mathbf{x}_k)$ . Note, that the evaluation of (4.23) involves two Monte Carlo integration approaches, namely the computation of the FIMs of the RTT and RSS measurements according to (3.56) and (3.59), and the computation of the expected value of the FIM according to (4.24). Finally, by insertion of (4.23) into (4.13), the MT location PCRLB for measurements affected by switching LOS/NLOS propagation conditions can be evaluated.

## 4.4 Kalman Filter-based Estimators

### 4.4.1 Introduction

In this section, KF-based estimators are proposed to solve the hybrid localization problem. KF-based estimators assume that all pdfs involved in the computation of the recursive solution, cf. (4.1c) and (4.3c), can be approximated with Gaussian pdfs, i.e.,

$$p(\mathbf{x}_{k-1}|\mathbf{Z}_{k-1}) \approx \mathcal{N}(\mathbf{x}_{k-1}; \hat{\mathbf{x}}_{k-1|k-1}, \mathbf{P}_{k-1|k-1}), \quad (4.25a)$$

$$p(\mathbf{x}_k|\mathbf{Z}_{k-1}) \approx \mathcal{N}(\mathbf{x}_k; \hat{\mathbf{x}}_{k|k-1}, \mathbf{P}_{k|k-1}), \quad (4.25b)$$

$$p(\mathbf{x}_k|\mathbf{Z}_k) \approx \mathcal{N}(\mathbf{x}_k; \hat{\mathbf{x}}_{k|k}, \mathbf{P}_{k|k}), \quad (4.25c)$$

[RAG04], which are completely specified by their mean vectors and covariance matrices. An appealing advantage of this approach is that the functional recursion in (4.1c) and (4.3c) reduces to an algebraic recursion, where only means and covariances have to be calculated. In Fig. 4.1, a block diagram showing the recursion of a KF-based estimator is depicted. At time  $k = 0$ , the filter is initialized with a Gaussian pdf  $p(\mathbf{x}_0)$  with mean vector  $\hat{\mathbf{x}}_{0|0}$  and covariance matrix  $\mathbf{P}_{0|0}$ . In the time update stage, a Gaussian approximation to the prediction density  $p(\mathbf{x}_k|\mathbf{Z}_{k-1})$  is calculated, which is represented by the mean  $\hat{\mathbf{x}}_{k|k-1}$  and covariance  $\mathbf{P}_{k|k-1}$ , cf. (4.1c) and (4.25b). Upon the arrival of a new measurement  $\mathbf{z}_k$ , the predicted mean  $\hat{\mathbf{x}}_{k|k-1}$  and covariance  $\mathbf{P}_{k|k-1}$  are corrected in the measurement update stage to follow the measurements. Here, a Gaussian approximation to the posterior pdf  $p(\mathbf{x}_k|\mathbf{Z}_k)$  is calculated, cf. (4.3c) and (4.25c). The corresponding mean  $\hat{\mathbf{x}}_{k|k}$  and covariance  $\mathbf{P}_{k|k}$  are the final estimates of the KF-based estimator and are used as approximations of the MMSE estimates defined in (4.5). In order to satisfy a recursion, the mean and covariance of the posterior pdf are used as input values for the time update stage at the next time instance.

In the following, three suboptimal algorithms, namely the EKF [BSLK01], the UKF [WvdM00], and the Cubature Kalman Filter (CKF) [AH09], are proposed to solve the underlying hybrid localization problem. While the filtering algorithms are well-known, the application of these algorithms to the hybrid localization problem can be regarded as the novel contribution. The filters can be straightforwardly applied to the scenario with LOS propagation conditions, where the transitional pdf  $p(\mathbf{x}_k|\mathbf{x}_{k-1})$  and the likelihood pdf  $p(\mathbf{z}_{\text{LOS},k}|\mathbf{x}_k)$  are assumed Gaussian, cf. (4.14) and (3.64). In scenarios, where the propagation conditions switch between LOS and NLOS, the likelihood pdf  $p(\mathbf{z}_k|\mathbf{x}_k)$  is a mixture of Gaussian pdfs, cf. (3.54). In order to apply the KF-based estimators to this scenario, the Gaussian mixture pdf has to be approximated with a single Gaussian

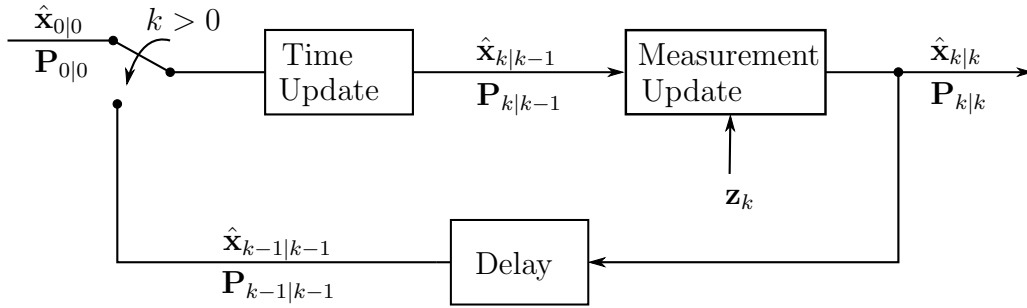


Figure 4.1. Block diagram showing the operation of KF-based estimators.

pdf using moment matching [BSLK01]. It can be straightforwardly shown that the covariance matrix of the moment-matched RSS measurement pdf is state-dependent, which prevents a direct application of the EKF, UKF and CKF to the hybrid localization problem. For these reasons, the KF-based estimators are only applied to the hybrid localization problem assuming LOS propagation conditions. In Section 4.4.2, the EKF is presented. In Section 4.4.3, the UKF is described and the CKF is briefly outlined in Section 4.4.4.

#### 4.4.2 Extended Kalman Filter

The EKF belongs to the class of nonlinear filters, where the nonlinear functions in the state and measurement models, cf. (2.1) and (2.8) are locally linearized using a Taylor series expansion [BSLK01]. It is assumed that the local linearization of the state and measurement models is a sufficient description of nonlinearity. The posterior pdf is approximated by a Gaussian density and relationships (4.25a)-(4.25c) are assumed to hold. For the hybrid localization problem, the state model is linear with additive Gaussian noise, cf. (2.49), so that there is no need for linearization in the time update. Since the measurement model is nonlinear with additive Gaussian noise, cf. (2.50), suitable approximations have to be introduced in the measurement update. The time update and measurement update of the EKF are presented next.

##### Time Update

Based on the assumption that the posterior pdf  $p(\mathbf{x}_{k-1}|\mathbf{Z}_{k-1})$  of the previous time step  $k-1$  is Gaussian, cf. (4.25a), and based on the fact that the transitional pdf

$p(\mathbf{x}_k|\mathbf{x}_{k-1})$  is linear Gaussian, cf. (4.14), the time update step, cf. (4.1c), can be evaluated in closed-form, and is given by

$$\begin{aligned} p(\mathbf{x}_k|\mathbf{Z}_{k-1}) &= \int_{\mathbb{R}^{n_x}} p(\mathbf{x}_k|\mathbf{x}_{k-1}) \cdot p(\mathbf{x}_{k-1}|\mathbf{Z}_{k-1}) d\mathbf{x}_{k-1} \\ &\approx \int_{\mathbb{R}^{n_x}} \mathcal{N}(\mathbf{x}_k; \mathbf{F} \cdot \mathbf{x}_{k-1}, \mathbf{\Gamma} \cdot \mathbf{Q} \cdot \mathbf{\Gamma}^\top) \cdot \mathcal{N}(\mathbf{x}_{k-1}; \hat{\mathbf{x}}_{k-1|k-1}, \mathbf{P}_{k-1|k-1}) d\mathbf{x}_{k-1} \\ &= \mathcal{N}(\mathbf{x}_k; \hat{\mathbf{x}}_{k|k-1}, \mathbf{P}_{k|k-1}), \end{aligned} \quad (4.26)$$

where

$$\hat{\mathbf{x}}_{k|k-1} = \mathbf{F} \cdot \hat{\mathbf{x}}_{k-1|k-1}, \quad (4.27a)$$

$$\mathbf{P}_{k|k-1} = \mathbf{F} \cdot \mathbf{P}_{k-1|k-1} \cdot \mathbf{F}^\top + \mathbf{\Gamma} \cdot \mathbf{Q} \cdot \mathbf{\Gamma}^\top. \quad (4.27b)$$

A proof of (4.26) can be found, for instance, in [HL64,BSLK01].

## Measurement Update

In the measurement update step, the posterior pdf is calculated according to (4.3c), which involves the evaluation of a multidimensional integral. Since for the hybrid localization problem the measurement model  $\mathbf{h}_{\text{LOS},k}(\mathbf{x}_k)$  is nonlinear, a closed-form solution of the integral given in (4.3c) does not exist. In the EKF, the nonlinear measurement model  $\mathbf{h}_{\text{LOS},k}(\mathbf{x}_k)$  is approximated with a first-order Taylor series expansion about  $\hat{\mathbf{x}}_{k|k-1}$ , which is given by

$$\mathbf{h}_{\text{LOS},k}(\mathbf{x}_k) \approx \mathbf{h}_{\text{LOS},k}(\hat{\mathbf{x}}_{k|k-1}) + \mathbf{H}_{\text{LOS},k}(\mathbf{x}_k)|_{\mathbf{x}_k=\hat{\mathbf{x}}_{k|k-1}} \cdot (\mathbf{x}_k - \hat{\mathbf{x}}_{k|k-1}), \quad (4.28)$$

where  $\mathbf{H}_{\text{LOS},k}(\mathbf{x}_k)$  denotes the Jacobian matrix of the measurements, cf. (3.68), evaluated for the complete MT state vector. Thus, the likelihood pdf can be approximated with

$$\begin{aligned} p(\mathbf{z}_k|\mathbf{x}_k) &= p(\mathbf{z}_{\text{LOS},k}|\mathbf{x}_k) = \mathcal{N}(\mathbf{z}_{\text{LOS},k}; \mathbf{h}_{\text{LOS},k}(\mathbf{x}_k), \mathbf{R}_{\text{LOS},k}) \\ &\approx \mathcal{N}(\mathbf{z}_{\text{LOS},k}; \mathbf{h}_{\text{LOS},k}(\hat{\mathbf{x}}_{k|k-1}) + \mathbf{H}_{\text{LOS},k}(\hat{\mathbf{x}}_{k|k-1}) \cdot (\mathbf{x}_k - \hat{\mathbf{x}}_{k|k-1}), \mathbf{R}_{\text{LOS},k}) \\ &= \mathcal{N}(\mathbf{z}_{\text{LOS},k}; \tilde{\mathbf{h}}_{\text{LOS},k}(\hat{\mathbf{x}}_{k|k-1}, \mathbf{x}_k), \mathbf{R}_{\text{LOS},k}). \end{aligned} \quad (4.29)$$

The measurement update step, can be written as

$$\begin{aligned} p(\mathbf{x}_k|\mathbf{Z}_k) &= \frac{p(\mathbf{z}_k|\mathbf{x}_k) \cdot p(\mathbf{x}_k|\mathbf{Z}_{k-1})}{\int_{\mathbb{R}^{n_x}} p(\mathbf{z}_k|\mathbf{x}_k) \cdot p(\mathbf{x}_k|\mathbf{Z}_{k-1}) d\mathbf{x}_k} \\ &\approx \frac{\mathcal{N}(\mathbf{z}_{\text{LOS},k}; \tilde{\mathbf{h}}_{\text{LOS},k}(\hat{\mathbf{x}}_{k|k-1}, \mathbf{x}_k), \mathbf{R}_{\text{LOS},k}) \cdot \mathcal{N}(\mathbf{x}_k; \hat{\mathbf{x}}_{k|k-1}, \mathbf{P}_{k|k-1})}{\int_{\mathbb{R}^{n_x}} \mathcal{N}(\mathbf{z}_{\text{LOS},k}; \tilde{\mathbf{h}}_{\text{LOS},k}(\hat{\mathbf{x}}_{k|k-1}, \mathbf{x}_k), \mathbf{R}_{\text{LOS},k}) \cdot \mathcal{N}(\mathbf{x}_k; \hat{\mathbf{x}}_{k|k-1}, \mathbf{P}_{k|k-1}) d\mathbf{x}_k} \\ &= \mathcal{N}(\mathbf{x}_k; \hat{\mathbf{x}}_{k|k}, \mathbf{P}_{k|k}), \end{aligned} \quad (4.30)$$

where

$$\hat{\mathbf{x}}_{k|k} = \hat{\mathbf{x}}_{k|k-1} + \mathbf{K}_k \cdot [\mathbf{z}_{\text{LOS},k} - \mathbf{h}_{\text{LOS},k}(\hat{\mathbf{x}}_{k|k-1})], \quad (4.31a)$$

$$\mathbf{P}_{k|k} = \mathbf{P}_{k|k-1} - \mathbf{K}_k \cdot \mathbf{P}_{\text{zz},k|k-1} \cdot \mathbf{K}_k^\top, \quad (4.31b)$$

$$\mathbf{P}_{\text{xz},k|k-1} = \mathbf{P}_{k|k-1} \cdot \mathbf{H}_{\text{LOS},k}^\top(\hat{\mathbf{x}}_{k|k-1}), \quad (4.31c)$$

$$\mathbf{P}_{\text{zz},k|k-1} = \mathbf{H}_{\text{LOS},k}(\hat{\mathbf{x}}_{k|k-1}) \cdot \mathbf{P}_{k|k-1} \cdot \mathbf{H}_{\text{LOS},k}^\top(\hat{\mathbf{x}}_{k|k-1}) + \mathbf{R}_{\text{LOS},k}, \quad (4.31d)$$

$$\mathbf{K}_k = \mathbf{P}_{\text{xz},k|k-1} \cdot [\mathbf{P}_{\text{zz},k|k-1}]^{-1}. \quad (4.31e)$$

A proof of (4.30) is given, for instance, in [BSLK01]. A pseudocode description of the EKF is given in Algorithm 4.1. Even though the EKF consists of an algebraic recursion, which allows a simple implementation and fast execution, it may have suboptimal performance or even will diverge, if  $\mathbf{h}_{\text{LOS},k}(\mathbf{x}_k)$  is highly nonlinear. In this case, the non-Gaussianity of the true posterior pdf  $p(\mathbf{x}_k|\mathbf{Z}_k)$  will be more pronounced and its Gaussian approximation is no longer justified.

---

**Algorithm 4.1** Extended Kalman Filter
 

---

```

1: // Initialization
2:  $\hat{\mathbf{x}}_{0|0} := \mathbb{E}\{\mathbf{x}_0\}$ 
3:  $\mathbf{P}_{0|0} := \mathbb{E}\{(\mathbf{x}_0 - \hat{\mathbf{x}}_{0|0})(\mathbf{x}_0 - \hat{\mathbf{x}}_{0|0})^\top\}$ 
4: // Recursion
5: for  $k = 1$  to  $k_{\text{max}}$  do
6:   // Time Update
7:    $\hat{\mathbf{x}}_{k|k-1} := \mathbf{F} \cdot \hat{\mathbf{x}}_{k-1|k-1}$ 
8:    $\mathbf{P}_{k|k-1} := \mathbf{F} \cdot \mathbf{P}_{k-1|k-1} \cdot \mathbf{F}^\top + \mathbf{\Gamma} \cdot \mathbf{Q} \cdot \mathbf{\Gamma}^\top$ 
9:   // Measurement Update
10:   $\mathbf{P}_{\text{xz},k|k-1} := \mathbf{P}_{k|k-1} \cdot \mathbf{H}_{\text{LOS},k}^\top(\hat{\mathbf{x}}_{k|k-1})$ 
11:   $\mathbf{P}_{\text{zz},k|k-1} := \mathbf{H}_{\text{LOS},k}(\hat{\mathbf{x}}_{k|k-1}) \cdot \mathbf{P}_{k|k-1} \cdot \mathbf{H}_{\text{LOS},k}^\top(\hat{\mathbf{x}}_{k|k-1}) + \mathbf{R}_{\text{LOS},k}$ 
12:   $\mathbf{K}_k := \mathbf{P}_{\text{xz},k|k-1} \cdot [\mathbf{P}_{\text{zz},k|k-1}]^{-1}$ 
13:   $\hat{\mathbf{x}}_{k|k} := \hat{\mathbf{x}}_{k|k-1} + \mathbf{K}_k \cdot [\mathbf{z}_{\text{LOS},k} - \mathbf{h}_{\text{LOS},k}(\hat{\mathbf{x}}_{k|k-1})]$ 
14:   $\mathbf{P}_{k|k} := \mathbf{P}_{k|k-1} - \mathbf{K}_k \cdot \mathbf{P}_{\text{zz},k|k-1} \cdot \mathbf{K}_k^\top$ 
15: end for

```

---

### 4.4.3 Unscented Kalman Filter

The UKF belongs to the class of nonlinear filters, where all involved pdfs, cf. (4.1c) and (4.3c), are approximated by Gaussian densities and whose mean and covariance is computed from a small number of deterministically chosen sample points and weights [WvdM00]. These sample points capture the true mean and covariance of the Gaussian densities and are often denoted as sigma points. When these sample points are propagated through a nonlinear transform, it can be shown that the transformed

sigma points exactly describe the true mean and covariance up to at least the second order of the Taylor series expansion of the nonlinearity, while the EKF achieves only first-order accuracy [Jul02]. Thus, instead of linearizing the state and measurement models, as it is done in the EKF, the UKF approximates pdfs, which is also known as statistical linearization [G<sup>+</sup>74]. The corresponding weights and sigma points are selected using the scaled unscented transformation [Jul02], which is presented next.

The scaled unscented transformation is a method for calculating the moments of a nonlinear transformed random variable. Let  $\mathbf{a}$  denote a vector of random variables of dimension  $n_a$  with mean  $\boldsymbol{\mu}_a$  and covariance  $\mathbf{P}_a$ . It is assumed that the random variable  $\mathbf{a}$  is propagated through an arbitrary nonlinear function  $\mathbf{g}(\cdot)$ , yielding the transformed random variable

$$\mathbf{b} = \mathbf{g}(\mathbf{a}) \quad (4.32)$$

of dimension  $n_b$ . The mean  $\boldsymbol{\mu}_b$  and covariance  $\mathbf{P}_b$  of  $\mathbf{b}$  are computed using the scaled unscented transformation. In the scaled unscented transformation,  $2 \cdot n_a + 1$  weighted sample points are deterministically chosen so that they completely describe the true mean  $\boldsymbol{\mu}_a$  and covariance  $\mathbf{P}_a$ . Let  $(\mathbf{A})_i$  denote the  $i$ -th row of the matrix  $\mathbf{A}$ . Further, let  $\mathbf{B} = \sqrt{\mathbf{A}}$  denote the matrix square root of  $\mathbf{A}$ , such that  $\mathbf{A} = \mathbf{B}^T \cdot \mathbf{B}$ . Then, a set of sigma points  $\mathcal{A}^{(i)}$  and weights  $W^{(i)}$  that satisfy the above requirements is given by

$$\mathcal{A}^{(0)} = \boldsymbol{\mu}_a, \quad (4.33a)$$

$$\mathcal{A}^{(i)} = \boldsymbol{\mu}_a + \left( \sqrt{(n_a + \gamma) \cdot \mathbf{P}_a} \right)_i, \quad i = 1, \dots, n_a, \quad (4.33b)$$

$$\mathcal{A}^{(i)} = \boldsymbol{\mu}_a - \left( \sqrt{(n_a + \gamma) \cdot \mathbf{P}_a} \right)_{i-n_a}, \quad i = n_a + 1, \dots, 2 \cdot n_a, \quad (4.33c)$$

$$W_m^{(0)} = \frac{\gamma}{n_a + \gamma}, \quad (4.33d)$$

$$W_c^{(0)} = \frac{\gamma}{n_a + \gamma} + (1 - \alpha^2 + \beta_2), \quad (4.33e)$$

$$W_m^{(i)} = W_c^{(i)} = \frac{1}{2 \cdot (n_a + \gamma)}, \quad i = 1, \dots, 2 \cdot n_a, \quad (4.33f)$$

where  $\gamma = \alpha^2(n_a + \beta_1) - n_a$  is a scaling parameter,  $\beta_1$  is a secondary scaling parameter,  $\alpha$  determines the spread of the sigma points around the mean  $\boldsymbol{\mu}_a$  and  $\beta_2$  is a weight parameter [Jul02]. Propagation of the sigma points  $\mathcal{A}^{(i)}$  through the true nonlinear function, yields the transformed sigma points

$$\mathcal{B}^{(i)} = \mathbf{g}(\mathcal{A}^{(i)}), \quad i = 1, \dots, 2 \cdot n_a. \quad (4.34)$$

The first two moments of  $\mathbf{b}$  are then approximated using a weighted mean and covari-

ance of the transformed sigma points, yielding

$$\boldsymbol{\mu}_b \approx \sum_{i=0}^{2 \cdot n_a} W_m^{(i)} \cdot \mathcal{B}^{(i)}, \quad (4.35a)$$

$$\mathbf{P}_b \approx \sum_{i=0}^{2 \cdot n_a} W_c^{(i)} \cdot (\mathcal{B}^{(i)} - \boldsymbol{\mu}_b) \cdot (\mathcal{B}^{(i)} - \boldsymbol{\mu}_b)^\top. \quad (4.35b)$$

Application of the scaled unscented transformation to the EKF framework, cf. (4.27) and (4.31), yields the UKF, whose time update and measurement update for the hybrid localization are presented in the following [BMW03].

### Time Update

Since the posterior pdf  $p(\mathbf{x}_{k-1} | \mathbf{Z}_{k-1})$  is assumed Gaussian and the transitional pdf  $p(\mathbf{x}_k | \mathbf{x}_{k-1})$  is linear Gaussian, there is no need to apply the scaled unscented transformation to the time update. In this case, the time update of the UKF is equivalent to the time update of the EKF, and the prediction pdf is given by

$$p(\mathbf{x}_k | \mathbf{Z}_{k-1}) \approx \mathcal{N}(\mathbf{x}_k; \hat{\mathbf{x}}_{k|k-1}, \mathbf{P}_{k|k-1}), \quad (4.36)$$

where  $\hat{\mathbf{x}}_{k|k-1}$  and  $\mathbf{P}_{k|k-1}$  are given in (4.27).

### Measurement Update

In order to apply the scaled unscented transformation to the measurement update, the update of the posterior pdf is expressed in terms of the conditional density of the joint state and the measurement  $p(\mathbf{x}_k, \mathbf{z}_k | \mathbf{Z}_{k-1})$ , yielding

$$p(\mathbf{x}_k | \mathbf{Z}_k) = \frac{p(\mathbf{x}_k, \mathbf{z}_k | \mathbf{Z}_{k-1})}{p(\mathbf{z}_k | \mathbf{Z}_{k-1})} = \frac{p(\mathbf{x}_k, \mathbf{z}_k | \mathbf{Z}_{k-1})}{\int_{\mathbb{R}^{n_x}} p(\mathbf{x}_k, \mathbf{z}_k | \mathbf{Z}_{k-1}) d\mathbf{x}_k}. \quad (4.37)$$

Since it is assumed that all pdfs involved in the recursive estimation of the posterior pdf are approximated by Gaussian pdfs, the pdf  $p(\mathbf{x}_k, \mathbf{z}_k | \mathbf{Z}_{k-1})$  is also Gaussian, and is given by

$$p(\mathbf{x}_k, \mathbf{z}_k | \mathbf{Z}_{k-1}) \approx \mathcal{N}([\mathbf{x}_k^\top, \mathbf{z}_k^\top]^\top; \boldsymbol{\mu}_{xz}, \tilde{\mathbf{P}}_{xz}), \quad (4.38)$$

with

$$\boldsymbol{\mu}_{xz} = \begin{bmatrix} \hat{\mathbf{x}}_{k|k-1} \\ \hat{\mathbf{z}}_{k|k-1} \end{bmatrix}, \quad \tilde{\mathbf{P}}_{xz} = \begin{bmatrix} \mathbf{P}_{k|k-1} & \mathbf{P}_{xz,k|k-1} \\ \mathbf{P}_{xz,k|k-1}^\top & \mathbf{P}_{zz,k|k-1} \end{bmatrix}. \quad (4.39)$$

Inserting (4.38) into (4.37) and evaluating the multidimensional integral, it follows that the posterior pdf  $p(\mathbf{x}_k|\mathbf{Z}_k)$  is Gaussian

$$p(\mathbf{x}_k|\mathbf{Z}_k) \approx \mathcal{N}(\mathbf{x}_k; \hat{\mathbf{x}}_{k|k-1}, \mathbf{P}_{k|k-1}), \quad (4.40)$$

where

$$\hat{\mathbf{x}}_{k|k} = \hat{\mathbf{x}}_{k|k-1} + \mathbf{K}_k \cdot [\mathbf{z}_k - \hat{\mathbf{z}}_{k|k-1}], \quad (4.41a)$$

$$\mathbf{P}_{k|k} = \mathbf{P}_{k|k-1} - \mathbf{K}_k \cdot \mathbf{P}_{zz,k|k-1} \cdot \mathbf{K}_k^\top, \quad (4.41b)$$

$$\mathbf{K}_k = \mathbf{P}_{xz,k|k-1} \cdot [\mathbf{P}_{zz,k|k-1}]^{-1}. \quad (4.41c)$$

A proof of this fact can be found in [BSLK01]. While  $\hat{\mathbf{x}}_{k|k-1}$  and  $\mathbf{P}_{k|k-1}$  are available from the time update, the predicted measurement  $\hat{\mathbf{z}}_{k|k-1}$ , the associated covariance  $\mathbf{P}_{zz,k|k-1}$  and the cross-covariance  $\mathbf{P}_{xz,k|k-1}$  have to be further evaluated. For measurement models of the form (2.50), these are given by

$$\hat{\mathbf{z}}_{k|k-1} = \int_{\mathbb{R}^{n_x}} \mathbf{h}_{\text{LOS},k}(\mathbf{x}_k) \cdot \mathcal{N}(\mathbf{x}_k; \hat{\mathbf{x}}_{k|k-1}, \mathbf{P}_{k|k-1}) d\mathbf{x}_k, \quad (4.42)$$

$$\mathbf{P}_{zz,k|k-1} = \int_{\mathbb{R}^{n_x}} (\mathbf{h}_{\text{LOS},k}(\mathbf{x}_k) - \hat{\mathbf{z}}_{k|k-1}) \cdot (\mathbf{h}_{\text{LOS},k}(\mathbf{x}_k) - \hat{\mathbf{z}}_{k|k-1})^\top \cdot \mathcal{N}(\mathbf{x}_k; \hat{\mathbf{x}}_{k|k-1}, \mathbf{P}_{k|k-1}) d\mathbf{x}_k + \mathbf{R}_{\text{LOS},k}, \quad (4.43)$$

$$\mathbf{P}_{xz,k|k-1} = \int_{\mathbb{R}^{n_x}} (\mathbf{x}_k - \hat{\mathbf{x}}_{k|k-1}) \cdot (\mathbf{h}_{\text{LOS},k}(\mathbf{x}_k) - \hat{\mathbf{z}}_{k|k-1})^\top \cdot \mathcal{N}(\mathbf{x}_k; \hat{\mathbf{x}}_{k|k-1}, \mathbf{P}_{k|k-1}) d\mathbf{x}_k. \quad (4.44)$$

The key idea in the UKF is now to approximate the multi-dimensional integrals in (4.42), (4.43) and (4.44) using the scaled unscented transformation [WvdM00, Jul02]. In the scaled unscented transformation, the prediction density  $p(\mathbf{x}_k|\mathbf{Z}_{k-1})$  is represented by  $2 \cdot n_x + 1$  sigma points  $\mathcal{X}_{k|k-1}^{(i)}$  and weights  $W^{(i)}$ , which are chosen according to the scheme given in (4.33). The sigma points are then transformed through the true nonlinear function according to

$$\mathcal{Z}_{k|k-1}^{(i)} = \mathbf{h}_{\text{LOS},k}(\mathcal{X}_{k|k-1}^{(i)}), \quad i = 0, \dots, 2 \cdot n_x. \quad (4.45)$$

Finally, estimates of  $\hat{\mathbf{z}}_{k|k-1}$ ,  $\mathbf{P}_{zz,k|k-1}$  and  $\mathbf{P}_{xz,k|k-1}$  can be determined from (4.35) and are given by

$$\hat{\mathbf{z}}_{k|k-1} \approx \sum_{i=0}^{2 \cdot n_x} W_m^{(i)} \cdot \mathcal{Z}_{k|k-1}^{(i)}, \quad (4.46)$$

$$\mathbf{P}_{zz,k|k-1} \approx \sum_{i=0}^{2 \cdot n_x} W_c^{(i)} \cdot (\mathcal{Z}_{k|k-1}^{(i)} - \hat{\mathbf{z}}_{k|k-1}) \cdot (\mathcal{Z}_{k|k-1}^{(i)} - \hat{\mathbf{z}}_{k|k-1})^\top + \mathbf{R}_{\text{LOS},k}, \quad (4.47)$$

$$\mathbf{P}_{xz,k|k-1} \approx \sum_{i=0}^{2 \cdot n_x} W_c^{(i)} \cdot (\mathcal{X}_{k|k-1}^{(i)} - \hat{\mathbf{x}}_{k|k-1}) \cdot (\mathcal{Z}_{k|k-1}^{(i)} - \hat{\mathbf{z}}_{k|k-1})^\top. \quad (4.48)$$

A pseudocode description of the UKF is given in Algorithm 4.2. Compared to the EKF the UKF does not require to evaluate Jacobian matrices, which is useful in cases, where no closed-form expression for  $\mathbf{h}_{\text{LOS},k}(\cdot)$  is available.



**Algorithm 4.2** Unscented Kalman Filter

---

```

1: // Initialization
2:  $\hat{\mathbf{x}}_{0|0} := \mathbb{E}\{\mathbf{x}_0\}$ 
3:  $\mathbf{P}_{0|0} := \mathbb{E}\{(\mathbf{x}_0 - \hat{\mathbf{x}}_{0|0})(\mathbf{x}_0 - \hat{\mathbf{x}}_{0|0})^\top\}$ 
4:  $\gamma := \alpha^2 \cdot (n_x + \beta_1) - n_x$ 
5:  $W_m^{(0)} := \gamma / (n_x + \gamma)$ 
6: for  $i = 1$  to  $n_x$  do
7:    $W_m^{(i)} := 1 / (2 \cdot (n_x + \gamma))$ 
8:    $W_c^{(0)} := W_m^{(0)} + (1 - \alpha^2 + \beta_2)$ 
9: end for
10: // Recursion
11: for  $k = 1$  to  $k_{\max}$  do
12:   // Time Update
13:    $\hat{\mathbf{x}}_{k|k-1} := \mathbf{F} \cdot \hat{\mathbf{x}}_{k-1|k-1}$ 
14:    $\mathbf{P}_{k|k-1} := \mathbf{F} \cdot \mathbf{P}_{k-1|k-1} \cdot \mathbf{F}^\top + \mathbf{\Gamma} \cdot \mathbf{Q} \cdot \mathbf{\Gamma}^\top$ 
15:   // Measurement Update
16:    $\mathcal{X}_{k|k-1}^{(0)} := \hat{\mathbf{x}}_{k|k-1}$ 
17:    $\mathcal{Z}_{k|k-1}^{(0)} := \mathbf{h}_{\text{LOS},k}(\mathcal{X}_{k|k-1}^{(0)})$ 
18:   for  $i = 1$  to  $n_x$  do
19:      $\mathcal{X}_{k|k-1}^{(i)} := \hat{\mathbf{x}}_{k|k-1} + (\sqrt{(n_x + \gamma) \cdot \mathbf{P}_{k|k-1}})_i$ 
20:      $\mathcal{X}_{k|k-1}^{(n_x+i)} := \hat{\mathbf{x}}_{k|k-1} - (\sqrt{(n_x + \gamma) \cdot \mathbf{P}_{k|k-1}})_i$ 
21:      $\mathcal{Z}_{k|k-1}^{(i)} := \mathbf{h}_{\text{LOS},k}(\mathcal{X}_{k|k-1}^{(i)})$ 
22:      $\mathcal{Z}_{k|k-1}^{(n_x+i)} := \mathbf{h}_{\text{LOS},k}(\mathcal{X}_{k|k-1}^{(n_x+i)})$ 
23:   end for
24:    $\hat{\mathbf{z}}_{k|k-1} := \sum_{i=0}^{2n_x} W_m^{(i)} \cdot \mathcal{Z}_{k|k-1}^{(i)}$ 
25:    $\mathbf{P}_{xz,k|k-1} := \sum_{i=0}^{2n_x} W_c^{(i)} \cdot (\mathcal{X}_{k|k-1}^{(i)} - \hat{\mathbf{x}}_{k|k-1}) \cdot (\mathcal{Z}_{k|k-1}^{(i)} - \hat{\mathbf{z}}_{k|k-1})^\top$ 
26:    $\mathbf{P}_{zz,k|k-1} := \sum_{i=0}^{2n_x} W_c^{(i)} \cdot (\mathcal{Z}_{k|k-1}^{(i)} - \hat{\mathbf{z}}_{k|k-1}) \cdot (\mathcal{Z}_{k|k-1}^{(i)} - \hat{\mathbf{z}}_{k|k-1})^\top + \mathbf{R}_{\text{LOS},k}$ 
27:    $\mathbf{K}_k := \mathbf{P}_{xz,k|k-1} \cdot [\mathbf{P}_{zz,k|k-1}]^{-1}$ 
28:    $\hat{\mathbf{x}}_{k|k} := \hat{\mathbf{x}}_{k|k-1} + \mathbf{K}_k \cdot [\mathbf{z}_{\text{LOS},k} - \hat{\mathbf{z}}_{k|k-1}]$ 
29:    $\mathbf{P}_{k|k} := \mathbf{P}_{k|k-1} - \mathbf{K}_k \cdot \mathbf{P}_{zz,k|k-1} \cdot \mathbf{K}_k^\top$ 
30: end for

```

---

**4.4.4 Cubature Kalman Filter**

The CKF is very similar to the UKF as it also calculates approximately the mean and covariances given in (4.46)-(4.48) by using a set of deterministically chosen sample points and weights. In the CKF, however, the sample points and weights result from

solving the multi-dimensional integrals in (4.42)-(4.44) with highly efficient numerical integration methods, which are known as cubature rules (see [AH09] for detailed derivations). One obtains a set of  $2 \cdot n_x$  cubature points and weights, from which the corresponding weighted mean and covariance can be computed. The set of cubature points and weights is very similar to the set of sigma points and weights of the UKF and can be determined from (4.33) by setting the parameters  $\alpha = 1$ ,  $\beta_1 = 0$  and  $\beta_2 = 0$ . The time update and the measurement update of the CKF for the hybrid localization problem is presented next.

### Time Update

The time update of the CKF is equivalent to the time update of the EKF and UKF, since the posterior pdf  $p(\mathbf{x}_k|\mathbf{Z}_k)$  is assumed Gaussian and the transitional pdf  $p(\mathbf{x}_k|\mathbf{x}_{k-1})$  is linear Gaussian. It follows, that

$$p(\mathbf{x}_k|\mathbf{Z}_{k-1}) \approx \mathcal{N}(\mathbf{x}_k; \hat{\mathbf{x}}_{k|k-1}, \mathbf{P}_{k|k-1}), \quad (4.49)$$

where  $\hat{\mathbf{x}}_{k|k-1}$  and  $\mathbf{P}_{k|k-1}$  are given in (4.27).

### Measurement Update

In the measurement update, the mean  $\hat{\mathbf{x}}_{k|k}$  and covariance  $\mathbf{P}_{k|k}$  of the Gaussian posterior pdf  $p(\mathbf{x}_k|\mathbf{Z}_k)$  is computed from (4.41). In [AH09], the mean  $\hat{\mathbf{z}}_{k|k-1}$  and the covariances  $\mathbf{P}_{zz,k|k-1}$  and  $\mathbf{P}_{xz,k|k-1}$  are given by

$$\hat{\mathbf{z}}_{k|k-1} = \int_{\mathbb{R}^{n_x}} \mathbf{h}_{\text{LOS},k}(\mathbf{x}_k) \cdot \mathcal{N}(\mathbf{x}_k; \hat{\mathbf{x}}_{k|k-1}, \mathbf{P}_{k|k-1}) d\mathbf{x}_k, \quad (4.50)$$

$$\begin{aligned} \mathbf{P}_{zz,k|k-1} &= \int_{\mathbb{R}^{n_x}} \mathbf{h}_{\text{LOS},k}(\mathbf{x}_k) \cdot \mathbf{h}_{\text{LOS},k}^\top(\mathbf{x}_k) \cdot \mathcal{N}(\mathbf{x}_k; \hat{\mathbf{x}}_{k|k-1}, \mathbf{P}_{k|k-1}) d\mathbf{x}_k \\ &\quad - \hat{\mathbf{z}}_{k|k-1} \cdot \hat{\mathbf{z}}_{k|k-1}^\top + \mathbf{R}_{\text{LOS},k}, \end{aligned} \quad (4.51)$$

$$\mathbf{P}_{xz,k|k-1} = \int_{\mathbb{R}^{n_x}} \mathbf{x}_k \cdot \mathbf{h}_{\text{LOS},k}^\top(\mathbf{x}_k) \cdot \mathcal{N}(\mathbf{x}_k; \hat{\mathbf{x}}_{k|k-1}, \mathbf{P}_{k|k-1}) d\mathbf{x}_k - \hat{\mathbf{x}}_{k|k-1} \cdot \hat{\mathbf{z}}_{k|k-1}^\top, \quad (4.52)$$

which is equivalent to (4.42)-(4.44). The multi-dimensional integrals are numerically approximated using cubature rules as described in [AH09], yielding

$$\hat{\mathbf{z}}_{k|k-1} \approx \frac{1}{2 \cdot n_x} \cdot \sum_{i=1}^{2 \cdot n_x} \mathcal{Z}_{k|k-1}^{(i)}, \quad (4.53)$$

$$\mathbf{P}_{zz,k|k-1} \approx \frac{1}{2 \cdot n_x} \cdot \sum_{i=1}^{2 \cdot n_x} \mathcal{Z}_{k|k-1}^{(i)} \cdot \mathcal{Z}_{k|k-1}^{(i)\top} - \hat{\mathbf{z}}_{k|k-1} \cdot \hat{\mathbf{z}}_{k|k-1}^\top + \mathbf{R}_{\text{LOS},k}, \quad (4.54)$$

$$\mathbf{P}_{xz,k|k-1} \approx \frac{1}{2 \cdot n_x} \cdot \sum_{i=1}^{2 \cdot n_x} \mathcal{X}_{k|k-1}^{(i)} \cdot \mathcal{Z}_{k|k-1}^{(i)\top} - \hat{\mathbf{x}}_{k|k-1} \cdot \hat{\mathbf{z}}_{k|k-1}^\top, \quad (4.55)$$

where  $\mathcal{Z}_{k|k-1}^{(i)}$  is defined in (4.45). A pseudocode description of the CKF is given in Table 4.3. Comparing the UKF and CKF with each other, it can be observed that the recursions are very similar, except that different sets of sample points and weights are used to approximate  $\hat{\mathbf{z}}_{k|k-1}$ ,  $\mathbf{P}_{zz,k|k-1}$  and  $\mathbf{P}_{xz,k|k-1}$ .

---

**Algorithm 4.3** Cubature Kalman Filter
 

---

```

1: // Initialization
2:  $\hat{\mathbf{x}}_{0|0} := \mathbb{E}\{\mathbf{x}_0\}$ 
3:  $\mathbf{P}_{0|0} := \mathbb{E}\{(\mathbf{x}_0 - \hat{\mathbf{x}}_{0|0})(\mathbf{x}_0 - \hat{\mathbf{x}}_{0|0})^\top\}$ 
4:  $W_m := 1/(2 \cdot n_x)$ 
5:  $W_c := W_m$ 
6:  $\Xi := \sqrt{n_x} \cdot [\mathbf{I}_{n_x}, -\mathbf{I}_{n_x}]$ 
7: // Recursion
8: for  $k = 1$  to  $k_{\max}$  do
9:   // Time Update
10:   $\hat{\mathbf{x}}_{k|k-1} := \mathbf{F} \cdot \hat{\mathbf{x}}_{k-1|k-1}$ 
11:   $\mathbf{P}_{k|k-1} := \mathbf{F} \cdot \mathbf{P}_{k-1|k-1} \cdot \mathbf{F}^\top + \Gamma \cdot \mathbf{Q} \cdot \Gamma^\top$ 
12:  // Measurement Update
13:   $\mathbf{S}_{k|k-1} := \sqrt{\mathbf{P}_{k|k-1}}$ 
14:  for  $i = 1$  to  $2 \cdot n_x$  do
15:     $\mathcal{X}_{k|k-1}^{(i)} := \hat{\mathbf{x}}_{k|k-1} + \mathbf{S}_{k|k-1} \cdot (\Xi)_i$ 
16:     $\mathcal{Z}_{k|k-1}^{(i)} := \mathbf{h}_{\text{LOS},k}(\mathcal{X}_{k|k-1}^{(i)})$ 
17:  end for
18:   $\hat{\mathbf{z}}_{k|k-1} := W_m \cdot \sum_{i=1}^{2n_x} \mathcal{Z}_{k|k-1}^{(i)}$ 
19:   $\mathbf{P}_{xz,k|k-1} := W_c \cdot \sum_{i=1}^{2n_x} \mathcal{X}_{k|k-1}^{(i)} \cdot \mathcal{Z}_{k|k-1}^{(i)} - \hat{\mathbf{x}}_{k|k-1} \cdot \hat{\mathbf{z}}_{k|k-1}^\top$ 
20:   $\mathbf{P}_{zz,k|k-1} := W_c \cdot \sum_{i=1}^{2n_x} \mathcal{Z}_{k|k-1}^{(i)} \cdot \mathcal{Z}_{k|k-1}^{(i)} - \hat{\mathbf{z}}_{k|k-1} \cdot \hat{\mathbf{z}}_{k|k-1}^\top + \mathbf{R}_{\text{LOS},k}$ 
21:   $\mathbf{K}_k := \mathbf{P}_{xz,k|k-1} \cdot [\mathbf{P}_{zz,k|k-1}]^{-1}$ 
22:   $\hat{\mathbf{x}}_{k|k} := \hat{\mathbf{x}}_{k|k-1} + \mathbf{K}_k \cdot [\mathbf{z}_{\text{LOS},k} - \hat{\mathbf{z}}_{k|k-1}]$ 
23:   $\mathbf{P}_{k|k} := \mathbf{P}_{k|k-1} - \mathbf{K}_k \cdot \mathbf{P}_{zz,k|k-1} \cdot \mathbf{K}_k^\top$ 
24: end for

```

---

## 4.5 Particle Filter-based Estimators

### 4.5.1 Introduction

In this section, PF-based estimators are proposed to solve the hybrid localization problem. PF-based estimators approximate the multi-dimensional integrals in the recursive Bayesian solution, cf. (4.1c) and (4.3c), using a Monte Carlo integration

technique, so that the posterior pdf  $p(\mathbf{x}_k|\mathbf{Z}_k)$  can be represented by a set of random samples (particles) with associated weights [GSS93]. It can be shown that the Monte Carlo approximation approaches the true posterior pdf and, thus, approaches the optimal recursive Bayesian solution, if the number of particles goes to infinity [dM04, HSL08]. In practice, however, an approximation is computed with a finite number of particles, due to the limited computational resources. The problem of using Monte Carlo integration techniques to recursive Bayesian estimation is degeneracy, i.e., after a certain number of recursive steps, all but one particle will have negligible weight [DGA00]. In order to overcome the degeneracy, the concept of resampling has been introduced, and the PF became useful in practice for the first time [GSS93]. Since then, several extensions and improvements have been proposed, see [DGA00, DdFG01, AMGC02, RAG04, CGM07, DJ09, Gus10a] for detailed surveys and tutorials on particle filtering. Compared to KF-based estimators, the PF-based estimators have the following advantageous properties:

- They can be applied to a very general class of nonlinear, non-Gaussian estimation problems
- They provide an approximation of the entire posterior pdf  $p(\mathbf{x}_k|\mathbf{Z}_k)$  and not only of its first two moments.
- It is very easy to incorporate hard constraints, e.g. road constraints or constraints on the MT velocity, into the PF.

However, since all PFs are based on the principle of Monte Carlo integration, the main disadvantage of using them is that they are orders of magnitudes computationally more complex than KF-based estimators. In the following, four different particle filter-based estimators are proposed to solve the hybrid localization problem. These are the PF as proposed in [GSS93], the Rao-Blackwellized Particle Filter (RBPF) [CL00, AD02, SGN05, Sch03], the Auxiliary Particle Filter (APF) [PS99, CCF99] and the recently proposed Rao-Blackwellized Auxiliary Particle Filter (RBAPF) [FSK09]. These filters can be applied to both scenarios with LOS and switching LOS/NLOS propagation conditions. In order to further improve the localization accuracy, road constraints have been incorporated into the PF and the RBPF. The novel contribution of this section is the application of the well-known PF, RBPF and APF to the hybrid localization problem. In addition to that a new filter, called the RBAPF is derived and applied to the hybrid localization problem. In Section 4.5.2 and 4.5.3, the PF and RBPF without road constraints are presented. In Section 4.5.4, the APF is described. In Section 4.5.5 the RBAPF is introduced. Finally, in Section 4.5.6 and 4.5.7, the road-constrained PF and RBPF are presented.

## 4.5.2 Particle Filter

### 4.5.2.1 Introduction

In this section, the PF is proposed as solution for the hybrid localization problem. The PF approximates the posterior pdf  $p(\mathbf{x}_k|\mathbf{Z}_k)$  with a discrete density, which can be obtained as follows: Let  $\delta(x)$  denote the Dirac delta function, which can be thought of as a function that is zero except at  $x = 0$  where it is infinite, and which has the following properties

$$\int_{-\infty}^{\infty} \delta(x) dx = 1, \quad \int_{-\infty}^{\infty} g(x) \cdot \delta(x - a) dx = g(a) \quad (4.56)$$

[Bra00]. The key idea is to rewrite the posterior pdf as follows

$$p(\mathbf{x}_k|\mathbf{Z}_k) = p(\mathbf{x}_k|\mathbf{Z}_k) \cdot \underbrace{\int_{\mathbb{R}^{n_x}} \delta(\mathbf{x}_k - \mathbf{x}'_k) d\mathbf{x}'_k}_{=1} = \int_{\mathbb{R}^{n_x}} \delta(\mathbf{x}_k - \mathbf{x}'_k) \cdot p(\mathbf{x}'_k|\mathbf{Z}_k) d\mathbf{x}'_k. \quad (4.57)$$

The trick is now to evaluate the above integral approximately using Monte Carlo integration, cf. Appendix A.10. Since, in most cases, the posterior pdf is known only up to a normalization constant, cf. (4.3c), direct sampling from the posterior pdf is often impossible. In these cases, samples are drawn from an importance density  $\mathbf{x}_k^{(i)} \sim q(\mathbf{x}_k|\mathbf{Z}_k)$ , which should be similar to the pdf  $p(\mathbf{x}_k|\mathbf{Z}_k)$ . Using this strategy, which is known as importance sampling, the posterior pdf can be approximated as follows

$$\begin{aligned} p(\mathbf{x}_k|\mathbf{Z}_k) &= \int_{\mathbb{R}^{n_x}} \delta(\mathbf{x}_k - \mathbf{x}'_k) \cdot \frac{p(\mathbf{x}'_k|\mathbf{Z}_k)}{q(\mathbf{x}'_k|\mathbf{Z}_k)} \cdot q(\mathbf{x}'_k|\mathbf{Z}_k) d\mathbf{x}'_k \\ &\approx \sum_{i=1}^N w_{k|k}^{(i)} \cdot \delta(\mathbf{x}_k - \mathbf{x}_k^{(i)}), \end{aligned} \quad (4.58)$$

where the normalized importance weights are defined as

$$w_{k|k}^{(i)} = \frac{\tilde{w}_{k|k}^{(i)}}{\sum_{j=1}^N \tilde{w}_{k|k}^{(j)}}, \quad \text{with} \quad \tilde{w}_{k|k}^{(i)} = \frac{p(\mathbf{x}_k^{(i)}|\mathbf{Z}_k)}{q(\mathbf{x}_k^{(i)}|\mathbf{Z}_k)} \quad (4.59)$$

[RAG04]. In the following, it is shown, how the concept of importance sampling can be applied to the optimal recursive Bayesian solution given by (4.1c) and (4.3c).

### 4.5.2.2 Derivations

In this section, the PF for hybrid localization is derived. In the literature, it is common to derive the PF from the pdf of the state trajectory  $p(\mathbf{X}_k|\mathbf{Z}_k)$  and then to discard the path  $\mathbf{X}_{k-1}$  to arrive at the desired posterior pdf of the current state  $p(\mathbf{x}_k|\mathbf{Z}_k)$  [DGA00,RAG04,Sch03]. In this work, the PF is derived from the posterior pdf  $p(\mathbf{x}_k|\mathbf{Z}_k)$  which is similar to the derivation given in [Tör08].

## Initialization

The PF is initialized by sampling  $N$  particles from the initial distribution  $p(\mathbf{x}_0)$  according to

$$\mathbf{x}_0^{(i)} \sim p(\mathbf{x}_0), \quad (4.60)$$

with corresponding weights  $w_{0|0}^{(i)}$  for  $i = 1, \dots, N$ . As a result, the initial pdf can be approximated with

$$p(\mathbf{x}_0) \approx \sum_{i=1}^N w_{0|0}^{(i)} \cdot \delta(\mathbf{x}_0 - \mathbf{x}_0^{(i)}). \quad (4.61)$$

## Time Update

In the time update, the Chapman-Kolmogorov equation (4.1c) has to be evaluated. Suppose that at time  $k - 1$ , a weighted discrete approximation of  $p(\mathbf{x}_{k-1}|\mathbf{Z}_{k-1})$  is available. This yields

$$\begin{aligned} p(\mathbf{x}_k|\mathbf{Z}_{k-1}) &= \int_{\mathbb{R}^{n_x}} p(\mathbf{x}_k|\mathbf{x}_{k-1}) \cdot p(\mathbf{x}_{k-1}|\mathbf{Z}_{k-1}) \, d\mathbf{x}_{k-1} \\ &\approx \int_{\mathbb{R}^{n_x}} p(\mathbf{x}_k|\mathbf{x}_{k-1}) \cdot \sum_{i=1}^N w_{k-1|k-1}^{(i)} \cdot \delta(\mathbf{x}_{k-1} - \mathbf{x}_{k-1}^{(i)}) \, d\mathbf{x}_{k-1} \\ &= \sum_{i=1}^N w_{k-1|k-1}^{(i)} \cdot p(\mathbf{x}_k|\mathbf{x}_{k-1}^{(i)}), \end{aligned} \quad (4.62)$$

where the last equality follows from (4.56). The prediction pdf in (4.62) is continuous with respect to  $\mathbf{x}_k$  and is composed of a weighted sum of  $N$  transitional pdfs. In the following, a weighted discrete approximation of  $p(\mathbf{x}_k|\mathbf{Z}_{k-1})$  is obtained using an importance sampling approach. In the PF, the key idea is to represent each component of the weighted sum by a single particle that is sampled from the following importance density

$$\mathbf{x}_k^{(i)} \sim q(\mathbf{x}_k|\mathbf{x}_{k-1}^{(i)}, \mathbf{z}_k), \quad i = 1, \dots, N, \quad (4.63)$$

where the latest measurement  $\mathbf{z}_k$  is taken into account in the importance density as this can improve the numerical properties of the PF [Dou98]. As a result, the prediction pdf can be approximated as

$$p(\mathbf{x}_k|\mathbf{Z}_{k-1}) \approx \sum_{i=1}^N w_{k|k-1}^{(i)} \cdot \delta(\mathbf{x}_k - \mathbf{x}_k^{(i)}), \quad (4.64)$$

where the unnormalized importance weights are given by

$$w_{k|k-1}^{(i)} \propto w_{k-1|k-1}^{(i)} \cdot \frac{p(\mathbf{x}_k^{(i)} | \mathbf{x}_{k-1}^{(i)})}{q(\mathbf{x}_k^{(i)} | \mathbf{x}_{k-1}^{(i)}, \mathbf{z}_k)}, \quad i = 1, \dots, N, \quad (4.65)$$

and “ $\propto$ ” denotes the proportionality operator. The importance weights have to be further normalized to ensure  $\sum_{j=1}^N w_{k|k-1}^{(j)} = 1$ .

### Measurement Update

In the measurement update, the posterior pdf  $p(\mathbf{x}_k | \mathbf{Z}_k)$  is updated according to (4.3c). Insertion of (4.64) into (4.3c) gives a weighted discrete approximation of the posterior pdf. Since this approximation is numerically normed, a calculation of the denominator in (4.3c) is not needed, yielding

$$\begin{aligned} p(\mathbf{x}_k | \mathbf{Z}_k) &= \frac{p(\mathbf{z}_k | \mathbf{x}_k) \cdot p(\mathbf{x}_k | \mathbf{Z}_{k-1})}{p(\mathbf{z}_k | \mathbf{Z}_{k-1})} \propto p(\mathbf{z}_k | \mathbf{x}_k) \cdot p(\mathbf{x}_k | \mathbf{Z}_{k-1}) \\ &\approx \sum_{i=1}^N w_{k|k-1}^{(i)} \cdot p(\mathbf{z}_k | \mathbf{x}_k^{(i)}) \cdot \delta(\mathbf{x}_k - \mathbf{x}_k^{(i)}) \\ &= \sum_{i=1}^N w_{k|k}^{(i)} \cdot \delta(\mathbf{x}_k - \mathbf{x}_k^{(i)}), \end{aligned} \quad (4.66)$$

where the normalized importance weights are given by

$$w_{k|k}^{(i)} = \frac{w_{k|k-1}^{(i)} \cdot p(\mathbf{z}_k | \mathbf{x}_k^{(i)})}{\sum_{j=1}^N w_{k|k-1}^{(j)} \cdot p(\mathbf{z}_k | \mathbf{x}_k^{(j)})}, \quad i = 1, \dots, N. \quad (4.67)$$

The PF recursion is now complete and consists of the recursive propagation of particles  $\mathbf{x}_k^{(i)}$  and importance weights  $w_{k|k}^{(i)}$  according to (4.63), (4.65) and (4.67). However, it has been shown in [DGA00] that the sequential application of importance sampling leads to the degeneracy problem, i.e., after a certain number of recursions, all but one particle will have close to zero importance weights. In order to overcome the degeneracy, the concept of resampling has been introduced in the PF.

### Estimation

The PF provides a discrete approximation of the posterior pdf according to (4.66), from which standard measures such as the MMSE  $\hat{\mathbf{x}}_{\text{MMSE},k|k}$  and its covariance  $\mathbf{P}_{\text{MMSE},k|k}$

can be computed [Sch03]. Numerical approximations of these quantities are given by

$$\hat{\mathbf{x}}_{\text{MMSE},k|k} \approx \sum_{i=1}^N w_{k|k}^{(i)} \cdot \mathbf{x}_k^{(i)}, \quad (4.68a)$$

$$\mathbf{P}_{\text{MMSE},k|k} \approx \sum_{i=1}^N w_{k|k}^{(i)} \cdot (\mathbf{x}_k^{(i)} - \hat{\mathbf{x}}_{\text{MMSE},k|k})(\mathbf{x}_k^{(i)} - \hat{\mathbf{x}}_{\text{MMSE},k|k})^\top. \quad (4.68b)$$

## Resampling

Particle filters with importance densities of the form (4.63) suffer from the degeneracy of particles. The resampling step was therefore included in the PF to solve this problem [GSS93]. The idea of resampling is to multiply particles with high importance weights and to discard particles having low importance weights. This can be done by drawing samples from the discrete approximation of  $p(\mathbf{x}_k|\mathbf{Z}_k)$  as follows: Take  $N$  samples from the set  $\{\mathbf{x}_k^{(i)}\}_{i=1}^N$ , where the probability to take sample  $i$  is given by  $w_{k|k}^{(i)}$ . Afterwards, replace the old weights with uniform weights. Until now, several resampling algorithms have been proposed that efficiently implement the above described procedure, see e.g. [DC05, HSG06] for a detailed description and comparison of different resampling algorithms. In this work, systematic resampling is used which is summarized in Algorithm 4.4 [CCF99, RAG04]. This algorithm also stores the index of the resampled parent particle, denoted as  $i^{(j)}$  or equivalently  $i^j$ , which is needed in the APF and RBAPF algorithms.

### 4.5.2.3 Choice of Importance Density

In the design of PFs, the choice of the importance density  $q(\mathbf{x}_k|\mathbf{x}_{k-1}^{(i)}, \mathbf{z}_k)$  plays a major role. The optimal importance density that minimizes the variance of the importance weights is given by  $q(\mathbf{x}_k|\mathbf{x}_{k-1}^{(i)}, \mathbf{z}_k)_{\text{opt}} = p(\mathbf{x}_k|\mathbf{x}_{k-1}^{(i)}, \mathbf{z}_k)$  [DGA00, RAG04]. However, for the hybrid localization problem, a closed-form expression for this density does not exist, so that one has resort to suboptimal importance densities. For the hybrid localization problem, the transitional pdf, cf. (3.14), is chosen as importance density, i.e.,

$$q(\mathbf{x}_k|\mathbf{x}_{k-1}^{(i)}, \mathbf{z}_k) = p(\mathbf{x}_k|\mathbf{x}_{k-1}^{(i)}), \quad (4.69)$$

which is the most popular suboptimal choice. In this case, the weights in the time update are given by  $w_{k|k-1}^{(i)} = w_{k-1|k-1}^{(i)}$ , cf. (4.65), and the weights in the measurement update simplify to

$$w_{k|k}^{(i)} = \frac{w_{k-1|k-1}^{(i)} \cdot p(\mathbf{z}_k|\mathbf{x}_k^{(i)})}{\sum_{j=1}^N w_{k-1|k-1}^{(j)} \cdot p(\mathbf{z}_k|\mathbf{x}_k^{(j)})}, \quad i = 1, \dots, N. \quad (4.70)$$



---

**Algorithm 4.4** Systematic Resampling

---

**Input:**  $\{\tilde{\mathbf{x}}_k^{(i)}, \tilde{w}_{k|k}^{(i)}\}_{i=1}^N$ **Output:**  $\{\mathbf{x}_k^{(j)}, w_{k|k}^{(j)}\}_{j=1}^N$ 

```

1:  $c_1 := \tilde{w}_{k|k}^{(1)}$ 
2: for  $i = 2$  to  $N$  do
3:    $c_i := c_{i-1} + \tilde{w}_{k|k}^{(i)}$ 
4: end for
5:  $i := 1$ 
6:  $u_1 \sim \mathcal{U}[0, N^{-1}]$ 
7: for  $j = 1$  to  $N$  do
8:    $u_j := u_1 + N^{-1} \cdot (j - 1)$ 
9:   while  $u_j > c_i$  do
10:     $i := i + 1$ 
11:   end while
12:    $\mathbf{x}_k^{(j)} := \tilde{\mathbf{x}}_k^{(i)}$ 
13:    $w_{k|k}^{(j)} := N^{-1}$ 
14:    $i^j := i$ 
15: end for

```

---

A pseudocode description of the PF for the hybrid localization is given in Algorithm 4.5. For the sake of clarity, a different notation for the description of the algorithm is used. The algorithm can be used for the scenario with LOS propagation conditions as well as for the scenario, where the propagation conditions switch between LOS and NLOS. The only difference is that the likelihood pdf  $p(\mathbf{z}_k|\mathbf{x}_k)$  for the former is given by (3.64) and for the latter is given by (3.83).

---

**Algorithm 4.5** Particle Filter
 

---

1. Initialization:

- For  $i = 1, \dots, N$ , initialize the particles  $\mathbf{x}_0^{(i)} \sim p(\mathbf{x}_0)$  and weights  $w_{0|0}^{(i)} = \frac{1}{N}$ .

2. Time Update:

- For  $i = 1, \dots, N$ , draw particles from the importance density according to

$$\mathbf{x}_k^{(i)} \sim p(\mathbf{x}_k | \mathbf{x}_{k-1}^{(i)}).$$

3. Measurement Update:

- For  $i = 1, \dots, N$ , evaluate the weights

$$w_{k|k}^{(i)} = \frac{w_{k-1|k-1}^{(i)} \cdot p(\mathbf{z}_k | \mathbf{x}_k^{(i)})}{\sum_{j=1}^N w_{k-1|k-1}^{(j)} \cdot p(\mathbf{z}_k | \mathbf{x}_k^{(j)})}.$$

4. Estimation:

- Determine an estimate of the state vector according to

$$\hat{\mathbf{x}}_k = \sum_{i=1}^N w_{k|k}^{(i)} \cdot \mathbf{x}_k^{(i)}.$$

5. Resampling:

- Perform systematic resampling using Algorithm 4.4. Take  $N$  samples with replacement from the set  $\{\mathbf{x}_k^{(i)}\}_{i=1}^N$ , where the probability to take sample  $i$  is  $w_{k|k}^{(i)}$ . Set  $w_{k|k}^{(i)} = \frac{1}{N}$  for  $i = 1, \dots, N$ .

6. Set  $k := k + 1$  and iterate from step 2.

---

### 4.5.3 Rao-Blackwellized Particle Filter

#### 4.5.3.1 Introduction

In state estimation problems, where the dimension of the state vector  $\mathbf{x}_k$  is high, the PF requires a large number of particles to obtain a good approximation of the posterior pdf  $p(\mathbf{x}_k | \mathbf{Z}_k)$  [DH03, Dau05]. In order to overcome this problem, a technique called

Rao-Blackwellization can be applied to PFs [CR96, CL00, AD02, SGN05, Sch03]. The RBPF exploits linear substructures in the state and measurement model equations, cf. Sections 2.3.2 and 2.3.3, so that the state space can be partitioned into two parts according to

$$\mathbf{x}_k = \begin{bmatrix} \mathbf{x}_k^n \\ \mathbf{x}_k^l \end{bmatrix}, \quad (4.71)$$

where  $\mathbf{x}_k^n$  denotes the vector of states with dimension  $n_{x_n}$  that enter nonlinearly into the model equations and  $\mathbf{x}_k^l$  denotes the vector of states with dimension  $n_{x_l}$  that enter linearly into the model equations. The resulting joint posterior pdf can be partitioned into two pdfs using Bayes' rule as follows

$$p(\mathbf{x}_k^n, \mathbf{x}_k^l | \mathbf{Z}_k) = p(\mathbf{x}_k^l | \mathbf{x}_k^n, \mathbf{Z}_k) \cdot p(\mathbf{x}_k^n | \mathbf{Z}_k). \quad (4.72)$$

The first pdf  $p(\mathbf{x}_k^l | \mathbf{x}_k^n, \mathbf{Z}_k)$  can be evaluated analytically using a KF, if the models are linear given the states  $\mathbf{x}_k^n$ , while the second pdf  $p(\mathbf{x}_k^n | \mathbf{Z}_k)$  is approximated using a PF. Since the dimension of the state  $\mathbf{x}_k^n$  is smaller than the dimension of the state  $\mathbf{x}_k$ , the RBPF generally requires fewer particles to obtain a good approximation of the posterior pdf  $p(\mathbf{x}_k | \mathbf{Z}_k)$ . This fact is proven theoretically in [DGK99], where it is shown that the variance of the state estimates provided by the RBPF is smaller than or equal to the variance of the state estimates provided by the standard PF. The RBPF has been extensively treated in the literature [CL00, AD02], and often is referred to as the marginalized particle filter [SGN05, Sch03].

#### 4.5.3.2 Derivations

In order to exploit the idea of Rao-Blackwellization in the PF for the hybrid localization problem, the following conditional linear system model is introduced:

$$\mathbf{x}_k^n = \mathbf{f}_{k-1}^n(\mathbf{x}_{k-1}^n) + \mathbf{F}_{k-1}^n(\mathbf{x}_{k-1}^n) \cdot \mathbf{x}_{k-1}^l + \mathbf{\Gamma}_{k-1}^n(\mathbf{x}_{k-1}^n) \cdot \mathbf{w}_{k-1}^n, \quad (4.73a)$$

$$\mathbf{x}_k^l = \mathbf{f}_{k-1}^l(\mathbf{x}_{k-1}^l) + \mathbf{F}_{k-1}^l(\mathbf{x}_{k-1}^l) \cdot \mathbf{x}_{k-1}^l + \mathbf{\Gamma}_{k-1}^l(\mathbf{x}_{k-1}^l) \cdot \mathbf{w}_{k-1}^l, \quad (4.73b)$$

$$\mathbf{z}_{1,k} = \mathbf{h}_{1,k}(\mathbf{x}_k^n) + \mathbf{H}_k(\mathbf{x}_k^n) \cdot \mathbf{x}_k^l + \mathbf{v}_{1,k}, \quad (4.73c)$$

$$\mathbf{z}_{2,k} = \mathbf{h}_{2,k}(\mathbf{x}_k^n, \mathbf{v}_{2,k}), \quad (4.73d)$$

where the measurement vector  $\mathbf{z}_k = [\mathbf{z}_{1,k}^\top, \mathbf{z}_{2,k}^\top]^\top$  is split into two statistically independent parts,  $\mathbf{f}_{k-1}^n(\cdot)$ ,  $\mathbf{f}_{k-1}^l(\cdot)$ ,  $\mathbf{h}_{1,k}(\cdot)$ ,  $\mathbf{h}_{2,k}(\cdot)$  are vector functions and  $\mathbf{F}_{k-1}^n(\cdot)$ ,  $\mathbf{F}_{k-1}^l(\cdot)$ ,  $\mathbf{\Gamma}_{k-1}^n(\cdot)$ ,  $\mathbf{\Gamma}_{k-1}^l(\cdot)$ ,  $\mathbf{H}_k(\cdot)$  are matrices of appropriate dimensions. The noises in the state and measurement models are denoted by  $\mathbf{w}_{k-1}^n$ ,  $\mathbf{w}_{k-1}^l$ ,  $\mathbf{v}_{1,k}$  and  $\mathbf{v}_{2,k}$  and are assumed to be white. In contrast to the approach presented in [SGN05, Sch03], a second measurement model, cf. (4.73d) is introduced, where the pdf of  $\mathbf{v}_{2,k}$  can be arbitrary and

$\mathbf{h}_{2,k}(\cdot)$  is any nonlinear function. The only restriction to (4.73d) is, that the model is independent of the linear state  $\mathbf{x}_k^1$  and that the corresponding likelihood pdf  $p(\mathbf{z}_{2,k}|\mathbf{x}_k^n)$  is available. The noise vectors  $[\mathbf{w}_{k-1}^{n,\top}, \mathbf{w}_{k-1}^{1,\top}]^\top$  and  $\mathbf{v}_{1,k}$  of dimensions  $n_w = n_{w_n} + n_{w_1}$  and  $n_{v,1}$  are assumed to be zero-mean Gaussian distributed according to

$$\begin{bmatrix} \mathbf{w}_{k-1}^n \\ \mathbf{w}_{k-1}^1 \end{bmatrix} \sim \mathcal{N}\left(\mathbf{0}_{n_w \times 1}, \begin{bmatrix} \mathbf{Q}_{k-1}^n & \mathbf{Q}_{k-1}^{n1} \\ \mathbf{Q}_{k-1}^{n1,\top} & \mathbf{Q}_{k-1}^1 \end{bmatrix}\right), \quad \mathbf{v}_{1,k} \sim \mathcal{N}(\mathbf{0}_{n_{v,1} \times 1}, \mathbf{R}_{1,k}). \quad (4.74)$$

Furthermore, it is assumed that  $\mathbf{x}_0^n$  and  $\mathbf{x}_0^1$  are white. The pdf of  $\mathbf{x}_0^n$  is arbitrary, but has to be known, and the pdf of  $\mathbf{x}_0^1$  is assumed Gaussian

$$\mathbf{x}_0^1 \sim \mathcal{N}(\hat{\mathbf{x}}_0^1, \mathbf{P}_0). \quad (4.75)$$

In order to derive the RBPF from the model given in (4.73), the two noise processes  $\mathbf{w}_{k-1}^n$  and  $\mathbf{w}_{k-1}^1$  have to be decorrelated using a Gram-Schmidt procedure, see [Sch03] for detailed derivations. The decorrelated system can be written as

$$\mathbf{x}_k^n = \mathbf{f}_{k-1}^n(\mathbf{x}_{k-1}^n) + \mathbf{F}_{k-1}^n(\mathbf{x}_{k-1}^n) \cdot \mathbf{x}_{k-1}^1 + \mathbf{\Gamma}_{k-1}^n(\mathbf{x}_{k-1}^n) \cdot \mathbf{w}_{k-1}^n, \quad (4.76a)$$

$$\mathbf{x}_k^1 = \mathbf{f}_{k-1}^1(\mathbf{x}_{k-1}^1) + \bar{\mathbf{F}}_{k-1}^1(\mathbf{x}_{k-1}^1) \cdot \mathbf{x}_{k-1}^1 + \bar{\mathbf{E}}_k(\mathbf{x}_k^n, \mathbf{x}_{k-1}^n) + \mathbf{\Gamma}_{k-1}^1(\mathbf{x}_{k-1}^1) \cdot \bar{\mathbf{w}}_{k-1}^1, \quad (4.76b)$$

$$\mathbf{z}_{1,k} = \mathbf{h}_{1,k}(\mathbf{x}_k^n) + \mathbf{H}_k(\mathbf{x}_k^n) \cdot \mathbf{x}_k^1 + \mathbf{v}_{1,k}, \quad (4.76c)$$

$$\mathbf{z}_{2,k} = \mathbf{h}_{2,k}(\mathbf{x}_k^n, \mathbf{v}_{2,k}), \quad (4.76d)$$

where

$$\bar{\mathbf{F}}_{k-1}^1(\mathbf{x}_{k-1}^1) = \mathbf{F}_{k-1}^1(\mathbf{x}_{k-1}^1) - \mathbf{\Gamma}_{k-1}^1(\mathbf{x}_{k-1}^1) \cdot \mathbf{Q}_{k-1}^{n1,\top} \cdot [\mathbf{\Gamma}_{k-1}^n(\mathbf{x}_{k-1}^n) \cdot \mathbf{Q}_{k-1}^n]^{-1} \cdot \mathbf{F}_{k-1}^n(\mathbf{x}_{k-1}^n), \quad (4.77a)$$

$$\bar{\mathbf{E}}_k(\mathbf{x}_k^n, \mathbf{x}_{k-1}^1) = \mathbf{\Gamma}_{k-1}^1(\mathbf{x}_{k-1}^1) \cdot \mathbf{Q}_{k-1}^{n1,\top} \cdot [\mathbf{\Gamma}_{k-1}^n(\mathbf{x}_{k-1}^n) \cdot \mathbf{Q}_{k-1}^n]^{-1} \cdot [\mathbf{x}_k^n - \mathbf{f}_{k-1}^n(\mathbf{x}_{k-1}^n)]. \quad (4.77b)$$

The noises  $\mathbf{w}_{k-1}^n$  and  $\bar{\mathbf{w}}_{k-1}^1$  are now uncorrelated and distributed according to

$$\begin{bmatrix} \mathbf{w}_{k-1}^n \\ \bar{\mathbf{w}}_{k-1}^1 \end{bmatrix} \sim \mathcal{N}(\mathbf{0}_{n_w \times 1}, \underbrace{\bar{\mathbf{Q}}_{k-1} = \text{diag}_{\text{gb}}[\mathbf{Q}_{k-1}^n, \mathbf{Q}_{k-1}^1 - \mathbf{Q}_{k-1}^{n1,\top} \cdot [\mathbf{Q}_{k-1}^n]^{-1} \cdot \mathbf{Q}_{k-1}^1]}_{\bar{\mathbf{Q}}_{k-1}^1}). \quad (4.78)$$

In order to simplify the notation, the following abbreviations are introduced

$$\begin{aligned} \mathbf{f}_{k-1}(\mathbf{x}_{k-1}^n) &= \begin{bmatrix} \mathbf{f}_{k-1}^n(\mathbf{x}_{k-1}^n) \\ \mathbf{f}_{k-1}^1(\mathbf{x}_{k-1}^1) \end{bmatrix}, \quad \mathbf{F}_{k-1} = \begin{bmatrix} \mathbf{F}_{k-1}^n(\mathbf{x}_{k-1}^n) \\ \bar{\mathbf{F}}_{k-1}^1(\mathbf{x}_{k-1}^1) \end{bmatrix}, \quad \mathbf{w}_{k-1} = \begin{bmatrix} \mathbf{w}_{k-1}^n \\ \bar{\mathbf{w}}_{k-1}^1 \end{bmatrix}, \\ \mathbf{E}_k(\mathbf{x}_k^n, \mathbf{x}_{k-1}^1) &= \begin{bmatrix} \mathbf{0}_{n_{x_n} \times 1} \\ \bar{\mathbf{E}}_k(\mathbf{x}_k^n, \mathbf{x}_{k-1}^1) \end{bmatrix}, \quad \mathbf{\Gamma}_{k-1} = \text{diag}_{\text{gb}}[\mathbf{\Gamma}_{k-1}^n(\mathbf{x}_{k-1}^n), \mathbf{\Gamma}_{k-1}^1(\mathbf{x}_{k-1}^1)]. \end{aligned}$$

Thus, the state model, cf. (4.76a) and (4.76b), can be written as

$$\mathbf{x}_k = \begin{bmatrix} \mathbf{x}_k^n \\ \mathbf{x}_k^1 \end{bmatrix} = \mathbf{f}_{k-1}(\mathbf{x}_{k-1}^n) + \mathbf{F}_{k-1} \cdot \mathbf{x}_{k-1}^1 + \mathbf{E}_k(\mathbf{x}_k^n, \mathbf{x}_{k-1}^1) + \mathbf{\Gamma}_{k-1} \cdot \mathbf{w}_{k-1}. \quad (4.79)$$

In the following, the RBPF is derived for the model given by (4.76). The derivation is based on the joint posterior pdf  $p(\mathbf{x}_k^n, \mathbf{x}_k^1 | \mathbf{Z}_k)$  and is similar to the derivation given in [Tör08].

## Initialization

The RBPF is initialized as follows:

$$p(\mathbf{x}_{k-1}^n, \mathbf{x}_{k-1}^l | \mathbf{Z}_{k-1}) \approx \sum_{i=1}^N w_{k-1|k-1}^{(i)} \cdot \mathcal{N}(\mathbf{x}_{k-1}^l; \mathbf{x}_{k-1|k-1}^{l,(i)}, \mathbf{P}_{k-1|k-1}^{(i)}) \cdot \delta(\mathbf{x}_{k-1}^n - \mathbf{x}_{k-1}^{n,(i)}). \quad (4.80)$$

## Time Update

The time update starts with evaluating the prediction density of the state at time  $k$  via the Chapman-Kolmogorov equation, cf. (4.1c):

$$\begin{aligned} p(\mathbf{x}_k^n, \mathbf{x}_k^l | \mathbf{Z}_{k-1}) &= \int_{\mathbb{R}^{n_{x_n}}} \int_{\mathbb{R}^{n_{x_1}}} p(\mathbf{x}_k^n, \mathbf{x}_k^l | \mathbf{x}_{k-1}^n, \mathbf{x}_{k-1}^l) \cdot \underbrace{p(\mathbf{x}_{k-1}^n, \mathbf{x}_{k-1}^l | \mathbf{Z}_{k-1})}_{(4.80)} d\mathbf{x}_{k-1}^n d\mathbf{x}_{k-1}^l \\ &\approx \sum_{i=1}^N w_{k-1|k-1}^{(i)} \\ &\quad \cdot \int_{\mathbb{R}^{n_{x_1}}} p(\mathbf{x}_k^n, \mathbf{x}_k^l | \mathbf{x}_{k-1}^{n,(i)}, \mathbf{x}_{k-1}^{l,(i)}) \cdot \mathcal{N}(\mathbf{x}_{k-1}^l; \mathbf{x}_{k-1|k-1}^{l,(i)}, \mathbf{P}_{k-1|k-1}^{(i)}) d\mathbf{x}_{k-1}^l. \end{aligned} \quad (4.81)$$

Due to the fact that the dynamic model, cf. (4.79), is conditional linear and the error is Gaussian distributed, the pdf  $p(\mathbf{x}_k^n, \mathbf{x}_k^l | \mathbf{x}_{k-1}^{n,(i)}, \mathbf{x}_{k-1}^{l,(i)})$  is also Gaussian

$$\begin{aligned} p(\mathbf{x}_k^n, \mathbf{x}_k^l | \mathbf{x}_{k-1}^{n,(i)}, \mathbf{x}_{k-1}^{l,(i)}) &= \mathcal{N}(\mathbf{x}_k; \mathbf{f}_{k-1}(\mathbf{x}_{k-1}^{n,(i)}) + \mathbf{F}_{k-1}^{(i)} \cdot \mathbf{x}_{k-1}^{l,(i)} + \mathbf{E}_k(\mathbf{x}_k^n, \mathbf{x}_{k-1}^{n,(i)}), \\ &\quad \mathbf{\Gamma}_{k-1}^{(i)} \cdot \bar{\mathbf{Q}}_{k-1} \cdot \mathbf{\Gamma}_{k-1}^{(i),\top}). \end{aligned} \quad (4.82)$$

The integral in (4.81) can be evaluated analytically since the integrand is a product of Gaussian densities. From this it follows, that an approximation of the prediction density is given by a weighted sum of Gaussian densities

$$p(\mathbf{x}_k^n, \mathbf{x}_k^l | \mathbf{Z}_{k-1}) \approx \sum_{i=1}^N w_{k-1|k-1}^{(i)} \cdot \mathcal{N}(\mathbf{x}_k; \bar{\mathbf{x}}_{k|k-1}^{(i)}, \bar{\mathbf{P}}_{k|k-1}^{(i)}), \quad (4.83)$$

where

$$\bar{\mathbf{x}}_{k|k-1}^{(i)} = \mathbf{f}_{k-1}(\mathbf{x}_{k-1}^{n,(i)}) + \mathbf{F}_{k-1}^{(i)} \cdot \mathbf{x}_{k-1|k-1}^{l,(i)} + \mathbf{E}_k(\mathbf{x}_k^n, \mathbf{x}_{k-1}^{n,(i)}), \quad (4.84a)$$

$$\bar{\mathbf{P}}_{k|k-1}^{(i)} = \mathbf{F}_{k-1}^{(i)} \cdot \mathbf{P}_{k-1|k-1}^{(i)} \cdot \mathbf{F}_{k-1}^{(i),\top} + \mathbf{\Gamma}_{k-1}^{(i)} \cdot \bar{\mathbf{Q}}_{k-1} \cdot \mathbf{\Gamma}_{k-1}^{(i),\top}. \quad (4.84b)$$

Note that (4.84) is similar to the KF time update. A proof of (4.84) can be found in [Sch03]. Unfortunately, the Gaussian mixture distribution is continuous in the linear and nonlinear part. In order to obtain a discrete weighted approximation of the

nonlinear part, the Gaussian pdfs in (4.83) have to be split into two parts. The mean vector and error covariance matrix can be split as follows:

$$\bar{\mathbf{x}}_{k|k-1}^{(i)} = \begin{bmatrix} \bar{\mathbf{x}}_{k|k-1}^{\text{n},(i)} \\ \bar{\mathbf{x}}_{k|k-1}^{\text{l},(i)} \\ \bar{\mathbf{x}}_{k|k-1}^{\text{n},(i)} \end{bmatrix}, \quad \bar{\mathbf{P}}_{k|k-1}^{(i)} = \begin{bmatrix} \bar{\mathbf{P}}_{k|k-1}^{\text{n},(i)} & \bar{\mathbf{P}}_{k|k-1}^{\text{nl},(i)} \\ \bar{\mathbf{P}}_{k|k-1}^{\text{nl},(i),\text{T}} & \bar{\mathbf{P}}_{k|k-1}^{\text{l},(i)} \end{bmatrix}. \quad (4.85)$$

It is well known [BSLK01], that a Gaussian density, with mean and covariance as given in (4.85), can be split into two parts according to

$$\mathcal{N}(\mathbf{x}_k; \bar{\mathbf{x}}_{k|k-1}^{(i)}, \bar{\mathbf{P}}_{k|k-1}^{(i)}) = \mathcal{N}(\mathbf{x}_k^{\text{l}}; \bar{\mathbf{x}}_{k|k-1}^{\text{l},(i)}, \bar{\mathbf{P}}_{k|k-1}^{\text{l},(i)}) \cdot \mathcal{N}(\mathbf{x}_k^{\text{n}}; \bar{\mathbf{x}}_{k|k-1}^{\text{n},(i)}, \bar{\mathbf{P}}_{k|k-1}^{\text{n},(i)}), \quad (4.86)$$

where

$$\bar{\mathbf{x}}_{k|k-1}^{\text{l},(i)} = \bar{\mathbf{x}}_{k|k-1}^{\text{l},(i)} + \bar{\mathbf{P}}_{k|k-1}^{\text{nl},(i),\text{T}} \cdot [\bar{\mathbf{P}}_{k|k-1}^{\text{n},(i)}]^{-1} \cdot (\mathbf{x}_k^{\text{n}} - \bar{\mathbf{x}}_{k|k-1}^{\text{n},(i)}), \quad (4.87\text{a})$$

$$\bar{\mathbf{P}}_{k|k-1}^{\text{l},(i)} = \bar{\mathbf{P}}_{k|k-1}^{\text{l},(i)} - \bar{\mathbf{P}}_{k|k-1}^{\text{nl},(i),\text{T}} \cdot [\bar{\mathbf{P}}_{k|k-1}^{\text{n},(i)}]^{-1} \cdot \bar{\mathbf{P}}_{k|k-1}^{\text{nl},(i)}. \quad (4.87\text{b})$$

Here, it should be noted that the first part is conditioned on the second through  $\mathbf{x}_k^{\text{n}}$ . As a result, the prediction density can be rewritten as

$$\begin{aligned} p(\mathbf{x}_k^{\text{n}}, \mathbf{x}_k^{\text{l}} | \mathbf{Z}_{k-1}) &= p(\mathbf{x}_k^{\text{l}} | \mathbf{x}_k^{\text{n}}, \mathbf{Z}_{k-1}) \cdot p(\mathbf{x}_k^{\text{n}} | \mathbf{Z}_{k-1}) \\ &\approx \sum_{i=1}^N w_{k-1|k-1}^{(i)} \cdot \mathcal{N}(\mathbf{x}_k^{\text{l}}; \bar{\mathbf{x}}_{k|k-1}^{\text{l},(i)}, \bar{\mathbf{P}}_{k|k-1}^{\text{l},(i)}) \cdot \mathcal{N}(\mathbf{x}_k^{\text{n}}; \bar{\mathbf{x}}_{k|k-1}^{\text{n},(i)}, \bar{\mathbf{P}}_{k|k-1}^{\text{n},(i)}). \end{aligned} \quad (4.88)$$

In the following, a weighted discrete approximation of  $p(\mathbf{x}_k^{\text{n}} | \mathbf{Z}_{k-1})$  is obtained using an importance sampling approach. In the RBPF, the key idea is to represent each component of the weighted sum by a single particle that is sampled from the following importance density

$$\mathbf{x}_k^{\text{n},(i)} \sim q(\mathbf{x}_k^{\text{n}} | \mathbf{X}_{k-1}^{\text{n},(i)}, \mathbf{Z}_k), \quad i = 1, \dots, N, \quad (4.89)$$

[DGA00, CGM07]. As a result, the prediction pdf can be approximated as

$$p(\mathbf{x}_k^{\text{n}}, \mathbf{x}_k^{\text{l}} | \mathbf{Z}_{k-1}) \approx \sum_{i=1}^N w_{k|k-1}^{(i)} \cdot \mathcal{N}(\mathbf{x}_k^{\text{l}}; \bar{\mathbf{x}}_{k|k-1}^{\text{l},(i)}, \bar{\mathbf{P}}_{k|k-1}^{\text{l},(i)}) \cdot \delta(\mathbf{x}_k^{\text{n}} - \mathbf{x}_k^{\text{n},(i)}), \quad (4.90)$$

where the unnormalized importance weights are given by

$$w_{k|k-1}^{(i)} \propto w_{k-1|k-1}^{(i)} \cdot \frac{\mathcal{N}(\mathbf{x}_k^{\text{n},(i)}; \bar{\mathbf{x}}_{k|k-1}^{\text{n},(i)}, \bar{\mathbf{P}}_{k|k-1}^{\text{n},(i)})}{q(\mathbf{x}_k^{\text{n},(i)} | \mathbf{X}_{k-1}^{\text{n},(i)}, \mathbf{Z}_k)}, \quad i = 1, \dots, N. \quad (4.91)$$

The importance weights have to be further normalized to ensure  $\sum_{j=1}^N w_{k|k-1}^{(j)} = 1$ .

## Measurement Update

The measurement update distribution can be split as follows:

$$p(\mathbf{x}_k^n, \mathbf{x}_k^1 | \mathbf{Z}_k) = p(\mathbf{x}_k^1 | \mathbf{x}_k^n, \mathbf{Z}_k) \cdot p(\mathbf{x}_k^n | \mathbf{Z}_k). \quad (4.92)$$

The two parts can be evaluated separately. The first distribution can be updated for each particle from the following relationship

$$p(\mathbf{x}_k^1 | \mathbf{x}_k^{n,(i)}, \mathbf{Z}_k) = \frac{p(\mathbf{z}_k | \mathbf{x}_k^{n,(i)}, \mathbf{x}_k^1) \cdot p(\mathbf{x}_k^1 | \mathbf{x}_k^{n,(i)}, \mathbf{Z}_{k-1})}{p(\mathbf{z}_k | \mathbf{x}_k^{n,(i)}, \mathbf{Z}_{k-1})}, \quad (4.93)$$

where

$$p(\mathbf{z}_k | \mathbf{x}_k^{n,(i)}, \mathbf{Z}_{k-1}) = \int_{\mathbb{R}^{n_{x_1}}} p(\mathbf{z}_k | \mathbf{x}_k^{n,(i)}, \mathbf{x}_k^1) \cdot p(\mathbf{x}_k^1 | \mathbf{x}_k^{n,(i)}, \mathbf{Z}_{k-1}) d\mathbf{x}_k^1. \quad (4.94)$$

For the measurement models given by (4.76c) and (4.76d), the likelihood function can be split into two parts according to

$$p(\mathbf{z}_k | \mathbf{x}_k^{n,(i)}, \mathbf{x}_k^1) = p(\mathbf{z}_{1,k} | \mathbf{x}_k^{n,(i)}, \mathbf{x}_k^1) \cdot p(\mathbf{z}_{2,k} | \mathbf{x}_k^{n,(i)}). \quad (4.95)$$

By insertion of (4.95) into (4.94), the pdf  $p(\mathbf{z}_{2,k} | \mathbf{x}_k^{n,(i)})$  can be canceled, since it is independent of the linear states  $\mathbf{x}_k^1$ , yielding

$$p(\mathbf{x}_k^1 | \mathbf{x}_k^{n,(i)}, \mathbf{Z}_k) = \frac{p(\mathbf{z}_{1,k} | \mathbf{x}_k^{n,(i)}, \mathbf{x}_k^1) \cdot p(\mathbf{x}_k^1 | \mathbf{x}_k^{n,(i)}, \mathbf{Z}_{k-1})}{p(\mathbf{z}_{1,k} | \mathbf{x}_k^{n,(i)}, \mathbf{Z}_{k-1})}, \quad (4.96)$$

where

$$p(\mathbf{z}_{1,k} | \mathbf{x}_k^{n,(i)}, \mathbf{Z}_{k-1}) = \int_{\mathbb{R}^{n_{x_1}}} p(\mathbf{z}_{1,k} | \mathbf{x}_k^{n,(i)}, \mathbf{x}_k^1) \cdot p(\mathbf{x}_k^1 | \mathbf{x}_k^{n,(i)}, \mathbf{Z}_{k-1}) d\mathbf{x}_k^1. \quad (4.97)$$

The likelihood pdf  $p(\mathbf{z}_{1,k} | \mathbf{x}_k^{n,(i)}, \mathbf{x}_k^1)$  can be determined from (4.76c) and is given by

$$p(\mathbf{z}_{1,k} | \mathbf{x}_k^{n,(i)}, \mathbf{x}_k^1) = \mathcal{N}(\mathbf{z}_{1,k}; \mathbf{h}_{1,k}(\mathbf{x}_k^n) + \mathbf{H}_k(\mathbf{x}_k^n) \cdot \mathbf{x}_k^1, \mathbf{R}_{1,k}). \quad (4.98)$$

The density  $p(\mathbf{x}_k^1 | \mathbf{x}_k^{n,(i)}, \mathbf{Z}_{k-1})$  is available from the time update stage and is given by

$$p(\mathbf{x}_k^1 | \mathbf{x}_k^{n,(i)}, \mathbf{Z}_{k-1}) = \mathcal{N}(\mathbf{x}_k^1; \mathbf{x}_{k|k-1}^{1,(i)}, \mathbf{P}_{k|k-1}^{(i)}). \quad (4.99)$$

The integral in (4.97) can be evaluated analytically since the integrand is a product of Gaussian densities. From this it follows,

$$p(\mathbf{z}_{1,k} | \mathbf{x}_k^{n,(i)}, \mathbf{Z}_{k-1}) = \mathcal{N}(\mathbf{z}_{1,k}; \hat{\mathbf{z}}_{1,k}^{(i)}, \mathbf{S}_k^{(i)}), \quad (4.100)$$

where

$$\hat{\mathbf{z}}_{1,k}^{(i)} = \mathbf{h}_{1,k}(\mathbf{x}_k^{n,(i)}) + \mathbf{H}_k(\mathbf{x}_k^{n,(i)}) \cdot \mathbf{x}_{k|k-1}^{1,(i)}, \quad (4.101a)$$

$$\mathbf{S}_k^{(i)} = \mathbf{H}_k(\mathbf{x}_k^{n,(i)}) \cdot \mathbf{P}_{k|k-1}^{(i)} \cdot \mathbf{H}_k^\top(\mathbf{x}_k^{n,(i)}) + \mathbf{R}_{1,k}. \quad (4.101b)$$

The densities involved in evaluating the measurement update, cf. (4.95), are all Gaussian. As a result, the density  $p(\mathbf{x}_k^1 | \mathbf{x}_k^{n,(i)}, \mathbf{Z}_k)$  is also Gaussian and is given by

$$p(\mathbf{x}_k^1 | \mathbf{x}_k^{n,(i)}, \mathbf{Z}_k) = \mathcal{N}(\mathbf{x}_k^1; \mathbf{x}_{k|k}^{1,(i)}, \mathbf{P}_{k|k}^{(i)}), \quad (4.102)$$

where

$$\mathbf{x}_{k|k}^{1,(i)} = \mathbf{x}_{k|k-1}^{1,(i)} + \mathbf{K}_k^{(i)} \cdot (\mathbf{z}_{1,k} - \hat{\mathbf{z}}_{1,k}^{(i)}), \quad (4.103a)$$

$$\mathbf{P}_{k|k}^{(i)} = \mathbf{P}_{k|k-1}^{(i)} - \mathbf{K}_k^{(i)} \cdot \mathbf{S}_k^{(i)} \cdot \mathbf{K}_k^{(i)\top}, \quad (4.103b)$$

$$\mathbf{K}_k^{(i)} = \mathbf{P}_{k|k-1}^{(i)} \cdot \mathbf{H}_k^\top(\mathbf{x}_k^{n,(i)}) \cdot [\mathbf{S}_k^{(i)}]^{-1}. \quad (4.103c)$$

Note, that (4.103) is similar to the Kalman measurement update. A proof of (4.103) can be found in [Sch03]. The measurement update for the nonlinear states  $\mathbf{x}_k^n$  is done as follows:

$$p(\mathbf{x}_k^n | \mathbf{Z}_k) = \frac{p(\mathbf{z}_k | \mathbf{x}_k^n, \mathbf{Z}_{k-1}) \cdot p(\mathbf{x}_k^n | \mathbf{Z}_{k-1})}{p(\mathbf{z}_k | \mathbf{Z}_{k-1})}. \quad (4.104)$$

Since the pdf  $p(\mathbf{x}_k^n | \mathbf{Z}_k)$  is approximated using an importance sampling approach, the denominator in (4.104) will be numerically normed and has not to be calculated. The measurement update can be written as

$$\begin{aligned} p(\mathbf{x}_k^n | \mathbf{Z}_k) &\propto p(\mathbf{z}_k | \mathbf{x}_k^n, \mathbf{Z}_{k-1}) \cdot p(\mathbf{x}_k^n | \mathbf{Z}_{k-1}) \\ &= \int_{\mathbb{R}^{n_{x1}}} p(\mathbf{z}_k | \mathbf{x}_k^n, \mathbf{x}_k^1) \cdot p(\mathbf{x}_k^1 | \mathbf{x}_k^n, \mathbf{Z}_{k-1}) d\mathbf{x}_k^1 \cdot p(\mathbf{x}_k^n | \mathbf{Z}_{k-1}) \\ &\approx \sum_{i=1}^N w_{k|k-1}^{(i)} \cdot \int_{\mathbb{R}^{n_{x1}}} \underbrace{p(\mathbf{z}_k | \mathbf{x}_k^{n,(i)}, \mathbf{x}_k^1)}_{(4.95)} \cdot p(\mathbf{x}_k^1 | \mathbf{x}_k^{n,(i)}, \mathbf{Z}_{k-1}) d\mathbf{x}_k^1 \cdot \delta(\mathbf{x}_k^n - \mathbf{x}_k^{n,(i)}) \\ &= \sum_{i=1}^N \underbrace{w_{k|k-1}^{(i)} \cdot \mathcal{N}(\mathbf{z}_{1,k}; \hat{\mathbf{z}}_{1,k}^{(i)}, \mathbf{S}_k^{(i)}) \cdot p(\mathbf{z}_{2,k} | \mathbf{x}_k^n)}_{w_{k|k}^{(i)}} \cdot \delta(\mathbf{x}_k^n - \mathbf{x}_k^{n,(i)}). \end{aligned} \quad (4.105)$$

Combining (4.102) and (4.105) according to (4.92) results in

$$p(\mathbf{x}_k^n, \mathbf{x}_k^1 | \mathbf{Z}_k) \approx \sum_{i=1}^N w_{k|k}^{(i)} \cdot \mathcal{N}(\mathbf{x}_k^1; \mathbf{x}_{k|k}^{1,(i)}, \mathbf{P}_{k|k}^{(i)}) \cdot \delta(\mathbf{x}_k^n - \mathbf{x}_k^{n,(i)}). \quad (4.106)$$

where the normalized weights are given by

$$w_{k|k}^{(i)} = \frac{w_{k|k-1}^{(i)} \cdot \mathcal{N}(\mathbf{z}_{1,k}; \hat{\mathbf{z}}_{1,k}^{(i)}, \mathbf{S}_k^{(i)}) \cdot p(\mathbf{z}_{2,k} | \mathbf{x}_k^{n,(i)})}{\sum_{j=1}^N w_{k|k-1}^{(j)} \cdot \mathcal{N}(\mathbf{z}_{1,k}; \hat{\mathbf{z}}_{1,k}^{(j)}, \mathbf{S}_k^{(j)}) \cdot p(\mathbf{z}_{2,k} | \mathbf{x}_k^{n,(j)})}. \quad (4.107)$$



## Estimation

The RBPF provides a discrete approximation of the posterior pdf according to (4.106), from which standard measures as the MMSE  $\hat{\mathbf{x}}_{\text{MMSE},k|k}$  and its covariance  $\mathbf{P}_{\text{MMSE},k|k}$  for the linear and nonlinear states can be computed [Sch03]. Numerical approximations of these quantities are given by

$$\hat{\mathbf{x}}_{\text{MMSE},k|k}^{\text{n}} \approx \sum_{i=1}^N w_{k|k}^{(i)} \cdot \mathbf{x}_k^{\text{n}(i)}, \quad (4.108\text{a})$$

$$\mathbf{P}_{\text{MMSE},k|k}^{\text{n}} \approx \sum_{i=1}^N w_{k|k}^{(i)} \cdot (\mathbf{x}_k^{\text{n}(i)} - \hat{\mathbf{x}}_{\text{MMSE},k|k}^{\text{n}}) \cdot (\mathbf{x}_k^{\text{n}(i)} - \hat{\mathbf{x}}_{\text{MMSE},k|k}^{\text{n}})^{\top}, \quad (4.108\text{b})$$

$$\hat{\mathbf{x}}_{\text{MMSE},k|k}^{\text{l}} \approx \sum_{i=1}^N w_{k|k}^{(i)} \cdot \mathbf{x}_k^{\text{l}(i)}, \quad (4.108\text{c})$$

$$\mathbf{P}_{\text{MMSE},k|k}^{\text{l}} \approx \sum_{i=1}^N w_{k|k}^{(i)} \cdot \left[ \mathbf{P}_{k|k}^{(i)} + (\mathbf{x}_k^{\text{l}(i)} - \hat{\mathbf{x}}_{\text{MMSE},k|k}^{\text{l}}) \cdot (\mathbf{x}_k^{\text{l}(i)} - \hat{\mathbf{x}}_{\text{MMSE},k|k}^{\text{l}})^{\top} \right]. \quad (4.108\text{d})$$

## Resampling

For the resampling step in the RBPF, systematic resampling is used which is explained in Section 4.5.2.2.

### 4.5.3.3 Choice of Importance Density

In the design of RBPFs, the choice of the importance density  $q(\mathbf{x}_k^{\text{n}} | \mathbf{X}_{k-1}^{\text{n}(i)}, \mathbf{Z}_k)$  plays a major role. The optimal importance density that minimizes the variance of the importance weights is given by  $q(\mathbf{x}_k^{\text{n}} | \mathbf{X}_{k-1}^{\text{n}(i)}, \mathbf{Z}_k)_{\text{opt}} = p(\mathbf{x}_k^{\text{n}} | \mathbf{X}_{k-1}^{\text{n}(i)}, \mathbf{Z}_k)$  [DGA00]. However, for the hybrid localization problem, a closed-form expression for this density does not exist, so that one has to resort to suboptimal importance densities. For the hybrid localization problem, the following pdf

$$q(\mathbf{x}_k | \mathbf{X}_{k-1}^{(i)}, \mathbf{Z}_k) = \mathcal{N}(\mathbf{x}_k^{\text{n}}; \bar{\mathbf{x}}_{k|k-1}^{\text{n}(i)}, \bar{\mathbf{P}}_{k|k-1}^{\text{n}(i)}), \quad (4.109)$$

is chosen as importance density, cf. (4.88), which is the most popular suboptimal choice. In this case, the weights in the time update are given by  $w_{k|k-1}^{(i)} = w_{k-1|k-1}^{(i)}$ , cf. (4.91), and the weights in the measurement update simplify to

$$w_{k|k}^{(i)} = \frac{w_{k-1|k-1}^{(i)} \cdot \mathcal{N}(\mathbf{z}_{1,k}; \hat{\mathbf{z}}_{1,k}^{(i)}, \mathbf{S}_k^{(i)}) \cdot p(\mathbf{z}_{2,k} | \mathbf{x}_k^{\text{n}(i)})}{\sum_{j=1}^N w_{k-1|k-1}^{(j)} \cdot \mathcal{N}(\mathbf{z}_{1,k}; \hat{\mathbf{z}}_{1,k}^{(j)}, \mathbf{S}_k^{(j)}) \cdot p(\mathbf{z}_{2,k} | \mathbf{x}_k^{\text{n}(j)})}. \quad (4.110)$$

A pseudocode description of the RBPF for the hybrid localization problem is given in Algorithm 4.6, where the following abbreviations have been introduced to simplify the notation:

$$\begin{aligned} \mathbf{f}_{k-1}^n(\mathbf{x}_{k-1}^{n,(i)}) &= \mathbf{f}_{k-1}^{n,(i)}, & \mathbf{F}_{k-1}^n(\mathbf{x}_{k-1}^{n,(i)}) &= \mathbf{F}_{k-1}^{n,(i)}, & \mathbf{\Gamma}_{k-1}^n(\mathbf{x}_{k-1}^{n,(i)}) &= \mathbf{\Gamma}_{k-1}^{n,(i)}, \\ \mathbf{f}_{k-1}^l(\mathbf{x}_{k-1}^{n,(i)}) &= \mathbf{f}_{k-1}^{l,(i)}, & \mathbf{F}_{k-1}^l(\mathbf{x}_{k-1}^{n,(i)}) &= \mathbf{F}_{k-1}^{l,(i)}, & \mathbf{\Gamma}_{k-1}^l(\mathbf{x}_{k-1}^{n,(i)}) &= \mathbf{\Gamma}_{k-1}^{l,(i)}, \\ \mathbf{h}_{1,k}(\mathbf{x}_k^{n,(i)}) &= \mathbf{h}_{1,k}^{(i)}, & \mathbf{H}_k(\mathbf{x}_k^{n,(i)}) &= \mathbf{H}_k^{(i)}, & \bar{\mathbf{E}}_k(\mathbf{x}_k^{n,(j)}, \mathbf{x}_{k-1}^{n,(i)}) &= \bar{\mathbf{E}}_k^{(i)}(\mathbf{x}_k^{n,(j)}). \end{aligned} \quad (4.111)$$

---

### Algorithm 4.6 Rao-Blackwellized Particle Filter

---

1. Initialization:

- For  $i = 1, \dots, N$ , initialize the particles  $\mathbf{x}_0^{n,(i)} \sim p(\mathbf{x}_0^n)$  and weights  $w_{0|0}^{(i)} = \frac{1}{N}$ , and set  $\{\hat{\mathbf{x}}_{0|0}^l, \mathbf{P}_{0|0}^{(i)}\} = \{\hat{\mathbf{x}}_0^l, \mathbf{P}_0\}$ .

2. Particle Filter Time Update:

- For  $i = 1, \dots, N$ , draw particles from the importance density according to

$$\mathbf{x}_k^{n,(i)} \sim \mathcal{N}(\bar{\mathbf{x}}_{k|k-1}^{n,(i)}, \bar{\mathbf{P}}_{k|k-1}^{n,(i)}),$$

where

$$\begin{aligned} \bar{\mathbf{x}}_{k|k-1}^{n,(i)} &= \mathbf{f}_{k-1}^{n,(i)} + \mathbf{F}_{k-1}^{n,(i)} \cdot \mathbf{x}_{k-1|k-1}^{l,(i)}, \\ \bar{\mathbf{P}}_{k|k-1}^{n,(i)} &= \mathbf{F}_{k-1}^{n,(i)} \cdot \mathbf{P}_{k-1|k-1}^{(i)} \cdot \mathbf{F}_{k-1}^{n,(i)\top} + \mathbf{\Gamma}_{k-1}^{n,(i)} \cdot \mathbf{Q}_{k-1}^n \cdot \mathbf{\Gamma}_{k-1}^{n,(i)\top}. \end{aligned}$$

3. Kalman Filter Time Update:

- For  $i = 1, \dots, N$ , evaluate

$$\begin{aligned} \mathbf{x}_{k|k-1}^{l,(i)} &= \bar{\mathbf{x}}_{k|k-1}^{n,(i)} + \bar{\mathbf{P}}_{k|k-1}^{nl,(i)\top} \cdot [\bar{\mathbf{P}}_{k|k-1}^{n,(i)}]^{-1} \cdot (\mathbf{x}_k^{n,(i)} - \bar{\mathbf{x}}_{k|k-1}^{n,(i)}), \\ \mathbf{P}_{k|k-1}^{(i)} &= \bar{\mathbf{P}}_{k|k-1}^{l,(i)} - \bar{\mathbf{P}}_{k|k-1}^{nl,(i)\top} \cdot [\bar{\mathbf{P}}_{k|k-1}^{n,(i)}]^{-1} \cdot \bar{\mathbf{P}}_{k|k-1}^{nl,(i)}, \end{aligned}$$

where

$$\begin{aligned} \bar{\mathbf{x}}_{k|k-1}^{l,(i)} &= \mathbf{f}_{k-1}^{l,(i)} + \bar{\mathbf{F}}_{k-1}^{l,(i)} \cdot \mathbf{x}_{k-1|k-1}^{l,(i)} + \bar{\mathbf{E}}_k^{(i)}(\mathbf{x}_{k-1}^{n,(i)}), \\ \bar{\mathbf{P}}_{k|k-1}^{nl,(i)} &= \mathbf{F}_{k-1}^{n,(i)} \cdot \mathbf{P}_{k-1|k-1}^{(i)} \cdot \bar{\mathbf{F}}_{k-1}^{l,(i)\top}, \\ \bar{\mathbf{P}}_{k|k-1}^{l,(i)} &= \bar{\mathbf{F}}_{k-1}^{l,(i)} \cdot \mathbf{P}_{k-1|k-1}^{(i)} \cdot \bar{\mathbf{F}}_{k-1}^{l,(i)\top} + \mathbf{\Gamma}_{k-1}^{l,(i)} \cdot \bar{\mathbf{Q}}_{k-1}^l \cdot \mathbf{\Gamma}_{k-1}^{l,(i)\top}, \\ \bar{\mathbf{E}}_k^{(i)}(\mathbf{x}_{k-1}^{n,(i)}) &= \mathbf{\Gamma}_{k-1}^{l,(i)} \cdot \mathbf{Q}_{k-1}^{nl,\top} \cdot [\mathbf{\Gamma}_{k-1}^{n,(i)} \cdot \mathbf{Q}_{k-1}^n]^{-1} \cdot (\mathbf{x}_{k-1}^{n,(i)} - \mathbf{f}_{k-1}^{n,(i)}), \\ \bar{\mathbf{F}}_{k-1}^{l,(i)} &= \mathbf{F}_{k-1}^{l,(i)} - \mathbf{\Gamma}_{k-1}^{l,(i)} \cdot \mathbf{Q}_{k-1}^{nl,\top} \cdot [\mathbf{\Gamma}_{k-1}^{n,(i)} \cdot \mathbf{Q}_{k-1}^n]^{-1} \cdot \mathbf{F}_{k-1}^{n,(i)}, \\ \bar{\mathbf{Q}}_{k-1}^l &= \mathbf{Q}_{k-1}^l - \mathbf{Q}_{k-1}^{nl,\top} \cdot [\mathbf{Q}_{k-1}^n]^{-1} \cdot \mathbf{Q}_{k-1}^{nl}. \end{aligned}$$

## 4. Particle Filter Measurement Update:

- For  $i = 1, \dots, N$ , evaluate the weights

$$w_{k|k}^{(i)} = \frac{w_{k-1|k-1}^{(i)} \cdot \mathcal{N}(\mathbf{z}_{1,k}; \hat{\mathbf{z}}_{1,k}^{(i)}, \mathbf{S}_k^{(i)}) \cdot p(\mathbf{z}_{2,k} | \mathbf{x}_k^{n,(i)})}{\sum_{j=1}^N w_{k-1|k-1}^{(j)} \cdot \mathcal{N}(\mathbf{z}_{1,k}; \hat{\mathbf{z}}_{1,k}^{(j)}, \mathbf{S}_k^{(j)}) \cdot p(\mathbf{z}_{2,k} | \mathbf{x}_k^{n,(j)})},$$

where

$$\begin{aligned} \hat{\mathbf{z}}_{1,k}^{(i)} &= \mathbf{h}_{1,k}^{(i)} + \mathbf{H}_k^{(i)} \cdot \mathbf{x}_{k|k-1}^{1,(i)}, \\ \mathbf{S}_k^{(i)} &= \mathbf{H}_k^{(i)} \cdot \mathbf{P}_{k|k-1}^{(i)} \cdot \mathbf{H}_k^{(i),\top} + \mathbf{R}_{1,k}. \end{aligned}$$

## 5. Kalman Filter Measurement Update:

- For  $i = 1, \dots, N$ , evaluate

$$\begin{aligned} \mathbf{x}_{k|k}^{1,(i)} &= \mathbf{x}_{k|k-1}^{1,(i)} + \mathbf{K}_k^{(i)} \cdot (\mathbf{z}_{1,k} - \hat{\mathbf{z}}_{1,k}^{(i)}), \\ \mathbf{P}_{k|k}^{(i)} &= \mathbf{P}_{k|k-1}^{(i)} - \mathbf{K}_k^{(i)} \cdot \mathbf{S}_k^{(i)} \cdot \mathbf{K}_k^{(i),\top}, \end{aligned}$$

where

$$\mathbf{K}_k^{(i)} = \mathbf{P}_{k|k-1}^{(i)} \cdot \mathbf{H}_k^{(i),\top} \cdot [\mathbf{S}_k^{(i)}]^{-1}.$$

## 6. Estimation:

- Determine estimates of the linear and nonlinear state vectors according to

$$\hat{\mathbf{x}}_{\text{MMSE},k|k}^n = \sum_{i=1}^N w_{k|k}^{(i)} \cdot \mathbf{x}_k^{n,(i)}, \quad \hat{\mathbf{x}}_{\text{MMSE},k|k}^1 = \sum_{i=1}^N w_{k|k}^{(i)} \cdot \mathbf{x}_{k|k}^{1,(i)}.$$

## 7. Resampling:

- Perform systematic resampling using Algorithm 4.4. Take  $N$  samples with replacement from the set  $\{\mathbf{x}_k^{n,(i)}, \mathbf{x}_{k|k}^{1,(i)}, \mathbf{P}_{k|k}^{(i)}\}_{i=1}^N$ , where the probability to take sample  $i$  is  $w_{k|k}^{(i)}$ . Set  $w_{k|k}^{(i)} = \frac{1}{N}$  for  $i = 1, \dots, N$ .

- 8. Set  $k := k + 1$  and iterate from step 2.

## 4.5.3.4 Application to the Hybrid Localization Problem

In this section, it is shown how the state and measurement models for the hybrid localization can be adopted to the conditional linear system model of the RBPF. For the hybrid localization problem, the state model is linear Gaussian and given by (2.49).

For the scenario with LOS propagation conditions, the measurement model is given by (2.50), and for the scenario, where the propagation conditions switch between LOS and NLOS, an approximation to the measurement model is used, whose likelihood pdf is given by (3.83). In order to relate the state and measurement models to the RBPF framework, the state vector is split into two parts. Due to the fact that only the MT location vector  $\mathbf{x}_{\text{MT},k}$  enters nonlinearly into the measurement model, the state vector is split as follows

$$\mathbf{x}_k^n = [x_{\text{MT},k}, y_{\text{MT},k}]^T, \quad (4.112)$$

$$\mathbf{x}_k^l = [\dot{x}_{\text{MT},k}, \dot{y}_{\text{MT},k}, c_0 \cdot \delta t_k, c_0 \cdot \delta \dot{t}_k]^T. \quad (4.113)$$

The resulting adapted state and measurement models are presented next.

## State Model

The state model can be adapted to the RBPF framework as follows:

$$\underbrace{\begin{bmatrix} x_{\text{MT},k} \\ y_{\text{MT},k} \end{bmatrix}}_{\mathbf{x}_k^n} = \underbrace{\begin{bmatrix} x_{\text{MT},k-1} \\ y_{\text{MT},k-1} \end{bmatrix}}_{\mathbf{f}_{k-1}^n(\mathbf{x}_{k-1}^n)} + \underbrace{\begin{bmatrix} T_S & 0 & 0 & 0 \\ 0 & T_S & 0 & 0 \end{bmatrix}}_{\mathbf{F}_{k-1}^n} \cdot \underbrace{\begin{bmatrix} \dot{x}_{\text{MT},k-1} \\ \dot{y}_{\text{MT},k-1} \\ c_0 \cdot \delta t_{k-1} \\ c_0 \cdot \delta \dot{t}_{k-1} \end{bmatrix}}_{\mathbf{x}_{k-1}^l} + \underbrace{\begin{bmatrix} \frac{T_S^2}{2} & 0 \\ 0 & \frac{T_S^2}{2} \end{bmatrix}}_{\mathbf{\Gamma}_{k-1}^n} \cdot \underbrace{\begin{bmatrix} w_{x,k-1} \\ w_{y,k-1} \end{bmatrix}}_{\mathbf{w}_{k-1}^n}, \quad (4.114)$$

$$\underbrace{\begin{bmatrix} \dot{x}_{\text{MT},k} \\ \dot{y}_{\text{MT},k} \\ c_0 \cdot \delta t_k \\ c_0 \cdot \delta \dot{t}_k \end{bmatrix}}_{\mathbf{x}_k^l} = \underbrace{\begin{bmatrix} 1 & 0 & 0 & 0 \\ 0 & 1 & 0 & 0 \\ 0 & 0 & 1 & T_S \\ 0 & 0 & 0 & 1 \end{bmatrix}}_{\mathbf{F}_{k-1}^l} \cdot \underbrace{\begin{bmatrix} \dot{x}_{\text{MT},k-1} \\ \dot{y}_{\text{MT},k-1} \\ c_0 \cdot \delta t_{k-1} \\ c_0 \cdot \delta \dot{t}_{k-1} \end{bmatrix}}_{\mathbf{x}_{k-1}^l} + \underbrace{\begin{bmatrix} T_S & 0 & 0 & 0 \\ 0 & T_S & 0 & 0 \\ 0 & 0 & c_0 & 0 \\ 0 & 0 & 0 & c_0 \end{bmatrix}}_{\mathbf{\Gamma}_{k-1}^l} \cdot \underbrace{\begin{bmatrix} w_{x,k-1} \\ w_{y,k-1} \\ w_{\delta t,k-1} \\ w_{\delta \dot{t},k-1} \end{bmatrix}}_{\mathbf{w}_{k-1}^l}. \quad (4.115)$$

Observe that the noises  $\mathbf{w}_{k-1}^n$  and  $\mathbf{w}_{k-1}^l$  are correlated, cf. (4.74), where the corresponding covariance matrices are given by  $\mathbf{Q}_{k-1}^n = \mathbf{Q}_{\text{CV}}$ ,  $\mathbf{Q}_{k-1}^{nl} = [\mathbf{Q}_{\text{CV}}, \mathbf{0}_{2 \times 2}]$  and  $\mathbf{Q}_{k-1}^l = \text{diag}_b[\mathbf{Q}_{\text{CV}}, \mathbf{Q}_{\text{CO}}]$ .

## Measurement Model - LOS Propagation Conditions

For the scenario with LOS propagation conditions, the measurement vector is split as follows

$$\mathbf{z}_{1,k} = [\mathbf{z}_{\text{PR},k}^T, \mathbf{z}_{\text{RTT,LOS},k}^T, \mathbf{z}_{\text{RSS,LOS},k}^T, z_{\text{BIAS},k}]^T, \quad (4.116)$$

i.e., all measurements can be expressed with (4.76c), while the measurement vector  $\mathbf{z}_{2,k}$  is empty. Thus, the corresponding measurement model can be rewritten as

$$\underbrace{\begin{bmatrix} \mathbf{z}_{\text{PR},k} \\ \mathbf{z}_{\text{RTT,LOS},k} \\ \mathbf{z}_{\text{RSS,LOS},k} \\ z_{\text{BIAS},k} \end{bmatrix}}_{\mathbf{z}_{1,k}} = \underbrace{\begin{bmatrix} \mathbf{d}_{\text{SAT},k}(\mathbf{x}_k^n) \\ \mathbf{h}_{\text{RTT},k}(\mathbf{x}_k^n) \\ \mathbf{h}_{\text{RSS,LOS},k}(\mathbf{x}_k^n) \\ 0 \end{bmatrix}}_{\mathbf{h}_{1,k}(\mathbf{x}_k^n)} + \underbrace{\begin{bmatrix} \mathbf{0}_{M_{\text{PR}} \times 2} & \mathbf{1}_{M_{\text{PR}} \times 1} & \mathbf{0}_{M_{\text{PR}} \times 1} \\ \mathbf{0}_{(M_{\text{RTT}}+M_{\text{RSS}}) \times 4} \\ \mathbf{0}_{1 \times 2} & 1 & 0 \end{bmatrix}}_{\mathbf{H}_k} \cdot \underbrace{\begin{bmatrix} \dot{x}_{\text{MT},k} \\ \dot{y}_{\text{MT},k} \\ c_0 \cdot \delta t_k \\ c_0 \cdot \delta \dot{t}_k \end{bmatrix}}_{\mathbf{x}_k^1} + \underbrace{\begin{bmatrix} \mathbf{v}_{\text{PR},k} \\ \mathbf{v}_{\text{RTT,LOS},k} \\ \mathbf{v}_{\text{RSS,LOS},k} \\ v_{\text{BIAS},k} \end{bmatrix}}_{\mathbf{v}_{1,k}}. \quad (4.117)$$

The measurement noise  $\mathbf{v}_{1,k}$  is zero-mean Gaussian distributed with covariance matrix  $\mathbf{R}_{1,k} = \mathbf{R}_{\text{LOS},k}$ . Since all measurements are expressed with model (4.76c), the likelihood function  $p(\mathbf{z}_{2,k}|\mathbf{x}_k^n)$  can be omitted in the calculation of the importance weights, cf. (4.110).

### Measurement Model - LOS/NLOS Propagation Conditions

For the scenario, where the propagation conditions switch between LOS and NLOS, the measurement vector is split as follows:

$$\mathbf{z}_{1,k} = [\mathbf{z}_{\text{PR},k}^\top, z_{\text{BIAS},k}^\top]^\top, \quad (4.118)$$

$$\mathbf{z}_{2,k} = [\mathbf{z}_{\text{RTT},k}^\top, \mathbf{z}_{\text{RSS},k}^\top]^\top. \quad (4.119)$$

The measurement model of  $\mathbf{z}_{1,k}$  can be rewritten as

$$\underbrace{\begin{bmatrix} \mathbf{z}_{\text{PR},k} \\ z_{\text{BIAS},k} \end{bmatrix}}_{\mathbf{z}_{1,k}} = \underbrace{\begin{bmatrix} \mathbf{d}_{\text{SAT},k}(\mathbf{x}_{\text{MT},k}) \\ 0 \end{bmatrix}}_{\mathbf{h}_{1,k}(\mathbf{x}_k^n)} + \underbrace{\begin{bmatrix} \mathbf{0}_{M_{\text{PR}} \times 2} & \mathbf{1}_{M_{\text{PR}} \times 1} & \mathbf{0}_{M_{\text{PR}} \times 1} \\ \mathbf{0}_{1 \times 2} & 1 & 0 \end{bmatrix}}_{\mathbf{H}_k} \cdot \underbrace{\begin{bmatrix} \dot{x}_{\text{MT},k} \\ \dot{y}_{\text{MT},k} \\ c_0 \cdot \delta t_k \\ c_0 \cdot \delta \dot{t}_k \end{bmatrix}}_{\mathbf{x}_k^1} + \underbrace{\begin{bmatrix} \mathbf{v}_{\text{PR},k} \\ v_{\text{BIAS},k} \end{bmatrix}}_{\mathbf{v}_{1,k}}, \quad (4.120)$$

where the measurement noise  $\mathbf{v}_{1,k}$  is zero-mean Gaussian distributed with covariance matrix  $\mathbf{R}_{1,k} = \mathbf{R}_{\text{SAT},k}$ . For the second measurement model (4.76d), it is sufficient to know the likelihood pdf  $p(\mathbf{z}_{2,k}|\mathbf{x}_k^n)$ , which is given by

$$p(\mathbf{z}_{2,k}|\mathbf{x}_k^n) = \prod_{\kappa_1=1}^{M_{\text{RTT}}} p(z_{\text{RTT},k}^{(\kappa_1)}|\mathbf{x}_k^n) \cdot \prod_{\kappa_2=1}^{M_{\text{RSS}}} p(z_{\text{RSS},k}^{(\kappa_2)}|\mathbf{x}_k^n), \quad (4.121)$$

where  $p(z_{\text{RTT},k}^{(\kappa_1)}|\mathbf{x}_k^n)$  and  $p(z_{\text{RSS},k}^{(\kappa_2)}|\mathbf{x}_k^n)$  are defined in (3.54) and (3.55).

## 4.5.4 Auxiliary Particle Filter

### 4.5.4.1 Introduction

In this section, the APF is proposed as a solution for the hybrid localization problem. Compared to the standard PF, the APF can be interpreted as a look ahead method, which at time  $k - 1$  predicts which samples will be in regions of high likelihood at time  $k$ . As a result, the cost of sampling particles from regions of very low likelihoods is reduced. Since its introduction in [PS99], several improvements were proposed to reduce the variance of the APF [CCF99, DdFG01]. In the following, the modified APF presented in [CCF99], is used for the hybrid localization problem. This algorithm has only one resampling step at each time instance and experimentally outperforms the original two-stage resampling algorithm proposed in [PS99].

### 4.5.4.2 Derivations

In this section, the APF for hybrid localization is derived. The APF can be derived based on pdf of the state trajectory  $p(\mathbf{X}_k | \mathbf{Z}_k)$ , which is presented in [CGM07], or from the posterior pdf  $p(\mathbf{x}_k | \mathbf{Z}_k)$  which is sketched in [RAG04]. In this work, the APF is derived from the posterior pdf  $p(\mathbf{x}_k | \mathbf{Z}_k)$  of the current state, so that a better comparison to the PF derivation is possible.

#### Initialization

The APF is initialized as follows:

$$p(\mathbf{x}_{k-1} | \mathbf{Z}_{k-1}) = \sum_{i=1}^N w_{k-1|k-1}^{(i)} \cdot \delta(\mathbf{x}_{k-1} - \mathbf{x}_{k-1}^{(i)}). \quad (4.122)$$

#### Time Update

In the time update, the Chapman-Kolmogorov equation has to be evaluated. Insertion of (4.122) into (4.1c), yields

$$p(\mathbf{x}_k | \mathbf{Z}_{k-1}) = \int_{\mathbb{R}^{n_x}} p(\mathbf{x}_k | \mathbf{x}_{k-1}) \cdot p(\mathbf{x}_{k-1} | \mathbf{Z}_{k-1}) d\mathbf{x}_{k-1} \approx \sum_{i=1}^N w_{k-1|k-1}^{(i)} \cdot p(\mathbf{x}_k | \mathbf{x}_{k-1}^{(i)}) \quad (4.123)$$

$$= \sum_{i=1}^N p(\mathbf{x}_k, i | \mathbf{Z}_{k-1}). \quad (4.124)$$

Comparison of (4.123) and (4.124) leads to

$$p(\mathbf{x}_k, i | \mathbf{Z}_{k-1}) = w_{k-1|k-1}^{(i)} \cdot p(\mathbf{x}_k | \mathbf{x}_{k-1}^{(i)}). \quad (4.125)$$

The idea of the APF is to approximate the joint density  $p(\mathbf{x}_k, i | \mathbf{Z}_k)$  and later on, omit the discrete index  $i$ , in order to arrive at the desired filtering distribution  $p(\mathbf{x}_k | \mathbf{Z}_k)$ . The joint prediction pdf  $p(\mathbf{x}_k, i | \mathbf{Z}_{k-1})$  is continuous with respect to  $\mathbf{x}_k$  and discrete with respect to  $i$ . In the following, a weighted discrete approximation of  $p(\mathbf{x}_k, i | \mathbf{Z}_{k-1})$  is obtained using an importance sampling approach. In the APF, the key idea is to represent each component of the weighted sum by a single particle and its corresponding discrete index, that is sampled from the following importance density

$$\mathbf{x}_k^{(j)}, i^{(j)} \sim q(\mathbf{x}_k, i | \mathbf{Z}_{k-1}, \mathbf{z}_k), \quad j = 1, \dots, N, \quad (4.126)$$

where the latest measurement  $\mathbf{z}_k$  is taken into account in the importance density. As a result, the prediction pdf can be approximated as

$$p(\mathbf{x}_k, i | \mathbf{Z}_{k-1}) \approx \sum_{j=1}^N w_{k|k-1}^{(j)} \cdot \delta(\mathbf{x}_k - \mathbf{x}_k^{(j)}, i - i^{(j)}), \quad (4.127)$$

where the unnormalized importance weights are given by

$$w_{k|k-1}^{(j)} \propto w_{k-1|k-1}^{(i^{(j)})} \cdot \frac{p(\mathbf{x}_k^{(j)} | \mathbf{x}_{k-1}^{(i^{(j)})})}{q(\mathbf{x}_k^{(j)}, i^{(j)} | \mathbf{Z}_k)}, \quad j = 1, \dots, N. \quad (4.128)$$

The importance weights have to be further normalized to ensure  $\sum_{m=1}^N w_{k|k-1}^{(m)} = 1$ .

## Measurement Update

In the measurement update, the joint posterior pdf  $p(\mathbf{x}_k, i | \mathbf{Z}_k)$  is updated according to

$$p(\mathbf{x}_k, i | \mathbf{Z}_k) = \frac{p(\mathbf{z}_k | \mathbf{x}_k, i, \mathbf{Z}_{k-1}) \cdot p(\mathbf{x}_k, i | \mathbf{Z}_{k-1})}{p(\mathbf{z}_k | \mathbf{Z}_{k-1})} = \frac{p(\mathbf{z}_k | \mathbf{x}_k) \cdot p(\mathbf{x}_k, i | \mathbf{Z}_{k-1})}{p(\mathbf{z}_k | \mathbf{Z}_{k-1})}. \quad (4.129)$$

Insertion of (4.127) into (4.129) gives a weighted discrete approximation of the joint posterior pdf. Since this approximation is numerically normed, a calculation of the denominator in (4.129) is not needed, yielding

$$\begin{aligned} p(\mathbf{x}_k, i | \mathbf{Z}_k) &\propto p(\mathbf{z}_k | \mathbf{x}_k) \cdot p(\mathbf{x}_k, i | \mathbf{Z}_{k-1}) \\ &\approx \sum_{j=1}^N \underbrace{w_{k|k-1}^{(j)} \cdot p(\mathbf{z}_k | \mathbf{x}_k^{(j)})}_{w_{k|k}^{(j)}} \cdot \delta(\mathbf{x}_k - \mathbf{x}_k^{(j)}, i - i^{(j)}) \\ &= \sum_{j=1}^N w_{k|k}^{(j)} \cdot \delta(\mathbf{x}_k - \mathbf{x}_k^{(j)}, i - i^{(j)}), \end{aligned} \quad (4.130)$$

where the normalized importance weights are given by

$$w_{k|k}^{(j)} = \frac{w_{k|k-1}^{(j)} \cdot p(\mathbf{z}_k | \mathbf{x}_k^{(j)})}{\sum_{m=1}^N w_{k|k-1}^{(m)} \cdot p(\mathbf{z}_k | \mathbf{x}_k^{(m)})}, \quad j = 1, \dots, N. \quad (4.131)$$

By finally omitting the index  $i$  in the discrete approximation, the desired posterior pdf of the current state is found which is given by

$$p(\mathbf{x}_k | \mathbf{Z}_k) \approx \sum_{j=1}^N w_{k|k}^{(j)} \cdot \delta(\mathbf{x}_k - \mathbf{x}_k^{(j)}). \quad (4.132)$$

## Estimation and Resampling

In the APF, the formulas for estimating the mean vector  $\hat{\mathbf{x}}_{\text{MMSE},k}$  and its covariance  $\hat{\mathbf{P}}_{\text{MMSE},k}$  are equivalent to the formulas given in (4.68). For the resampling step in the APF, systematic resampling is used which is explained in Section 4.5.2.2.

### 4.5.4.3 Choice of Importance Density

In the design of APFs, the choice of the importance density  $q(\mathbf{x}_k, i | \mathbf{Z}_k)$  plays a major role. For the APF, the importance density used to draw the sample  $\{\mathbf{x}_k^{(j)}, i^{(j)}\}_{j=1}^N$  is defined to satisfy the following proportionality

$$q(\mathbf{x}_k, i | \mathbf{Z}_k) \propto p(\mathbf{z}_k | \boldsymbol{\xi}_k^{(i)}) \cdot p(\mathbf{x}_k | \mathbf{x}_{k-1}^{(i)}) \cdot w_{k-1|k-1}^{(i)}, \quad (4.133)$$

[DdFG01, RAG04]. Here,  $\boldsymbol{\xi}_k^{(i)}$  is some characterization of  $\mathbf{x}_k$ , given  $\mathbf{x}_{k-1}^{(i)}$ , for instance, the conditional mean, i.e.,  $\boldsymbol{\xi}_k^{(i)} = \mathbb{E}_{p(\mathbf{x}_k | \mathbf{x}_{k-1}^{(i)})} \{\mathbf{x}_k\}$ , or a sample  $\boldsymbol{\xi}_k^{(i)} \sim p(\mathbf{x}_k | \mathbf{x}_{k-1}^{(i)})$ . The importance density can be further decomposed using Bayes' rule, yielding

$$q(\mathbf{x}_k, i | \mathbf{Z}_k) = q(\mathbf{x}_k | i, \mathbf{Z}_k) \cdot q(i | \mathbf{Z}_k). \quad (4.134)$$

By defining

$$q(\mathbf{x}_k | i, \mathbf{Z}_k) = p(\mathbf{x}_k | \mathbf{x}_{k-1}^{(i)}), \quad (4.135)$$

it follows from (4.133) that

$$q(i | \mathbf{Z}_k) \propto w_{k-1|k-1}^{(i)} \cdot p(\mathbf{z}_k | \boldsymbol{\xi}_k^{(i)}). \quad (4.136)$$

As a result, the weights can be updated according to

$$w_{k|k}^{(j)} \propto w_{k-1|k-1}^{(i^j)} \cdot \frac{p(\mathbf{z}_k | \mathbf{x}_k^{(j)}) \cdot p(\mathbf{x}_k^{(j)} | \mathbf{x}_{k-1}^{(i^j)})}{q(\mathbf{x}_k^{(j)}, i^{(j)} | \mathbf{Z}_k)} = \frac{p(\mathbf{z}_k | \mathbf{x}_k^{(j)})}{p(\mathbf{z}_k | \boldsymbol{\xi}_k^{(i^j)})}. \quad (4.137)$$



The idea of the decomposition in (4.134), is to first sample the discrete index  $i$  of the weighted sum according to  $q(i|\mathbf{Z}_k)$  and then draw particles from the importance density  $q(\mathbf{x}_k|i, \mathbf{Z}_k)$ . By first sampling the discrete index  $i$ , it is possible to find out which components of the weighted sum are most likely to be in the region of high likelihood. This information can be then used to draw particles only from those components of the weighted sum providing high likelihoods and, thus, inefficient sampling from sum components with low likelihoods is avoided. A pseudocode description of the APF is given in Algorithm 4.7. Note that the algorithm can be used for the scenario with LOS propagation conditions as well as for the scenario, where the propagation conditions switch between LOS and NLOS. The only difference is that the likelihood pdf  $p(\mathbf{z}_k|\mathbf{x}_k)$  for the former is given by (3.64) and for the latter is given by (3.83).

### 4.5.5 Rao-Blackwellized Auxiliary Particle Filter

#### 4.5.5.1 Introduction

In this section, the idea of Rao-Blackwellization is applied to the APF. By partitioning the state space into two parts according to (4.71), the corresponding joint posterior pdf can be decomposed into two pdfs using Bayes' rule as follows

$$p(\mathbf{x}_k^n, \mathbf{x}_k^l | \mathbf{Z}_k) = p(\mathbf{x}_k^l | \mathbf{x}_k^n, i, \mathbf{Z}_k) \cdot p(\mathbf{x}_k^n, i | \mathbf{Z}_k). \quad (4.138)$$

The first pdf  $p(\mathbf{x}_k^l | \mathbf{x}_k^n, i, \mathbf{Z}_k)$  can be evaluated analytically using the KF and the second pdf  $p(\mathbf{x}_k^n, i | \mathbf{Z}_k)$  is approximated using the APF. By using this technique, it is possible to reduce the variance of the state estimates of the APF. The resulting filter is called the RBAPF and is also known as the marginalized auxiliary particle filter [FSK09].

#### 4.5.5.2 Derivations

The idea of Rao-Blackwellization can be exploited in the APF, if the system model is conditionally linear. A system model that fulfills this requirement is given by (4.73), which can be further simplified to (4.76). In the following, the RBAPF is derived for the hybrid localization problem using the decorrelated system model as given in (4.76).

---

**Algorithm 4.7** Auxiliary Particle Filter
 

---

## 1. Initialization:

- For  $i = 1, \dots, N$ , initialize the particles  $\mathbf{x}_0^{(i)} \sim p(\mathbf{x}_0)$  and weights  $w_{0|0}^{(i)} = \frac{1}{N}$ .

## 2. Time Update and Measurement Update (First Stage Weights):

- For  $i = 1, \dots, N$ , determine  $\boldsymbol{\xi}_k^{(i)}$  according to

$$\boldsymbol{\xi}_k^{(i)} = \mathbb{E}_{p(\mathbf{x}_k|\mathbf{x}_{k-1}^{(i)})} \{\mathbf{x}_k\}.$$

- For  $i = 1, \dots, N$ , evaluate the first stage weights

$$w_{k|k-1}^{(i)} = q(i|\mathbf{Z}_k) = \frac{w_{k-1|k-1}^{(i)} \cdot p(\mathbf{z}_k|\boldsymbol{\xi}_k^{(i)})}{\sum_{m=1}^N w_{k-1|k-1}^{(m)} \cdot p(\mathbf{z}_k|\boldsymbol{\xi}_k^{(m)})}.$$

## 3. Resampling:

- Perform systematic resampling using Algorithm 4.4. Take  $N$  samples with replacement from the set  $\{\boldsymbol{\xi}_k^{(i)}\}_{i=1}^N$ , where the probability to take sample  $i$  is  $w_{k|k-1}^{(i)}$ . Store for each resampled particle the parent index, denoted by  $i^{(j)}$ .

## 4. Time Update and Measurement Update (Second Stage Weights):

- For  $j = 1, \dots, N$ , draw particles from the importance density according to

$$\mathbf{x}_k^{(j)} \sim q(\mathbf{x}_k|i, \mathbf{Z}_k) = p(\mathbf{x}_k|\mathbf{x}_{k-1}^{(i^{(j)})}).$$

- For  $j = 1, \dots, N$ , evaluate the second stage weights

$$\tilde{w}_{k|k}^{(j)} = \frac{p(\mathbf{z}_k|\mathbf{x}_k^{(j)})}{p(\mathbf{z}_k|\boldsymbol{\xi}_k^{(i^{(j)})})},$$

and normalize the weights according to  $w_{k|k}^{(j)} = \tilde{w}_{k|k}^{(j)} / \sum_{m=1}^N \tilde{w}_{k|k}^{(m)}$ .

## 5. Estimation:

- Determine an estimate of the state vector according to

$$\hat{\mathbf{x}}_k = \sum_{j=1}^N w_{k|k}^{(j)} \cdot \mathbf{x}_k^{(j)}.$$

6. Set  $k := k + 1$  and iterate from step 2.

## Initialization

The RBAPF is initialized as follows:

$$p(\mathbf{x}_{k-1}^n, \mathbf{x}_{k-1}^1 | \mathbf{Z}_{k-1}) \approx \sum_{i=1}^N w_{k-1|k-1}^{(i)} \cdot \mathcal{N}(\mathbf{x}_{k-1}^1; \mathbf{x}_{k-1|k-1}^{1,(i)}, \mathbf{P}_{k-1|k-1}^{(i)}) \cdot \delta(\mathbf{x}_{k-1}^n - \mathbf{x}_{k-1}^{n,(i)}). \quad (4.139)$$

## Time Update

The time update starts with evaluating the prediction density  $p(\mathbf{x}_k^n, \mathbf{x}_k^1 | \mathbf{Z}_{k-1})$ . Following the same derivation steps as in the RBPF, cf. Section 4.5.3.2, this density can be written as

$$\begin{aligned} p(\mathbf{x}_k^n, \mathbf{x}_k^1 | \mathbf{Z}_{k-1}) &= \sum_{i=1}^N p(\mathbf{x}_k^n, \mathbf{x}_k^1, i | \mathbf{Z}_{k-1}) \\ &= \sum_{i=1}^N p(\mathbf{x}_k^1 | \mathbf{x}_k^n, i, \mathbf{Z}_{k-1}) \cdot p(\mathbf{x}_k^n, i | \mathbf{Z}_{k-1}) \\ &\approx \sum_{i=1}^N w_{k-1|k-1}^{(i)} \cdot \mathcal{N}(\mathbf{x}_k^1; \mathbf{x}_{k|k-1}^{1,(i)}, \mathbf{P}_{k|k-1}^{(i)}) \cdot \mathcal{N}(\mathbf{x}_k^n; \bar{\mathbf{x}}_{k|k-1}^{n,(i)}, \bar{\mathbf{P}}_{k|k-1}^{n,(i)}), \end{aligned} \quad (4.140)$$

where  $\mathbf{x}_{k|k-1}^{1,(i)}$  and  $\mathbf{P}_{k|k-1}^{(i)}$  are given by (4.87) and  $\bar{\mathbf{x}}_{k|k-1}^{n,(i)}$  and  $\bar{\mathbf{P}}_{k|k-1}^{n,(i)}$  are given by (4.85), respectively. Comparing (4.140) with (4.141) leads to

$$p(\mathbf{x}_k^1 | \mathbf{x}_k^n, i, \mathbf{Z}_{k-1}) = \mathcal{N}(\mathbf{x}_k^1; \mathbf{x}_{k|k-1}^{1,(i)}, \mathbf{P}_{k|k-1}^{(i)}), \quad (4.142)$$

$$p(\mathbf{x}_k^n, i | \mathbf{Z}_{k-1}) = w_{k-1|k-1}^{(i)} \cdot \mathcal{N}(\mathbf{x}_k^n; \bar{\mathbf{x}}_{k|k-1}^{n,(i)}, \bar{\mathbf{P}}_{k|k-1}^{n,(i)}). \quad (4.143)$$

The joint prediction pdf  $p(\mathbf{x}_k^n, i | \mathbf{Z}_{k-1})$  is continuous with respect to the nonlinear state  $\mathbf{x}_k^n$  and discrete with respect to  $i$ . In the following, a weighted discrete approximation of  $p(\mathbf{x}_k^n, i | \mathbf{Z}_{k-1})$  is obtained using an importance sampling approach. The key idea is to represent each component of the weighted sum by a single particle and its corresponding discrete index, that is sampled from the following importance density

$$\mathbf{x}_k^{n,(j)}, i^{(j)} \sim q(\mathbf{x}_k^n, i | \mathbf{Z}_{k-1}, \mathbf{z}_k), \quad j = 1, \dots, N, \quad (4.144)$$

where the latest measurement  $\mathbf{z}_k$  is taken into account in the importance density. As a result, the joint prediction pdf can be approximated as

$$p(\mathbf{x}_k^n, \mathbf{x}_k^1, i | \mathbf{Z}_{k-1}) \approx \sum_{j=1}^N w_{k|k-1}^{(j)} \cdot \mathcal{N}(\mathbf{x}_k^1; \mathbf{x}_{k|k-1}^{1,(j)}, \mathbf{P}_{k|k-1}^{(j)}) \cdot \delta(\mathbf{x}_k^n - \mathbf{x}_k^{n,(j)}, i - i^{(j)}), \quad (4.145)$$

where

$$\mathbf{x}_{k|k-1}^{1,(j)} = \bar{\mathbf{x}}_{k|k-1}^{1,(ij)} + \bar{\mathbf{P}}_{k|k-1}^{\text{nl},(ij),\text{T}} \cdot [\bar{\mathbf{P}}_{k|k-1}^{\text{n},(ij)}]^{-1} \cdot (\mathbf{x}_k^{\text{n},(j)} - \bar{\mathbf{x}}_{k|k-1}^{\text{n},(ij)}), \quad (4.146\text{a})$$

$$\mathbf{P}_{k|k-1}^{(j)} = \bar{\mathbf{P}}_{k|k-1}^{1,(ij)} - \bar{\mathbf{P}}_{k|k-1}^{\text{nl},(ij),\text{T}} \cdot [\bar{\mathbf{P}}_{k|k-1}^{\text{n},(ij)}]^{-1} \cdot \bar{\mathbf{P}}_{k|k-1}^{\text{nl},(ij)}, \quad (4.146\text{b})$$

and

$$w_{k|k-1}^{(j)} \propto w_{k-1|k-1}^{(ij)} \cdot \frac{\mathcal{N}(\mathbf{x}_k^{\text{n},(j)}; \bar{\mathbf{x}}_{k|k-1}^{\text{n},(ij)}, \bar{\mathbf{P}}_{k|k-1}^{\text{n},(ij)})}{q(\mathbf{x}_k^{\text{n},(j)}, i^{(j)} | \mathbf{Z}_k)}, \quad j = 1, \dots, N. \quad (4.147)$$

The importance weights have to be further normalized to ensure  $\sum_{m=1}^N w_{k|k-1}^{(m)} = 1$ .

## Measurement Update

The measurement update distribution can be split as follows:

$$p(\mathbf{x}_k^{\text{n}}, \mathbf{x}_k^1, i | \mathbf{Z}_k) = p(\mathbf{x}_k^1 | \mathbf{x}_k^{\text{n}}, i, \mathbf{Z}_k) \cdot p(\mathbf{x}_k^{\text{n}}, i | \mathbf{Z}_k). \quad (4.148)$$

The two parts can be evaluated separately. The first distribution can be updated for each particle from the following relationship

$$\begin{aligned} p(\mathbf{x}_k^1 | \mathbf{x}_k^{\text{n},(j)}, i^{(j)}, \mathbf{Z}_k) &= \frac{p(\mathbf{z}_k | \mathbf{x}_k^1, \mathbf{x}_k^{\text{n},(j)}, i^{(j)}, \mathbf{Z}_{k-1}) \cdot p(\mathbf{x}_k^1 | \mathbf{x}_k^{\text{n},(j)}, i^{(j)}, \mathbf{Z}_{k-1})}{p(\mathbf{z}_k | \mathbf{x}_k^{\text{n},(j)}, i^{(j)}, \mathbf{Z}_{k-1})} \\ &= \frac{p(\mathbf{z}_k | \mathbf{x}_k^1, \mathbf{x}_k^{\text{n},(j)}) \cdot p(\mathbf{x}_k^1 | \mathbf{x}_k^{\text{n},(j)}, i^{(j)}, \mathbf{Z}_{k-1})}{p(\mathbf{z}_k | \mathbf{x}_k^{\text{n},(j)}, \mathbf{Z}_{k-1})}, \end{aligned} \quad (4.149)$$

where

$$p(\mathbf{z}_k | \mathbf{x}_k^{\text{n},(j)}, \mathbf{Z}_{k-1}) = \int_{\mathbb{R}^{n_x}} p(\mathbf{z}_k | \mathbf{x}_k^1, \mathbf{x}_k^{\text{n},(j)}) \cdot p(\mathbf{x}_k^1 | \mathbf{x}_k^{\text{n},(j)}, i^{(j)}, \mathbf{Z}_{k-1}) \, d\mathbf{x}_k^1. \quad (4.150)$$

For the measurement models given by (4.76c) and (4.76d), the relationship in (4.149) can be simplified, cf. Section 4.5.3.2, yielding

$$p(\mathbf{x}_k^1 | \mathbf{x}_k^{\text{n},(j)}, i^{(j)}, \mathbf{Z}_k) = \frac{p(\mathbf{z}_{1,k} | \mathbf{x}_k^{\text{n},(j)}, \mathbf{x}_k^1) \cdot p(\mathbf{x}_k^1 | \mathbf{x}_k^{\text{n},(j)}, i^{(j)}, \mathbf{Z}_{k-1})}{p(\mathbf{z}_{1,k} | \mathbf{x}_k^{\text{n},(j)}, \mathbf{Z}_{k-1})}, \quad (4.151)$$

where

$$p(\mathbf{z}_{1,k} | \mathbf{x}_k^{\text{n},(j)}, \mathbf{Z}_{k-1}) = \int_{\mathbb{R}^{n_{x_1}}} p(\mathbf{z}_{1,k} | \mathbf{x}_k^{\text{n},(j)}, \mathbf{x}_k^1) \cdot p(\mathbf{x}_k^1 | \mathbf{x}_k^{\text{n},(j)}, i^{(j)}, \mathbf{Z}_{k-1}) \, d\mathbf{x}_k^1. \quad (4.152)$$

The likelihood pdf  $p(\mathbf{z}_{1,k} | \mathbf{x}_k^{\text{n},(j)}, \mathbf{x}_k^1)$  is Gaussian and given by (4.98) and the density  $p(\mathbf{x}_k^1 | \mathbf{x}_k^{\text{n},(j)}, i^{(j)}, \mathbf{Z}_{k-1})$  is available from the time update stage and is given by

$$p(\mathbf{x}_k^1 | \mathbf{x}_k^{\text{n},(j)}, i^{(j)}, \mathbf{Z}_{k-1}) = \mathcal{N}(\mathbf{x}_k^1; \bar{\mathbf{x}}_{k|k-1}^{1,(j)}, \mathbf{P}_{k|k-1}^{(j)}). \quad (4.153)$$

Since both pdfs are Gaussian, the integral in (4.152) can be evaluated analytically, yielding

$$p(\mathbf{z}_{1,k} | \mathbf{x}_k^{n,(j)}, \mathbf{Z}_{k-1}) = \mathcal{N}(\mathbf{z}_{1,k}; \hat{\mathbf{z}}_{1,k}^{(j)}, \mathbf{S}_k^{(j)}), \quad (4.154)$$

where  $\hat{\mathbf{z}}_{1,k}^{(j)}$  and  $\mathbf{S}_k^{(j)}$  are obtained from (4.101) by replacing the index  $i$  with the new index  $j$ . Since the densities involved in evaluating the measurement update, cf. (4.151), are all Gaussian, the density  $p(\mathbf{x}_k^1 | \mathbf{x}_k^{n,(j)}, i^{(j)}, \mathbf{Z}_k)$  is also Gaussian and is given by

$$p(\mathbf{x}_k^1 | \mathbf{x}_k^{n,(j)}, i^{(j)}, \mathbf{Z}_k) = \mathcal{N}(\mathbf{x}_k^1; \mathbf{x}_{k|k}^{1,(j)}, \mathbf{P}_{k|k}^{(j)}), \quad (4.155)$$

where  $\mathbf{x}_{k|k}^{1,(j)}$  and  $\mathbf{P}_{k|k}^{(j)}$  are obtained from (4.103) by replacing the index  $i$  with the new index  $j$ .

The measurement update for the nonlinear states  $\mathbf{x}_k^n$  is done as follows:

$$p(\mathbf{x}_k^n, i | \mathbf{Z}_k) = \frac{p(\mathbf{z}_k | \mathbf{x}_k^n, i, \mathbf{Z}_{k-1}) \cdot p(\mathbf{x}_k^n, i | \mathbf{Z}_{k-1})}{p(\mathbf{z}_k | \mathbf{Z}_{k-1})}. \quad (4.156)$$

Since the pdf  $p(\mathbf{x}_k^n, i | \mathbf{Z}_k)$  is approximated using an importance sampling approach, the denominator in (4.156) will be numerically normed and has not to be calculated. The measurement update can be written as

$$\begin{aligned} p(\mathbf{x}_k^n, i | \mathbf{Z}_k) &\propto p(\mathbf{z}_k | \mathbf{x}_k^n, i, \mathbf{Z}_{k-1}) \cdot p(\mathbf{x}_k^n, i | \mathbf{Z}_{k-1}) \\ &= \int_{\mathbb{R}^{n_{x_1}}} p(\mathbf{z}_k | \mathbf{x}_k^n, \mathbf{x}_k^1, i, \mathbf{Z}_{k-1}) \cdot p(\mathbf{x}_k^1 | \mathbf{x}_k^n, i, \mathbf{Z}_{k-1}) d\mathbf{x}_k^1 \cdot p(\mathbf{x}_k^n, i | \mathbf{Z}_{k-1}) \\ &= \int_{\mathbb{R}^{n_{x_1}}} p(\mathbf{z}_{1,k} | \mathbf{x}_k^n, \mathbf{Z}_{k-1}) \cdot p(\mathbf{x}_k^1 | \mathbf{x}_k^n, i, \mathbf{Z}_{k-1}) d\mathbf{x}_k^1 \cdot p(\mathbf{z}_{2,k} | \mathbf{x}_k^n) \cdot p(\mathbf{x}_k^n, i | \mathbf{Z}_{k-1}) \\ &\approx \sum_{j=1}^N w_{k|k-1}^{(ij)} \cdot \underbrace{p(\mathbf{z}_{1,k} | \mathbf{x}_k^{n,(j)}, \mathbf{Z}_{k-1})}_{(4.154)} \cdot p(\mathbf{z}_{2,k} | \mathbf{x}_k^{n,(j)}) \cdot \delta(\mathbf{x}_k^n - \mathbf{x}_k^{n,(j)}, i - i^{(j)}) \\ &= \sum_{j=1}^N w_{k|k}^{(ij)} \cdot \delta(\mathbf{x}_k^n - \mathbf{x}_k^{n,(j)}, i - i^{(j)}), \end{aligned} \quad (4.157)$$

where the normalized importance weights are given by

$$w_{k|k}^{(j)} = \frac{w_{k|k-1}^{(ij)} \cdot \mathcal{N}(\mathbf{z}_{1,k}; \hat{\mathbf{z}}_{1,k}^{(j)}, \mathbf{S}_k^{(j)}) \cdot p(\mathbf{z}_{2,k} | \mathbf{x}_k^{n,(j)})}{\sum_{m=1}^N w_{k|k-1}^{(im)} \cdot \mathcal{N}(\mathbf{z}_{1,k}; \hat{\mathbf{z}}_{1,k}^{(m)}, \mathbf{S}_k^{(m)}) \cdot p(\mathbf{z}_{2,k} | \mathbf{x}_k^{n,(m)})}, \quad j = 1, \dots, N. \quad (4.158)$$

Combining (4.153) and (4.158) according to (4.148) results in

$$p(\mathbf{x}_k^n, \mathbf{x}_k^1, i | \mathbf{Z}_k) \approx \sum_{j=1}^N w_{k|k}^{(j)} \mathcal{N}(\mathbf{x}_k^1; \mathbf{x}_{k|k}^{1,(j)}, \mathbf{P}_{k|k}^{(j)}) \cdot \delta(\mathbf{x}_k^n - \mathbf{x}_k^{n,(j)}, i - i^{(j)}). \quad (4.159)$$

By finally omitting the index  $i$  in the discrete approximation, the posterior pdf is found which is given by

$$p(\mathbf{x}_k^n, \mathbf{x}_k^1 | \mathbf{Z}_k) \approx \sum_{j=1}^N w_{k|k}^{(j)} \mathcal{N}(\mathbf{x}_k^1; \mathbf{x}_{k|k}^{1,(j)}, \mathbf{P}_{k|k}^{(j)}) \cdot \delta(\mathbf{x}_k^n - \mathbf{x}_k^{n,(j)}). \quad (4.160)$$

## Estimation and Resampling

In the RBAPF, the formulas for estimating the mean vector  $\hat{\mathbf{x}}_{\text{MMSE},k}$  and its covariance  $\hat{\mathbf{P}}_{\text{MMSE},k}$  of the linear and nonlinear states are equivalent to the formulas given in (4.108). For the resampling step in the RBAPF, systematic resampling is used which is explained in Section 4.5.2.2.

### 4.5.5.3 Choice of Importance Density

In the design of RBAPFs, the choice of the importance density  $q(\mathbf{x}_k^n, i | \mathbf{Z}_k)$  plays a major role. Similar to the APF, the importance density used to draw the sample  $\{\mathbf{x}_k^{n,(j)}, i^{(j)}\}_{j=1}^N$  is defined to satisfy the following proportionality

$$q(\mathbf{x}_k^n, i | \mathbf{Z}_k) \propto p(\mathbf{z}_{1,k} | \boldsymbol{\xi}_k^{n,(i)}, \mathbf{Z}_{k-1}) \cdot p(\mathbf{z}_{2,k} | \boldsymbol{\xi}_k^{n,(i)}) \cdot \mathcal{N}(\mathbf{x}_k^n; \bar{\mathbf{x}}_{k|k-1}^{n,(i)}, \bar{\mathbf{P}}_{k|k-1}^{n,(i)}) \cdot w_{k-1|k-1}^{(i)}, \quad (4.161)$$

where  $\boldsymbol{\xi}_k^{n,(i)}$  is some characterization of  $\mathbf{x}_k^n$  (e.g. the mean, mode or a sample) that is associated to the density  $\mathcal{N}(\mathbf{x}_k^n; \bar{\mathbf{x}}_{k|k-1}^{n,(i)}, \bar{\mathbf{P}}_{k|k-1}^{n,(i)})$ . The importance density can be further decomposed using Bayes' rule, yielding

$$q(\mathbf{x}_k^n, i | \mathbf{Z}_k) = q(\mathbf{x}_k^n | i, \mathbf{Z}_k) \cdot q(i | \mathbf{Z}_k). \quad (4.162)$$

By defining

$$q(\mathbf{x}_k^n | i, \mathbf{Z}_k) = \mathcal{N}(\mathbf{x}_k^n; \bar{\mathbf{x}}_{k|k-1}^{n,(i)}, \bar{\mathbf{P}}_{k|k-1}^{n,(i)}), \quad (4.163)$$

it follows from (4.161) that

$$q(i | \mathbf{Z}_k) \propto w_{k-1|k-1}^{(i)} \cdot p(\mathbf{z}_{1,k} | \boldsymbol{\xi}_k^{n,(i)}, \mathbf{Z}_k) \cdot p(\mathbf{z}_{2,k} | \boldsymbol{\xi}_k^{n,(i)}). \quad (4.164)$$

As a result, the weights can be updated according to

$$\begin{aligned} w_{k|k}^{(j)} &\propto w_{k-1|k-1}^{(j)} \cdot \frac{\mathcal{N}(\mathbf{x}_k^{n,(j)}; \bar{\mathbf{x}}_{k|k-1}^{n,(j)}, \bar{\mathbf{P}}_{k|k-1}^{n,(j)}) \cdot p(\mathbf{z}_{1,k} | \mathbf{x}_k^{n,(j)}, \mathbf{Z}_k) \cdot p(\mathbf{z}_{2,k} | \mathbf{x}_k^{n,(j)})}{q(\mathbf{x}_k^{n,(j)}, i^{(j)} | \mathbf{Z}_k)} \\ &= \frac{p(\mathbf{z}_{1,k} | \mathbf{x}_k^{n,(j)}, \mathbf{Z}_k) \cdot p(\mathbf{z}_{2,k} | \mathbf{x}_k^{n,(j)})}{p(\mathbf{z}_{1,k} | \boldsymbol{\xi}_k^{n,(j)}, \mathbf{Z}_k) \cdot p(\mathbf{z}_{2,k} | \boldsymbol{\xi}_k^{n,(j)})}, \quad j = 1, \dots, N. \end{aligned} \quad (4.165)$$

A pseudocode description of the RBAPF with the abbreviations introduced in (4.111) is given in Algorithm 4.8. Note that the algorithm can be used for the scenario with LOS propagation conditions as well as for the scenario, where the propagation conditions switch between LOS and NLOS. The necessary decompositions of the state and measurement models are equivalent to the decompositions presented in Section 4.5.3.4.

---

**Algorithm 4.8** Rao-Blackwellized Auxiliary Particle Filter
 

---

1. Initialization:

- For  $i = 1, \dots, N$ , initialize the particles  $\mathbf{x}_0^{n,(i)} \sim p(\mathbf{x}_0^n)$  and weights  $w_{0|0}^{(i)} = \frac{1}{N}$ , and set  $\{\hat{\mathbf{x}}_{0|0}^{1,(i)}, \mathbf{P}_{0|0}^{(i)}\} = \{\hat{\mathbf{x}}_0^1, \mathbf{P}_0\}$ .

2. Particle Filter Time Update and Measurement Update (First Stage Weights):

- For  $i = 1, \dots, N$ , determine  $\boldsymbol{\xi}_k^{n,(i)}$  from  $\mathcal{N}(\mathbf{x}_k^n; \bar{\mathbf{x}}_{k|k-1}^{n,(i)}, \bar{\mathbf{P}}_{k|k-1}^{n,(i)})$ , e.g., take the mean  $\boldsymbol{\xi}_k^{n,(i)} = \bar{\mathbf{x}}_{k|k-1}^{n,(i)}$ , where

$$\begin{aligned}\bar{\mathbf{x}}_{k|k-1}^{n,(i)} &= \mathbf{f}_{k-1}^{n,(i)} + \mathbf{F}_{k-1}^{n,(i)} \cdot \mathbf{x}_{k-1|k-1}^{1,(i)}, \\ \bar{\mathbf{P}}_{k|k-1}^{n,(i)} &= \mathbf{F}_{k-1}^{n,(i)} \cdot \mathbf{P}_{k-1|k-1}^{(i)} \cdot \mathbf{F}_{k-1}^{n,(i)\top} + \mathbf{\Gamma}_{k-1}^{n,(i)} \cdot \mathbf{Q}_{k-1}^n \cdot \mathbf{\Gamma}_{k-1}^{n,(i)\top}.\end{aligned}$$

- For  $i = 1, \dots, N$ , evaluate the first stage weights

$$w_{k|k-1}^{(i)} = q(i|\mathbf{Z}_k) = \frac{w_{k-1|k-1}^{(i)} \cdot \mathcal{N}(\mathbf{z}_{1,k}; \tilde{\mathbf{z}}_{1,k}^{(i)}, \tilde{\mathbf{S}}_k^{(i)}) \cdot p(\mathbf{z}_{2,k}|\boldsymbol{\xi}_k^{(i)})}{\sum_{m=1}^N w_{k-1|k-1}^{(m)} \cdot \mathcal{N}(\mathbf{z}_{1,k}; \tilde{\mathbf{z}}_{1,k}^{(m)}, \tilde{\mathbf{S}}_k^{(m)}) \cdot p(\mathbf{z}_{2,k}|\boldsymbol{\xi}_k^{(m)})}.$$

where

$$\begin{aligned}\tilde{\mathbf{z}}_k^{(i)} &= \mathbf{h}_k(\boldsymbol{\xi}_k^{n,(i)}) + \mathbf{H}_k(\boldsymbol{\xi}_k^{n,(i)}) \cdot \tilde{\mathbf{x}}_{k|k-1}^{1,(i)}, \\ \tilde{\mathbf{S}}_k^{(i)} &= \mathbf{H}_k(\boldsymbol{\xi}_k^{n,(i)}) \cdot \tilde{\mathbf{P}}_{k|k-1}^{1,(i)} \cdot \mathbf{H}_k(\boldsymbol{\xi}_k^{n,(i)\top}) + \mathbf{R}_{1,k}, \\ \tilde{\mathbf{x}}_{k|k-1}^{1,(i)} &= \bar{\mathbf{x}}_{k|k-1}^{1,(i)} + \bar{\mathbf{P}}_{k|k-1}^{nl,(i)\top} \cdot [\bar{\mathbf{P}}_{k|k-1}^{nl,(i)}]^{-1} \cdot (\boldsymbol{\xi}_k^{n,(i)} - \bar{\mathbf{x}}_{k|k-1}^{n,(i)}), \\ \tilde{\mathbf{P}}_{k|k-1}^{1,(i)} &= \bar{\mathbf{P}}_{k|k-1}^{1,(i)} - \bar{\mathbf{P}}_{k|k-1}^{nl,(i)\top} \cdot [\bar{\mathbf{P}}_{k|k-1}^{nl,(i)}]^{-1} \cdot \bar{\mathbf{P}}_{k|k-1}^{nl,(i)},\end{aligned}$$

and

$$\begin{aligned}\bar{\mathbf{x}}_{k|k-1}^{1,(i)} &= \mathbf{f}_{k-1}^{1,(i)} + \bar{\mathbf{F}}_{k-1}^{1,(i)} \cdot \mathbf{x}_{k-1|k-1}^{1,(i)} + \bar{\mathbf{E}}_k^{(i)}(\boldsymbol{\xi}_k^{n,(i)}), \\ \bar{\mathbf{P}}_{k|k-1}^{1,(i)} &= \bar{\mathbf{F}}_{k-1}^{1,(i)} \cdot \mathbf{P}_{k-1|k-1}^{(i)} \cdot \bar{\mathbf{F}}_{k-1}^{1,(i)\top} + \mathbf{\Gamma}_{k-1}^{1,(i)} \cdot \bar{\mathbf{Q}}_{k-1}^1 \cdot \mathbf{\Gamma}_{k-1}^{1,(i)\top}, \\ \bar{\mathbf{P}}_{k|k-1}^{nl,(i)} &= \mathbf{F}_{k-1}^{n,(i)} \cdot \mathbf{P}_{k-1|k-1}^{(i)} \cdot \bar{\mathbf{F}}_{k-1}^{1,(i)\top}, \\ \bar{\mathbf{E}}_k^{(i)}(\boldsymbol{\xi}_k^{n,(i)}) &= \mathbf{\Gamma}_{k-1}^{1,(i)} \cdot \mathbf{Q}_{k-1}^{nl,\top} \cdot [\mathbf{\Gamma}_{k-1}^{n,(i)} \cdot \mathbf{Q}_{k-1}^n]^{-1} \cdot (\boldsymbol{\xi}_k^{n,(i)} - \mathbf{f}_{k-1}^{n,(i)}), \\ \bar{\mathbf{F}}_{k-1}^{1,(i)} &= \mathbf{F}_{k-1}^{1,(i)} - \mathbf{\Gamma}_{k-1}^{1,(i)} \cdot \mathbf{Q}_{k-1}^{nl,\top} \cdot [\mathbf{\Gamma}_{k-1}^{n,(i)} \cdot \mathbf{Q}_{k-1}^n]^{-1} \cdot \mathbf{F}_{k-1}^{n,(i)}, \\ \bar{\mathbf{Q}}_{k-1}^1 &= \mathbf{Q}_{k-1}^1 - \mathbf{Q}_{k-1}^{nl,\top} \cdot [\mathbf{Q}_{k-1}^n]^{-1} \cdot \mathbf{Q}_{k-1}^{nl}.\end{aligned}$$

3. Resampling:

- Perform systematic resampling using Algorithm 4.4. Take  $N$  samples with replacement from the set  $\{\boldsymbol{\xi}_k^{n,(i)}\}_{i=1}^N$ , where the probability to take sample  $i$  is  $w_{k|k-1}^{(i)}$ . Store for each resampled particle the parent index denoted by  $i^{(j)}$ .

## 4. Particle Filter Time Update:

- For  $j = 1, \dots, N$ , draw particles from the importance density according to

$$\mathbf{x}_k^{n,(j)} \sim q(\mathbf{x}_k^n | i^{(j)}, \mathbf{Z}_k) = \mathcal{N}(\mathbf{x}_k^n; \bar{\mathbf{x}}_{k|k-1}^{n,(i^j)}, \bar{\mathbf{P}}_{k|k-1}^{n,(i^j)}).$$

## 5. Kalman Filter Time Update:

- For  $j = 1, \dots, N$ , evaluate

$$\begin{aligned} \mathbf{x}_{k|k-1}^{1,(j)} &= \bar{\mathbf{x}}_{k|k-1}^{1,(j)} + \bar{\mathbf{P}}_{k|k-1}^{nl,(i^j),\top} \cdot [\bar{\mathbf{P}}_{k|k-1}^{n,(i^j)}]^{-1} \cdot (\mathbf{x}_k^{n,(j)} - \bar{\mathbf{x}}_{k|k-1}^{n,(i^j)}), \\ \mathbf{P}_{k|k-1}^{(j)} &= \bar{\mathbf{P}}_{k|k-1}^{1,(i^j)} - \bar{\mathbf{P}}_{k|k-1}^{nl,(i^j),\top} \cdot [\bar{\mathbf{P}}_{k|k-1}^{n,(i^j)}]^{-1} \cdot \bar{\mathbf{P}}_{k|k-1}^{n,(i^j)}, \end{aligned}$$

where

$$\bar{\mathbf{x}}_{k|k-1}^{1,(j)} = \mathbf{f}_{k-1}^{n,(i^j)} + \mathbf{F}_{k-1}^{n,(i^j)} \cdot \mathbf{x}_{k-1|k-1}^{1,(i^j)} + \bar{\mathbf{E}}_k^{(i^j)}(\mathbf{x}_k^{n,(j)}).$$

## 6. Particle Filter Measurement Update (Second Stage Weights):

- For  $j = 1, \dots, N$ , evaluate the second stage weights

$$\tilde{w}_{k|k}^{(j)} = \frac{\mathcal{N}(\mathbf{z}_{1,k}; \hat{\mathbf{z}}_{1,k}^{(j)}, \mathbf{S}_k^{(j)}) \cdot p(\mathbf{z}_{2,k} | \mathbf{x}_k^{n,(j)})}{\mathcal{N}(\mathbf{z}_{1,k}; \tilde{\mathbf{z}}_{1,k}^{(j)}, \tilde{\mathbf{S}}_k^{(j)}) \cdot p(\mathbf{z}_{2,k} | \xi_k^{n,(i^j)})},$$

where

$$\begin{aligned} \hat{\mathbf{z}}_{1,k}^{(j)} &= \mathbf{h}_{1,k}^{(j)} + \mathbf{H}_k^{(j)} \cdot \mathbf{x}_{k|k-1}^{1,(j)}, \\ \mathbf{S}_k^{(j)} &= \mathbf{H}_k^{(j)} \cdot \mathbf{P}_{k|k-1}^{(j)} \cdot \mathbf{H}_k^{(j),\top} + \mathbf{R}_{1,k}, \end{aligned}$$

and normalize the weights according to  $w_{k|k}^{(j)} = \tilde{w}_{k|k}^{(j)} / \sum_{m=1}^N \tilde{w}_{k|k}^{(m)}$ .

## 7. Kalman Filter Measurement Update:

- For  $j = 1, \dots, N$ , evaluate

$$\begin{aligned} \mathbf{x}_{k|k}^{1,(j)} &= \mathbf{x}_{k|k-1}^{1,(j)} + \mathbf{K}_k^{(j)} \cdot (\mathbf{z}_{1,k} - \hat{\mathbf{z}}_{1,k}^{(j)}), \\ \mathbf{P}_{k|k}^{(j)} &= \mathbf{P}_{k|k-1}^{(j)} - \mathbf{K}_k^{(j)} \cdot \mathbf{S}_k^{(j)} \cdot \mathbf{K}_k^{(j),\top}, \end{aligned}$$

where

$$\mathbf{K}_k^{(j)} = \mathbf{P}_{k|k-1}^{(j)} \cdot \mathbf{H}_k^{(j),\top} \cdot [\mathbf{S}_k^{(j)}]^{-1}.$$

## 8. Estimation:

- Determine estimates of the linear and nonlinear state vectors according to

$$\hat{\mathbf{x}}_{\text{MMSE},k|k}^n = \sum_{j=1}^N w_{k|k}^{(j)} \cdot \mathbf{x}_k^{n,(j)}, \quad \hat{\mathbf{x}}_{\text{MMSE},k|k}^1 = \sum_{j=1}^N w_{k|k}^{(j)} \cdot \mathbf{x}_{k|k}^{1,(j)}.$$

9. Set  $i := j$  and  $k := k + 1$  and iterate from step 2.



## 4.5.6 Particle Filter with Road Constraints

### 4.5.6.1 Introduction

In many situations, additional information such as road maps are available to the MT, that can be additionally used to further constrain the MT movement to roads. If such an information is available to the MT, it should be taken into account in the hybrid localization algorithm, since it further improves the performance. Until now, several approaches have been proposed to efficiently incorporate road constraints into PF-based estimators, see for instance [AMGC02, RAG04, UK06, ES07, CS07, OSG09]. The vast majority of approaches consider that the movement of the MT can switch between on-road and off-road, which is described by different state models. These models are then incorporated into a multiple model filtering approach that can efficiently keep track of the different MT movements [CS07, OSG09]. In this work, it is assumed that the MT is restricted to on-road movements and no off-road movement is considered. Hence, a multiple model filtering approach is no longer necessary and a PF can be used to implement the road-constrained approach.

### 4.5.6.2 Incorporation of Road Constraints

In this section, it is shown how road constraints can be incorporated into the PF for hybrid localization. The road-constrained approach presented in this work is taken from [OSG09], where it was used to track targets, which can move both on-road and off-road, with a multiple model particle filter approach.

It is assumed that a road network database  $\mathcal{T}_{RN}$  is available to the MT. A road is assumed to be represented by straight line segments with corresponding endpoints that are connected with each other. Each line segment is assigned a different road identity denoted by  $s_{ID}$ , which is stored together with the corresponding endpoints in the road network database  $\mathcal{T}_{RN}$ . The key idea of the approach presented in [OSG09], is to express the MT state model, cf. Section 2.3.2, in a local coordinate system and the measurement model, cf. Section 2.3.3, in a global coordinate system. The local coordinate system is road-segment based. The origin (or the reference point) of the local coordinate system is placed at one of the endpoints of the corresponding road segment, where the local  $x_L$ - and  $y_L$ -axes are aligned along and perpendicular to the road as shown in Fig. 4.2. In the following, only MT movement along the road is considered, so that the position and speed of the MT on the road segment can be expressed by the scalar variables  $p_{MT}$  and  $\dot{p}_{MT}$ . Since the state and measurement models

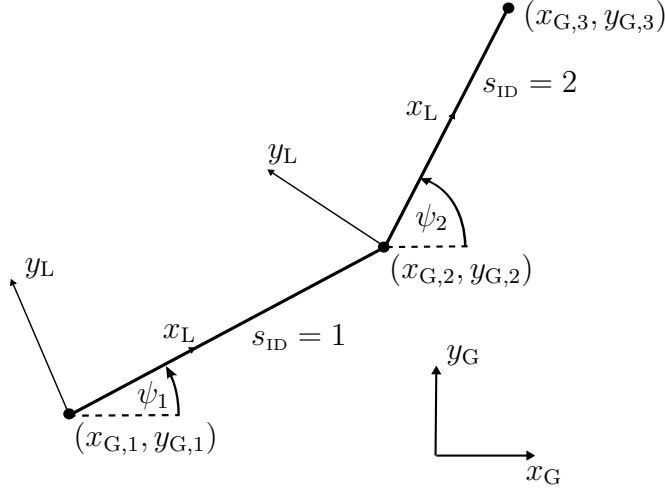


Figure 4.2. Relationship between global coordinate system and local, road-constrained, coordinate system.

use different coordinate systems, appropriate functions to convert the state vector from one coordinate system representation into the other coordinate system representation are needed. For the road-constrained approach investigated in this work, only the transformation  $\mathbf{T}_{LG}(\cdot)$  from local coordinates to global coordinates is required, which is given by

$$\begin{bmatrix} x_{MT} \\ y_{MT} \\ \dot{x}_{MT} \\ \dot{y}_{MT} \end{bmatrix} = \mathbf{T}_{LG} \left( \begin{bmatrix} p_{MT} \\ \dot{p}_{MT} \\ s_{ID} \end{bmatrix}, \mathcal{T}_{RN} \right) = \begin{bmatrix} p_{MT} \cdot \cos(\psi_{s_{ID}}) + x_{G,s_{ID}} \\ p_{MT} \cdot \sin(\psi_{s_{ID}}) + y_{G,s_{ID}} \\ \dot{p}_{MT} \cdot \cos(\psi_{s_{ID}}) \\ \dot{p}_{MT} \cdot \sin(\psi_{s_{ID}}) \end{bmatrix}, \quad (4.166)$$

where  $\psi_{s_{ID}}$  denotes the angle between the  $s_{ID}$ -th road segment and the  $x_G$ -axis of the global coordinate system, and  $\mathbf{x}_{G,s_{ID}} = [x_{G,s_{ID}}, y_{G,s_{ID}}]^T$  denotes the reference endpoint of the  $s_{ID}$ -th road segment in global coordinates, cf. Fig. 4.2. In the PF with road constraints, the on-road movement of the MT is described by the following model

$$\begin{bmatrix} p'_{MT,k} \\ \dot{p}'_{MT,k} \end{bmatrix} = \begin{bmatrix} 1 & T_S \\ 0 & 1 \end{bmatrix} \cdot \begin{bmatrix} p_{MT,k-1} \\ \dot{p}_{MT,k-1} \end{bmatrix} + \begin{bmatrix} \frac{T_S^2}{2} \\ T_S \end{bmatrix} \cdot w_{1,k-1}, \quad (4.167)$$

where  $w_{1,k-1}$  denotes zero-mean white Gaussian noise with standard deviation  $\sigma_P$ . Since the predicted position and speed values  $p'_{MT,k}$ ,  $\dot{p}'_{MT,k}$  might not be on the road segment indicated by  $s_{ID,k-1}$ , the function  $\mathbf{f}_{P,k-1}(\cdot)$  is introduced which projects the values  $p'_{MT,k}$ ,  $\dot{p}'_{MT,k}$  into the next road segment indicated by  $s_{ID,k}$ . If there are several candidates for the next road segment in the road database  $\mathcal{T}_{RN}$ , e.g., the MT crosses a road junction, the function  $\mathbf{f}_{P,k-1}(\cdot)$  also selects at random one road segment according to the discrete process noise term  $w_{2,k-1} \in \{1, \dots, N_r\}$ , where  $N_r$  denotes the number

of candidates for the next road segment. As a result, the model describing road-constrained MT movement for hybrid localization can be written as

$$\begin{bmatrix} p_{\text{MT},k} \\ \dot{p}_{\text{MT},k} \\ s_{\text{ID},k} \\ c_0 \cdot \delta t_k \\ c_0 \cdot \delta \dot{t}_k \end{bmatrix} = \begin{bmatrix} \mathbf{f}_{\text{P},k-1} \left( \begin{bmatrix} p'_{\text{MT},k} \\ \dot{p}'_{\text{MT},k} \\ s_{\text{ID},k-1} \end{bmatrix}, \mathcal{T}_{\text{RN}}, w_{2,k-1} \right) \\ \begin{bmatrix} 1 & T_{\text{S}} \\ 0 & 1 \end{bmatrix} \cdot \begin{bmatrix} c_0 \cdot \delta t_{k-1} \\ c_0 \cdot \delta \dot{t}_{k-1} \end{bmatrix} + \begin{bmatrix} c_0 & 0 \\ 0 & c_0 \end{bmatrix} \cdot \begin{bmatrix} w_{\delta t,k-1} \\ w_{\delta \dot{t},k-1} \end{bmatrix} \end{bmatrix}. \quad (4.168)$$

In the following, let  $\mathbf{x}_{\text{R},k} = [p_{\text{MT},k}, \dot{p}_{\text{MT},k}, s_{\text{ID},k}, c_0 \cdot \delta t_k, c_0 \cdot \delta \dot{t}_k]^{\text{T}}$  denote the state vector for road-constrained hybrid localization, let  $\mathbf{w}_{\text{R},k-1} = [w_{1,k-1}, w_{2,k-1}]^{\text{T}}$  denote the corresponding noise term and let  $\mathbf{f}_{\text{R},k-1}(\cdot)$  denote a nonlinear function, so that (4.168) is fulfilled. Then, the model in (4.168) can be written more compactly, yielding

$$\mathbf{x}_{\text{R},k} = \mathbf{f}_{\text{R},k-1}(\mathbf{x}_{\text{R},k-1}, \mathcal{I}_{\text{RN}}, \mathbf{w}_{\text{R},k-1}, \mathbf{w}_{\text{CO},k-1}). \quad (4.169)$$

The measurement models and the corresponding likelihood pdfs depend on the MT state, which is commonly expressed in global coordinates, cf. (3.64) and (3.83). In order to evaluate the importance weights in the measurement update of the PF with road constraints, the corresponding likelihood functions have to be related to the MT state  $\mathbf{x}_{\text{R},k}$  in local coordinates. The function  $\mathbf{T}_{\text{G},k}(\cdot)$  is therefore introduced that converts a state vector  $\mathbf{x}_{\text{R},k}$  given in local coordinates to a state vector  $\mathbf{x}_k$  in global coordinates according to

$$\underbrace{\begin{bmatrix} x_{\text{MT},k} \\ y_{\text{MT},k} \\ \dot{x}_{\text{MT},k} \\ \dot{y}_{\text{MT},k} \\ c_0 \cdot \delta t_k \\ c_0 \cdot \delta \dot{t}_k \end{bmatrix}}_{\mathbf{x}_k} = \underbrace{\begin{bmatrix} \mathbf{T}_{\text{LG},k} \left( \begin{bmatrix} p_{\text{MT},k} \\ \dot{p}_{\text{MT},k} \\ s_{\text{ID},k} \end{bmatrix}, \mathcal{T}_{\text{RN}} \right) \\ c_0 \cdot \delta t_k \\ c_0 \cdot \delta \dot{t}_k \end{bmatrix}}_{\mathbf{T}_{\text{G},k}(\mathbf{x}_{\text{R},k}, \mathcal{T}_{\text{RN}})}, \quad (4.170)$$

which is equivalent to

$$\mathbf{x}_k = \mathbf{T}_{\text{G},k}(\mathbf{x}_{\text{R},k}, \mathcal{T}_{\text{RN}}). \quad (4.171)$$

Using this approach, the likelihood pdfs can be expressed as  $p(\mathbf{z}_k | \mathbf{x}_k = \mathbf{T}_{\text{G},k}(\mathbf{x}_{\text{R},k}, \mathcal{T}_{\text{RN}}))$ . A pseudocode description of the PF with road constraints is given in Algorithm 4.9. The algorithm can be used for the scenario with LOS propagation conditions as well as for the scenario, where the propagation conditions switch between LOS and NLOS. The only difference is that the likelihood pdf for the former is given by (3.64) and for the latter is given by (3.83).

---

**Algorithm 4.9** Particle Filter with Road Constraints
 

---

## 1. Initialization:

- For  $i = 1, \dots, N$ , initialize the particles  $\mathbf{x}_{R,0}^{(i)} \sim p(\mathbf{x}_{R,0})$  and weights  $w_{0|0}^{(i)} = \frac{1}{N}$ .

## 2. Time Update:

- For  $i = 1, \dots, N$ , generate particles  $\mathbf{x}_{R,k}^{(i)}$  from  $\mathbf{x}_{R,k-1}^{(i)}$  by using samples from the process noise sequences  $\mathbf{w}_{R,k-1}^{(i)} \sim p_{\mathbf{w}_{R,k-1}}(\cdot)$  and  $\mathbf{w}_{CO,k-1}^{(i)} \sim p_{\mathbf{w}_{CO,k-1}}(\cdot)$  as shown in (4.169).

## 3. Measurement Update:

- For  $i = 1, \dots, N$ , evaluate the weights

$$w_{k|k}^{(i)} = \frac{w_{k-1|k-1}^{(i)} \cdot p(\mathbf{z}_k | \mathbf{T}_{G,k}(\mathbf{x}_{R,k}^{(i)}, \mathcal{I}_{RN}))}{\sum_{j=1}^N w_{k-1|k-1}^{(j)} \cdot p(\mathbf{z}_k | \mathbf{T}_{G,k}(\mathbf{x}_{R,k}^{(j)}, \mathcal{I}_{RN}))}.$$

## 4. Estimation:

- Determine an estimate of the state vector according to

$$\hat{\mathbf{x}}_k = \sum_{i=1}^N w_{k|k}^{(i)} \cdot \mathbf{T}_{G,k}(\mathbf{x}_{R,k}^{(i)}, \mathcal{I}_{RN}).$$

## 5. Resampling:

- Perform systematic resampling using Algorithm 4.4. Take  $N$  samples with replacement from the set  $\{\mathbf{x}_{R,k}^{(i)}\}_{i=1}^N$ , where the probability to take sample  $i$  is  $w_{k|k}^{(i)}$ . Set  $w_{k|k}^{(i)} = \frac{1}{N}$  for  $i = 1, \dots, N$ .

- 6. Set  $k := k + 1$  and iterate from step 2.
- 

### 4.5.7 Rao-Blackwellized Particle Filter with Road Constraints

In this section, it is shown how the state and measurement models of the road-constrained approach, presented in the previous section, can be rewritten to fit into the RBPF framework. By using this strategy, it is expected to further reduce the variance of the state estimates compared to the PF approach.

Due to the fact that the one-dimensional MT location vector  $p_{\text{MT},k}$  and velocity vector  $\dot{p}_{\text{MT},k}$  enters nonlinearly into the state equation and the two-dimensional MT location vector  $\mathbf{x}_{\text{MT},k}$  enters nonlinearly into the measurement model, the state vector  $\mathbf{x}_{\text{R},k}$  is split as follows

$$\mathbf{x}_{\text{R},k}^{\text{n}} = [p_{\text{MT},k}, \dot{p}_{\text{MT},k}, s_{\text{ID},k}]^{\text{T}}, \quad (4.172)$$

$$\mathbf{x}_{\text{R},k}^{\text{l}} = [c_0 \cdot \delta t_k, c_0 \cdot \delta \dot{t}_k]^{\text{T}}. \quad (4.173)$$

The resulting adapted state and measurement models are presented next.

### State Model

The state model can be adapted to the RBPF framework as follows:

$$\underbrace{\begin{bmatrix} p_{\text{MT},k} \\ \dot{p}_{\text{MT},k} \\ s_{\text{ID},k} \end{bmatrix}}_{\mathbf{x}_{\text{R},k}^{\text{n}}} = \underbrace{\mathbf{f}_{\text{P},k-1} \left( \begin{bmatrix} \dot{p}'_{\text{MT},k} \\ \dot{p}'_{\text{MT},k} \\ s_{\text{ID},k-1} \end{bmatrix}, \mathcal{T}_{\text{RN}}, w_{2,k-1} \right)}_{\mathbf{f}_{k-1}^{\text{n}}(\mathbf{x}_{\text{R},k-1}^{\text{n}}, \mathbf{w}_{k-1}^{\text{n}})}, \quad (4.174)$$

$$\underbrace{\begin{bmatrix} c_0 \cdot \delta t_k \\ c_0 \cdot \delta \dot{t}_k \end{bmatrix}}_{\mathbf{x}_{\text{R},k}^{\text{l}}} = \underbrace{\begin{bmatrix} 1 & T_{\text{S}} \\ 0 & 1 \end{bmatrix}}_{\mathbf{F}_{k-1}^{\text{l}}} \cdot \underbrace{\begin{bmatrix} c_0 \cdot \delta t_{k-1} \\ c_0 \cdot \delta \dot{t}_{k-1} \end{bmatrix}}_{\mathbf{x}_{\text{R},k-1}^{\text{l}}} + \underbrace{\begin{bmatrix} c_0 & 0 \\ 0 & c_0 \end{bmatrix}}_{\mathbf{\Gamma}_{k-1}^{\text{l}}} \cdot \underbrace{\begin{bmatrix} w_{\delta t,k-1} \\ w_{\delta \dot{t},k-1} \end{bmatrix}}_{\mathbf{w}_{k-1}^{\text{l}}}. \quad (4.175)$$

Observe that the noises  $\mathbf{w}_{k-1}^{\text{n}} = [w_{1,k-1}, w_{2,k-1}]^{\text{T}}$  and  $\mathbf{w}_{k-1}^{\text{l}} = [w_{\delta t,k-1}, w_{\delta \dot{t},k-1}]^{\text{T}}$  are uncorrelated and that the state equation (4.174) is independent of the linear states. This is another special case of a conditional linear model, where the RBPF can be applied to. An appealing advantage of the model structure given in (4.174) is that the time update stage in the RBPF can be greatly simplified [SGN05, Sch03].

### Measurement Model - LOS Propagation Conditions

For the scenario with LOS propagation conditions, the measurement vector is split as follows

$$\mathbf{z}_{1,k} = [\mathbf{z}_{\text{PR},k}^{\text{T}}, \mathbf{z}_{\text{RTT,LOS},k}^{\text{T}}, \mathbf{z}_{\text{RSS,LOS},k}^{\text{T}}, z_{\text{BIAS},k}]^{\text{T}}, \quad (4.176)$$

The corresponding measurement model can be rewritten as

$$\underbrace{\begin{bmatrix} \mathbf{z}_{\text{PR},k} \\ \mathbf{z}_{\text{RTT,LOS},k} \\ \mathbf{z}_{\text{RSS,LOS},k} \\ z_{\text{BIAS},k} \end{bmatrix}}_{\mathbf{z}_{1,k}} = \underbrace{\begin{bmatrix} \mathbf{d}_{\text{SAT},k}(\mathbf{x}_{\text{MT},k}) \\ \mathbf{h}_{\text{RTT},k}(\mathbf{x}_{\text{MT},k}) \\ \mathbf{h}_{\text{RSS,LOS},k}(\mathbf{x}_{\text{MT},k}) \\ 0 \end{bmatrix}}_{\mathbf{h}_{1,k}(\mathbf{T}_{\text{LG},k}(\mathbf{x}_{\text{R},k}^{\text{n}}, \mathcal{T}_{\text{RN}}))} + \underbrace{\begin{bmatrix} \mathbf{1}_{M_{\text{PR}} \times 1} & \mathbf{0}_{M_{\text{PR}} \times 1} \\ \mathbf{0}_{(M_{\text{RTT}} + M_{\text{RSS}}) \times 2} & 1 \end{bmatrix}}_{\mathbf{H}_k} \cdot \underbrace{\begin{bmatrix} c_0 \cdot \delta t_k \\ c_0 \cdot \delta \dot{t}_k \end{bmatrix}}_{\mathbf{x}_{\text{R},k}^{\text{l}}} + \underbrace{\begin{bmatrix} \mathbf{v}_{\text{PR},k} \\ \mathbf{v}_{\text{RTT,LOS},k} \\ \mathbf{v}_{\text{RSS,LOS},k} \\ v_{\text{BIAS},k} \end{bmatrix}}_{\mathbf{v}_{1,k}}. \quad (4.177)$$

The measurement noise  $\mathbf{v}_{1,k}$  is zero-mean Gaussian distributed with covariance matrix  $\mathbf{R}_1 = \mathbf{R}_{\text{LOS},k}$ .

### Measurement Model - LOS/NLOS Propagation Conditions

For the scenario, where the propagation conditions switch between LOS and NLOS, the measurement vector is split as follows:

$$\mathbf{z}_{1,k} = [\mathbf{z}_{\text{PR},k}^{\text{T}}, z_{\text{BIAS},k}]^{\text{T}}, \quad (4.178)$$

$$\mathbf{z}_{2,k} = [\mathbf{z}_{\text{RTT},k}^{\text{T}}, \mathbf{z}_{\text{RSS},k}^{\text{T}}]^{\text{T}}. \quad (4.179)$$

The measurement model of  $\mathbf{z}_{1,k}$  can be rewritten as

$$\underbrace{\begin{bmatrix} \mathbf{z}_{\text{PR},k} \\ z_{\text{BIAS},k} \end{bmatrix}}_{\mathbf{z}_{1,k}} = \underbrace{\begin{bmatrix} \mathbf{d}_{\text{SAT},k}(\mathbf{x}_{\text{MT},k}) \\ 0 \end{bmatrix}}_{\mathbf{h}_{1,k}(\mathbf{T}_{\text{LG},k}(\mathbf{x}_{\text{R},k}^{\text{n}}, \mathcal{T}_{\text{RN}}))} + \underbrace{\begin{bmatrix} \mathbf{1}_{M_{\text{PR}} \times 1} & \mathbf{0}_{M_{\text{PR}} \times 1} \\ 1 & 0 \end{bmatrix}}_{\mathbf{H}_k} \cdot \underbrace{\begin{bmatrix} c_0 \cdot \delta t_k \\ c_0 \cdot \delta t_k \end{bmatrix}}_{\mathbf{x}_{\text{R},k}^1} + \underbrace{\begin{bmatrix} \mathbf{v}_{\text{PR},k} \\ v_{\text{BIAS},k} \end{bmatrix}}_{\mathbf{v}_{1,k}}, \quad (4.180)$$

where the measurement noise  $\mathbf{v}_{1,k}$  is zero-mean Gaussian distributed with covariance matrix  $\mathbf{R}_1 = \mathbf{R}_{\text{SAT},k}$ . The second measurement model is expressed in terms of the likelihood pdf  $p(\mathbf{z}_{2,k} | \mathbf{T}_{\text{LG},k}(\mathbf{x}_{\text{R},k}^{\text{n}}, \mathcal{T}_{\text{RN}}))$ , which is given by

$$p(\mathbf{z}_{2,k} | \mathbf{T}_{\text{LG},k}(\mathbf{x}_{\text{R},k}^{\text{n}}, \mathcal{T}_{\text{RN}})) = \prod_{\kappa_1=1}^{M_{\text{RTT}}} p(z_{\text{RTT},k}^{(\kappa_1)} | \mathbf{T}_{\text{LG},k}(\mathbf{x}_{\text{R},k}^{\text{n}}, \mathcal{T}_{\text{RN}})) \cdot \prod_{\kappa_2=1}^{M_{\text{RSS}}} p(z_{\text{RSS},k}^{(\kappa_2)} | \mathbf{T}_{\text{LG},k}(\mathbf{x}_{\text{R},k}^{\text{n}}, \mathcal{T}_{\text{RN}})), \quad (4.181)$$

where the pdfs  $p(z_{\text{RTT},k}^{(\kappa_1)} | \mathbf{T}_{\text{LG},k}(\mathbf{x}_{\text{R},k}^{\text{n}}, \mathcal{T}_{\text{RN}}))$  and  $p(z_{\text{RSS},k}^{(\kappa_2)} | \mathbf{T}_{\text{LG},k}(\mathbf{x}_{\text{R},k}^{\text{n}}, \mathcal{T}_{\text{RN}}))$  are given by (3.54) and (3.55). A pseudocode description of the RBPF with road constraints is given in Algorithm 4.10.

---

#### Algorithm 4.10 Rao-Blackwellized Particle Filter with Road Constraints

---

1. Initialization:

- For  $i = 1, \dots, N$ , initialize the particles  $\mathbf{x}_{\text{R},0}^{\text{n},(i)} \sim p(\mathbf{x}_{\text{R},0}^{\text{n}})$  and the weights  $w_{0|0}^{(i)} = \frac{1}{N}$ , and set  $\mathbf{x}_{0|0}^1 = \hat{\mathbf{x}}_{\text{R},0}^1$  and  $\mathbf{P}_{0|0} = \mathbf{P}_{\text{R},0}$ .

2. Particle Filter Time Update:

- For  $i = 1, \dots, N$ , generate particles  $\mathbf{x}_{\text{R},k}^{\text{n},(i)}$  from  $\mathbf{x}_{\text{R},k-1}^{\text{n},(i)}$  by using samples from the process noise sequences  $\mathbf{w}_{k-1}^{\text{n},(i)} \sim p_{\mathbf{w}_{k-1}^{\text{n}}}(\cdot)$  as shown in (4.174).

3. Kalman Filter Time Update:

- For  $i = 1, \dots, N$ , evaluate

$$\begin{aligned}\mathbf{x}_{k|k-1}^{1,(i)} &= \mathbf{F}_{k-1}^1 \cdot \mathbf{x}_{k-1|k-1}^{1,(i)}, \\ \mathbf{P}_{k|k-1} &= \mathbf{F}_{k-1}^1 \cdot \mathbf{P}_{k-1|k-1} \cdot \mathbf{F}_{k-1}^{1,\top} + \mathbf{\Gamma}_{k-1}^1 \cdot \mathbf{Q}_{k-1}^1 \cdot \mathbf{\Gamma}_{k-1}^{1,\top}.\end{aligned}$$

#### 4. Particle Filter Measurement Update:

- For  $i = 1, \dots, N$ , evaluate the weights

$$w_{k|k}^{(i)} = \frac{w_{k-1|k-1}^{(i)} \cdot \mathcal{N}(\mathbf{z}_{1,k}; \hat{\mathbf{z}}_{1,k}^{(i)}, \mathbf{S}_k) \cdot p(\mathbf{z}_{2,k} | \mathbf{T}_{\text{LG},k}(\mathbf{x}_k^{\text{n},(i)}, \mathcal{T}_{\text{RN}}))}{\sum_{j=1}^N w_{k-1|k-1}^{(j)} \cdot \mathcal{N}(\mathbf{z}_{1,k}; \hat{\mathbf{z}}_{1,k}^{(j)}, \mathbf{S}_k) \cdot p(\mathbf{z}_{2,k} | \mathbf{T}_{\text{LG},k}(\mathbf{x}_k^{\text{n},(j)}, \mathcal{T}_{\text{RN}}))},$$

where

$$\begin{aligned}\hat{\mathbf{z}}_{1,k}^{(i)} &= \mathbf{h}_{1,k}(\mathbf{T}_{\text{LG},k}(\mathbf{x}_{\text{R},k}^{\text{n},(i)}, \mathcal{T}_{\text{RN}})) + \mathbf{H}_k \cdot \mathbf{x}_{k|k-1}^{1,(i)}, \\ \mathbf{S}_k &= \mathbf{H}_k \cdot \mathbf{P}_{k|k-1} \cdot \mathbf{H}_k^\top + \mathbf{R}_k.\end{aligned}$$

#### 5. Kalman Filter Measurement Update:

- For  $i = 1, \dots, N$ , evaluate

$$\begin{aligned}\mathbf{x}_{k|k}^{1,(i)} &= \mathbf{x}_{k|k-1}^{1,(i)} + \mathbf{K}_k \cdot (\mathbf{z}_{1,k} - \hat{\mathbf{z}}_{1,k}^{(i)}), \\ \mathbf{P}_{k|k} &= \mathbf{P}_{k|k-1} - \mathbf{K}_k \cdot \mathbf{S}_k \cdot \mathbf{K}_k^\top,\end{aligned}$$

where

$$\mathbf{K}_k = \mathbf{P}_{k|k-1} \cdot \mathbf{H}_k^\top \cdot [\mathbf{S}_k]^{-1}.$$

#### 6. Estimation:

- Determine estimates of the linear and nonlinear state vectors according to

$$\hat{\mathbf{x}}_{\text{MMSE},k|k}^{\text{n}} = \sum_{i=1}^N w_{k|k}^{(i)} \cdot \mathbf{T}_{\text{LG},k}(\mathbf{x}_{\text{R},k}^{\text{n},(i)}, \mathcal{T}_{\text{RN}}), \quad \hat{\mathbf{x}}_{\text{MMSE},k|k}^1 = \sum_{i=1}^N w_{k|k}^{(i)} \cdot \mathbf{x}_{k|k}^{1,(i)}.$$

#### 7. Resampling:

- Perform systematic resampling using Algorithm 4.4. Take  $N$  samples with replacement from the set  $\{\mathbf{x}_{\text{R},k}^{\text{n},(i)}, \mathbf{x}_{k|k}^{1,(i)}\}_{i=1}^N$ , where the probability to take sample  $i$  is  $w_{k|k}^{(i)}$ . Set  $w_{k|k}^{(i)} = \frac{1}{N}$  for  $i = 1, \dots, N$ .

- 8. Set  $k := k + 1$  and iterate from step 2.

## 4.6 Performance Evaluation

### 4.6.1 Introduction

In this Section 4.6, the hybrid localization algorithms of Sections 4.4 and 4.5 are evaluated by means of Monte Carlo simulations and their average performance is compared to the PCRLB. The performance metrics that will be used are the RMSE of the MT location and time averaged RMSE of the MT location as defined in (3.95) and (3.96). The corresponding PCRLBs for these metrics are given by

$$\text{PCRLB}_k = \sqrt{[[\mathbf{J}_k]^{-1}]_{1,1} + [[\mathbf{J}_k]^{-1}]_{2,2}} \quad (4.182)$$

and

$$\overline{\text{PCRLB}} = \frac{1}{k_{\max}} \sum_{k=1}^{k_{\max}} \sqrt{[[\mathbf{J}_k]^{-1}]_{1,1} + [[\mathbf{J}_k]^{-1}]_{2,2}}, \quad (4.183)$$

where the Bayesian information submatrix  $\mathbf{J}_k$  is defined in (4.9). Since it is not otherwise stated, the results are averaged over  $N_{\text{MC}} = 500$  Monte Carlo runs. The Monte Carlo simulations are performed for Scenario I, cf. Section 2.3.4.2, and the results are presented in Section 4.6.2. The algorithms of Section 4.5 are further evaluated for experimental data available from a field trial, which is presented in Section 4.6.3. Finally, the computational complexity of the different algorithms is investigated in Section 4.6.4.

### 4.6.2 Simulation Results for Scenario I

#### 4.6.2.1 Simulation Results for LOS Propagation Conditions

In this section, the performance of the KF-based algorithms and PF-based algorithms introduced in Sections 4.4 and 4.5 is evaluated for the different combinations of measurements of Scenario I as given in Section 2.3.4.2. The PCRLBs for the different combinations of measurements are computed to indicate the best possible performance that one can expect for the given scenario and set of parameters.

Since all algorithms are recursive, proper initialization is required. For the KF-based estimators, the initial state estimate  $\hat{\mathbf{x}}_{0|0}$  is assumed to be the true state with initial covariance matrix  $\mathbf{P}_{0|0} = \text{diag}[200^2, 10^2, 200^2, 10^2, 100^2/3, 5^2]$ . The initial pdf of the PF-based estimators without road constraints is assumed to be Gaussian with mean  $\hat{\mathbf{x}}_{0|0}$



and covariance  $\mathbf{P}_{0|0}$ . The initial pdf of the PF-based estimators with road constraints is assumed to be Gaussian with mean  $\hat{\mathbf{x}}_{R,0|0}$  equal to the true state and covariance matrix  $\mathbf{P}_{R,0|0} = \text{diag}[200^2, 10^2, 100^2/3, 5^2]$ . Here, it is worth noting that the true initial state for the hybrid localization scenario is a fixed known quantity. This requirement, however, violates the assumption for the optimal Bayesian solution, cf. Section 4.2, where the true initial state is a random variable with pdf  $p(\mathbf{x}_0)$ . Thus, it is expected that the reuse of the same initial conditions in the algorithms for each Monte Carlo run will lead to biased estimates [BSLK01].

In order to apply the algorithms to the hybrid localization problem, the parameters included in the measurement model  $\mathbf{h}_{\text{LOS},k}(\mathbf{x}_k)$ , as well as the noise statistics given by the covariance matrices  $\mathbf{R}_{\text{LOS},k}$  and  $\mathbf{Q}$  have to be specified. In order to account for possible MT maneuvers and clock uncertainties  $\mathbf{Q}$  is chosen in the algorithms as  $\mathbf{Q} = \text{diag}_b[\mathbf{Q}_{\text{CV}}, 100 \cdot \mathbf{Q}_{\text{CO}}]$  with  $\mathbf{Q}_{\text{CV}} = \text{diag}[9, 9]$  ( $\mathbf{Q} = \text{diag}_b[\sigma_p^2, 100 \cdot \mathbf{Q}_{\text{CO}}]$  with  $\sigma_p^2 = 9$  for PF-based algorithms with road constraints), where the parameters of the covariance matrix  $\mathbf{Q}_{\text{CO}}$  are given in Table 2.2. The parameters that specify the measurement model  $\mathbf{h}_{\text{LOS},k}(\mathbf{x}_k)$  and the covariance matrix  $\mathbf{R}_{\text{LOS},k}$  are assumed to be equal to the parameters with which the measurements have been generated. In practice, however, these parameters are unknown and have to be estimated in advance from field trial data. For the computation of the PCRLB, the covariance matrices  $\mathbf{R}_{\text{LOS},k}$  and  $\mathbf{Q}$ , as well as the parameters included in the measurement model  $\mathbf{h}_{\text{LOS},k}(\mathbf{x}_k)$  are chosen such that they are equal to the parameters with which the measurements have been generated. The pdf required to initialize the PCRLBs, cf. (4.12), is assumed to be Gaussian with mean  $\hat{\mathbf{x}}_{0|0}$  and covariance matrix  $\mathbf{P}_{0|0}$ .

In Fig. 4.3 the MT location RMSEs in m vs. the time index  $k$  for the Cellular, Hybrid 1 and Hybrid 2 methods are shown for the EKF, UKF and CKF together with the corresponding PCRLBs. It can be seen that the performance of the three filters for the different methods is practically equivalent. The Cellular method provides the worst performance, small improvements can be obtained with the Hybrid 1 method and large improvements are possible using the Hybrid 2 method. The equivalent performance of the three filters can be explained by the fact that the distances between the BSs/satellites and the MT are large and, thus, the impact of the nonlinearities, inherent in the RSS and RTT and PR measured values, is small. At time steps  $k = 160$  and  $k = 320$ , the performance of the filters become worse for a certain period of time. These peaks can be explained by the fact that at these time steps, the MT is located in a curve, cf. Fig. 2.3, and has to perform a maneuver to change the direction of movement. Since the filter has no knowledge about the maneuver, it has to adapt to this new situation, resulting in the worse performance. The magnitude of the peak errors can be controlled by the choice of the covariance matrix  $\mathbf{Q}_{\text{CV}}$  in the filters. While

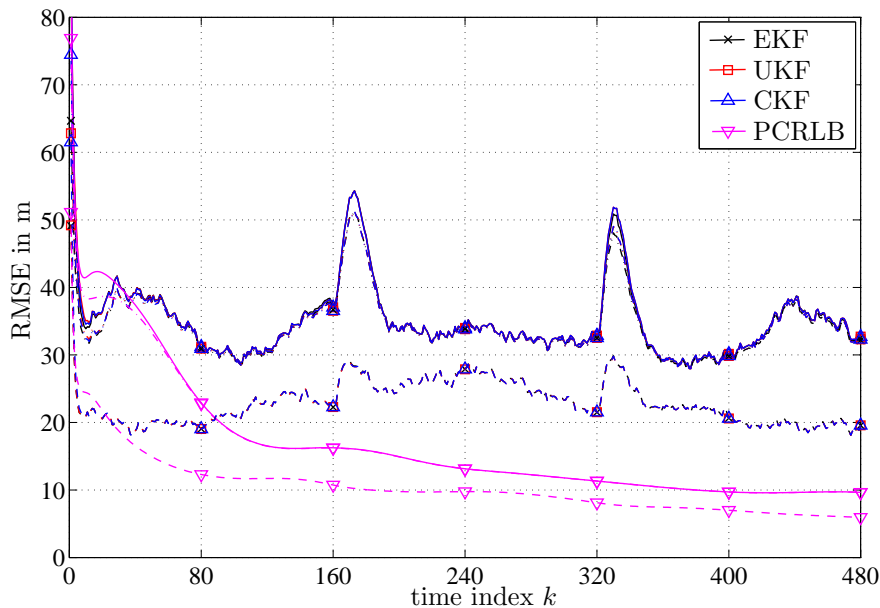


Figure 4.3. MT location RMSE vs. time index  $k$  for EKF, UKF, CKF and PCRLB assuming LOS propagation conditions, solid lines: Cellular method, dash-dotted lines: Hybrid 1 method, dashed lines: Hybrid 2 method.

small values for  $\mathbf{Q}_{CV}$  can decrease the RMSE during periods of straight and uniform MT movement, it will result in larger peak errors during maneuvers. Furthermore, it can be observed that the peaks resulting from the maneuver of the MT are smaller for the Hybrid 1 and Hybrid 2 method than for the Cellular method. This fact can be explained as follows. Since the filters extract their information about the MT state from the measurements, more accurate measurements, as it is the case for the Hybrid 1 and Hybrid 2 method, will yield an improved filter performance during maneuvers.

Comparing the performance of the filters to the PCRLB, it can be seen that the filters are biased for small values of  $k$ , which is a result of the chosen initialization strategy. Furthermore, it can be observed that the filters cannot attain the PCRLB. Comparing the PCRLBs of the Cellular and Hybrid 1 method, it can be observed that small improvements are possible for small values of  $k$ . However, after a certain number of time steps, the two bounds coincide with each other and from a theoretical point of view, no improvements using the Hybrid 1 method instead of the Cellular method are possible.

This behaviour can be explained best by looking at the computation of the Bayesian information submatrix  $\mathbf{J}_k$ , cf. (4.19). The first term in (4.19) is composed of the information from previous time steps and the information available from the state model,

while the second term describes the contribution of the measurements. Recall from Section 3.3.2, that the CRLBs of the Cellular and Hybrid 1 method are equal. Due to the fact that (4.22) holds, the measurements cannot be responsible for the performance improvements of the Hybrid 1 method. Thus, the performance improvements exclusively depend on the state model and the information that is contained in the initial Bayesian information submatrix  $\mathbf{J}_0$ . Since the first term in the sum of (4.19) has the effect of averaging the information from previous time steps with the information available from the state model, the initial information becomes less important as the number of time steps  $k$  increases. Due to the fact that the measurements of the Hybrid 1 method do not contribute to the improvement of the PCRLB, the PCRLBs of the Cellular and Hybrid 1 methods finally coincide with each other.

In Figs. 4.4, 4.5 and 4.6 the MT location RMSEs in m vs. the time index  $k$  for the Cellular, Hybrid 1 and Hybrid 2 methods are shown for the PF, APF, RBPF and RBAPF using  $N = 1000$  particles, together with the corresponding PCRLBs. From this results, the same conclusions as those for the KF-based estimators can be drawn. For the Cellular method, the performance of the four filters without taking into account road constraints is practically equivalent, and compared to the KF-based estimators, no performance improvements are possible. By additionally considering road constraints in the PF, the performance can be significantly improved. The worse performance

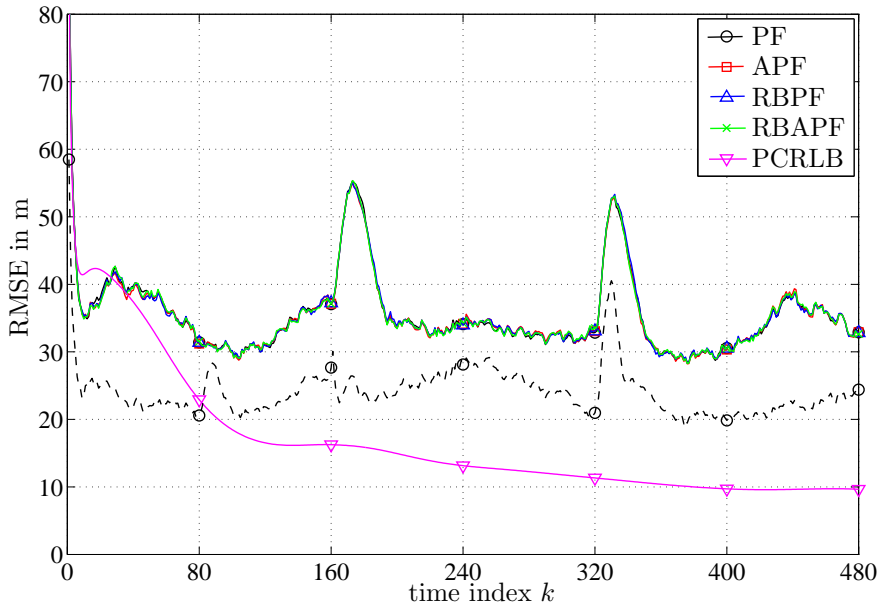


Figure 4.4. MT location RMSE vs. time index  $k$  for PF, APF, RBPF, RBAPF and PCRLB assuming LOS propagation conditions and Cellular method, solid lines: No road constraints, dashed lines: Road constraints.

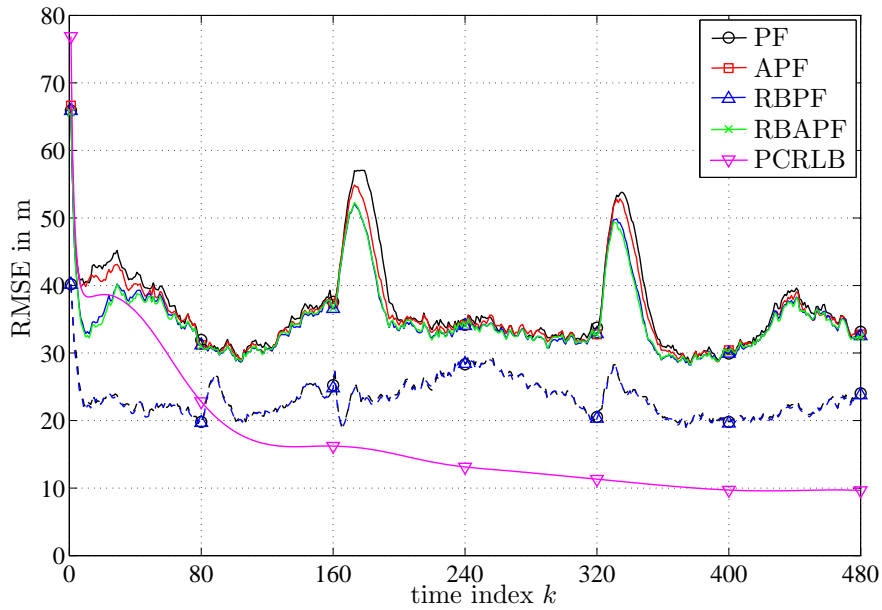


Figure 4.5. MT location RMSE vs. time index  $k$  for PF, APF, RBPF, RBAPF and PCRLB assuming LOS propagation conditions and Hybrid 1 method, solid lines: No road constraints, dashed lines: Road constraints.

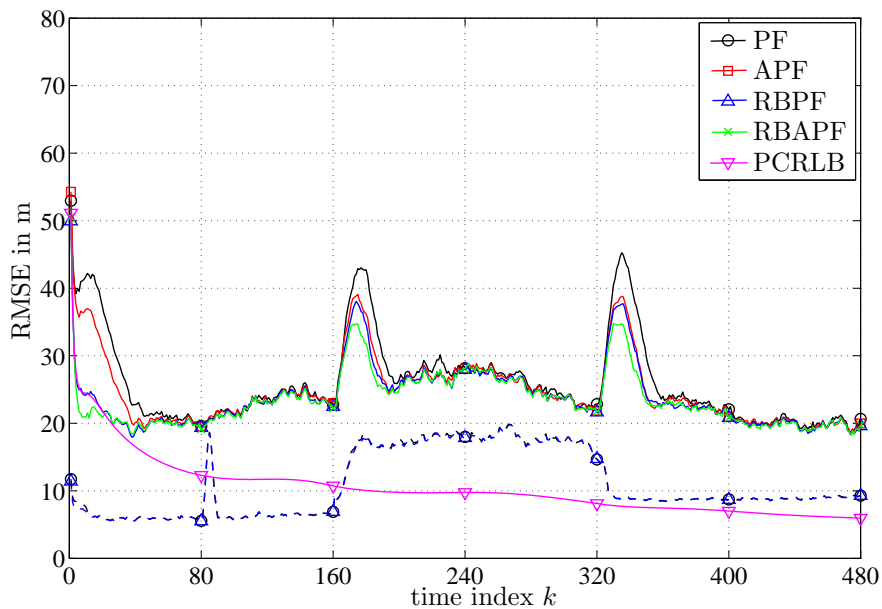


Figure 4.6. MT location RMSE vs. time index  $k$  for PF, APF, RBPF, RBAPF and PCRLB assuming LOS propagation conditions and Hybrid 2 method, solid lines: No road constraints, dashed lines: Road constraints.

beginning at  $k = 80$  and  $k = 320$  can be explained by the fact that at these time steps, the MT is located in a road junction, cf. Fig. 2.3. Since at  $k = 320$  three roads meet at the junction and the MT is additionally changing the direction of its movement, the peak is larger compared to the peak at  $k = 80$ . For the Hybrid 1 method shown in Fig. 4.5, differences in the performance of the four filters without taking into account road constraints can be observed. It can be seen that for small values of  $k$  and when the MT is performing a maneuver, the RBPF and RBAPF clearly outperform the PF and APF. The reason for this is the increased state dimension, the PF and APF have to deal with. While the nonlinear state dimension of the RBPF and RBAPF remains unchanged at two, the state dimension in the PF and APF has increased from four to six. Thus, in order to obtain a good approximation of the posterior pdf in the PF and APF, a larger number of particles in these filters are necessary. With the given number of  $N = 1000$  particles, only the RBPF and RBAPF can achieve a performance similar to the KF-based estimators. By additionally considering road constraints in the PF and RBPF, the performance can be significantly improved. However, the performance improvements of the RBPF compared to the PF are marginal. The reason for this is the relatively small state dimension. While the nonlinear state dimension of the RBPF with road constraints remains unchanged at two, the state dimension in the PF with road constraints has increased from two to four. With the given number of particles, this is enough to obtain a good approximation of the posterior pdf. Comparing these results with the results of the Cellular method, it can be observed that small improvements are possible with the Hybrid 1 method especially in situations, where the MT is performing a maneuver or is located in a road junction.

For the Hybrid 2 method shown in Fig. 4.6, the same conclusions as those for the Hybrid 1 method can be drawn. However, compared to the Hybrid 1 method, it can be seen that for small values of  $k$  and when the MT is performing a maneuver, the RBAPF now clearly outperforms the other filters without road constraints. The additional incorporation of road constraints into the PF and RBPF can further improve the performance and strongly depends on the orientation of the street and the location of the satellites and BSs relative to the street, cf. Fig. 2.3. It can be observed that good performance is achieved when the MT is moving on street segments oriented parallel to the  $x$ -axis. This is the case for time steps  $0 \leq k < 160$  and  $320 < k \leq 480$ . The performance is worse when the MT is moving on street segments oriented parallel to the  $y$ -axis, which is the case for time steps  $160 \leq k < 320$ .

In Fig. 4.7 the MT location  $\overline{\text{RMSE}}$  in m vs. particle number  $N$  for the Cellular, Hybrid 1 and Hybrid 2 methods are shown for the PF, APF, RBPF, RBAPF together with the  $\overline{\text{PCRLB}}$ . It can be observed that for the Cellular method, the performance of the different filters is practically equivalent and only small performance improvements

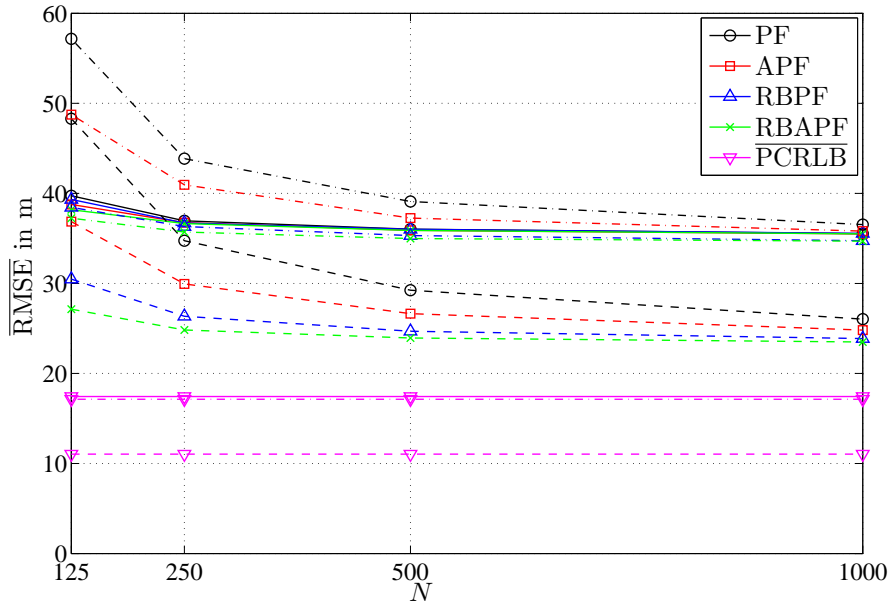


Figure 4.7. MT location  $\overline{\text{RMSE}}$  vs. particle number  $N$  for PF, APF, RBPF, RBAPF and  $\overline{\text{PCRLB}}$  assuming LOS propagation conditions, solid lines: Cellular method, dash-dotted lines: Hybrid 1 method, dashed lines: Hybrid 2 method.

can be achieved by increasing the number of particles in the filters. For the Hybrid 1 method, the same conclusions as those for the Cellular method can be drawn for the RBPF and RBAPF. It can be noticed that for all tested number of particles, the performance of the RBPF and RBAPF is always better than the performance of these filters for the Cellular method. The  $\overline{\text{RMSE}}$ s of the PF and APF are worse compared to the  $\overline{\text{RMSE}}$ s of the RBPF and RBAPF and results from the increased state dimension, the PF and APF have to deal with. Even though the performance of these filters can be improved by increasing the number of particles, they cannot reach the performance of the RBPF and RBAPF. More interestingly, they cannot even reach the performance of the Cellular method. For the Hybrid 2 method, the RBAPF provides the best performance even for small numbers of particles, which is followed by the RBPF. The PF and APF generally require more particles to obtain acceptable results.

In Fig. 4.8 the MT location  $\overline{\text{RMSE}}$  in m vs. particle number  $N$  for the Cellular, Hybrid 1 and Hybrid 2 methods are shown for the PF and RBPF with road constraints. It can be observed that the performance of the RBPF with road constraints is practically equivalent for all investigated numbers of particles. Compared to the RBPF with road constraints, the performance of the PF with road constraints is slightly worse, especially when the number of particles is small.

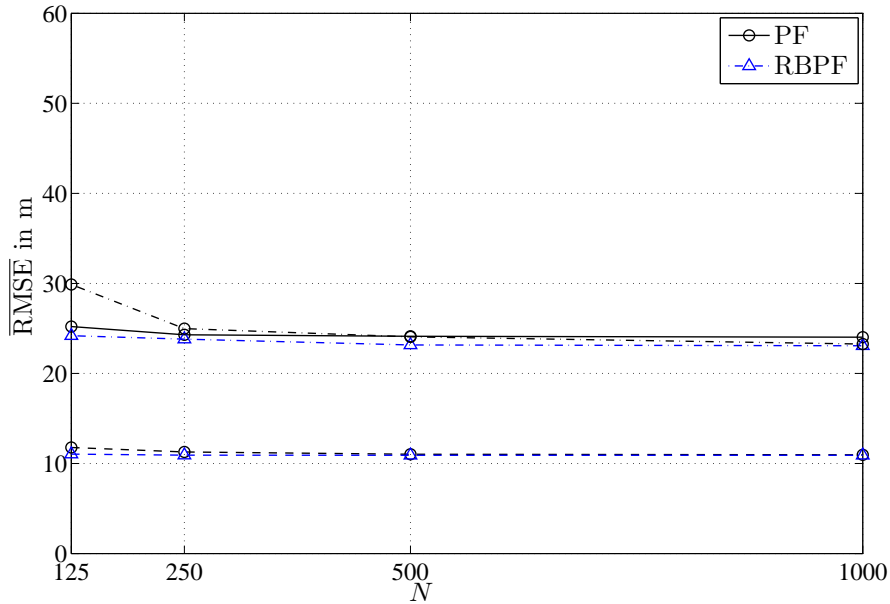


Figure 4.8. MT location  $\overline{\text{RMSE}}$  vs. particle number  $N$  for PF and RBPF with road constraints assuming LOS propagation conditions, solid lines: Cellular method, dash-dotted lines: Hybrid 1 method, dashed lines: Hybrid 2 method.

In Fig. 4.9, the MT location  $\overline{\text{RMSE}}$  in m vs. the GRT error standard deviation  $\sigma_{\text{GRT}}$  in s for the Hybrid 1+ and Hybrid 2+ method are shown for the EKF, UKF and CKF together with the corresponding  $\overline{\text{PCRLB}}$ . The results are obtained from  $N_{\text{MC}} = 100$  Monte Carlo runs. It can be observed that all three filters have practically the same performance. For  $\sigma_{\text{GRT}} \geq 5 \cdot 10^{-6}$ , the  $\overline{\text{RMSE}}$  of the Hybrid 1+ method reaches an upper bound, which is equivalent to the  $\overline{\text{RMSE}}$  of the Hybrid 1 method. Large performance improvements can be obtained for  $\sigma_{\text{GRT}} < 5 \cdot 10^{-6}$ . For values of  $\sigma_{\text{GRT}}$  smaller than  $10^{-8}$  the Hybrid 1+ method reaches a lower bound and no significant performance improvements are possible. For the Hybrid 2+ method, similar conclusions can be drawn. For  $\sigma_{\text{GRT}} \geq 5 \cdot 10^{-7}$  the  $\overline{\text{RMSE}}$  of the Hybrid 2+ method reaches an upper bound which is equivalent to the  $\overline{\text{RMSE}}$  of the Hybrid 2 method. Small performance improvements can be obtained for  $\sigma_{\text{GRT}} < 5 \cdot 10^{-7}$ . For values of  $\sigma_{\text{GRT}}$  smaller than  $10^{-9}$  the Hybrid 2+ method reaches a lower bound and no significant performance improvements are possible. The performance improvements of the Hybrid 2+ method are smaller than the performance improvements of the Hybrid 1+ method. It can be observed that all three filters cannot attain the corresponding PCRLB. In Fig. 4.10, the MT location  $\overline{\text{RMSE}}$  in m vs. the GRT error standard deviation  $\sigma_{\text{GRT}}$  in s for the Hybrid 1+ and Hybrid 2+ method are shown for the PF, APF, RBPF and RBAPF using  $N = 1000$  particles, together with the corresponding  $\overline{\text{PCRLB}}$ . The results are

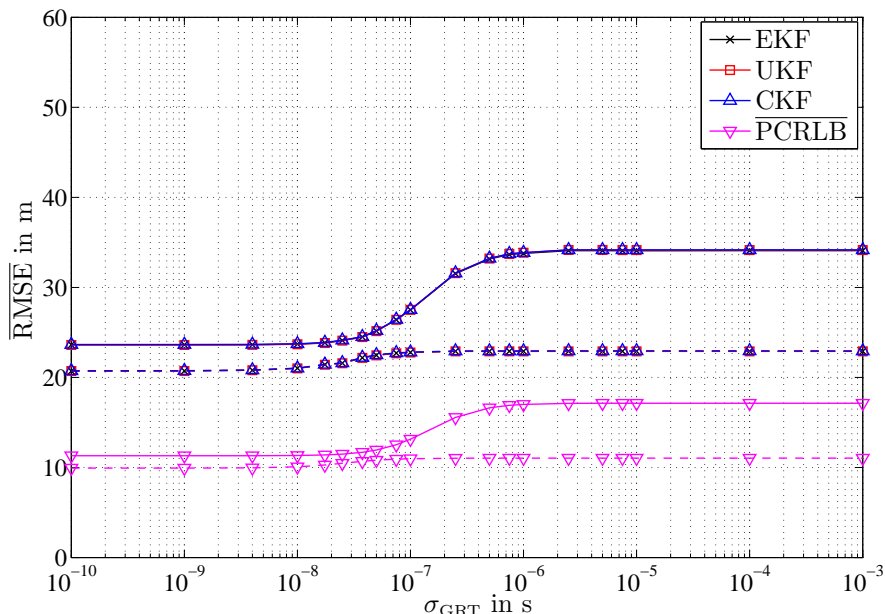


Figure 4.9. MT location  $\overline{\text{RMSE}}$  vs. GRT error standard deviation  $\sigma_{\text{GRT}}$  for EKF, UKF, CKF and corresponding PCRLB assuming LOS propagation conditions, solid lines: Hybrid 1+ method, dashed lines: Hybrid 2+ method.

obtained from  $N_{\text{MC}} = 100$  Monte Carlo runs and the same conclusions as those for the KF-based estimators can be drawn. It can be observed that only the RBPF and RBAPF can approximately achieve the performance of the KF-based estimators. The PF and APF diverge for small values of  $\sigma_{\text{GRT}}$ . The reason for divergence is that for small values of  $\sigma_{\text{GRT}}$ , the likelihood pdf of the GRT measurement becomes highly peaked. Since the particles in the PF and APF are drawn from the transitional pdf which is not peaked, and the weights are updated using the likelihood pdf, the corresponding weights will have very low weights resulting in a poor representation of the posterior pdf. In the RBPF and RBAPF, the peaked likelihood pdf of the GRT measurement cancels out in the PF measurement update of the nonlinear states, cf. (4.104) and (4.156), since it depends only on the bias which is a linear state. Thus, the RBPF and RBAPF are not influenced by this effect. In Fig. 4.11, the MT location  $\overline{\text{RMSE}}$  in m vs. the GRT error standard deviation  $\sigma_{\text{GRT}}$  in s for the Hybrid 1+ and Hybrid 2+ method are shown for the PF and RBPF with road constraints using  $N = 1000$  particles. The results are obtained from  $N_{\text{MC}} = 100$  Monte Carlo runs and the same conclusions as those for the PF-based estimators without road constraints can be drawn from these results. It can be noticed, that with the Hybrid 2+ method practically no performance gains can be achieved compared to the Hybrid 2 method. Furthermore, compared to the PF, the effect of the peaked likelihood is less pronounced for the PF



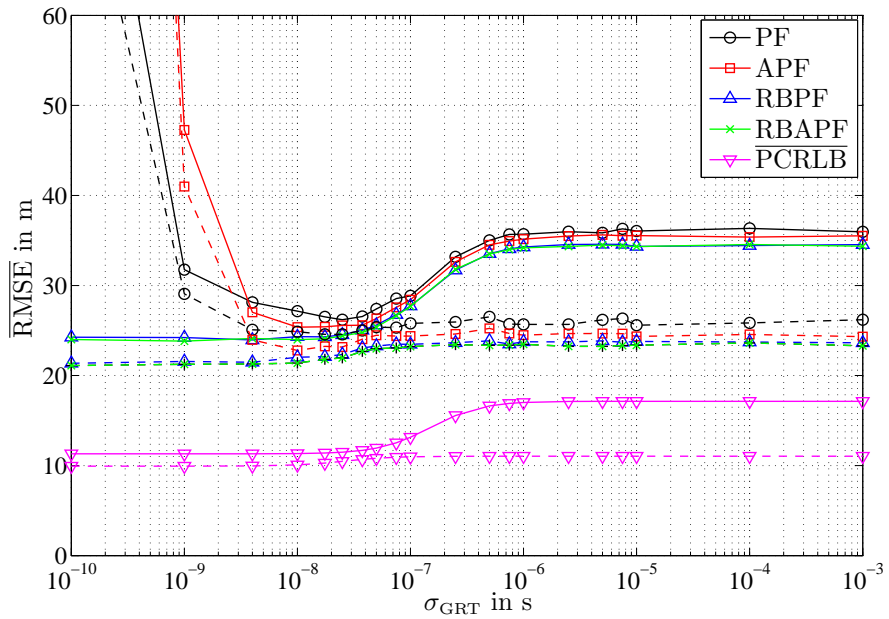


Figure 4.10. MT location  $\overline{\text{RMSE}}$  vs. GRT error standard deviation  $\sigma_{\text{GRT}}$  for PF, APF, RBPF, RBAPF and corresponding PCRLB assuming LOS propagation conditions, solid lines: Hybrid 1+ method, dashed lines: Hybrid 2+ method.

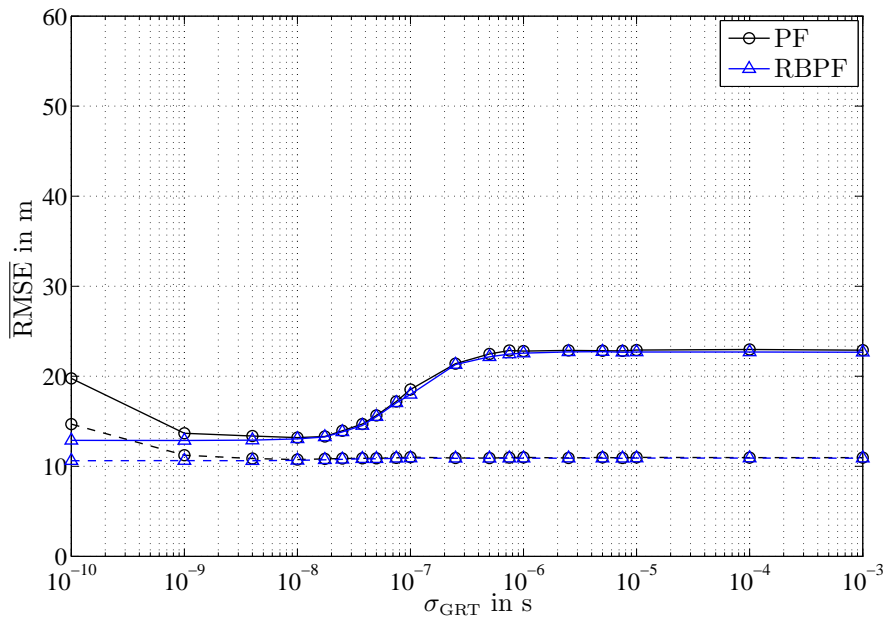


Figure 4.11. MT location  $\overline{\text{RMSE}}$  vs. GRT error standard deviation  $\sigma_{\text{GRT}}$  for PF and RBPF with road constraints assuming LOS propagation conditions, solid lines: Hybrid 1+ method, dashed lines: Hybrid 2+ method.

with road constraints. In Fig. 4.12, the MT location  $\overline{\text{RMSE}}$  in m vs. GDOP for the Satellite and Hybrid 3 method are shown for the EKF, UKF and CKF together with the corresponding  $\overline{\text{PCRLBs}}$ . The results show that all three filters provide the same performance and that they cannot achieve the corresponding  $\overline{\text{PCRLBs}}$ . For small GDOP values, the performance improvements of the Hybrid 3 method compared to the Satellite method are small. For large GDOP values, the Hybrid 3 method significantly outperforms the Satellite method. In Fig. 4.13, the MT location  $\overline{\text{RMSE}}$  in m vs. GDOP for the Satellite and Hybrid 3 method are shown for the PF, APF, RBPF, RBAPF using  $N = 1000$  particles, together with the corresponding  $\overline{\text{PCRLBs}}$ . For the PF-based estimators without road constraints, the same conclusions can be drawn from these results as those for the KF-based estimators. It can be noticed that the RBPF and RBAPF provide the best performance, which is practically identical, while the performance of the PF and APF is worse. For the PF and RBPF with road constraints, significant performance improvements can be obtained. However, using the Hybrid 3 method rather than the Satellite method will yield only small improvements, which is true for all tested GDOP values. It can be further seen that the performance is approximately equal for all GDOP values. This can be explained by the fact that the additional consideration of road information in the filter can be interpreted as an additional and very accurate measurement. Depending on the orientation of the road

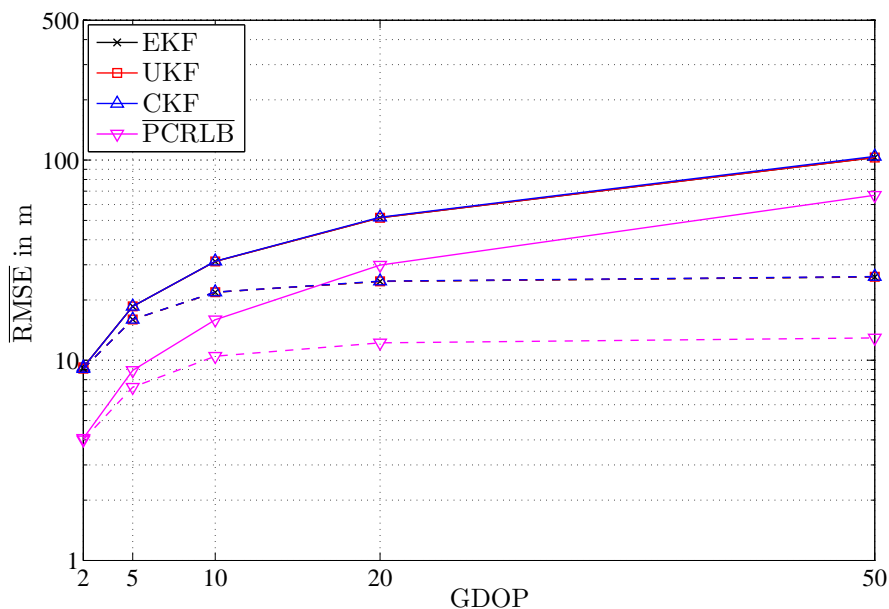


Figure 4.12. MT location  $\overline{\text{RMSE}}$  vs. GDOP for EKF, UKF, CKF and corresponding PCRLB assuming LOS propagation conditions, solid lines: Satellite method, dashed lines: Hybrid 3 method.

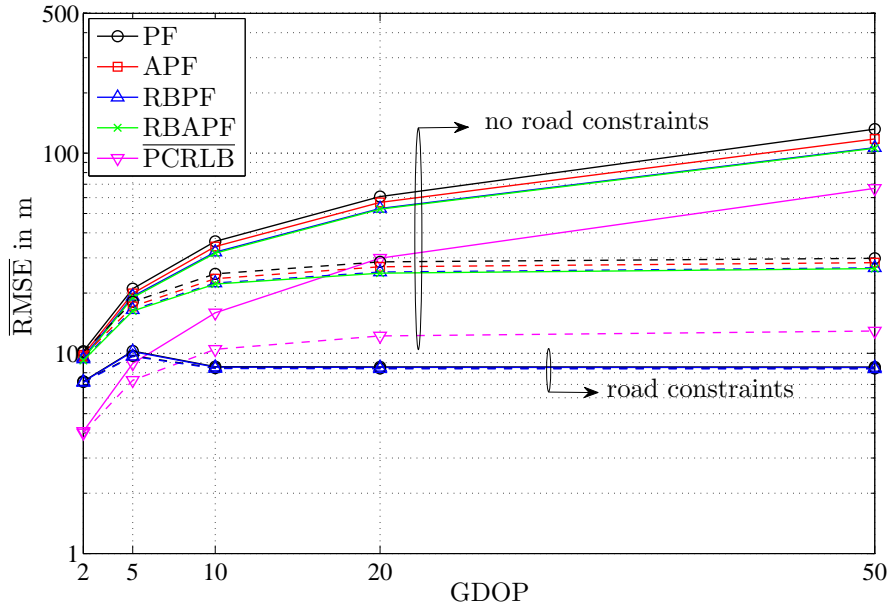


Figure 4.13. MT location  $\overline{\text{RMSE}}$  vs. GDOP for PF, APF, RBPF, RBAPF and corresponding PCRLB assuming LOS propagation conditions, solid lines: Satellite method, dashed lines: Hybrid 3 method.

with respect to the locations of the satellites and BSs, the road information can help to further improve the performance. Comparing the results of this section with the results of the non-recursive estimators, cf. Section 3.5.2.1, it can be observed that due to the additional consideration of the state model in the estimation process, large performance gains due to time averaging effects are possible for all investigated methods.

#### 4.6.2.2 Simulation Results for Propagation Conditions that switch between LOS and NLOS

In this section, the performance of the PF-based algorithms introduced in Section 4.5 is evaluated for the different combinations of measurements of Scenario I as given in Section 2.3.4.2. In contrast to Section 4.6.2.1, it is now assumed that the RSS and RTT measurements are affected by switching LOS/NLOS propagation conditions. The PCRLBs for the different combinations of measurements are computed according to Section 4.3.3 using  $N = 10000$  samples, in order to indicate the best possible performance that one can expect for the given scenario and set of parameters.

For the initialization of the filters, the same strategy is used as explained in Section 4.6.2.1. In order to apply the algorithms to the hybrid localization problem, the pa-

parameters of the likelihood pdf and transitional pdf have to be specified, cf. (3.83) and (4.14). In the following, the covariance matrix  $\mathbf{Q}$  is chosen as in Section 4.6.2.1 and the parameters of the likelihood pdf are chosen such that they are equal to the parameters with which the measurements have been generated, cf. Table 2.2. The stationary probabilities of the Markov chain can be computed from (2.15) and (2.51). In practice, however, these parameters are unknown and have to be estimated in advance from field trial data. For the computation of the PCRLB, the parameters of the likelihood pdf and transitional pdf are assumed to be equal to the parameters with which the measurements have been generated, cf. Table 2.2. The pdf required to initialize the PCRLBs, cf. (4.12), is assumed to be Gaussian with mean  $\hat{\mathbf{x}}_{0|0}$  and covariance  $\mathbf{P}_{0|0}$ .

In Figs. 4.14, 4.15 and 4.16, the MT location RMSEs in m vs. the time index  $k$  for the Cellular, Hybrid 1 and Hybrid 2 methods are shown for the PF, APF, RBPF and RBAPF using  $N = 1000$  particles, together with the corresponding PCRLBs. From these results, the same conclusions as those for the PF-based estimators assuming LOS propagation conditions can be drawn. It can be observed that compared to the LOS case, the RMSEs for the different methods are larger. This can be explained by the fact that in NLOS situations, the noise with which the measurements are affected with is larger. This, in turn, means that the measurements provide less information about the MT state, which leads to the inferior performance. It can be further noticed that the performance of the PF and RBPF with road constraints for the Hybrid 2 method, cf. Fig 4.16, is practically equivalent to the performance of the same filters assuming LOS propagation conditions, cf. Fig. 4.6. From these results one can conclude that the performance is dominated by the information available from the PR measurements and the road, and less influenced by the RSS and RTT measurements.

In Figs. 4.17 and 4.18, the MT location  $\overline{\text{RMSE}}$  in m vs. the GRT error standard deviation  $\sigma_{\text{GRT}}$  in s for the Hybrid 1+ and Hybrid 2+ method are shown for the PF, APF, RBPF, RBAPF, PF with road constraints and RBPF with road constraints using  $N = 1000$  particles, together with the corresponding  $\overline{\text{PCRLB}}$ . The results are obtained from  $N_{\text{MC}} = 100$  Monte Carlo runs. For the shown results, the same conclusions as those drawn for the results assuming LOS propagation conditions can be drawn. It can be noticed that compared to the LOS case, the performance of the PF-based estimators without road constraints is worse for the Hybrid 1+ and Hybrid 2+ method. However, the possible performance improvements using the Hybrid 1+ method instead of the Hybrid 1 method are larger compared to the LOS case. In Fig. 4.19, the MT location  $\overline{\text{RMSE}}$  in m vs. GDOP for the Satellite and Hybrid 3 method are shown for the PF, APF, RBPF, RBAPF using  $N = 1000$  particles, together with the corresponding  $\overline{\text{PCRLBs}}$ . The same conclusions can be drawn from these results as those for the PF-based estimators assuming LOS propagation conditions. It can be observed that for

the PF-based estimators without road constraints the results are worse compared to the LOS case, which is due to the different assumptions for the measurement noise in LOS and NLOS propagation conditions.

### 4.6.3 Field Trial Results

In this section, the expected performance of the hybrid localization method is tested on experimental data available from a field trial. Since the RTT and RSS measurements are highly affected by switching LOS/NLOS propagation conditions the PF-based algorithms have been used for the hybrid localization method. The unknown parameters of the RTT and RSS model as well as the stationary values of the Markov chain, which are necessary to evaluate the likelihood function, cf. (3.83), have been estimated from the available field trial data using the Expectation-Maximization algorithm [DLR77, MK97]. For the initialization of the filters, the strategy presented in Section 4.6.2.1 is used. The initial state vector is obtained from the geometric approach presented in Section 3.5.3 and the initial MT velocity and the MT clock drift is set to zero. The movement of the MT during the field trial can be described with the movement of a car in a city. The MT experiences many accelerations and deaccelerations,

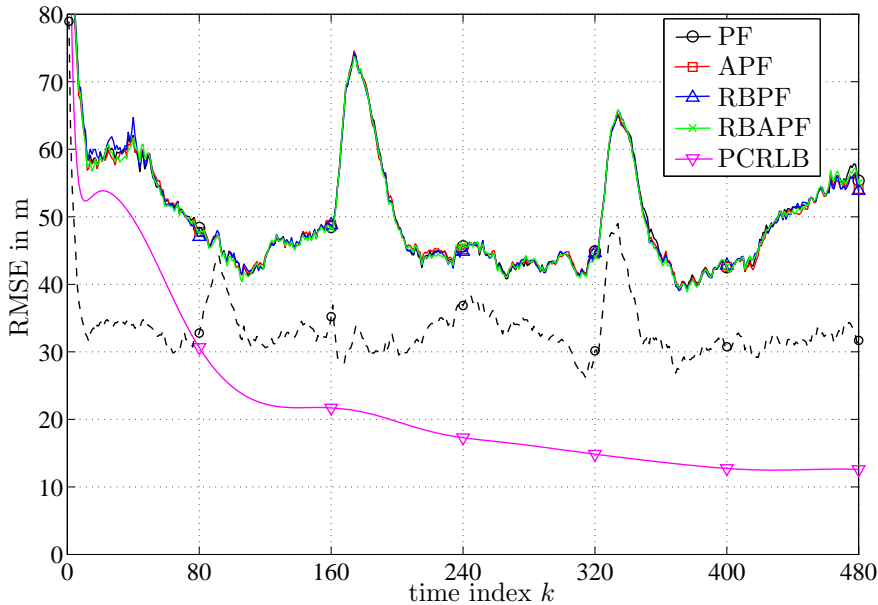


Figure 4.14. MT location RMSE vs. time index  $k$  for PF, APF, RBPF, RBAPF and PCRLB assuming switching LOS/NLOS propagation conditions and Cellular method, solid lines: No road constraints, dashed lines: Road constraints.

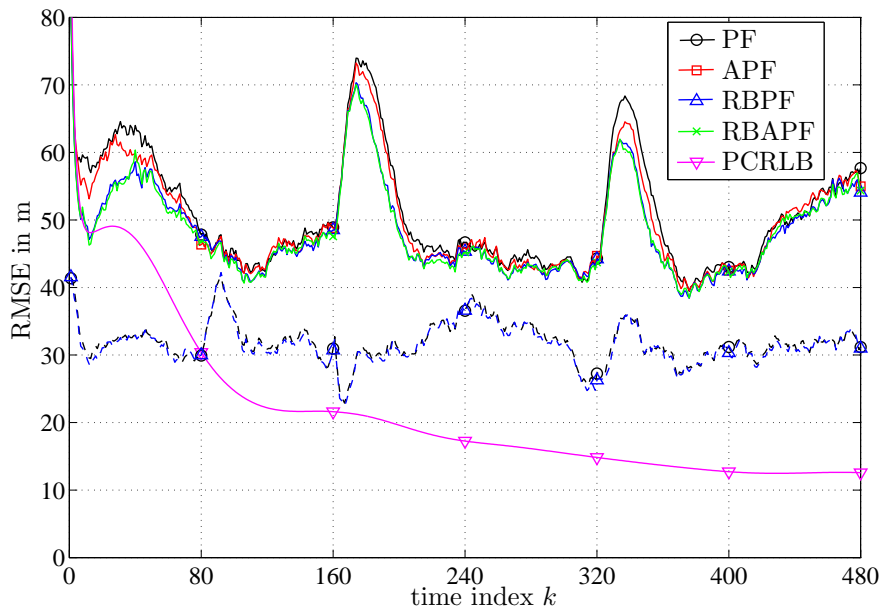


Figure 4.15. MT location RMSE vs. time index  $k$  for PF, APF, RBPF, RBAPF and PCRLB assuming switching LOS/NLOS propagation conditions and Hybrid 1 method, solid lines: No road constraints, dashed lines: Road constraints.

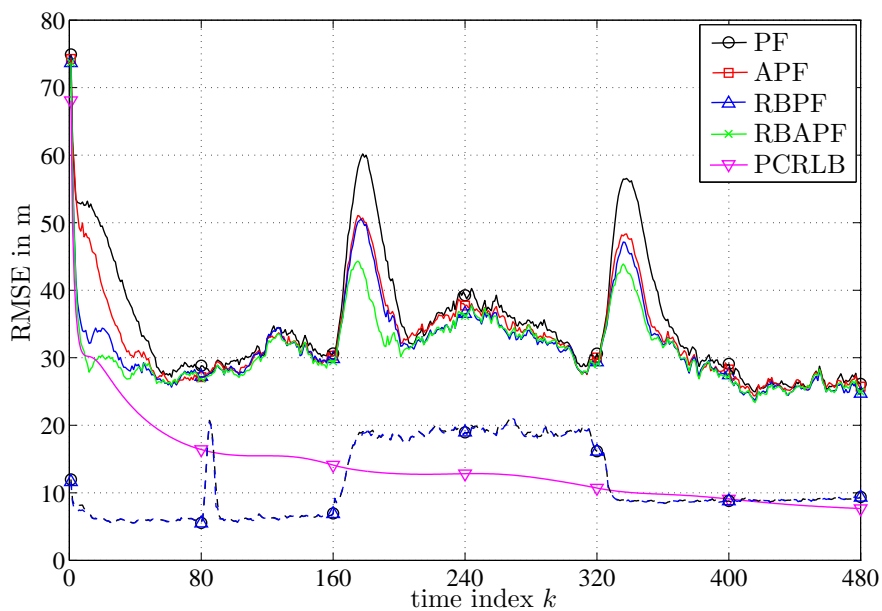


Figure 4.16. MT location RMSE vs. time index  $k$  for PF, APF, RBPF, RBAPF and PCRLB assuming switching LOS/NLOS propagation conditions and Hybrid 2 method, solid lines: No road constraints, dashed lines: Road constraints.

followed by periods of no movement, since the car has to stop at traffic lights. In order to take into account the different maneuvers of the MT, the covariance matrix  $\mathbf{Q}$ , which is a filter design parameter, is chosen in the algorithms as  $\mathbf{Q} = \text{diag}_b[\mathbf{Q}_{\text{CV}}, 100 \cdot \mathbf{Q}_{\text{CO}}]$  with  $\mathbf{Q}_{\text{CV}} = \text{diag}[100, 100]$  ( $\mathbf{Q} = \text{diag}_b[\sigma_p^2, 100 \cdot \mathbf{Q}_{\text{CO}}]$  with  $\sigma_p^2 = 100$  for PF-based algorithms with road constraints), where the parameters of the covariance matrix  $\mathbf{Q}_{\text{CO}}$  are given in Table 2.2. Note that the algorithms have been also tested for smaller values of  $\mathbf{Q}_{\text{CV}}$ , but this yielded no performance improvements. In order to obtain an average performance of the PF-based estimators,  $N_{\text{MC}} = 100$  Monte Carlo runs are performed, where in each run the same set of measurement data is used.

In Fig. 4.20, the MT location  $\overline{\text{RMSE}}$  vs. particle number  $N$  for the Cellular, Hybrid 1 and Hybrid 2 method is shown for the PF, APF, RBPF and RBAPF. It can be seen that the performance of the different filters for the Cellular method is practically equivalent for all tested numbers of particles. Small performance gains can be obtained using the Hybrid 1 method rather than the Cellular method, where the PF and APF are outperformed by the RBPF and RBAPF for small  $N$ . Significant performance improvements are possible with the Hybrid 2 method. In Fig. 4.21, the MT location RMSE vs. time index  $k$  for the Cellular, Hybrid 1 and Hybrid 2 method is shown for the PF using  $N = 1000$ . Here, only the results for the PF are shown since for  $N = 1000$ , all investigated algorithms have approximately the same performance, cf. Fig. 4.20. It can

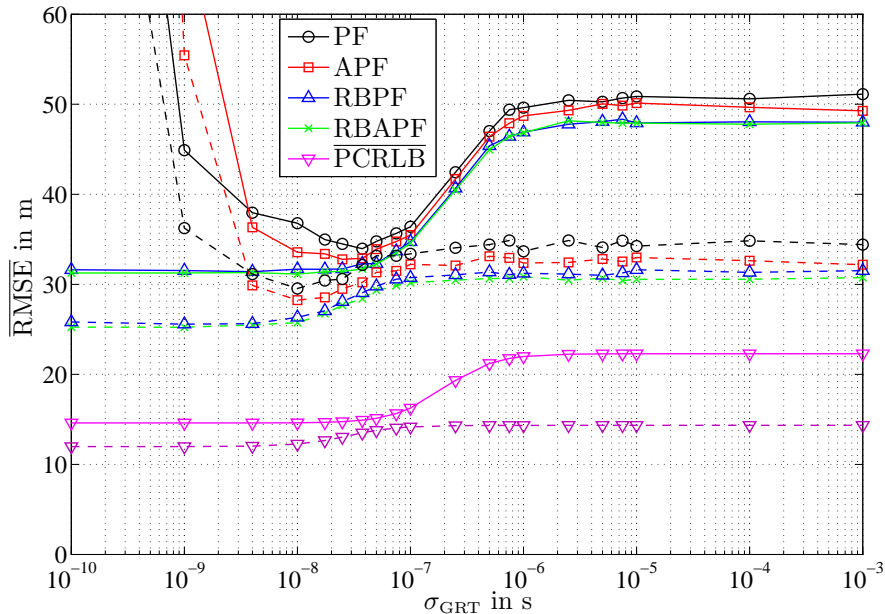


Figure 4.17. MT location  $\overline{\text{RMSE}}$  vs. GRT error standard deviation  $\sigma_{\text{GRT}}$  for PF, APF, RBPF, RBAPF and  $\overline{\text{PCRLB}}$  assuming switching LOS/NLOS propagation conditions, solid lines: Hybrid 1+ method, dashed lines: Hybrid 2+ method.

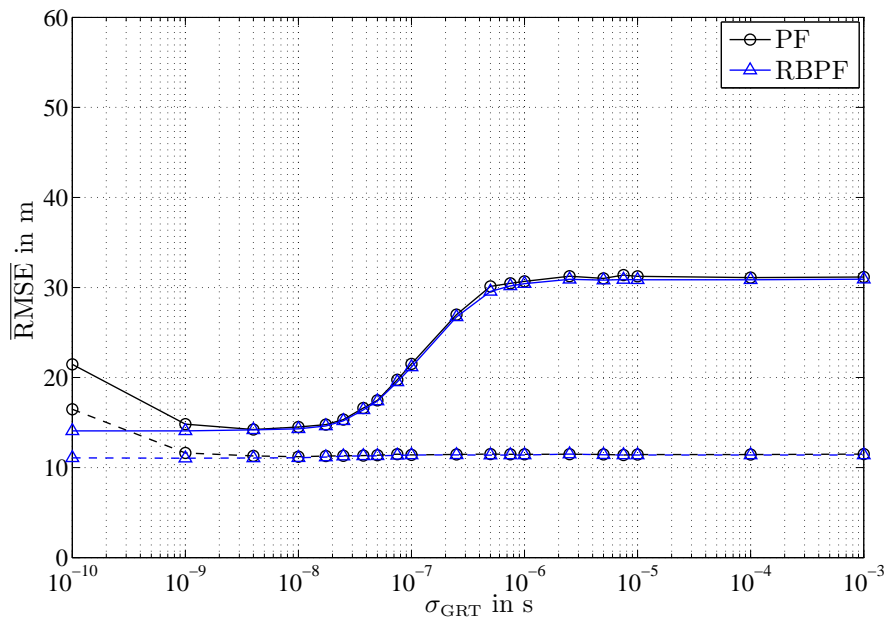


Figure 4.18. MT location  $\overline{\text{RMSE}}$  vs. GRT error standard deviation  $\sigma_{\text{GRT}}$  for PF and RBPF with road constraints assuming switching LOS/NLOS propagation conditions, solid lines: Hybrid 1+ method, dashed lines: Hybrid 2+ method.

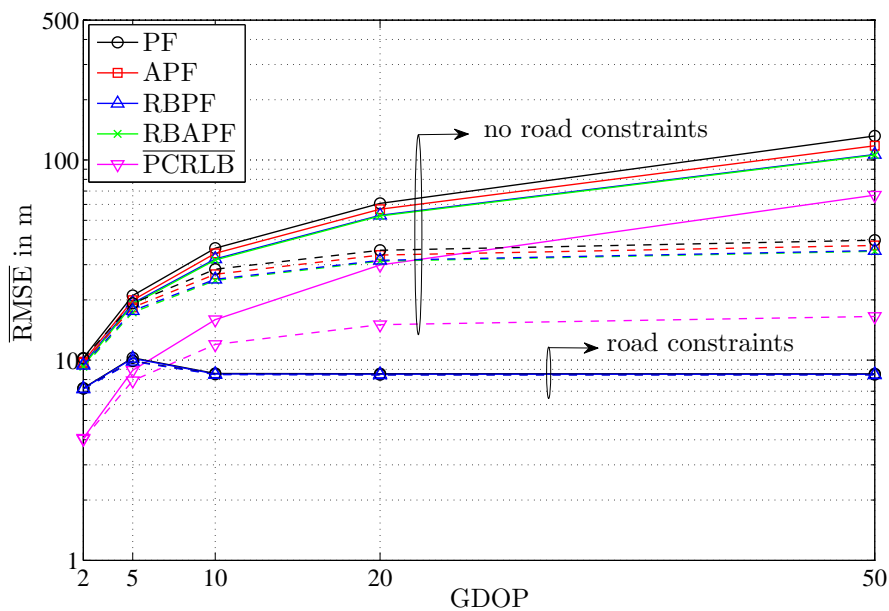


Figure 4.19. MT location  $\overline{\text{RMSE}}$  vs. GDOP for PF, APF, RBPF, RBAPF and  $\overline{\text{PCRLB}}$  assuming switching LOS/NLOS propagation conditions, solid lines: Satellite method, dashed lines: Hybrid 3 method.



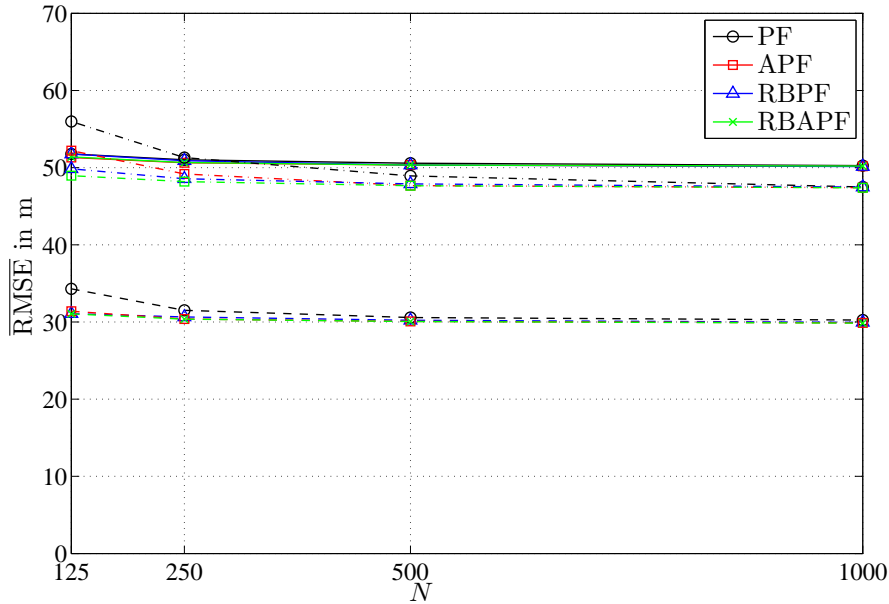


Figure 4.20. MT location  $\overline{\text{RMSE}}$  vs. particle number  $N$  for PF, APF, RBPF and RBAPF, solid lines: Cellular method, dash-dotted lines: Hybrid 1 method, dashed lines: Hybrid 2 method.

be seen that the Cellular method provides the worst performance. Small performance improvements can be obtained using the Hybrid 1 method and significant performance gains are possible using the Hybrid 2 method. The peaks in the RMSE result from the mismatch between the state model assumptions and the true MT movement, and the geometric relationships between the satellites, BS and the MT during the field trial. In Fig. 4.22, the MT location RMSE vs. time index  $k$  for the Cellular, Hybrid 1 and Hybrid 2 method is shown for the PF with road constraints using  $N = 1000$ . From these results the same conclusions as those for the PF can be drawn. Note that the results for the RBPF with road constraints are practically equivalent and are not shown. It can be seen that the incorporation of road constraints into the PF for the Cellular method does not yield the performance improvements that have been obtained in the simulations. The reason for this result is the investigated field trial scenario, which is much more challenging than the simulation scenario, since it contains much more road junctions and less favourable geometries between the MT and the BSs, cf. Fig. 2.6. These facts in combination with the availability of inaccurate RTT and RSS measurements result in the described performance. The performance can be significantly improved using the Hybrid 2 method. In this case, two very accurate PR measurements are available that help to improve the overall performance. In Table 4.1, the MT location  $\overline{\text{RMSE}}$  in m for the Cellular, Hybrid 1 and Hybrid 2 methods are shown for the PF and PF

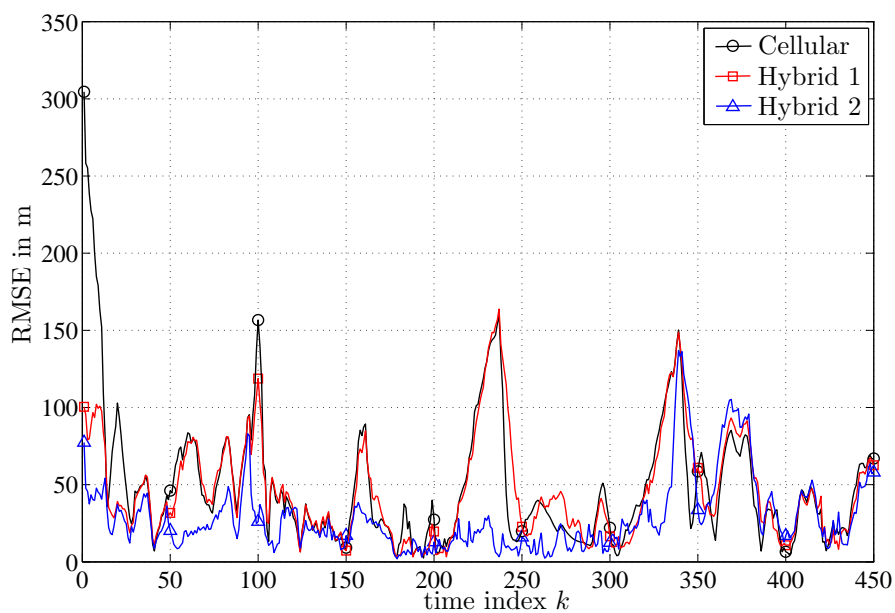


Figure 4.21. MT location RMSE vs. time index  $k$  for the Cellular, Hybrid 1 and Hybrid 2 methods shown for the PF.

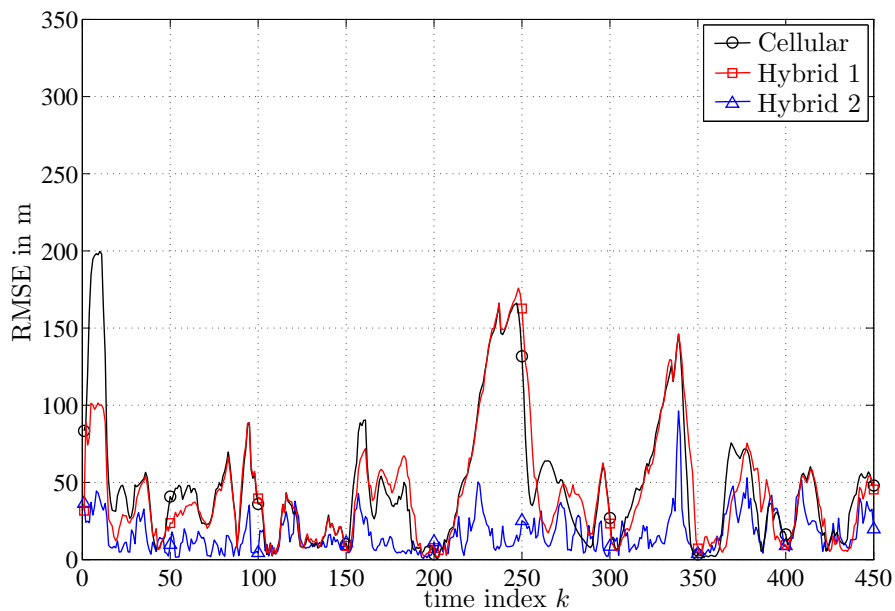


Figure 4.22. MT location RMSE vs. time index  $k$  for the Cellular, Hybrid 1 and Hybrid 2 methods shown for the PF with road constraints.

with road constraints using  $N = 1000$  particles. The results show that in terms of  $\overline{\text{RMSE}}$ , the PF with road constraints always outperforms the PF. However, only large improvements are possible using the Hybrid 2 method. Comparing these results with the results of the non-recursive estimator, cf. Table 4.1, it can be concluded that the results of the PF are similar to the results obtained with the non-recursive estimator assuming optimal initial values. The performance using the PF is not further improved due to the choice of  $\mathbf{Q}_{CV}$ . Even though the choice of  $\mathbf{Q}_{CV}$  helps to cover the different maneuvers of the MT during the field trial, it also leads to higher uncertainty meaning less confidence in the state model. This, in turn, means that performance of the filter is dominated by the information that is contained in the measurements. Nevertheless, compared to the non-recursive estimator, the PF-based estimators have the advantage that they are relatively insensitive to badly chosen initial values.

Table 4.1. MT location  $\overline{\text{RMSE}}$  for the Cellular, Hybrid 1 and Hybrid 2 method using the PF and PF with road constraints for  $N = 1000$  particles.

Method	MT location $\overline{\text{RMSE}}$ in m	
	PF	PF with road constraints
Cellular	50.26	49.42
Hybrid 1	47.49	46.30
Hybrid 2	29.85	19.76

#### 4.6.4 Computational Complexity

In order to complement the performance analysis, this section deals with the complexity of the different hybrid localization algorithms. With the obtained results, it is possible to identify which algorithm presents the best trade-off between complexity and performance.

In the following, the complexity of the EKF, UKF and CKF algorithms is evaluated in terms of FLOPs. In the PF-based algorithms, essential steps such as the generation of random variables cannot be measured in FLOPs. These steps, however, significantly contribute to the computational complexity and cannot be neglected. The complexity analysis of PF-based estimators can be found in [KSG05] and is not further treated in this work, since a fair comparison to KF-based estimators in terms of FLOPs is not possible. However, as a rule, one can safely say that the PF-based estimators are orders of magnitude more complex than the KF-based estimators. In Table 4.2, the

Table 4.2. Computational complexity of some common matrix operations [KSG05]

Operation	Size	Mult.	Add.	Other
$\mathbf{A} + \mathbf{A}$	$\mathbf{A} \in \mathbb{R}^{n \times m}$	–	$nm$	–
$\mathbf{A} \cdot \mathbf{B}$	$\mathbf{A} \in \mathbb{R}^{n \times m}, \mathbf{B} \in \mathbb{R}^{m \times l}$	$lmn$	$(m-1)ln$	–
$\mathbf{C}^{-1}$	$\mathbf{C} \in \mathbb{R}^{n \times n}$	$n^3$	–	–
$\sqrt{\mathbf{C}}$	$\mathbf{C} \in \mathbb{R}^{n \times n}$	–	–	$n^3/3 + 2n^2$

computational complexity of some common matrix operations is summarized [KSG05]. Here, it is worth noting that the matrix square root, which is needed to evaluate the set of cubature and sigma points, is computed using Cholesky decomposition, whose complexity grows cubically. In the EKF as well as in the UKF and CKF, there are certain steps that cannot be measured in FLOPs. In the EKF, for example, one has to evaluate at every time step  $k$  the Jacobian matrix  $\mathbf{H}_{\text{LOS},k}$  and the nonlinear function  $\mathbf{h}_{\text{LOS},k}(\cdot)$ , cf. Algorithm 4.1. In the UKF and CKF, one has to propagate at every time step  $2 \cdot n_x + 1$  sigma points and  $2 \cdot n_x$  cubature points through the nonlinear function  $\mathbf{h}_{\text{LOS},k}(\cdot)$  (cf. Algorithms 4.2 and 4.3). In the following, the cost of evaluating a certain nonlinear function and Jacobian matrix is neglected. Furthermore, the computation of the weights in the UKF and CKF, as well as the initialization of all three filters can be neglected, since these steps are done only once. In Table 4.3, the computational complexity of the different quantities that have to be evaluated in the EKF, UKF and CKF is presented. Summing up the computational complexity of the different

Table 4.3. Computational complexity of the EKF, UKF and CKF.  $\mathcal{X}_{k|k-1}$  denotes the matrix composed of sigma/cubature point vectors.

Quantity	Complexity in FLOPs		
	EKF	UKF	CKF
$\hat{\mathbf{x}}_{k k-1}$	$2n_x^2 - n_x$	$2n_x^2 - n_x$	$2n_x^2 - n_x$
$\mathbf{P}_{k k-1}$	$8n_x^3 - 15n_x^2 + 10n_x$	$8n_x^3 - 15n_x^2 + 10n_x$	$8n_x^3 - 15n_x^2 + 10n_x$
$\mathcal{X}_{k k-1}$	–	$13n_x^3/3 + 2n_x^2$	$13n_x^3/3 + 2n_x^2$
$\hat{\mathbf{z}}_{k k-1}$	–	$2n_x n_z + 2n_z$	$2n_x n_z$
$\mathbf{P}_{\mathbf{zz},k k-1}$	$2n_z^2 n_x + 2n_x^2 n_z - n_x n_z$	$4n_z^2 n_x + 2n_x n_z + 4n_z^2 + n_z$	$4n_z^2 n_x + 3n_z^2$
$\mathbf{P}_{\mathbf{xz},k k-1}$	$2n_x^2 n_z - n_x n_z$	$4n_x^2 n_z + 3n_x n_z + 2n_x^2 + n_x$	$4n_x^2 n_z + 2n_x n_z$
$\mathbf{K}_k$	$n_z^3 + 2n_z^2 n_x - n_x n_z$	$n_z^3 + 2n_z^2 n_x - n_x n_z$	$n_z^3 + 2n_z^2 n_x - n_x n_z$
$\hat{\mathbf{x}}_{k k}$	$2n_x n_z + 2n_z$	$2n_x n_z + 2n_z$	$2n_x n_z + 2n_z$
$\mathbf{P}_{k k}$	$2n_z^2 n_x + 2n_x^2 n_z - n_x n_z$	$2n_z^2 n_x + 2n_x^2 n_z - n_x n_z$	$2n_z^2 n_x + 2n_x^2 n_z - n_x n_z$

quantities results in the total FLOP complexity of the EKF, UKF and CKF for one time step which is given by

$$\mathcal{C}_{\text{EKF}}(n_x, n_z) = 8n_x^3 + n_z^3 + 6n_x^2n_z + 6n_z^2n_x - 13n_x^2 - 2n_xn_z + 9n_x + 2n_z, \quad (4.184)$$

$$\mathcal{C}_{\text{UKF}}(n_x, n_z) = \frac{37}{3}n_x^3 + n_z^3 + 6n_x^2n_z + 8n_z^2n_x - 9n_x^2 + 7n_xn_z + 4n_z^2 + 10n_x + 5n_z, \quad (4.185)$$

$$\mathcal{C}_{\text{CKF}}(n_x, n_z) = \frac{37}{3}n_x^3 + n_z^3 + 6n_x^2n_z + 8n_z^2n_x - 11n_x^2 + 4n_xn_z + 3n_z^2 + 9n_x + 2n_z. \quad (4.186)$$

Table 4.4 shows the complexity of the algorithms in terms of FLOPs per time step  $k$  for the different methods and Scenario I. It can be seen that for all investigated methods, the EKF has the lowest computational complexity, followed by the CKF and UKF. The complexity reduction of the EKF compared to the UKF is about 30%. Using a CKF rather than a UKF results in a complexity reduction of only 4%.

Table 4.4. Computational complexity of the hybrid localization algorithms in FLOPs per time step  $k$  for Scenario I.

Method	Complexity in FLOPs per Time Step		
	EKF	UKF	CKF
Cellular	3108	4534	4314
Hybrid 1	6813	9708	9360
Hybrid 1+	7974	11230	10842
Hybrid 2	7974	11230	10842
Hybrid 2+	9267	12916	12486
Hybrid 3	9267	12916	12486
Satellite	2283	3684	3534

## 4.7 Conclusions

In this chapter, the hybrid localization problem has been reformulated as a recursive state estimation problem, where the MT state is assumed to be a Markov process. Various well-known KF-based estimators and PF-based estimators have been proposed to solve the hybrid localization problem. The RBAPF has been newly proposed and derived in the framework of a general conditional linear system model. Road constraints have been incorporated into the PF and RBPF to further improve the performance. The performance of the different algorithms has been compared to the theoretically

best achievable performance, which is given by the PCRLB. For the case of LOS propagation conditions, the PCRLB has been newly derived in the hybrid localization framework. For the case of switching LOS/NLOS propagation conditions, a numerical solution of the PCRLB based on Monte Carlo integration has been newly proposed. The presented hybrid localization algorithms have been extensively analyzed in terms of performance. The KF-based algorithms are further investigated in terms of their complexity. If it is not otherwise stated, the following main conclusions hold for both cases assuming LOS and switching LOS/NLOS propagation conditions:

- The performance gains of the Hybrid 1 method with respect to the Cellular method strongly depend on the accuracy of the initial values.
- Compared to the hybrid localization algorithms presented in Chapter 3, large performance improvements can be obtained with the KF-based algorithms and PF-based algorithms for all investigated methods.
- The proposed KF-based algorithms and PF-based algorithms cannot achieve the corresponding PCRLBs.
- The RBPF and RBAPF show good performance for the Hybrid 1+ and Hybrid 2+ method for all investigated accuracies of the GRT measurements. The PF and APF diverge for highly accurate GRT measurements due to a peaked likelihood pdf.
- For the case of LOS propagation conditions and having no road information available, the EKF provides the best trade-off between complexity and performance.
- Significantly performance improvements can be achieved for all investigated methods by incorporating road-constraints into the PF and RBPF. Good performance results can be obtained already with a small number of particles.
- The RBPF always outperforms the PF and the RBAPF always outperforms the APF. The achievable performance gains strongly depend on the dimension of the state space and the number of particles used in the corresponding filters.

---

## Chapter 5

# Recursive State Estimation with Adaptive LOS/NLOS Detection for Hybrid Localization

## 5.1 Introduction

In this chapter, the hybrid localization problem is solved using recursive state estimation techniques with adaptive LOS/NLOS detection <sup>1</sup>. In recursive state estimation with adaptive LOS/NLOS detection, the MT state and the mode variable is taken into account in the estimation process. These quantities are estimated for each time step  $k$  recursively, by taking into account the information available from the measurements, MT state estimates and estimates related to the mode variable from previous time steps.

The concept of adaptive recursive Bayesian state estimation is introduced in Section 5.2 and two solutions to the optimal adaptive recursive Bayesian solution are presented. In order to assess the theoretical best achievable performance of adaptive recursive estimators, the PCRLB is evaluated for the hybrid localization problem in Section 5.3. Since an analytical solution of the optimal adaptive recursive Bayesian solution for hybrid localization does not exist, suboptimal adaptive recursive estimators are proposed. In Section 5.4, IMM algorithm-based estimators are introduced to solve the hybrid localization problem, and in Section 5.5, multiple model PF-based estimators are proposed. The performance of the different hybrid localization algorithms is analyzed by means of simulations in Section 5.6. Finally, the main conclusions of this chapter are drawn in Section 5.7.

---

<sup>1</sup>In the literature, recursive state estimation with adaptive detection is also known as adaptive state estimation, adaptive filtering, jump Markov state estimation or hybrid state estimation [SB99, BSLK01, RAG04, GG05].

## 5.2 Concept of Adaptive Recursive Bayesian Estimation

### 5.2.1 Introduction

In this section, the concept of adaptive recursive Bayesian estimation is presented. In adaptive recursive Bayesian estimation, the discrete-valued mode variable  $r_k$  is introduced to model possible jumps among different models that occur randomly between two consecutive time steps, see for instance [SB99, BSLK01, RAG04, LJ05]. Since the actual value of the mode variable  $r_k$  at every time step is unknown, it has to be considered as unknown in the corresponding adaptive recursive estimator. In the following, two approaches are presented, with which the adaptive Bayesian estimation problem can be solved.

The first approach is based on mode sequence conditioning and is presented in Section 5.2.2. The second approach is based on state vector augmentation and is presented in Section 5.2.3.

### 5.2.2 Mode Sequence Conditioning

In this section, the conceptual solution for the adaptive recursive Bayesian estimation problem using the mode sequence conditioning approach is presented [AF70, BSLK01, RAG04]. The idea of the mode sequence conditioning approach is to calculate posterior pdfs that are conditioned on particular mode sequences. Thus, instead of estimating the current mode  $r_k$ , all possible mode sequences that might occur through time  $k$  are evaluated in this approach.

Let  $r_\kappa^l$  denote the particular value of the mode variable at time  $\kappa$  in the  $l$ -th mode sequence. Since at each time step  $k$  the mode variable is assumed to be among the possible  $s$  modes, the number of mode sequences increase exponentially with  $s^k$ . In the following, the sequence of modes up to time index  $k$  is denoted with

$$\mathcal{R}_k^l = \{r_1^l, r_2^l, \dots, r_k^l\} = \{\mathcal{R}_{k-1}^l, r_k^l\}, \quad \text{for } l = 1, \dots, s^k. \quad (5.1)$$

Let  $\Pr\{\mathcal{R}_k^l | \mathbf{Z}_k\}$  denote the probability of a particular mode sequence given the measurements  $\mathbf{Z}_k$ , and let  $p(\mathbf{x}_k | \mathcal{R}_k^l, \mathbf{Z}_k)$  denote the posterior pdf conditioned on a particular



mode sequence. Then, the posterior pdf  $p(\mathbf{x}_k|\mathbf{Z}_k)$  can be expressed as a weighted sum of pdfs according to

$$p(\mathbf{x}_k|\mathbf{Z}_k) = \sum_{l=1}^{s^k} p(\mathbf{x}_k, \mathcal{R}_k^l|\mathbf{Z}_k) = \sum_{l=1}^{s^k} \Pr\{\mathcal{R}_k^l|\mathbf{Z}_k\} \cdot p(\mathbf{x}_k|\mathcal{R}_k^l, \mathbf{Z}_k). \quad (5.2)$$

Note that the number of sum components increase exponentially with time. According to [AF70], the posterior pdf  $p(\mathbf{x}_k|\mathcal{R}_k^l, \mathbf{Z}_k)$  conditioned on a particular mode sequence as well as the probability  $\Pr\{\mathcal{R}_k^l|\mathbf{Z}_k\}$  can be updated recursively. The corresponding time update and measurement update equations can be written as follows. In the time update step, the prediction density  $p(\mathbf{x}_k|\mathcal{R}_k^l, \mathbf{Z}_{k-1})$  conditioned on the mode sequence  $\mathcal{R}_k^l$  is computed according to

$$p(\mathbf{x}_k|\mathcal{R}_k^l, \mathbf{Z}_{k-1}) = \int_{\mathbb{R}^{n_x}} p(\mathbf{x}_k|\mathbf{x}_{k-1}, r_k^l) \cdot p(\mathbf{x}_{k-1}|\mathcal{R}_{k-1}^l, \mathbf{Z}_{k-1}) d\mathbf{x}_{k-1}. \quad (5.3)$$

For state models of the form (2.2), the transitional pdf  $p(\mathbf{x}_k|\mathbf{x}_{k-1}, r_k)$  can be reduced to

$$p(\mathbf{x}_k|\mathbf{x}_{k-1}, r_k) = p(\mathbf{x}_k|\mathbf{x}_{k-1}), \quad (5.4)$$

where  $p(\mathbf{x}_k|\mathbf{x}_{k-1})$  is given by (4.2). In the measurement update step, the posterior pdf  $p(\mathbf{x}_k|\mathcal{R}_k^l, \mathbf{Z}_k)$  conditioned on the mode sequence is calculated from the following relationship

$$p(\mathbf{x}_k|\mathcal{R}_k^l, \mathbf{Z}_k) = \frac{p(\mathbf{z}_k|\mathbf{x}_k, r_k^l) \cdot p(\mathbf{x}_k|\mathcal{R}_k^l, \mathbf{Z}_{k-1})}{p(\mathbf{z}_k|\mathcal{R}_k^l, \mathbf{Z}_{k-1})} = \frac{p(\mathbf{z}_k|\mathbf{x}_k, r_k^l) \cdot p(\mathbf{x}_k|\mathcal{R}_k^l, \mathbf{Z}_{k-1})}{\int_{\mathbb{R}^{n_x}} p(\mathbf{z}_k|\mathbf{x}_k, r_k^l) \cdot p(\mathbf{x}_k|\mathcal{R}_k^l, \mathbf{Z}_{k-1}) d\mathbf{x}_{k-1}}. \quad (5.5)$$

For measurement models of the form (2.18), the pdf  $p(\mathbf{z}_k|\mathbf{x}_k, r_k^l)$  (or mode-conditioned likelihood function) is given by

$$p(\mathbf{z}_k|\mathbf{x}_k, r_k^l) = p_{\mathbf{v}_k(r_k^l)}(\mathbf{x}_k - \mathbf{h}_k(\mathbf{x}_k, r_k^l)). \quad (5.6)$$

The probability  $\Pr\{\mathcal{R}_k^l|\mathbf{Z}_k\}$  can be evaluated recursively from

$$\Pr\{\mathcal{R}_k^l|\mathbf{Z}_k\} = \frac{p(\mathbf{z}_k|\mathcal{R}_k^l, \mathbf{Z}_{k-1}) \cdot \Pr\{r_k^l|r_{k-1}^l\} \cdot \Pr\{\mathcal{R}_{k-1}^l|\mathbf{Z}_{k-1}\}}{p(\mathbf{z}_k|\mathbf{Z}_{k-1})}, \quad (5.7)$$

and the recursions are initiated with  $p(\mathbf{x}_0)$  and  $\Pr\{r_1\}$  [AF70,BSLK01]. Note that if the mode variable  $r_k$  in effect at every time step  $k$  is known, then the adaptive recursive solution given by (5.2), reduces to the recursive solution presented in Section 4.2. Knowledge of the posterior pdf  $p(\mathbf{x}_k|\mathbf{Z}_k)$  enables one to obtain MT state estimates with respect to any criterion. In the following, the MMSE estimator for recursive adaptive

estimation and the corresponding covariance using the mode sequence conditioning approach are introduced that can be obtained from inserting (5.2) into (4.5), yielding

$$\hat{\mathbf{x}}_{\text{MMSE},k|k} = \sum_{l=1}^{s^k} \Pr\{\mathcal{R}_k^l | \mathbf{Z}_k\} \cdot \int_{\mathbb{R}^{n_x}} \mathbf{x}_k \cdot p(\mathbf{x}_k | \mathcal{R}_k^l, \mathbf{Z}_k) d\mathbf{x}_k, \quad (5.8a)$$

$$\mathbf{P}_{\text{MMSE},k|k} = \sum_{l=1}^{s^k} \Pr\{\mathcal{R}_k^l | \mathbf{Z}_k\} \cdot \int_{\mathbb{R}^{n_x}} (\mathbf{x}_k - \hat{\mathbf{x}}_{\text{MMSE},k|k})(\mathbf{x}_k - \hat{\mathbf{x}}_{\text{MMSE},k|k})^\top p(\mathbf{x}_k | \mathcal{R}_k^l | \mathbf{Z}_k) d\mathbf{x}_k. \quad (5.8b)$$

For the hybrid localization problem, an analytical solution for  $p(\mathbf{x}_k | \mathcal{R}_k^l, \mathbf{Z}_k)$  does not exist, since the measurement model  $\mathbf{h}_k(\mathbf{x}_k, r_k)$  is nonlinear. In this case, one has to resort to suboptimal approaches. In addition to that, the exponentially increasing number of mode sequences prevent the evaluation of (5.2) for large values of  $k$  in practice, so that further approximations have to be introduced.

### 5.2.3 State Vector Augmentation

In this section, the conceptual solution for the adaptive recursive Bayesian estimation problem using the state vector augmentation approach is presented [RAG04]. In the state vector augmentation approach, the continuous-valued state vector  $\mathbf{x}_k$  is augmented by the unknown discrete-valued mode variable  $r_k$ , yielding  $\mathbf{y}_k = [\mathbf{x}_k^\top, r_k]^\top$ . Since the augmented state vector  $\mathbf{y}_k$  is composed of continuous-valued and discrete-valued states, the corresponding estimation problem is also known as hybrid-state estimation problem [RAG04, SB99].

The aim in hybrid-state estimation is to recursively compute estimates of the state  $\mathbf{x}_k$  and the mode  $r_k$  using the sequence of all available measurements  $\mathbf{Z}_k$ . From a Bayesian point of view, the aim is to recursively compute the joint posterior pdf  $p(\mathbf{x}_k, r_k | \mathbf{Z}_k)$ , since it provides a complete statistical description of the state  $\mathbf{x}_k$  and mode  $r_k$  at that time. The recursive solution to the hybrid state estimation problem is divided into a time update step and measurement update step [RAG04]. In the time update step, the joint prediction density  $p(\mathbf{x}_k, r_k | \mathbf{Z}_{k-1})$  is computed according to

$$p(\mathbf{x}_k, r_k | \mathbf{Z}_{k-1}) = \sum_{r_{k-1}} \Pr\{r_k | r_{k-1}\} \cdot \int_{\mathbb{R}^{n_x}} p(\mathbf{x}_k | \mathbf{x}_{k-1}, r_k) \cdot p(\mathbf{x}_{k-1}, r_{k-1} | \mathbf{Z}_k) d\mathbf{x}_{k-1}. \quad (5.9)$$

Note that for state models of the form (2.2) the pdf  $p(\mathbf{x}_k | \mathbf{x}_{k-1}, r_k^l)$  can be replaced by the expression in (5.4). When a new measurement becomes available at time step  $k$ ,

the measurement update step is performed. Using Bayes' theorem, the joint posterior pdf  $p(\mathbf{x}_k, r_k | \mathbf{Z}_k)$  can be updated according to

$$p(\mathbf{x}_k, r_k | \mathbf{Z}_k) = \frac{p(\mathbf{z}_k | \mathbf{x}_k, r_k) \cdot p(\mathbf{x}_k, r_k | \mathbf{Z}_{k-1})}{\sum_{r_k} \int_{\mathbb{R}^{n_x}} p(\mathbf{z}_k | \mathbf{x}_k, r_k) \cdot p(\mathbf{x}_k, r_k | \mathbf{Z}_{k-1}) d\mathbf{x}_k}, \quad (5.10)$$

where the pdf  $p(\mathbf{z}_k | \mathbf{x}_k, r_k)$  is given by (5.6), and the recursions are initiated with  $p(\mathbf{x}_0)$  and  $\Pr\{r_1\}$  [RAG04]. The posterior pdf of the current state, given the measurements can be finally obtained from

$$p(\mathbf{x}_k | \mathbf{Z}_k) = \sum_{r_k} p(\mathbf{x}_k, r_k | \mathbf{Z}_k). \quad (5.11)$$

Note that if  $r_k$  is known at each time step  $k$ , then the adaptive recursive solution given by (5.11) reduces to the recursive solution presented in Section 4.2. Knowledge of the posterior pdf  $p(\mathbf{x}_k | \mathbf{Z}_k)$  enables one to obtain MT state estimates with respect to any criterion. In the following the MMSE estimator for recursive adaptive estimation and the corresponding covariance using the state vector augmentation approach are presented that can be obtained from inserting (5.11) into (4.5), yielding

$$\hat{\mathbf{x}}_{\text{MMSE},k|k} = \sum_{r_k} \int_{\mathbb{R}^{n_x}} \mathbf{x}_k \cdot p(\mathbf{x}_k, r_k | \mathbf{Z}_k) d\mathbf{x}_k, \quad (5.12a)$$

$$\mathbf{P}_{\text{MMSE},k|k} = \sum_{r_k} \int_{\mathbb{R}^{n_x}} (\mathbf{x}_k - \hat{\mathbf{x}}_{\text{MMSE},k|k}) \cdot (\mathbf{x}_k - \hat{\mathbf{x}}_{\text{MMSE},k|k})^T \cdot p(\mathbf{x}_k, r_k | \mathbf{Z}_k) d\mathbf{x}_k. \quad (5.12b)$$

For the hybrid localization method, an analytical solution to the recursion given by (5.9) and (5.11) does not exist, since the mode-dependent measurement function  $\mathbf{h}_k(\mathbf{x}_k, r_k)$  is nonlinear. In this case, one has to resort to suboptimal approaches.

## 5.3 Posterior Cramér-Rao Lower Bound

### 5.3.1 Introduction

In this section, the PCRLB for the hybrid localization method is presented, where the switching between LOS and NLOS propagation conditions is modeled with a Markov chain. The calculation of the PCRLB for this case is more difficult, since a discrete valued model index  $r_k$  is introduced in addition to the continuous valued state vector  $\mathbf{x}_k$ . As the evaluation of the PCRLB involves derivatives with respect to the state

vector of interest,  $r_k$  cannot be included into the state vector, since then, the regularity conditions for computing the PCRLB are no longer satisfied [vT68].

In the following, two approaches for the evaluation of the PCRLB are presented, that avoid the incorporation of  $r_k$  into the state vector of interest. In Section 5.3.2, the enumeration method is presented, where the PCRLB is approximated as the expected value of the mode sequence [BRF<sup>+</sup>03, RAG04, HRF05]. In Section 5.3.3, the marginalization method is proposed, where the discrete mode index  $r_k$  is marginalized from all pdfs that are involved in the computation of the PCRLB. The main contributions in this section are the application of the well-known enumeration method to the hybrid localization problem, so that suitable performance bounds for the corresponding estimators can be established. In addition to that, a new performance bound is proposed, which is derived for a more general setting and then applied to the hybrid localization problem.

### 5.3.2 Enumeration Method

The idea of the enumeration method is to condition the PCRLB on the mode sequence, yielding a conditional PCRLB. The unconditional PCRLB is then found, by evaluating the expected value of the conditional PCRLB, where the expectation is taken over the mode sequence [BRF<sup>+</sup>03, RAG04, HRF05].

Let  $p(\mathbf{X}_k, \mathbf{Z}_k | \mathcal{R}_k^l)$  denote the joint pdf of the sequence of states  $\mathbf{X}_k$  and measurements  $\mathbf{Z}_k$ , conditioned on a particular sequence of modes  $\mathcal{R}_k^l$ . Let further  $\hat{\mathbf{x}}_{k|k}(\mathbf{Z}_k)$  denote an unbiased estimate of  $\mathbf{x}_k$  and let  $\hat{\mathbf{x}}_{k|k}(\mathbf{Z}_k) - \mathbf{x}_k$  denote the estimation error. Then, for a given mode sequence  $\mathcal{R}_k^l$ , the covariance matrix of the estimation error has a lower bound, referred to as conditional PCRLB, and is defined as the inverse of the  $(n_x \times n_x)$  conditional Bayesian information submatrix  $\mathbf{J}_k^l$ . Then, the covariance matrix of the estimation error satisfies the following inequality

$$\mathbb{E}_{p(\mathbf{x}_k, \mathbf{z}_k | \mathcal{R}_k^l)} \{ (\hat{\mathbf{x}}_{k|k}(\mathbf{Z}_k) - \mathbf{x}_k) (\hat{\mathbf{x}}_{k|k}(\mathbf{Z}_k) - \mathbf{x}_k)^\top \} \geq [\mathbf{J}_k^l]^{-1}. \quad (5.13)$$

According to [BRF<sup>+</sup>03, RAG04, HRF05], the conditional Bayesian information submatrix  $\mathbf{J}_k^l$  for estimating the state vector  $\mathbf{x}_k$  can be calculated recursively using the following formula

$$\mathbf{J}_k^l = \mathbf{D}_{k-1}^{l,22} - \mathbf{D}_{k-1}^{l,21} (\mathbf{J}_{k-1}^l + \mathbf{D}_{k-1}^{l,11})^{-1} \mathbf{D}_{k-1}^{l,12} + \mathbf{D}_{k-1}^{l,33}, \quad (k \geq 1) \quad (5.14)$$

where

$$\mathbf{D}_{k-1}^{l,11} = \mathbb{E}_{p(\mathbf{x}_k|\mathcal{R}_k^l)} \left\{ -\Delta_{\mathbf{x}_{k-1}}^{\mathbf{x}_k} \log_e p(\mathbf{x}_k|\mathbf{x}_{k-1}, r_k^l) \right\}, \quad (5.15a)$$

$$\mathbf{D}_{k-1}^{l,12} = \mathbb{E}_{p(\mathbf{x}_k|\mathcal{R}_k^l)} \left\{ -\Delta_{\mathbf{x}_{k-1}}^{\mathbf{x}_k} \log_e p(\mathbf{x}_k|\mathbf{x}_{k-1}, r_k^l) \right\} = [\mathbf{D}_k^{l,21}]^\top, \quad (5.15b)$$

$$\mathbf{D}_{k-1}^{l,22} = \mathbb{E}_{p(\mathbf{x}_k|\mathcal{R}_k^l)} \left\{ -\Delta_{\mathbf{x}_k}^{\mathbf{x}_k} \log_e p(\mathbf{x}_k|\mathbf{x}_{k-1}, r_k^l) \right\}, \quad (5.15c)$$

$$\mathbf{D}_{k-1}^{l,33} = \mathbb{E}_{p(\mathbf{x}_k|\mathcal{R}_k^l)} \left\{ \mathbb{E}_{p(\mathbf{z}_k|\mathbf{x}_k, \mathcal{R}_k^l)} \left\{ -\Delta_{\mathbf{x}_k}^{\mathbf{x}_k} \log_e p(\mathbf{z}_k|\mathbf{x}_k, r_k^l) \right\} \right\}. \quad (5.15d)$$

The recursion (5.14) is initialized with  $\mathbf{J}_0$  which is defined in (4.12). The unconditional PCRLB is defined as the expected value of the conditional PCRLB and can be determined from the following relationship

$$\begin{aligned} & \mathbb{E}_{p(\mathbf{x}_k, \mathbf{z}_k, \mathcal{R}_k^l)} \left\{ (\hat{\mathbf{x}}_{k|k}(\mathbf{Z}_k) - \mathbf{x}_k)(\hat{\mathbf{x}}_{k|k}(\mathbf{Z}_k) - \mathbf{x}_k)^\top \right\} \\ &= \mathbb{E}_{\Pr\{\mathcal{R}_k^l\}} \left\{ \mathbb{E}_{p(\mathbf{x}_k, \mathbf{z}_k|\mathcal{R}_k^l)} \left\{ (\hat{\mathbf{x}}_{k|k}(\mathbf{Z}_k) - \mathbf{x}_k)(\hat{\mathbf{x}}_{k|k}(\mathbf{Z}_k) - \mathbf{x}_k)^\top \right\} \right\} \\ &\geq \mathbb{E}_{\Pr\{\mathcal{R}_k^l\}} \left\{ [\mathbf{J}_k^l]^{-1} \right\} \end{aligned} \quad (5.16)$$

$$= \sum_{l=1}^{s^k} \Pr\{\mathcal{R}_k^l\} [\mathbf{J}_k^l]^{-1} = \mathcal{P}_{\text{E-PCRLB}}, \quad (5.17)$$

where  $\Pr\{\mathcal{R}_k^l\}$  is the probability that a particular mode sequence  $\mathcal{R}_k^l$  will occur. Observe that the number of sum components grows exponentially with time  $k$ . Since the calculation of the probabilities  $\Pr\{\mathcal{R}_k^l\}$  requires the enumeration of all possible mode sequences, the bound given in (5.17) is called the Enumeration Posterior Cramér-Rao Lower Bound (E-PCRLB) [RAG04].

For the hybrid localization method, the Markov chain is assumed to have  $s = 2^{N_{\text{BS}}}$  different modes with  $r_k \in \{1, \dots, 2^{N_{\text{BS}}}\}$ , cf. Section 2.3.5. Thus, a calculation of (5.17) for large values of  $k$  is practically impossible (e.g. assuming  $N_{\text{BS}} = 3$  and  $k = 100$ , one has to calculate and sum up  $8^{100}$  unconditional PCRLBs). In this case, it is possible to approximate the expectation given in (5.16) using a Monte Carlo integration approach [BRF<sup>+</sup>03]. The idea is to sample  $N_{\text{MC}}$  mode sequences  $\mathcal{R}_k^i$ ,  $i = 1, \dots, N_{\text{MC}}$ , using the prior mode probabilities  $\Pr\{r_k = i\}$ ,  $i = 1, \dots, 2^{N_{\text{BS}}}$ , and the mode transition probabilities  $\pi_{ij}$ ,  $i, j = 1, \dots, 2^{N_{\text{BS}}}$ . Then, the expectation (5.16) can be approximated as follows

$$\mathbb{E}_{\Pr\{\mathcal{R}_k^l\}} \left\{ [\mathbf{J}_k^l]^{-1} \right\} \approx \frac{1}{N_{\text{MC}}} \sum_{i=1}^{N_{\text{MC}}} [\mathbf{J}_k^i]^{-1}. \quad (5.18)$$

Using this strategy, one naturally considers those mode sequences in the computation of the bound that are most likely and discard the ones that are very unlikely. A proof that the approximation in (5.18) converges to the E-PCRLB for large  $N_{\text{MC}}$  can be found in [BRF<sup>+</sup>03]. As a result, the E-PCRLB can be approximated with

$$\mathcal{P}_{\text{E-PCRLB}} \approx \frac{1}{N_{\text{MC}}} \sum_{i=1}^{N_{\text{MC}}} [\mathbf{J}_k^i]^{-1}. \quad (5.19)$$

From (5.19), the MSE of the MT location can be determined which satisfies the following inequality

$$\mathbb{E}_{p(\mathbf{x}_k, \mathbf{z}_k, \mathbf{r}_k)} \{ \|\hat{\mathbf{x}}_{\text{MT},k|k}(\mathbf{z}_k) - \mathbf{x}_{\text{MT},k} \|^2 \} \geq [\mathcal{P}_{\text{E-PCRLB},k}]_{1,1} + [\mathcal{P}_{\text{E-PCRLB},k}]_{2,2}. \quad (5.20)$$

In order to evaluate the E-PCRLB for the hybrid localization method, it is necessary to determine the unknown matrices  $\mathbf{D}_{k-1}^{l,11}$ ,  $\mathbf{D}_{k-1}^{l,12}$ ,  $\mathbf{D}_{k-1}^{l,21}$ ,  $\mathbf{D}_{k-1}^{l,22}$  and  $\mathbf{D}_{k-1}^{l,33}$ , cf. (5.15). Since the switching between LOS and NLOS propagation conditions is modeled with a Markov chain, the hybrid localization method is fully described by the models given in (2.49) and (2.53). The model in (2.49) is linear Gaussian and independent of the mode variable  $r_k^l$ , so that the matrices  $\mathbf{D}_{k-1}^{l,11}$ ,  $\mathbf{D}_{k-1}^{l,12}$ ,  $\mathbf{D}_{k-1}^{l,21}$  and  $\mathbf{D}_{k-1}^{l,22}$  simplify to

$$\mathbf{D}_{k-1}^{l,11} = \mathbf{D}_{k-1}^{11}, \quad \mathbf{D}_{k-1}^{l,12} = \mathbf{D}_{k-1}^{12}, \quad \mathbf{D}_{k-1}^{l,21} = \mathbf{D}_{k-1}^{21}, \quad \mathbf{D}_{k-1}^{l,22} = \mathbf{D}_{k-1}^{22}, \quad (5.21)$$

where  $\mathbf{D}_{k-1}^{11}$ ,  $\mathbf{D}_{k-1}^{12}$ ,  $\mathbf{D}_{k-1}^{21}$  and  $\mathbf{D}_{k-1}^{22}$  are defined in (4.15). The likelihood function  $p(\mathbf{z}_k | \mathbf{x}_k, r_k)$ , necessary to evaluate the matrix  $\mathbf{D}_{k-1}^{l,33}$ , can be determined from the measurement model (2.53), and is given by

$$p(\mathbf{z}_k | \mathbf{x}_k, r_k) = \mathcal{N}(\mathbf{z}_k; \mathbf{h}_k(\mathbf{x}_k, r_k) + \boldsymbol{\mu}_k(r_k), \mathbf{R}_k(r_k)). \quad (5.22)$$

Let  $\tilde{\mathbf{H}}_k(\mathbf{x}_k, r_k)$  denote the mode-conditioned Jacobian matrix, which is given by

$$\tilde{\mathbf{H}}_k(\mathbf{x}_k, r_k) = \begin{bmatrix} \frac{\partial h_k^{(1)}(\mathbf{x}_k, r_k)}{\partial x_k^{(1)}} & \frac{\partial h_k^{(1)}(\mathbf{x}_k, r_k)}{\partial x_k^{(2)}} & \dots & \frac{\partial h_k^{(1)}(\mathbf{x}_k, r_k)}{\partial x_k^{(n_x)}} \\ \frac{\partial h_k^{(2)}(\mathbf{x}_k, r_k)}{\partial x_k^{(1)}} & \frac{\partial h_k^{(2)}(\mathbf{x}_k, r_k)}{\partial x_k^{(2)}} & \dots & \frac{\partial h_k^{(2)}(\mathbf{x}_k, r_k)}{\partial x_k^{(n_x)}} \\ \vdots & \vdots & & \vdots \\ \frac{\partial h_k^{(M)}(\mathbf{x}_k, r_k)}{\partial x_k^{(1)}} & \frac{\partial h_k^{(M)}(\mathbf{x}_k, r_k)}{\partial x_k^{(2)}} & \dots & \frac{\partial h_k^{(M)}(\mathbf{x}_k, r_k)}{\partial x_k^{(n_x)}} \end{bmatrix}, \quad (5.23)$$

and let  $\mathcal{F}(\mathbf{x}_k, r_k)$  denote the mode-conditioned FIM. Then, the matrix  $\mathbf{D}_{k-1}^{l,33}$  can be written as

$$\mathbf{D}_{k-1}^{l,33} = \mathbb{E}_{p(\mathbf{x}_k)} \{ \mathcal{F}(\mathbf{x}_k, r_k^l) \} = \mathbb{E}_{p(\mathbf{x}_k)} \{ \tilde{\mathbf{H}}_k^T(\mathbf{x}_k, r_k^l) \cdot [\mathbf{R}_k(r_k^l)]^{-1} \cdot \tilde{\mathbf{H}}_k(\mathbf{x}_k, r_k^l) \}. \quad (5.24)$$

Note that the bound is independent of the mean vector  $\boldsymbol{\mu}_k(r_k^l)$ . By insertion of (5.21) and (5.24) into (5.14) and by application of the matrix inversion lemma (4.18) to (5.14), the expression for the recursive calculation of the conditional Bayesian information submatrix can be rewritten as

$$\mathbf{J}_k^l = [\boldsymbol{\Gamma} \cdot \mathbf{Q} \cdot \boldsymbol{\Gamma}^T + \mathbf{F} \cdot [\mathbf{J}_{k-1}^l]^{-1} \cdot \mathbf{F}^T]^{-1} + \mathbb{E}_{p(\mathbf{x}_k)} \{ \tilde{\mathbf{H}}_k^T(\mathbf{x}_k, r_k^l) \cdot [\mathbf{R}_k(r_k^l)]^{-1} \cdot \tilde{\mathbf{H}}_k(\mathbf{x}_k, r_k^l) \}. \quad (5.25)$$

The expected value of the mode-conditioned FIM is approximated in the following using a Monte-Carlo integration approach, cf. Appendix A.10, yielding

$$\mathbb{E}_{p(\mathbf{x}_k)}\{\mathcal{F}(\mathbf{x}_k, r_k^l)\} \approx \frac{1}{N_{\text{MC}}} \sum_{n=1}^{N_{\text{MC}}} \tilde{\mathbf{H}}_k^T(\mathbf{x}_k^{(n)}, r_k^l) \cdot [\mathbf{R}_k(r_k^l)]^{-1} \cdot \tilde{\mathbf{H}}_k(\mathbf{x}_k^{(n)}, r_k^l), \quad (5.26)$$

where  $\mathbf{x}_k^{(n)}$ ,  $n = 1, \dots, N_{\text{MC}}$ , are i.i.d. state vector realizations, such that  $\mathbf{x}_k^{(n)} \sim p(\mathbf{x}_k)$ . Finally, by insertion of (5.25) into (5.19) and evaluation of (5.20), the MT location E-PCRLB can be found. The E-PCRLB is overly optimistic, because in calculating each conditional Bayesian information submatrix  $\mathbf{J}_k^l$ , it is implicitly assumed that the mode sequence  $\mathcal{R}_k^l$  is known [BRF<sup>+</sup>03, RAG04, HRF05]. In reality, however, the mode sequence is not known and the corresponding filter algorithm has to account for this added uncertainty. As a result, it is expected, that the estimation errors of the corresponding adaptive recursive algorithms are greater than the bound.

### 5.3.3 Marginalization Method

The idea of the marginalization method is to marginalize the discrete mode index  $r_k$  from all pdfs that are necessary to evaluate the PCRLB. This approach is not new and has been recently proposed in [Sve10] to compute the PCRLB for a nonlinear, additive Gaussian state model that depends on the discrete model index  $r_k$  and a linear, additive Gaussian measurement model that is independent of  $r_k$ . However, the algorithm presented in [Sve10] cannot be applied to evaluate the PCRLB for the hybrid localization method, since in our case, the state model is linear, additive Gaussian and independent of  $r_k$ , cf. (2.49), and the measurement model is nonlinear, additive Gaussian and depends on  $r_k$ , cf. (2.53). In the following, it is shown how the idea of marginalization can be applied to evaluate the PCRLB for the hybrid localization method. The corresponding PCRLB is termed hereinafter the Marginalization Posterior Cramér-Rao Lower Bound (M-PCRLB).

The main objective is to evaluate the PCRLB for the current state  $\mathbf{x}_k$  given the sequence of measurements  $\mathbf{Z}_k$ . Recall from Section 4.3 that the Bayesian information submatrix  $\mathbf{J}_k$  for the parameter of interest  $\mathbf{x}_k$ , is defined as the inverse of the  $(n_x \times n_x)$  lower-right submatrix of  $[\mathbf{I}_{\text{B},k}]^{-1}$ . Thus, in order to obtain the PCRLB for  $\mathbf{x}_k$ , the inverse of  $\mathbf{J}_k$  has to be calculated. According to (4.7), the BIM for estimating the sequence of states  $\mathbf{X}_k$  depends on the joint density  $p(\mathbf{X}_k, \mathbf{Z}_k)$ . For the general state and measurement model given in (2.1) and (2.17), which include the models (2.49) and (2.53) for the hybrid

localization method, the joint density  $p(\mathbf{X}_k, \mathbf{Z}_k)$  can be decomposed as follows

$$\begin{aligned} p(\mathbf{X}_k, \mathbf{Z}_k) &= p(\mathbf{x}_k, \mathbf{X}_{k-1}, \mathbf{z}_k, \mathbf{Z}_{k-1}) \\ &= p(\mathbf{z}_k | \mathbf{x}_k, \mathbf{X}_{k-1}, \mathbf{Z}_{k-1}) \cdot p(\mathbf{x}_k | \mathbf{X}_{k-1}, \mathbf{Z}_{k-1}) \cdot p(\mathbf{X}_{k-1}, \mathbf{Z}_{k-1}) \\ &= p(\mathbf{z}_k | \mathbf{x}_k, \mathbf{Z}_{k-1}) \cdot p(\mathbf{x}_k | \mathbf{x}_{k-1}) \cdot p(\mathbf{X}_{k-1}, \mathbf{Z}_{k-1}), \end{aligned} \quad (5.27)$$

where the third equality follows from the fact that  $\mathbf{x}_k$  is Markov. Note that the pdf  $p(\mathbf{z}_k | \mathbf{x}_k, \mathbf{Z}_{k-1})$  implicitly takes into account the dependency of the measurements on the Markov chain by conditioning the pdf on the sequence of measurements  $\mathbf{Z}_{k-1}$ . This, in turn, means that the conditional independence assumption does not hold any longer for models of the form (2.17), i.e.,  $p(\mathbf{z}_k | \mathbf{x}_k, \mathbf{Z}_{k-1}) \neq p(\mathbf{z}_k | \mathbf{x}_k)$ . Since  $\mathbf{x}_k$  is Markov, the BIM has a block diagonal structure that enables a recursive calculation of the PCRLB [TMN98]. In the following, a recursive formula for evaluating the Bayesian information submatrix is presented. The Bayesian information submatrix  $\mathbf{J}_k$  for estimating the state vector  $\mathbf{x}_k$  can be calculated recursively using the following formula

$$\mathbf{J}_k = \mathbf{D}_{k-1}^{22} - \mathbf{D}_{k-1}^{21} (\mathbf{J}_{k-1} + \mathbf{D}_{k-1}^{11})^{-1} \mathbf{D}_{k-1}^{12} + \mathbf{D}_{k-1}^{33}, \quad (k \geq 1) \quad (5.28)$$

where  $\mathbf{D}_{k-1}^{11}$ ,  $\mathbf{D}_{k-1}^{12}$ ,  $\mathbf{D}_{k-1}^{21}$  and  $\mathbf{D}_{k-1}^{22}$  are given by (4.10a)-(4.10c) and

$$\mathbf{D}_{k-1}^{33} = \mathbb{E}_{p(\mathbf{x}_k, \mathbf{z}_k)} \{ -\Delta_{\mathbf{x}_k}^{\mathbf{x}_k} \log_e p(\mathbf{z}_k | \mathbf{x}_k, \mathbf{Z}_{k-1}) \}. \quad (5.29)$$

A proof of (5.28) can be found in Appendix A.11. For the hybrid localization method, the matrices  $\mathbf{D}_{k-1}^{11}$ ,  $\mathbf{D}_{k-1}^{12}$ ,  $\mathbf{D}_{k-1}^{21}$  and  $\mathbf{D}_{k-1}^{22}$  are given by (4.15). Following the same derivation steps as in Section 4.3.2, the recursive formula for computing the Bayesian information submatrix for the hybrid localization method can be written as

$$\mathbf{J}_k = [\mathbf{\Gamma} \cdot \mathbf{Q} \cdot \mathbf{\Gamma}^T + \mathbf{F} \cdot [\mathbf{J}_{k-1}]^{-1} \cdot \mathbf{F}^T]^{-1} + \mathbf{D}_{k-1}^{33}. \quad (5.30)$$

The matrix  $\mathbf{D}_{k-1}^{33}$  is approximated numerically, using a Monte Carlo integration approach. The expectation in (5.29) can be written as

$$\mathbf{D}_{k-1}^{33} = \int_{(\mathbb{R}^{n_x})^k} \left[ \int_{(\mathbb{R}^{n_z})^k} [-\Delta_{\mathbf{x}_k}^{\mathbf{x}_k} \log_e p(\mathbf{z}_k | \mathbf{x}_k, \mathbf{Z}_{k-1})] \cdot p(\mathbf{Z}_k | \mathbf{X}_k) d\mathbf{Z}_k \right] \cdot p(\mathbf{X}_k) d\mathbf{X}_k. \quad (5.31)$$

Often, it is more convenient to express  $\mathbf{D}_{k-1}^{33}$  as follows

$$\mathbf{D}_{k-1}^{33} = \int_{(\mathbb{R}^{n_x})^k} \left[ \int_{(\mathbb{R}^{n_z})^k} \frac{\nabla_{\mathbf{x}_k} p(\mathbf{z}_k | \mathbf{x}_k, \mathbf{Z}_{k-1}) \cdot [\nabla_{\mathbf{x}_k} p(\mathbf{z}_k | \mathbf{x}_k, \mathbf{Z}_{k-1})]^T}{[p(\mathbf{z}_k | \mathbf{x}_k, \mathbf{Z}_{k-1})]^2} p(\mathbf{Z}_k | \mathbf{X}_k) d\mathbf{Z}_k \right] p(\mathbf{X}_k) d\mathbf{X}_k. \quad (5.32)$$

A Monte Carlo approximation of (5.32) is, thus, given by

$$\mathbf{D}_{k-1}^{33} \approx \frac{1}{N_{\text{MC}}} \sum_{n=1}^{N_{\text{MC}}} \frac{\nabla_{\mathbf{x}_k} p(\mathbf{z}_k^{(n)} | \mathbf{x}_k^{(n)}, \mathbf{Z}_{k-1}^{(n)}) \cdot [\nabla_{\mathbf{x}_k} p(\mathbf{z}_k^{(n)} | \mathbf{x}_k^{(n)}, \mathbf{Z}_{k-1}^{(n)})]^T}{[p(\mathbf{z}_k^{(n)} | \mathbf{x}_k^{(n)}, \mathbf{Z}_{k-1}^{(n)})]^2}, \quad (5.33)$$



where  $\mathbf{X}_k^{(n)}$ ,  $n = 1, \dots, N_{\text{MC}}$ , are i.i.d. vectors such that  $\mathbf{X}_k^{(n)} \sim p(\mathbf{X}_k)$  and  $\mathbf{Z}_k^{(n)}$ ,  $n = 1, \dots, N_{\text{MC}}$ , are i.i.d. vectors such that  $\mathbf{Z}_k^{(n)} \sim p(\mathbf{Z}_k | \mathbf{X}_k^{(n)})$ . In order to approximate  $\mathbf{D}_{k-1}^{33}$  as in (5.33), a recursive algorithm has to be developed to generate  $\mathbf{X}_k^{(n)}$  and  $\mathbf{Z}_k^{(n)}$  and to evaluate

$$\frac{\nabla_{\mathbf{x}_k} p(\mathbf{z}_k^{(n)} | \mathbf{x}_k^{(n)}, \mathbf{Z}_{k-1}^{(n)}) \cdot \left[ \nabla_{\mathbf{x}_k} p(\mathbf{z}_k^{(n)} | \mathbf{x}_k^{(n)}, \mathbf{Z}_{k-1}^{(n)}) \right]^\top}{\left[ p(\mathbf{z}_k^{(n)} | \mathbf{x}_k^{(n)}, \mathbf{Z}_{k-1}^{(n)}) \right]^2}. \quad (5.34)$$

Note, if  $\mathbf{X}_k^{(n)}$  can be generated recursively, it is also possible to evaluate the approximation of the expectation (5.33) for each  $k$ . For the state and measurement model given by (2.1) and (2.17), the joint density of  $\mathbf{X}_k$  and  $\mathbf{Z}_k$  can be written for  $k > 0$  as

$$p(\mathbf{X}_k, \mathbf{Z}_k) = p(\mathbf{x}_0) \cdot p(\mathbf{z}_1 | \mathbf{x}_1) \cdot \prod_{t=1}^k p(\mathbf{x}_t | \mathbf{x}_{t-1}) \cdot \prod_{s=2}^k p(\mathbf{z}_s | \mathbf{x}_s, \mathbf{Z}_{s-1}), \quad (5.35)$$

which allows a recursive generation of  $\mathbf{X}_k^{(n)}$  and  $\mathbf{Z}_k^{(n)}$ . To compute  $\nabla_{\mathbf{x}_k} p(\mathbf{z}_k^{(n)} | \mathbf{x}_k^{(n)}, \mathbf{Z}_{k-1}^{(n)})$  and  $p(\mathbf{z}_k^{(n)} | \mathbf{x}_k^{(n)}, \mathbf{Z}_{k-1}^{(n)})$ , one has to calculate  $\Pr\{r_k\}$ ,  $p(\mathbf{z}_k^{(n)} | \mathbf{x}_k^{(n)}, r_k)$  and  $\nabla_{\mathbf{x}_k} p(\mathbf{z}_k^{(n)} | \mathbf{x}_k^{(n)}, r_k)$  for all values of  $r_k$  and  $k$ . An algorithm to do this and with which the M-PCRLB can be evaluated is given in Algorithm 5.1.

---

**Algorithm 5.1** Computation of the Marginalization PCRLB

---

1. At time  $k = 0$ , initialize  $\mathbf{x}_0^n \sim p(\mathbf{x}_0)$  for  $n = 1, \dots, N_{\text{MC}}$ . Evaluate  $\mathbf{J}_0$  from (4.12) and determine the M-PCRLB which is given by  $[\mathbf{J}_0]^{-1}$ .
2. At time  $k = 1$ , initialize  $r_1^{(n)} \sim \Pr\{r_1\}$  and generate  $\mathbf{x}_1^{(n)} \sim p(\mathbf{x}_1 | \mathbf{x}_0^{(n)})$  and  $\mathbf{z}_1^{(n)} \sim p(\mathbf{z}_1 | \mathbf{x}_1^{(n)}, r_1^{(n)})$  for  $n = 1, \dots, N_{\text{MC}}$ .

- Evaluate  $\nabla_{\mathbf{x}_1} p(\mathbf{z}_1^{(n)} | \mathbf{x}_1^{(n)})$  and  $p(\mathbf{z}_1^{(n)} | \mathbf{x}_1^{(n)})$  for each  $n$  as follows:

$$\begin{aligned} \nabla_{\mathbf{x}_1} p(\mathbf{z}_1^{(n)} | \mathbf{x}_1^{(n)}) &= \sum_{r_1} \nabla_{\mathbf{x}_1} p(\mathbf{z}_1^{(n)} | \mathbf{x}_1^{(n)}, r_1) \cdot \Pr\{r_1\}, \\ p(\mathbf{z}_1^{(n)} | \mathbf{x}_1^{(n)}) &= \sum_{r_1} p(\mathbf{z}_1^{(n)} | \mathbf{x}_1^{(n)}, r_1) \cdot \Pr\{r_1\}. \end{aligned}$$

- Evaluate  $\mathbf{D}_0^{33}$  given in (5.33). Afterwards, evaluate  $\mathbf{J}_1$  according to (5.28) and obtain the M-PCRLB which is given by  $[\mathbf{J}_1]^{-1}$ .

3. For  $k = 2, 3, \dots$ , and  $n = 1, \dots, N_{\text{MC}}$ , do:

- Generate  $r_k^{(n)} \sim \Pr\{r_k | r_{k-1}^{(n)}\}$ ,  $\mathbf{x}_k^{(n)} \sim p(\mathbf{x}_k | \mathbf{x}_{k-1}^{(n)})$  and  $\mathbf{z}_k^{(n)} \sim p(\mathbf{z}_k | \mathbf{x}_k^{(n)}, r_k^{(n)})$ .

- Update the stored quantity  $\Pr\{r_{k-1}\}$  using the relation

$$\Pr\{r_k\} = \sum_{r_{k-1}} \Pr\{r_k|r_{k-1}\}\Pr\{r_{k-1}\}. \quad (5.36)$$

- Evaluate  $\nabla_{\mathbf{x}_k} p(\mathbf{z}_k^{(n)}|\mathbf{x}_k^{(n)}, \mathbf{Z}_{k-1})$  and  $p(\mathbf{z}_k^{(n)}|\mathbf{x}_k^{(n)}, \mathbf{Z}_{k-1})$  as follows:

$$\begin{aligned} \nabla_{\mathbf{x}_k} p(\mathbf{z}_k^{(n)}|\mathbf{x}_k^{(n)}, \mathbf{Z}_{k-1}) &= \sum_{r_1} \nabla_{\mathbf{x}_k} p(\mathbf{z}_k^{(n)}|\mathbf{x}_k^{(n)}, r_k) \cdot \Pr\{r_k\}, \\ p(\mathbf{z}_k^{(n)}|\mathbf{x}_k^{(n)}, \mathbf{Z}_{k-1}) &= \sum_{r_1} p(\mathbf{z}_k^{(n)}|\mathbf{x}_k^{(n)}, r_k) \cdot \Pr\{r_k\}. \end{aligned} \quad (5.37)$$

- Evaluate  $\mathbf{D}_{k-1}^{33}$  given in (5.33). Afterwards, evaluate  $\mathbf{J}_k$  according to (5.28) and obtain the M-PCRLB which is given by  $[\mathbf{J}_k]^{-1}$ .

Note that (5.37) can be derived as follows

$$\begin{aligned} p(\mathbf{z}_k^{(n)}|\mathbf{x}_k^{(n)}, \mathbf{Z}_{k-1}) &= \sum_{r_k} p(\mathbf{z}_k^{(n)}, r_k|\mathbf{x}_k^{(n)}, \mathbf{Z}_{k-1}) \\ &= \sum_{r_k} \frac{p(\mathbf{z}_k^{(n)}|\mathbf{x}_k^{(n)}, r_k, \mathbf{Z}_{k-1}) \cdot p(\mathbf{x}_k, \mathbf{Z}_{k-1}|r_k) \cdot \Pr\{r_k\}}{p(\mathbf{x}_k, \mathbf{Z}_{k-1})} \\ &= \sum_{r_k} \frac{p(\mathbf{z}_k^{(n)}|\mathbf{x}_k^{(n)}, r_k) \cdot p(\mathbf{x}_k, \mathbf{Z}_{k-1}) \cdot \Pr\{r_k\}}{p(\mathbf{x}_k, \mathbf{Z}_{k-1})} \\ &= \sum_{r_k} p(\mathbf{z}_k^{(n)}|\mathbf{x}_k^{(n)}, r_k) \cdot \Pr\{r_k\}, \end{aligned} \quad (5.38)$$

where the third equality follows from the fact that the joint distribution of  $\mathbf{x}_k$  and  $\mathbf{Z}_{k-1}$  is conditionally independent of  $r_k$ . Note further that (5.36) reduces to  $\Pr\{r_k\} = \Pr\{r_{k-1}\}, \forall r_k = r_{k-1}$ , for time-homogeneous Markov chains with symmetric TPMs, which are initialized with their stationary values. In order to evaluate the M-PCRLB for the hybrid localization method, the gradient  $\nabla_{\mathbf{x}_k} p(\mathbf{z}_k|\mathbf{x}_k, r_k)$  and the transitional pdf has to be known. Recall that the pdfs  $p(\mathbf{x}_k|\mathbf{x}_{k-1})$  and  $p(\mathbf{z}_k|\mathbf{x}_k, r_k)$  are given by (4.14) and (5.22). Then, the gradient is given as follows

$$\nabla_{\mathbf{x}_k} p(\mathbf{z}_k|\mathbf{x}_k, r_k) = p(\mathbf{z}_k|\mathbf{x}_k, r_k) \cdot \mathbf{H}_k^T(\mathbf{x}_k, r_k) \cdot [\mathbf{R}_k(r_k)]^{-1} \cdot [\mathbf{z}_k - \mathbf{h}_k(\mathbf{x}_k, r_k) - \boldsymbol{\mu}_k(r_k)]. \quad (5.39)$$

The MT location PCRLB can be determined by evaluating the Bayesian information submatrix  $\mathbf{J}_k$  according to (5.30) and then inserting the result into (4.13). In contrast to the E-PCRLB, the M-PCRLB does not assume that the mode sequence  $\mathcal{R}_k^l$  is known. Thus, it is expected, that the M-PCRLB is greater than the E-PCRLB.

## 5.4 Interacting Multiple Model Algorithm-based Estimators

### 5.4.1 Introduction

In this section, suboptimal estimators for the hybrid localization problem are developed that are based on the mode sequence conditioning approach presented in Section 5.2.2. In order to avoid the exponential increasing number of mode sequences in the optimal approach, the idea of suboptimal solutions is to keep a fixed number of mode sequences with the largest probabilities and discard the rest. The probabilities of the remaining mode sequences are then renormalized such that they sum up to unity.

Suboptimal approaches for solving the adaptive recursive Bayesian estimation problem using the mode sequence conditioning approach are the generalized pseudo-Bayesian and the IMM algorithm [AF70, BBS88, MABSD98, BSLK01, DB04, LJ05]. These approaches have in common that a certain number of filters (e.g. EKFs, CKFs or PFs) operate in parallel, where each filter is matched to a certain mode sequence. In the following, the IMM algorithm is proposed to solve the adaptive recursive Bayesian estimation problem, since it only requires  $s$  filters in parallel and best trades off performance versus computational complexity [BSLK01]. Any filter proposed in Section 4.4 and 4.5 or a combination of them can be used in conjunction with the IMM algorithm. For the hybrid localization problem, however, the IMM algorithm in conjunction with the EKF is proposed as solution, since with the other, computationally more complex filters, no significant performance improvements are expected, as long as road constraints are not included in the algorithm. Even though PF-based estimators using road constraints can be used in the IMM algorithm as well, it turned out that these approaches cannot reach the performance of the multiple-model particle filter based approaches, cf. Section 5.5, and thus, are not further considered. The main contribution of this section is the application of the well-known IMM-EKF to the hybrid localization problem with adaptive LOS/NLOS detection.

### 5.4.2 Interacting Multiple Model Extended Kalman Filter

In this section, the IMM-EKF is proposed as a solution to the hybrid localization problem with adaptive LOS/NLOS detection. In the IMM algorithm, the posterior pdf, cf. (5.2), is approximated as

$$p(\mathbf{x}_k | \mathbf{Z}_k) \approx \sum_{r_k} \Pr\{r_k | \mathbf{Z}_k\} \cdot p(\mathbf{x}_k | r_k, \mathbf{Z}_k) \quad (5.40)$$

[BBS88,BSLK01]. Observe that the number of components in the sum is reduced from  $s^k$  to  $s$ , which leads to a substantial complexity reduction. The quantities  $\Pr\{r_k|\mathbf{Z}_k\}$  and  $p(\mathbf{x}_k|r_k, \mathbf{Z}_k)$  can be calculated recursively by introducing a mixing stage at the beginning of each recursion, where the history through  $k-1$  is summarized by merging the mode-conditioned posterior pdfs of the previous time step into  $s$  new mixing pdfs. The mixing stage is the key feature of the IMM algorithm, and enables one to use  $s$  mode-conditioned filters in parallel rather than  $s^k$  filters. The IMM algorithm can be decomposed into the following stages: Mixing probability calculation, mixing, mode-conditioned filtering and mode update. The corresponding IMM recursions are summarized below (for detailed derivations, see for instance [BBS88,BSLK01]).

- Mixing probability calculation ( $r_k, r_{k-1} = 1, \dots, s$ )

$$\Pr\{r_{k-1}|r_k, \mathbf{Z}_{k-1}\} = \frac{\Pr\{r_k|r_{k-1}\} \cdot \Pr\{r_{k-1}|\mathbf{Z}_{k-1}\}}{\Pr\{r_k|\mathbf{Z}_{k-1}\}}, \quad (5.41)$$

where

$$\Pr\{r_k|\mathbf{Z}_{k-1}\} = \sum_{r_{k-1}} \Pr\{r_k|r_{k-1}\} \cdot \Pr\{r_{k-1}|\mathbf{Z}_{k-1}\}. \quad (5.42)$$

- Mixing ( $r_k = 1, \dots, s$ )

$$p(\mathbf{x}_{k-1}|r_k, \mathbf{Z}_{k-1}) = \sum_{r_{k-1}} \Pr\{r_{k-1}|r_k, \mathbf{Z}_{k-1}\} \cdot p(\mathbf{x}_{k-1}|r_{k-1}, \mathbf{Z}_{k-1}). \quad (5.43)$$

- Mode-conditioned filtering ( $r_k = 1, \dots, s$ )

– Mode-conditioned Time Update

$$p(\mathbf{x}_k|r_k, \mathbf{Z}_{k-1}) = \int p(\mathbf{x}_k|\mathbf{x}_{k-1}, r_k) \cdot p(\mathbf{x}_{k-1}|r_k, \mathbf{Z}_{k-1}) \, d\mathbf{x}_{k-1}. \quad (5.44)$$

– Mode-conditioned Measurement Update

$$p(\mathbf{x}_k|r_k, \mathbf{Z}_k) = \frac{p(\mathbf{z}_k|\mathbf{x}_k, r_k) \cdot p(\mathbf{x}_k|r_k, \mathbf{Z}_{k-1})}{p(\mathbf{z}_k|r_k, \mathbf{Z}_{k-1})}, \quad (5.45)$$

where

$$p(\mathbf{z}_k|r_k, \mathbf{Z}_{k-1}) = \int p(\mathbf{z}_k|\mathbf{x}_k, r_k) \cdot p(\mathbf{x}_k|r_k, \mathbf{Z}_{k-1}) \, d\mathbf{x}_k. \quad (5.46)$$

- Mode Update ( $r_k = 1, \dots, s$ )

$$\Pr\{r_k|\mathbf{Z}_k\} = \frac{p(\mathbf{z}_k|r_k, \mathbf{Z}_{k-1}) \cdot \Pr\{r_k|\mathbf{Z}_{k-1}\}}{\sum_{r_k} p(\mathbf{z}_k|r_k, \mathbf{Z}_{k-1}) \cdot \Pr\{r_k|\mathbf{Z}_{k-1}\}}. \quad (5.47)$$

The IMM recursions are initiated with  $p(\mathbf{x}_0)$  and  $\Pr\{r_1\}$ . By using the mode probabilities  $\Pr\{r_k|\mathbf{Z}_k\}$ , obtained from the mode update, and the mode-conditioned pdfs  $p(\mathbf{x}_k|r_k, \mathbf{Z}_k)$ , obtained from the mode-conditioned measurement update, an approximation to the posterior pdf  $p(\mathbf{x}_k|\mathbf{Z}_k)$  can be finally determined according to (5.40).

In the IMM-EKF the idea is to evaluate the mode-conditioned filtering stage using a bank of  $s$  EKF, operating in parallel, where each of the EKFs is matched to a specific mode. In each mode-conditioned EKF, the posterior pdf  $p(\mathbf{x}_{k-1}|r_{k-1}, \mathbf{Z}_{k-1})$  is approximated with a Gaussian pdf, i.e.,

$$p(\mathbf{x}_{k-1}|r_{k-1}, \mathbf{Z}_{k-1}) \approx \mathcal{N}(\mathbf{x}_{k-1}; \hat{\mathbf{x}}_{k-1|k-1}(r_{k-1}), \mathbf{P}_{k-1|k-1}(r_{k-1})), \quad \text{for } r_{k-1} = 1, \dots, s. \quad (5.48)$$

Thus, the mixing pdf  $p(\mathbf{x}_{k-1}|r_k, \mathbf{Z}_{k-1})$ , cf. (5.43), is composed of a sum of Gaussian pdfs (or Gaussian mixture pdf) given by

$$p(\mathbf{x}_{k-1}|r_k, \mathbf{Z}_{k-1}) \approx \sum_{r_{k-1}} \Pr\{r_{k-1}|r_k, \mathbf{Z}_{k-1}\} \cdot \mathcal{N}(\mathbf{x}_{k-1}; \hat{\mathbf{x}}_{k-1|k-1}(r_{k-1}), \mathbf{P}_{k-1|k-1}(r_{k-1})), \quad (5.49)$$

with  $r_k = 1, \dots, s$ , respectively. Since the mixing pdfs  $p(\mathbf{x}_{k-1}|r_k, \mathbf{Z}_{k-1})$  serve as input to the  $s$  mode-conditioned EKF, and the mode-conditioned EKF can handle only Gaussian pdfs, the mixing pdfs have to be further approximated with a single Gaussian pdf using moment matching [BSLK01], yielding

$$p(\mathbf{x}_{k-1}|r_k, \mathbf{Z}_{k-1}) \approx \mathcal{N}(\mathbf{x}_{k-1}; \hat{\mathbf{x}}_{m,k-1|k-1}(r_k), \mathbf{P}_{m,k-1|k-1}(r_k)), \quad \text{for } r_k = 1, \dots, s, \quad (5.50)$$

where

$$\hat{\mathbf{x}}_{m,k-1|k-1}(r_k) = \sum_{r_{k-1}} \Pr\{r_{k-1}|r_k, \mathbf{Z}_{k-1}\} \cdot \hat{\mathbf{x}}_{k-1|k-1}(r_{k-1}), \quad (5.51a)$$

$$\mathbf{P}_{m,k-1|k-1}(r_k) = \sum_{r_{k-1}} \Pr\{r_{k-1}|r_k, \mathbf{Z}_{k-1}\} \cdot \left\{ \mathbf{P}_{k-1|k-1}(r_{k-1}) + [\hat{\mathbf{x}}_{k-1|k-1}(r_{k-1}) - \hat{\mathbf{x}}_{m,k-1|k-1}(r_k)] \cdot [\hat{\mathbf{x}}_{k-1|k-1}(r_{k-1}) - \hat{\mathbf{x}}_{m,k-1|k-1}(r_k)]^\top \right\}. \quad (5.51b)$$

After having completed the mode-matched filtering and mode update stage,  $s$  different state estimates  $\hat{\mathbf{x}}_{k|k}(r_k)$ , covariances  $\mathbf{P}_{k|k}(r_k)$  and mode probabilities  $\Pr\{r_k|\mathbf{Z}_k\}$  are available, from which approximations of the estimates  $\hat{\mathbf{x}}_{\text{MMSE},k|k}$  and  $\mathbf{P}_{\text{MMSE},k|k}$ , cf. (5.8), can be computed according to

$$\hat{\mathbf{x}}_{\text{MMSE},k|k} \approx \sum_{r_k} \Pr\{r_k|\mathbf{Z}_k\} \cdot \hat{\mathbf{x}}_{k|k}(r_k), \quad (5.52a)$$

$$\mathbf{P}_{\text{MMSE},k|k} \approx \sum_{r_k} \Pr\{r_k|\mathbf{Z}_k\} \cdot \left\{ \mathbf{P}_{k|k}(r_k) + [\hat{\mathbf{x}}_{k|k}(r_k) - \hat{\mathbf{x}}_{\text{MMSE},k|k}] \cdot [\hat{\mathbf{x}}_{k|k}(r_k) - \hat{\mathbf{x}}_{\text{MMSE},k|k}]^\top \right\} \quad (5.52b)$$

[BSLK01]. For the hybrid localization method, where the switching between LOS and NLOS propagation conditions is modeled with a Markov chain having  $s = 2^{N_{\text{BS}}}$  different modes,  $2^{N_{\text{BS}}}$  EKF's have to be operated in parallel. Thus, the proposed IMM-EKF-based solution is especially suitable for scenarios where measurements are received from a small number of BSs. In addition to that, if the number of possible modes is too large, another problem occurs which degrades the performance and which is known as competition among the modes [MABSD98]. A pseudocode description of the IMM-EKF for hybrid localization is summarized in Algorithm 5.2. Note that after the initialization, the mixing probability calculation and the mixing are left out and one directly performs the mode-conditioned extended Kalman filtering.

---

**Algorithm 5.2** Interacting Multiple Model Extended Kalman Filter

---

1. Initialization:

- For  $r_1 = 1, \dots, 2^{N_{\text{BS}}}$ , initialize the  $2^{N_{\text{BS}}}$  mode-conditioned EKF's with  $\{\mathbf{x}_{m,0|0}(r_1), \mathbf{P}_{m,0|0}(r_1)\} = \{\hat{\mathbf{x}}_0, \mathbf{P}_0\}$  and set the initial mode probabilities to  $\Pr\{r_1\} = 1/2^{N_{\text{BS}}}$ .

2. Mixing Probability Calculation:

- For  $r_{k-1} = r_k = 1, \dots, 2^{N_{\text{BS}}}$ , evaluate the mixing probabilities according to

$$\Pr\{r_{k-1}|r_k, \mathbf{Z}_{k-1}\} = \frac{\Pr\{r_k|r_{k-1}\} \cdot \Pr\{r_{k-1}|\mathbf{Z}_{k-1}\}}{\Pr\{r_k|\mathbf{Z}_{k-1}\}},$$

and store the predicted mode probabilities

$$\Pr\{r_k|\mathbf{Z}_{k-1}\} = \sum_{r_{k-1}} \Pr\{r_k|r_{k-1}\} \cdot \Pr\{r_{k-1}|\mathbf{Z}_{k-1}\}.$$

3. Mixing:

- For  $r_k = 1, \dots, 2^{N_{\text{BS}}}$ , evaluate the moment matched means and covariances of the mixing pdfs according to

$$\begin{aligned} \hat{\mathbf{x}}_{m,k-1|k-1}(r_k) &= \sum_{r_{k-1}} \Pr\{r_{k-1}|r_k, \mathbf{Z}_{k-1}\} \cdot \hat{\mathbf{x}}_{k-1|k-1}(r_{k-1}), \\ \mathbf{P}_{m,k-1|k-1}(r_k) &= \sum_{r_{k-1}} \Pr\{r_{k-1}|r_k, \mathbf{Z}_{k-1}\} \cdot \left\{ \mathbf{P}_{k-1|k-1}(r_{k-1}) + \left[ \hat{\mathbf{x}}_{k-1|k-1}(r_{k-1}) - \hat{\mathbf{x}}_{m,k-1|k-1}(r_k) \right] \cdot \left[ \hat{\mathbf{x}}_{k-1|k-1}(r_{k-1}) - \hat{\mathbf{x}}_{m,k-1|k-1}(r_k) \right]^T \right\}. \end{aligned}$$

4. Mode-conditioned Extended Kalman Filtering:

- For  $r_k = 1, \dots, 2^{N_{\text{BS}}}$ , evaluate

$$\begin{aligned}\hat{\mathbf{x}}_{k|k-1}(r_k) &= \mathbf{F} \cdot \hat{\mathbf{x}}_{m,k-1|k-1}(r_k), \\ \mathbf{P}_{k|k-1}(r_k) &= \mathbf{F} \cdot \mathbf{P}_{m,k-1|k-1}(r_k) \cdot \mathbf{F}^\top + \mathbf{\Gamma} \cdot \mathbf{Q} \cdot \mathbf{\Gamma}^\top, \\ \mathbf{P}_{\text{zz},k|k-1}(r_k) &= \mathbf{P}_{k|k-1}(r_k) \cdot \tilde{\mathbf{H}}_k^\top(\hat{\mathbf{x}}_{k|k-1}(r_k), r_k), \\ \mathbf{P}_{\text{zz},k|k-1}(r_k) &= \tilde{\mathbf{H}}_k(\hat{\mathbf{x}}_{k|k-1}(r_k), r_k) \cdot \mathbf{P}_{k|k-1}(r_k) \cdot \tilde{\mathbf{H}}_k^\top(\hat{\mathbf{x}}_{k|k-1}(r_k), r_k) + \mathbf{R}_k(r_k), \\ \mathbf{K}_k(r_k) &= \mathbf{P}_{\text{zz},k|k-1}(r_k) \cdot [\mathbf{P}_{\text{zz},k|k-1}(r_k)]^{-1}, \\ \hat{\mathbf{x}}_{k|k}(r_k) &= \hat{\mathbf{x}}_{k|k-1}(r_k) + \mathbf{K}_k(r_k) \cdot [\mathbf{z}_k - \mathbf{h}_k(\hat{\mathbf{x}}_{k|k-1}(r_k), r_k) - \boldsymbol{\mu}_k(r_k)], \\ \mathbf{P}_{k|k}(r_k) &= \mathbf{P}_{k|k-1}(r_k) - \mathbf{K}_k(r_k) \cdot \mathbf{P}_{\text{zz},k|k-1}(r_k) \cdot \mathbf{K}_k^\top(r_k),\end{aligned}$$

and approximate

$$p(\mathbf{z}_k | r_k, \mathbf{Z}_{k-1}) = \mathcal{N}(\mathbf{z}_k; \mathbf{h}_k(\hat{\mathbf{x}}_{k|k-1}(r_k), r_k) + \boldsymbol{\mu}_k(r_k), \mathbf{P}_{\text{zz},k|k-1}(r_k)).$$

## 5. Mode Update

- For  $r_k = 1, \dots, 2^{N_{\text{BS}}}$ , evaluate

$$\Pr\{r_k | \mathbf{Z}_k\} = \frac{p(\mathbf{z}_k | r_k, \mathbf{Z}_{k-1}) \cdot \Pr\{r_k | \mathbf{Z}_{k-1}\}}{\sum_{r_k} p(\mathbf{z}_k | r_k, \mathbf{Z}_{k-1}) \cdot \Pr\{r_k | \mathbf{Z}_{k-1}\}},$$

where  $\Pr\{r_k | \mathbf{Z}_{k-1}\}$  and  $p(\mathbf{z}_k | r_k, \mathbf{Z}_{k-1})$  are available from step 2 and 4.

## 6. Estimation:

- Determine an estimate of the state vector according to

$$\hat{\mathbf{x}}_{\text{MMSE},k|k} = \sum_{r_k} \Pr\{r_k | \mathbf{Z}_k\} \cdot \hat{\mathbf{x}}_{k|k}(r_k).$$

7. Set  $k := k + 1$  and iterate from step 2.

# 5.5 Multiple Model Particle Filter-based Estimators

## 5.5.1 Introduction

In this section, suboptimal estimators for the hybrid localization problem are developed that are based on the state vector augmentation approach presented in Section 5.2.3.

Suboptimal approaches for solving the adaptive recursive Bayesian estimation problem using the state vector augmentation approach are generally PF-based [RAG04]. These approaches have in common that the posterior pdf of the augmented state vector  $p(\mathbf{x}_k, r_k | \mathbf{Z}_k)$  is represented by particles and corresponding weights, from which relevant quantities such as  $\hat{\mathbf{x}}_{\text{MMSE},k|k}$ ,  $\mathbf{P}_{\text{MMSE},k|k}$  and mode probabilities  $\Pr\{r_k | \mathbf{Z}_k\}$  can be computed. An appealing advantage of this approach is that, compared to the IMM-EKF, the mode probabilities can be estimated without merging mode histories and it is not necessary to linearize the measurement model.

For any PF-based estimator proposed in Section 4.5, a corresponding multiple-model-based estimator can be constructed. In the literature, this has been done for the PF [MI00], yielding the multiple-model particle filter (MM-PF), for the APF [KB00], yielding the multiple-model auxiliary particle filter and for the RBPF, yielding the multiple-model Rao-Blackwellized particle filter (MM-RBPF) [MAH<sup>+</sup>07]. In the following, the MM-PF and the MM-RBPF are proposed as solution for the hybrid localization problem. Road constraints are incorporated into these filters in order to further improve the performance. In Section 5.5.2 the MM-PF is presented and in Section 5.5.3 the MM-RBPF is introduced. The main contributions of this section are the application of the well-known MM-PF to the hybrid localization problem. In addition to that, the MM-RBPF presented in [MAH<sup>+</sup>07] is derived for a more general setting and then applied to the hybrid localization problem.

## 5.5.2 Multiple Model Particle Filter

### 5.5.2.1 Introduction

In this section, the MM-PF is proposed as a solution to the hybrid localization problem. The MM-PF is a sequential Monte Carlo approximation of the conceptual solution of the adaptive recursive Bayesian estimation given by (5.9) and (5.10). In the MM-PF, the posterior pdf, cf. (5.2) is approximated by a set of particles and weights  $\{\mathbf{y}_k^{(i)}, w_{k|k}^{(i)}\}_{i=1}^N$ , where each particle  $\mathbf{y}_k^{(i)}$  consists of two components, namely  $\mathbf{x}_k^{(i)}$  and  $r_k^{(i)}$  [MI00, RAG04]. The corresponding discrete approximation to the posterior pdf is given by

$$p(\mathbf{x}_k, r_k | \mathbf{Z}_{k-1}) \approx \sum_{i=1}^N w_{k|k}^{(i)} \cdot \delta(\mathbf{x}_k - \mathbf{x}_k^{(i)}, r_k - r_k^{(i)}). \quad (5.53)$$

In the following, it is shown how the particles and weights can be updated recursively, resulting in the MM-PF.



### 5.5.2.2 Derivations

In this section, the MM-PF for hybrid localization is derived. The derivation of the MM-PF is based on the posterior pdf  $p(\mathbf{x}_k, r_k | \mathbf{Z}_k)$  [MI00, DdFG01].

#### Initialization

The MM-PF is initialized as follows:

$$p(\mathbf{x}_{k-1}, r_{k-1} | \mathbf{Z}_{k-1}) \approx \sum_{i=1}^N w_{k-1|k-1}^{(i)} \cdot \delta(\mathbf{x}_{k-1} - \mathbf{x}_{k-1}^{(i)}, r_{k-1} - r_{k-1}^{(i)}). \quad (5.54)$$

#### Time Update

The time update starts with evaluating the joint prediction density  $p(\mathbf{x}_k, r_k | \mathbf{Z}_{k-1})$ , cf. (5.9), yielding

$$\begin{aligned} p(\mathbf{x}_k, r_k | \mathbf{Z}_{k-1}) &= \sum_{r_{k-1}} \Pr\{r_k | r_{k-1}\} \cdot \int_{\mathbb{R}^{n_x}} p(\mathbf{x}_k | \mathbf{x}_{k-1}, r_k) \cdot \underbrace{p(\mathbf{x}_{k-1}, r_{k-1} | \mathbf{Z}_k)}_{(5.54)} d\mathbf{x}_{k-1} \\ &\approx \sum_{i=1}^N w_{k-1|k-1}^{(i)} \cdot \Pr\{r_k | r_{k-1}^{(i)}\} \cdot p(\mathbf{x}_k | \mathbf{x}_{k-1}^{(i)}, r_k). \end{aligned} \quad (5.55)$$

In the following, a weighted discrete approximation of  $p(\mathbf{x}_k, r_k | \mathbf{Z}_{k-1})$  is obtained using an importance sampling approach. In the MM-PF, the key idea is to represent each component of the weighted sum in (5.55) by a single particle, which is composed of  $\mathbf{x}_k^{(i)}$  and  $r_k^{(i)}$ . While the mode  $r_k$  is sampled from  $\Pr\{r_k | r_{k-1}^{(i)}\}$ , the state  $\mathbf{x}_k$  is sampled from a mode-conditioned importance density, yielding

$$r_k^{(i)} \sim \Pr\{r_k | r_{k-1}^{(i)}\}, \quad \text{and} \quad \mathbf{x}_k^{(i)} \sim q(\mathbf{x}_k | \mathbf{x}_{k-1}^{(i)}, r_k^{(i)}, \mathbf{z}_k), \quad i = 1, \dots, N, \quad (5.56)$$

where the latest measurement  $\mathbf{z}_k$  is taken into account in the mode-conditioned importance density [RAG04]. As a result, the prediction pdf can be approximated as

$$p(\mathbf{x}_k, r_k | \mathbf{Z}_{k-1}) \approx \sum_{i=1}^N w_{k|k-1}^{(i)} \cdot \delta(\mathbf{x}_k - \mathbf{x}_k^{(i)}, r_k - r_k^{(i)}), \quad (5.57)$$

where the unnormalized importance weights are given by

$$w_{k|k-1}^{(i)} \propto w_{k-1|k-1}^{(i)} \cdot \frac{p(\mathbf{x}_k^{(i)} | \mathbf{x}_{k-1}^{(i)}, r_k^{(i)})}{q(\mathbf{x}_k^{(i)} | \mathbf{x}_{k-1}^{(i)}, r_k^{(i)}, \mathbf{z}_k)}, \quad i = 1, \dots, N. \quad (5.58)$$

The importance weights have to be further normalized to ensure  $\sum_{j=1}^N w_{k|k-1}^{(j)} = 1$ .

## Measurement Update

In the measurement update, the joint posterior pdf  $p(\mathbf{x}_k, r_k | \mathbf{Z}_k)$  is updated according to (5.10). Insertion of (5.58) into (5.10) gives a weighted discrete approximation of the joint posterior pdf. Since this approximation is numerically normed, a calculation of the denominator in (5.10) is not needed, yielding

$$\begin{aligned}
 p(\mathbf{x}_k, r_k | \mathbf{Z}_k) &\propto p(\mathbf{z}_k | \mathbf{x}_k, r_k) \cdot p(\mathbf{x}_k, r_k | \mathbf{Z}_{k-1}) \\
 &\approx \sum_{i=1}^N \underbrace{w_{k|k-1}^{(i)} \cdot p(\mathbf{z}_k | \mathbf{x}_k^{(i)}, r_k^{(i)})}_{w_{k|k-1}^{(i)}} \cdot \delta(\mathbf{x}_k - \mathbf{x}_k^{(i)}, r_k - r_k^{(i)}) \\
 &= \sum_{i=1}^N w_{k|k}^{(i)} \cdot \delta(\mathbf{x}_k - \mathbf{x}_k^{(i)}, r_k - r_k^{(i)}), \tag{5.59}
 \end{aligned}$$

where the normalized importance weights are given by

$$w_{k|k}^{(i)} = \frac{w_{k|k-1}^{(i)} \cdot p(\mathbf{z}_k | \mathbf{x}_k^{(i)}, r_k^{(i)})}{\sum_{j=1}^N w_{k|k-1}^{(j)} \cdot p(\mathbf{z}_k | \mathbf{x}_k^{(j)}, r_k^{(j)})}, \quad i = 1, \dots, N. \tag{5.60}$$

By finally omitting the mode  $r_k$  in the discrete approximation (5.59), the desired posterior pdf of the current state is found which is given by

$$p(\mathbf{x}_k | \mathbf{Z}_k) \approx \sum_{i=1}^N w_{k|k}^{(i)} \cdot \delta(\mathbf{x}_k - \mathbf{x}_k^{(i)}). \tag{5.61}$$

## Estimation and Resampling

In the MM-PF, the formulas for estimating the mean vector  $\hat{\mathbf{x}}_{\text{MMSE},k}$  and its covariance  $\hat{\mathbf{P}}_{\text{MMSE},k}$  are equivalent to the formulas given in (4.68), since the posterior pdf is approximated with (5.61). For the resampling step in the MM-PF, systematic resampling is used which is explained in Section 4.5.2.2.

### 5.5.2.3 Choice of Importance Density

In the design of MM-PFs, the choice of the mode-conditioned importance density  $q(\mathbf{x}_k | \mathbf{x}_{k-1}^{(i)}, r_k^{(i)}, \mathbf{z}_k)$  plays a major role. The optimal mode-conditioned importance density that minimizes the variance of the importance weights is given by

$q(\mathbf{x}_k | \mathbf{x}_{k-1}^{(i)}, r_k^{(i)}, \mathbf{z}_k)_{\text{opt}} = p(\mathbf{x}_k | \mathbf{x}_{k-1}^{(i)}, r_k, \mathbf{z}_k)$  [RAG04]. However, for the hybrid localization problem, a closed-form expression for the density  $p(\mathbf{x}_k | \mathbf{x}_{k-1}^{(i)}, r_k, \mathbf{z}_k)$  does not exist, so that one has resort to suboptimal choices. For the hybrid localization problem, the following importance density is chosen

$$q(\mathbf{x}_k | \mathbf{x}_{k-1}^{(i)}, r_k^{(i)}, \mathbf{z}_k) = p(\mathbf{x}_k | \mathbf{x}_{k-1}^{(i)}, r_k^{(i)}) = p(\mathbf{x}_k | \mathbf{x}_{k-1}^{(i)}). \quad (5.62)$$

In this case, the weights in the time update are given by  $w_{k|k-1}^{(i)} = w_{k-1|k-1}^{(i)}$ , cf. (5.58), and the weights in the measurement update simplify to

$$w_{k|k}^{(i)} = \frac{w_{k-1|k-1}^{(i)} \cdot p(\mathbf{z}_k | \mathbf{x}_k^{(i)}, r_k^{(i)})}{\sum_{j=1}^N w_{k-1|k-1}^{(j)} \cdot p(\mathbf{z}_k | \mathbf{x}_k^{(j)}, r_k^{(j)})}, \quad i = 1, \dots, N. \quad (5.63)$$

A pseudocode description of the MM-PF for the hybrid localization is given in Algorithm 5.3. Note that the pdfs  $p(\mathbf{x}_k | \mathbf{x}_{k-1})$  and  $p(\mathbf{z}_k | \mathbf{x}_k, r_k)$ , and the TPM  $\Pr\{r_k | r_{k-1}\}$ , necessary to evaluate Algorithm 5.3, are given by (4.14), (5.22) and (2.52), respectively. Note further that after the initialization, the sampling of mode variables in the time update step is left out, and one directly starts with the sampling of the states.

#### 5.5.2.4 Incorporation of Road Constraints

In this section, it is explained how road constraints can be incorporated into the MM-PF for hybrid localization. For incorporating road constraints into the MM-PF, the approach presented in Section 4.5.6.2 is used. Since the mode variable is included only in the measurement model, the incorporation of road constraints into the MM-PF can be done as follows. The model for generating the state  $\mathbf{x}_k$  is replaced with the model for generating road-constrained states  $\mathbf{x}_{R,k}$ , cf. (4.169). The mode-conditioned likelihood function has to be rewritten as

$$p(\mathbf{z}_k | \mathbf{x}_k, r_k) = p(\mathbf{z}_k | \mathbf{T}_{G,k}(\mathbf{x}_{R,k}, \mathcal{T}_{RN}), r_k). \quad (5.64)$$

A pseudocode description of the MM-PF with road-constraints for hybrid localization is given in Algorithm 5.4. Note that after the initialization, the sampling of mode variables in the time update step is left out, and one directly starts with the sampling of the road-constrained states.

---

**Algorithm 5.3** Multiple-Model Particle Filter
 

---

## 1. Initialization:

- For  $i = 1, \dots, N$ , initialize the particles  $\mathbf{x}_0^{(i)} \sim p(\mathbf{x}_0)$ , the weights  $w_{0|0}^{(i)} = \frac{1}{N}$  and the mode probabilities  $r_1^{(i)} \sim \Pr\{r_1\}$ .

## 2. Time Update:

- For  $i = 1, \dots, N$ , draw mode probabilities according to

$$r_k^{(i)} \sim \Pr\{r_k | r_{k-1}^{(i)}\},$$

and draw states from the importance density

$$\mathbf{x}_k^{(i)} \sim p(\mathbf{x}_k | \mathbf{x}_{k-1}^{(i)}).$$

## 3. Measurement Update:

- For  $i = 1, \dots, N$ , evaluate the weights

$$w_{k|k}^{(i)} = \frac{w_{k-1|k-1}^{(i)} \cdot p(\mathbf{z}_k | \mathbf{x}_k^{(i)}, r_k^{(i)})}{\sum_{j=1}^N w_{k-1|k-1}^{(j)} \cdot p(\mathbf{z}_k | \mathbf{x}_k^{(j)}, r_k^{(j)})}.$$

## 4. Estimation:

- Determine an estimate of the state vector according to

$$\hat{\mathbf{x}}_k = \sum_{i=1}^N w_{k|k}^{(i)} \cdot \mathbf{x}_k^{(i)}.$$

## 5. Resampling:

- Perform systematic resampling using Algorithm 4.4. Take  $N$  samples with replacement from the set  $\{\mathbf{x}_k^{(i)}, r_k^{(i)}\}_{i=1}^N$ , where the probability to take sample  $i$  is  $w_{k|k}^{(i)}$ . Set  $w_{k|k}^{(i)} = \frac{1}{N}$  for  $i = 1, \dots, N$ .

6. Set  $k := k + 1$  and iterate from step 2.

---

---

**Algorithm 5.4** Multiple-Model Particle Filter with Road Constraints
 

---

## 1. Initialization:

- For  $i = 1, \dots, N$ , initialize the particles  $\mathbf{x}_{R,0}^{(i)} \sim p(\mathbf{x}_{R,0})$ , the weights  $w_{0|0}^{(i)} = \frac{1}{N}$  and the mode probabilities  $r_1^{(i)} \sim \Pr\{r_1\}$ .

## 2. Time Update:

- For  $i = 1, \dots, N$ , draw mode probabilities according to

$$r_k^{(i)} \sim \Pr\{r_k | r_{k-1}^{(i)}\},$$

- For  $i = 1, \dots, N$ , generate particles  $\mathbf{x}_{R,k}^{(i)}$  from  $\mathbf{x}_{R,k-1}^{(i)}$  by using samples from the process noise sequences  $\mathbf{w}_{R,k-1}^{(i)} \sim p_{\mathbf{w}_{R,k-1}}(\cdot)$  and  $\mathbf{w}_{CO,k-1}^{(i)} \sim p_{\mathbf{w}_{CO,k-1}}(\cdot)$  as shown in (4.169).

## 3. Measurement Update:

- For  $i = 1, \dots, N$ , evaluate the weights

$$w_{k|k}^{(i)} = \frac{w_{k-1|k-1}^{(i)} \cdot p(\mathbf{z}_k | \mathbf{T}_{G,k}(\mathbf{x}_{R,k}^{(i)}, \mathcal{I}_{RN}), r_k^{(i)})}{\sum_{j=1}^N w_{k-1|k-1}^{(j)} \cdot p(\mathbf{z}_k | \mathbf{T}_{G,k}(\mathbf{x}_{R,k}^{(j)}, \mathcal{T}_{RN}), r_k^{(j)})}.$$

## 4. Estimation:

- Determine an estimate of the state vector according to

$$\hat{\mathbf{x}}_k = \sum_{i=1}^N w_{k|k}^{(i)} \cdot \mathbf{T}_{G,k}(\mathbf{x}_{R,k}^{(i)}, \mathcal{T}_{RN}).$$

## 5. Resampling:

- Perform systematic resampling using Algorithm 4.4. Take  $N$  samples with replacement from the set  $\{\mathbf{x}_{R,k}^{(i)}, r_k^{(i)}\}_{i=1}^N$ , where the probability to take sample  $i$  is  $w_{k|k}^{(i)}$ . Set  $w_{k|k}^{(i)} = \frac{1}{N}$  for  $i = 1, \dots, N$ .

6. Set  $k := k + 1$  and iterate from step 2.

### 5.5.3 Multiple Model Rao-Blackwellized Particle Filter

#### 5.5.3.1 Introduction

The MM-PF requires a large number of particles to obtain a good approximation of the joint posterior pdf  $p(\mathbf{x}_k, r_k | \mathbf{Z}_k)$  in state estimation problems, where the dimension of the state vector  $\mathbf{x}_k$  is high. In order to overcome this problem, Rao-Blackwellization can be applied to the MM-PF. The corresponding MM-RBPF exploits linear substructures in the state and measurement model equations, cf. Sections 2.3.2 and 2.3.3, so that the state space can be partitioned into two parts according to (4.71). The resulting joint posterior pdf can be partitioned into two pdfs using Bayes' rule as follows

$$p(\mathbf{x}_k^n, \mathbf{x}_k^l, r_k | \mathbf{Z}_k) = p(\mathbf{x}_k^l | \mathbf{x}_k^n, r_k, \mathbf{Z}_k) \cdot p(\mathbf{x}_k^n, r_k | \mathbf{Z}_k). \quad (5.65)$$

The first pdf  $p(\mathbf{x}_k^l | \mathbf{x}_k^n, r_k, \mathbf{Z}_k)$  can be evaluated analytically using a mode-conditioned Kalman filter, if the models are linear given  $\mathbf{x}_k^n$  and  $r_k$ , while the second pdf  $p(\mathbf{x}_k^n, r_k | \mathbf{Z}_k)$  is approximated using an MM-PF. Since the dimension of the state  $\mathbf{x}_k^n$  is smaller than the dimension of the state  $\mathbf{x}_k$ , the MM-RBPF generally requires fewer particles to obtain a good approximation of the posterior pdf  $p(\mathbf{x}_k, r_k | \mathbf{Z}_k)$ .

#### 5.5.3.2 Derivations

In this section, the MM-RBPF is derived for the hybrid localization method. The MM-RBPF approach is not new and has been proposed in [MAH<sup>+</sup>07] to derive an estimator for mobility tracking in cellular radio networks, where the mode variable  $r_k$  is included only in the state model and the measurement model is independent of the linear states. However, the algorithm presented in [MAH<sup>+</sup>07] cannot be applied to the hybrid localization problem, since in our case, the measurement model depends on the mode variable  $r_k$  and the linear states, cf. (2.53). In the following, the MM-RBPF is derived for a more general mode-dependent conditional linear system model, where both, the state model and the measurement model, depend on the mode variable  $r_k$ . The resulting MM-RBPF can be applied to a broader class of problems and, thus, the results in this work can be regarded as an extension of what has been presented in [MAH<sup>+</sup>07]. In order to exploit the idea of Rao-Blackwellization in the MM-PF, the following mode-dependent conditional linear system model is introduced:

$$\mathbf{x}_k^n = \mathbf{f}_{k-1}^n(\mathbf{x}_{k-1}^n, r_k) + \mathbf{F}_{k-1}^n(\mathbf{x}_{k-1}^n, r_k) \cdot \mathbf{x}_{k-1}^l + \mathbf{\Gamma}_{k-1}^n(\mathbf{x}_{k-1}^n, r_k) \cdot \mathbf{w}_{k-1}^n(r_k), \quad (5.66a)$$

$$\mathbf{x}_k^l = \mathbf{f}_{k-1}^l(\mathbf{x}_{k-1}^n, r_k) + \mathbf{F}_{k-1}^l(\mathbf{x}_{k-1}^n, r_k) \cdot \mathbf{x}_{k-1}^l + \mathbf{\Gamma}_{k-1}^l(\mathbf{x}_{k-1}^n, r_k) \cdot \mathbf{w}_{k-1}^l(r_k), \quad (5.66b)$$

$$\mathbf{z}_{1,k} = \mathbf{h}_{1,k}(\mathbf{x}_k^n, r_k) + \mathbf{H}_k(\mathbf{x}_k^n, r_k) \cdot \mathbf{x}_k^l + \mathbf{v}_{1,k}(r_k), \quad (5.66c)$$

$$\mathbf{z}_{2,k} = \mathbf{h}_{2,k}(\mathbf{x}_k^n, r_k, \mathbf{v}_{2,k}(r_k)). \quad (5.66d)$$

Note, that in contrast to (4.73), the discrete mode variable  $r_k$  is included into the equations, in order to account for the possible switching between different models. The measurement vector  $\mathbf{z}_k = [\mathbf{z}_{1,k}^\top, \mathbf{z}_{2,k}^\top]^\top$  is split into two statistically independent parts,  $\mathbf{f}_{k-1}^n(\cdot)$ ,  $\mathbf{f}_{k-1}^l(\cdot)$ ,  $\mathbf{h}_{1,k}(\cdot)$ ,  $\mathbf{h}_{2,k}(\cdot)$  are vector functions and  $\mathbf{F}_{k-1}^n(\cdot)$ ,  $\mathbf{F}_{k-1}^l(\cdot)$ ,  $\mathbf{\Gamma}_{k-1}^n(\cdot)$ ,  $\mathbf{\Gamma}_{k-1}^l(\cdot)$ ,  $\mathbf{H}_k(\cdot)$  are matrices of appropriate dimensions. The mode-dependent noises in the state and measurement models are denoted by  $\mathbf{w}_{k-1}^n(r_k)$ ,  $\mathbf{w}_{k-1}^l(r_k)$ ,  $\mathbf{v}_{1,k}(r_k)$  and  $\mathbf{v}_{2,k}(r_k)$  and are assumed to be white. The noise vector  $[\mathbf{w}_{k-1}^{n,\top}(r_k), \mathbf{w}_{k-1}^{l,\top}(r_k)]^\top$ , with dimension  $n_w$ , and the vector  $\mathbf{v}_{1,k}(r_k)$  are assumed Gaussian distributed according to

$$\begin{bmatrix} \mathbf{w}_{k-1}^n(r_k) \\ \mathbf{w}_{k-1}^l(r_k) \end{bmatrix} \sim \mathcal{N}\left(\mathbf{0}_{n_w \times 1}, \begin{bmatrix} \mathbf{Q}_{k-1}^n(r_k) & \mathbf{Q}_{k-1}^{nl}(r_k) \\ \mathbf{Q}_{k-1}^{nl,\top}(r_k) & \mathbf{Q}_{k-1}^l(r_k) \end{bmatrix}\right), \mathbf{v}_{1,k}(r_k) \sim \mathcal{N}(\boldsymbol{\mu}_{1,k}(r_k), \mathbf{R}_{1,k}(r_k)). \quad (5.67)$$

Furthermore, it is assumed that  $\mathbf{x}_0^n$  and  $\mathbf{x}_0^l$  are white. The pdfs  $p(\mathbf{x}_0^n)$  and  $p(\mathbf{z}_{2,k} | \mathbf{x}_k, r_k)$  can be arbitrary, but have to be known. The pdf of  $\mathbf{x}_0^l$  is Gaussian, cf. (4.75) and the initial mode probabilities  $\Pr\{r_1\}$ ,  $r_1 \in \{1, \dots, s\}$ , are assumed known. In order to derive the MM-RBPF from the model given in (5.66), the two noise processes  $\mathbf{w}_{k-1}^n(r_k)$  and  $\mathbf{w}_{k-1}^l(r_k)$  have to be decorrelated using a Gram-Schmidt procedure [Sch03]. Similar to (4.76), the decorrelated system can be written as

$$\mathbf{x}_k^n = \mathbf{f}_{k-1}^n(\mathbf{x}_{k-1}^n, r_k) + \mathbf{F}_{k-1}^n(\mathbf{x}_{k-1}^n, r_k) \cdot \mathbf{x}_{k-1}^l + \mathbf{\Gamma}_{k-1}^n(\mathbf{x}_{k-1}^n, r_k) \cdot \mathbf{w}_{k-1}^n(r_k), \quad (5.68a)$$

$$\begin{aligned} \mathbf{x}_k^l &= \mathbf{f}_{k-1}^l(\mathbf{x}_{k-1}^n, r_k) + \bar{\mathbf{F}}_{k-1}^l(\mathbf{x}_{k-1}^n, r_k) \cdot \mathbf{x}_{k-1}^l + \bar{\mathbf{E}}_k(\mathbf{x}_k^n, \mathbf{x}_{k-1}^n, r_k) \\ &\quad + \mathbf{\Gamma}_{k-1}^l(\mathbf{x}_{k-1}^n, r_k) \cdot \bar{\mathbf{w}}_{k-1}^l(r_k), \end{aligned} \quad (5.68b)$$

$$\mathbf{z}_{1,k} = \mathbf{h}_{1,k}(\mathbf{x}_k^n, r_k) + \mathbf{H}_k(\mathbf{x}_k^n, r_k) \cdot \mathbf{x}_k^l + \mathbf{v}_{1,k}(r_k), \quad (5.68c)$$

$$\mathbf{z}_{2,k} = \mathbf{h}_{2,k}(\mathbf{x}_k^n, r_k, \mathbf{v}_{2,k}(r_k)), \quad (5.68d)$$

where

$$\begin{aligned} \bar{\mathbf{F}}_{k-1}^l(\mathbf{x}_{k-1}^n, r_k) &= \mathbf{F}_{k-1}^l(\mathbf{x}_{k-1}^n, r_k) - \mathbf{\Gamma}_{k-1}^l(\mathbf{x}_{k-1}^n, r_k) \cdot \mathbf{Q}_{k-1}^{nl,\top}(r_k) \\ &\quad \cdot [\mathbf{\Gamma}_{k-1}^n(\mathbf{x}_{k-1}^n, r_k) \cdot \mathbf{Q}_{k-1}^n(r_k)]^{-1} \cdot \mathbf{F}_{k-1}^n(\mathbf{x}_{k-1}^n, r_k), \end{aligned} \quad (5.69a)$$

$$\begin{aligned} \bar{\mathbf{E}}_k(\mathbf{x}_k^n, \mathbf{x}_{k-1}^n, r_k) &= \mathbf{\Gamma}_{k-1}^l(\mathbf{x}_{k-1}^n, r_k) \cdot \mathbf{Q}_{k-1}^{nl,\top}(r_k) \cdot [\mathbf{\Gamma}_{k-1}^n(\mathbf{x}_{k-1}^n, r_k) \cdot \mathbf{Q}_{k-1}^n(r_k)]^{-1} \\ &\quad \cdot [\mathbf{x}_k^n - \mathbf{f}_{k-1}^n(\mathbf{x}_{k-1}^n, r_k)]. \end{aligned} \quad (5.69b)$$

The noises  $\mathbf{w}_{k-1}^n(r_k)$  and  $\bar{\mathbf{w}}_{k-1}^l(r_k)$  are now uncorrelated and distributed according to

$$\begin{bmatrix} \mathbf{w}_{k-1}^n(r_k) \\ \bar{\mathbf{w}}_{k-1}^l(r_k) \end{bmatrix} \sim \mathcal{N}(\mathbf{0}_{n_w \times 1}, \bar{\mathbf{Q}}_{k-1}(r_k)), \quad (5.70)$$

with

$$\bar{\mathbf{Q}}_{k-1}(r_k) = \text{diag}_{\mathcal{S}_b}[\mathbf{Q}_{k-1}^n(r_k), \underbrace{\mathbf{Q}_{k-1}^l(r_k) - \mathbf{Q}_{k-1}^{nl,\top}(r_k) \cdot [\mathbf{Q}_{k-1}^n(r_k)]^{-1} \cdot \mathbf{Q}_{k-1}^{nl}(r_k)}_{\bar{\mathbf{Q}}_{k-1}^l(r_k)}]. \quad (5.71)$$

In order to simplify the notation, the following abbreviations are introduced

$$\begin{aligned} \mathbf{f}_{k-1}(\mathbf{x}_{k-1}^n, r_k) &= \begin{bmatrix} \mathbf{f}_{k-1}^n(\mathbf{x}_{k-1}^n, r_k) \\ \mathbf{f}_{k-1}^l(\mathbf{x}_{k-1}^n, r_k) \end{bmatrix}, \quad \mathbf{F}_{k-1}(r_k) = \begin{bmatrix} \mathbf{F}_{k-1}^n(\mathbf{x}_{k-1}^n, r_k) \\ \mathbf{F}_{k-1}^l(\mathbf{x}_{k-1}^n, r_k) \end{bmatrix}, \\ \mathbf{E}_k(\mathbf{x}_k^n, \mathbf{x}_{k-1}^n, r_k) &= \begin{bmatrix} \mathbf{0}_{n_{x_n} \times 1} \\ \bar{\mathbf{E}}_k(\mathbf{x}_k^n, \mathbf{x}_{k-1}^n, r_k) \end{bmatrix}, \quad \mathbf{w}_{k-1}(r_k) = \begin{bmatrix} \mathbf{w}_{k-1}^n(r_k) \\ \bar{\mathbf{w}}_{k-1}^l(r_k) \end{bmatrix}, \\ \mathbf{\Gamma}_{k-1}(r_k) &= \text{diag}_b[\mathbf{\Gamma}_{k-1}^n(\mathbf{x}_{k-1}^n, r_k), \mathbf{\Gamma}_{k-1}^l(\mathbf{x}_{k-1}^n, r_k)]. \end{aligned}$$

Thus, the state model, cf. (5.68a) and (5.68b), can be written as

$$\begin{bmatrix} \mathbf{x}_k^n \\ \mathbf{x}_k^l \end{bmatrix} = \mathbf{f}_{k-1}(\mathbf{x}_{k-1}^n, r_k) + \mathbf{F}_{k-1}(r_k) \cdot \mathbf{x}_{k-1}^l + \mathbf{E}_k(\mathbf{x}_k^n, \mathbf{x}_{k-1}^n, r_k) + \mathbf{\Gamma}_{k-1}(r_k) \cdot \mathbf{w}_{k-1}(r_k). \quad (5.72)$$

In the following, the MM-RBPF is derived for the model given by (5.68). The derivation is based on the joint posterior pdf  $p(\mathbf{x}_k^n, \mathbf{x}_k^l, r_k | \mathbf{Z}_k)$ .

## Initialization

The MM-RBPF is initialized as follows:

$$\begin{aligned} p(\mathbf{x}_{k-1}^n, \mathbf{x}_{k-1}^l, r_{k-1} | \mathbf{Z}_{k-1}) &\approx \sum_{i=1}^N w_{k-1|k-1}^{(i)} \cdot \mathcal{N}(\mathbf{x}_{k-1}^l; \mathbf{x}_{k-1}^{l,(i)}, \mathbf{P}_{k-1|k-1}^{(i)}) \\ &\quad \cdot \delta(\mathbf{x}_{k-1}^n - \mathbf{x}_{k-1}^{n,(i)}, r_{k-1} - r_{k-1}^{(i)}). \end{aligned} \quad (5.73)$$

## Time Update

The time update starts with evaluating the prediction density  $p(\mathbf{x}_k^n, \mathbf{x}_k^l, r_k | \mathbf{Z}_{k-1})$ , cf. (5.9), yielding

$$\begin{aligned} p(\mathbf{x}_k^n, \mathbf{x}_k^l, r_k | \mathbf{Z}_{k-1}) &= \sum_{r_{k-1}} \Pr\{r_k | r_{k-1}\} \cdot \int_{\mathbb{R}^{n_{x_n}}} \int_{\mathbb{R}^{n_{x_l}}} p(\mathbf{x}_k^n, \mathbf{x}_k^l | \mathbf{x}_{k-1}^n, \mathbf{x}_{k-1}^l, r_k) \\ &\quad \cdot \underbrace{p(\mathbf{x}_{k-1}^n, \mathbf{x}_{k-1}^l, r_{k-1} | \mathbf{Z}_{k-1})}_{(5.73)} d\mathbf{x}_{k-1}^n d\mathbf{x}_{k-1}^l \\ &\approx \sum_{i=1}^N w_{k-1|k-1}^{(i)} \cdot \Pr\{r_k | r_{k-1}^{(i)}\} \\ &\quad \cdot \int_{\mathbb{R}^{n_{x_l}}} p(\mathbf{x}_k^n, \mathbf{x}_k^l | \mathbf{x}_{k-1}^{n,(i)}, \mathbf{x}_{k-1}^l, r_k) \cdot \mathcal{N}(\mathbf{x}_{k-1}^l; \mathbf{x}_{k-1}^{l,(i)}, \mathbf{P}_{k-1|k-1}^{(i)}) d\mathbf{x}_{k-1}^l. \end{aligned} \quad (5.74)$$



Since the dynamic model, cf. (5.72), is conditional linear and the error is Gaussian distributed, the pdf  $p(\mathbf{x}_k^n, \mathbf{x}_k^1 | \mathbf{x}_{k-1}^{n,(i)}, \mathbf{x}_{k-1}^1, r_k)$  is also Gaussian and given by

$$p(\mathbf{x}_k^n, \mathbf{x}_k^1 | \mathbf{x}_{k-1}^{n,(i)}, \mathbf{x}_{k-1}^1, r_k) = \mathcal{N}(\mathbf{x}_k; \mathbf{f}_{k-1}(\mathbf{x}_{k-1}^{n,(i)}, r_k) + \mathbf{F}_{k-1}^{(i)}(r_k) \cdot \mathbf{x}_{k-1}^1 + \mathbf{E}_k(\mathbf{x}_k^n, \mathbf{x}_{k-1}^{n,(i)}, r_k), \mathbf{\Gamma}_{k-1}^{(i)}(r_k) \cdot \bar{\mathbf{Q}}_{k-1}(r_k) \cdot \mathbf{\Gamma}_{k-1}^{(i),\top}(r_k)). \quad (5.75)$$

As a result, the integral in (5.74) can be evaluated analytically, yielding

$$p(\mathbf{x}_k^n, \mathbf{x}_k^1, r_k | \mathbf{Z}_{k-1}) \approx \sum_{i=1}^N w_{k-1|k-1}^{(i)} \cdot \Pr\{r_k | r_{k-1}^{(i)}\} \cdot \mathcal{N}(\mathbf{x}_k; \bar{\mathbf{x}}_{k|k-1}^{(i)}, \bar{\mathbf{P}}_{k|k-1}^{(i)}), \quad (5.76)$$

where

$$\bar{\mathbf{x}}_{k|k-1}^{(i)} = \mathbf{f}_{k-1}(\mathbf{x}_{k-1}^{n,(i)}, r_k) + \mathbf{F}_{k-1}^{(i)}(r_k) \cdot \mathbf{x}_{k-1|k-1}^1 + \mathbf{E}_k(\mathbf{x}_k^n, \mathbf{x}_{k-1}^{n,(i)}, r_k), \quad (5.77a)$$

$$\bar{\mathbf{P}}_{k|k-1}^{(i)} = \mathbf{F}_{k-1}^{(i)}(r_k) \cdot \mathbf{P}_{k-1|k-1}^{(i)} \cdot \mathbf{F}_{k-1}^{(i),\top}(r_k) + \mathbf{\Gamma}_{k-1}^{(i)}(r_k) \cdot \bar{\mathbf{Q}}_{k-1}(r_k) \cdot \mathbf{\Gamma}_{k-1}^{(i),\top}(r_k). \quad (5.77b)$$

By splitting the mean vector  $\bar{\mathbf{x}}_{k|k-1}^{(i)}$  and covariance matrix  $\bar{\mathbf{P}}_{k|k-1}^{(i)}$  according to (4.85), the Gaussian density in (5.76) can be split into two parts, cf. (4.86). Note that the consideration of the mode variable  $r_k$  in (5.77) does not affect the splitting. Thus, the prediction pdf  $p(\mathbf{x}_k^n, \mathbf{x}_k^1, r_k | \mathbf{Z}_{k-1})$  can be further rewritten as

$$\begin{aligned} p(\mathbf{x}_k^n, \mathbf{x}_k^1, r_k | \mathbf{Z}_{k-1}) &= p(\mathbf{x}_k^1 | \mathbf{x}_k^n, r_k, \mathbf{Z}_{k-1}) \cdot p(\mathbf{x}_k^n, r_k | \mathbf{Z}_{k-1}) \\ &\approx \sum_{i=1}^N w_{k-1|k-1}^{(i)} \cdot \Pr\{r_k | r_{k-1}^{(i)}\} \cdot \mathcal{N}(\mathbf{x}_k^n; \bar{\mathbf{x}}_{k|k-1}^{n,(i)}, \bar{\mathbf{P}}_{k|k-1}^{n,(i)}) \\ &\quad \cdot \mathcal{N}(\mathbf{x}_k^1; \mathbf{x}_{k|k-1}^{1,(i)}, \mathbf{P}_{k|k-1}^{(i)}), \end{aligned} \quad (5.78)$$

with

$$\mathbf{x}_{k|k-1}^{1,(i)} = \bar{\mathbf{x}}_{k|k-1}^{1,(i)} + \bar{\mathbf{P}}_{k|k-1}^{1,(i),\top} \cdot [\bar{\mathbf{P}}_{k|k-1}^{n,(i)}]^{-1} \cdot (\mathbf{x}_k^n - \bar{\mathbf{x}}_{k|k-1}^{n,(i)}), \quad (5.79a)$$

$$\mathbf{P}_{k|k-1}^{(i)} = \bar{\mathbf{P}}_{k|k-1}^{1,(i)} - \bar{\mathbf{P}}_{k|k-1}^{1,(i),\top} \cdot [\bar{\mathbf{P}}_{k|k-1}^{n,(i)}]^{-1} \cdot \bar{\mathbf{P}}_{k|k-1}^{n,(i)}, \quad (5.79b)$$

where  $\bar{\mathbf{x}}_{k|k-1}^{n,(i)}$ ,  $\bar{\mathbf{x}}_{k|k-1}^{1,(i)}$ ,  $\bar{\mathbf{P}}_{k|k-1}^{1,(i)}$ ,  $\bar{\mathbf{P}}_{k|k-1}^{n,(i)}$ , and  $\bar{\mathbf{P}}_{k|k-1}^{n,(i)}$  are defined in (4.85). In the following, a weighted discrete approximation of  $p(\mathbf{x}_k^n, r_k | \mathbf{Z}_{k-1})$  is obtained using an importance sampling approach. In the MM-RBPF, the key idea is to represent each component of the weighted sum by a single particle which is composed of  $\mathbf{x}_k^{(i)}$  and  $r_k^{(i)}$ . While the mode  $r_k$  is sampled from  $\Pr\{r_k | r_{k-1}^{(i)}\}$ , the nonlinear state  $\mathbf{x}_k^n$  is sampled from the following importance density

$$\mathbf{x}_k^{n,(i)} \sim q(\mathbf{x}_k^n | \mathbf{X}_{k-1}^{n,(i)}, r_k^{(i)}, \mathbf{Z}_k), \quad i = 1, \dots, N. \quad (5.80)$$

As a result, the prediction pdf can be approximated as

$$p(\mathbf{x}_k^n, \mathbf{x}_k^1, r_k | \mathbf{Z}_{k-1}) \approx \sum_{i=1}^N w_{k|k-1}^{(i)} \cdot \mathcal{N}(\mathbf{x}_k^1; \mathbf{x}_{k|k-1}^{1,(i)}, \mathbf{P}_{k|k-1}^{(i)}) \cdot \delta(\mathbf{x}_k^n - \mathbf{x}_k^{n,(i)}, r_k - r_k^{(i)}), \quad (5.81)$$

where the unnormalized importance weights are given by

$$w_{k|k-1}^{(i)} \propto w_{k-1|k-1}^{(i)} \cdot \frac{\mathcal{N}(\mathbf{x}_k^{n,(i)}; \bar{\mathbf{x}}_{k|k-1}^{n,(i)}, \bar{\mathbf{P}}_{k|k-1}^{n,(i)})}{q(\mathbf{x}_k^{n,(i)} | \mathbf{X}_{k-1}^{n,(i)}, r_k^{(i)}, \mathbf{Z}_k)}, \quad i = 1, \dots, N. \quad (5.82)$$

The importance weights have to be further normalized to ensure  $\sum_{j=1}^N w_{k|k-1}^{(j)} = 1$ .

## Measurement Update

The measurement update distribution can be split as follows:

$$p(\mathbf{x}_k^n, \mathbf{x}_k^1, r_k | \mathbf{Z}_k) = p(\mathbf{x}_k^1 | \mathbf{x}_k^n, r_k, \mathbf{Z}_k) \cdot p(\mathbf{x}_k^n, r_k | \mathbf{Z}_k). \quad (5.83)$$

The two parts can be evaluated separately. The first distribution can be updated for each particle from the following relationship

$$p(\mathbf{x}_k^1 | \mathbf{x}_k^{n,(i)}, r_k^{(i)}, \mathbf{Z}_k) = \frac{p(\mathbf{z}_k | \mathbf{x}_k^{n,(i)}, \mathbf{x}_k^1, r_k^{(i)}) \cdot p(\mathbf{x}_k^1 | \mathbf{x}_k^{n,(i)}, r_k^{(i)}, \mathbf{Z}_{k-1})}{p(\mathbf{z}_k | \mathbf{x}_k^{n,(i)}, r_k^{(i)}, \mathbf{Z}_{k-1})}, \quad (5.84)$$

where

$$p(\mathbf{z}_k | \mathbf{x}_k^{n,(i)}, r_k^{(i)}, \mathbf{Z}_{k-1}) = \int_{\mathbb{R}^{n_{x_1}}} p(\mathbf{z}_k | \mathbf{x}_k^{n,(i)}, \mathbf{x}_k^1, r_k^{(i)}) \cdot p(\mathbf{x}_k^1 | \mathbf{x}_k^{n,(i)}, r_k^{(i)}, \mathbf{Z}_{k-1}) d\mathbf{x}_k^1. \quad (5.85)$$

For the measurement models given by (5.68c) and (5.68d), the likelihood function can be split into two parts according to

$$p(\mathbf{z}_k | \mathbf{x}_k^{n,(i)}, \mathbf{x}_k^1, r_k^{(i)}) = p(\mathbf{z}_{1,k} | \mathbf{x}_k^{n,(i)}, \mathbf{x}_k^1, r_k^{(i)}) \cdot p(\mathbf{z}_{2,k} | \mathbf{x}_k^{n,(i)}, r_k^{(i)}). \quad (5.86)$$

By insertion of (5.86) into (5.84), the pdf  $p(\mathbf{z}_{2,k} | \mathbf{x}_k^{n,(i)}, r_k^{(i)})$  can be canceled, since it is independent of the linear states  $\mathbf{x}_k^1$ , yielding

$$p(\mathbf{x}_k^1 | \mathbf{x}_k^{n,(i)}, \mathbf{Z}_k) = \frac{p(\mathbf{z}_{1,k} | \mathbf{x}_k^{n,(i)}, \mathbf{x}_k^1, r_k^{(i)}) \cdot p(\mathbf{x}_k^1 | \mathbf{x}_k^{n,(i)}, r_k^{(i)}, \mathbf{Z}_{k-1})}{p(\mathbf{z}_{1,k} | \mathbf{x}_k^{n,(i)}, r_k^{(i)}, \mathbf{Z}_{k-1})}, \quad (5.87)$$

where

$$p(\mathbf{z}_{1,k} | \mathbf{x}_k^{n,(i)}, r_k^{(i)}, \mathbf{Z}_{k-1}) = \int_{\mathbb{R}^{n_{x_1}}} p(\mathbf{z}_{1,k} | \mathbf{x}_k^{n,(i)}, \mathbf{x}_k^1, r_k^{(i)}) \cdot p(\mathbf{x}_k^1 | \mathbf{x}_k^{n,(i)}, r_k^{(i)}, \mathbf{Z}_{k-1}) d\mathbf{x}_k^1. \quad (5.88)$$

The likelihood pdf  $p(\mathbf{z}_{1,k} | \mathbf{x}_k^{n,(i)}, \mathbf{x}_k^1, r_k^{(i)})$  can be determined from (5.68c) and is given by

$$p(\mathbf{z}_{1,k} | \mathbf{x}_k^{n,(i)}, \mathbf{x}_k^1, r_k^{(i)}) = \mathcal{N}(\mathbf{z}_{1,k}; \mathbf{h}_{1,k}(\mathbf{x}_k^n, r_k^{(i)}) + \mathbf{H}_k(\mathbf{x}_k^n, r_k^{(i)}) \cdot \mathbf{x}_k^1 + \boldsymbol{\mu}_{1,k}(r_k^{(i)}), \mathbf{R}_{1,k}(r_k^{(i)})). \quad (5.89)$$

The density  $p(\mathbf{x}_k^1 | \mathbf{x}_k^{n,(i)}, r_k^{(i)}, \mathbf{Z}_{k-1})$  is available from the time update stage and is given by

$$p(\mathbf{x}_k^1 | \mathbf{x}_k^{n,(i)}, \mathbf{Z}_{k-1}) = \mathcal{N}(\mathbf{x}_k^1; \mathbf{x}_{k|k-1}^{1,(i)}, \mathbf{P}_{k|k-1}^{(i)}). \quad (5.90)$$

The integral in (5.88) can be evaluated analytically since the integrand is a product of Gaussian densities. From this it follows that

$$p(\mathbf{z}_{1,k} | \mathbf{x}_k^{n,(i)}, r_k^{(i)}, \mathbf{Z}_{k-1}) = \mathcal{N}(\mathbf{z}_{1,k}; \hat{\mathbf{z}}_{1,k}^{(i)}, \mathbf{S}_k^{(i)}), \quad (5.91)$$

where

$$\hat{\mathbf{z}}_{1,k}^{(i)} = \mathbf{h}_{1,k}(\mathbf{x}_k^{n,(i)}, r_k^{(i)}) + \mathbf{H}_k(\mathbf{x}_k^{n,(i)}, r_k^{(i)}) \cdot \mathbf{x}_{k|k-1}^{1,(i)} + \boldsymbol{\mu}_{1,k}(r_k^{(i)}), \quad (5.92a)$$

$$\mathbf{S}_k^{(i)} = \mathbf{H}_k(\mathbf{x}_k^{n,(i)}, r_k^{(i)}) \cdot \mathbf{P}_{k|k-1}^{(i)} \cdot \mathbf{H}_k^\top(\mathbf{x}_k^{n,(i)}, r_k^{(i)}) + \mathbf{R}_{1,k}(r_k^{(i)}). \quad (5.92b)$$

The densities involved in evaluating the measurement update, cf. (5.84), are all Gaussian. As a result, the density  $p(\mathbf{x}_k^1 | \mathbf{x}_k^{n,(i)}, r_k^{(i)}, \mathbf{Z}_k)$  is also Gaussian and is given by

$$p(\mathbf{x}_k^1 | \mathbf{x}_k^{n,(i)}, r_k^{(i)}, \mathbf{Z}_k) = \mathcal{N}(\mathbf{x}_k^1; \mathbf{x}_{k|k}^{1,(i)}, \mathbf{P}_{k|k}^{(i)}), \quad (5.93)$$

where

$$\mathbf{x}_{k|k}^{1,(i)} = \mathbf{x}_{k|k-1}^{1,(i)} + \mathbf{K}_k^{(i)} \cdot (\mathbf{z}_{1,k} - \hat{\mathbf{z}}_{1,k}^{(i)}), \quad (5.94a)$$

$$\mathbf{P}_{k|k}^{(i)} = \mathbf{P}_{k|k-1}^{(i)} - \mathbf{K}_k^{(i)} \cdot \mathbf{S}_k^{(i)} \cdot \mathbf{K}_k^{(i)\top}, \quad (5.94b)$$

$$\mathbf{K}_k^{(i)} = \mathbf{P}_{k|k-1}^{(i)} \cdot \mathbf{H}_k^\top(\mathbf{x}_k^{n,(i)}, r_k^{(i)}) \cdot [\mathbf{S}_k^{(i)}]^{-1}. \quad (5.94c)$$

The measurement update for the nonlinear states  $\mathbf{x}_k^n$  is done as follows:

$$p(\mathbf{x}_k^n, r_k | \mathbf{Z}_k) = \frac{p(\mathbf{z}_k | \mathbf{x}_k^n, r_k, \mathbf{Z}_{k-1}) \cdot p(\mathbf{x}_k^n, r_k | \mathbf{Z}_{k-1})}{p(\mathbf{z}_k | \mathbf{Z}_{k-1})}. \quad (5.95)$$

Since the pdf  $p(\mathbf{x}_k^n, r_k | \mathbf{Z}_k)$  is approximated using an importance sampling approach, the denominator in (5.95) will be numerically normed and has not to be calculated.

The measurement update can be written as

$$\begin{aligned} p(\mathbf{x}_k^n, r_k | \mathbf{Z}_k) &\propto p(\mathbf{z}_k | \mathbf{x}_k^n, r_k, \mathbf{Z}_{k-1}) \cdot p(\mathbf{x}_k^n, r_k | \mathbf{Z}_{k-1}) \\ &= \int_{\mathbb{R}^{n_{x_1}}} p(\mathbf{z}_k | \mathbf{x}_k^n, \mathbf{x}_k^1, r_k) \cdot p(\mathbf{x}_k^1 | \mathbf{x}_k^n, r_k, \mathbf{Z}_{k-1}) \, d\mathbf{x}_k^1 \cdot p(\mathbf{x}_k^n, r_k | \mathbf{Z}_{k-1}) \\ &\approx \sum_{i=1}^N w_{k|k-1}^{(i)} \cdot \int_{\mathbb{R}^{n_{x_1}}} \underbrace{p(\mathbf{z}_k | \mathbf{x}_k^{n,(i)}, \mathbf{x}_k^1, r_k^{(i)})}_{(5.86)} \cdot p(\mathbf{x}_k^1 | \mathbf{x}_k^{n,(i)}, r_k^{(i)}, \mathbf{Z}_{k-1}) \, d\mathbf{x}_k^1 \\ &\quad \cdot \delta(\mathbf{x}_k^n - \mathbf{x}_k^{n,(i)}, r_k - r_k^{(i)}) \\ &= \sum_{i=1}^N \underbrace{w_{k|k-1}^{(i)} \cdot \mathcal{N}(\mathbf{z}_{1,k}; \hat{\mathbf{z}}_{1,k}^{(i)}, \mathbf{S}_k^{(i)})}_{w_{k|k}^{(i)}} \cdot p(\mathbf{z}_{2,k} | \mathbf{x}_k^n, r_k) \cdot \delta(\mathbf{x}_k^n - \mathbf{x}_k^{n,(i)}, r_k - r_k^{(i)}). \end{aligned} \quad (5.96)$$

Combining (5.93) and (5.96) according to (5.83) results in

$$p(\mathbf{x}_k^n, \mathbf{x}_k^l, r_k | \mathbf{Z}_k) \approx \sum_{i=1}^N w_{k|k}^{(i)} \cdot \mathcal{N}(\mathbf{x}_k^l; \mathbf{x}_{k|k}^{l,(i)}, \mathbf{P}_{k|k}^{(i)}) \cdot \delta(\mathbf{x}_k^n - \mathbf{x}_k^{n,(i)}, r_k - r_k^{(i)}). \quad (5.97)$$

where the normalized weights are given by

$$w_{k|k}^{(i)} = \frac{w_{k|k-1}^{(i)} \cdot \mathcal{N}(\mathbf{z}_{1,k}; \hat{\mathbf{z}}_{1,k}^{(i)}, \mathbf{S}_k^{(i)}) \cdot p(\mathbf{z}_{2,k} | \mathbf{x}_k^{n,(i)}, r_k^{(i)})}{\sum_{j=1}^N w_{k|k-1}^{(j)} \cdot \mathcal{N}(\mathbf{z}_{1,k}; \hat{\mathbf{z}}_{1,k}^{(j)}, \mathbf{S}_k^{(j)}) \cdot p(\mathbf{z}_{2,k} | \mathbf{x}_k^{n,(j)}, r_k^{(j)})}. \quad (5.98)$$

By finally omitting the mode  $r_k$  in the discrete approximation (5.97), the desired posterior pdf of the current state is found which is given by

$$p(\mathbf{x}_k^n, \mathbf{x}_k^l | \mathbf{Z}_k) \approx \sum_{i=1}^N w_{k|k}^{(i)} \cdot \mathcal{N}(\mathbf{x}_k^l; \mathbf{x}_{k|k}^{l,(i)}, \mathbf{P}_{k|k}^{(i)}) \cdot \delta(\mathbf{x}_k^n - \mathbf{x}_k^{n,(i)}). \quad (5.99)$$

## Estimation and Resampling

In the MM-RBPF, the formulas for estimating the mean vector  $\hat{\mathbf{x}}_{\text{MMSE},k}$  and its covariance  $\mathbf{P}_{\text{MMSE},k}$  of the linear and nonlinear states are equivalent to the formulas given in (4.108), since the joint posterior pdf is approximated with (5.99). For the resampling step in the MM-RBPF, systematic resampling is used which is explained in Section 4.5.2.2.

### 5.5.3.3 Choice of Importance Density

In the design of MM-RBPFs, the choice of the mode-conditioned importance density  $q(\mathbf{x}_k^n | \mathbf{X}_{k-1}^{n,(i)}, r_k^{(i)}, \mathbf{Z}_k)$  plays a major role. The optimal mode-conditioned importance density that minimizes the variance of the importance weights is given by  $q(\mathbf{x}_k^n | \mathbf{X}_{k-1}^{n,(i)}, r_k^{(i)}, \mathbf{Z}_k)_{\text{opt}} = p(\mathbf{x}_k^n | \mathbf{X}_{k-1}^{n,(i)}, r_k^{(i)}, \mathbf{Z}_k)$ . The proof is similar to the proof given in [DGA00]. However, for the hybrid localization problem, a closed-form expression for this density does not exist, so that one has to resort to suboptimal importance densities. For the hybrid localization problem, the following pdf

$$q(\mathbf{x}_k^n | \mathbf{X}_{k-1}^{n,(i)}, r_k^{(i)}, \mathbf{Z}_k) = \mathcal{N}(\mathbf{x}_k^n; \bar{\mathbf{x}}_{k|k-1}^{n,(i)}, \bar{\mathbf{P}}_{k|k-1}^{n,(i)}) \quad (5.100)$$

is chosen as importance density, cf. (5.78). In this case, the weights in the time update are given by  $w_{k|k-1}^{(i)} = w_{k-1|k-1}^{(i)}$ , cf. (5.72), and the weights in the measurement update simplify to

$$w_{k|k}^{(i)} = \frac{w_{k-1|k-1}^{(i)} \cdot \mathcal{N}(\mathbf{z}_{1,k}; \hat{\mathbf{z}}_{1,k}^{(i)}, \mathbf{S}_k^{(i)}) \cdot p(\mathbf{z}_{2,k} | \mathbf{x}_k^{n,(i)}, r_k^{(i)})}{\sum_{j=1}^N w_{k-1|k-1}^{(j)} \cdot \mathcal{N}(\mathbf{z}_{1,k}; \hat{\mathbf{z}}_{1,k}^{(j)}, \mathbf{S}_k^{(j)}) \cdot p(\mathbf{z}_{2,k} | \mathbf{x}_k^{n,(j)}, r_k^{(j)})}. \quad (5.101)$$

A pseudocode description of the MM-RBPF is given in Algorithm 5.5, where the following abbreviations have been introduced in order to simplify the notation:

$$\begin{aligned} \mathbf{f}_{k-1}^{\mathbf{n}}(\mathbf{x}_{k-1}^{\mathbf{n},(i)}, r_k^{(i)}) &= \mathbf{f}_{k-1}^{\mathbf{n},(i)}, & \mathbf{F}_{k-1}^{\mathbf{n}}(\mathbf{x}_{k-1}^{\mathbf{n},(i)}, r_k^{(i)}) &= \mathbf{F}_{k-1}^{\mathbf{n},(i)}, & \mathbf{\Gamma}_{k-1}^{\mathbf{n}}(\mathbf{x}_{k-1}^{\mathbf{n},(i)}, r_k^{(i)}) &= \mathbf{\Gamma}_{k-1}^{\mathbf{n},(i)}, \\ \mathbf{f}_{k-1}^{\mathbf{l}}(\mathbf{x}_{k-1}^{\mathbf{n},(i)}, r_k^{(i)}) &= \mathbf{f}_{k-1}^{\mathbf{l},(i)}, & \mathbf{F}_{k-1}^{\mathbf{l}}(\mathbf{x}_{k-1}^{\mathbf{n},(i)}, r_k^{(i)}) &= \mathbf{F}_{k-1}^{\mathbf{l},(i)}, & \mathbf{\Gamma}_{k-1}^{\mathbf{l}}(\mathbf{x}_{k-1}^{\mathbf{n},(i)}, r_k^{(i)}) &= \mathbf{\Gamma}_{k-1}^{\mathbf{l},(i)}, \\ \mathbf{h}_{1,k}(\mathbf{x}_k^{\mathbf{n},(i)}, r_k^{(i)}) &= \mathbf{h}_{1,k}^{(i)}, & \mathbf{H}_k(\mathbf{x}_k^{\mathbf{n},(i)}, r_k^{(i)}) &= \mathbf{H}_k^{(i)}, & \bar{\mathbf{E}}_k(\mathbf{x}_k^{\mathbf{n},(i)}, \mathbf{x}_{k-1}^{\mathbf{n},(i)}, r_k^{(i)}) &= \bar{\mathbf{E}}_k^{(i)}. \end{aligned} \quad (5.102)$$

Note that after the initialization, the sampling of mode variables in the time update step is left out, and one directly starts with the sampling of the nonlinear states.

---

**Algorithm 5.5** Multiple-Model Rao-Blackwellized Particle Filter

---

1. Initialization:

- For  $i = 1, \dots, N$ , initialize the particles  $\mathbf{x}_0^{\mathbf{n},(i)} \sim p(\mathbf{x}_0^{\mathbf{n}})$ , the mode probabilities  $r_1^{(i)} \sim \Pr\{r_1\}$  and the weights  $w_{0|0}^{(i)} = \frac{1}{N}$ , and set  $\{\mathbf{x}_{0|0}^{\mathbf{l},(i)}, \mathbf{P}_{0|0}^{(i)}\} = \{\hat{\mathbf{x}}_0^{\mathbf{l}}, \mathbf{P}_0\}$ .

2. Particle Filter Time Update:

- For  $i = 1, \dots, N$ , draw mode probabilities according to

$$r_k^{(i)} \sim \Pr\{r_k | r_{k-1}^{(i)}\},$$

- For  $i = 1, \dots, N$ , draw particles from the importance density according to

$$\mathbf{x}_k^{\mathbf{n},(i)} \sim \mathcal{N}(\bar{\mathbf{x}}_{k|k-1}^{\mathbf{n},(i)}, \bar{\mathbf{P}}_{k|k-1}^{\mathbf{n},(i)}),$$

where

$$\begin{aligned} \bar{\mathbf{x}}_{k|k-1}^{\mathbf{n},(i)} &= \mathbf{f}_{k-1}^{\mathbf{n},(i)} + \mathbf{F}_{k-1}^{\mathbf{n},(i)} \cdot \mathbf{x}_{k-1|k-1}^{\mathbf{l},(i)}, \\ \bar{\mathbf{P}}_{k|k-1}^{\mathbf{n},(i)} &= \mathbf{F}_{k-1}^{\mathbf{n},(i)} \cdot \mathbf{P}_{k-1|k-1}^{(i)} \cdot \mathbf{F}_{k-1}^{\mathbf{n},(i),\top} + \mathbf{\Gamma}_{k-1}^{\mathbf{n},(i)} \cdot \mathbf{Q}_{k-1}^{\mathbf{n}} \cdot \mathbf{\Gamma}_{k-1}^{\mathbf{n},(i),\top}. \end{aligned}$$

3. Kalman Filter Time Update:

- For  $i = 1, \dots, N$ , evaluate

$$\begin{aligned} \mathbf{x}_{k|k-1}^{\mathbf{l},(i)} &= \bar{\mathbf{x}}_{k|k-1}^{\mathbf{l},(i)} + \bar{\mathbf{P}}_{k|k-1}^{\mathbf{nl},(i),\top} \cdot [\bar{\mathbf{P}}_{k|k-1}^{\mathbf{n},(i)}]^{-1} \cdot (\mathbf{x}_k^{\mathbf{n},(i)} - \bar{\mathbf{x}}_{k|k-1}^{\mathbf{n},(i)}), \\ \mathbf{P}_{k|k-1}^{(i)} &= \bar{\mathbf{P}}_{k|k-1}^{\mathbf{l},(i)} - \bar{\mathbf{P}}_{k|k-1}^{\mathbf{nl},(i),\top} \cdot [\bar{\mathbf{P}}_{k|k-1}^{\mathbf{n},(i)}]^{-1} \cdot \bar{\mathbf{P}}_{k|k-1}^{\mathbf{nl},(i)}, \end{aligned}$$

where

$$\begin{aligned}
\bar{\mathbf{x}}_{k|k-1}^{1,(i)} &= \mathbf{f}_{k-1}^{1,(i)} + \bar{\mathbf{F}}_{k-1}^{1,(i)} \cdot \mathbf{x}_{k-1|k-1}^{1,(i)} + \bar{\mathbf{E}}_k^{(i)}, \\
\bar{\mathbf{P}}_{k|k-1}^{nl,(i)} &= \mathbf{F}_{k-1}^{n,(i)} \cdot \mathbf{P}_{k-1|k-1}^{(i)} \cdot \bar{\mathbf{F}}_{k-1}^{1,(i),\top}, \\
\bar{\mathbf{P}}_{k|k-1}^{1,(i)} &= \bar{\mathbf{F}}_{k-1}^{1,(i)} \cdot \mathbf{P}_{k-1|k-1}^{(i)} \cdot \bar{\mathbf{F}}_{k-1}^{1,(i),\top} + \mathbf{\Gamma}_{k-1}^{1,(i)} \cdot \bar{\mathbf{Q}}_{k-1}^1 \cdot \mathbf{\Gamma}_{k-1}^{1,(i),\top}, \\
\bar{\mathbf{E}}_k^{(i)} &= \mathbf{\Gamma}_{k-1}^{1,(i)} \cdot \mathbf{Q}_{k-1}^{nl,\top} \cdot [\mathbf{\Gamma}_{k-1}^{n,(i)} \cdot \mathbf{Q}_{k-1}^n]^{-1} \cdot (\mathbf{x}_k^{n,(i)} - \mathbf{f}_{k-1}^{n,(i)}), \\
\bar{\mathbf{F}}_{k-1}^{1,(i)} &= \mathbf{F}_{k-1}^{1,(i)} - \mathbf{\Gamma}_{k-1}^{1,(i)} \cdot \mathbf{Q}_{k-1}^{nl,\top} \cdot [\mathbf{\Gamma}_{k-1}^{n,(i)} \cdot \mathbf{Q}_{k-1}^n]^{-1} \cdot \mathbf{F}_{k-1}^{n,(i)}, \\
\bar{\mathbf{Q}}_{k-1}^1 &= \mathbf{Q}_{k-1}^1 - \mathbf{Q}_{k-1}^{nl,\top} \cdot [\mathbf{Q}_{k-1}^n]^{-1} \cdot \mathbf{Q}_{k-1}^{nl}.
\end{aligned}$$

#### 4. Particle Filter Measurement Update:

- For  $i = 1, \dots, N$ , evaluate the weights

$$w_{k|k}^{(i)} = \frac{w_{k-1|k-1}^{(i)} \cdot \mathcal{N}(\mathbf{z}_{1,k}; \hat{\mathbf{z}}_{1,k}^{(i)}, \mathbf{S}_k^{(i)}) \cdot p(\mathbf{z}_{2,k} | \mathbf{x}_k^{n,(i)}, r_k^{(i)})}{\sum_{j=1}^N w_{k-1|k-1}^{(j)} \cdot \mathcal{N}(\mathbf{z}_{1,k}; \hat{\mathbf{z}}_{1,k}^{(j)}, \mathbf{S}_k^{(j)}) \cdot p(\mathbf{z}_{2,k} | \mathbf{x}_k^{n,(j)}, r_k^{(j)})},$$

where

$$\begin{aligned}
\hat{\mathbf{z}}_{1,k}^{(i)} &= \mathbf{h}_{1,k}^{(i)} + \mathbf{H}_k^{(i)} \cdot \mathbf{x}_{k|k-1}^{1,(i)} + \boldsymbol{\mu}_k(r_k^{(i)}), \\
\mathbf{S}_k^{(i)} &= \mathbf{H}_k^{(i)} \cdot \mathbf{P}_{k|k-1}^{(i)} \cdot \mathbf{H}_k^{(i),\top} + \mathbf{R}_{1,k}(r_k^{(i)}).
\end{aligned}$$

#### 5. Kalman Filter Measurement Update:

- For  $i = 1, \dots, N$ , evaluate

$$\begin{aligned}
\mathbf{x}_{k|k}^{1,(i)} &= \mathbf{x}_{k|k-1}^{1,(i)} + \mathbf{K}_k^{(i)} \cdot (\mathbf{z}_{1,k} - \hat{\mathbf{z}}_{1,k}^{(i)}), \\
\mathbf{P}_{k|k}^{(i)} &= \mathbf{P}_{k|k-1}^{(i)} - \mathbf{K}_k^{(i)} \cdot \mathbf{S}_k^{(i)} \cdot \mathbf{K}_k^{(i),\top},
\end{aligned}$$

where

$$\mathbf{K}_k^{(i)} = \mathbf{P}_{k|k-1}^{(i)} \cdot \mathbf{H}_k^{(i),\top} \cdot [\mathbf{S}_k^{(i)}]^{-1}.$$

#### 6. Estimation:

- Determine estimates of the linear and nonlinear state vectors according to

$$\hat{\mathbf{x}}_{\text{MMSE},k|k}^n = \sum_{i=1}^N w_{k|k}^{(i)} \cdot \mathbf{x}_k^{n,(i)}, \quad \hat{\mathbf{x}}_{\text{MMSE},k|k}^1 = \sum_{i=1}^N w_{k|k}^{(i)} \cdot \mathbf{x}_{k|k}^{1,(i)}.$$

#### 7. Resampling:

- Perform systematic resampling using Algorithm 4.4. Take  $N$  samples with replacement from the set  $\{\mathbf{x}_k^{n,(i)}, \mathbf{x}_{k|k}^{1,(i)}, \mathbf{P}_{k|k}^{(i)}, r_k^{(i)}\}_{i=1}^N$ , where the probability to take sample  $i$  is  $w_{k|k}^{(i)}$ . Set  $w_{k|k}^{(i)} = \frac{1}{N}$  for  $i = 1, \dots, N$ .

8. Set  $k := k + 1$  and iterate from step 2.

### 5.5.3.4 Application to the Hybrid Localization Problem

In this section, the state and measurement models for the hybrid localization are adopted to the conditional linear system model of the MM-RBPF, cf. 5.66. For the hybrid localization problem, the state model is given by (2.49). The measurement model, where the switching between LOS and NLOS propagation conditions is modeled with a Markov chain, is given by (2.53). In order to relate the state and measurement models to the MM-RBPF framework, the state vector is split into two parts according to (4.112) and (4.113). Due to the fact that the state model is linear Gaussian and independent of the mode variable  $r_k$ , the models for the linear and nonlinear states can be written as in (4.114) and (4.115). For the mode-dependent measurement model, the measurement vector is split as follows

$$\mathbf{z}_{1,k} = [\mathbf{z}_{\text{PR},k}^\top, \mathbf{z}_{\text{RTT,LOS},k}^\top, \mathbf{z}_{\text{RSS,LOS},k}^\top, z_{\text{BIAS},k}]^\top, \quad (5.103)$$

i.e., all measurements can be expressed with (5.68c), while the measurement vector  $\mathbf{z}_{2,k}$  is empty. Thus, the corresponding measurement model can be rewritten as

$$\underbrace{\begin{bmatrix} \mathbf{z}_{\text{PR},k} \\ \mathbf{z}_{\text{RTT},k} \\ \mathbf{z}_{\text{RSS},k} \\ z_{\text{BIAS},k} \end{bmatrix}}_{\mathbf{z}_{1,k}} = \underbrace{\begin{bmatrix} \mathbf{d}_{\text{SAT},k}(\mathbf{x}_k^n) \\ \mathbf{h}_{\text{RTT},k}(\mathbf{x}_k^n) \\ \mathbf{h}_{\text{RSS},k}(\mathbf{x}_k^n, r_k) \\ 0 \end{bmatrix}}_{\mathbf{h}_{1,k}(\mathbf{x}_k^n, r_k)} + \underbrace{\begin{bmatrix} \mathbf{0}_{M_{\text{PR}} \times 2} & \mathbf{1}_{M_{\text{PR}} \times 1} & \mathbf{0}_{M_{\text{PR}} \times 1} \\ \mathbf{0}_{(M_{\text{RTT}} + M_{\text{RSS}}) \times 4} \\ \mathbf{0}_{1 \times 2} & 1 & 0 \end{bmatrix}}_{\mathbf{H}_k} \cdot \underbrace{\begin{bmatrix} \dot{x}_{\text{MT},k} \\ \dot{y}_{\text{MT},k} \\ c_0 \cdot \delta t_k \\ c_0 \cdot \delta t_k \end{bmatrix}}_{\mathbf{x}_k^1} + \underbrace{\begin{bmatrix} \mathbf{v}_{\text{PR},k} \\ \mathbf{v}_{\text{RTT},k}(r_k) \\ \mathbf{v}_{\text{RSS},k}(r_k) \\ v_{\text{BIAS},k} \end{bmatrix}}_{\mathbf{v}_{1,k}(r_k)}. \quad (5.104)$$

The mode-dependent measurement noise  $\mathbf{v}_{1,k}(r_k)$  is Gaussian distributed with mean vector  $\boldsymbol{\mu}_{1,k}(r_k) = \boldsymbol{\mu}_k(r_k)$  and covariance matrix  $\mathbf{R}_{1,k}(r_k) = \mathbf{R}_k(r_k)$ . Since all measurements are expressed with model (5.68c), the likelihood function  $p(\mathbf{z}_{2,k} | \mathbf{x}_k^n, r_k)$  can be omitted in the calculation of the importance weights, cf. (5.101).

### 5.5.3.5 Incorporation of Road Constraints

In this section, it is explained how road constraints can be incorporated into the MM-RBPF for hybrid localization. For incorporating road constraints into the MM-RBPF, the approach presented in Section 4.5.6.2 is used. Since the mode variable is included only in the measurement model, the incorporation of road constraints into the MM-RBPF can be done as follows. The state vector is split into two parts according to (4.172) and (4.173). The model for generating the state  $\mathbf{x}_k$  is replaced with the model for generating road-constrained states  $\mathbf{x}_{\text{R},k}$ , cf. (4.174) and (4.175). The measurement

vector is split according to (5.103), so that the mode-conditioned measurement model can be written as

$$\underbrace{\begin{bmatrix} \mathbf{z}_{\text{PR},k} \\ \mathbf{z}_{\text{RTT},k} \\ \mathbf{z}_{\text{RSS},k} \\ z_{\text{BIAS},k} \end{bmatrix}}_{\mathbf{z}_{1,k}} = \underbrace{\begin{bmatrix} \mathbf{d}_{\text{SAT},k}(\mathbf{x}_{\text{MT},k}) \\ \mathbf{h}_{\text{RTT},k}(\mathbf{x}_{\text{MT},k}) \\ \mathbf{h}_{\text{RSS},k}(\mathbf{x}_{\text{MT},k}, r_k) \\ 0 \end{bmatrix}}_{\mathbf{h}_{1,k}(\mathbf{T}_{\text{LG},k}(\mathbf{x}_{\text{R},k}^{\text{n}}, \mathcal{T}_{\text{RN}}))} + \underbrace{\begin{bmatrix} \mathbf{1}_{M_{\text{PR}} \times 1} & \mathbf{0}_{M_{\text{PR}} \times 1} \\ \mathbf{0}_{(M_{\text{RTT}} + M_{\text{RSS}}) \times 2} & \mathbf{0} \\ 1 & 0 \end{bmatrix}}_{\mathbf{H}_k} \cdot \underbrace{\begin{bmatrix} c_0 \cdot \delta t_k \\ c_0 \cdot \delta \dot{t}_k \end{bmatrix}}_{\mathbf{x}_{\text{R},k}^1} + \underbrace{\begin{bmatrix} \mathbf{v}_{\text{PR},k} \\ \mathbf{v}_{\text{RTT},k}(r_k) \\ \mathbf{v}_{\text{RSS},k}(r_k) \\ v_{\text{BIAS},k} \end{bmatrix}}_{\mathbf{v}_{1,k}(r_k)}. \quad (5.105)$$

The mode-dependent measurement noise  $\mathbf{v}_{1,k}(r_k)$  is Gaussian distributed with mean vector  $\boldsymbol{\mu}_{1,k}(r_k) = \boldsymbol{\mu}_k(r_k)$  and covariance matrix  $\mathbf{R}_{1,k}(r_k) = \mathbf{R}_k(r_k)$ , and the corresponding mode-conditioned likelihood function is given by

$$p(\mathbf{z}_{1,k} | \mathbf{x}_k, r_k) = p(\mathbf{z}_{1,k} | \mathbf{T}_{\text{G},k}(\mathbf{x}_{\text{R},k}, \mathcal{T}_{\text{RN}}), r_k). \quad (5.106)$$

A pseudocode description of the MM-RBPF with road-constraints for hybrid localization is given in Algorithm 5.6. Note that after the initialization, the sampling of mode variables in the time update step can be left out, and one can directly start with the sampling of the road-constrained states.

---

**Algorithm 5.6** Multiple-Model Rao-Blackwellized Particle Filter with Road Constraints

---

1. Initialization:

- For  $i = 1, \dots, N$ , initialize the particles  $\mathbf{x}_{\text{R},0}^{\text{n},(i)} \sim p(\mathbf{x}_{\text{R},0}^{\text{n}})$ , mode probabilities  $r_1 \sim \text{Pr}\{r_1\}$  and weights  $w_{0|0}^{(i)} = \frac{1}{N}$ , and set  $\{\mathbf{x}_{0|0}^{1,(i)}, \mathbf{P}_{0|0}^{(i)}\} = \{\hat{\mathbf{x}}_{\text{R},0}^1, \mathbf{P}_{\text{R},0}\}$ .

2. Particle Filter Time Update:

- For  $i = 1, \dots, N$ , draw mode probabilities according to

$$r_k^{(i)} \sim \text{Pr}\{r_k | r_{k-1}^{(i)}\},$$

- For  $i = 1, \dots, N$ , generate particles  $\mathbf{x}_{\text{R},k}^{\text{n},(i)}$  from  $\mathbf{x}_{\text{R},k-1}^{\text{n},(i)}$  by using samples from the process noise sequences  $\mathbf{w}_{k-1}^{\text{n},(i)} \sim p_{\mathbf{w}_{k-1}^{\text{n}}}(\cdot)$  as shown in (4.174).

3. Kalman Filter Time Update:

- For  $i = 1, \dots, N$ , evaluate

$$\begin{aligned} \mathbf{x}_{k|k-1}^{1,(i)} &= \mathbf{F}_{k-1}^1 \cdot \mathbf{x}_{k-1|k-1}^{1,(i)}, \\ \mathbf{P}_{k|k-1}^{(i)} &= \mathbf{F}_{k-1}^1 \cdot \mathbf{P}_{k-1|k-1}^{(i)} \cdot \mathbf{F}_{k-1}^{1,\top} + \mathbf{\Gamma}_{k-1}^1 \cdot \mathbf{Q}_{k-1}^1 \cdot \mathbf{\Gamma}_{k-1}^{1,\top}. \end{aligned}$$



## 4. Particle Filter Measurement Update:

- For  $i = 1, \dots, N$ , evaluate the weights

$$w_{k|k}^{(i)} = \frac{w_{k-1|k-1}^{(i)} \cdot \mathcal{N}(\mathbf{z}_{1,k}; \hat{\mathbf{z}}_{1,k}^{(i)}, \mathbf{S}_k^{(i)})}{\sum_{j=1}^N w_{k-1|k-1}^{(j)} \cdot \mathcal{N}(\mathbf{z}_{1,k}; \hat{\mathbf{z}}_{1,k}^{(j)}, \mathbf{S}_k^{(j)})},$$

where

$$\begin{aligned} \hat{\mathbf{z}}_{1,k}^{(i)} &= \mathbf{h}_{1,k}(\mathbf{T}_{\text{LG},k}(\mathbf{x}_{\text{R},k}^{\text{n},(i)}, \mathcal{T}_{\text{RN}})) + \mathbf{H}_k \cdot \mathbf{x}_{k|k-1}^{1,(i)} + \boldsymbol{\mu}_{1,k}(r_k^{(i)}), \\ \mathbf{S}_k^{(i)} &= \mathbf{H}_k \cdot \mathbf{P}_{k|k-1}^{(i)} \cdot \mathbf{H}_k^\top + \mathbf{R}_{1,k}(r_k^{(i)}). \end{aligned}$$

## 5. Kalman Filter Measurement Update:

- For  $i = 1, \dots, N$ , evaluate

$$\begin{aligned} \mathbf{x}_{k|k}^{1,(i)} &= \mathbf{x}_{k|k-1}^{1,(i)} + \mathbf{K}_k^{(i)} \cdot (\mathbf{z}_{1,k} - \hat{\mathbf{z}}_{1,k}^{(i)}), \\ \mathbf{P}_{k|k}^{(i)} &= \mathbf{P}_{k|k-1}^{(i)} - \mathbf{K}_k^{(i)} \cdot \mathbf{S}_k^{(i)} \cdot \mathbf{K}_k^{(i)\top}, \end{aligned}$$

where

$$\mathbf{K}_k^{(i)} = \mathbf{P}_{k|k-1}^{(i)} \cdot \mathbf{H}_k^\top \cdot [\mathbf{S}_k^{(i)}]^{-1}.$$

## 6. Estimation:

- Determine estimates of the linear and nonlinear state vectors according to

$$\hat{\mathbf{x}}_{\text{MMSE},k|k}^{\text{n}} = \sum_{i=1}^N w_{k|k}^{(i)} \cdot \mathbf{T}_{\text{LG},k}(\mathbf{x}_{\text{R},k}^{\text{n},(i)}, \mathcal{T}_{\text{RN}}), \quad \hat{\mathbf{x}}_{\text{MMSE},k|k}^1 = \sum_{i=1}^N w_{k|k}^{(i)} \cdot \mathbf{x}_{k|k}^{1,(i)}.$$

## 7. Resampling:

- Perform systematic resampling using Algorithm 4.4. Take  $N$  samples with replacement from the set  $\{\mathbf{x}_{\text{R},k}^{\text{n},(i)}, \mathbf{x}_{k|k}^{1,(i)}, \mathbf{P}_{k|k}^{(i)}\}_{i=1}^N$ , where the probability to take sample  $i$  is  $w_{k|k}^{(i)}$ . Set  $w_{k|k}^{(i)} = \frac{1}{N}$  for  $i = 1, \dots, N$ .

- 8. Set  $k := k + 1$  and iterate from step 2.

## 5.6 Performance Evaluation

### 5.6.1 Introduction

In this Section 5.6, the hybrid localization algorithms of Sections 5.4 and 5.5 are evaluated by means of Monte Carlo simulations and their average performance is compared

to the PCRLB. The performance metrics that will be used are the RMSE of the MT location and time averaged RMSE of the MT location as defined in (3.95) and (3.96), as well as the corresponding PCRLBs given by (4.182) and (4.183). Note that the Bayesian information submatrix  $\mathbf{J}_k$  for the M-PCRLB is defined in (5.30). For the evaluation of the E-PCRLB, the terms  $[[\mathbf{J}_k]^{-1}]_{1,1}$  and  $[[\mathbf{J}_k]^{-1}]_{2,2}$  in (4.182) and (4.183) have to be replaced with the terms  $[\mathcal{P}_{\text{E-PCRLB}}]_{1,1}$  and  $[\mathcal{P}_{\text{E-PCRLB}}]_{2,2}$ , defined in (5.17), respectively. All results have been obtained by performing  $N_{\text{MC}} = 100$  Monte Carlo runs. The Monte Carlo simulations are performed for Scenario II, cf. Section 2.3.4.3, and the results are presented in Section 5.6.2. Finally, comments on the computational complexity of the different algorithms are given in Section 5.6.3.

## 5.6.2 Simulation Results for Scenario II

### 5.6.2.1 Simulation Results for LOS Propagation Conditions

In this section, the performance of the IMM-based algorithm and multiple model-based algorithms introduced in Sections 5.4 and 5.5 is evaluated for the different combinations of measurements of Scenario II assuming LOS propagation conditions, cf. Section 2.3.4.3. The PCRLB for this case is defined in Section 4.3.2 and is computed for the different combinations of measurements to indicate the best possible performance that one can expect for the given scenario and set of parameters. All filters are initialized using the strategy explained in Section 4.6.2.1 and the initial mode probabilities are set to  $\Pr\{r_1\} = 1/8$ , for  $r_1 = 1, \dots, 8$ .

In order to apply the algorithms to the hybrid localization problem, the parameters included in the mode-dependent measurement model  $\mathbf{h}_k(\mathbf{x}_k, r_k)$ , as well as the noise statistics given by the mode-dependent mean vector  $\boldsymbol{\mu}_k(r_k)$  and covariance matrices  $\mathbf{R}_k(r_k)$  and  $\mathbf{Q}$  have to be specified. In the following,  $\mathbf{Q}$  is chosen as described in Section 4.6.2.1 and the parameters of the mode-dependent covariance matrix  $\mathbf{R}_k(r_k)$  are assumed to be equal to the parameters with which the measurements have been generated, cf. Table 2.2. The parameters of the Markov chain used in the algorithms are assumed to be a-priori known and are given in (2.51). In practice, however, these parameters are unknown and have to be estimated in advance from field trial data. The computation of the PCRLB follows the same strategy as described in Section 4.6.2.1.

In Fig. 5.1, the MT location RMSEs in m vs. the time index  $k$  for the Cellular method is shown for the RBPF, MM-RBPF, PF with road constraints and MM-PF with road constraints using  $N = 8000$  particles, together with the IMM-EKF and the

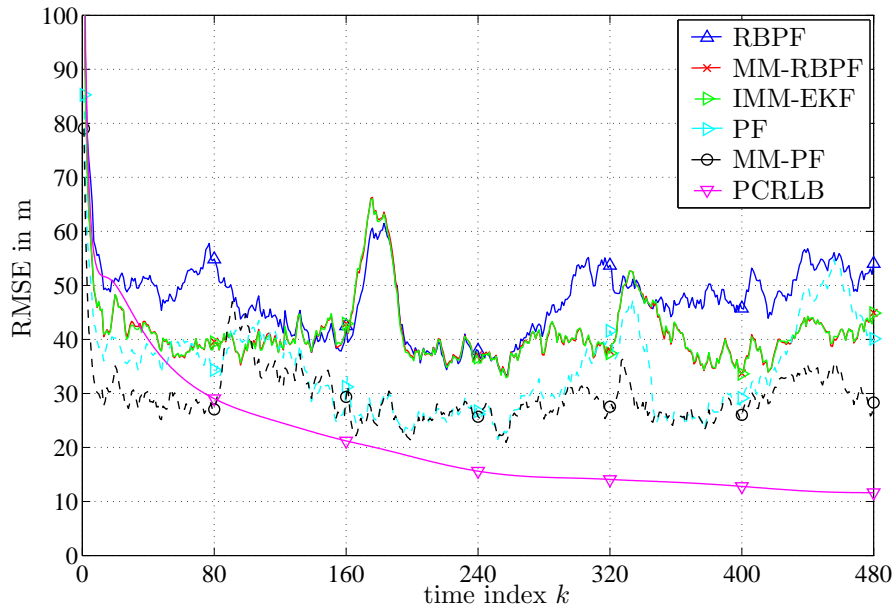


Figure 5.1. MT location RMSE vs. time index  $k$  for RBPF, MM-RBPF, IMM-EKF, PF, MM-PF and PCRLB assuming LOS propagation conditions and Cellular method, solid lines: No road constraints, dashed lines: Road constraints.

corresponding PCRLBs. Note that for comparison purposes, the results for the RBPF and PF with road constraints introduced in Sections 4.5.3 and 4.5.6 are also shown. These two filters use the likelihood pdf given in (3.83), i.e., there is an intentional mismatch between the statistics with which the measurements have been generated and the statistics used in the filter, in order to evaluate the expected degradation in performance. The results show that the RBPF provides the worst results. The performance can be improved using the IMM-EKF and MM-RBPF, which have approximately the same performance. The performance improvements of the IMM-EKF and MM-RBPF are a result of the efficient estimation of the current propagation conditions, which are modeled with the mode variable  $r_k$ . Since the filters additionally estimate the mode variable  $r_k$  based on the measurements, they can quickly adapt to new propagation conditions. It can be further noticed that the filters cannot attain the PCRLB. This is mainly due to the choice of the covariance matrix  $\mathbf{Q}$ , which is different in the filters and in the computation of the PCRLB. Comparing the performance of the PF with road constraints and the MM-PF with road constraints, it can be seen that the MM-PF outperforms the PF. Again, the additional estimation of the mode variable  $r_k$  helps to improve the performance.

In Fig. 5.2, the MT location RMSEs in m vs. the time index  $k$  for the Hybrid 1 method is shown for the RBPF, MM-RBPF, RBPF with road constraints and MM-

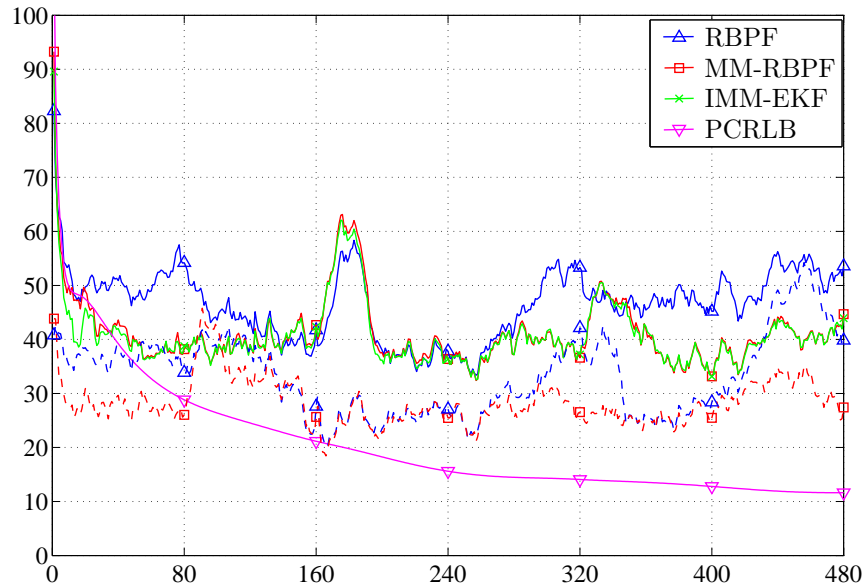


Figure 5.2. MT location RMSE vs. time index  $k$  for RBPf, MM-RBPf, IMM-EKF and PCRLB assuming LOS propagation conditions and Hybrid 1 method, solid lines: No road constraints, dashed lines: Road constraints.

RBPf with road constraints using  $N = 8000$  particles, together with the IMM-EKF and the corresponding PCRLBs. For these results, the same conclusions as those for the Cellular method can be drawn. It can be noticed, that using the Hybrid 1 method rather than the Cellular method yields small performance improvements.

In Fig. 5.3, the MT location RMSEs in m vs. the time index  $k$  for the Hybrid 2 method is shown for the RBPf, MM-RBPf, RBPf with road constraints and MM-RBPf with road constraints using  $N = 8000$  particles, together with the IMM-EKF and the corresponding PCRLBs. It can be seen that on average, the RBPf provides the worst results. For the estimators without road constraints, the IMM-EKF provides the best results, followed by the MM-RBPf. The RBPf provides on average the worst results. However, it can be also noticed that the performance differences between the RBPf and the IMM-EKF and MM-RBPf are smaller. This is due to the fact that in the Hybrid 2 method, two very accurate pseudorange measurements are available. From this it follows, that the performance is dominated by the information available from the PR measurements and less influenced by the RSS and RTT measurements. It can be further noticed that the performance of the RBPf and MM-RBPf with road constraints is practically equivalent. Again, it can be concluded that the performance is dominated by the information available from the PR measurements and the road, and less influenced by the RSS and RTT measurements. In Fig. 5.4 the MT location

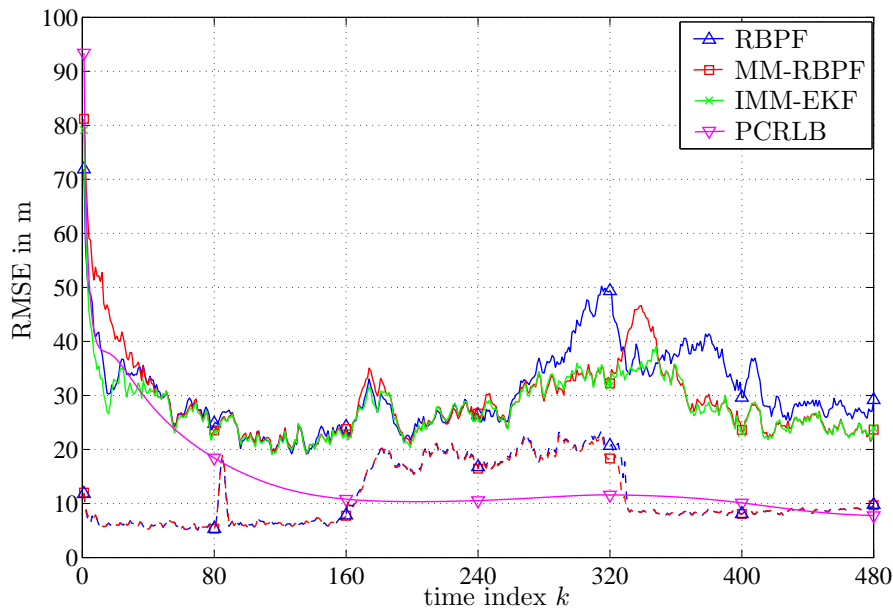


Figure 5.3. MT location RMSE vs. time index  $k$  for RBPf, MM-RBPf, IMM-EKF and PCRLB assuming LOS propagation conditions and Hybrid 2 method, solid lines: No road constraints, dashed lines: Road constraints.

$\overline{\text{RMSE}}$  in m vs. particle number  $N$  for the Cellular, Hybrid 1 and Hybrid 2 methods are shown for the MM-PF, MM-RBPf, RBPf and IMM-EKF, together with the  $\overline{\text{PCRLB}}$ . It can be noticed that for the Cellular and Hybrid 1 method, the RBPf provides the worst performance and practically no performance improvements can be achieved by increasing the number of particles in the filter. These results can be explained by the intentional mismatch between the statistics with which the measurements have been generated and the statistics used in the filter, that cannot be compensated to yield better performance results. This also holds for the RBPf and the Hybrid 2 method. It can be further observed that the IMM-EKF provides the best results for all three methods. The MM-PF and MM-RBPf achieve slightly worse results for  $N = 8000$ . The MM-RBPf is always better than the MM-PF, which is a result of the increased state dimension, the MM-PF has to deal with. It can be further noticed that by increasing the number of particles in these filters, the performance can be improved. It is expected that a performance similar to the IMM-EKF can be obtained, by further increasing the number of particles beyond values of  $N = 8000$ . Another option is to consider a different mode-conditioned importance density in these filters, cf. (5.62) and (5.100), that takes into account the latest measurement. With this strategy it is expected that a good approximation of the posterior pdf can be obtained by using a fewer number of particles. In Fig. 5.5 the MT location  $\overline{\text{RMSE}}$  in m vs.

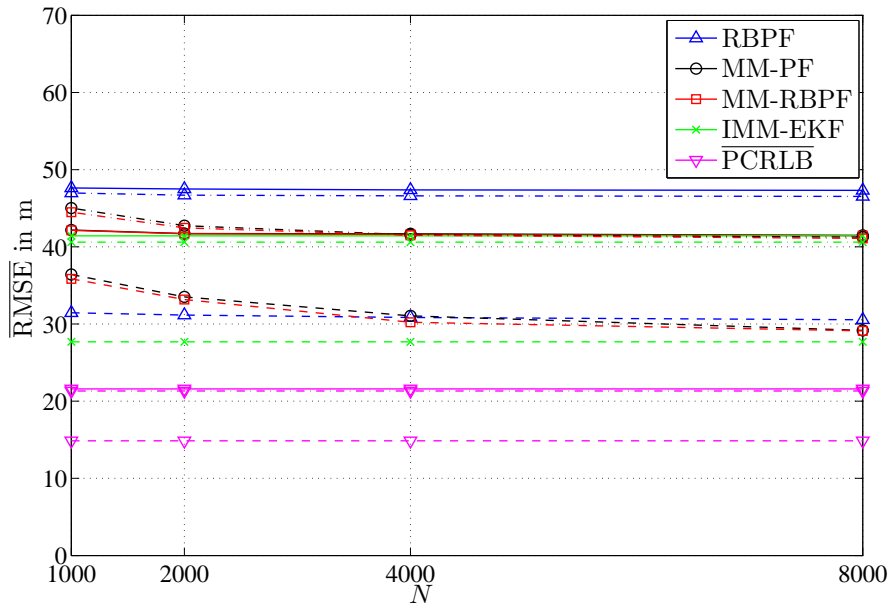


Figure 5.4. MT location  $\overline{\text{RMSE}}$  vs. particle number  $N$  for MM-PF, MM-RBPF, RBPF, IMM-EKF and  $\overline{\text{PCRLB}}$  assuming LOS propagation conditions, solid lines: Cellular method, dash-dotted lines: Hybrid 1 method, dashed lines: Hybrid 2 method.

particle number  $N$  for the Cellular, Hybrid 1 and Hybrid 2 methods are shown for the MM-PF, MM-RBPF, PF and RBPF with road constraints. It can be noticed that the performance results for the different filters do not significantly change for different numbers of particles. Thus, it is not necessary to use a large number of particles in these filters, since acceptable results can be already obtained with  $N = 1000$  particles. The multiple model-based estimators generally outperform the PF and RBPF, due to the mismatch of statistics inherent in the PF and RBPF. However, for the Hybrid 2 method, the performance of the different filters is practically equivalent. The reason for this result is that the performance is dominated by the information available from the PR measurements and the road, and less influenced by the mismatch of the statistics that is related to the RSS and RTT measurements. In Fig. 5.6, the MT location  $\overline{\text{RMSE}}$  in m vs. GDOP for the Hybrid 3 method are shown for the MM-PF, MM-RBPF, RBPF with and without road constraints using  $N = 8000$  particles, together with the IMM-EKF and corresponding  $\overline{\text{PCRLBs}}$ . Note that for comparison purposes the performance of the RBPF with and without road constraints for the Satellite method is also shown. It can be seen that the Hybrid 3 method yields large performance improvements for large GDOP values, as long as no road constraints are considered in the filters. In this case, the IMM-EKF and RBPF yield the best performance. The performance is slightly worse for the MM-PF and MM-RBPF. The performance differences can be

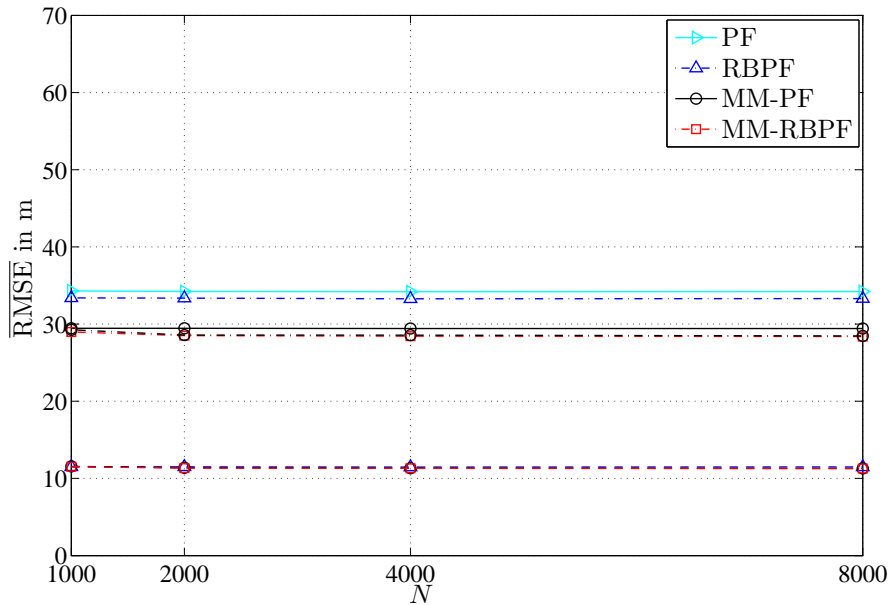


Figure 5.5. MT location  $\overline{\text{RMSE}}$  vs. particle number  $N$  for PF, RBPF, MM-PF and MM-RBPF with road constraints assuming LOS propagation conditions, solid lines: Cellular method, dash-dotted lines: Hybrid 1 method, dashed lines: Hybrid 2 method.

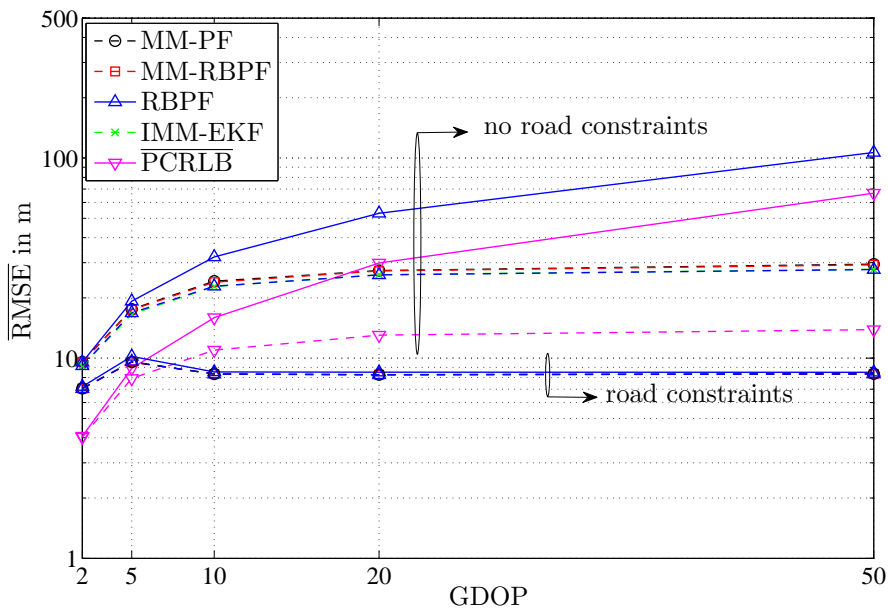


Figure 5.6. MT location  $\overline{\text{RMSE}}$  vs. GDOP for MM-PF, MM-RBPF, RBPF, IMM-EKF and  $\overline{\text{PCRLB}}$  assuming LOS propagation conditions, solid lines: Satellite method, dashed lines: Hybrid 3 method.

explained by the fact that the dimension of the augmented state vector in the multiple model-based estimators is generally larger than the dimension of the state vector in the RBPF. Thus, in the multiple model-based estimators a large number of particles is required to obtain a good approximation of the posterior pdf. Even though there is an intentional mismatch between the statistics with which the measurements have been generated and the statistics used in the RBPF, this has less influence on its performance in the LOS case, since three very accurate pseudorange measurements are available. For the RBPF, MM-PF and MM-RBPF with road constraints, significant performance improvements can be obtained. Using the Hybrid 3 method rather than the Satellite method will yield only small improvements, which is true for all tested GDOP values.

### 5.6.2.2 Simulation Results for Propagation conditions that switch between LOS and NLOS

In this section, the performance of the IMM-based algorithm and multiple model-based algorithms introduced in Sections 5.4 and 5.5 is evaluated for the different combinations of measurements of Scenario II assuming switching LOS/NLOS propagation conditions, cf. Section 2.3.4.3. The E-PCRLB and M-PCRLB are computed for the different combinations of measurements to indicate the best possible performance that one can expect for the given scenario and set of parameters. All filters are initialized using the strategy explained in Section 4.6.2.1. The parameters included in the mode-dependent measurement model  $\mathbf{h}_k(\mathbf{x}_k, r_k)$ , the parameters of the Markov chain, as well as the noise statistics given by the mode-dependent mean vector  $\boldsymbol{\mu}_k(r_k)$  and covariance matrices  $\mathbf{R}_k(r_k)$  and  $\mathbf{Q}$  are chosen for the algorithms as in Section 5.6.2.1. The computation of the E-PCRLB and M-PCRLB follows the same strategy as described in Section 4.6.2.1.

In Fig. 5.7, the E-PCRLB and M-PCRLB on the MT location RMSE in m vs. time index  $k$  for the Cellular, Hybrid 1 and Hybrid 2 are shown. The bounds have been calculated using  $N_{MC} = 10000$  mode sequences/samples. It can be noticed that the E-PCRLB is lower than the M-PCRLB for all three methods. The reason for this can be explained by the fact that in the computation of the E-PCRLB, the mode sequence is explicitly known, while in the calculation of the M-PCRLB it is not. In Figs. 5.8, 5.9 and 5.10, the MT location RMSEs in m vs. the time index  $k$  for the Cellular, Hybrid 1 and Hybrid 2 methods are shown for the PF, RBPF, MM-PF and MM-RBPF using  $N = 8000$  particles, together with the corresponding IMM-EKF and M-PCRLBs. Note that the likelihood pdf of the PF and RBPF is given by (3.83). From these results, the same conclusions as those for the case of LOS propagation conditions



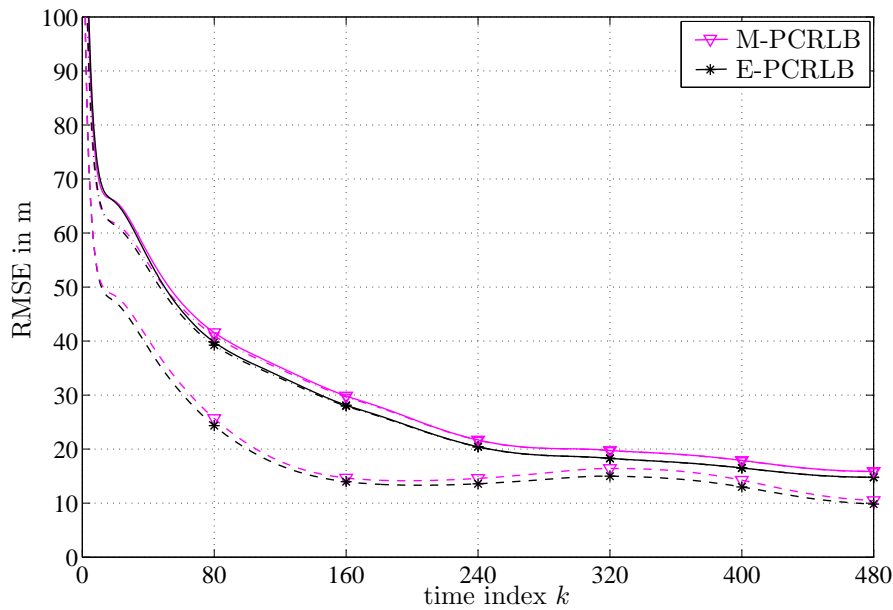


Figure 5.7. MT location RMSE vs. time index  $k$  for E-PCRLB and M-PCRLB, solid lines: Cellular method, , dash-dotted lines: Hybrid 1 method, dashed lines: Hybrid 2 method.

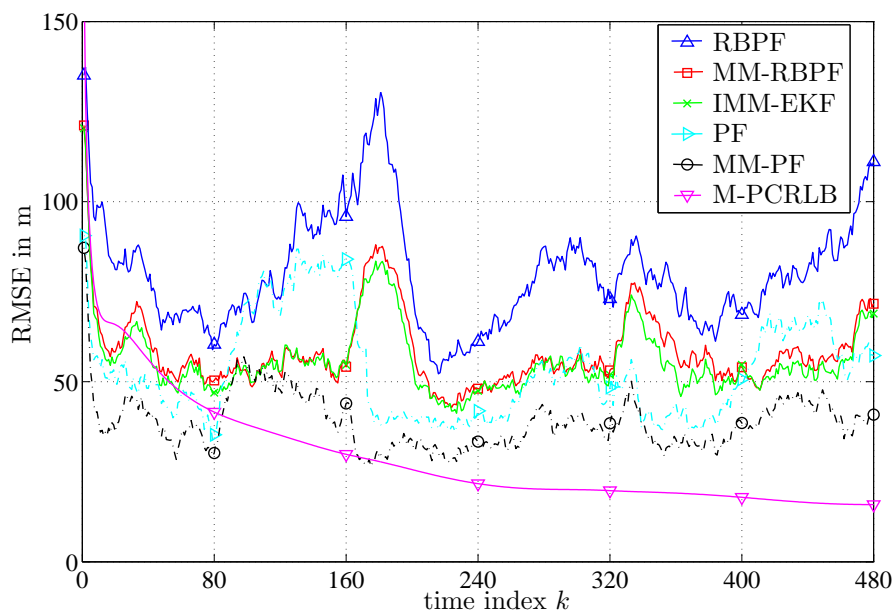


Figure 5.8. MT location RMSE vs. time index  $k$  for RBPF, MM-RBPF, IMM-EKF and M-PCRLB assuming switching LOS/NLOS propagation conditions and Cellular method, solid lines: No road constraints, dashed lines: Road constraints.

can be drawn. It can be further observed that compared to the LOS case, the RMSEs for the different methods are larger. On the one hand, this can be explained by the fact that in NLOS situations, the measurement noise is larger, which leads to the inferior performance. On the other hand, compared to the LOS scenario, this scenario is much more challenging, since the filters have to adapt themselves continuously to the switching LOS/NLOS propagation conditions. It is expected that the performance of all PF-based estimators can be improved by including the latest measurement into the corresponding importance density. In Fig. 5.11, the MT location  $\overline{\text{RMSE}}$  in m vs. GDOP for the Hybrid 3 method are shown for the MM-PF, MM-RBPF, RBPF with and without road constraints using  $N = 8000$  particles, together with the IMM-EKF and corresponding  $\overline{\text{M-PCRLB}}$ s. Note that for comparison purposes the performance of the RBPF with and without road constraints for the Satellite method is also shown. From these results, the same conclusions can be drawn as those for the case of LOS propagation conditions. It can be further observed that compared to the LOS case, the RMSEs for the estimators without road constraints are larger, while for the PF-based estimators with road constraints the RMSEs are practically equivalent.

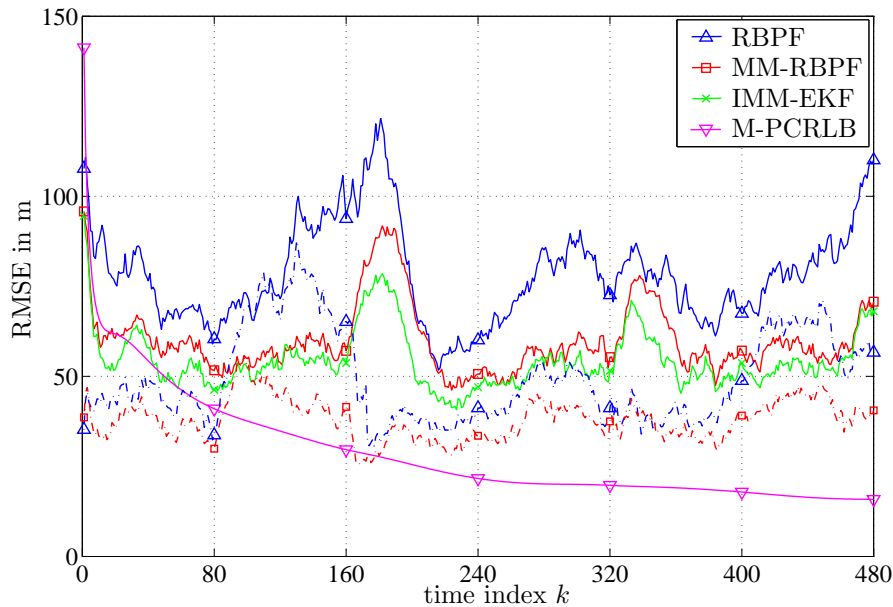


Figure 5.9. MT location RMSE vs. time index  $k$  for RBPF, MM-RBPF, IMM-EKF and M-PCRLB assuming switching LOS/NLOS propagation conditions and Hybrid 1 method, solid lines: No road constraints, dashed lines: Road constraints.

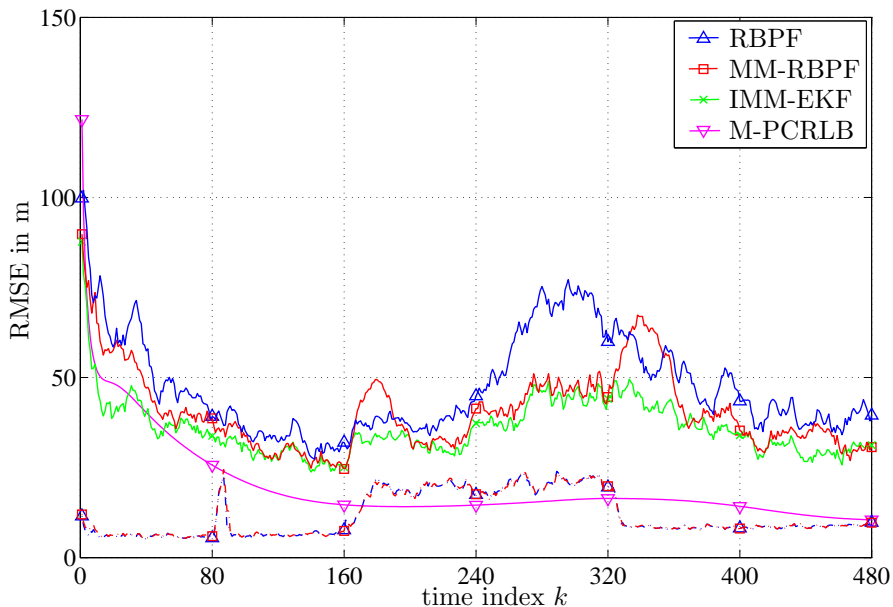


Figure 5.10. MT location RMSE vs. time index  $k$  for RBPf, MM-RBPf, IMM-EKF and M-PCRLB assuming switching LOS/NLOS propagation conditions and Hybrid 2 method, solid lines: No road constraints, dashed lines: Road constraints.

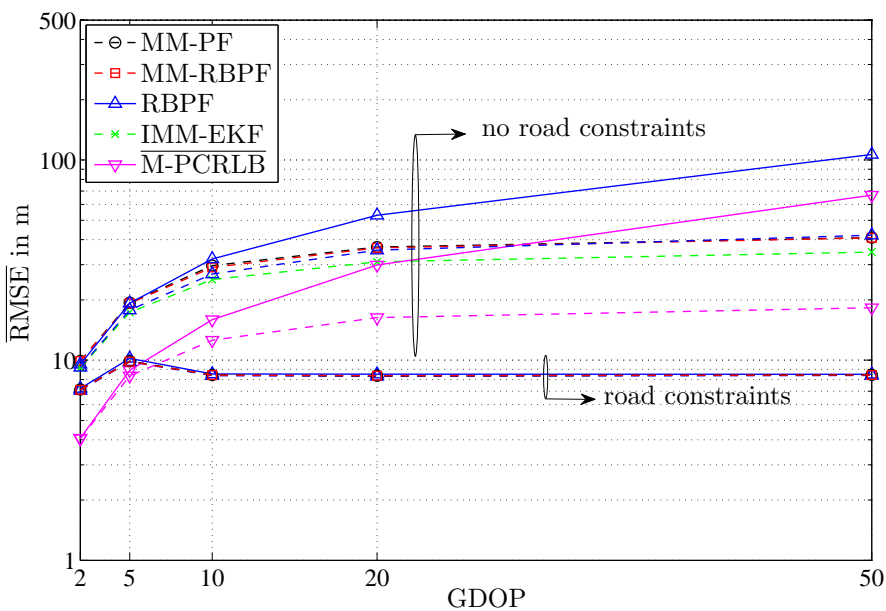


Figure 5.11. MT location  $\overline{\text{RMSE}}$  vs. GDOP for MM-PF, MM-RBPf, RBPf, IMM-EKF and M-PCRLB assuming switching LOS/NLOS propagation conditions, solid lines: Satellite method, dashed lines: Hybrid 3 method.

### 5.6.3 Comments on Computational Complexity

In this section, comments are given on the computational complexity of the different algorithms, which have been introduced in this chapter. The computational complexity of the IMM-EKF grows exponentially with  $s = 2^{N_{BS}}$ . Thus, this algorithm is especially useful in situations, where  $N_{BS}$  is small. Since in the algorithm,  $2^{N_{BS}}$  are operated in parallel, the computational complexity of the IMM-EKF is roughly  $2^{N_{BS}}$ -times larger than the conventional EKF, cf. Section 4.6.4. The multiple model PF-based estimators are generally orders of magnitudes more complex than the IMM-EKF. In terms of execution time, a large amount of time is spent in the PF-based estimators to generate random variables, which scales with the number of particles  $N$  [KSG05]. Comparing the computational complexity of the MM-PF with the MM-RBPF, cf. Algorithm 5.3 and 5.5, it can be concluded that for a given number  $N$  of particles, the MM-RBPF is generally more complex than the MM-PF, since in the MM-RBPF for each particle an KF time update and measurement update step has to be performed, which may considerably increase the computational complexity. The MM-PF and MM-RBPF are generally more complex than the corresponding PF and RBPF, since in the PF and RBPF the generation of realizations of the mode variable can be omitted.

## 5.7 Conclusions

In this chapter, the hybrid localization problem has been reformulated as an adaptive recursive state estimation problem, where the switching between LOS and NLOS propagation conditions has been modeled in the estimator with a Markov chain. Three different estimators, namely the IMM-EKF, MM-PF and MM-RBPF have been proposed to solve the hybrid localization problem and have been compared to the PF and RBPF proposed in Chapter 4. The MM-RBPF has been newly derived for the general, mode-dependent, conditional linear system model, cf. (5.66). Road constraints have been incorporated into the MM-PF and MM-RBPF to further improve the performance. The performance of the different algorithms has been compared to the theoretically best achievable performance, which is given by the PCRLB. Two different bounds have been calculated, namely the E-PCRLB and the newly proposed M-PCRLB. All presented hybrid localization algorithms have been extensively analyzed in terms of performance and comments on the complexity are given. If it is not otherwise stated, the following main conclusions hold for both cases assuming LOS and switching LOS/NLOS propagation conditions:

- 
- For switching LOS/NLOS propagation conditions and all investigated methods, the E-PCRLBs are lower than the M-PCRLBs.
  - The proposed IMM-based algorithms and multiple model-based algorithms cannot achieve the corresponding M-PCRLBs.
  - For the case of having no road information available, the IMM-EKF provides the best trade-off between complexity and performance.
  - For the case of having no road information available, a relatively large number of particles is required in the MM-PF and MM-RBPF to obtain a performance similar to the IMM-EKF.
  - Significantly performance improvements can be achieved for all investigated methods by incorporating road-constraints into the MM-PF and MM-RBPF.
  - The MM-RBPF always outperforms the MM-PF. The achievable performance gains strongly depend on the dimension of the state space and the number of particles used in the corresponding filters.



---

## Chapter 6

### Conclusions

This thesis deals with the problem of finding the location of an MT by using PR measurements from GPS and RTT, RSS and GRT measurements from GSM, which is termed hybrid localization problem. The signals from the cellular radio network are assumed to be further affected by interferences due to NLOS propagation, which can severely affect the localization accuracy of the corresponding algorithms. Several new localization algorithms based on statistical data fusion are proposed in this thesis to solve the hybrid localization problem for the case of LOS propagation conditions as well as for NLOS propagation conditions.

In order to analyze the hybrid localization algorithms, a mathematical framework is introduced in Chapter 2 that describes the hybrid localization scenario. The hybrid localization scenario is further decomposed into the simulations and the field trial. In the former, models for the MT movement and clock, as well as models for the measurements assuming LOS and NLOS propagation conditions are introduced, so that MT trajectories and measurements can be generated artificially. In the latter, the MT movement as well as the measurements from the cellular radio network are available from a field trial, which was performed in an operating GSM network.

In Chapter 3, hybrid localization algorithms based on the ML principle have been derived that do not take into account temporal dependencies between MT states and between measurements. The corresponding ML estimators have been derived for measurements affected by LOS propagation conditions as well as for measurements affected by switching LOS/NLOS propagation conditions. For both cases, suboptimal algorithms are proposed to numerically obtain ML estimates. The performance of these algorithms has been compared to the CRLB, which has been determined for measurements affected by LOS propagation conditions as well as propagation conditions that switch between LOS and NLOS. The algorithms have been applied to simulated data as well as data available from a field trial, and the performance of the algorithms has been analyzed in terms of MT location RMSE and time averaged MT location RMSE. The results have shown that additionally taking into account PR measurements from GPS and GRT from GSM in the algorithms can significantly improve the localization accuracy compared to algorithms that only take into account RTT and RSS measurements from GSM. It has been further proven that additionally taking into account only one PR measurement from GPS cannot improve the localization accuracy.

The case where temporal dependencies are taken into account in the hybrid localization algorithms is treated in Chapter 4. In these algorithms, models describing the MT movement and clock have been taken into account to further improve the localization accuracy. KF-based estimators and PF-based estimators are introduced to solve the hybrid localization problem. KF-based estimators are proposed for the case that measurements are affected by LOS propagation conditions. The PF-based estimators have been derived for the case that measurements are affected by LOS propagation conditions as well as switching LOS/NLOS propagation conditions. Road constraints have been incorporated into the PF-based estimators to further improve the localization accuracy. The performance of these algorithms has been compared to the PCRLB, which has been determined for measurements affected by LOS propagation conditions as well as switching LOS/NLOS propagation conditions. The results have shown that PF-based estimators with road constraints generally outperform KF-based estimators and PF-based estimators that do not take into account road constraints. In scenarios, where the measurements are affected by LOS propagation conditions, the analysis of the results revealed that the best trade-off between performance and computational complexity was achieved by the EKF.

Since the switching between LOS propagation conditions and NLOS propagation conditions is expected to have a significant impact on the achievable performance of the hybrid localization algorithms, this issue has been further addressed in Chapter 5. The IMM-EKF-based estimator and two different multiple model PF-based estimators are introduced to solve the hybrid localization problem. These algorithms take into account models for the MT movement and clock, and model the switching between LOS and NLOS propagation conditions with a Markov chain. Road constraints have been incorporated into the PF-based estimators to further improve the localization accuracy. The performance of these algorithms has been compared to the PCRLB, which has been calculated using two different approaches. The results have shown that multiple model PF-based estimators with road constraints generally outperform the IMM-EKF and the multiple model PF-based estimators that do not take into account road constraints. When road constraints are not considered in the algorithms, the IMM-EKF achieves the best trade-off between performance and computational complexity.



# Appendix

## A.1 Coordinate Transformations for Hybrid Localization

### A.1.1 Introduction

In this section, the transformations between different coordinate systems is presented [RAG04, GWA07]. In general, three coordinate systems are involved when hybrid localization algorithms are applied to real data: the geodetic coordinate system, the ECEF coordinate system and the ENU coordinate system. Since the transformation between the geodetic coordinates and the ENU coordinates is done via the ECEF coordinates, only two different transformations have to be considered in the following. The transformation from geodetic coordinates to ECEF coordinates, which is described in Section A.1.2, and the transformation from ECEF coordinates to ENU coordinates, which is described in Section A.1.3.

### A.1.2 Transformation from Geodetic Coordinates to ECEF Coordinates

In this section, the transformation from geodetic coordinates to ECEF coordinates is explained. In the geodetic coordinate system, the Earth's surface is modeled by an ellipsoid, hereinafter called the reference ellipsoid. The parameters that completely describe the reference ellipsoid are the semi-major axis  $a_{\text{geo}}$  and the semi-minor axis  $b_{\text{geo}}$ , which are dependent on the underlying geodetic system. In the following, the parameters of the World Geodetic System 1984 (WGS-84) are used, since this is the geodetic system that describes the reference coordinate system used by GPS. The corresponding parameters for the WGS-84, are  $a_{\text{geo}} = 6378137\text{ m}$  and  $b_{\text{geo}} = 6356752.314245\text{ m}$ , respectively.

In the WGS-84, the coordinate origin is located at the Earth's center of mass. Locations near the reference ellipsoid are described in terms of latitude  $\lambda_{\text{geo}}$ , longitude  $\phi_{\text{geo}}$  and altitude  $h_{\text{geo}}$  above the reference ellipsoid. The latitude defines the angular distance between the Equator and points north or south of it on the Earth's surface. The latitude is counted counterclockwise and ranges from  $0^\circ$  at the Equator to  $\pm 90^\circ$  at the poles. The longitude defines the angular distance between the Prime Meridian and

points east or west of it on the Earth's surface. The longitude is counted counterclockwise and ranges from  $0^\circ$  at the Prime Meridian to  $180^\circ$  eastward and  $-180^\circ$  westward. The ECEF coordinate system is closely related to the geodetic coordinate system. The ECEF coordinate system is a Cartesian coordinate system, and a point in ECEF coordinates is described by the vector  $\mathbf{x}_{\text{ECEF}} = [x_{\text{ECEF}}, y_{\text{ECEF}}, z_{\text{ECEF}}]^\top$ . The ECEF coordinate system rotates with Earth and its origin is located at the mass center of the Earth. The  $x_{\text{ECEF}}$ -axis intersects the reference ellipsoid at the Prime Meridian ( $0^\circ$  longitude) and the Equator ( $0^\circ$  latitude). The  $z_{\text{ECEF}}$ -axis is defined to coincide with the earth rotational axis and is pointing towards the North Pole. The  $y_{\text{ECEF}}$ -axis passes through the Equator at  $90^\circ$  longitude and completes the right-handed coordinate system. For the sake of clarity, the basic relationships between the geodetic coordinate system and the ECEF coordinate system are depicted in Fig. A.1. Let  $e_{\text{geo}} = \sqrt{1 - b_{\text{geo}}^2/a_{\text{geo}}^2}$  denote the eccentricity of the reference ellipsoid and let  $N_{\text{geo}}$  denote the radius of curvature in prime vertical, which is given by

$$N_{\text{geo}} = \frac{a}{\sqrt{1 - e_{\text{geo}}^2 \cdot \sin^2(\lambda_{\text{geo}})}}. \quad (\text{A.1})$$

Then, the coordinate transformations from geodetic to ECEF coordinates are as follows

$$x_{\text{ECEF}} = [N_{\text{geo}} + h_{\text{geo}}] \cdot \cos(\lambda_{\text{geo}}) \cdot \cos(\phi_{\text{geo}}), \quad (\text{A.2})$$

$$y_{\text{ECEF}} = [N_{\text{geo}} + h_{\text{geo}}] \cdot \cos(\lambda_{\text{geo}}) \cdot \sin(\phi_{\text{geo}}), \quad (\text{A.3})$$

$$z_{\text{ECEF}} = [(1 - e_{\text{geo}}^2) \cdot N_{\text{geo}} + h_{\text{geo}}] \cdot \sin(\lambda_{\text{geo}}). \quad (\text{A.4})$$

### A.1.3 Transformation from ECEF Coordinates to ENU Coordinates

In this section, the transformation from ECEF coordinates to ENU coordinates is explained. The ENU coordinate system is a local Cartesian coordinate system, and a point in ENU coordinates is described by the vector  $\mathbf{x}_{\text{ENU}} = [x_{\text{ENU}}, y_{\text{ENU}}, z_{\text{ENU}}]^\top$ . The ENU coordinate system is determined by the fitting of a tangent plane to the Earth's surface at a fixed reference point, where the reference point is the origin of the local ENU coordinate system. The  $x_{\text{ENU}}$ -axis points to true east, the  $y_{\text{ENU}}$ -axis points north, and  $z_{\text{ENU}}$ -axis points up, in order to complete the right-handed coordinate system. For the sake of clarity, the basic relationships between the ECEF coordinate system and the ENU coordinate system are depicted in Fig. A.1. Let the reference point in ECEF coordinates be given by the vector  $\mathbf{x}_{\text{ECEF},0}$  and let the rotation matrix for the conversion of ECEF coordinates to ENU coordinates be given by

$$\mathbf{M} = \begin{bmatrix} \sin(\phi_{\text{geo}}) & \cos(\phi_{\text{geo}}) & 0 \\ -\sin(\lambda_{\text{geo}}) \cos(\phi_{\text{geo}}) & -\sin(\lambda_{\text{geo}}) \sin(\phi_{\text{geo}}) & \cos(\lambda_{\text{geo}}) \\ \cos(\lambda_{\text{geo}}) \cos(\phi_{\text{geo}}) & \cos(\lambda_{\text{geo}}) \sin(\phi_{\text{geo}}) & \sin(\lambda_{\text{geo}}) \end{bmatrix}. \quad (\text{A.5})$$

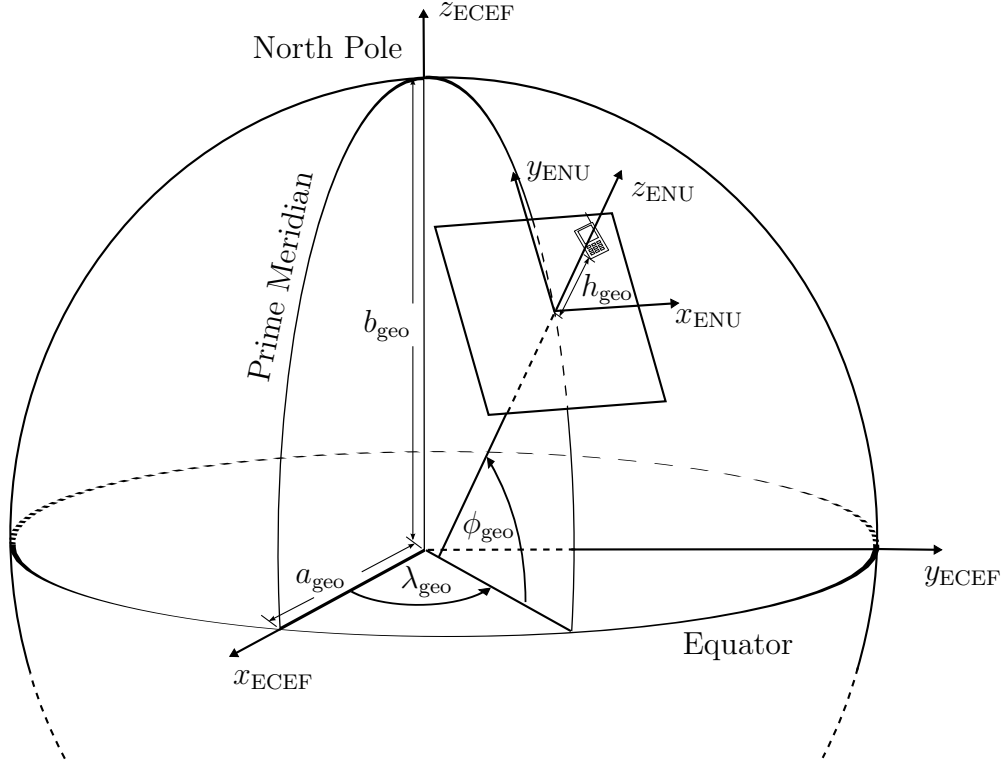


Figure A.1. Relationship between Geodetic coordinate system, ENU coordinate system and ECEF coordinate system.

Then, the coordinate transformations from ECEF coordinates to ENU coordinates are as follows

$$\mathbf{x}_{\text{ENU}} = \mathbf{M} \cdot (\mathbf{x}_{\text{ECEF}} - \mathbf{x}_{\text{ECEF},0}). \quad (\text{A.6})$$

## A.2 Derivation of (3.19) describing the FIM for measurements corrupted by zero-mean Gaussian errors

In this section, the FIM for measurements corrupted by zero-mean Gaussian distributed errors is determined, since it forms the basis of determining the FIMs for PR, RTT and RSS measurements in LOS propagation conditions. The general expression for the FIM is given by

$$\mathcal{F}(\mathbf{x}_k) = \mathbb{E}_{p(\mathbf{z}_k|\mathbf{x}_k)} \{ [\nabla_{\mathbf{x}_k} \log_e p(\mathbf{z}_k|\mathbf{x}_k)] [\nabla_{\mathbf{x}_k} \log_e p(\mathbf{z}_k|\mathbf{x}_k)]^T \}, \quad (\text{A.7})$$

[Kay93]. For measurement models of the form (2.9), the above expression can be decomposed using the chain rule [LC98]. Let

$$\tilde{\mathbf{H}}_k(\mathbf{x}_k) = \begin{bmatrix} \frac{\partial h_k^{(1)}(\mathbf{x}_k)}{\partial x_k^{(1)}} & \frac{\partial h_k^{(1)}(\mathbf{x}_k)}{\partial x_k^{(2)}} & \cdots & \frac{\partial h_k^{(1)}(\mathbf{x}_k)}{\partial x_k^{(n_x)}} \\ \frac{\partial h_k^{(2)}(\mathbf{x}_k)}{\partial x_k^{(1)}} & \frac{\partial h_k^{(2)}(\mathbf{x}_k)}{\partial x_k^{(2)}} & \cdots & \frac{\partial h_k^{(2)}(\mathbf{x}_k)}{\partial x_k^{(n_x)}} \\ \vdots & \vdots & \ddots & \vdots \\ \frac{\partial h_k^{(n_z)}(\mathbf{x}_k)}{\partial x_k^{(1)}} & \frac{\partial h_k^{(n_z)}(\mathbf{x}_k)}{\partial x_k^{(2)}} & \cdots & \frac{\partial h_k^{(n_z)}(\mathbf{x}_k)}{\partial x_k^{(n_x)}} \end{bmatrix}. \quad (\text{A.8})$$

denote the Jacobian matrix of  $\mathbf{h}_k(\mathbf{x}_k)$  evaluated at the true state vector  $\mathbf{x}_k$ . Let further  $\mathcal{F}(\mathbf{h}_k(\mathbf{x}_k))$  denote the FIM for the  $n_z$ -vector function  $\mathbf{h}_k(\mathbf{x}_k)$ . Then, the FIM can be determined from the chain rule

$$\mathcal{F}(\mathbf{x}_k) = \tilde{\mathbf{H}}_k^\top(\mathbf{x}_k) \cdot \mathcal{F}(\mathbf{h}_k(\mathbf{x}_k)) \cdot \tilde{\mathbf{H}}_k(\mathbf{x}_k), \quad (\text{A.9})$$

[LC98]. Here, it is worth noting that the application of the chain rule is independent of the assumption on the pdf of the errors  $p_{\mathbf{v}_k}(\mathbf{v}_k)$ . For the measurement model assuming LOS propagation conditions, cf. (2.50), the errors are zero-mean Gaussian distributed, so that  $\mathcal{F}(\mathbf{h}_{\text{LOS},k}(\mathbf{x}_k)) = \mathbf{R}_{\text{LOS},k}^{-1}$  holds [Kay93]. If the errors are further assumed mutually independent, this matrix reduces to a diagonal matrix and is given by

$$\mathcal{F}(\mathbf{h}_{\text{LOS},k}(\mathbf{x}_k)) = \mathbf{R}_{\text{LOS},k}^{-1} = \text{diag}[\sigma_{\text{LOS},k}^{(1),-2}, \dots, \sigma_{\text{LOS},k}^{(n_z),-2}]. \quad (\text{A.10})$$

The  $(i, j)$ -th element of  $\mathcal{F}(\mathbf{x}_k)$  is, thus, given by

$$[\mathcal{F}(\mathbf{x}_k)]_{(i,j)} = \sum_{\nu=1}^{n_z} \sigma_{\text{LOS},k}^{(\nu),-2} \cdot \left[ \frac{\partial h_{\text{LOS},k}^{(\nu)}(\mathbf{x}_k)}{\partial x_k^{(i)}} \cdot \frac{\partial h_{\text{LOS},k}^{(\nu)}(\mathbf{x}_k)}{\partial x_k^{(j)}} \right], \quad i, j = 1, \dots, n_x. \quad (\text{A.11})$$

### A.3 Derivation of (3.23) describing the FIM for PR measurements

In this section, the derivation of the FIM  $\mathcal{F}_{\text{PR}}(\tilde{\mathbf{x}}_k)$  for the PR measurements given by (3.23) is sketched. The Jacobian matrix  $\mathbf{H}_{\text{PR},k}(\tilde{\mathbf{x}}_k)$  for the  $M_{\text{PR}}$  PR measurements can be found from inserting (2.20) into (A.8). The elements of the Jacobian matrix

$\mathbf{H}_{\text{PR},k}(\tilde{\mathbf{x}}_k)$  are given by

$$\frac{\partial h_{\text{PR},k}^{(m)}(\mathbf{x}_{\text{MT},k}, c_0 \cdot \delta t_k)}{\partial x_{\text{MT},k}} = \frac{x_{\text{MT},k} - x_{\text{SAT},k}^{(m)}}{d_{\text{SAT},k}^{(m)}(\mathbf{x}_{\text{MT},k})} = u_{\text{SAT},k}^{(m)}, \quad (\text{A.12a})$$

$$\frac{\partial h_{\text{PR},k}^{(m)}(\mathbf{x}_{\text{MT},k}, c_0 \cdot \delta t_k)}{\partial y_{\text{MT},k}} = \frac{y_{\text{MT},k} - y_{\text{SAT},k}^{(m)}}{d_{\text{SAT},k}^{(m)}(\mathbf{x}_{\text{MT},k})} = u_{\text{SAT},k}^{(m)}, \quad (\text{A.12b})$$

$$\frac{\partial h_{\text{PR},k}^{(m)}(\mathbf{x}_{\text{MT},k}, c_0 \cdot \delta t_k)}{\partial (c_0 \cdot \delta t_k)} = 1, \quad (\text{A.12c})$$

where  $m = 1, \dots, M_{\text{PR}}$ . Let  $\mathbf{H}_{\text{PR}}$  denote the Jacobian matrix of the MT location vector  $\mathbf{x}_{\text{MT},k}$ , which is given by

$$\mathbf{H}_{\text{PR}} = \begin{bmatrix} \frac{\partial h_{\text{PR},k}^{(1)}(\tilde{\mathbf{x}}_k)}{\partial x_{\text{MT},k}} & \frac{\partial h_{\text{PR},k}^{(1)}(\tilde{\mathbf{x}}_k)}{\partial y_{\text{MT},k}} \\ \frac{\partial h_{\text{PR},k}^{(2)}(\tilde{\mathbf{x}}_k)}{\partial x_{\text{MT},k}} & \frac{\partial h_{\text{PR},k}^{(2)}(\tilde{\mathbf{x}}_k)}{\partial y_{\text{MT},k}} \\ \vdots & \vdots \\ \frac{\partial h_{\text{PR},k}^{(M_{\text{PR}})}(\tilde{\mathbf{x}}_k)}{\partial x_{\text{MT},k}} & \frac{\partial h_{\text{PR},k}^{(M_{\text{PR}})}(\tilde{\mathbf{x}}_k)}{\partial y_{\text{MT},k}} \end{bmatrix}. \quad (\text{A.13})$$

Then, the Jacobian matrix  $\mathbf{H}_{\text{PR},k}(\tilde{\mathbf{x}}_k)$  of the vector  $\tilde{\mathbf{x}}_k$  can be partitioned as follows

$$\mathbf{H}_{\text{PR},k}(\tilde{\mathbf{x}}_k) = \left[ \mathbf{H}_{\text{PR}} \mid \mathbf{1}_{M_{\text{PR}} \times 1} \right], \quad (\text{A.14})$$

where  $\mathbf{1}_{M_{\text{PR}} \times 1}$  denotes the all-ones vector of size  $M_{\text{PR}} \times 1$ . Let  $\mathbf{\Lambda}_{\text{PR}}$  denote the FIM  $\mathcal{F}(\mathbf{h}_{\text{PR},k}(\tilde{\mathbf{x}}_k))$ , which is given by

$$\mathbf{\Lambda}_{\text{PR}} = \text{diag}[\sigma_{\text{PR},k}^{(1),-2}, \dots, \sigma_{\text{PR},k}^{(M_{\text{PR}}),-2}]. \quad (\text{A.15})$$

Then, the FIM  $\mathcal{F}_{\text{PR}}(\tilde{\mathbf{x}}_k)$  can be found from inserting (A.14) and (A.15) into (A.9) yielding

$$\mathcal{F}_{\text{PR}}(\tilde{\mathbf{x}}_k) = \begin{bmatrix} \mathbf{H}_{\text{PR}}^{\text{T}} \mathbf{\Lambda}_{\text{PR}} \mathbf{H}_{\text{PR}} & \mathbf{H}_{\text{PR}}^{\text{T}} \mathbf{\Lambda}_{\text{PR}} \mathbf{1}_{M_{\text{PR}} \times 1} \\ \mathbf{1}_{M_{\text{PR}} \times 1}^{\text{T}} \mathbf{\Lambda}_{\text{PR}} \mathbf{H}_{\text{PR}} & \mathbf{1}_{M_{\text{PR}} \times 1}^{\text{T}} \mathbf{\Lambda}_{\text{PR}} \mathbf{1}_{M_{\text{PR}} \times 1} \end{bmatrix}. \quad (\text{A.16})$$

By further evaluating (A.16), the elements of the FIM can be found. These are given by

$$[\mathcal{F}_{\text{PR}}(\tilde{\mathbf{x}}_k)]_{1,1} = \sum_{m=1}^{M_{\text{PR}}} \sigma_{\text{PR},k}^{(m),-2} \cdot u_{\text{SAT}_x,k}^{(m),2}, \quad (\text{A.17a})$$

$$[\mathcal{F}_{\text{PR}}(\tilde{\mathbf{x}}_k)]_{1,2} = [\mathcal{F}_{\text{PR}}(\tilde{\mathbf{x}}_k)]_{2,1} = \sum_{m=1}^{M_{\text{PR}}} \sigma_{\text{PR},k}^{(m),-2} \cdot u_{\text{SAT}_x,k}^{(m)} \cdot u_{\text{SAT}_y,k}^{(m)}, \quad (\text{A.17b})$$

$$[\mathcal{F}_{\text{PR}}(\tilde{\mathbf{x}}_k)]_{2,2} = \sum_{m=1}^{M_{\text{PR}}} \sigma_{\text{PR},k}^{(m),-2} \cdot u_{\text{SAT}_y,k}^{(m),2}, \quad (\text{A.17c})$$

$$[\mathcal{F}_{\text{PR}}(\tilde{\mathbf{x}}_k)]_{1,3} = [\mathcal{F}_{\text{PR}}(\tilde{\mathbf{x}}_k)]_{3,1} = \sum_{m=1}^{M_{\text{PR}}} \sigma_{\text{PR},k}^{(m),-2} \cdot u_{\text{SAT}_x,k}^{(m)}, \quad (\text{A.17d})$$

$$[\mathcal{F}_{\text{PR}}(\tilde{\mathbf{x}}_k)]_{2,3} = [\mathcal{F}_{\text{PR}}(\tilde{\mathbf{x}}_k)]_{3,2} = \sum_{m=1}^{M_{\text{PR}}} \sigma_{\text{PR},k}^{(m),-2} \cdot u_{\text{SAT}_y,k}^{(m)}, \quad (\text{A.17e})$$

$$[\mathcal{F}_{\text{PR}}(\tilde{\mathbf{x}}_k)]_{3,3} = \sum_{m=1}^{M_{\text{PR}}} \sigma_{\text{PR},k}^{(m),-2}. \quad (\text{A.17f})$$

## A.4 Derivation of (3.25) describing the FIM for RTT measurements

In this section, the derivation of the FIM  $\mathcal{F}_{\text{RTT}}(\tilde{\mathbf{x}}_k)$  for the RTT measurements given by (3.25) is sketched. The Jacobian matrix  $\mathbf{H}_{\text{RTT},k}(\tilde{\mathbf{x}}_k)$  for the  $M_{\text{RTT}}$  RTT measurements can be found from inserting (2.23) into (A.8). The elements of the Jacobian matrix  $\mathbf{H}_{\text{RTT},k}(\tilde{\mathbf{x}}_k)$  are given by

$$\frac{\partial h_{\text{RTT},k}^{(m)}(\mathbf{x}_{\text{MT},k})}{\partial x_{\text{MT},k}} = \frac{x_{\text{MT},k} - x_{\text{BS},k}^{(m)}}{d_{\text{BS},k}^{(m)}(\mathbf{x}_{\text{MT},k})} = u_{\text{BS}_x,k}^{(m)}, \quad (\text{A.18a})$$

$$\frac{\partial h_{\text{RTT},k}^{(m)}(\mathbf{x}_{\text{MT},k})}{\partial y_{\text{MT},k}} = \frac{y_{\text{MT},k} - y_{\text{BS},k}^{(m)}}{d_{\text{BS},k}^{(m)}(\mathbf{x}_{\text{MT},k})} = u_{\text{BS}_y,k}^{(m)}, \quad (\text{A.18b})$$

$$\frac{\partial h_{\text{RTT},k}^{(m)}(\mathbf{x}_{\text{MT},k})}{\partial (c_0 \cdot \delta t_k)} = 0, \quad (\text{A.18c})$$

where  $m = 1, \dots, M_{\text{RTT}}$ . Let  $\mathbf{H}_{\text{RTT}}$  denote the Jacobian matrix of the MT location vector  $\mathbf{x}_{\text{MT},k}$ , which is given by

$$\mathbf{H}_{\text{RTT}} = \begin{bmatrix} \frac{\partial h_{\text{RTT},k}^{(1)}(\mathbf{x}_{\text{MT},k})}{\partial x_{\text{MT},k}} & \frac{\partial h_{\text{RTT},k}^{(2)}(\mathbf{x}_{\text{MT},k})}{\partial y_{\text{MT},k}} \\ \frac{\partial h_{\text{RTT},k}^{(1)}(\mathbf{x}_{\text{MT},k})}{\partial x_{\text{MT},k}} & \frac{\partial h_{\text{RTT},k}^{(2)}(\mathbf{x}_{\text{MT},k})}{\partial y_{\text{MT},k}} \\ \vdots & \vdots \\ \frac{\partial h_{\text{RTT},k}^{(M_{\text{RTT}})}(\mathbf{x}_{\text{MT},k})}{\partial x_{\text{MT},k}} & \frac{\partial h_{\text{RTT},k}^{(M_{\text{RTT}})}(\mathbf{x}_{\text{MT},k})}{\partial y_{\text{MT},k}} \end{bmatrix}. \quad (\text{A.19})$$

Then, the Jacobian matrix  $\mathbf{H}_{\text{RTT},k}(\tilde{\mathbf{x}}_k)$  of the vector  $\tilde{\mathbf{x}}_k$  can be partitioned as follows

$$\mathbf{H}_{\text{RTT},k}(\tilde{\mathbf{x}}_k) = \left[ \mathbf{H}_{\text{RTT}} \mid \mathbf{0}_{M_{\text{RTT}} \times 1} \right]. \quad (\text{A.20})$$

Let  $\mathbf{\Lambda}_{\text{RTT}}$  denote the FIM  $\mathcal{F}(\mathbf{h}_{\text{RTT},k}(\mathbf{x}_{\text{MT},k}))$  for the case of LOS propagation conditions, which is given by

$$\mathbf{\Lambda}_{\text{RTT}} = \text{diag}[\sigma_{\text{RTT,LOS},k}^{(1),-2}, \dots, \sigma_{\text{RTT,LOS},k}^{(M_{\text{RTT}}),-2}]. \quad (\text{A.21})$$

Then, the FIM  $\mathcal{F}_{\text{RTT}}(\tilde{\mathbf{x}}_k)$  can be found from inserting (A.20) and (A.21) into (A.9) yielding

$$\mathcal{F}_{\text{RTT}}(\tilde{\mathbf{x}}_k) = \begin{bmatrix} \mathbf{H}_{\text{RTT}}^{\text{T}} \mathbf{\Lambda}_{\text{RTT}} \mathbf{H}_{\text{RTT}} & \mathbf{0}_{2 \times 1} \\ \mathbf{0}_{1 \times 2} & 0 \end{bmatrix}. \quad (\text{A.22})$$

By further evaluating (A.22), the elements of the FIM can be found. The non-zero elements are given by

$$[\mathcal{F}_{\text{RTT}}(\tilde{\mathbf{x}}_k)]_{1,1} = \sum_{m=1}^{M_{\text{RTT}}} \sigma_{\text{RTT,LOS},k}^{(m),-2} \cdot u_{\text{BS}_x,k}^{(m),2}, \quad (\text{A.23a})$$

$$[\mathcal{F}_{\text{RTT}}(\tilde{\mathbf{x}}_k)]_{1,2} = [\mathcal{F}_{\text{RTT}}(\tilde{\mathbf{x}}_k)]_{2,1} = \sum_{m=1}^{M_{\text{RTT}}} \sigma_{\text{RTT,LOS},k}^{(m),-2} \cdot u_{\text{BS}_x,k}^{(m)} \cdot u_{\text{BS}_y,k}^{(m)}, \quad (\text{A.23b})$$

$$[\mathcal{F}_{\text{RTT}}(\tilde{\mathbf{x}}_k)]_{2,2} = \sum_{m=1}^{M_{\text{RTT}}} \sigma_{\text{RTT,LOS},k}^{(m),-2} \cdot u_{\text{BS}_y,k}^{(m),2}. \quad (\text{A.23c})$$

## A.5 Derivation of (3.28) describing the FIM for RSS measurements

In this section, the derivation of the FIM  $\mathcal{F}_{\text{RSS}}(\tilde{\mathbf{x}}_k)$  for the RSS measurements given by (3.28) is sketched. The Jacobian matrix  $\mathbf{H}_{\text{RSS},k}(\tilde{\mathbf{x}}_k)$  for the  $M_{\text{RSS}}$  RSS measurements

can be found from inserting  $\mathbf{h}_{\text{RSS,LOS},k}(\mathbf{x}_{\text{MT},k})$  defined in (2.42) into (A.8). The elements of the Jacobian matrix  $\mathbf{H}_{\text{RSS},k}(\tilde{\mathbf{x}}_k)$  are given by

$$\begin{aligned} \frac{\partial h_{\text{RSS},k}^{(m)}(\mathbf{x}_{\text{MT},k})}{\partial x_{\text{MT},k}} &= -b^{(m)} \cdot \frac{x_{\text{MT},k} - x_{\text{BS},k}^{(m)}}{[d_{\text{BS},k}^{(m)}(\mathbf{x}_{\text{MT},k})]^2} - g^{(m)} \cdot \frac{y_{\text{MT},k} - y_{\text{BS},k}^{(m)}}{[d_{\text{BS},k}^{(m)}(\mathbf{x}_{\text{MT},k})]^2} \\ &= -\frac{b^{(m)} \cdot u_{\text{BS},k}^{(m)} + g^{(m)} \cdot u_{\text{BS},k}^{(m)}}{d_{\text{BS},k}^{(m)}(\mathbf{x}_{\text{MT},k})}, \end{aligned} \quad (\text{A.24a})$$

$$\begin{aligned} \frac{\partial h_{\text{RSS},k}^{(m)}(\mathbf{x}_{\text{MT},k})}{\partial y_{\text{MT},k}} &= -b^{(m)} \cdot \frac{y_{\text{MT},k} - y_{\text{BS},k}^{(m)}}{[d_{\text{BS},k}^{(m)}(\mathbf{x}_{\text{MT},k})]^2} + g^{(m)} \cdot \frac{x_{\text{MT},k} - x_{\text{BS},k}^{(m)}}{[d_{\text{BS},k}^{(m)}(\mathbf{x}_{\text{MT},k})]^2} \\ &= -\frac{b^{(m)} \cdot u_{\text{BS},k}^{(m)} - g^{(m)} \cdot u_{\text{BS},k}^{(m)}}{d_{\text{BS},k}^{(m)}(\mathbf{x}_{\text{MT},k})}, \end{aligned} \quad (\text{A.24b})$$

$$\frac{\partial h_{\text{RSS},k}^{(m)}(\mathbf{x}_{\text{MT},k})}{\partial (c_0 \cdot \delta t_k)} = 0, \quad (\text{A.24c})$$

where  $m = 1, \dots, M_{\text{RSS}}$ . Let  $\mathbf{H}_{\text{RSS}}$  denote the Jacobian matrix of the MT location vector  $\mathbf{x}_{\text{MT},k}$ , which is given by

$$\mathbf{H}_{\text{RSS}} = \begin{bmatrix} \frac{\partial h_{\text{RSS},k}^{(1)}(\mathbf{x}_{\text{MT},k})}{\partial x_{\text{MT},k}} & \frac{\partial h_{\text{RSS},k}^{(1)}(\mathbf{x}_{\text{MT},k})}{\partial y_{\text{MT},k}} \\ \frac{\partial h_{\text{RSS},k}^{(2)}(\mathbf{x}_{\text{MT},k})}{\partial x_{\text{MT},k}} & \frac{\partial h_{\text{RSS},k}^{(2)}(\mathbf{x}_{\text{MT},k})}{\partial y_{\text{MT},k}} \\ \vdots & \vdots \\ \frac{\partial h_{\text{RSS},k}^{(M_{\text{RSS}})}(\mathbf{x}_{\text{MT},k})}{\partial x_{\text{MT},k}} & \frac{\partial h_{\text{RSS},k}^{(M_{\text{RSS}})}(\mathbf{x}_{\text{MT},k})}{\partial y_{\text{MT},k}} \end{bmatrix}. \quad (\text{A.25})$$

Then, the Jacobian matrix  $\mathbf{H}_{\text{RSS},k}(\tilde{\mathbf{x}}_k)$  of the vector  $\tilde{\mathbf{x}}_k$  can be partitioned as follows

$$\mathbf{H}_{\text{RSS},k}(\tilde{\mathbf{x}}_k) = \left[ \mathbf{H}_{\text{RSS}} \mid \mathbf{0}_{M_{\text{RSS}} \times 1} \right]. \quad (\text{A.26})$$

Let  $\mathbf{\Lambda}_{\text{RSS}}$  denote the FIM  $\mathcal{F}(\mathbf{h}_{\text{RSS,LOS},k}(\mathbf{x}_{\text{MT},k}))$  for the case of LOS propagation conditions, which is given by

$$\mathbf{\Lambda}_{\text{RSS}} = \text{diag}[\sigma_{\text{RSS,LOS},k}^{(1),-2}, \dots, \sigma_{\text{RSS,LOS},k}^{(M_{\text{RSS}}),-2}]. \quad (\text{A.27})$$

Then, the FIM  $\mathcal{F}_{\text{RSS}}(\tilde{\mathbf{x}}_k)$  can be found from inserting (A.26) and (A.27) into (A.9) yielding

$$\mathcal{F}_{\text{RSS}}(\tilde{\mathbf{x}}_k) = \begin{bmatrix} \mathbf{H}_{\text{RSS}}^T \mathbf{\Lambda}_{\text{RSS}} \mathbf{H}_{\text{RSS}} & \mathbf{0}_{2 \times 1} \\ \mathbf{0}_{1 \times 2} & 0 \end{bmatrix}. \quad (\text{A.28})$$



By further evaluating (A.28), the elements of the FIM can be found. The non-zero elements are given by

$$[\mathcal{F}_{\text{RSS}}(\tilde{\mathbf{x}}_k)]_{1,1} = \sum_{m=1}^{M_{\text{RSS}}} \sigma_{\text{RSS,LOS},k}^{(m),-2} \cdot \left[ \frac{b^{(m)} \cdot u_{\text{BSx},k}^{(m)} + g^{(m)} \cdot u_{\text{BSy},k}^{(m)}}{d_{\text{BS},k}^{(m)}(\mathbf{x}_{\text{MT},k})} \right]^2, \quad (\text{A.29a})$$

$$\begin{aligned} [\mathcal{F}_{\text{RSS}}(\tilde{\mathbf{x}}_k)]_{1,2} = [\mathcal{F}_{\text{RSS}}(\tilde{\mathbf{x}}_k)]_{2,1} &= \sum_{m=1}^{M_{\text{RSS}}} \sigma_{\text{RSS,LOS},k}^{(m),-2} \cdot \left[ \left( \frac{b^{(m)} \cdot u_{\text{BSx},k}^{(m)} + g^{(m)} \cdot u_{\text{BSy},k}^{(m)}}{d_{\text{BS},k}^{(m)}(\mathbf{x}_{\text{MT},k})} \right) \right. \\ &\quad \left. \times \left( \frac{b^{(m)} \cdot u_{\text{BSy},k}^{(m)} - g^{(m)} \cdot u_{\text{BSx},k}^{(m)}}{d_{\text{BS},k}^{(m)}(\mathbf{x}_{\text{MT},k})} \right) \right], \end{aligned} \quad (\text{A.29b})$$

$$[\mathcal{F}_{\text{RSS}}(\tilde{\mathbf{x}}_k)]_{2,2} = \sum_{m=1}^{M_{\text{RSS}}} \sigma_{\text{RSS,LOS},k}^{(m),-2} \cdot \left[ \frac{b^{(m)} \cdot u_{\text{BSy},k}^{(m)} - g^{(m)} \cdot u_{\text{BSx},k}^{(m)}}{d_{\text{BS},k}^{(m)}(\mathbf{x}_{\text{MT},k})} \right]^2. \quad (\text{A.29c})$$

## A.6 Derivation of (3.36) describing the MT location Fisher information submatrix for hybrid localization

In this section, the elements for the MT location Fisher information submatrix  $\mathcal{F}_{\text{L}}(\tilde{\mathbf{x}}_k)$  of the hybrid localization are derived. The FIM for hybrid localization can be found from inserting (A.16), (A.22), (A.28) and (3.29) into (3.20), yielding

$$\mathcal{F}(\tilde{\mathbf{x}}_k) = \left[ \begin{array}{c|c} \mathcal{F}_1(\tilde{\mathbf{x}}_k) & \mathcal{F}_2(\tilde{\mathbf{x}}_k) \\ \hline \mathcal{F}_3(\tilde{\mathbf{x}}_k) & \mathcal{F}_4(\tilde{\mathbf{x}}_k) \end{array} \right], \quad (\text{A.30})$$

where

$$\mathcal{F}_1(\tilde{\mathbf{x}}_k) = \mathbf{H}_{\text{PR}}^{\text{T}} \mathbf{\Lambda}_{\text{PR}} \mathbf{H}_{\text{PR}} + \mathbf{H}_{\text{RTT}}^{\text{T}} \mathbf{\Lambda}_{\text{RTT}} \mathbf{H}_{\text{RTT}} + \mathbf{H}_{\text{RSS}}^{\text{T}} \mathbf{\Lambda}_{\text{RSS}} \mathbf{H}_{\text{RSS}}, \quad (\text{A.31a})$$

$$\mathcal{F}_2(\tilde{\mathbf{x}}_k) = \mathbf{H}_{\text{PR}}^{\text{T}} \mathbf{\Lambda}_{\text{PR}} \mathbf{1}_{M_{\text{PR}} \times 1}, \quad (\text{A.31b})$$

$$\mathcal{F}_3(\tilde{\mathbf{x}}_k) = \mathbf{1}_{M_{\text{PR}} \times 1}^{\text{T}} \mathbf{\Lambda}_{\text{PR}} \mathbf{H}_{\text{PR}}, \quad (\text{A.31c})$$

$$\mathcal{F}_4(\tilde{\mathbf{x}}_k) = \mathbf{1}_{M_{\text{PR}} \times 1}^{\text{T}} \mathbf{\Lambda}_{\text{PR}} \mathbf{1}_{M_{\text{PR}} \times 1} + \sigma_{\text{BIAS},k}^{-2}. \quad (\text{A.31d})$$

According to (3.32), the first  $2 \times 2$  diagonal submatrix  $\mathcal{P}_1(\tilde{\mathbf{x}}_k)$  is given by

$$\begin{aligned} \mathcal{P}_1(\tilde{\mathbf{x}}_k) &= [\mathcal{F}_{\text{L}}(\tilde{\mathbf{x}}_k)]^{-1} = [\mathbf{H}_{\text{PR}}^{\text{T}} \mathbf{\Lambda}_{\text{PR}} \mathbf{H}_{\text{PR}} + \mathbf{H}_{\text{RTT}}^{\text{T}} \mathbf{\Lambda}_{\text{RTT}} \mathbf{H}_{\text{RTT}} + \mathbf{H}_{\text{RSS}}^{\text{T}} \mathbf{\Lambda}_{\text{RSS}} \mathbf{H}_{\text{RSS}} \\ &\quad - \mathbf{H}_{\text{PR}}^{\text{T}} \mathbf{\Lambda}_{\text{PR}} \mathbf{1}_{M_{\text{PR}} \times 1} [\mathbf{1}_{M_{\text{PR}} \times 1}^{\text{T}} \mathbf{\Lambda}_{\text{PR}} \mathbf{1}_{M_{\text{PR}} \times 1} + \sigma_{\text{BIAS},k}^{-2}]^{-1} \mathbf{1}_{M_{\text{PR}} \times 1}^{\text{T}} \mathbf{\Lambda}_{\text{PR}} \mathbf{H}_{\text{PR}}]^{-1}. \end{aligned} \quad (\text{A.32})$$

The elements of the matrix  $\mathcal{F}_L(\tilde{\mathbf{x}}_k)$  can be found by evaluating the expression in (A.32). These are given by

$$\begin{aligned}
[\mathcal{F}_L(\tilde{\mathbf{x}}_k)]_{1,1} &= \sum_{\kappa_1=1}^{M_{\text{PR}}} \sigma_{\text{PR},k}^{(\kappa_1),-2} \cdot u_{\text{SAT}_x,k}^{(\kappa_1),2} + \sum_{\kappa_1=1}^{M_{\text{RTT}}} \sigma_{\text{RTT,LOS},k}^{(\kappa_1),-2} \cdot u_{\text{BS}_x,k}^{(\kappa_1),2} \\
&\quad + \sum_{\kappa_1=1}^{M_{\text{RSS}}} \sigma_{\text{RSS,LOS},k}^{(\kappa_1),-2} \cdot \left[ \frac{b^{(\kappa_1)} \cdot u_{\text{BS}_x,k}^{(\kappa_1)} + g^{(\kappa_1)} \cdot u_{\text{BS}_y,k}^{(\kappa_1)}}{d_{\text{BS},k}^{(\kappa_1)}(\mathbf{x}_{\text{MT},k})} \right]^2 \\
&\quad - \left[ \sigma_{\text{BIAS},k}^{-2} + \sum_{\kappa_3=1}^{M_{\text{PR}}} \sigma_{\text{PR},k}^{(\kappa_3),-2} \right]^{-1} \sum_{\kappa_1=1}^{M_{\text{PR}}} \sum_{\kappa_2=1}^{M_{\text{PR}}} \sigma_{\text{PR},k}^{(\kappa_1),-2} \cdot \sigma_{\text{PR},k}^{(\kappa_2),-2} \cdot u_{\text{SAT}_x,k}^{(\kappa_1)} \cdot u_{\text{SAT}_x,k}^{(\kappa_2)},
\end{aligned} \tag{A.33a}$$

$$\begin{aligned}
[\mathcal{F}_L(\tilde{\mathbf{x}}_k)]_{1,2} &= \sum_{\kappa_1=1}^{M_{\text{PR}}} \sigma_{\text{PR},k}^{(\kappa_1),-2} \cdot u_{\text{SAT}_x,k}^{(\kappa_1)} \cdot u_{\text{SAT}_y,k}^{(\kappa_1)} + \sum_{\kappa_1=1}^{M_{\text{RTT}}} \sigma_{\text{RTT,LOS},k}^{(\kappa_1),-2} \cdot u_{\text{BS}_x,k}^{(\kappa_1)} \cdot u_{\text{BS}_y,k}^{(\kappa_1)} \\
&\quad + \sum_{\kappa_1=1}^{M_{\text{RSS}}} \sigma_{\text{RSS,LOS},k}^{(\kappa_1),-2} \cdot \left[ \left( \frac{b^{(\kappa_1)} \cdot u_{\text{BS}_x,k}^{(\kappa_1)} + g^{(\kappa_1)}(\mathbf{x}_{\text{MT},k}) \cdot u_{\text{BS}_y,k}^{(\kappa_1)}}{d_{\text{BS},k}^{(\kappa_1)}(\mathbf{x}_{\text{MT},k})} \right) \right. \\
&\quad \times \left. \left( \frac{b^{(\kappa_1)} \cdot u_{\text{BS}_y,k}^{(\kappa_1)} - g^{(\kappa_1)} \cdot u_{\text{BS}_x,k}^{(\kappa_1)}}{d_{\text{BS},k}^{(\kappa_1)}(\mathbf{x}_{\text{MT},k})} \right) \right] \\
&\quad - \left[ \sigma_{\text{BIAS},k}^{-2} + \sum_{\kappa_3=1}^{M_{\text{PR}}} \sigma_{\text{PR},k}^{(\kappa_3),-2} \right]^{-1} \sum_{\kappa_1=1}^{M_{\text{PR}}} \sum_{\kappa_2=1}^{M_{\text{PR}}} \sigma_{\text{PR},k}^{(\kappa_1),-2} \cdot \sigma_{\text{PR},k}^{(\kappa_2),-2} \cdot u_{\text{SAT}_x,k}^{(\kappa_1)} \cdot u_{\text{SAT}_y,k}^{(\kappa_2)} \\
&= [\mathcal{F}_L(\tilde{\mathbf{x}}_k)]_{2,1},
\end{aligned} \tag{A.33b}$$

$$\begin{aligned}
[\mathcal{F}_L(\tilde{\mathbf{x}}_k)]_{2,2} &= \sum_{\kappa_1=1}^{M_{\text{PR}}} \sigma_{\text{PR},k}^{(\kappa_1),-2} \cdot u_{\text{SAT}_y,k}^{(\kappa_1),2} + \sum_{\kappa_1=1}^{M_{\text{RTT}}} \sigma_{\text{RTT,LOS},k}^{(\kappa_1),-2} \cdot u_{\text{BS}_y,k}^{(\kappa_1),2} \\
&\quad + \sum_{\kappa_1=1}^{M_{\text{RSS}}} \sigma_{\text{RSS,LOS},k}^{(\kappa_1),-2} \cdot \left[ \frac{b^{(\kappa_1)} \cdot u_{\text{BS}_y,k}^{(\kappa_1)} - g^{(\kappa_1)} \cdot u_{\text{BS}_x,k}^{(\kappa_1)}}{d_{\text{BS},k}^{(\kappa_1)}(\mathbf{x}_{\text{MT},k})} \right]^2 \\
&\quad - \left[ \sigma_{\text{BIAS},k}^{-2} + \sum_{\kappa_3=1}^{M_{\text{PR}}} \sigma_{\text{PR},k}^{(\kappa_3),-2} \right]^{-1} \sum_{\kappa_1=1}^{M_{\text{PR}}} \sum_{\kappa_2=1}^{M_{\text{PR}}} \sigma_{\text{PR},k}^{(\kappa_1),-2} \cdot \sigma_{\text{PR},k}^{(\kappa_2),-2} \cdot u_{\text{SAT}_y,k}^{(\kappa_1)} \cdot u_{\text{SAT}_y,k}^{(\kappa_2)}.
\end{aligned} \tag{A.33c}$$

The expressions in (A.33) can be further simplified by combining the sum components that depend on the PR measurements. For  $[\mathcal{F}_L(\tilde{\mathbf{x}}_k)]_{1,1}$ , the sum component of the PR

measurement can be written as

$$\begin{aligned} \sum_{\kappa_1=1}^{M_{\text{PR}}} \sigma_{\text{PR},k}^{(\kappa_1),-2} \cdot u_{\text{SAT}_x,k}^{(\kappa_1),2} - \frac{\sum_{\kappa_1=1}^{M_{\text{PR}}} \sum_{\kappa_2=1}^{M_{\text{PR}}} \sigma_{\text{PR},k}^{(\kappa_1),-2} \cdot \sigma_{\text{PR},k}^{(\kappa_2),-2} \cdot u_{\text{SAT}_x,k}^{(\kappa_1)} \cdot u_{\text{SAT}_x,k}^{(\kappa_2)}}{\sigma_{\text{BIAS},k}^{-2} + \sum_{\kappa_3=1}^{M_{\text{PR}}} \sigma_{\text{PR},k}^{(\kappa_3),-2}} = \\ \sum_{\kappa_1=1}^{M_{\text{PR}}} e^{(\kappa_1)} \cdot u_{\text{SAT}_x,k}^{(\kappa_1),2} + \sum_{\kappa_1=1}^{M_{\text{PR}}} \sum_{\kappa_2=1}^{M_{\text{PR}}} c^{(\kappa_1,\kappa_2)} \cdot (u_{\text{SAT}_x,k}^{(\kappa_1),2} - u_{\text{SAT}_x,k}^{(\kappa_1)} \cdot u_{\text{SAT}_x,k}^{(\kappa_2)}), \end{aligned} \quad (\text{A.34})$$

where  $e^{(\kappa_1)}$  and  $c^{(\kappa_1,\kappa_2)}$  are defined in (3.35) and (3.34). For  $[\mathcal{F}_L(\tilde{\mathbf{x}}_k)]_{1,2}$ ,  $[\mathcal{F}_L(\tilde{\mathbf{x}}_k)]_{2,1}$  and  $[\mathcal{F}_L(\tilde{\mathbf{x}}_k)]_{2,2}$ , similar expressions can be found for the sum components of the PR measurement. As a result, the elements of the matrix  $\mathcal{F}_L(\tilde{\mathbf{x}}_k)$  can be rewritten as

$$\begin{aligned} [\mathcal{F}_L(\tilde{\mathbf{x}}_k)]_{1,1} = & \sum_{\kappa_1=1}^{M_{\text{PR}}} e^{(\kappa_1)} \cdot u_{\text{SAT}_x,k}^{(\kappa_1),2} + \sum_{\kappa_1=1}^{M_{\text{RTT}}} \sigma_{\text{RTT,LOS},k}^{(\kappa_1),-2} \cdot u_{\text{BS}_x,k}^{(\kappa_1),2} \\ & + \sum_{\kappa_1=1}^{M_{\text{PR}}} \sum_{\kappa_2=1}^{M_{\text{PR}}} c^{(\kappa_1,\kappa_2)} \cdot (u_{\text{SAT}_x,k}^{(\kappa_1),2} - u_{\text{SAT}_x,k}^{(\kappa_1)} \cdot u_{\text{SAT}_x,k}^{(\kappa_2)}) \\ & + \sum_{\kappa_1=1}^{M_{\text{RSS}}} \sigma_{\text{RSS,LOS},k}^{(\kappa_1),-2} \cdot \left[ \frac{b^{(\kappa_1)} \cdot u_{\text{BS}_x,k}^{(\kappa_1)} + g^{(\kappa_1)} \cdot u_{\text{BS}_y,k}^{(\kappa_1)}}{d_{\text{BS},k}^{(\kappa_1)}(\mathbf{x}_{\text{MT},k})} \right]^2, \end{aligned} \quad (\text{A.35a})$$

$$\begin{aligned} [\mathcal{F}_L(\tilde{\mathbf{x}}_k)]_{1,2} = & \sum_{\kappa_1=1}^{M_{\text{PR}}} e^{(\kappa_1)} \cdot u_{\text{SAT}_x,k}^{(\kappa_1)} \cdot u_{\text{SAT}_y,k}^{(\kappa_1)} + \sum_{\kappa_1=1}^{M_{\text{RTT}}} \sigma_{\text{RTT,LOS},k}^{(\kappa_1),-2} \cdot u_{\text{BS}_x,k}^{(\kappa_1)} \cdot u_{\text{BS}_y,k}^{(\kappa_1)} \\ & + \sum_{\kappa_1=1}^{M_{\text{PR}}} \sum_{\kappa_2=1}^{M_{\text{PR}}} c^{(\kappa_1,\kappa_2)} \cdot (u_{\text{SAT}_x,k}^{(\kappa_1)} \cdot u_{\text{SAT}_y,k}^{(\kappa_1)} - u_{\text{SAT}_y,k}^{(\kappa_1)} \cdot u_{\text{SAT}_y,k}^{(\kappa_2)}) \\ & + \sum_{\kappa_1=1}^{M_{\text{RSS}}} \sigma_{\text{RSS,LOS},k}^{(\kappa_1),-2} \cdot \left[ \left( \frac{b^{(\kappa_1)} \cdot u_{\text{BS}_x,k}^{(\kappa_1)} + g^{(\kappa_1)} \cdot u_{\text{BS}_y,k}^{(\kappa_1)}}{d_{\text{BS},k}^{(\kappa_1)}(\mathbf{x}_{\text{MT},k})} \right) \right. \\ & \left. \times \left( \frac{b^{(\kappa_1)} \cdot u_{\text{BS}_y,k}^{(\kappa_1)} - g^{(\kappa_1)} \cdot u_{\text{BS}_x,k}^{(\kappa_1)}}{d_{\text{BS},k}^{(\kappa_1)}(\mathbf{x}_{\text{MT},k})} \right) \right] = [\mathcal{F}_L(\tilde{\mathbf{x}}_k)]_{2,1}, \end{aligned} \quad (\text{A.35b})$$

$$\begin{aligned} [\mathcal{F}_L(\tilde{\mathbf{x}}_k)]_{2,2} = & \sum_{\kappa_1=1}^{M_{\text{PR}}} e^{(\kappa_1)} \cdot u_{\text{SAT}_y,k}^{(\kappa_1),2} + \sum_{\kappa_1=1}^{M_{\text{RTT}}} \sigma_{\text{RTT,LOS},k}^{(\kappa_1),-2} \cdot u_{\text{BS}_y,k}^{(\kappa_1),2} \\ & + \sum_{\kappa_1=1}^{M_{\text{PR}}} \sum_{\kappa_2=1}^{M_{\text{PR}}} c^{(\kappa_1,\kappa_2)} \cdot (u_{\text{SAT}_y,k}^{(\kappa_1),2} - u_{\text{SAT}_y,k}^{(\kappa_1)} \cdot u_{\text{SAT}_y,k}^{(\kappa_2)}) \\ & + \sum_{\kappa_1=1}^{M_{\text{RSS}}} \sigma_{\text{RSS,LOS},k}^{(\kappa_1),-2} \cdot \left[ \frac{b^{(\kappa_1)} \cdot u_{\text{BS}_y,k}^{(\kappa_1)} - g^{(\kappa_1)} \cdot u_{\text{BS}_x,k}^{(\kappa_1)}}{d_{\text{BS},k}^{(\kappa_1)}(\mathbf{x}_{\text{MT},k})} \right]^2. \end{aligned} \quad (\text{A.35c})$$

## A.7 Derivation of (3.37) describing the numerator of the MT location CRLB

In this section, the numerator of the MT location CRLB is derived. The numerator can be found from the addition of  $[\mathcal{F}_L(\tilde{\mathbf{x}}_k)]_{1,1}$  and  $[\mathcal{F}_L(\tilde{\mathbf{x}}_k)]_{2,2}$  which are defined in (3.36a) and (3.36c), yielding

$$\begin{aligned}
[\mathcal{F}_L(\tilde{\mathbf{x}}_k)]_{1,1} + [\mathcal{F}_L(\tilde{\mathbf{x}}_k)]_{2,2} &= \sum_{\kappa_1=1}^{M_{\text{PR}}} e^{(\kappa_1)} \cdot (u_{\text{SAT}_x,k}^{(\kappa_1),2} + u_{\text{SAT}_y,k}^{(\kappa_1),2}) \\
&+ \sum_{\kappa_1=1}^{M_{\text{RTT}}} \sigma_{\text{RTT,LOS},k}^{(\kappa_1),-2} \cdot (u_{\text{BS}_x,k}^{(\kappa_1),2} + u_{\text{BS}_y,k}^{(\kappa_1),2}) \\
&+ \sum_{\kappa_1=1}^{M_{\text{PR}}} \sum_{\kappa_2=1}^{M_{\text{PR}}} c^{(\kappa_1,\kappa_2)} \cdot (u_{\text{SAT}_x,k}^{(\kappa_1),2} + u_{\text{SAT}_y,k}^{(\kappa_1),2}) \\
&- \sum_{\kappa_1=1}^{M_{\text{PR}}} \sum_{\kappa_2=1}^{M_{\text{PR}}} c^{(\kappa_1,\kappa_2)} \cdot (u_{\text{SAT}_x,k}^{(\kappa_1)} \cdot u_{\text{SAT}_x,k}^{(\kappa_2)} + u_{\text{SAT}_y,k}^{(\kappa_1)} \cdot u_{\text{SAT}_y,k}^{(\kappa_2)}) \\
&+ \sum_{\kappa_1=1}^{M_{\text{RSS}}} \sigma_{\text{RSS,LOS},k}^{(\kappa_1),-2} \cdot \left[ \frac{b^{(\kappa_1),2} \cdot (u_{\text{BS}_x,k}^{(\kappa_1),2} + u_{\text{BS}_y,k}^{(\kappa_1),2})}{d_{\text{BS},k}^{(\kappa_1)}(\mathbf{x}_{\text{MT},k})} \right. \\
&\left. + \frac{g^{(\kappa_1),2} \cdot (u_{\text{BS}_x,k}^{(\kappa_1),2} + u_{\text{BS}_y,k}^{(\kappa_1),2})}{d_{\text{BS},k}^{(\kappa_1)}(\mathbf{x}_{\text{MT},k})} \right]. \tag{A.36}
\end{aligned}$$

By taking into account that  $\|\mathbf{p}_{\text{SAT},k}^{(\kappa_1)}\|^2 = u_{\text{SAT}_x,k}^{(\kappa_1),2} + u_{\text{SAT}_y,k}^{(\kappa_1),2}$ ,  $\|\mathbf{u}_{\text{BS},k}\|^2 = u_{\text{BS}_x,k}^{(\kappa_1),2} + u_{\text{BS}_y,k}^{(\kappa_1),2} = 1$  and  $\mathbf{p}_{\text{SAT},k}^{(\kappa_1)} \cdot \mathbf{p}_{\text{SAT},k}^{(\kappa_2)} = u_{\text{SAT}_x,k}^{(\kappa_1)} \cdot u_{\text{SAT}_x,k}^{(\kappa_2)} + u_{\text{SAT}_y,k}^{(\kappa_1)} \cdot u_{\text{SAT}_y,k}^{(\kappa_2)}$  holds, the above expression simplifies to

$$\begin{aligned}
[\mathcal{F}_L(\tilde{\mathbf{x}}_k)]_{1,1} + [\mathcal{F}_L(\tilde{\mathbf{x}}_k)]_{2,2} &= \sum_{\kappa_1=1}^{M_{\text{PR}}} e^{(\kappa_1)} \cdot \|\mathbf{p}_{\text{SAT},k}^{(\kappa_1)}\|^2 + \sum_{\kappa_1=1}^{M_{\text{RTT}}} \sigma_{\text{RTT,LOS},k}^{(\kappa_1),-2} \\
&+ \sum_{\kappa_1=1}^{M_{\text{PR}}} \sum_{\substack{\kappa_2=1 \\ \kappa_2 \neq \kappa_1}}^{M_{\text{PR}}} c^{(\kappa_1,\kappa_2)} \cdot (\|\mathbf{p}_{\text{SAT}_{xy},k}^{(\kappa_1)}\|^2 - \mathbf{p}_{\text{SAT},k}^{(\kappa_1)} \cdot \mathbf{p}_{\text{SAT},k}^{(\kappa_2)}) \\
&+ \sum_{\kappa_1=1}^{M_{\text{RSS}}} \sigma_{\text{RSS,LOS},k}^{(\kappa_1),-2} \cdot \left[ \frac{b^{(\kappa_1),2} + g^{(\kappa_1),2}}{d_{\text{BS},k}^{(\kappa_1),2}(\mathbf{x}_{\text{MT},k})} \right]. \tag{A.37}
\end{aligned}$$

The double sum in (A.37) can be further modified by excluding the terms occurring when  $\kappa_1 = \kappa_2$ , since  $\|\mathbf{p}_{\text{SAT},k}^{(\kappa_1)}\|^2 - \mathbf{p}_{\text{SAT},k}^{(\kappa_1)} \cdot \mathbf{p}_{\text{SAT},k}^{(\kappa_1)} = 0$ . In this case, the formula

$$\sum_{\kappa_1} \sum_{\substack{\kappa_2 \\ \kappa_2 \neq \kappa_1}} a_{\kappa_1} b_{\kappa_2} = \sum_{\kappa_1} \sum_{\substack{\kappa_2 \\ \kappa_2 > \kappa_1}} (a_{\kappa_1} b_{\kappa_2} + a_{\kappa_2} b_{\kappa_1}), \tag{A.38}$$

valid for  $\kappa_1$  and  $\kappa_2$  spanning the same set of ordered values can be used and (A.37) becomes

$$\begin{aligned}
[\mathcal{F}_L(\tilde{\mathbf{x}}_k)]_{1,1} + [\mathcal{F}_L(\tilde{\mathbf{x}}_k)]_{2,2} &= \sum_{\kappa_1=1}^{M_{\text{PR}}} e^{(\kappa_1)} \cdot \|\mathbf{p}_{\text{SAT},k}^{(\kappa_1)}\|^2 + \sum_{\kappa_1=1}^{M_{\text{RTT}}} \sigma_{\text{RTT,LOS},k}^{(\kappa_1),-2} \\
&+ \sum_{\kappa_1=1}^{M_{\text{PR}}} \sum_{\substack{\kappa_2=1 \\ \kappa_2 > \kappa_1}}^{M_{\text{PR}}} c^{(\kappa_1, \kappa_2)} \cdot \|\mathbf{p}_{\text{SAT},k}^{(\kappa_1)} - \mathbf{p}_{\text{SAT},k}^{(\kappa_2)}\|^2 \\
&+ \sum_{\kappa_1=1}^{M_{\text{RSS}}} \sigma_{\text{RSS,LOS},k}^{(\kappa_1),-2} \cdot \left[ \frac{b^{(\kappa_1),2} + g^{(\kappa_1),2}}{d_{\text{BS},k}^{(\kappa_1),2}(\mathbf{x}_{\text{MT},k})} \right]. \quad (\text{A.39})
\end{aligned}$$

## A.8 Derivation of (3.47) describing the denominator of the MT location CRLB

In this section, the derivation of the denominator of the MT location CRLB is sketched. The denominator can be found from inserting (3.36) into (3.38). For notational convenience, the time step  $k$  is suppressed in the following. For the same reasons,  $\sigma_{\text{RTT,LOS},k}^{(\kappa_1),-2}$  is replaced by  $\sigma_{\text{RTT}}^{(\kappa_1),-2}$  and  $\sigma_{\text{RSS,LOS},k}^{(\kappa_1),-2}$  is replaced by  $\sigma_{\text{RSS}}^{(\kappa_1),-2}$ . The direct evaluation of (3.38) results in 10 different terms, yielding

$$\det[\mathcal{F}_L(\tilde{\mathbf{x}}_k)] = \sum_{\kappa_1=1}^{10} \mathcal{F}_{L,\kappa_1}, \quad (\text{A.40})$$

where the summands are given as follows

$$\mathcal{F}_{L,1} = \sum_{\kappa_1=1}^{M_{\text{PR}}} \sum_{\kappa_2=1}^{M_{\text{PR}}} e^{(\kappa_1)} e^{(\kappa_2)} \left[ u_{\text{SAT}_x}^{(\kappa_1),2} u_{\text{SAT}_y}^{(\kappa_2),2} - u_{\text{SAT}_x}^{(\kappa_1)} u_{\text{SAT}_y}^{(\kappa_1)} u_{\text{SAT}_x}^{(\kappa_2)} u_{\text{SAT}_y}^{(\kappa_2)} \right], \quad (\text{A.41})$$

$$\begin{aligned}
\mathcal{F}_{L,2} &= \sum_{\kappa_1=1}^{M_{\text{RTT}}} \sum_{\kappa_2=1}^{M_{\text{PR}}} \sigma_{\text{RTT}}^{(\kappa_1),-2} e^{(\kappa_2)} \left[ (u_{\text{BS}_x}^{(\kappa_1),2} u_{\text{SAT}_y}^{(\kappa_2),2} - u_{\text{SAT}_x}^{(\kappa_2)} u_{\text{SAT}_y}^{(\kappa_2)} u_{\text{BS}_x}^{(\kappa_1)} u_{\text{BS}_y}^{(\kappa_1)}) \right. \\
&+ \left. (u_{\text{BS}_y}^{(\kappa_1),2} u_{\text{SAT}_x}^{(\kappa_2),2} - u_{\text{SAT}_x}^{(\kappa_2)} u_{\text{SAT}_y}^{(\kappa_2)} u_{\text{BS}_x}^{(\kappa_1)} u_{\text{BS}_y}^{(\kappa_1)}) \right], \quad (\text{A.42})
\end{aligned}$$

$$\begin{aligned}
\mathcal{F}_{L,3} &= \sum_{\kappa_1=1}^{M_{\text{PR}}} \sum_{\kappa_2=1}^{M_{\text{PR}}} \sum_{\kappa_3=1}^{M_{\text{PR}}} e^{(\kappa_1)} c^{(\kappa_2, \kappa_3)} \left[ u_{\text{SAT}_x}^{(\kappa_1),2} (u_{\text{SAT}_y}^{(\kappa_2),2} - u_{\text{SAT}_y}^{(\kappa_2)} u_{\text{SAT}_y}^{(\kappa_3)}) \right. \\
&- u_{\text{SAT}_x}^{(\kappa_1)} u_{\text{SAT}_y}^{(\kappa_1)} (u_{\text{SAT}_y}^{(\kappa_2)} u_{\text{SAT}_x}^{(\kappa_2)} - u_{\text{SAT}_y}^{(\kappa_2)} u_{\text{SAT}_x}^{(\kappa_3)}) + u_{\text{SAT}_y}^{(\kappa_1),2} (u_{\text{SAT}_x}^{(\kappa_2),2} - u_{\text{SAT}_x}^{(\kappa_2)} u_{\text{SAT}_x}^{(\kappa_3)}) \\
&\left. - u_{\text{SAT}_y}^{(\kappa_1)} u_{\text{SAT}_x}^{(\kappa_1)} (u_{\text{SAT}_x}^{(\kappa_2)} u_{\text{SAT}_y}^{(\kappa_2)} - u_{\text{SAT}_x}^{(\kappa_2)} u_{\text{SAT}_y}^{(\kappa_3)}) \right], \quad (\text{A.43})
\end{aligned}$$

$$\mathcal{F}_{L,4} = \sum_{\kappa_1=1}^{M_{\text{RSS}}} \sum_{\kappa_2=1}^{M_{\text{PR}}} \sigma_{\text{RSS}}^{(\kappa_1),-2} e^{(\kappa_2)} \left[ \left( \frac{b^{(\kappa_1)} u_{\text{BSx}}^{(\kappa_1)} + g^{(\kappa_1)} u_{\text{BSy}}^{(\kappa_1)}}{d_{\text{BS}}^{(\kappa_1)}(\mathbf{x}_{\text{MT}})} \right) u_{\text{SATy}}^{(\kappa_2)} - \left( \frac{b^{(\kappa_1)} u_{\text{BSy}}^{(\kappa_1)} - g^{(\kappa_1)} u_{\text{BSx}}^{(\kappa_1)}}{d_{\text{BS}}^{(\kappa_1)}(\mathbf{x}_{\text{MT}})} \right) u_{\text{SATx}}^{(\kappa_2)} \right]^2, \quad (\text{A.44})$$

$$\mathcal{F}_{L,5} = \sum_{\kappa_1=1}^{M_{\text{RTT}}} \sum_{\kappa_2=1}^{M_{\text{RTT}}} \sigma_{\text{RTT}}^{(\kappa_1),-2} \sigma_{\text{RTT}}^{(\kappa_2),-2} \left[ u_{\text{BSx}}^{(\kappa_1),2} u_{\text{BSy}}^{(\kappa_2),2} - u_{\text{BSx}}^{(\kappa_1)} u_{\text{BSy}}^{(\kappa_1)} u_{\text{BSx}}^{(\kappa_2)} u_{\text{BSy}}^{(\kappa_2)} \right], \quad (\text{A.45})$$

$$\mathcal{F}_{L,6} = \sum_{\kappa_1=1}^{M_{\text{RTT}}} \sum_{\kappa_2=1}^{M_{\text{PR}}} \sum_{\kappa_3=1}^{M_{\text{PR}}} \sigma_{\text{RTT}}^{(\kappa_1),-2} c^{(\kappa_2,\kappa_3)} \left[ u_{\text{BSx}}^{(\kappa_1),2} (u_{\text{SATy}}^{(\kappa_2),2} - u_{\text{SATy}}^{(\kappa_2)} u_{\text{SATy}}^{(\kappa_3)}) - u_{\text{BSx}}^{(\kappa_1)} u_{\text{BSy}}^{(\kappa_1)} (u_{\text{SATy}}^{(\kappa_2)} u_{\text{SATx}}^{(\kappa_2)} - u_{\text{SATy}}^{(\kappa_2)} u_{\text{SATx}}^{(\kappa_3)}) + u_{\text{BSy}}^{(\kappa_1),2} (u_{\text{SATx}}^{(\kappa_2)} - u_{\text{SATx}}^{(\kappa_2)} u_{\text{SATx}}^{(\kappa_3)}) - u_{\text{BSy}}^{(\kappa_1)} u_{\text{BSx}}^{(\kappa_1)} (u_{\text{SATx}}^{(\kappa_2)} u_{\text{SATy}}^{(\kappa_2)} - u_{\text{SATx}}^{(\kappa_2)} u_{\text{SATy}}^{(\kappa_3)}) \right], \quad (\text{A.46})$$

$$\mathcal{F}_{L,7} = \sum_{\kappa_1=1}^{M_{\text{RTT}}} \sum_{\kappa_2=1}^{M_{\text{RSS}}} \sigma_{\text{RTT}}^{(\kappa_1),-2} \sigma_{\text{RSS}}^{(\kappa_2),-2} \left[ u_{\text{BSx}}^{(\kappa_1)} \left( \frac{b^{(\kappa_2)} u_{\text{BSy}}^{(\kappa_2)} - g^{(\kappa_2)} u_{\text{BSx}}^{(\kappa_2)}}{d_{\text{BS}}^{(\kappa_2)}(\mathbf{x}_{\text{MT}})} \right) - u_{\text{BSy}}^{(\kappa_1)} \left( \frac{b^{(\kappa_2)} u_{\text{BSx}}^{(\kappa_2)} + g^{(\kappa_2)} u_{\text{BSy}}^{(\kappa_2)}}{d_{\text{BS}}^{(\kappa_2)}(\mathbf{x}_{\text{MT}})} \right) \right]^2, \quad (\text{A.47})$$

$$\mathcal{F}_{L,8} = \sum_{\kappa_1=1}^{M_{\text{PR}}} \sum_{\kappa_2=1}^{M_{\text{PR}}} \sum_{\kappa_3=1}^{M_{\text{PR}}} \sum_{\kappa_4=1}^{M_{\text{PR}}} c^{(\kappa_1,\kappa_2)} c^{(\kappa_3,\kappa_4)} \left[ (u_{\text{SATx}}^{(\kappa_1),2} - u_{\text{SATx}}^{(\kappa_1)} u_{\text{SATx}}^{(\kappa_2)}) (u_{\text{SATy}}^{(\kappa_3),2} - u_{\text{SATy}}^{(\kappa_3)} u_{\text{SATy}}^{(\kappa_4)}) - (u_{\text{SATx}}^{(\kappa_1)} u_{\text{SATy}}^{(\kappa_1)} - u_{\text{SATx}}^{(\kappa_1)} u_{\text{SATy}}^{(\kappa_2)}) (u_{\text{SATy}}^{(\kappa_3)} u_{\text{SATx}}^{(\kappa_3)} - u_{\text{SATy}}^{(\kappa_3)} u_{\text{SATx}}^{(\kappa_4)}) \right], \quad (\text{A.48})$$

$$\mathcal{F}_{L,9} = \sum_{\kappa_1=1}^{M_{\text{RSS}}} \sum_{\kappa_2=1}^{M_{\text{PR}}} \sum_{\kappa_3=1}^{M_{\text{PR}}} \sigma_{\text{RSS}}^{(\kappa_1),-2} c^{(\kappa_2,\kappa_3)} \left[ \left( \frac{b^{(\kappa_1)} u_{\text{BSx}}^{(\kappa_1)} + g^{(\kappa_1)} u_{\text{BSy}}^{(\kappa_1)}}{d_{\text{BS}}^{(\kappa_1)}(\mathbf{x}_{\text{MT}})} \right)^2 (u_{\text{SATy}}^{(\kappa_2),2} - u_{\text{SATy}}^{(\kappa_2)} u_{\text{SATy}}^{(\kappa_3)}) - \left( \frac{(b^{(\kappa_1)} u_{\text{BSx}}^{(\kappa_1)} + g^{(\kappa_1)} u_{\text{BSy}}^{(\kappa_1)}) (b^{(\kappa_1)} u_{\text{BSy}}^{(\kappa_1)} - g^{(\kappa_1)} u_{\text{BSx}}^{(\kappa_1)})}{d_{\text{BS}}^{(\kappa_1),2}(\mathbf{x}_{\text{MT}})} \right) \cdot \left[ (u_{\text{SATy}}^{(\kappa_2)} u_{\text{SATx}}^{(\kappa_2)} - u_{\text{SATy}}^{(\kappa_2)} u_{\text{SATx}}^{(\kappa_3)}) + (u_{\text{SATx}}^{(\kappa_2)} u_{\text{SATy}}^{(\kappa_2)} - u_{\text{SATx}}^{(\kappa_2)} u_{\text{SATy}}^{(\kappa_3)}) \right] + \left( \frac{b^{(\kappa_1)} u_{\text{BSy}}^{(\kappa_1)} - g^{(\kappa_1)} u_{\text{BSx}}^{(\kappa_1)}}{d_{\text{BS}}^{(\kappa_1)}(\mathbf{x}_{\text{MT}})} \right)^2 (u_{\text{SATx}}^{(\kappa_2),2} - u_{\text{SATx}}^{(\kappa_2)} u_{\text{SATx}}^{(\kappa_3)}) \right], \quad (\text{A.49})$$

$$\mathcal{F}_{L,10} = \sum_{\kappa_1=1}^{M_{\text{RSS}}} \sum_{\kappa_2=1}^{M_{\text{RSS}}} \sigma_{\text{RSS}}^{(\kappa_1),-2} \sigma_{\text{RSS}}^{(\kappa_2),-2} \left[ \left( \frac{b^{(\kappa_1)} u_{\text{BSx}}^{(\kappa_1)} + g^{(\kappa_1)} u_{\text{BSy}}^{(\kappa_1)}}{d_{\text{BS}}^{(\kappa_1)}(\mathbf{x}_{\text{MT}})} \cdot \frac{b^{(\kappa_2)} u_{\text{BSy}}^{(\kappa_2)} - g^{(\kappa_2)} u_{\text{BSx}}^{(\kappa_2)}}{d_{\text{BS}}^{(\kappa_2)}(\mathbf{x}_{\text{MT}})} \right)^2 - \left( \frac{(b^{(\kappa_1)} u_{\text{BSx}}^{(\kappa_1)} + g^{(\kappa_1)} u_{\text{BSy}}^{(\kappa_1)}) (b^{(\kappa_1)} u_{\text{BSy}}^{(\kappa_1)} - g^{(\kappa_1)} u_{\text{BSx}}^{(\kappa_1)})}{d_{\text{BS}}^{(\kappa_1),2}(\mathbf{x}_{\text{MT}})} \right) \cdot \left( \frac{(b^{(\kappa_2)} u_{\text{BSy}}^{(\kappa_2)} - g^{(\kappa_2)} u_{\text{BSx}}^{(\kappa_2)}) (b^{(\kappa_2)} u_{\text{BSx}}^{(\kappa_2)} + g^{(\kappa_2)} u_{\text{BSy}}^{(\kappa_2)})}{d_{\text{BS}}^{(\kappa_2),2}(\mathbf{x}_{\text{MT}})} \right) \right]. \quad (\text{A.50})$$

In the following, the summands are further simplified in order to arrive at the expression given in (3.47). This is done as follows:

- The summand  $\mathcal{F}_{L,1}$  can be expressed in terms of  $\mathcal{A}^{(\kappa_1, \kappa_2)}$  defined in (3.39), yielding

$$\mathcal{F}_{L,1} = \sum_{\kappa_1=1}^{M_{\text{PR}}} \sum_{\kappa_2=1}^{M_{\text{PR}}} e^{(\kappa_1)} \cdot e^{(\kappa_2)} \cdot \left[ u_{\text{SAT}_x}^{(\kappa_1)} u_{\text{SAT}_y}^{(\kappa_2)} \cdot \mathcal{A}^{(\kappa_1, \kappa_2)} \right]. \quad (\text{A.51})$$

The double sum in (A.51) can be further modified by excluding the terms occurring when  $\kappa_1 = \kappa_2$ , since  $\mathcal{A}^{(\kappa_1, \kappa_1)} = 0$ . In this case, the formula in (A.38) can be used and  $\mathcal{F}_{L,1}$  can be rewritten as

$$\mathcal{F}_{L,1} = \sum_{\kappa_1=1}^{M_{\text{PR}}} \sum_{\substack{\kappa_2=1 \\ \kappa_2 > \kappa_1}}^{M_{\text{PR}}} e^{(\kappa_1)} \cdot e^{(\kappa_2)} \cdot \mathcal{A}^{(\kappa_1, \kappa_2), 2}. \quad (\text{A.52})$$

- The summand  $\mathcal{F}_{L,2}$  can be expressed in terms of  $\mathcal{B}^{(\kappa_1, \kappa_2)}$  defined in (3.40), yielding

$$\mathcal{F}_{L,2} = \sum_{\kappa_1=1}^{M_{\text{RTT}}} \sum_{\kappa_2=1}^{M_{\text{PR}}} \sigma_{\text{RTT}}^{(\kappa_1), -2} \cdot e^{(\kappa_2)} \cdot \mathcal{B}^{(\kappa_1, \kappa_2), 2}. \quad (\text{A.53})$$

- The summand  $\mathcal{F}_{L,3}$  can be expressed in terms of  $\mathcal{A}^{(\kappa_1, \kappa_2)}$  defined in (3.39), yielding

$$\mathcal{F}_{L,3} = \sum_{\kappa_1=1}^{M_{\text{PR}}} \sum_{\kappa_2=1}^{M_{\text{PR}}} \sum_{\kappa_3=1}^{M_{\text{PR}}} e^{(\kappa_1)} \cdot c^{(\kappa_2, \kappa_3)} \cdot \left[ \mathcal{A}^{(\kappa_1, \kappa_2), 2} - \mathcal{A}^{(\kappa_1, \kappa_2)} \cdot \mathcal{A}^{(\kappa_1, \kappa_3)} \right]. \quad (\text{A.54})$$

The triple sum in (A.54) can be further modified by excluding the terms occurring when  $\kappa_2 = \kappa_3$ , since  $\mathcal{A}^{(\kappa_1, \kappa_2), 2} - \mathcal{A}^{(\kappa_1, \kappa_2)} \cdot \mathcal{A}^{(\kappa_1, \kappa_2)} = 0$ . In this case, the formula

$$\sum_{\kappa_1} \sum_{\kappa_2} \sum_{\substack{\kappa_3 \\ \kappa_3 \neq \kappa_2}} a_{\kappa_1} b_{\kappa_2} c_{\kappa_3} = \sum_{\kappa_1} \sum_{\kappa_2} \sum_{\substack{\kappa_3 \\ \kappa_3 > \kappa_2}} a_{\kappa_1} (b_{\kappa_2} c_{\kappa_3} + b_{\kappa_3} c_{\kappa_2}), \quad (\text{A.55})$$

valid for  $\kappa_2$  and  $\kappa_3$  spanning the same set of ordered values can be used and (A.54) becomes

$$\mathcal{F}_{L,3} = \sum_{\kappa_1=1}^{M_{\text{PR}}} \sum_{\kappa_2=1}^{M_{\text{PR}}} \sum_{\substack{\kappa_3=1 \\ \kappa_3 > \kappa_2}}^{M_{\text{PR}}} e^{(\kappa_1)} \cdot c^{(\kappa_2, \kappa_3)} \cdot \left[ \mathcal{A}^{(\kappa_1, \kappa_2)} - \mathcal{A}^{(\kappa_1, \kappa_3)} \right]^2. \quad (\text{A.56})$$

- The summand  $\mathcal{F}_{L,4}$  can be expressed in terms of  $\mathcal{B}^{(\kappa_1, \kappa_2)}$  and  $\mathcal{D}^{(\kappa_1, \kappa_2)}$  defined in (3.40) and (3.42), yielding

$$\mathcal{F}_{L,4} = \sum_{\kappa_1=1}^{M_{\text{RSS}}} \sum_{\kappa_2=1}^{M_{\text{PR}}} \sigma_{\text{RSS}}^{(\kappa_1), -2} \cdot e^{(\kappa_2)} \cdot \left[ \frac{b^{(\kappa_1)} \cdot \mathcal{B}^{(\kappa_1, \kappa_2)} + g^{(\kappa_1)} \cdot \mathcal{D}^{(\kappa_1, \kappa_2)}}{d_{\text{BS}}^{(\kappa_1)}(\mathbf{x}_{\text{MT}})} \right]^2. \quad (\text{A.57})$$

- The summand  $\mathcal{F}_{L,5}$  can be expressed in terms of  $\mathcal{C}^{(\kappa_1, \kappa_2)}$  defined in (3.41). Following the same derivation steps as for  $\mathcal{F}_{L,1}$ ,  $\mathcal{F}_{L,5}$  is given by

$$\mathcal{F}_{L,5} = \sum_{\kappa_1=1}^{M_{\text{RTT}}} \sum_{\substack{\kappa_2=1 \\ \kappa_2 > \kappa_1}}^{M_{\text{RTT}}} \sigma_{\text{RTT}}^{(\kappa_1), -2} \cdot \sigma_{\text{RTT}}^{(\kappa_2), -2} \cdot \mathcal{C}^{(\kappa_1, \kappa_2), 2}. \quad (\text{A.58})$$

- The summand  $\mathcal{F}_{L,6}$  can be expressed in terms of  $\mathcal{B}^{(\kappa_1, \kappa_2)}$  defined in (3.40). Following the same derivation steps as for  $\mathcal{F}_{L,3}$ ,  $\mathcal{F}_{L,6}$  is given by

$$\mathcal{F}_{L,6} = \sum_{\kappa_1=1}^{M_{\text{RTT}}} \sum_{\kappa_2=1}^{M_{\text{PR}}} \sum_{\substack{\kappa_3 \\ \kappa_3 > \kappa_2}}^{M_{\text{PR}}} \sigma_{\text{RTT}}^{(\kappa_1), -2} \cdot c^{(\kappa_2, \kappa_3)} \cdot [\mathcal{B}^{(\kappa_1, \kappa_2)} - \mathcal{B}^{(\kappa_1, \kappa_3)}]^2. \quad (\text{A.59})$$

- The summand  $\mathcal{F}_{L,7}$  can be expressed in terms of  $\mathcal{C}^{(\kappa_1, \kappa_2)}$  and  $\mathcal{E}^{(\kappa_1, \kappa_2)}$  defined in (3.41) and (3.43), yielding

$$\mathcal{F}_{L,7} = \sum_{\kappa_1=1}^{M_{\text{RTT}}} \sum_{\kappa_2=1}^{M_{\text{RSS}}} \sigma_{\text{RTT}}^{(\kappa_1), -2} \cdot \sigma_{\text{RSS}}^{(\kappa_2), -2} \cdot \left[ \frac{b^{(\kappa_2)} \cdot \mathcal{C}^{(\kappa_1, \kappa_2)} - g^{(\kappa_2)} \cdot \mathcal{E}^{(\kappa_1, \kappa_2)}}{d_{\text{BS}}^{(\kappa_2)}(\mathbf{x}_{\text{MT}})} \right]^2. \quad (\text{A.60})$$

- The summand  $\mathcal{F}_{L,8}$  can be rewritten by evaluating the expression in the square brackets of (A.48). After a cumbersome rearrangement of the terms,  $\mathcal{F}_{L,8}$  can be rewritten as

$$\begin{aligned} \mathcal{F}_{L,8} = & \sum_{\kappa_1=1}^{M_{\text{PR}}} \sum_{\kappa_2=1}^{M_{\text{PR}}} \sum_{\kappa_3=1}^{M_{\text{PR}}} \sum_{\kappa_4=1}^{M_{\text{PR}}} c^{(\kappa_1, \kappa_2)} \cdot c^{(\kappa_3, \kappa_4)} \cdot u_{\text{SAT}_x}^{(\kappa_1)} \cdot u_{\text{SAT}_y}^{(\kappa_4)} \\ & \cdot \left[ (\mathbf{p}_{\text{SAT}}^{(\kappa_1)} - \mathbf{p}_{\text{SAT}}^{(\kappa_2)}) \times (\mathbf{p}_{\text{SAT}}^{(\kappa_3)} - \mathbf{p}_{\text{SAT}}^{(\kappa_4)}) \right]^{\text{T}} \cdot \mathbf{u}_z. \end{aligned} \quad (\text{A.61})$$

The expression in the square brackets of (A.61) equals zero for the two cases  $\kappa_1 = \kappa_2$  and  $\kappa_3 = \kappa_4$ . Thus, the quadruple sum in (A.61) can be further modified by excluding the terms occurring when  $\kappa_1 = \kappa_2$  and  $\kappa_3 = \kappa_4$ . In this case, the formula

$$\sum_{\kappa_1} \sum_{\substack{\kappa_2 \\ \kappa_2 \neq \kappa_1}} \sum_{\kappa_3} \sum_{\substack{\kappa_4 \\ \kappa_4 \neq \kappa_3}} a_{\kappa_1} b_{\kappa_2} c_{\kappa_3} d_{\kappa_4} = \sum_{\kappa_1} \sum_{\substack{\kappa_2 \\ \kappa_2 > \kappa_1}} \sum_{\kappa_3} \sum_{\substack{\kappa_4 \\ \kappa_4 > \kappa_3}} (a_{\kappa_1} b_{\kappa_2} + a_{\kappa_2} b_{\kappa_1}) (c_{\kappa_3} d_{\kappa_4} + c_{\kappa_4} d_{\kappa_3}), \quad (\text{A.62})$$

valid for  $\kappa_1, \kappa_2, \kappa_3, \kappa_4$  spanning the same set of ordered values can be used and (A.61) can be expressed in terms of  $\mathcal{G}^{(\kappa_1, \kappa_2, \kappa_3, \kappa_4)}$  defined in (3.46), yielding

$$\mathcal{F}_{L,8} = \sum_{\substack{\kappa_1=1 \\ \kappa_2 > \kappa_1}}^{M_{\text{PR}}} \sum_{\substack{\kappa_2=1 \\ \kappa_2 > \kappa_1}}^{M_{\text{PR}}} \sum_{\substack{\kappa_3=1 \\ \kappa_3 > \kappa_2}}^{M_{\text{PR}}} \sum_{\substack{\kappa_4=1 \\ \kappa_4 > \kappa_3}}^{M_{\text{PR}}} c^{(\kappa_1, \kappa_2)} \cdot c^{(\kappa_3, \kappa_4)} \cdot \mathcal{G}^{(\kappa_1, \kappa_2, \kappa_3, \kappa_4)}. \quad (\text{A.63})$$



- The summand  $\mathcal{F}_{L,9}$  can be rewritten by evaluating the expression in the square brackets of (A.49). After a cumbersome rearrangement of the terms,  $\mathcal{F}_{L,9}$  can be rewritten in terms of  $\mathcal{B}^{(\kappa_1, \kappa_2)}$  and  $\mathcal{D}^{(\kappa_1, \kappa_2)}$  defined in (3.40) and (3.42), yielding

$$\mathcal{F}_{L,9} = \sum_{\kappa_1=1}^{M_{\text{RSS}}} \sum_{\kappa_2=1}^{M_{\text{PR}}} \sum_{\kappa_3=1}^{M_{\text{PR}}} \sigma_{\text{RSS}}^{(\kappa_1), -2} \cdot c^{(\kappa_2, \kappa_3)} \cdot \left[ \left( \frac{b^{(\kappa_1)} \mathcal{B}^{(\kappa_1, \kappa_2)} + g^{(\kappa_1)} \mathcal{D}^{(\kappa_1, \kappa_2)}}{d_{\text{BS}}^{(\kappa_1)}(\mathbf{x}_{\text{MT}})} \right)^2 - \frac{(b^{(\kappa_1)} \mathcal{B}^{(\kappa_1, \kappa_2)} + g^{(\kappa_1)} \mathcal{D}^{(\kappa_1, \kappa_2)})(b^{(\kappa_1)} \mathcal{B}^{(\kappa_1, \kappa_3)} + g^{(\kappa_1)} \mathcal{D}^{(\kappa_1, \kappa_3)})}{d_{\text{BS}}^{(\kappa_1), 2}(\mathbf{x}_{\text{MT}})} \right]. \quad (\text{A.64})$$

The expression in the square brackets of (A.64) equals zero for the case  $\kappa_2 = \kappa_3$ . Thus, the triple sum in (A.64) can be further modified by excluding the terms occurring when  $\kappa_2 = \kappa_3$ . In this case, the formula in (A.55) can be used, so that  $\mathcal{F}_{L,9}$  can be written as

$$\mathcal{F}_{L,9} = \sum_{\kappa_1=1}^{M_{\text{RSS}}} \sum_{\kappa_2=1}^{M_{\text{PR}}} \sum_{\substack{\kappa_3=1 \\ \kappa_3 > \kappa_2}}^{M_{\text{PR}}} \sigma_{\text{RSS}}^{(\kappa_1), -2} \cdot c^{(\kappa_2, \kappa_3)} \cdot \left[ \frac{b^{(\kappa_1)} \mathcal{B}^{(\kappa_1, \kappa_2)} + g^{(\kappa_1)} \mathcal{D}^{(\kappa_1, \kappa_2)}}{d_{\text{BS}}^{(\kappa_1)}(\mathbf{x}_{\text{MT}})} - \frac{b^{(\kappa_1)} \mathcal{B}^{(\kappa_1, \kappa_3)} + g^{(\kappa_1)} \mathcal{D}^{(\kappa_1, \kappa_3)}}{d_{\text{BS}}^{(\kappa_1)}(\mathbf{x}_{\text{MT}})} \right]^2. \quad (\text{A.65})$$

- The summand  $\mathcal{F}_{L,10}$  can be expressed in terms of  $\mathcal{C}^{(\kappa_1, \kappa_2)}$  and  $\mathcal{E}^{(\kappa_1, \kappa_2)}$  defined in (3.41) and (3.43), yielding

$$\mathcal{F}_{L,10} = \sum_{\kappa_1=1}^{M_{\text{RSS}}} \sum_{\kappa_2=1}^{M_{\text{RSS}}} \sigma_{\text{RSS}}^{(\kappa_1), -2} \cdot \sigma_{\text{RSS}}^{(\kappa_2), -2} \cdot \left[ \frac{b^{(\kappa_1)} u_{\text{BSx}}^{(\kappa_1)} + g^{(\kappa_1)} u_{\text{BSy}}^{(\kappa_1)}}{d_{\text{BS}}^{(\kappa_1)}(\mathbf{x}_{\text{MT}})} \cdot \frac{b^{(\kappa_2)} u_{\text{BSy}}^{(\kappa_2)} - g^{(\kappa_2)} u_{\text{BSx}}^{(\kappa_2)}}{d_{\text{BS}}^{(\kappa_2)}(\mathbf{x}_{\text{MT}})} \cdot \left( \frac{(b^{(\kappa_1)} \cdot b^{(\kappa_2)} + g^{(\kappa_1)} \cdot g^{(\kappa_2)}) \cdot \mathcal{C}^{(\kappa_1, \kappa_2)}}{d_{\text{BS}}^{(\kappa_1)}(\mathbf{x}_{\text{MT}}) \cdot d_{\text{BS}}^{(\kappa_2)}(\mathbf{x}_{\text{MT}})} + \frac{(b^{(\kappa_2)} \cdot g^{(\kappa_1)} - b^{(\kappa_1)} \cdot g^{(\kappa_2)}) \cdot \mathcal{E}^{(\kappa_1, \kappa_2)}}{d_{\text{BS}}^{(\kappa_1)}(\mathbf{x}_{\text{MT}}) \cdot d_{\text{BS}}^{(\kappa_2)}(\mathbf{x}_{\text{MT}})} \right) \right]. \quad (\text{A.66})$$

The double sum in (A.66) can be further modified by excluding the terms occurring when  $\kappa_1 = \kappa_2$ , since  $\mathcal{C}^{(\kappa_1, \kappa_1)} = 0$  and  $b^{(\kappa_1)} \cdot g^{(\kappa_1)} - b^{(\kappa_1)} \cdot g^{(\kappa_1)} = 0$ . In this case, the formula in (A.38) can be used and  $\mathcal{F}_{L,10}$  can be rewritten as

$$\mathcal{F}_{L,10} = \sum_{\kappa_1=1}^{M_{\text{RSS}}} \sum_{\substack{\kappa_1=1 \\ \kappa_2 > \kappa_1}}^{M_{\text{RSS}}} \sigma_{\text{RSS}}^{(\kappa_1), -2} \cdot \sigma_{\text{RSS}}^{(\kappa_2), -2} \cdot \left[ \frac{(b^{(\kappa_1)} \cdot b^{(\kappa_2)} + g^{(\kappa_1)} \cdot g^{(\kappa_2)}) \cdot \mathcal{C}^{(\kappa_1, \kappa_2)}}{d_{\text{BS}}^{(\kappa_1)}(\mathbf{x}_{\text{MT}}) \cdot d_{\text{BS}}^{(\kappa_2)}(\mathbf{x}_{\text{MT}})} + \frac{(b^{(\kappa_2)} \cdot g^{(\kappa_1)} - b^{(\kappa_1)} \cdot g^{(\kappa_2)}) \cdot \mathcal{E}^{(\kappa_1, \kappa_2)}}{d_{\text{BS}}^{(\kappa_1)}(\mathbf{x}_{\text{MT}}) \cdot d_{\text{BS}}^{(\kappa_2)}(\mathbf{x}_{\text{MT}})} \right]^2. \quad (\text{A.67})$$

According to (A.40), the denominator of the MT location CRLB is, thus, given by

$$\begin{aligned}
\det[\mathcal{F}_L(\tilde{\mathbf{x}}_k)] &= \sum_{\kappa_1=1}^{M_{\text{PR}}} \sum_{\substack{\kappa_2=1 \\ \kappa_2 > \kappa_1}}^{M_{\text{PR}}} e^{(\kappa_1)} \cdot e^{(\kappa_2)} \cdot \mathcal{A}^{(\kappa_1, \kappa_2), 2} \\
&+ \sum_{\kappa_1=1}^{M_{\text{RTT}}} \sum_{\kappa_2=1}^{M_{\text{PR}}} \sigma_{\text{RTT,LOS},k}^{(\kappa_1), -2} \cdot e^{(\kappa_2)} \cdot \mathcal{B}^{(\kappa_1, \kappa_2), 2} \\
&+ \sum_{\kappa_1=1}^{M_{\text{PR}}} \sum_{\kappa_2=1}^{M_{\text{PR}}} \sum_{\substack{\kappa_3=1 \\ \kappa_3 > \kappa_2}}^{M_{\text{PR}}} e^{(\kappa_1)} \cdot c^{(\kappa_2, \kappa_3)} \cdot [\mathcal{A}^{(\kappa_1, \kappa_2)} - \mathcal{A}^{(\kappa_1, \kappa_3)}]^2 \\
&+ \sum_{\kappa_1=1}^{M_{\text{RSS}}} \sum_{\kappa_2=1}^{M_{\text{PR}}} \sigma_{\text{RSS,LOS},k}^{(\kappa_1), -2} \cdot e^{(\kappa_2)} \cdot \left[ \frac{b^{(\kappa_1)} \cdot \mathcal{B}^{(\kappa_1, \kappa_2)} + g^{(\kappa_1)} \cdot \mathcal{D}^{(\kappa_1, \kappa_2)}}{d_{\text{BS},k}^{(\kappa_1)}(\mathbf{x}_{\text{MT},k})} \right]^2 \\
&+ \sum_{\kappa_1=1}^{M_{\text{RTT}}} \sum_{\substack{\kappa_2=1 \\ \kappa_2 > \kappa_1}}^{M_{\text{RTT}}} \sigma_{\text{RTT,LOS},k}^{(\kappa_1), -2} \cdot \sigma_{\text{RTT,LOS},k}^{(\kappa_2), -2} \cdot \mathcal{C}^{(\kappa_1, \kappa_2), 2} \\
&+ \sum_{\kappa_1=1}^{M_{\text{RTT}}} \sum_{\kappa_2=1}^{M_{\text{PR}}} \sum_{\substack{\kappa_3=1 \\ \kappa_3 > \kappa_2}}^{M_{\text{PR}}} \sigma_{\text{RTT,LOS},k}^{(\kappa_1), -2} \cdot c^{(\kappa_2, \kappa_3)} \cdot [\mathcal{B}^{(\kappa_1, \kappa_2)} - \mathcal{B}^{(\kappa_1, \kappa_3)}]^2 \\
&+ \sum_{\kappa_1=1}^{M_{\text{RTT}}} \sum_{\kappa_2=1}^{M_{\text{RSS}}} \sigma_{\text{RTT,LOS},k}^{(\kappa_1), -2} \cdot \sigma_{\text{RSS,LOS},k}^{(\kappa_2), -2} \cdot \left[ \frac{b^{(\kappa_2)} \cdot \mathcal{C}^{(\kappa_1, \kappa_2)} - g^{(\kappa_2)} \cdot \mathcal{E}^{(\kappa_1, \kappa_2)}}{d_{\text{BS},k}^{(\kappa_2)}(\mathbf{x}_{\text{MT},k})} \right]^2 \\
&+ \sum_{\kappa_1=1}^{M_{\text{PR}}} \sum_{\substack{\kappa_2=1 \\ \kappa_2 > \kappa_1}}^{M_{\text{PR}}} \sum_{\kappa_3=1}^{M_{\text{PR}}} \sum_{\substack{\kappa_4=1 \\ \kappa_4 > \kappa_3}}^{M_{\text{PR}}} c^{(\kappa_1, \kappa_2)} \cdot c^{(\kappa_3, \kappa_4)} \cdot \mathcal{G}^{(\kappa_1, \kappa_2, \kappa_3, \kappa_4)} \\
&+ \sum_{\kappa_1=1}^{M_{\text{RSS}}} \sum_{\kappa_2=1}^{M_{\text{PR}}} \sum_{\substack{\kappa_3=1 \\ \kappa_3 > \kappa_2}}^{M_{\text{PR}}} \sigma_{\text{RSS,LOS},k}^{(\kappa_1), -2} \cdot c^{(\kappa_2, \kappa_3)} \cdot \left[ \frac{b^{(\kappa_1)} \cdot \mathcal{B}^{(\kappa_1, \kappa_2)} + g^{(\kappa_1)} \cdot \mathcal{D}^{(\kappa_1, \kappa_2)}}{d_{\text{BS},k}^{(\kappa_1)}(\mathbf{x}_{\text{MT},k})} \right. \\
&\quad \left. + \frac{b^{(\kappa_1)} \cdot \mathcal{B}^{(\kappa_1, \kappa_3)} + g^{(\kappa_1)} \cdot \mathcal{D}^{(\kappa_1, \kappa_3)}}{d_{\text{BS},k}^{(\kappa_1)}(\mathbf{x}_{\text{MT},k})} \right]^2 \\
&+ \sum_{\kappa_1=1}^{M_{\text{RSS}}} \sum_{\substack{\kappa_1=1 \\ \kappa_2 > \kappa_1}}^{M_{\text{RSS}}} \sigma_{\text{RSS,LOS},k}^{(\kappa_1), -2} \cdot \sigma_{\text{RSS,LOS},k}^{(\kappa_2), -2} \cdot \left[ \frac{(b^{(\kappa_1)} \cdot b^{(\kappa_2)} + g^{(\kappa_1)} \cdot g^{(\kappa_2)}) \cdot \mathcal{C}^{(\kappa_1, \kappa_2)}}{d_{\text{BS},k}^{(\kappa_1)}(\mathbf{x}_{\text{MT},k}) \cdot d_{\text{BS},k}^{(\kappa_2)}(\mathbf{x}_{\text{MT},k})} \right. \\
&\quad \left. + \frac{(b^{(\kappa_2)} \cdot g^{(\kappa_1)} - b^{(\kappa_1)} \cdot g^{(\kappa_2)}) \cdot \mathcal{E}^{(\kappa_1, \kappa_2)}}{d_{\text{BS},k}^{(\kappa_1)}(\mathbf{x}_{\text{MT},k}) \cdot d_{\text{BS},k}^{(\kappa_2)}(\mathbf{x}_{\text{MT},k})} \right]^2. \tag{A.68}
\end{aligned}$$

## A.9 Proof showing that the MT location CRLBs of the Cellular and Hybrid 1 method are equal.

In this section, it is proven that the MT location CRLB of the Cellular and Hybrid 1 method are equal. The FIM of the Cellular method with respect to  $\mathbf{x}_{\text{MT},k}$  is given by

$$\mathcal{F}_{\text{Cellular}}(\mathbf{x}_{\text{MT},k}) = \mathcal{F}_{\text{RTT}}(x_{\text{MT},k}) + \mathcal{F}_{\text{RSS}}(x_{\text{MT},k}), \quad (\text{A.69})$$

By inserting (A.22), (A.28) into (A.69), it follows for the FIM of the Cellular method

$$\mathcal{F}_{\text{Cellular}}(\mathbf{x}_{\text{MT},k}) = \mathbf{H}_{\text{RTT}}^{\text{T}} \mathbf{\Lambda}_{\text{RTT}} \mathbf{H}_{\text{RTT}} + \mathbf{H}_{\text{RSS}}^{\text{T}} \mathbf{\Lambda}_{\text{RSS}} \mathbf{H}_{\text{RSS}}. \quad (\text{A.70})$$

The CRLB matrix of the Cellular method is, thus, given by

$$\mathcal{P}_{\text{CRLB,Cellular}} = [\mathbf{H}_{\text{RTT}}^{\text{T}} \mathbf{\Lambda}_{\text{RTT}} \mathbf{H}_{\text{RTT}} + \mathbf{H}_{\text{RSS}}^{\text{T}} \mathbf{\Lambda}_{\text{RSS}} \mathbf{H}_{\text{RSS}}]^{-1}. \quad (\text{A.71})$$

The FIM of the Hybrid 1 method with respect to  $\tilde{\mathbf{x}}_k$  is given by

$$\mathcal{F}_{\text{Hybrid 1}}(\tilde{\mathbf{x}}_k) = \mathcal{F}_{\text{PR}}(\tilde{\mathbf{x}}_k) + \mathcal{F}_{\text{RTT}}(\tilde{\mathbf{x}}_k) + \mathcal{F}_{\text{RSS}}(\tilde{\mathbf{x}}_k). \quad (\text{A.72})$$

By inserting (A.16), (A.22), (A.28) into (A.72), the FIM of the Hybrid 1 method can be found

$$\mathcal{F}_{\text{Hybrid 1}}(\tilde{\mathbf{x}}_k) = \left[ \begin{array}{c|c} \mathbf{H}_{\text{PR}}^{\text{T}} \sigma_{\text{PR},k}^{(1),-2} \mathbf{H}_{\text{PR}} + \mathbf{H}_{\text{RTT}}^{\text{T}} \mathbf{\Lambda}_{\text{RTT}} \mathbf{H}_{\text{RTT}} + \mathbf{H}_{\text{RSS}}^{\text{T}} \mathbf{\Lambda}_{\text{RSS}} \mathbf{H}_{\text{RSS}} & \mathbf{H}_{\text{PR}}^{\text{T}} \sigma_{\text{PR},k}^{(1),-2} \\ \hline \sigma_{\text{PR},k}^{(1),-2} \mathbf{H}_{\text{PR}} & \sigma_{\text{PR},k}^{(1),-2} \end{array} \right]. \quad (\text{A.73})$$

According to (3.32), the first  $2 \times 2$  diagonal submatrix  $\mathcal{P}_1(\tilde{\mathbf{x}}_k)$  gives the MT location CRLB matrix of the Hybrid 1 method, which is given by

$$\begin{aligned} \mathcal{P}_1(\tilde{\mathbf{x}}_k) &\triangleq \mathcal{P}_{\text{CRLB,Hybrid 1}} = \left[ \begin{array}{c} \mathbf{H}_{\text{PR}}^{\text{T}} \sigma_{\text{PR},k}^{(1),-2} \mathbf{H}_{\text{PR}} + \mathbf{H}_{\text{RTT}}^{\text{T}} \mathbf{\Lambda}_{\text{RTT}} \mathbf{H}_{\text{RTT}} + \mathbf{H}_{\text{RSS}}^{\text{T}} \mathbf{\Lambda}_{\text{RSS}} \mathbf{H}_{\text{RSS}} \\ -\mathbf{H}_{\text{PR}}^{\text{T}} \sigma_{\text{PR},k}^{(1),-2} \sigma_{\text{PR},k}^{(1),2} \sigma_{\text{PR},k}^{(1),-2} \mathbf{H}_{\text{PR}} \end{array} \right]^{-1} \\ &= [\mathbf{H}_{\text{RTT}}^{\text{T}} \mathbf{\Lambda}_{\text{RTT}} \mathbf{H}_{\text{RTT}} + \mathbf{H}_{\text{RSS}}^{\text{T}} \mathbf{\Lambda}_{\text{RSS}} \mathbf{H}_{\text{RSS}}]^{-1}. \end{aligned} \quad (\text{A.74})$$

Now, since  $\mathcal{P}_{\text{CRLB,Cellular}} = \mathcal{P}_{\text{CRLB,Hybrid 1}}$ , it directly follows that  $\mathcal{P}_{\text{CRLB,Cellular}} = \mathcal{P}_{\text{CRLB,Hybrid 1}}$  holds, which concludes our proof.  $\square$

## A.10 Monte Carlo Integration

In this section, the concept of Monte Carlo integration is reviewed [MU49,NB99,RC99,RAG04]. Let  $g(\mathbf{x})$  denote an arbitrary function depending on  $\mathbf{x} \in \mathbb{R}^{n_x}$  and let the multidimensional integral of  $g(\mathbf{x})$  be given by

$$I = \int_{\mathbb{R}^{n_x}} g(\mathbf{x}) \, \text{d}\mathbf{x}. \quad (\text{A.75})$$

The idea of Monte Carlo integration is to factorize  $g(\mathbf{x}) = f(\mathbf{x}) \cdot p(\mathbf{x})$  in such a way that  $p(\mathbf{x})$  is interpreted as a pdf. Thus, the above integral can be rewritten as the expected value of a function of a random variable  $\mathbf{x}$ , yielding

$$I = \mathbb{E}_{p(\mathbf{x})}\{f(\mathbf{x})\} = \int_{\mathbb{R}^{n_x}} f(\mathbf{x}) \cdot p(\mathbf{x}) \, d\mathbf{x}. \quad (\text{A.76})$$

By drawing  $N_{\text{MC}} \gg 1$  i.i.d. samples  $\{\mathbf{x}^{(i)}\}_{i=1}^{N_{\text{MC}}}$  from  $p(\mathbf{x})$ , an unbiased estimate  $I_{\text{MC}}$  of the integral can be determined, which is given by the sample mean

$$I \approx I_{\text{MC}} = \mathbb{E}_{p(\mathbf{x})}\{f(\mathbf{x})\} = \frac{1}{N_{\text{MC}}} \sum_{i=1}^{N_{\text{MC}}} f(\mathbf{x}^{(i)}). \quad (\text{A.77})$$

Let  $\sigma_{\text{MC}}^2$  denote the variance of the Monte Carlo estimate  $I_{\text{MC}}$  and let  $\sigma_f^2 < \infty$  denote the finite variance of  $f(\mathbf{x})$ . Then,

$$\sigma_{\text{MC}}^2 = \frac{\sigma_f^2}{N_{\text{MC}}} \quad (\text{A.78})$$

holds. The above result is the key to Monte Carlo integration and states that the variance  $\sigma_{\text{MC}}^2$  of the sample mean is by the factor  $1/N_{\text{MC}}$  smaller than the variance of  $f(\mathbf{x})$ , i.e., the variance  $\sigma_{\text{MC}}^2$  decreases asymptotically to zero as  $1/N_{\text{MC}}$ . Thus, the larger the sample size  $N_{\text{MC}}$ , the better the approximation of the integral given by (A.77) holds. Further theoretical results on the convergence of the Monte Carlo integration method can be found in [NB99, RAG04].

## A.11 Proof of (5.28) showing that the Bayesian information submatrix can be calculated recursively.

In this section, it is proven that the Bayesian information submatrix  $\mathbf{J}_k$  can be calculated recursively for state and measurement models given by (2.1) and (2.17). The proof presented in this section is similar to the proof given in [TMN98]. The proof starts with relating the BIM  $\mathbf{I}_{\text{B},k}$ , cf. (4.7), to the Bayesian information submatrix  $\mathbf{J}_k$ . Decomposing  $\mathbf{X}_k$  as  $\mathbf{X}_k = [\mathbf{X}_{k-1}^\top, \mathbf{x}_k^\top]^\top$ , the BIM can be written as

$$\begin{aligned} \mathbf{I}_{\text{B},k} &= \begin{bmatrix} \mathbf{A}_k & \mathbf{B}_k \\ \mathbf{B}_k^\top & \mathbf{C}_k \end{bmatrix} \\ &= \begin{bmatrix} \mathbb{E}_{p(\mathbf{X}_k, \mathbf{Z}_k)}\{-\Delta_{\mathbf{X}_{k-1}}^{\mathbf{X}_{k-1}} \log_e p(\mathbf{X}_k, \mathbf{Z}_k)\} & \mathbb{E}_{p(\mathbf{X}_k, \mathbf{Z}_k)}\{-\Delta_{\mathbf{x}_k}^{\mathbf{X}_{k-1}} \log_e p(\mathbf{X}_k, \mathbf{Z}_k)\} \\ \mathbb{E}_{p(\mathbf{X}_k, \mathbf{Z}_k)}\{-\Delta_{\mathbf{x}_k}^{\mathbf{x}_k} \log_e p(\mathbf{X}_k, \mathbf{Z}_k)\} & \mathbb{E}_{p(\mathbf{X}_k, \mathbf{Z}_k)}\{-\Delta_{\mathbf{x}_k}^{\mathbf{x}_k} \log_e p(\mathbf{X}_k, \mathbf{Z}_k)\} \end{bmatrix} \quad (\text{A.79}) \end{aligned}$$

Recall that the Bayesian information submatrix  $\mathbf{J}_k$  is the inverse of the  $(n_x \times n_x)$  lower-right submatrix of  $[\mathbf{I}_{B,k}]^{-1}$ . Thus,  $\mathbf{J}_k$  can be obtained from block-matrix inversion [Ber09], yielding

$$\mathbf{J}_k = \mathbf{C}_k - \mathbf{B}_k^\top \mathbf{A}_k^{-1} \mathbf{B}_k. \quad (\text{A.80})$$

In order to evaluate the  $(n_x \times n_x)$  matrix  $\mathbf{J}_k$ , it is necessary to either calculate the inverse of the  $(kn_x \times kn_x)$  matrix  $\mathbf{A}_k$  or the inverse of the  $[(k+1)n_x \times (k+1)n_x]$  matrix  $\mathbf{I}_{B,k}$ , which makes it practically impossible to evaluate  $\mathbf{J}_k$  for large values of  $k$ .

In the following, a recursive formula is developed which allows the computation of the Bayesian information submatrix  $\mathbf{J}_k$  without calculating the inverse of large matrices such as  $\mathbf{I}_{B,k}$  and  $\mathbf{A}_k$ . According to (5.27), the joint probability density function of  $\mathbf{X}_{k+1}$  and  $\mathbf{Z}_{k+1}$  can be rewritten as

$$p(\mathbf{X}_{k+1}, \mathbf{Z}_{k+1}) = p(\mathbf{z}_{k+1} | \mathbf{x}_{k+1}, \mathbf{Z}_k) \cdot p(\mathbf{x}_{k+1} | \mathbf{x}_k) \cdot p(\mathbf{X}_k, \mathbf{Z}_k), \quad (\text{A.81})$$

Using (A.81) and decomposing the vector  $\mathbf{X}_k = [\mathbf{X}_{k-1}^\top, \mathbf{x}_k^\top, \mathbf{x}_{k+1}^\top]^\top$ , it is very easy to verify that the Bayesian information matrix  $\mathbf{I}_{B,k+1}$  can be written in block diagonal form, yielding

$$\mathbf{I}_{B,k+1} = \begin{bmatrix} \mathbf{A}_k & \mathbf{B}_k & \mathbf{0} \\ \mathbf{B}_k^\top & \mathbf{C}_k + \mathbf{D}_k^{11} & \mathbf{D}_k^{12} \\ \mathbf{0} & \mathbf{D}_k^{21} & \mathbf{D}_k^{22} + \mathbf{D}_k^{33} \end{bmatrix}, \quad (\text{A.82})$$

where  $\mathbf{0}$  are all-zero matrices of appropriate dimension, and where the matrices  $\mathbf{D}_k^{11}$ ,  $\mathbf{D}_k^{12}$ ,  $\mathbf{D}_k^{21}$ ,  $\mathbf{D}_k^{22}$  and  $\mathbf{D}_k^{33}$  can be obtained from the definitions in (4.10a)-(4.10d) and (5.29), by replacing the time index  $k-1$  with the new index  $k$ , respectively. The Bayesian information submatrix  $\mathbf{J}_{k+1}$  is computed as the inverse of the  $(n_x \times n_x)$  right-lower submatrix of  $[\mathbf{I}_{B,k+1}]^{-1}$ . Thus, it follows

$$\begin{aligned} \mathbf{J}_{k+1} &= \mathbf{D}_k^{22} - [\mathbf{0} \ \mathbf{D}_k^{21}] \begin{bmatrix} \mathbf{A}_k & \mathbf{B}_k \\ \mathbf{B}_k^\top & \mathbf{C}_k + \mathbf{D}_k^{11} \end{bmatrix}^{-1} \begin{bmatrix} \mathbf{0} \\ \mathbf{D}_k^{12} \end{bmatrix} + \mathbf{D}_k^{33} \\ &= \mathbf{D}_k^{22} - \mathbf{D}_k^{21} [\mathbf{C}_k + \mathbf{D}_k^{11} - \mathbf{B}_k^\top \mathbf{A}_k^{-1} \mathbf{B}_k]^{-1} \mathbf{D}_k^{12} + \mathbf{D}_k^{33}. \end{aligned} \quad (\text{A.83})$$

Inserting the definition of  $\mathbf{J}_{k+1}$  given in (A.80) into (A.83) and replacing the index  $k$  with the new index  $k-1$ , yields the desired recursive formula for computing  $\mathbf{J}_k$ . This concludes our proof of (5.28).  $\square$



---

## List of Acronyms

<b>AoA</b>	Angle of Arrival
<b>APF</b>	Auxiliary Particle Filter
<b>BIM</b>	Bayesian Information Matrix
<b>BS</b>	Base Station
<b>CKF</b>	Cubature Kalman Filter
<b>CO</b>	Clock Offset
<b>CRLB</b>	Cramér-Rao Lower Bound
<b>CV</b>	Constant Velocity
<b>ECEF</b>	Earth Centered Earth Fixed
<b>EKF</b>	Extended Kalman Filter
<b>ENU</b>	East-North-Up
<b>E-OTD</b>	Enhanced Observed Time Difference
<b>E-PCRLB</b>	Enumeration Posterior Cramér-Rao Lower Bound
<b>FCC</b>	Federal Communications Commission
<b>FIM</b>	Fisher Information Matrix
<b>FLOP</b>	Floating-Point Operation
<b>GDOP</b>	Geometric Dilution of Precision
<b>GNSS</b>	Global Navigation Satellite System
<b>GRT</b>	GNSS Reference Time
<b>GPS</b>	Global Positioning System
<b>GSM</b>	Global System for Mobile communications
<b>i.i.d.</b>	independent and identically distributed
<b>IMM</b>	Interacting Multiple Model
<b>KF</b>	Kalman filter

---

<b>LOS</b>	Line-Of-Sight
<b>MAP</b>	Maximum A Posteriori
<b>MC</b>	Monte Carlo
<b>ML</b>	Maximum Likelihood
<b>MM-PF</b>	multiple-model particle filter
<b>MM-RBPF</b>	multiple-model Rao-Blackwellized particle filter
<b>MMSE</b>	Minimum Mean Square Error
<b>M-PCRLB</b>	Marginalization Posterior Cramér-Rao Lower Bound
<b>MSE</b>	Mean Square Error
<b>MT</b>	Mobile Terminal
<b>NLOS</b>	Non-Line-Of-Sight
<b>PCRLB</b>	Posterior Cramér-Rao Lower Bound
<b>pdf</b>	probability density function
<b>PF</b>	Particle Filter
<b>PR</b>	Pseudorange
<b>RBAPF</b>	Rao-Blackwellized Auxiliary Particle Filter
<b>RBPF</b>	Rao-Blackwellized Particle Filter
<b>RMSE</b>	Root Mean Square Error
<b>RRLP</b>	Radio Ressource Location Protocol
<b>RSS</b>	Received Signal Strength
<b>RTT</b>	Round Trip Time
<b>RXLEV</b>	Received Signal Level
<b>SAT</b>	Satellite
<b>TA</b>	Timing Advance
<b>ToA</b>	Time of Arrival



<b>TDoA</b>	Time Difference of Arrival
<b>TPM</b>	Transition Probability Matrix
<b>UKF</b>	Unscented Kalman Filter
<b>UMTS</b>	Universal Mobile Telecommunications System
<b>WGS-84</b>	World Geodetic System 1984
<b>WLAN</b>	Wireless Local Area Network



# List of Symbols

$\arg \max_x f(x)$	The $x$ maximizing $f(x)$
$\arg \min_x f(x)$	The $x$ minimizing $f(x)$
$A(\cdot)$	Mode-dependent reference path loss
$A_{LOS}^{(m)}$	Reference path loss of the $m$ -th RSS measurement affected by LOS propagation conditions
$A_{NLOS}^{(m)}$	Reference path loss of the $m$ -th RSS measurement affected by NLOS propagation conditions
$b^{(m)}$	Constant related to the FIM of RSS measurements, cf. Section 3.3.2
$B(\cdot)$	Mode-dependent path loss exponent
$B_{LOS}^{(m)}$	Path loss exponent of the $m$ -th RSS measurement affected by LOS propagation conditions
$B_{NLOS}^{(m)}$	Path loss exponent of the $m$ -th RSS measurement affected by NLOS propagation conditions
$c_0$	speed of light
$c^{(\cdot)}$	Constant related to the equivalent FIM of the MT location, cf. Section 3.3.2
$\text{CRLB}_k$	MT location CRLB at time step $k$
$\overline{\text{CRLB}}$	Time averaged MT location CRLB
$d_{\text{BS},k}^{(n)}(\cdot)$	Euclidean distance between the MT and the $n$ -th BS at time step $k$
$d_{\text{SAT},k}^{(l)}(\cdot)$	Euclidean distance between the MT and the $l$ -th SAT at time step $k$
$\det[\cdot]$	Determinant of a matrix
$\text{diag}[\cdot]$	Diagonal matrix consisting of the elements of a vector
$\text{diag}_b[\cdot]$	Composes a block diagonal matrix of the matrix arguments
$\mathbf{D}(\cdot)$	Hessian matrix related to the Gauss-Newton algorithm, cf. Section 3.4.2.2
$e$	Base of the natural logarithm, also called Napier's constant
$e^{(\cdot)}$	Constant related to the equivalent FIM of the MT location, cf. Section 3.3.2
$\mathbf{f}_{k-1}(\cdot)$	State transition function relating the state $\mathbf{x}_{k-1}$ to the state $\mathbf{x}_k$
$\mathbf{f}_{k-1}^{(l)}(\cdot)$	State transition function relating the state $\mathbf{x}_{k-1}^{(l)}$ to the state $\mathbf{x}_k^{(l)}$
$\mathbf{f}_{k-1}^{(n)}(\cdot)$	State transition function relating the state $\mathbf{x}_{k-1}^{(n)}$ to the state $\mathbf{x}_k^{(n)}$
$\mathbf{f}_{\text{P},k-1}(\cdot)$	Projection function, that projects the on-road MT state vector into the next road segment
$\mathbf{f}_{\text{R},k-1}(\cdot)$	Function relating the state $\mathbf{x}_{\text{R},k-1}$ to the state $\mathbf{x}_{\text{R},k}$
$\mathbf{F}$	State transition matrix related to the state vector $\mathbf{x}_k$

$\mathbf{F}_{k-1}^l(\cdot)$	State transition matrix at time step $k - 1$ related to the vector $\mathbf{x}_k^l$
$\mathbf{F}_{k-1}^n(\cdot)$	State transition matrix at time step $k - 1$ related to the vector $\mathbf{x}_k^n$
$\mathbf{F}_{\text{CO}}$	State transition matrix related to the state vector $\mathbf{x}_{\text{CO},k}$
$\mathbf{F}_{\text{CV}}$	State transition matrix related to the state vector $\mathbf{x}_{\text{CV},k}$
$g^{(m)}$	Constant related to the FIM of the $m$ -th RSS measurement, cf. Section 3.3.2
$G^{(m)}(\cdot)$	Mode-dependent normalized antenna gain of the $m$ -th BS antenna
$G_{\text{ANT}}(\cdot)$	Normalized antenna gain of the $m$ -th BS antenna
$G_{\text{min}}$	Minimum antenna gain of the $m$ -th BS antenna
$\mathbf{g}(\cdot)$	Gradient vector related to the Gauss-Newton algorithm, cf. Section 3.4.2.2
$h_i$	Allan variance parameters ( $i = -2, -1, 0$ )
$h_k^{(l)}(\cdot)$	$l$ -th element of the vector $\mathbf{h}_k(\cdot)$
$h_{\text{BIAS},k}(\cdot)$	Function relating the MT state to the MT clock bias measurement
$h_{\text{LOS},k}^{(m)}(\cdot)$	$m$ -th element of the vector $\mathbf{h}_{\text{LOS},k}(\cdot)$
$h_{\text{RSS},k}^{(m)}(\cdot)$	$m$ -th element of the vector $\mathbf{h}_{\text{RSS},k}(\cdot)$
$h_{\text{RTT},k}^{(m)}(\cdot)$	$m$ -th element of the vector $\mathbf{h}_{\text{RTT},k}(\cdot)$
$\mathbf{h}_k(\cdot)$	Vector of measurement functions, related to the vector $\mathbf{z}_k$
$\mathbf{h}_{1,k}(\cdot)$	Vector of measurement functions, related to the vector $\mathbf{z}_{1,k}$
$\mathbf{h}_{2,k}(\cdot)$	Vector of measurement functions, related to the vector $\mathbf{z}_{2,k}$
$\mathbf{h}_{\text{LOS},k}(\cdot)$	Vector of functions relating the MT state to the measurements, where each measurement is affected by LOS propagation conditions at time step $k$
$\mathbf{h}_{\text{PR},k}(\cdot)$	Vector of functions relating the MT state to the PR measurements at time step $k$
$\mathbf{h}_{\text{RSS},k}(\cdot)$	Vector of mode-dependent functions relating the MT state to the RSS measurements at time step $k$
$\mathbf{h}_{\text{RSS,LOS},k}(\cdot)$	Vector of functions relating the MT state to the RSS measurements, where each measurement is affected by LOS propagation conditions at time step $k$
$\mathbf{h}_{\text{RTT},k}(\cdot)$	Vector of functions relating the MT state to the RTT measurements at time step $k$
$\mathbf{h}_{\text{SAT},k}(\cdot)$	Vector of functions relating the MT state to the PR and GRT measurements at time step $k$
$\mathbf{H}_k(\cdot)$	Matrix relating the state vector $\mathbf{x}_k^l$ to the measurement vector $\mathbf{z}_{1,k}$
$\tilde{\mathbf{H}}_k(\cdot)$	Jacobian matrix of $\mathbf{h}_k(\cdot)$
$\mathbf{H}_{\text{LOS},k}(\cdot)$	Jacobian matrix of $\mathbf{h}_{\text{LOS},k}(\cdot)$
$i^j, i^{(j)}$	index of the resampled parent particle

---

$\mathbf{I}_n$	Identity matrix of size $n$
$\mathbf{I}_{B,k}$	BIM at time step $k$
$\mathbf{J}_k$	Bayesian information submatrix at time step $k$
$\mathbf{J}_k^l$	Bayesian information submatrix at time step $k$ conditioned on the $l$ -th mode sequence $\mathcal{R}_k^l$
$k$	discrete time index
$k_{\max}$	Total number of time steps
$\mathbf{K}_k$	Kalman gain matrix at time step $k$
$l_1$	Edge length of initial simplex
$\log_{10}$	Logarithm to the base 10
$\log_e$	Natural logarithm
$L^{(m)}(\cdot)$	Mode-dependent path loss of the $m$ -th RSS measurement
$M$	Number of measurements
$M_{\text{PR}}$	Number of PR measurements
$M_{\text{RSS}}$	Number of RSS measurements
$M_{\text{RTT}}$	Number of RTT measurements
$n_w$	Dimension of state noise vector $\mathbf{w}_{k-1}$
$n_v$	Dimension of measurement noise vector $\mathbf{v}_k$
$n_x$	Dimension of state vector $\mathbf{x}_k$
$n_{x_1}$	Dimension of state vector $\mathbf{x}_k^1$
$n_{x_n}$	Dimension of state vector $\mathbf{x}_k^n$
$n_{\tilde{\mathbf{x}}}$	Dimension of reduced state vector $\tilde{\mathbf{x}}_k$
$n_z$	Dimension of measurement vector $\mathbf{z}_k$
$N$	Number of particles
$N_{\text{BS}}$	Number of BSs
$N_{\text{MC}}$	Number of Monte Carlo simulations
$N_r$	Number of candidate road segments
$N_{\text{SAT}}$	Number of satellites
$\tilde{\mathbf{n}}_{n,k}^{(\eta)}$	$n$ -th vertex of the simplex after shrinkage at time step $k$ and at the $\eta$ -th iteration of the Nelder-Mead simplex algorithm
$p(\cdot)$	pdf
$p(\cdot \cdot)$	conditional pdf
$p_{\text{LOS}}^{(m)}$	stationary mode probability of the $m$ -th Markov chain corresponding to the $m$ -th measurement being affected by LOS propagation conditions
$p_{\text{MT}}$	MT location in local, road-based coordinates

$\dot{p}_{\text{MT}}$	MT velocity in local, road-based coordinates
$P_{\text{NLOS}}^{(m)}$	stationary mode probabilities of the $m$ -th Markov chain corresponding to the $m$ -th measurement being affected by NLOS propagation conditions
$\mathbf{P}_{\text{SAT},k}^{(m)}$	Projection of the unit vector $\mathbf{u}_{\text{SAT},k}^{(m)}$ into the $xy$ -plane
$P_{\text{T}}^{(m)}$	Equivalent isotropic radiated power of the $m$ -th BS antenna
$\Pr\{\cdot\}$	Probability of an event
$\Pr\{\cdot \cdot\}$	Conditional probability of an event
$\text{PCRLB}_k$	MT location PCRLB at time step $k$
$\overline{\text{PCRLB}}$	Time averaged MT location PCRLB
$\mathbf{P}_{k k-1}$	Prediction covariance matrix
$\mathbf{P}_{k k}$	Posterior covariance matrix
$\mathbf{P}_{\text{m},k k}$	Moment-matched posterior covariance matrix in the IMM algorithm
$\mathbf{P}_{\text{MMSE},k k}$	Covariance matrix of MMSE estimation error related to the state vector $\mathbf{x}_k$
$\mathbf{P}_{\text{MMSE},k k}^{\text{l}}$	Covariance matrix of MMSE estimation error related to the state vector $\mathbf{x}_k^{\text{l}}$
$\mathbf{P}_{\text{MMSE},k k}^{\text{n}}$	Covariance matrix of MMSE estimation error related to the state vector $\mathbf{x}_k^{\text{n}}$
$\mathbf{P}_{\text{xz},k k-1}$	Cross-covariance matrix
$\mathbf{P}_{\text{zz},k k-1}$	Innovation covariance matrix
$q(\cdot)$	importance density
$q(\cdot)_{\text{opt.}}$	optimal importance density
$\mathbf{Q}$	Covariance matrix of the noise vector $\mathbf{w}_{k-1}$
$\mathbf{Q}_{k-1}^{\text{l}}$	Covariance matrix of the noise vector $\mathbf{w}_{k-1}^{\text{l}}$
$\bar{\mathbf{Q}}_{k-1}^{\text{l}}$	Covariance matrix of the noise vector $\bar{\mathbf{w}}_{k-1}^{\text{l}}$
$\mathbf{Q}_{k-1}^{\text{n}}$	Covariance matrix of the noise vector $\mathbf{w}_{k-1}^{\text{n}}$
$\mathbf{Q}_{k-1}^{\text{nl}}$	Cross-covariance matrix between the noise vectors $\mathbf{w}_{k-1}^{\text{l}}$ and $\mathbf{w}_{k-1}^{\text{n}}$
$\mathbf{Q}_{\text{CO}}$	Covariance matrix of the noise vector $\mathbf{w}_{\text{CO},k-1}$
$\mathbf{Q}_{\text{CV}}$	Covariance matrix of the noise vector $\mathbf{w}_{\text{CV},k-1}$
$r_k$	mode variable of the augmented Markov chain at time step $k$
$r_k^{(m)}$	mode variable of the $m$ -th Markov chain at time step $k$
$r_{\kappa}^{\text{l}}$	Value of the mode variable at time $\kappa = 1, \dots, k$ in the $l$ -th mode sequence $\mathcal{R}_k^{\text{l}}$
$\text{RMSE}_k$	MT location RMSE at time step $k$
$\overline{\text{RMSE}}$	Time averaged MT location RMSE
$\mathbf{R}_k$	Covariance matrix of the noise vector $\mathbf{v}_k$

---

$\mathbf{R}_{1,k}(\cdot)$	Covariance matrix of the noise vector $\mathbf{v}_{1,k}$
$\mathbf{R}_{\text{LOS},k}$	Covariance matrix of the noise vector $\mathbf{v}_{\text{LOS},k}$
$\mathbf{R}_{\text{PR},k}$	Covariance matrix of the noise vector $\mathbf{v}_{\text{PR},k}$
$\mathbf{R}_{\text{RSS},k}(\cdot)$	Mode-dependent covariance matrix of the noise vector $\mathbf{v}_{\text{RSS},k}(\cdot)$
$\mathbf{R}_{\text{RSS,LOS},k}$	Covariance matrix of the noise vector $\mathbf{v}_{\text{RSS,LOS},k}$
$\mathbf{R}_{\text{RTT},k}(\cdot)$	Mode-dependent covariance matrix of the noise vector $\mathbf{v}_{\text{RTT},k}(\cdot)$
$\mathbf{R}_{\text{RTT,LOS},k}$	Covariance matrix of the noise vector $\mathbf{v}_{\text{RTT,LOS},k}$
$\mathbf{R}_{\text{SAT},k}$	Covariance matrix of the combined noise vector $[\mathbf{v}_{\text{PR},k}^{\top}, \mathbf{v}_{\text{GRT},k}^{\top}]^{\top}$
$s$	Number of discrete states in the augmented Markov chain
$s^{(m)}$	Number of discrete states in the $m$ -th Markov chain
$s_{\text{ID}}$	Road identity value assigned to each road segment
$S_1^{(\eta)}$	Set of vectors forming the vertices of the simplex at the $\eta$ -th iteration of the Nelder-Mead simplex algorithm
$S_2^{(\eta)}$	Set of cost function values evaluated at the vertices of the simplex at the $\eta$ -th iteration of the Nelder-Mead simplex algorithm
$\tilde{S}_1^{(\eta)}$	Set of vertices of the simplex excluding the vertex $\mathbf{x}_{\text{H},k}^{(\eta)}$ at the $\eta$ -th iteration of the Nelder-Mead simplex algorithm
$\tilde{S}_2^{(\eta)}$	Set of cost function values evaluated at the vertices contained in the set $\tilde{S}_1^{(\eta)}$ at the $\eta$ -th iteration of the Nelder-Mead simplex algorithm
$\mathbf{S}_k$	Innovation covariance matrix
$t_k$	Time scale sampled at time instance $k \cdot T_{\text{S}}$
$t_{\text{GNSS},k}$	Sampled GNSS time scale
$t_{\text{MTC},k}$	Sampled MT clock time scale
$T_{\text{S}}$	Sampling interval of GSM measurements
$T'_{\text{S}}$	Sampling interval of GNSS measurements
$\mathbf{T}_{\text{G}}$	Transformation operator, that converts the state vector $\mathbf{x}_{\text{R},k}$ into the state vector $\mathbf{x}_k$
$\mathbf{T}_{\text{LG}}$	Transformation operator, that transforms local coordinates into global coordinates
$\text{tr}[\cdot]$	Trace of a matrix
$u_{\text{BS}_x,k}^{(m)}$	$x$ -component of unit vector $\mathbf{u}_{\text{BS},k}^{(m)}$
$u_{\text{BS}_y,k}^{(m)}$	$y$ -component of unit vector $\mathbf{u}_{\text{BS},k}^{(m)}$
$u_{\text{SAT}_x,k}^{(m)}$	$x$ -component of unit vector $\mathbf{u}_{\text{SAT},k}^{(m)}$
$u_{\text{SAT}_y,k}^{(m)}$	$y$ -component of unit vector $\mathbf{u}_{\text{SAT},k}^{(m)}$
$u_{\text{SAT}_z,k}^{(m)}$	$z$ -component of unit vector $\mathbf{u}_{\text{SAT},k}^{(m)}$
$\mathbf{u}_x$	unit vector in $x$ -direction
$\mathbf{u}_y$	unit vector in $y$ -direction

$\mathbf{u}_z$	unit vector in $z$ -direction
$\mathbf{u}_{\text{BS},k}^{(m)}$	Unit vector originating at the true MT location and directed towards the $m$ -th BS at time step $k$
$\mathbf{u}_{\text{SAT},k}^{(m)}$	Unit vector originating at the true MT location and directed towards the $m$ -th satellite at time step $k$
$v_k^{(l)}$	$l$ -th element of the measurement noise vector $\mathbf{v}_k$
$v_{\text{BIAS},k}$	MT clock bias measurement noise variable at time step $k$
$v_{\text{GRT},k}$	GRT measurement noise variable at time step $k$
$v_{\text{RSS,LOS},k}^{(m)}$	Noise variable for the $m$ -th RSS measurement affected by LOS propagation conditions at time step $k$
$v_{\text{RSS,NLOS},k}^{(m)}$	Noise variable for the $m$ -th RSS measurement affected by NLOS propagation conditions at time step $k$
$v_{\text{RTT,LOS},k}^{(m)}$	Noise variable for the $m$ -th RTT measurement affected by LOS propagation conditions at time step $k$
$v_{\text{RTT,NLOS},k}^{(m)}$	Noise variable for the $m$ -th RTT measurement affected by NLOS propagation conditions at time step $k$
$V_1(\cdot)$	Cost function of ML estimator assuming that all measurements are affected by LOS propagation conditions
$V_1'(\cdot)$	Gradient of the cost function $V_1(\cdot)$
$V_2(\cdot)$	Approximative cost function of ML estimator assuming that measurements are affected by LOS or NLOS propagation conditions
$\tilde{V}_1(\cdot)$	Cost function of Gauss-Newton algorithm
$\check{V}_1(\cdot)$	Cost function of Levenberg-Marquardt algorithm
$\mathbf{v}_k$	Measurement noise vector at time step $k$ , which is related to the measurement vector $\mathbf{z}_k$
$\mathbf{v}_{1,k}$	Measurement noise vector at time step $k$ , which is related to the measurement vector $\mathbf{z}_{1,k}$
$\mathbf{v}_{2,k}$	Measurement noise vector at time step $k$ , which is related to the measurement vector $\mathbf{z}_{2,k}$
$\mathbf{v}_{\text{LOS},k}$	Noise vector for measurements affected by LOS propagation conditions at time step $k$
$\mathbf{v}_{\text{PR},k}$	PR measurement noise vector at time step $k$
$\mathbf{v}_{\text{RSS},k}(\cdot)$	Mode-dependent RSS measurement noise vector at time step $k$
$\mathbf{v}_{\text{RSS,LOS},k}$	Noise vector for RSS measurements affected by LOS propagation conditions at time step $k$
$\mathbf{v}_{\text{RTT},k}(\cdot)$	Mode-dependent RTT measurement noise vector at time step $k$
$\mathbf{v}_{\text{RTT,LOS},k}$	Noise vector for RTT measurements affected by LOS propagation conditions at time step $k$
$w_{k-1}^{(l)}$	$l$ -th element of the state noise vector $\mathbf{w}_{k-1}$



---

$w_{1,k-1}$	State noise variable at time step $k - 1$ related to the on-road state vector $\mathbf{x}_{\text{MT},k}$
$w_{2,k-1}$	Discrete state noise variable at time step $k - 1$ that selects between $N_r$ candidate road segments
$w_{\delta t,k-1}$	clock bias component of $\mathbf{w}_{\text{CO},k-1}$
$w_{\delta t,k-1}$	clock drift component of $\mathbf{w}_{\text{CO},k-1}$
$w_{x,k-1}$	$x$ -component of $\mathbf{w}_{\text{CO},k-1}$
$w_{y,k-1}$	$y$ -component of $\mathbf{w}_{\text{CO},k-1}$
$w_{k k}^{(i)}$	importance weight related to the $i$ -th particle in the PF-based algorithms
$W_m^{(i)}$	$i$ -th weight used to calculate the mean vector of the transformed sigma point/cubature point vector
$W_c^{(i)}$	$i$ -th weight used to calculate the covariance matrix of the transformed sigma point/cubature point vector
$\mathbf{w}_{k-1}$	State noise vector at time step $k - 1$ related to $\mathbf{x}_k$
$\mathbf{w}_{k-1}^1$	State noise vector at time step $k - 1$ related to $\mathbf{x}_k^1$
$\bar{\mathbf{w}}_{k-1}^1$	Decorrelated state noise vector of $\mathbf{w}_{k-1}^1$
$\mathbf{w}_{k-1}^n$	State noise vector at time step $k - 1$ related to $\mathbf{x}_k^n$
$\mathbf{w}_{\text{CO},k-1}$	State noise vector at time step $k - 1$ related to $\mathbf{x}_{\text{CO},k}$
$\mathbf{w}_{\text{CV},k-1}$	State noise vector at time step $k - 1$ related to $\mathbf{x}_{\text{CV},k}$
$\mathbf{w}_{\text{R},k-1}$	State noise vector at time step $k - 1$ related to $\mathbf{x}_{\text{R},k}$
$x_k^{(l)}$	$l$ -th element of the state vector $\mathbf{x}_k$
$\tilde{x}_k^{(l)}$	$l$ -th element of the reduced state vector $\tilde{\mathbf{x}}_k$
$x_{\text{BS}}^{(n)}$	$x$ -coordinate of the $n$ -th BS
$x_G$	$x$ -coordinate of global coordinate system
$x_L$	$x$ -coordinate of local coordinate system
$x_{\text{MT},k}$	$x$ -coordinate of the MT at time step $k$
$\dot{x}_{\text{MT},k}$	MT velocity in $x$ -direction at time step $k$
$x_{\text{SAT},k}^{(l)}$	$x$ -coordinate of the $l$ -th satellite at time step $k$
$\mathbf{x}_k$	State vector at time step $k$
$\hat{\mathbf{x}}_k(\cdot)$	Estimate of the state vector $\mathbf{x}_k$ (given the measurement $\mathbf{z}_k$ )
$\tilde{\mathbf{x}}_k$	Reduced state vector at time step $k$
$\hat{\tilde{\mathbf{x}}}_k^{(\eta)}$	Estimate of the reduced state vector $\tilde{\mathbf{x}}_k$ at the $\eta$ -th iteration
$\mathbf{x}_k^1$	State vector at time step $k$ composed of linear states
$\mathbf{x}_k^n$	State vector at time step $k$ composed of nonlinear states
$\hat{\mathbf{x}}_{k \kappa}$	Estimate of the state vector $\mathbf{x}_k$ given the measurements $\mathbf{Z}_\kappa$

$\hat{\mathbf{x}}_{k k-1}$	Predicted state vector
$\hat{\mathbf{x}}_{m,k k}$	Moment-matched mean vector in the IMM algorithm
$\tilde{\mathbf{x}}_{n,k}^{(\eta)}$	$n$ -th vertex of the simplex at the $\eta$ -th iteration at time step $k$ and the $\eta$ -th iteration of the Nelder-Mead simplex algorithm
$\mathbf{x}_{BS}^{(n)}$	Vector of coordinates of the $n$ -th BS
$\mathbf{x}_{CO,k}$	State vector of the CO model at time step $k$ , cf. Section 2.3.2.4
$\mathbf{x}_{CV,k}$	State vector of the CV model at time step $k$ , cf. Section 2.3.2.3
$\tilde{\mathbf{x}}_{E,k}^{(\eta)}$	Expansion vector at time step $k$ and at the $\eta$ -th iteration of the Nelder-Mead simplex algorithm
$\tilde{\mathbf{x}}_{H,k}^{(\eta)}$	Vertex providing the largest cost function value of the set $S_2^{(\eta)}$ at time step $k$ and at the $\eta$ -th iteration of the Nelder-Mead simplex algorithm
$\tilde{\mathbf{x}}_{IC,k}^{(\eta)}$	Inside contraction vector at time step $k$ and the $\eta$ -th iteration of the Nelder-Mead simplex algorithm
$\tilde{\mathbf{x}}_{L,k}^{(\eta)}$	Vertex providing the smallest cost function value of the set $S_2^{(\eta)}$ at time step $k$ and at the $\eta$ -th iteration of the Nelder-Mead simplex algorithm
$\tilde{\mathbf{x}}_{M,k}^{(\eta)}$	Center of gravity of all vectors contained in the set $\tilde{S}_1^{(\eta)}$ at time step $k$ and at the $\eta$ -th iteration of the Nelder-Mead simplex algorithm
$\hat{\mathbf{x}}_{MAP,k}$	MAP estimate of the state vector $\mathbf{x}_k$
$\hat{\mathbf{x}}_{ML,k}$	ML estimate of the state vector $\mathbf{x}_k$
$\hat{\tilde{\mathbf{x}}}_{ML,k}$	ML estimate of the reduced state vector $\tilde{\mathbf{x}}_k$
$\hat{\mathbf{x}}_{MMSE,k}$	MMSE estimate of the state vector $\mathbf{x}_k$ (given the measurement $\mathbf{z}_k$ )
$\hat{\mathbf{x}}_{MMSE,k k}$	MMSE estimate of the state vector $\mathbf{x}_k$ given the measurements $\mathbf{Z}_k$
$\hat{\mathbf{x}}_{MMSE,k k}^1$	MMSE estimate of the state vector $\mathbf{x}_k^1$ given the measurements $\mathbf{Z}_k$
$\hat{\mathbf{x}}_{MMSE,k k}^n$	MMSE estimate of the state vector $\mathbf{x}_k^n$ given the measurements $\mathbf{Z}_k$
$\mathbf{x}_{MT,k}$	Vector of MT coordinates at time step $k$
$\dot{\mathbf{x}}_{MT,k}$	Vector of MT velocity components at time step $k$
$\hat{\mathbf{x}}_{MT,k}$	Estimate of the MT location vector $\mathbf{x}_{MT,k}$ (given the measurement $\mathbf{z}_k$ )
$\hat{\mathbf{x}}_{MT,k k}$	Estimate of the MT location vector $\mathbf{x}_{MT,k}$ given the measurements $\mathbf{Z}_k$
$\tilde{\mathbf{x}}_{OC,k}^{(\eta)}$	Outside contraction vector at time step $k$ and at the $\eta$ -th iteration of the Nelder-Mead simplex algorithm
$\tilde{\mathbf{x}}_{R,k}^{(\eta)}$	Reflection vector at time step $k$ and at the $\eta$ -th iteration of the Nelder-Mead simplex algorithm
$\mathbf{x}_{R,k}$	On-road state vector at time step $k$
$\mathbf{x}_{R,k}^1$	On-road state vector at time step $k$ composed of linear states
$\mathbf{x}_{R,k}^n$	On-road state vector at time step $k$ composed of nonlinear states
$\tilde{\mathbf{x}}_{S,k}^{(\eta)}$	Vertex providing the second largest cost function value of the set $S_2^{(\eta)}$ at time step $k$ and at the $\eta$ -th iteration of the Nelder-Mead simplex algorithm

---

$\mathbf{x}_{\text{SAT},k}^{(l)}$	Vector of coordinates of the $l$ -th satellite at time step $k$
$\mathbf{X}_k$	Sequence of states $\{\mathbf{x}_0, \dots, \mathbf{x}_k\}$ up to and including time $k$
$\hat{\mathbf{X}}_k(\cdot)$	Estimate of $\mathbf{X}_k$
$y_{\text{BS}}^{(n)}$	$y$ -coordinate of the $n$ -th BS
$y_{\text{G}}$	$y$ -coordinate of global coordinate system
$y_{\text{L}}$	$y$ -coordinate of local coordinate system
$y_{\text{MT},k}$	$y$ -coordinate of the MT at time step $k$
$\dot{y}_{\text{MT},k}$	MT velocity in $y$ -direction at time step $k$
$y_{\text{SAT},k}^{(l)}$	$y$ -coordinate of the $l$ -th satellite at time step $k$
$\mathbf{y}_k$	augmented state vector at time step $k$ , consisting of the state vector $\mathbf{x}_k$ and mode variable $r_k$
$z_k^{(l)}$	$l$ -th element of the measurement vector $\mathbf{z}_k$
$z_{\text{BIAS},k}$	MT clock bias measurement at time step $k$
$z_{\text{GRT},k}$	GRT measurement at time step $k$
$z_{\text{RSS},k}^{(m)}$	$m$ -th element of the vector $\mathbf{z}_{\text{RSS},k}$
$z_{\text{RTT},k}^{(m)}$	$m$ -th element of the vector $\mathbf{z}_{\text{RTT},k}$
$z_{\text{SAT},k}^{(l)}$	$z$ -coordinate of the $l$ -th satellite at time step $k$
$\mathbf{z}_k$	Vector of measurements at time step $k$
$\hat{\mathbf{z}}_{k k-1}$	Prediction estimate of the measurement vector $\mathbf{z}_k$
$\mathbf{z}_{1,k}$	Vector of measurements at time step $k$ , where each measurement depends on the state vectors $\mathbf{x}_k^n$ and/or $\mathbf{x}_k^1$
$\hat{\mathbf{z}}_{1,k}$	Prediction estimate of the measurement vector $\mathbf{z}_{1,k}$
$\mathbf{z}_{2,k}$	Vector of measurements at time step $k$ , where each measurement depends only on the state vector $\mathbf{x}_k^n$
$\mathbf{z}_{\text{LOS},k}$	Vector of measurements at time step $k$ , where all measurements are affected by LOS propagation conditions
$\mathbf{z}_{\text{PR},k}$	Vector of PR measurements at time step $k$
$\mathbf{z}_{\text{RSS},k}$	Vector of RSS measurements at time step $k$ , where each measurement is affected by LOS or NLOS propagation conditions
$\mathbf{z}_{\text{RSS,LOS},k}$	Vector of RSS measurements at time step $k$ , where all measurements are affected by LOS propagation conditions
$\mathbf{z}_{\text{RTT},k}$	Vector of RTT measurements at time step $k$ , where each measurement is affected by LOS or NLOS propagation conditions
$\mathbf{z}_{\text{RTT,LOS},k}$	Vector of RTT measurements at time step $k$ , where all measurements are affected by LOS propagation conditions
$\mathbf{z}_{\text{SAT},k}$	Vector of PR and GRT measurements at time step $k$
$\mathbf{Z}_k$	Sequence of measurements $\{\mathbf{z}_1, \dots, \mathbf{z}_k\}$ up to and including time $k$

$\alpha$	Parameter describing the spread of sigma point vectors around the mean in the scaled unscented transformation, cf. Section 4.4.3
$\alpha_1$	Reflection coefficient in the Nelder-Mead simplex algorithm, cf. Section 3.4.3
$\alpha_2$	Expansion coefficient in the Nelder-Mead simplex algorithm, cf. Section 3.4.3
$\alpha_3$	Contraction coefficient in the Nelder-Mead simplex algorithm, cf. Section 3.4.3
$\alpha_4$	Shrinkage coefficient in the Nelder-Mead simplex algorithm, cf. Section 3.4.3
$\beta_1$	Scaling parameter in the scaled unscented transformation, cf. Section 4.4.3
$\beta_2$	Weight parameter in the scaled unscented transformation, cf. Section 4.4.3
$\gamma$	Scaling parameter in the scaled unscented transformation, cf. Section 4.4.3
$\mathbf{\Gamma}_{k-1}$	Noise gain matrix at time step $k - 1$ related to $\mathbf{w}_{k-1}$
$\mathbf{\Gamma}_{k-1}^1$	Noise gain matrix at time step $k - 1$ related to $\mathbf{w}_{k-1}^{(1)}$
$\mathbf{\Gamma}_{k-1}^n$	Noise gain matrix at time step $k - 1$ related to $\mathbf{w}_{k-1}^{(n)}$
$\mathbf{\Gamma}_{\text{CO}}$	Noise gain matrix related to $\mathbf{w}_{\text{CO},k-1}$
$\mathbf{\Gamma}_{\text{CV}}$	Noise gain matrix related to $\mathbf{w}_{\text{CV},k-1}$
$\delta(\cdot)$	Dirac delta
$\delta t_k$	MT clock bias state at time step $k$
$\delta \dot{t}_k$	MT clock drift state at time step $k$
$\Delta$	Laplace operator
$\epsilon_1$	Constant related to the stopping criterion of the Gauss-Newton algorithm, cf. Section 3.4.2.2
$\epsilon_2$	Constant related to the stopping criterion of the Gauss-Newton algorithm, cf. Section 3.4.2.2
$\epsilon_3$	Constant related to the stopping criterion of the Nelder-Mead simplex algorithm, cf. Section 3.4.3
$\zeta^{(\cdot)}$	Damping parameter of the Levenberg-Marquardt algorithm
$\eta$	iteration index
$\eta_{\text{max}}$	Maximum number of iterations
$\mu_{\text{ANT}}^{(m)}$	Mean value of the pdf describing the antenna gain of the $m$ -th BS in NLOS propagation conditions
$\mu_{\text{RTT},k}(\cdot)$	Element of the mean vector $\boldsymbol{\mu}_{\text{RTT},k}(\cdot)$
$\mu_{\text{RTT,NLOS},k}^{(m)}$	Mean value of the $m$ -th noise variable $v_{\text{RTT,NLOS},k}^{(m)}$

---

$\boldsymbol{\mu}_k$	Mean vector of the noise vector $\mathbf{v}_k$
$\boldsymbol{\mu}_{1,k}$	Mean vector of the noise vector $\mathbf{v}_{1,k}$
$\boldsymbol{\mu}_{\text{RTT},k}(\cdot)$	Mode-dependent mean vector of the noise vector $\mathbf{v}_{\text{RTT},k}(\cdot)$
$\pi_i$	Initial mode probabilities of the $m$ -th Markov chain ( $i = 1, 2$ )
$\pi_{ij}^{(m)}$	Transition probability from mode $i$ to mode $j$ for the $m$ -th Markov chain ( $i, j = 1, 2$ )
$\mathbf{\Pi}_m$	TPM of the $m$ -th Markov chain
$\mathbf{\Pi}$	TPM of the augmented Markov chain
$\rho^{(\cdot)}$	Parameter related to the Levenberg-Marquardt algorithm, cf. Section 3.4.2.3
$\varrho$	Gain ratio used in the Levenberg-Marquardt algorithm, cf. Section 3.4.2.3
$\sigma_{\text{ANT}}^{(m)}$	Standard deviation of the pdf describing the antenna gain of the $m$ -th BS in NLOS propagation conditions
$\sigma_{\text{BIAS},k}$	Standard deviation of the noise variable $v_{\text{BIAS},k}$
$\sigma_{\text{GRT},k}$	Standard deviation of the noise variable $v_{\text{GRT},k}$
$\sigma_{\text{LOS},k}^{(m)}$	Standard deviation of the noise variable related to the $m$ -th measurement, which is affected by LOS propagation conditions
$\sigma_{\text{P}}$	Standard deviation of the noise vector $\mathbf{w}_{1,k-1}$
$\sigma_{\text{PR},k}^{(l)}$	Standard deviation of the $l$ -th element of the noise vector $\mathbf{v}_{\text{PR},k}$
$\sigma_{\text{RSS},k}^{(m)}$	Mode-dependent standard deviation of the $m$ -th element of the noise vector $\mathbf{v}_{\text{RSS},k}(\cdot)$
$\sigma_{\text{RSS,LOS},k}^{(m)}$	Standard deviation of the $m$ -th noise variable $v_{\text{RSS,LOS},k}^{(m)}$
$\sigma_{\text{RSS,NLOS},k}^{(m)}$	Standard deviation of the $m$ -th noise variable $v_{\text{RSS,NLOS},k}^{(m)}$
$\sigma_{\text{RTT},k}^{(m)}$	Mode-dependent standard deviation of the $m$ -th element of the noise vector $\mathbf{v}_{\text{RTT},k}(\cdot)$
$\sigma_{\text{RTT,LOS},k}^{(m)}$	Standard deviation of the $m$ -th noise variable $v_{\text{RTT,LOS},k}^{(m)}$
$\sigma_{\text{RTT,NLOS},k}^{(m)}$	Standard deviation of the $m$ -th noise variable $v_{\text{RTT,NLOS},k}^{(m)}$
$\sigma_{\text{SHA},k}^{(m)}$	Standard deviation of the $m$ -th noise variable describing RSS measurement errors due to shadowing
$\sigma_x$	Standard deviation of the noise vector $w_{x,k-1}$
$\sigma_y$	Standard deviation of the noise vector $w_{y,k-1}$
$\tau$	Constant related to the Levenberg-Marquardt algorithm, cf. Section 3.4.2.3
$\varphi_0^{(m)}$	Azimuth angle between the positive $x$ -axis of the Cartesian coordinate system with the $m$ -th BS location as origin, and the vector pointing in the boresight direction of the $m$ -th BS antenna
$\varphi_{3\text{dB}}^{(m)}$	3 dB beamwidth of the $m$ -th BS antenna

$\varphi_{\text{BS}}^{(m)}(\cdot)$	Azimuth angle between the vector pointing into the boresight direction of the $m$ -th BS antenna and the vector that is directed towards the mode-dependent (LOS or NLOS) propagation path of the radio signal that is received by the MT
$\varphi_{\text{LOS}}^{(m)}(\cdot)$	Azimuth angle between the vector pointing into the boresight direction of the $m$ -th BS antenna and the vector that is directed towards the LOS propagation path of the radio signal that is received by the MT
$\varphi_{\text{NLOS}}^{(m)}$	Azimuth angle between the vector pointing into the boresight direction of the $m$ -th BS antenna and the vector that is directed towards the NLOS propagation path of the radio signal that is received by the MT
$\psi_{s_{\text{ID}}}$	Angle between the $s_{\text{ID}}$ -th road segment and the $x_{\text{G}}$ -axis of the global coordinate system
$\mathcal{A}^{(\kappa_1, \kappa_2)}$	Signed area of the parallelogram determined by $\mathbf{p}_{\text{SAT},k}^{(\kappa_1)}$ and $\mathbf{p}_{\text{SAT},k}^{(\kappa_2)}$
$\mathcal{B}^{(\kappa_1, \kappa_2)}$	Signed area of the parallelogram determined by $\mathbf{u}_{\text{BS},k}^{(\kappa_1)}$ and $\mathbf{p}_{\text{SAT},k}^{(\kappa_2)}$
$\mathcal{C}^{(\kappa_1, \kappa_2)}$	Signed area of the parallelogram determined by $\mathbf{u}_{\text{BS},k}^{(\kappa_1)}$ and $\mathbf{u}_{\text{BS},k}^{(\kappa_2)}$
$\mathcal{C}_{\text{CKF}}(\cdot)$	Computational complexity in FLOPs per time step of the CKF
$\mathcal{C}_{\text{EKF}}(\cdot)$	Computational complexity in FLOPs per time step of the EKF
$\mathcal{C}_{\text{GN}}(\cdot)$	Computational complexity in FLOPs per iteration of Gauss-Newton algorithm
$\mathcal{C}_{\text{LM}}(\cdot)$	Computational complexity in FLOPs per iteration of Levenberg-Marquardt algorithm
$\mathcal{C}_{\text{UKF}}(\cdot)$	Computational complexity in FLOPs per time step of the UKF
$\mathcal{D}^{(\kappa_1, \kappa_2)}$	Dot product of $\mathbf{u}_{\text{BS},k}^{(\kappa_1)}$ and $\mathbf{p}_{\text{SAT},k}^{(\kappa_2)}$
$\mathcal{E}^{(\kappa_1, \kappa_2)}$	Dot product of $\mathbf{u}_{\text{BS},k}^{(\kappa_1)}$ and $\mathbf{u}_{\text{BS},k}^{(\kappa_2)}$
$\mathcal{F}(\cdot)$	FIM
$\mathcal{F}_{\text{L}}(\cdot)$	Equivalent FIM of the MT location
$\mathcal{F}_{\text{GRT}}(\cdot)$	FIM of GRT measurements
$\mathcal{F}_{\text{PR}}(\cdot)$	FIM of PR measurements
$\mathcal{F}_{\text{RSS}}(\cdot)$	FIM of RSS measurements
$\mathcal{F}_{\text{RSS}}^{(m)}(\cdot)$	FIM of the $m$ -th RSS measurement
$\mathcal{F}_{\text{RTT}}(\cdot)$	FIM of RTT measurements
$\mathcal{F}_{\text{RTT}}^{(m)}(\cdot)$	FIM of the $m$ -th RTT measurement
$\mathcal{G}^{(\kappa_1, \kappa_2, \kappa_3, \kappa_4)}$	Product of the signed areas $\mathcal{G}_1^{(\kappa_1, \kappa_2, \kappa_3, \kappa_4)}$ and $\mathcal{G}_2^{(\kappa_1, \kappa_2, \kappa_3, \kappa_4)}$
$\mathcal{G}_1^{(\kappa_1, \kappa_2, \kappa_3, \kappa_4)}$	Signed area of the rectangle determined by $[\mathbf{p}_{\text{SAT},k}^{(\kappa_1)} - \mathbf{p}_{\text{SAT},k}^{(\kappa_2)}]^\top \cdot \mathbf{u}_x$ and $[\mathbf{p}_{\text{SAT},k}^{(\kappa_3)} - \mathbf{p}_{\text{SAT},k}^{(\kappa_4)}]^\top \cdot \mathbf{u}_x$
$\mathcal{G}_2^{(\kappa_1, \kappa_2, \kappa_3, \kappa_4)}$	Signed area of the parallelogram determined by $(\mathbf{p}_{\text{SAT},k}^{(\kappa_1)} - \mathbf{p}_{\text{SAT},k}^{(\kappa_2)})$ and $(\mathbf{p}_{\text{SAT},k}^{(\kappa_3)} - \mathbf{p}_{\text{SAT},k}^{(\kappa_4)})$
$\mathcal{N}(z; \mu_z, \sigma_z^2)$	pdf of a Gaussian random variable $z$ with mean $\mu_z$ and variance $\sigma_z^2$

---

$\mathcal{N}(\mathbf{z}; \boldsymbol{\mu}_{\mathbf{z}}, \mathbf{P}_{\mathbf{z}})$	pdf of a Gaussian random vector $\mathbf{z}$ with mean vector $\boldsymbol{\mu}_{\mathbf{z}}$ and covariance matrix $\mathbf{P}_{\mathbf{z}}$
$\mathcal{P}_{\text{CRLB},k}$	MT location CRLB at time step $k$
$\mathcal{P}(\cdot)$	CRLB matrix
$\mathcal{P}_{\text{E-PCRLB}}$	E-PCRLB matrix
$\mathcal{R}_k^l$	$l$ -th mode sequence $\{r_1^l, \dots, r_k^l\}$ up to and including time $k$
$\mathcal{T}_{\text{RN}}$	Road network database
$\mathcal{U}[a, b]$	Uniform distribution over the interval $[a, b]$
$\mathcal{X}_{k k-1}^{(i)}$	$i$ -th sigma/cubature point vector of the predicted state vector $\hat{\mathbf{x}}_{k k-1}$
$\mathcal{Z}_{k k-1}^{(i)}$	$i$ -th transformed sigma/cubature point vector of the predicted measurement vector $\hat{\mathbf{z}}_{k k-1}$
$\mathbb{E}_{p(\cdot)}\{\cdot\}$	Expectation operator with respect to the pdf $p(\cdot)$
$\mathbb{R}$	Set of real numbers
$\mathbb{N}$	Set of natural numbers
$\mathbf{0}_{i \times j}$	All-zeros matrix with $i$ rows and $j$ columns
$\mathbf{1}_{i \times j}$	All-ones matrix with $i$ rows and $j$ columns
$[\cdot]^{\text{T}}$	Transpose of a vector or matrix
$[\cdot]^{-1}$	Inverse of a square matrix
$[\cdot]_{i,j}$	element at the $i$ -th row and $j$ -th column of a matrix
$(\cdot)_i$	$i$ -th row of a matrix
$\triangleq$	Equal by definition
$\equiv$	identically equal
$\propto$	proportional to
$\sim$	distributed as
$\in$	Element of
$\times$	Vector cross product
$\otimes$	Kronecker product operator
$\nabla$	Gradient operator
$\ \cdot\ $	Euclidean norm or 2-norm of a vector
$\ \cdot\ _{\infty}$	Infinite norm of a vector
$\sqrt{\cdot}$	Square root of a scalar or square matrix





---

## Bibliography

- [3GP07] 3GPP TR 25.996, “Technical specification group radio access network; Spatial channel model for MIMO simulations,” European Telecommunications Standards Institute (ETSI), Version 6.1.0, Sept. 2007.
- [3GP09] 3GPP TS 44.031, “Location services LCS; Mobile Station (MS) - Serving Mobile Location Centre (SMLC) - Radio Resource LCS Protocol (RRLP),” European Telecommunications Standards Institute (ETSI), Version 8.3.0, May. 2009.
- [AD02] C. Andrieu and A. Doucet, “Particle filtering for partially observed Gaussian state space models,” *Journal of the Royal Statistical Society: Series B (Statistical Methodology)*, vol. 64, no. 4, pp. 827–836, 2002.
- [AF70] G. A. Ackerson and K. S. Fu, “On state estimation in switching environments,” *IEEE Trans. Autom. Control*, vol. 15, no. 1, pp. 10–17, 1970.
- [AH09] I. Arasaratnam and S. Haykin, “Cubature Kalman filters,” *IEEE Trans. Autom. Control*, vol. 54, no. 6, pp. 1254–1269, Jun 2009.
- [AJC02] S. Al-Jazzar and J. Caffery, “ML and Bayesian TOA location estimators for NLOS environments,” in *IEEE Vehicular Technology Conference*, Vancouver, BC, Canada, Sept 2002, pp. 1178–1181.
- [AL09] S. Ali-Löytty, “Gaussian mixture filters for hybrid positioning,” Ph.D. dissertation, Tampere University of Technology, Tampere, Finland, 2009.
- [AM79] B. Anderson and J. Moore, *Optimal filtering*, ser. Information and System Science Series. Englewood Cliffs, NJ, USA: Prentice Hall, 1979.
- [AMGC02] M. S. Arulampalam, S. Maskell, N. Gordon, and T. Clapp, “A tutorial on particle filters for online nonlinear/non-Gaussian Bayesian tracking,” *IEEE Trans. Signal Process.*, vol. 50, no. 2, pp. 174–188, Feb. 2002.
- [Ban85] S. Bancroft, “An algebraic solution for the GPS equations,” *IEEE Trans. Aerosp. Electron. Syst.*, vol. 21, no. 7, pp. 56–59, 1985.
- [BBS88] H. A. P. Blom and Y. Bar-Shalom, “The interacting multiple model algorithm for systems with markovian switching coefficients,” *IEEE Trans. Autom. Control*, vol. 33, no. 8, pp. 780–783, 1988.
- [Ber09] D. S. Bernstein, *Matrix mathematics: theory, facts and formulas*, 2nd ed. Princeton, NJ, USA: Princeton University Press, 2009.
- [BGRS02] N. Bourdeau, M. Gibeaux, J. Riba, and F. Sansone, “Hybridised GPS and GSM positioning technology for high performance location based services,” in *Proc. IST Mobile & Wireless Communications Summit*, Jun. 2002.

- [BHM98] J. Borras, P. Hatrack, and N. B. Mandayam, "Decision theoretic framework for NLOS mitigation," in *IEEE Vehicular Technology Conference*, Ottawa, Ontario, Canada, Apr 1998, pp. 1583–1587.
- [BMW03] M. Briers, S. Maskell, and R. Wright, "A Rao-Blackwellised unscented Kalman filter," in *Proceedings of the 6th International Conference of Information Fusion*, vol. 1, Jul. 2003, pp. 55–61.
- [Bra00] R. Bracewell, *The Fourier Transform and Its Applications*, 3rd ed. New York, NY, USA: Mc-Graw Hill, 2000.
- [BRF<sup>+</sup>03] A. Bessell, B. Ristic, A. Farina, X. Wang, and M. S. Arulampalam, "Error performance bounds for tracking a manoeuvring target," in *Proceedings of the International Conference on Information Fusion*, Cairns, Queensland, Australia, 2003, pp. 903–910.
- [BSLK01] Y. Bar-Shalom, X. R. Li, and T. Kirubarajan, *Estimation with Applications to Tracking and Navigation*. New York, NY, USA: Wiley-Interscience, 2001.
- [Caf99] J. Caffery, *Wireless location in CDMA cellular radio systems*. Norwell, MA, USA: Kluwer Academic Publishers, 1999.
- [Car05] G. C. Carter, "Coherence and time delay estimation," *Proceedings of the IEEE*, vol. 75, no. 2, pp. 236–255, 2005.
- [CCF99] J. Carpenter, P. Clifford, and P. Fearnhead, "An improved particle filter for non-linear problems," in *IEE Proceedings - Radar, Sonar and Navigation*, vol. 146, 1999, pp. 2–7.
- [CGM07] O. Cappé, S. J. Godsill, and E. Moulines, "An overview of existing methods and recent advances in sequential monte carlo," *Proceedings of the IEEE*, vol. 95, no. 5, pp. 899–924, May 2007.
- [Che99] P.-C. Chen, "A non-line-of-sight error mitigation algorithm in location estimation," in *IEEE Wireless Communications and Networking Conference*, New Orleans, LA, USA, 1999, pp. 316–320.
- [CL00] R. Chen and J. Liu, "Mixture Kalman filters," *Journal of the Royal Statistical Society: Series B (Statistical Methodology)*, vol. 62, no. 3, pp. 493–508, 2000.
- [CR96] G. Casella and C. P. Robert, "Rao-Blackwellization of sampling schemes," *Biometrika*, vol. 83, no. 1, pp. 84–94, 1996.
- [CS04] A. Catovic and Z. Sahinoglu, "The Cramer-Rao bounds of hybrid TOA/RSS and TDOA/RSS location estimation schemes," *IEEE Commun. Lett.*, vol. 8, no. 10, pp. 626–628, Oct. 2004.
- [CS07] Y. Cheng and T. Singh, "Efficient particle filtering for road-constrained target tracking," *IEEE Trans. Aerosp. Electron. Syst.*, vol. 43, no. 4, pp. 1454–1469, 2007.

- [CSMC06] K. W. Cheung, H. C. So, W.-K. Ma, and Y. T. Chan, "A constrained least squares approach to mobile positioning: Algorithms and optimality," *EURASIP Journal on Applied Signal Processing*, vol. 2006, pp. 1–23, 2006.
- [CYLL09] B.-S. Chen, C.-Y. Yang, F.-K. Liao, and J.-F. Liao, "Mobile location estimator in rough wireless environment using extended Kalman-based IMM and data fusion," *IEEE Trans. Veh. Technol.*, vol. 58, no. 3, pp. 1157 – 1169, 2009.
- [CZ01] L. Cong and W. Zhuang, "Non-line-of-sight error mitigation in tdoa mobile location," in *Global Communications Conference (GLOBECOM)*, San Antonio, Texas, USA, Nov 2001, pp. 680–684.
- [CZ02] ———, "Hybrid tdoa/aoa mobile user location for wideband CDMA cellular systems," *IEEE Trans. Wireless Commun.*, vol. 1, no. 3, pp. 439–447, 2002.
- [CZ05] ———, "Nonline-of-sight error mitigation in mobile location," *IEEE Trans. Wireless Commun.*, vol. 4, no. 2, pp. 560–573, 2005.
- [Dau05] F. Daum, "Nonlinear filters: Beyond the Kalman filter," *IEEE Aerospace and Electronic Systems Magazine*, vol. 20, no. 8, pp. 57–69, Aug 2005.
- [DB04] J. N. Driessen and Y. Boers, "An efficient particle filter for nonlinear jump Markov systems," in *Proceedings of IEE Colloquium on Target Tracking*, Sussex, UK, Mar 2004.
- [DC99] E. Damasso and L. M. Correia, Eds., *Digital mobile radio towards future generation systems*. Brussels, Belgium: European Cooperation in the field of Scientific and Technical research (COST), 1999.
- [DC05] R. Douc and O. Cappe, "Comparison of resampling schemes for particle filtering," in *4th International Symposium on Image and Signal Processing and Analysis*, Zagreb, Croatia, Sept 2005, pp. 64–69.
- [DdFG01] A. Doucet, N. de Freitas, and N. Gordon, Eds., *Sequential Monte Carlo Methods in Practice*. New York, NY, USA: Springer-Verlag, 2001.
- [DGA00] A. Doucet, S. J. Godsill, and C. Andrieu, "On sequential Monte Carlo methods for Bayesian filtering," *Statistics and Computing*, vol. 10, no. 3, pp. 197–208, 2000.
- [DGK99] A. Doucet, N. Gordon, and V. Krishnamurthy, "Particle filters for state estimation of jump Markov linear systems," University of Cambridge, Cambridge, UK, Tech. Rep., 1999.
- [DH03] F. Daum and J. Huang, "Curse of dimensionality and particle filters," in *IEEE Aerospace Conference*, vol. 4, Big Sky, USA, Mar 2003, pp. 1979–1993.

- [DJ09] A. Doucet and A. M. Johansen, “A tutorial on particle filtering and smoothing: Fifteen years later,” in *Handbook of Nonlinear Filtering*, D. Crisan and B. Rozovsky, Eds. Oxford, UK: Oxford University Press, 2009.
- [DKK00] D. Drakoulis, S. Kyriazakos, and G. Karetsos, “Improving subscriber position location using a hybrid satellite-assisted and network-based technique,” in *IEEE Vehicular Technology Conference*, Boston, MA, USA, Sept 2000, pp. 1887–1893.
- [DLR77] A. P. Dempster, N. M. Laird, and D. B. Rubin, “Maximum likelihood from incomplete data via the EM algorithm,” *Journal of the Royal Statistical Society. Series B (Methodological)*, vol. 39, no. 1, pp. 1–38, 1977.
- [dM04] P. del Moral, *Feynman-Kac formulae: Genealogical and interacting particle systems with applications*, ser. Probability and Applications. New York, NY, USA: Springer-Verlag, 2004.
- [Do08] J.-Y. Do, “Road to seamless positioning: Hybrid positioning system combining GPS and television signals,” Ph.D. dissertation, Stanford University, Stanford, CA, USA, 2008.
- [Dou98] A. Doucet, “On sequential simulation-based methods for Bayesian filtering,” University of Cambridge, Cambridge, UK, Tech. Rep., 1998.
- [ES07] M. Ekman and E. Sviestins, “Multiple model algorithm based on particle filters for ground target tracking,” in *Proceedings of International Conference on Information Fusion*, Quebec, Canada, 2007, pp. 1–8.
- [EVB01] J. Eberspächer, H.-J. Vögel, and C. Bettstetter, *GSM Global System for Mobile Communication*, 3rd ed. Wiesbaden, Germany: B. G. Teubner, 2001.
- [Fis22] R. A. Fisher, “On the foundations of mathematical statistics,” *The Philosophical Transactions of the Royal Society of London*, vol. A, no. 222, pp. 309–368, 1922.
- [Fis25] ———, “Theory of statistical estimation,” in *Proceedings of the Cambridge Philosophical Society*, vol. 22, 1925.
- [FK08] C. Fritsche and A. Klein, “Cramér-Rao lower bounds for hybrid localization of mobile terminals,” in *Proc. 5th Workshop on Positioning, Navigation and Communication (WPNC’08)*, Mar. 2008, pp. 157–164.
- [FK09] ———, “On the performance of mobile terminal tracking in urban gsm networks using particle filters,” in *European Signal Processing Conference (EUSIPCO)*, Glasgow, Scotland, Aug 2009.
- [FKS06] C. Fritsche, A. Klein, and H. Schmitz, “Mobile station localization by combining measurements from different sources including reliability information,” in *Proc. ITG Fachtagung Innovations for Europe - Mobility*, Aachen, Germany, Oct. 2006, pp. 169–174.

- [FKSP07] C. Fritsche, A. Klein, H. Schmitz, and M. Pakulski, “A hybrid localization method for mobile station location estimation,” in *Proc. ITG Fachgruppensitzung Angewandte Informationstheorie: Signalverarbeitung in der Navigation*, Oberpfaffenhofen, Germany, Oct. 2007, pp. 66–73.
- [FPCFR07] C. Fernández-Prades, P. Closas, and J. A. Fernández-Rubio, “Rao-Blackwellized variable rate particle filtering for handset tracking in communication and sensor networks,” in *Proc. European Signal Processing Conference*, Poznań, Poland, Sept. 2007, pp. 111–115.
- [FSK09] C. Fritsche, T. B. Schön, and A. Klein, “The marginalized auxiliary particle filter,” in *3rd IEEE International Workshop on Computational Advances in Multi-Sensor Adaptive Processing*, Aruba, Dutch Antilles, Dec 2009.
- [G<sup>+</sup>74] A. Gelb *et al.*, *Applied Optimal Estimation*, A. Gelb, Ed. Cambridge, MA, USA: MIT Press, 1974.
- [GAM05] E. Grosicki and K. Abed-Meraim, “A new trilateration method to mitigate the impact of some non-line-of-sight errors in TOA measurements for mobile localization,” in *IEEE International Conference on Acoustics, Speech and Signal Processing*, Philadelphia, PA, USA, Mar 2005, pp. 1045–1048.
- [GG05] F. Gustafsson and F. Gunnarsson, “Mobile positioning using wireless networks,” *IEEE Signal Process. Mag.*, vol. 22, no. 4, pp. 41–53, Jul. 2005.
- [GKP03] S. Gezici, H. Kobayashi, and H. V. Poor, “Non-parametric non-line-of-sight identification,” in *IEEE Vehicular Technology Conference*, Orlando, Florida, USA, Oct 2003, pp. 2544–2548.
- [GP09] S. Gezici and H. V. Poor, “Position estimation via ultra-wideband signals,” *Proceedings of the IEEE*, vol. 97, no. 2, pp. 386–403, 2009.
- [GSS93] N. J. Gordon, D. J. Salmond, and A. F. M. Smith, “Novel approach to nonlinear/non-Gaussian Bayesian state estimation,” in *IEE Proceedings on Radar and Signal Processing*, vol. 140, 1993, pp. 107–113.
- [Gus10a] F. Gustafsson, “Particle filter theory and practice with positioning applications,” *IEEE Aerospace and Electronic Systems Magazine*, vol. 25, no. 7, pp. 53–82, Jul 2010.
- [Gus10b] —, *Statistical Sensor Fusion*. Lund, Sweden: Studentlitteratur AB, 2010.
- [GWA07] M. S. Grewal, L. R. Weill, and A. P. Andrews, *Global positioning systems, inertial navigation and integration*, 2nd ed. New York, NY, USA: John Wiley & Sons, 2007.
- [Hat80] M. Hata, “Empirical formula for propagation loss in land mobile radio services,” *IEEE Trans. Veh. Technol.*, vol. 29, no. 3, pp. 317–325, Aug. 1980.

- [HGVT07] J. M. Huerta, A. Giremus, J. Vidal, and J.-Y. Tournet, “Joint particle filter and UKF position tracking under strong NLOS situation,” in *IEEE Workshop on Statistical Signal Processing*, Madison, WI, USA, Aug 2007, pp. 547–541.
- [HL64] Y. C. Ho and R. C. K. Lee, “A Bayesian approach to problems in stochastic estimation and control,” *IEEE Trans. Autom. Control*, vol. 9, pp. 333–338, 1964.
- [HMD04] G. Heinrichs, P. Mulassano, and F. Dervis, “A hybrid positioning algorithm for cellular radio networks by using a common rake receiver architecture,” in *Proc. 15th International Symposium Personal Indoor and Mobile Communications*, vol. 4, Sept. 2004, pp. 2347–2351.
- [HRF05] M. L. Hernandez, B. Risic, and A. Farina, “A performance bound for manoeuvring target tracking using best-fitting gaussian distributions,” in *Proceeding of International Conference on Information Fusion*, Philadelphia, PA, USA, 2005, pp. 1–8.
- [HSG06] J. D. Hol, T. B. Schön, and F. Gustafsson, “On resampling algorithms for particle filters,” in *IEEE Workshop on Nonlinear Statistical Signal Processing*, Cambridge, UK, Sept 2006, pp. 79–82.
- [HSL08] X.-L. Hu, T. B. Schön, and L. Ljung, “A basic convergence result for particle filtering,” *IEEE Trans. Signal Process.*, vol. 4, pp. 1337–1348, 2008.
- [HWZ08] U. Hammes, E. Wolsztynski, and A. M. Zoubir, “Semi-parametric geolocation estimation in NLOS environments,” in *European Signal Processing Conference*, Lausanne, Switzerland, Aug 2008.
- [HWZ09] —, “Robust tracking and geolocation for wireless networks in NLOS environments,” *IEEE Journal of Selected Topics in Signal Processing*, vol. 3, no. 5, pp. 889–901, 2009.
- [HZ10] U. Hammes and A. Zoubir, “Robust mobile terminal tracking in NLOS environments based on data association,” *IEEE Trans. Signal Process.*, vol. 58, no. 11, pp. 5872 – 5882, 2010.
- [Jaz70] A. H. Jazwinski, *Stochastic Processes and Filtering Theory*, ser. Mathematics in Science and Engineering. New York, NY, USA: Academic Press, 1970, vol. 64.
- [JCS98] J. James Caffery and G. L. Stüber, “Subscriber location in cdma cellular networks,” *IEEE Trans. Veh. Technol.*, vol. 47, no. 2, pp. 406–416, 1998.
- [JEDS83] J. J. E. Dennis and R. B. Schnabel, *Numerical Methods for Unconstrained Optimization and Nonlinear Equations*. Upper Saddle River, NJ, USA: Prentice-Hall, 1983.
- [Jul02] S. Julier, “The scaled unscented transformation,” in *Proc. of American Control Conference*, vol. 6, May 2002, pp. 4555–4559.

- [Kal60] R. E. Kalman, "A new approach to linear filtering and prediction problems," *Transactions of the American Society of Mechanical Engineering-Journal Basic Engineering*, vol. 82, no. 1, pp. 35–45, Mar. 1960.
- [Kap96] E. D. Kaplan, Ed., *Understanding GPS: principles and applications*, 1st ed. Boston, MA, USA: Artech-House, 1996.
- [Kay93] S. M. Kay, *Fundamentals of statistical signal processing: estimation theory*, 1st ed. Upper Saddle River, NJ, USA: Prentice-Hall, 1993.
- [KB00] R. Karlsson and N. Bergman, "Auxiliary particle filters for tracking a maneuvering target," in *Proceedings of the IEEE Conference on Decision and Control*, Sydney, Australia, Dec 2000, pp. 3891–3895.
- [KDTSP00] S. Kyriazakos, D. Drakoulis, M. Theologou, and J.-A. Sanchez-P., "Localization of mobile terminals, based on a hybrid satellite-assisted and network-based techniques," in *Proc. of IEEE Wireless Communications and Networking Conference (WCNC)*, vol. 2, Sept. 2000, pp. 798–802.
- [Kel99] C. T. Kelley, *Iterative Methods for Optimization*. Philadelphia, PA, USA: SIAM Publications, 1999.
- [KGP05] M. Kuipers, P. Gradalski, and M. Pakulski, "Low cost positioning and efficient fallback in GSM and UTRAN networks," in *Workshop on Positioning, Navigation and Communication*, Hanover, Germany, Mar. 2005, pp. 57–62.
- [KOB01] T. Kleine-Ostmann and A. E. Bell, "A data fusion architecture for enhanced position estimation in wireless networks," *IEEE Commun. Lett.*, vol. 5, no. 8, pp. 343–345, 2001.
- [Küp05] A. Küpper, *Location-based services*, 1st ed. New York, NY, USA: John Wiley & Sons, 2005.
- [KR99] L. Koolen and T. Rantalainen, "Mobile standardization and regulatory issues - an European perspective," in *IBC Conference on Mobile Location Services*, London, UK, Nov 1999.
- [KSG05] R. Karlsson, T. Schön, and F. Gustafsson, "Complexity analysis of the marginalized particle filter," *IEEE Trans. Signal Process.*, vol. 53, no. 11, pp. 4408–4411, Nov. 2005.
- [KV99] H. Krim and M. Viberg, "Two decades of array signal processing research: the parametric approach," *IEEE Signal Processing Magazine*, vol. 13, no. 4, pp. 67–94, 1999.
- [LC98] E. Lehmann and G. Casella, *Theory of point estimation*, 2nd ed., ser. Springer Texts in Statistics. New York, NY, USA: Springer-Verlag, 1998.
- [LC06] J.-F. Liao and B.-S. Chen, "Robust mobile location estimator with NLOS mitigation using IMM algorithm," *IEEE Trans. Wireless Commun.*, vol. 5, no. 11, pp. 3002–3006, Nov 2006.

- [Lev44] K. Levenberg, "A method for the solution of certain problems in least squares," *Quarterly of Applied Mathematics*, vol. 2, pp. 164–168, 1944.
- [Lev00] N. Levanon, "Lowest GDOP in 2-D scenarios," in *IEE Proc. Radar, Sonar and Navigation.*, vol. 147, no. 3, Jun. 2000, pp. 149–155.
- [Lip74] S. Lipschutz, *Schaum's Outline of Theory and Problems of Probability*. New York, NY, USA: Mc-Graw Hill, 1974.
- [LJ03] X. R. Li and V. P. Jilkov, "Survey of maneuvering target tracking. part i: Dynamic models," *IEEE Trans. Aerosp. Electron. Syst.*, vol. 39, no. 4, pp. 1333–1364, 2003.
- [LJ05] X.-R. Li and V. P. Jilkov, "Survey of maneuvering target tracking. part v: Multiple-model methods," *IEEE Trans. Aerosp. Electron. Syst.*, vol. 41, no. 4, pp. 1255–1321, 2005.
- [LLP09] C. Liang, W. Lenan, and R. Piche, "Posterior Cramer-Rao lower bound for mobile tracking in mixed LOS/NLOS conditions," in *European Signal Processing Conference*, Glasgow, Scotland, Aug 2009, pp. 90–94.
- [LRWW98] J. C. Lagarias, J. A. Reeds, M. H. Wright, and P. E. Wright, "Convergence properties of the Nelder-Mead simplex method in low dimensions," *SIAM J. OPTIM.*, vol. 9, no. 1, pp. 112–147, Dec. 1998.
- [MABSD98] E. Mazor, A. Averbuch, Y. Bar-Shalom, and J. Dayan, "Interacting multiple model methods in target tracking: A survey," *IEEE Trans. Aerosp. Electron. Syst.*, vol. 34, no. 1, pp. 103–123, 1998.
- [MAH<sup>+</sup>07] L. Mihaylova, D. Angelova, S. Honary, D. Bull, C. N. Canagarajah, and B. Ristic, "Mobility tracking in cellular networks using particle filtering," *IEEE Trans. Wireless Commun.*, vol. 6, pp. 3589–3599, Oct. 2007.
- [Mar63] D. Marquardt, "An algorithm for least squares estimation on nonlinear parameters," *SIAM J. APPL. MATH.*, vol. 11, pp. 431–441, 1963.
- [ME06] P. Misra and P. Enge, *Global Positioning System: Signals, Measurements, and Performance*, 2nd ed. Lincoln, MA, USA: Ganga-Jamuna Press, 2006.
- [MI00] S. McGinnity and G. W. Irwin, "Multiple model bootstrap filter for maneuvering target tracking," *IEEE Trans. Aerosp. Electron. Syst.*, vol. 36, no. 3, pp. 1006–1012, 2000.
- [MK97] G. J. McLachlan and T. Krishnan, *The EM algorithm and extensions*, ser. Wiley Series in Probability and Statistics. New York, NY, USA: John Wiley & Sons, Inc., 1997.
- [MNT04] K. Madsen, H. Nielsen, and O. Tingleff, "Methods for non-linear least squares problems," [http://www2.imm.dtu.dk/pubdb/views/publication\\_details.php?id=3215](http://www2.imm.dtu.dk/pubdb/views/publication_details.php?id=3215), Kongens Lyngby, Denmark, 2004.



- [MPV00] M. McGuire, K. N. Plataniotis, and A. N. Venetsanopoulos, “Robust estimation of mobile terminal position,” *Electronics Letters*, vol. 36, no. 16, pp. 1426–1428, 2000.
- [MPV03] ———, “Location of mobile terminals using time measurements and survey points,” *IEEE Trans. Veh. Technol.*, vol. 52, no. 4, pp. 999–1011, 2003.
- [MPV05] ———, “Data fusion of power and time measurements for mobile terminal location,” *IEEE Trans. Mobile Comput.*, vol. 4, no. 2, pp. 142–153, 2005.
- [MSD09] C. Mensing, S. Sand, and A. Damman, “GNSS positioning in critical scenarios: Hybrid data fusion with communication signals,” in *International Conference of Communications, International Workshop on Synergies in Communications and Localization*, Dresden, Germany, Jun 2009.
- [MSD10] ———, “Hybrid data fusion and tracking for positioning with GNSS and 3GPP-LTE,” *International Journal of Navigation and Observation*, vol. 2010, pp. 1–12, 2010.
- [MU49] N. Metropolis and S. Ulam, “The monte carlo method,” *Journal of the American Statistical Association*, vol. 44, no. 247, pp. 335–341, 1949.
- [NB99] M. E. J. Newman and G. T. Barkema, *Monte Carlo Methods in Statistical Physics*. Oxford, UK: Oxford University Press, 1999.
- [NHVC04] M. Najar, J. M. Huerta, J. Vidal, and J. A. Castro, “Mobile location with bias tracking in non-line-of-sight,” in *IEEE International Conference on Acoustics, Speech and Signal Processing*, Montreal, Quebec, Canada, May 2004, pp. 956–959.
- [Nie99] H. B. Nielsen, “Damping parameter in Marquardt’s method,” IMM DTU, Tech. Rep., 1999.
- [NM65] J. A. Nelder and R. Mead, “A simplex method for function minimization,” *Computer Journal*, vol. 7, pp. 308–313, 1965.
- [NV03] M. Najar and J. Vidal, “Kalman tracking for mobile location in NLOS environments,” in *Proceedings of IEEE Conference on Personal, Indoor and Mobile Communications*, Beijing, China, Sept 2003, pp. 2203–2207.
- [OOKF68] Y. Okumura, E. Ohmori, T. Kawano, and K. Fukuda, “Field strength and its variability in VHF and UHF land-mobile radio service,” *Rev. Elec. Commun. Lab.*, vol. 16, pp. 9–10, 1968.
- [OSG09] U. Orguner, T. B. Schön, and F. Gustafsson, “Improved target tracking with road network information,” in *IEEE Aerospace Conference*, Big Sky, MT, USA, Mar 2009, pp. 1–11.
- [Pap84] A. Papoulis, *Probability, random variables, and stochastic processes*, 2nd ed. New York, NY, USA: McGraw-Hill, 1984.

- [PP07] T. Perala and R. Piche, “Robust extended kalman filtering in hybrid positioning applications,” in *Workshop on Positioning, Navigation and Communication*, Hanover, Germany, Mar 2007, pp. 55–63.
- [PS99] M. Pitt and N. Shephard, “Filtering via simulation: Auxiliary particle filters,” *Journal of the American Statistical Association*, vol. 94, no. 446, pp. 590–599, 1999.
- [PST97] M. Pent, M. A. Spirito, and E. Turco, “Method for positioning GSM mobile stations using absolute time delay measurements,” *IEEE Electronic Letters*, vol. 33, no. 24, pp. 2019–2020, Nov. 1997.
- [PZV02] A. Pages-Zamora and J. Vidal, “Evaluation of the improvement in the position estimate accuracy of UMTS mobiles with hybrid positioning techniques,” in *IEEE Vehicular Technology Conference*, Birmingham, AL, USA, May 2002, pp. 1631–1635.
- [Qi03] Y. Qi, “Wireless geolocation in a non-line-of-sight environment,” Ph.D. dissertation, Princeton University, Princeton, New Jersey, USA, 2003.
- [QKS06] Y. Qi, H. Kobayashi, and H. Suda, “Analysis of wireless geolocation in a non-line-of-sight environment,” *IEEE Trans. Wireless Commun.*, vol. 5, no. 3, pp. 672–681, Mar. 2006.
- [RAG04] B. Ristic, S. Arulampalam, and N. Gordon, *Beyond the Kalman Filter: Particle Filters for Tracking Applications*. Boston, MA, USA: Artech-House, 2004.
- [Rao46] C. R. Rao, “Minimum variance and the estimation of several parameters,” in *Proceedings of the Cambridge Philosophical Society*, vol. 43, 1946, pp. 280–283.
- [Rap02] T. S. Rappaport, *Wireless Communications: Principles and Practice*, 2nd ed. Upper Saddle River, NJ, USA: Prentice Hall, 2002.
- [RC99] C. P. Robert and G. Casella, *Monte Carlo Statistical Methods*, ser. Springer Texts in Statistics. New York, NY, USA: Springer-Verlag, 1999.
- [RCC+00] S. Rooney, P. Chippendale, R. Choony, C. L. Roux, and B. Honary, “Accurate vehicular positioning using a DAB-GSM hybrid system,” in *IEEE Vehicular Technology Conference*, Tokyo, Japan, Sept 2000, pp. 97–101.
- [RNALP08] M. Raitoharju, N. Sirola, S. Ali-Loytty, and R. Piche, “Pnaff: A modular software platform for testing hybrid position estimation algorithms,” in *Workshop on Positioning, Navigation and Communication*, Hanover, Germany, 2008, pp. 137 – 141.
- [RU04] J. Riba and A. Urruela, “A non-line-of-sight mitigation technique based on ML detection,” in *IEEE International Conference on Acoustics, Speech and Signal Processing*, Montreal, Quebec, Canada, May 2004, pp. 153–156.

- [SAF<sup>+</sup>00] S. Soliman, P. Agashe, I. Fernandez, A. Vayanos, P. Gaal, and M. Oljaca, “gpsOne<sup>tm</sup>: a hybrid position location system,” in *Proc. International Symposium on Spread Spectrum Techniques and Applications*, vol. 1, Sept. 2000, pp. 330–335.
- [SB99] D. D. Sworder and J. E. Boyd, *Estimation Problems in Hybrid Systems*. Cambridge, UK: Cambridge University Press, 1999.
- [SC04] Z. Sahinoglu and A. Catovic, “A hybrid location estimation scheme (HLES) for partially synchronized wireless sensor networks,” in *Proceedings of International Conference on Communications*, Paris, France, Jun 2004, pp. 3797–3801.
- [SCGL05] G. Sun, J. Chen, W. Guo, and K. J. R. Liu, “Signal processing techniques in network-aided positioning: a survey of state-of-the-art positioning designs,” *IEEE Signal Process. Mag.*, vol. 22, no. 4, pp. 12–23, Jul. 2005.
- [Sch03] T. Schön, “On computational methods for nonlinear estimation,” Licentiate Thesis, Linköping University, Linköping, Sweden, 2003.
- [SG04] G. Sun and W. Guo, “Bootstrapping M-estimators for reducing errors due to non-line-of-sight (NLOS) propagation,” *IEEE Commun. Lett.*, vol. 8, no. 8, pp. 509–510, 2004.
- [SGKJ07] J. Schroeder, S. Galler, K. Kyamakya, and K. Jobmann, “NLOS detection algorithms for ultra-wideband localization,” in *Workshop on Positioning, Navigation and Communication*, Hanover, Germany, 2007, pp. 159–166.
- [SGN05] T. Schön, F. Gustafsson, and P.-J. Nordlund, “Marginalized particle filters for mixed linear/nonlinear state-space models,” *IEEE Trans. Signal Process.*, vol. 53, no. 7, pp. 2279–2289, Jul. 2005.
- [SGR04] R. Singh, M. Guainazzo, and C. R. Regazzoni, “Location determination using WLAN in conjunction with GPS network,” in *Vehicular Technology Conference*, Milan, Italy, May 2004, pp. 2695–2699.
- [Sim06] D. Simon, *Optimal State Estimation*. New York, NY, USA: John Wiley & Sons, 2006.
- [SLJ03] H. C. Son, J. G. Lee, and G. I. Jee, “Mobile station location using hybrid GPS and a wireless network,” in *IEEE Vehicular Technology Conference*, Jeju Island, Korea, Apr 2003, pp. 2716–2720.
- [SM99] M. A. Spirito and A. G. Mattioli, “Preliminary experimental results of a GSM mobile phones positioning system based on timing advance,” *IEEE VTS 50th Vehicular Technology Conference*, vol. 4, pp. 2072–2076, Sept. 1999.
- [Spi01] M. A. Spirito, “On the accuracy of cellular mobile station location estimation,” *IEEE Trans. Veh. Technol.*, vol. 50, no. 3, pp. 674–685, May. 2001.

- [SPK01] M. A. Spirito, S. Pöykkö, and O. Knuuttila, “Experimental performance of methods to estimate the location of legacy handsets in GSM,” in *Proc. Vehicular Technology Conference*, vol. 4, Oct. 2001, pp. 2716–2720.
- [SR96] M. I. Silventoinen and T. Rantalainen, “Mobile station emergency locating in gsm,” in *IEEE International Conference on Personal Wireless Communications*, New Dehli, India, Feb 1996.
- [SS99] S. Singer and S. Singer, “Complexity analysis of nelder-mead search iterations,” in *1st Conference on Applied Mathematics and Computation*, Dubrovnik, Croatia, Sept 1999, pp. 185–196.
- [STK05] A. H. Sayed, A. Tarighat, and N. Khajehnouri, “Network-based wireless location: challenges faced in developing techniques for accurate wireless location information,” *IEEE Signal Process. Mag.*, vol. 22, no. 4, pp. 24–40, Jul. 2005.
- [Sve10] L. Svensson, “On the Bayesian Cramér-Rao bound for Markovian switching systems,” *IEEE Trans. Signal Process.*, vol. 58, no. 9, pp. 4507–4516, 2010.
- [TCL01a] N. J. Thomas, D. G. M. Cruickshank, and D. I. Laurenson, “Performance of a TDOA-AOA hybrid mobile location system,” in *Conference on 3G Mobile Communications Technologies*, London, UK, Mar 2001, pp. 216–220.
- [TCL01b] N. J. Thomas, D. G. M. Cruickshank, and D. Laurenson, “Calculation of mobile location using scatterer information,” *Electronics Letters*, vol. 37, no. 19, pp. 1193–1194, 2001.
- [TMN98] P. Tichavský, C. H. Muravchik, and A. Nehorai, “Posterior Cramér-Rao bounds for discrete-time nonlinear filtering,” *IEEE Trans. Signal Process.*, vol. 46, no. 5, pp. 1386–1396, May. 1998.
- [Tor84] D. J. Torrieri, “Statistical theory of passive location systems,” *IEEE Trans. Aerosp. Electron. Syst.*, vol. 20, no. 2, pp. 183–198, 1984.
- [Tör08] D. Törnqvist, “Estimation and detection with applications to navigation,” Ph.D. dissertation, Linköpings Univeristet, Linköping, Sweden, 2008.
- [Tri99] G. Tristani, “FCC 99-245: Third report and order,” Federal Communications Commission, <http://www.fcc.gov/911/enhanced>, Tech. Rep., Oct. 1999.
- [UK06] M. Ulmke and W. Koch, “Road-map assisted ground target tracking,” *IEEE Trans. Aerosp. Electron. Syst.*, vol. 42, no. 3, pp. 1264–1274, 2006.
- [VC02] S. Venkatraman and J. Caffery, “Statistical approach to non-line-of-sight BS identification,” in *International Symposium on Wireless Personal Multimedia Communications*, Honolulu, Hawaii, USA, Oct 2002, pp. 296–300.

- [vDBB84] A. J. van Dierendonck, J. B. Brown, and R. Brown, "Relationship between allan variances and kalman filter parameters," in *16th Annual Precise Time and Time Interval (PTTI) Applications and Planning Meeting*, Greenbelt, Maryland, USA, Nov 1984, pp. 273–292.
- [vT68] H. L. van Trees, *Detection, Estimation and Modulation Theory Part I*. New York, NY, USA: John Wiley & Sons, 1968.
- [VWG<sup>+</sup>04] M. Vossiek, L. Wiebking, P. Gulden, J. Wiegardt, C. Hoffmann, and P. Heide, "Wireless local positioning," *IEEE Microwave Magazine*, vol. 4, pp. 77–86, 2004.
- [WB01] G. Welch and G. Bishop, "An introduction to the Kalman filter," in *Proceedings of SIGGRAPH conference*, Los Angeles, CA, USA, Aug. 2001.
- [WH96] M. P. Wylie and J. Holtzmann, "The non-line of sight problem in mobile location estimation," in *IEEE International Conference on Universal Personal Communications*, vol. 2, Cambridge, Massachussets, USA, Sept 1996, pp. 827–831.
- [WvdM00] E. A. Wan and R. van der Merwe, "The unscented Kalman filter for nonlinear estimation," in *Proceedings of Symposium 2000 on Adaptive Systems for Signal Processing, Communication and Control (AS-SPCC)*, Oct. 2000, pp. 153–158.
- [WWO03] X. Wang, Z. Wang, and B. O’Dea, "A TOA-based location algorithm reducing the errors due to non-line-of-sight (NLOS) propagation," *IEEE Trans. Veh. Technol.*, vol. 52, no. 1, pp. 112–116, 2003.
- [YG09] K. Yu and Y. J. Gu, "Statistical nlos identification based on aoa, toa, and signal strength," *IEEE Trans. Veh. Technol.*, vol. 58, no. 1, pp. 274–286, 2009.
- [ZKUL06] M. Zhang, S. Knedlik, P. Ubolkosold, and O. Loffeld, "A data fusion approach for improved positioning in GSM networks," in *Proc. IEEE/ION Position, Location, and Navigation Symposium*, San Diego, USA, Apr. 2006, pp. 218–222.
- [ZLB08] M. Zhaounia, M. A. Landolsi, and R. Bouallegue, "Hybrid TOA/AOA mobile localization with NLOS mitigation in ring scattering environments," in *3rd International Symposium of Wireless Pervasive Computing*, Santorini, Greece, May 2008, pp. 370–373.



# Lebenslauf

Name: Carsten Fritsche  
Anschrift: Schlosserstraße 1, 64287 Darmstadt  
Geburtsdatum: 20.07.1978  
Geburtsort: Groß-Gerau  
Familienstand: ledig

## Schulbildung

08/1985-06/1989 Grundschule in Reinheim  
08/1989-06/1998 Albert-Einstein Schule in Groß-Bieberau

## Studium

10/1999-03/2005 Studium der Elektro- und Informationstechnik  
an der Technischen Universität Darmstadt,  
Studienabschluß: Diplom

## Berufstätigkeit

07/2005-06/2010 wissenschaftlicher Mitarbeiter am  
Fachgebiet Kommunikationstechnik,  
Institut für Nachrichtentechnik,  
Technische Universität Darmstadt





Erklärung laut §9 der Promotionsordnung

Ich versichere hiermit, dass ich die vorliegende Dissertation allein und nur unter Verwendung der angegebenen Literatur verfasst habe. Die Arbeit hat bisher noch nicht zu Prüfungszwecken gedient.

Darmstadt, 14. Januar 2008,

